Université de Neuchâtel

Geochemical and Environmental Analysis

Palaeoceanographic and palaeoclimatic changes during the Late Hauterivian - Barremian and their impact on the northern Tethyan margin:

A combined sedimentological and geochemical approach

Stéphane Bodin

Institut de Géologie et d'Hydrogéologie
Université de Neuchâtel

Jury:

Prof. Karl B. Föllmi (Neuchâtel)	Directeur
Prof. Thierry Adatte (Neuchâtel)	Rapporteur
Dr. Virginie Matera (Neuchâtel)	Rapporteur
Prof. André Strasser (Fribourg)	Rapporteur
Prof. François Baudin (Paris VI)	Rapporteur

27 Novembre 2006

Palaeoceanographic and palaeoclimatic changes during the Late Hauterivian - Barremian and their impact on the northern Tethyan margin:

A combined sedimentological and geochemical approach

Thèse présentée à la Faculté des Sciences
Institut de Géologie et d'Hydrogéologie
Université de Neuchâtel

Pour l'obtention du grade de docteur ès Sciences

Par

Stéphane Bodin

Acceptée sur la proposition du jury :

Prof. Karl B. Föllmi, directeur de thèse
Prof. Thierry Adatte, rapporteur
Dr. Virginie Matera, rapporteur
Prof. André Strasser, rapporteur
Prof. François Baudin, rapporteur

Soutenue le 27 Novembre 2006

Université de Neuchâtel
2006

Université de Neuchâtel

FACULTE DES SCIENCES
Secrétariat-Décanat de la faculté
- Rue Emile-Argand 11
- CP 158
- CH-2009 Neuchâtel

IMPRIMATUR POUR LA THESE

Palaeoceanographic and palaeoclimatic changes during the Late Hauterivian - Barremian and their impact on the northern Tethyan margin : a combined sedimentological and geochemical approach

Stéphane BODIN

UNIVERSITE DE NEUCHATEL

FACULTE DES SCIENCES

La Faculté des sciences de l'Université de Neuchâtel,
sur le rapport des membres du jury

Mme V. Matera,
MM. K. Föllmi (directeur de thèse), T. Adatte, A. Strasser (Fribourg),
et B. Baudin (Paris)

autorise l'impression de la présente thèse.

Neuchâtel, le 12 décembre 2006

Le doyen :
J.-P. Derendinger

UNIVERSITE DE NEUCHATEL
FACULTE DES SCIENCES
Secrétariat-décanat de la faculté
Rue Emile-Argand 11 - CP 158
CH-2009 Neuchâtel

■ Téléphone : +41 32 718 21 00 ■ Fax : +41 32 718 21 03 ■ E-mail : secretariat.sciences@unine.ch ■ www.unine.ch/sciences

Keywords

Hauterivian; Barremian; northern Tethyan margin; photozoan; heterozoan; carbonate platform drowning; Altmann Member; Urgonian limestone; ammonite biostratigraphy; belemnites; Faraoni Level; redox-sensitive trace metals; phosphorus burial rates; carbon and oxygen isotopes.

Mots clés: Hauterivien; Barrémien ; marge Nord-Tethysienne ; photozoaire ; hétérozoaire ; ennoiement de plate-forme carbonatée ; membre d'Altmann ; calcaire urgonien ; biostratigraphie des ammonites ; bélemnites ; niveau Faraoni ; métaux traces sensibles aux conditions redox ; taux d'enfouissement du phophore ; isotopes du carbone et de l'oxygène.

Abstract

The goal of this PhD study was to decipher the mechanisms responsible for changes in the carbonate platform factory accompanied by incipient drowning. For this purpose, a peculiar condensed level called the Altmann Member, which recorded the northern Tethyan margin drowning during the latest Hauterivian – Early Barremian, and which is now locked up in the Helvetic realm, was studied. Indeed, this horizon is situated at the verge of a major change in the carbonate platform production mode. On one hand, during the Hauterivian, heterotrophic organisms such as crinoids and bryozoans dominated the northern Tethyan carbonate platforms. On the other hand, phototrophic organisms such as corals, green algae and rudists dominated during the Late Barremian. This important transition and its documentation in the shelf and basinal realms of the Tethys offered the framework of this study.

Helvetic realm: A first step was to establish as precisely as possible the time range of the Late Hauterivian – Barremian sediments in the Helvetic realm. Thanks to numerous ammonite findings, it was possible to determine that the Altmann Member spans from the *Pseudothurmannia seitzi* (latest Hauterivian) to the *Coronites darsi* (latest Early Barremian) ammonite zones. The onset of the Schrattenkalk Formation is dated by sequence stratigraphy correlation and by ammonite findings in the Chopf Member. This event is dated as belonging to the *Gerhardtia sartousiana* zone.

Sedimentology and sequence stratigraphy studies helped to determine the unfolding of the Altmann Member drowning episode, which has proceeded in two steps. The first one is coeval with the Faraoni event, which was thus far only reported from basinal settings. The second step is coeval with the Barremian second-order sea-level rise occurring at the Early – Late Barremian transition. During the Early Barremian second-order sea-level lowstand, the Helvetic platform was submitted to winnowing currents leading to the formation of phosphatized crusts.

Basin sections: In order to understand the link between carbonate platform factory changes and drowning events, geochemical studies were done on bulk-rock and belemnite samples from (hemi-) pelagic sections. These include redox-sensitive trace metals, phosphorus, carbon and oxygen isotopes. Four sections were chosen: the Angles section, SE France, which is the Barremian stratotype section; the Veveyse de Châtel – St. Denis section, Ultrahelvetic realm, Switzerland: the Fiume-Bosso and Gorgo a Cerbara sections, Umbria-Marche basin, Italy. These four sections offer a good coverage of the western Tethys and allow thus to establish general trends in the paleoceanographic conditions of the western Tethys at that time.

Enrichments of redox-sensitive trace metals were used to trace oceanic anoxic events during the Late Hauterivian – Early Barremian, because numerous black-shale horizons are recognized in the corresponding rocks. Only one level, corresponding to the Faraoni Level, was identified as the result of an oceanic anoxic event. This result is confirmed by the C/P ratio that shows a positive shift associated to the Faraoni Level.

Phosphorus burial rates were used to trace nutrient contents in the ocean during the Late Hauterivian – Barremian. They have resulted in a tripartite division of trophic conditions during the studied time interval. Thus, the middle Late Hauterivian is associated to mesotrophic conditions, the latest Hauterivian – Early Barremian to eutrophic conditions and the Late Barremian to oligotrophic conditions.

Bulk rock carbon isotopes were investigated in order to obtain information about the carbon cycle and its link to the carbonate platform. It appears that the bulk-rock carbon isotope signal in basinal sections situated close to the northern Tethyan margin is strongly influenced by carbonate factory changes due to carbonate platform shedding into the basin. During the time of heterozoan-dominated platform growth, the pelagic carbon isotope signal is buffered by the shedding of calcite-dominated fragments and dissolved inorganic carbon. During the time of photozoan-dominated platform growth, the pelagic carbon isotope signal is pushed to heavier values due to the export of aragonite.

Finally, in order to better understand the interactions between palaeoenvironmental changes and carbonate platform, an integrated approach, coupling numerous geochemical data as well as clay minerals, sea-level changes and others information, was done. This approach allows to conclude that changes in the northern Tethyan carbonate platform factory were driven by the overall nutrient content in seawater. During times of oligotrophic conditions, photozoan carbonate systems dominated the neritic realm whereas during times of meso-eutrophic conditions, heterozoan carbonate systems developed. Moreover, carbonate platform drowning events were linked to changes in ocean current pattern during time of sea-level highstand, together with high seawater nutrient levels. These changes have favored winnowing of platform-surface sediments and the deposition of phosphate-rich layers, and precluded carbonate platform growth along the northern Tethyan margin.

Acknowledgment

First of all, I would like to thank my supervisor Karl Föllmi, who set up this project and allow me to work on it. His door was always open for questions and comments on the latest results and crucial interrogations. His curiosity, open-mindedness and skills were much appreciated and I have learned many basics of the carbonate system from him.
I could never see so far if I did not climb on the shoulder of my master…

This work was done in close collaboration with Alexis Godet. During four years, we have shared lots of things (office, lab, coffee-break, field-trip, cigarettes, etc…) and numerous hours of discussion. I have very much appreciated him as my colleague and, above all, as my friend.

In the GEA laboratory, skills and advices of Virginie Matera (*ICP Queen*), Thierry Adatte (*Perturbator*) and Philipp Steinmann have considerably helped to improve my work. This PhD thesis benefited greatly from their comments.

A scientific project cannot be achieved without money, and I therefore gratefully acknowledge the Swiss National Science Foundation who financially supported this work (projects 2100-067807/1 and 200020-105206/1). I also acknowledge André Strasser (Fribourg) and François Baudin (Paris VI) who have accepted to be member of the jury.

Jean Vermeulen is the "official" ammonite specialist of this work. Nothing would be possible at the same level of precision in biostratigraphy without his expertise. I would acknowledge him for being always present when needed, and for many hours we spend together in his house to identify the ammonites, and on the field to sample the "route d'Angles" section.

I thank Nicolas Fiet and Zsolt Berner, who have done the carbon and oxygen isotope analyses. The expertise of Haydon Mort with the SEDEX method, as well as the numerous hours of phosphorus cycle discussion, was much appreciated. Tiffany Monnier assisted us considerably for preparing the ICP-MS samples. In the domain of Helvetic realm ammonite collection, the help of Hans-Peter Funk was very helpful. I would like to thank him for the interest he has shown in my work. The great knowledge of the Urgonian limestone system of Annie Arnaud-Vanneau and Hubert Arnaud was also much appreciated. I also thank Bas van de Schootbrugge for his advices on belemnites preparation. André Villard is acknowledged for the preparation of thin-sections and for numerous discussions about car, fish, and life at the institute.

The Museums of Natural History of St. Gallen and Dornbirn, and the ETH Zürich, are acknowledged for providing Altmann Member ammonites from their collections. The same goes for the Reserve Géologique de Haute-Provence and Myette Guiomar for providing fieldwork pass in the Vocontian trough. The help of Elisabeth Kuster was much appreciated when I was lost in the library. The secretariat work by Cianfranca Cerrito and Sabine Erb helped to make administrative stuff easier. Manuel Da Silvia is also acknowledged for its everyday smile.

Walking and sampling alone in the mountain, or along a hot macadam road, was not so frequent thanks to the researchers or students that helped me during my numerous field-trip. I therefore want to thank Karl Föllmi, Thierry Adatte, Hans-Peter Funk, Urs Oberli, Ueli Briegel, Pascal Linder, Laure Pelletier, Laureline Scherler, Charles Robert-Charrue, Claire Rambeau, Stéphane Westermann and Haydon Mort for their help on the field.

My co-authors, Alexis Godet, Karl Föllmi, Thierry Adatte, Virginie Matera, Philipp Steinmann, Jean Vermeulen, Nicolas Fiet, Arnaud Clément, Nico Janssen, André Strasser, Hubert Arnaud, Bas

Van de Schootbrugge, Pascal Linder, Silvia Gardin and Rodolfo Coccioni are gratefully acknowledge for their comments and suggestions on the papers.

Friends in Neuchâtel helped to make life easier: Alex, Mary-Alix, Laure, Beni, Charles, Erwan, Stéphane, Virginie, Flurin, Laureline, Haydon, Gilles, Nico, Ivan, Marie-Eve, Mousse.
Vive les soirées bêtes mortes !

I will never forget my two first year in Neuchâtel with my "roomies" Sergio and Matheo. I would also like to thank all the others people at the institute for lots of funny moment in front of a coffee cup: Guillaume, Olivier, Cyril, Laurent, Cécile, Kaspar, Rachel, Claire, Bastos, JD, Christina, Ronny, Julien, Christophe, Mélody, Pierre-André, Roberto and Martin.
It's friday-beer time.

Going back in the past, I remember the good moment that I had with Mathieu Schuster (*Comment ???)* during my DEA at Strasbourg. I do not forget our six-month office sharing and that he was the person who forwarded me this PhD position announcement. I also thank Philippe Duringer (Strasbourg) that gives me the passion of sedimentology and for all the good moment at Digne-les-Bains. The supervision of my internship at Total by Christian Blanpied was also very much appreciated. Friends from Alsace were good reference point when I was back in Brumath: Matthieu, Sandrine, Christophe, Claude, Patrick, Rosita, Sébastien, Christian and many others. Big kiss to Lucie.

A big thank goes to Violaine (*mon projet qui marche)* for her love during all the good and the bad moments. Love.

Last, but definitively not least, I would like to thank my parents, who have always supported me. Nothing would be possible without them. Big kiss to the "Badaclic".

In the memory of Martin Burkhard,
who left us too early.

Palaeoceanographic and palaeoclimatic changes during the Late Hauterivian - Barremian and their impact on the Northern Tethyan margin: a combined sedimentological and geochemical approach

Chapter A.

General introduction

View on the Churfirsten from the Säntis (ct. St. Gallen, Switzerland)

"La science est toujours utile, on ne perd pas le temps employé à l'acquérir"

Proverbe chinois

A.1

Introduction

A.1.1. Foreword

Facing today's global changes and the profound impact of human activity on the Earth system, geologists have the means to look into the past in order to appreciate, and perhaps predict, what is happening and what will happen if we do not change our way of life. Indeed, the Earth history presents a wide variety of climatic and oceanographic conditions that followed one another and which are a thus an example of how the Earth system is reacting. The knowledge of these past processes and interactions may thus help us to better understand present environmental change.

One of the most studied time periods is the Cretaceous (from 145.5 to 65.5 Myr ago, following Gradstein et al., 2004). The main reason for this is that we know that the Cretaceous as a whole was a warm period (Hallam, 1984; Barron et al., 1984; Francis and Frakes, 1993), sometimes interrupted by cooler conditions (e.g., Kemper, 1987). The presence of polar ice cap is however still debated. Previous studies have concluded that the atmospheric pCO_2 was 2 to 6 times higher during the Cretaceous than todays pre-industrial values (e.g., Barron & Washington, 1985; Berner, 1994; Veizer et al., 1999; Retallack, 2001; Wallmann, 2001; Heimhofer et al., 2004; Haworth et al., 2005). It is thus representative of a greenhouse world and may therefore serve as an example mirroring what may happen on Earth if human activity (increased CO_2 input into the atmosphere, eutrophication of ocean…) continues at the same rate as today.

Today's carbonate platforms are suffering from climate change (coral bleaching, seawater pollution, calcification crises; *e.g.,* Bryant et al., 1998; Kleypas et al., 1999; Kayanne et al., 2005). Following the previous described philosophy, one main purpose of the research done at the University of Neuchâtel is thus to study the remains of past carbonate platforms and how they have reacted to global changes. For this purpose, the Alps are a good place. Indeed, thanks to tectonic activity, the Northern parts of the Alps (the Helvetic nappes) have conserved the record of an ancient carbonate platform that evolved during the Cretaceous along the northern Tethyan margin. They serve thus as a natural laboratory to study the impact of global changes on carbonate platform. Of special interest are the links between palaeoceanographic, as well as palaeoclimatic changes, and the time of carbonate platform demise, also called "drowning events".

The red line of this PhD thesis is the so-called Altmann Member, which constitute the basal part of the Drusberg Formation. It is mainly composed of highly condensed, phosphate-bearing sediments. The Altmann Member has recorded the northern Tethyan margin drowning during the Hauterivian – Barremian transition. It is situated on the edge of two different carbonate platform factories. On one hand, during the Valanginian – Hauterivian, the northern Tethyan margin was dominated by heterozoan biota such as crinoids and bryozoans. On the other hand, during the latest Barremian – earliest Aptian, photozoan biota such as corals, stromatoporoids, rudists, green algae have dominated the neritic record and formed the famous Urgonian limestone (Schrattenkalk Formation in the Helvetic realm).

A.1.2. Aims, questions and hypotheses

The aim of this PhD thesis project was to better understand the northern Tethyan carbonate platform dynamic during the latest Hauterivian – Barremian (with a focus on the Altmann Member) and to place it within a more global palaeoceanographic context. For this purpose, a dual study was done: Firstly, a precise documentation was obtained of the Helvetic realm during the latest Hauterivian – Barremian using ammonite biostratigraphy and sedimentological tools. Secondly, time-equivalent basinal deposits were studied for their geochemical content. The final goal of this PhD thesis was to compile all the obtained results, and integrate results on this period published by others, in order to have an integrated view on carbonate platform drowning events and their link to global change.

A.1.2.1. The Helvetic realm

A first step of this PhD thesis is thus to date as precise as possible the Hauterivian – Barremian deposits in the Helvetic realm using newly collected ammonites as well as a reevaluation of previous findings. Indeed, within the Helvetic realm, the condensed horizons are known to be relatively rich in ammonites (*e.g.,* Heim, 1910-1917; Fichter, 1934; Wyssling, 1986; Kuhn, 1996; Van de Schootbrugge, 2001) and this is of great assistance to refine the dating of this event. Coupled with sedimentological and sequence stratigraphic interpretations, the resulting biostratigraphic information may also help to develop a complete history on this drowning event and the sedimentary dynamics before and after it.

An interesting question concerns the relationship between the Altmann Member drowning event and a specific organic-rich level (the Faraoni Level), suspected to be the result of an oceanic anoxic event (*e.g.,* Baudin, 2005), which was deposited during the latest Hauterivian in basinal settings. Does this event have an impact on the onset of the Altmann Member drowning episode? Is it possible to recognize it within the Altmann Member?

A.1.2.2. The pelagic realm

In order to understand the palaeoceanographic context of the Altmann Member drowning event, an integrated geochemical study of (hemi-) pelagic sections was done. This may help to investigate many palaeoceanographic parameters such as seawater temperature, carbon cycle, nutrient level, palaeoclimate, redox conditions, etc… To obtain results reliable for the entire western Tethyan realm, sections in three different domains were studied. Two sections were studied in Italy (Fiume-Bosso and Gorgo a Cerbara), one in Switzerland (Veveyse de Châtel-St. Denis) and one in the Vocontian trough (France; Angles). During the Early Cretaceous, the Angles and the Veveyse de Châtel-St. Denis sections were situated along the northern Tethyan margin. The Veveyse de Châtel-St. Denis section is part of the Ultrahelvetic realm, which is considered as the deeper offshore prolongation of the Vocontian Trough to the northeast (Trümpy 1960). The Fiume-Bosso and the Gorgo a Cerbara sections, which represent the deepest sections, were situated in the southern part of the Tethys, in the Umbria-Marche Basin, remote from any continent. These sections offer thus a good coverage of the western Tethys. A common geochemical signal obtained for all these sections may thus be interpreted as a signal of wider importance (at least for the western Tethyan realm).

A first step with regards to the geochemical analyses was to characterize the redox state of the bottom water during the latest Hauterivian – Barremian using the distribution of redox-sensitive trace metals. This may help to better characterize the Faraoni Level, and also to identify further eventual ocean anoxia. This is especially needed during the Early Barremian where several organic-carbon enriched levels were recognized in the Tethyan realm (*e.g.,* Bréhéret, 1994; Erba et al., 1999; Bersezio et al., 2002).

Secondly, in order to better understand the nutrient cycle, phosphorus analyses will be performed and compared to the reference curve of Föllmi (1995) with the aim of deciphering local to global variations in nutrient levels in the ocean. Two interesting points will be the behavior of phosphorus during the Faraoni Level (how did anoxic conditions interact with the marine phosphorus cycle?) and to determine if there is a link between nutrient levels and the carbonate-platform factory.

Carbon and oxygen isotope analyses were performed on both bulk-rock carbonate and belemnites. They help to characterize the carbon cycle and palaeotemperature variations during the latest Hauterivian – Barremian. An interesting problem is to look whether carbon and phosphorus cycles were coupled or not during this period (*e.g.,* Van de Schootbrugge et al., 2003). Owing to the fact that bulk-rock carbonates are mainly constituted by organisms living close to the sea surface and that the ecological habitats of belemnites were deeper (they were nektonic animals; *e.g.,* Van de Schootbrugge et al., 2000), another interesting point was to trace water-mass mixing or stratification. Does such phenomena have an impact on carbonate platforms?

A.1.3. Organization of the thesis

This PhD thesis was done in close collaboration with Alexis Godet, who has worked on Hauterivian – Barremian sediments from the Jura Mountains. Our two themes included geochemical work on pelagic sediments. We have thus carried out a large part of the field work and laboratory analyses together. With the exception of Chapter A, B.3 and D, each Chapter of this thesis has been submitted to a peer-reviewed journal. Except for Chapter C.5, each paper has been accepted for publication or is already published (please refer to the title page of each Chapter to have precise references). Two papers on the Hauterivian – Barremian are attached in Appendix 1 for which I am co-author, but not the principal contributor.

A.1.4. References

Barron, E.J., Hay, W.W. and Kauffman, E.G. 1984. Cretaceous climates. Geology, 12: 377-378.

Barron, E.J. and Washington, W.M. 1985. Warm Cretaceous climates: High atmospheric CO2 as a plausible mechanism. In: The carbon cycle and atmospheric CO2: Natural variations Archean to present (Eds E.T. Sundquist and W.S. Broecker), 32, pp. 546-553. Geophysical monograph, Washington, American Geophysical Union.

Baudin, F. 2005. A Late Hauterivian short-lived anoxic event in the Mediterranean Tethys: the «Faraoni Event». Comptes Rendus Geoscience, 337: 1532-1540.

Berner, R.A. 1994. GEOCARB II: a revised model of atmospheric CO2 over Phanerozoic time. American Journal of Science, 294: 56-91.

Bersezio, R., Erba, E., Gorza, M. and Riva, A. 2002. Berriasian-Aptian black shales of the Maiolica formation (Lombardian Basin, Southern Alps, Northern Italy): local to global events. Palaeogeography, Palaeoclimatology, Palaeoecology, 180: 253-275.

Bryant, D.B., L., McManus, J.W. and Spalding, M. 1998. Reefs at risk: A map-based indicator of potential threats to the World's Coral Reef. Worlds Resources Institute, Washington D.C., 60 pp.

Bréhéret, J.-G. 1994. The Mid-Cretaceous organic-rich sediments from the Vocontian zone of the French Southeast basin. In: Hydrocarbon and Petroleum Geology of France (Ed A. Mascle), Special Publication of the European Association of Petroleum Geoscientists, 4, 4, pp. 295-320.

Erba, E., Channell, J.E.T., Claps, M., Jones, C.E., Larson, R.L., Opdyke, B., Premoli-Silva, I., Riva, A., Salvini, G. and Torriceli, S. 1999. Integrated stratigraphy of the Cismon APTICORE (Southern Alps, Italy): A «reference section» for

the Barremian-Aptian interval at low latitudes. Journal of Foraminiferal Research, 29: 371-391.

Fichter, H.J. 1934. Geologie der Bauen-Brisen-Kette am Vierwaldstaettersee und die zyklische Gliederung der Kreide und des Malm der helvetischen Decken. Bretträge zur Geologischen Karte, 128 pp.

Francis, J.E. and Frakes, L.A. 1993. Cretaceous climates. Sedimentology Review, 1: 17-30.

Föllmi, K.B. 1995. 160 m.y. record of marine sedimentary phosphorus burial: Coupling of climate and continental weathering under greenhouse and icehouse conditions. Geology, 23: 859-862.

Gradstein, F.M., Ogg, J.G., Smith, A.G., Bleeker, W. and Lourens, L.J. 2004. A new Geologic Time Scale with special reference to Precambrian and Neogene. Episodes, 27: 83-100.

Hallam, A. 1984. Continental humid and arid zones during the Jurassic and Cretaceous. Palaeogeography Palaeoclimatology Palaeoecology, 47: 195-223.

Haworth, M., Hesselbo, S.P., McElwain, J.C., Robinson, S.A. and Brunt, J.W. 2005. Mid-Cretaceous pCO_2 based on stomata of the extinct conifer Pseudofrenelopsis (Cheirolepidisceae). Geology, 33: 749-752.

Heim, A. 1910-1916. Monographie der Churfirsten-Mattstock-Gruppe. Beiträge zur Geologischen Karte der Schweiz, 50, Bern, 662 pp.

Heimhofer, U., Hochuli, P.A., Herrle, J.O., Andersen, N. and Weissert, H. 2004. Absence of major vegetation and palaeoatmospheric pCO2 changes associated with oceanic anoxic event 1a (Early aptian, SE France). Earth and Planetary Science Letters, 223: 303-318.

Kayanne, H., Hata, H., Kudo, S., Yamano, H., Watanabe, A., Ikeda, Y., Nozaki, k., Kato, K., Negishi, A. and Saito, H. 2005. Seasonal and bleaching-induced changes in coral reef metabolism and CO_2 flux. Global Biogeochemical Cycles, 19, GB3015: 1-11.

Kemper, E. 1987. Das klima der Kreide-zeit. Geologisches Jahrbuch, Reihe A, 96: 5-185.

Kleypas, J.A., Buddemeier, R.W., Archer, D., Gattuso, J.-P., Langdon, C. and Opdyke, B.N. 1999. Geochemical Consequences of Increased Atmospheric Carbon Dioxide on Coral Reefs. Nature, 284: 118-120.

Kuhn, O. 1996. Der Einfluss von Verwitterung auf die Paläozeanographie zu Beginn des Kreide-Treibhausklimas (Valanginian und Hauterivian) in der West-Tethys, Universität Zürich, Zürich, 380 pp.

Retallack, G.J. 2001. A 300-million-year record of atmospheric carbon dioxide from fossil plant cuticles. Nature, 411: 287-290.

Trümpy, R. 1960. Paleotectonic evolution of the Central and Western Alps. Bulletin of the Geological Society of America, 71: 843-908.

Van de Schootbrugge, B. 2001. Influence of paleo-environmental changes during the Hauterivian (Early Cretaceous) on carbonate deposition along the northern margin of the Tethys: Evidence from geochimical records (C, O, and Sr-isotopes, P, Fe, Mn). Thèse de Doctorat ès Sciences, spécialité Géologie, Université de Neuchâtel, Institut de Géologie, Neuchâtel (Switzerland), 268 pp.

Van de Schootbrugge, B., Föllmi, K.B., Bulot, L.G. and Burns, S.J. 2000. Paleoceanographic changes during the early Cretaceous (Valanginian-Hauterivian): evidence from oxygen and carbon stable isotopes. Earth and Planetary Science Letters, 181: 15-31.

Van de Schootbrugge, B., Kuhn, O., Adatte, T., Steinmann, P. and Föllmi, K.B. 2003. Decoupling of P- and Corg-burial following Early Cretaceous (Valanginian-Hauterivian) platform drowning along the NW Tethyan margin. Palaeogeography, Palaeoclimatology, Palaeoecology, 199: 315-331.

Veizer, J., Ala, D., Azmy, K., Bruckschen, P., Buhl, D., Bruhn, F., Carden, G.A.F.,

Diener, A., Ebneth, S. and Godderis, Y. 1999. 87Sr/86Sr, δ13C and δ18O evolution of Phanerozoic seawater. Chemical Geology, 161: 59-88.

Wallmann, K. 2001. Controls on the Cretaceous and Cenozoic evolution of seawater composition, atmospheric CO2 and climate. Geochimica et Cosmochimica Acta, 65: 3005-3025.

Wyssling, G.W. 1986. Der frühkretazische helvetische Schelf in Vorarlberg und im Allgäu - Stratigraphie, Sedimentologie und Paläogeographie. Jb. Geol. Bund., 129: 161-265.

A.2.

The Early Cretaceous

This chapter aims at providing a short general background on palaeoenvironmental change during the Early Cretaceous in order to place this study in a more general context. Essential information on the record of the Helvetic realm is also given here.

A.2.1. Palaeoenvironmental change

A.2.1.1. Palaeogeography and palaeoceanography

The palaeogeography of the Early Cretaceous was slightly different from today (Fig. A.2.1). The North Atlantic has just begun its opening during the Late Jurassic. India and Australia were attached to Antarctica. A wide east-west directed ocean was separating these three continents, together with Africa, from Eurasia: the Tethys. To the north, the Boreal realm was separated from the Tethys by the Eurasian continent.

Palaeoceanographic currents were mostly oriented east-west in the Tethys (Fig. A.2.2; *e.g.*, Pucéat et al., 2005). The Pacific was probably characterized by two giant gyres (Barron and Peterson, 1989; Stille et al., 1996). This is however still the matter of numerous debates. Indeed, as argued by Hay & Flögel (2004), in a Cretaceous greenhouse world, the subtropical ocean gyres would have been weakened leading to an ocean circulation dominated by eddies. Opening of connections between the Tethys and the Boreal realm during high sea-level stand lead to the influx of cooler water in the Tethys realm through the Polish Furrow and the Moscow platform (*e.g.*, Van de Schootbrugge, 2001).

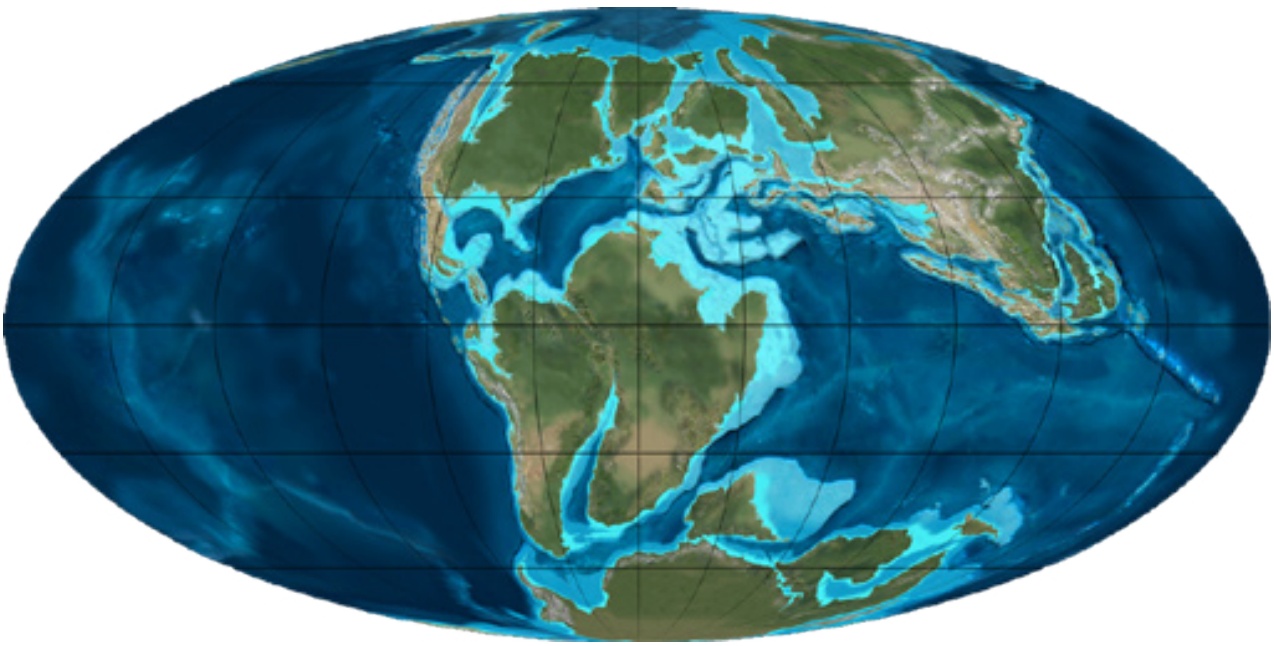

Fig. A.2.1: Earth palaeogeographic map during the Early Cretaceous (Aptian; © Blakey R.; http://jan.ucc.nau.edu/~rcb7/RCB.html).

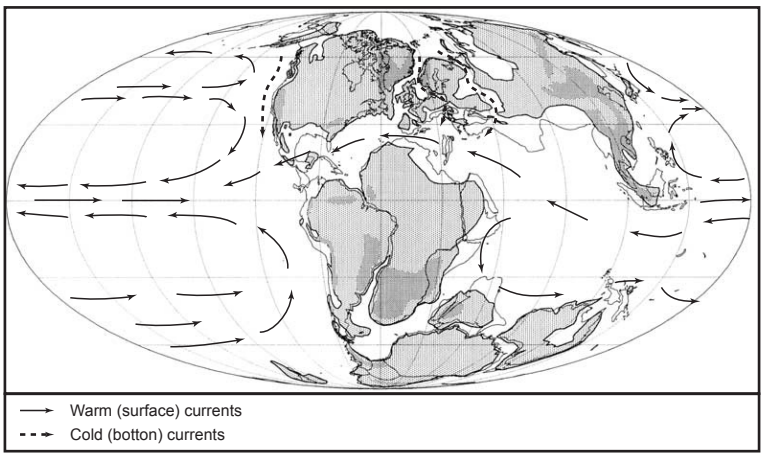

Fig. A.2.2: Main surface and bottom palaeocurrents during the Early Cretaceous (adapted from Van de Schootbrugge, 2001 and Pucéat et al., 2005).

A.2.1.2. Greenhouse versus icehouse

It is generally admitted that the Cretaceous as a whole was a warm period (*e.g.,* Hallam, 1984; Barron et al., 1984; Francis and Frakes, 1993). This can be inferred from tree fossils and crocodilian remains that have been found in Antarctica as well as from vegetation reconstructions showing that subtropical plants prospered 20° further north than today (Vakhrameev, 1978). Different studies have concluded that the atmospheric pCO_2 was 2 to 6 times higher during the Cretaceous than the today's pre-industrial value (e.g., Barron & Washington, 1985; Berner, 1994; Veizer et al., 1999; Retallack, 2001; Wallmann, 2001; Heimhofer et al., 2004; Haworth et al., 2005). This high atmospheric pCO_2 may thus explain the warm period by enhanced greenhouse conditions.

Kemper (1987) however questioned the statement of an exclusively warm Early Cretaceous period with the discovery of glendonites and glaciomarine drift ("dropstones") within Valanginian and Upper Aptian-Albian sedimentary sequences in Arctic Canada. Glendonites are indicators of temperatures of 0°C or less. This may indicate that, at least during the Valanginian and the Upper Aptian-Albian, polar regions may have experienced the growth of ice caps and thus icehouse conditions may be inferred from these periods instead of greenhouse ones (see also Price, 1999). Sea-level variations may also be an indicator of icehouse conditions during the Early Cretaceous. Indeed, certain rates of sea-level change deducted from Early Cretaceous 3rd order sequences are difficult to be explained without implying glacio-eustacy (*e.g.,* Immenhauser, 2005). These interpretations are in contradiction with the calculated high atmospheric pCO_2 during the Cretaceous. Veizer et al. (2000) argued that either the reconstructed pCO_2 values are incorrect, or the role of pCO_2 as the main driving force of past global climate change is partially questionable, or that climatic models are unable to reproduce correctly the past climates modes. This problem remains unresolved.

A.2.1.3. Oceanic Anoxic Events (OAE)

During the Cretaceous, certain coeval black-shale deposits horizons have been recognized worldwide. They have been attributed to Oceanic Anoxic Events (*e.g.,* Schlanger & Jenkins, 1976). In the Early Cretaceous, these deposits occur during the latest Hauterivian (Faraoni Level; *e.g.,* Cecca et al., 1994; Baudin, 2005), the Early Aptian (Selli Level, OAE1a; *e.g.,* Erba et al., 1999), the Aptian-Albian transition (OAE1b; *e.g.,* Herrle et al., 2004) and the Late Albian (OAE1c and 1d). In addition, during the Valanginian, a major excursion of the $\partial^{13}C$ signal is reported and assumed by some authors to represent another

Oceanic Anoxic Event (Lini et al., 1992; Erba et al., 2004). However, the lack of major black-shale deposits associated with this event makes this interpretation questionable. The major AOEs seem to be contemporaneous with major volcanic activity associated with the installation of Large Igneous Provinces (LIP).

Even if each OAE may have its own triggering mechanisms, a general scheme implying eutrophication of seawater leading to the slowdown of carbonate production relative to organic carbon production can be advanced (*e.g.,* Meyers, 2006). The general model proposed by Jenkyns (1999, 2003) is the following: LIP activity results in excess volcanogenic CO_2 supplied to the ocean and the atmosphere. This may result in a global temperature rise leading to an accelerated hydrological cycle and an increased nutrient flux into the ocean. A global temperature rise may also be responsible of the dissociation of methane gas hydrates from the seafloor which may contribute to a positive feedback loop and further increase global temperature. Plankton productivity is then enhanced and leads to the development of anoxic conditions due to oxygen depletion by organic matter oxidation. The OAE begins and is characterized by an high amount of organic matter deposition. Finally, increased basalt weathering and organic matter deposit lead to CO_2 drawdown, resulting in the decrease of nutrient input into the ocean and cooling, that ended the OAE. In addition, Weissert & Erba (2004) pointed out the role of seawater pCO_2 as an influential factor in biocalcification processes. Indeed, an excess of seawater pCO_2 leads to ocean acidification which may lead to a biocalcification crisis and thus to the slowdown of carbonate production (see Orr et al., 2005).

A.2.2. The Helvetic record

A.2.2.1. Geological setting

The Helvetic nappes or rather: tectonic unit are situated in the northern part of the Alps (Fig. A.2.3). It documents the sedimentary cover of the northern Tethyan, southern European shelf, which became thrusted, overthrusted and folded in a northward direction during Alpine orogenesis. This fossil shelf succession includes the remnants of a vast carbonate platform system that evolved during the Late Jurassic to the early Late Cretaceous along the northern Tethyan margin (*e.g.,* Funk et al., 1993; Föllmi et al., 1994, 2006). These platform remains document periods of carbonate production alternating with periods of platform demise, also called drowning event (*e.g.,* Schlager, 1981; Föllmi et al., 1994).

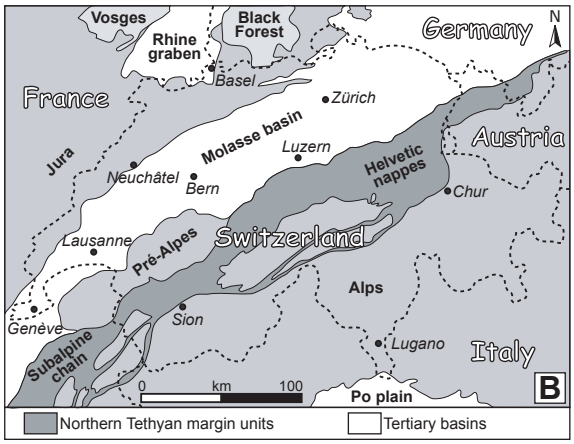

Fig. A.2.3: Tectonic map of Switzerland with the location of the Helvetic realm (dark grey colored).

A.2.2.2. Carbonate platform factories

Two types of carbonate platform factory are recognized within the Helvetic realm: the photozoan and the heterozoan biogenic association. The photozoan association (Coral-oolite carbonate production mode after Föllmi et al., 1994) is composed of reef-related organisms such as coral, chaetetids, stromatoporoids, rudists and green algae. Abundant crinoids and bryozoans, as well as bivalves, brachiopods and siliceous sponges, characterize the heterozoan association (Crinoid-bryozoan carbonate production mode after Föllmi et al., 1994). It is also characterized by the absence of reef-related organisms.

Following numerous studies (*e.g.,* Föllmi et al., 1994; James, 1997; Halfar et al., 2004), the

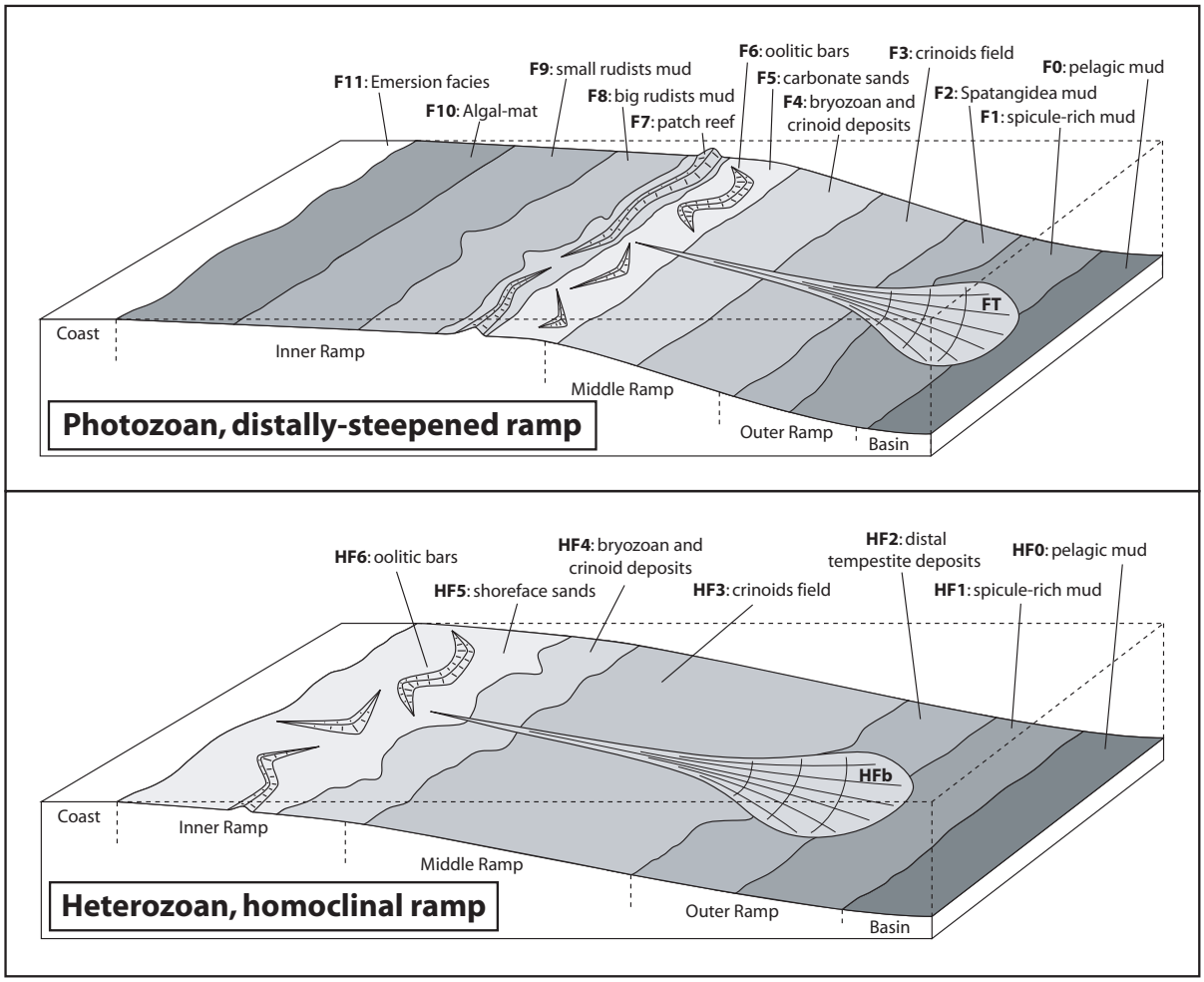

Fig. A.2.4: Synthetic bloc diagram showing the repartition of facies belts within photozoan and heterozoan-dominated carbonate platforms during the Early Cretaceous (after Arnaud-Vanneau, 1980; Bodin et al., 2006).

photozoan association discriminates warm and oligotrophic sea water whereas the heterozoan association is related to cool, or warm and meso-eutrophic, sea water. The photozoan-dominated carbonate platform is composed of photozoan biota in the photic zone and heterozoan biota in deeper settings, whereas the heterozoan-dominated carbonate platform is only composed of heterozoan biota (Fig. A.2.4; Bodin et al., 2006).

A.2.2.3. Drowning events

Minimized carbonate production, thin horizons with high amounts of glaucony and phosphatized nodules or crusts, and the presence of hiatuses and erosive surfaces characterize condensed levels that are associated with the Helvetic shelf drowning events (Föllmi et al., 1994). These events are related to palaeoceanographic and palaeoclimatic perturbations leading to carbonate platform growth crises (Weissert et al., 1998).

Five drowning unconformities have been recognized within the Early Cretaceous Helvetic record (Funk et al., 1993). They are named D1 to D5 (Fig A.2.5). The D1, D2 and D5 events were already the subject of detailed studies (Kuhn, 1996; Van de Schootbrugge, 2001; Föllmi, 1989; respectively). The drowning event D3, recorded in the Altmann Member, is the subject of this PhD thesis whereas the D4 event is the subject of an ongoing PhD thesis by Pascal Linder (University of Neuchâtel).

Föllmi et al. (1994) and Weissert et al. (1998) suggested the following model in order to explain the two major drowning events of the

Valanginian and the Aptian: Intensified volcanic activity resulted in reinforced greenhouse conditions, an eustatic sea level rise and in the acceleration of the hydrological cycle. This may have lead to elevated marine nutrient levels through the increased nutrient flux from the continents, thereby increasing primary productivity. Carbonate platform drowning may be linked to an elevated nutrient and clastic load leading to the demise of benthic carbonate

Fig. A.2.5: Time-space transect through the Helvetic zone (modified after Föllmi et al., 2006).

productivity. This global scenario is however difficult to apply to all drowning events, and especially the D3 event, because of the lack of major volcanic activity during the time of this event.

A.2.3. Conclusions

The Early Cretaceous time as a whole was a time of intensified greenhouse conditions, interrupted by short-lived cooling periods during the Valanginian and the Late Aptian-Albian. It experienced the widespread deposition of several black-shale layers that are related to oceanic anoxic events. Palaeoenvironmental changes have not only affected basinal settings, but also the neritic realm. These changes are marked on carbonate platforms by carbonate-producing factory changes and drowning events.

A.2.4. References

Arnaud-Vanneau, A. 1980. Micropaléontologie, paléoécologie et sédimentologie d'une plate-forme carbonatée de la marge passive de la Téthys; L'Urgonien du Vercors septentrional et de la Chartreuse (Alpes occidentales). Géologie Alpine, Mémoire Hors-Série, 11.

Barron, E.J., Hay, W.W. and Kauffman, E.G. 1984. Cretaceous climates. Geology, 12: 377-378.

Barron, E.J. and Peterson, W.H. 1989. Model simulation of the Cretaceous ocean circulation. Science, 244: 684-686.

Barron, E.J. and Washington, W.M. 1985. Warm Cretaceous climates: High atmospheric CO_2 as a plausible mechanism. In: The carbon cycle and atmospheric CO_2: Natural variations Archean to present (Eds E.T. Sundquist and W.S. Broecker), 32, pp. 546-553. Geophysical monograph, Washington, American Geophysical Union.

Baudin, F. 2005. A Late Hauterivian short-lived anoxic event in the Mediterranean Tethys: the «Faraoni Event». Comptes Rendus Geoscience, 337: 1532-1540.

Berner, R.A. 1994. GEOCARB II: a revised model of atmospheric CO_2 over Phanerozoic time. American Journal of Science, 294: 56-91.

Bodin, S., Godet, A., Vermeulen, J., Linder, P. and Föllmi, K.B. 2006. Biostratigraphy, sedimentology and sequence stratigraphy of the latest Hauterivian - early Barremian drowning episode of the Northern Tethyan margin (Altmann Member, Helvetic nappes, Switzerland). Eclogae geologicae Helvetiae, 99: 157-174.

Cecca, F., Marini, A., Pallini, G., Baudin, F. and Begouen, V. 1994. A guide-level of the uppermost Hauterivian (Lower Cretaceous) in the pelagic succession of Umbria-Marche Apennines (Central Italy): the Faraoni Level. Riv. Ital. Paleontol. Stratigr., 99: 551-568.

Erba, E., Bartolini, A. and Larson, R.L. 2004. Valanginian Weissert oceanic anoxic event. Geology, 32: 149-152.

Erba, E., Channell, J.E.T., Claps, M., Jones, C.E., Larson, R.L., Opdyke, B., Premoli-Silva, I., Riva, A., Salvini, G. and Torriceli, S. 1999. Integrated stratigraphy of the Cismon APTICORE (Southern Alps, Italy): A «reference section» for the Barremian-Aptian interval at low latitudes. Journal of Foraminiferal Research, 29: 371-391.

Francis, J.E. and Frakes, L.A. 1993. Cretaceous climates. Sedimentology Review, 1: 17-30.

Funk, H., Föllmi, K.B. and Mohr, H. 1993. Evolution of the Tithonian-Aptian carbonate platform along the northern Tethyan margin, eastern Helvetic Alps. In: Cretaceous carbonates platforms (Eds Simo J.A.T., Scott R.W. and Masse J.-P.), AAPG Memoir, 56, pp. 387-407. American Association of Petroleum Geologists. Tulsa, OK, United States.

Föllmi, K.B. 1989. Evolution of the Mid-Cretaceous Triad. Platform Carbonates, Phosphatic Sediments, and Pelagic

Carbonates along the Northern Tethys margin. Lecture Notes in Earth Sciences, 23. Springer-Verlag, 153 pp.

Föllmi, K.B., Godet, A., Bodin, S. and Linder, P. 2006. Interactions between environmental change and shallow-water carbonate build-up along the northern Tethyan margin and their impact on the early Cretaceous carbon-isotope record. Paleoceanography, 21, PA4211.

Föllmi, K.B., Weissert, H., Bisping, M. and Funk, H. 1994. Phosphogenesis, carbon-isotope stratigraphy, and carbonate-platform evolution along the Lower Cretaceous northern Tethyan margin. Geological Society of America Bulletin, 106: 729-746.

Halfar, J., Godinez-Orta, L., Mutti, M., Valdez-Holguin, J.E. and Borges, J.M. 2004. Nutrient and temperature controls on modern carbonate production: An example from the Gulf of California, Mexico. Geology, 32: 213-216.

Hallam, A. 1984. Continental humid and arid zones during the Jurassic and Cretaceous. Palaeogeography Palaeoclimatology Palaeoecology, 47: 195-223.

Haworth, M., Hesselbo, S.P., McElwain, J.C., Robinson, S.A. and Brunt, J.W. 2005. Mid-Cretaceous pCO_2 based on stomata of the extinct conifer Pseudofrenelopsis (Cheirolepidisceae). Geology, 33: 749-752.

Hay, W.W. and Flögel, S. 2004. Organic carbon deposition in eddy-filled Cretaceous oceans. In: 32nd IGC, Florence, Italy, August 20-28, 2004.

Heimhofer, U., Hochuli, P.A., Herrle, J.O., Andersen, N. and Weissert, H. 2004. Absence of major vegetation and palaeoatmospheric pCO_2 changes associated with oceanic anoxic event 1a (Early aptian, SE France). Earth and Planetary Science Letters, 223: 303-318.

Herrle, J.O., Kössler, P., Friedrich, O., Erlenkeuser, H. and Hemleben, C. 2004. High-resolution carbon isotope records of the Aptian to Lower Albian from SE France and the Mazagan Plateau (DSDP Site 545): a stratigraphic tool for paleoceanographic and paleobiologic reconstruction. Earth and Planetary Science Letters, 218: 149-161.

Immenhauser, A. 2005. High-rate sea-level change during the Mesozoic: New approaches to an old problem. Sedimentary Geology, 175: 277-296.

James, N.P. 1997. The cool-water carbonate depositional realm. In: Cool water carbonates (Eds N.P. James and J.A.D. Clarke), 56, pp. 1-22. Society for Sedimentary Geology, Spec. Pub.

Jenkyns, H.C. 1999. Mesozoic anoxic events and palaeoclimate. Zentralblatt Geologie und Paläontologie, 1, Heft 7-9: 943-949.

Jenkyns, H.C. 2003. Evidence for rapid climate change in the Mesozoic-Palaeogene greenhouse world. Philosophical Transactions of the Royal Society, London, A, 361: 1885-1916.

Kemper, E. 1987. Das klima der Kreide-zeit. Geologisches Jahrbuch, Reihe A, 96: 5-185.

Kuhn, O. 1996. Der Einfluss von Verwitterung auf die Paläozeanographie zu Beginn des Kreide-Treibhausklimas (Valanginian und Hauterivian) in der West-Tethys, Universität Zürich, Zürich, 380 pp.

Lini, A., Weissert, H. and Erba, E. 1992. The Valanginian carbon isotope event; a first episode of greenhouse climate conditions during the Cretaceous. Terra Nova, 4: 374-384.

Meyers, P.A. 2006. Paleoceanographic and paleoclimatic similarities between Mediterranean sapropels and Cretaceous black shales. Palaeogeography, Palaeoclimatology, Palaeoecology, 235: 305-320.

Orr, J.C., Fabry, V.J., Aumont, O., Bopp, L., Doney, S.C., Feely, R.A., Gnanadesikan, A., Gruber, N., Ishida, A., Joos, F., Key, R.M., Lindsay, K., Maier-Reimer, E., Matear, R., Monfray, P., Mouchet, A., Najjar, R.G., Plattner, G.-K., Rodgers, K.B., Sabine, C.L., Sarmiento, J.L.,

Schlitzer, R., Slater, R.D., Totterdell, I.J., Weirig, M.-F., Yamanaka, Y. and Yool, A. 2005. Anthropogenic ocean acidification over the twnty-first century and its impact on calcifying organisms. Nature, 437: 681-686.

Price, G.D. 1999. The evidence and implications of polar ice during the Mesozoic. Earth-Science Reviews, 48: 183-210.

Pucéat, E., Lécuyer, C. and Reisberg, L. 2005. Neodymium isotope evolution of NW Tethyan upper ocean waters throughout the Cretaceous. Earth and Planetary Science Letters, 236: 705-720.

Retallack, G.J. 2001. A 300-million-year record of atmospheric carbon dioxide from fossil plant cuticles. Nature, 411: 287-290.

Schlager, W. 1981. The paradox of drowned reefs and carbonates platforms. Geological Society of America Bulletin, 92: 197-211.

Schlanger, S.O. and Jenkyns, H.C. 1976. Cretaceous oceanic anoxic events: causes and consequences. Geologie en Mijnbouw, 55: 179-184.

Stille, P., Steinmann, M. and Riggs, S.R. 1996. Nd isotope evidence for the evolution of the paleocurrents in the Atlantic and Tethys Oceans during the past 180 Ma. Earth and Planetary Science Letters, 144: 9-19.

Vakhrameev, V.A. 1978. The climates of the northern hemisphere in the Cretaceous in light of paleobotanical data. Paleontological Journal, 12: 143-154.

Van de Schootbrugge, B. 2001. Influence of paleo-environmental changes during the Hauterivian (Early Cretaceous) on carbonate deposition along the northern margin of the Tethys: Evidence from geochimical records (C, O, and Sr-isotopes, P, Fe, Mn). Thèse de Doctorat ès Sciences, spécialité Géologie, Université de Neuchâtel, Institut de Géologie, Neuchâtel (Switzerland), 268 pp.

Veizer, J., Ala, D., Azmy, K., Bruckschen, P., Buhl, D., Bruhn, F., Carden, G.A.F., Diener, A., Ebneth, S. and Godderis, Y. 1999. $^{87}Sr/^{86}Sr$, $\partial^{13}C$ and $\partial^{18}O$ evolution of Phanerozoic seawater. Chemical Geology, 161: 59-88.

Veizer, J., Godderis, Y. and François, L.M. 2000. Evidence for decoupling of atmospheric CO_2 and global climate during the Phanerozoic eon. Nature, 408: 698-701.

Wallmann, K. 2001. Controls on the Cretaceous and Cenozoic evolution of seawater composition, atmospheric CO_2 and climate. Geochimica et Cosmochimica Acta, 65: 3005-3025.

Weissert, H. and Erba, E. 2004. Volcanism, CO_2 and palaeoclimate; a Late Jurassic-Early Cretaceous carbon and oxygen isotope record. Journal of the Geological Society of London, 161: 695-702.

Weissert, H., Lini, A., Föllmi, K.B. and Kuhn, O. 1998. Correlation of Early Cretaceous carbon isotope stratigraphy and platform drowning events: a possible link? Palaeogeography, Palaeoclimatology, Palaeoecology, 137: 189-203.

Chapter B.

The Helvetic - Jura shelf record

Tierwis refuge and Säntis summit (ct. St. Gallen, Switzerland)

"N'a de convictions que celui qui n'a rien approfondi"

Emil Michel Cioran, *De l'inconvénient d'être né*

B.1.

Introduction

In order to better understand the changes in the shallow-water carbonate factory and drowning of the northern Tethyan platform during the Late Hauterivian – Barremian, a first step undertaken during this PhD thesis was to precisely date the Altmann and the Chopf Members. Indeed, these two members are key marker successions deposited during this time interval in the Helvetic realm. They provide not only a precise age indication of the periods of major environmental change associated with these sediments, but also maximal and minimal age dates of the under- and overlying members. A further focus of the research project described here was on the sedimentology and sequence stratigraphy of the Altmann Member with the goal of establishing a model for the unfolding of the D3 drowning event. Two published papers and an additional chapter resulted from this work.

Foreword to "Biostratigraphy, sedimentology and sequence stratigraphy of the latest Hauterivian – early Barremian drowning episode of the Northern Tethyan margin (Altmann Member, Helvetic nappes, Switzerland)"

The main goal of this paper, published in *Eclogae Geologicae Helvetiae*, is to provide an improved time resolution of the Altmann Member using newly collected ammonite as well as those already collected. Using sequence stratigraphy, it includes also a proposal of a model for the unfolding of the drowning episode.

Foreword to "Biostratigraphy of the Chopf Member (Helvetic Alps, eastern Switzerland): New data on the age of the installation of Urgonian-type carbonates along the northern Tethyan margin"

This paper, published in *Comptes Rendus Geoscience*, provides an ammonite-based age date of the Chopf Member. This dating is important because it allows to better constrain the onset of the Schrattenkalk Formation (Urgonian-like limestone) in the Helvetic realm.

Foreword to "Correlation between the Helvetic and the Jura realm during the Hauterivian – Barremian by means of biostratigraphy, sequence stratigraphy and carbonate platform factory changes"

This chapter aims at providing a high-resolution correlation between the Helvetic and the Jura realm. It demonstrates that the observed changes in the Helvetic realm can be traced in other part of the Tethyan realm and are thus of supra-regional nature.

B.2.

Biostratigraphy, sedimentology and sequence stratigraphy of the latest Hauterivian – Early Barremian drowning episode of the Northern Tethyan margin (Altmann Member, Helvetic nappes, Switzerland)

Stéphane Bodin [1], Alexis Godet [1], Jean Vermeulen [2], Pascal Linder [1] & Karl B. Föllmi [1]

[1] Institut de Géologie, Université de Neuchâtel, Rue Emile Argand 11, CP 158, 2009 Neuchâtel, Switzerland

[2] Grand Rue, 04330 Barrême, France

Keywords: Early Cretaceous; Platform Drowning; Phosphatization; Condensation; Heterozoan; Northern Tethyan margin

Published in: Eclogae Geologicae Helvetiae **99** (2006), 157-174

Abstract

During the Early Cretaceous, major palaeoceanographic changes are mirrored on the northern Tethyan carbonate platform by changes in the carbonate factory and by platform drowning. The Altmann Member of the central European, northern Alpine Helvetic thrust and fold belt, contains the sedimentary record of one of these drowning events which occurred during the Late Hauterivian – Early Barremian. It consists mainly of highly condensed beds, which are rich in glaucony and phosphates. The Altmann Member was hitherto only poorly dated. New ammonite findings and a re-evaluation of existing ammonite fauna allow to precisely date this drowning episode, starting in the *Pseudothurmannia seitzi* biozone (latest Hauterivian) and lasting until the *Coronites darsi* biozone (latest Early Barremian). These new age dates, coupled with sequence stratigraphic interpretations allow to better understand the unfolding of the drowning episode, which proceeded in two stages: The first stage consisted in an important phase of marine transgression during the latest Hauterivian, during which carbonate production was highly reduced; the second stage is recorded during the latest Early Barremian by an important sequence boundary, which is associated with a phosphatized hardground, followed by rapid sea-level rise and the deposition of outer ramp sediment associated with the backstepping of the platform. Almost the whole early Barremian is likely to be condensed in this phosphatized hardground, which is associated to a second order sea-level lowstand. The onset of the drowning event is linked to the Faraoni oceanic anoxic event, whereas during the Early Barremian, phosphatization might be the result of important winnowing during a period of highly eutrophic conditions.

Résumé

Durant le Crétacé inférieur, les changements paléoceanographiques sont enregistrés sur la marge nord-Téthysienne par des fluctuations du mode de production des carbonates ainsi que des épisodes d'ennoiement de plate-forme. Le Membre d'Altmann, qui affleure en Europe centrale, dans les nappes plissées et charriées du domaine Helvétique, est le résultat d'un de ces ennoiements de la plate-forme carbonatée se déroulant durant l'Hauterivien tardif et le Barrémien précoce. Principalement constitué de couches fortement condensées riches en glauconie et phosphate, le Membre d'Altmann, qui peut être relié à des changements paléocéanographiques majeurs durant le Crétacé inférieur, n'a pour l'instant été que faiblement daté. De nouvelles datations biostratigraphiques basées sur des ammonites nouvellement trouvées, ainsi que sur une réévaluation de celles précédemment publiées, permettent de précisément dater cet épisode d'ennoiement de plate-forme. Celui-ci débute dans la zone d'ammonites à *Pseudothurmannia seitzi* (Hauterivien tardif) et se termine dans la zone à *Coronites darsi* (dernière zone du Barrémien inférieur). Ces nouvelles datations, couplées avec des interprétations en stratigraphie séquentielle, permettent de mieux appréhender le déroulement de cet épisode d'ennoiement de plate-forme qui se développe en deux temps : une première étape correspond à une importante phase de transgression marine durant l'Hauterivien terminal, accompagnée par une réduction importante de la production carbonatée. Une seconde étape est enregistrée durant la fin du Barrémien précoce par la formation d'un fond induré phosphaté associé à un bas niveau marin, suivie par une remontée rapide du niveau marin et le dépôt de sédiments de rampe carbonatée externe associé à une forte rétrogradation de la plateforme. De plus, la majeure partie du Barrémien précoce est condensée dans ce fond induré phosphaté associé à un bas niveau marin de second ordre. Le début de cet épisode d'ennoiement de plate-forme semble être lié à l'événement d'anoxie océanique du niveau Faraoni, tandis que durant le Barrémien inférieur, la phosphatogenèse semble être le résultat d'un important vannage des fonds océaniques durant une période d'eutrophie marine.

B.2.1. Introduction

The Early Cretaceous record on the Helvetic platform is characterized by several drowning episodes expressed in highly condensed and phosphatized beds (Funk *et al*., 1993; Föllmi *et al*., 1994). These beds are relatively rich in macrofossils (ammonites, belemnites, bivalves, brachiopods, sponges and echinoids) and have been the focus of several studies for nearly a century (e.g., Heim, 1910-1916; Goldschmid, 1927; Fichter, 1934; Hantke, 1961; Funk, 1971; Briegel, 1972; Wyssling, 1986; Föllmi, 1989; Kuhn, 1996; van de Schootbrugge, 2001) due to their importance to date the intercalated sediments poor in biostratigraphically significant fossils.

This paper focuses on one of these condensed horizons, the Altmann Member (Mb), which separates the Kieselkalk Formation (Fm; Hauterivian) from the rest of the Drusberg Fm (latest Early to early Late Barremian). Previously, the Altmann Mb has not been dated precisely although a latest Hauterivian to earliest Barremian age was assumed (e.g., Funk, 1969; Briegel, 1972; Rick, 1985; Wyssling, 1986; Funk *et al*., 1993; Föllmi *et al*., 1994). Thus, a first goal of this study is to provide a high-resolution biostratigraphy for the Altmann Mb using newly collected ammonites, as well as a reevaluation of those already collected during previous studies and stored in different museums.

The drowning horizons of the Lower Cretaceous Helvetic platform are of great interest since Föllmi *et al*. (1994) and Weissert *et al*. (1998) (see also Kuhn, 1996; van de Schootbrugge, 2001) have postulated links between these episodes and global palaeoceanographic events, as expressed by the carbon-isotope record. The Altmann Mb documents an episode for which no clear explanation has been yet formulated. On the other hand, major palaeoceanographic changes are present in the Tethyan realm during the Late Hauterivian – Early Barremian, such as the Faraoni oceanic anoxic event (Late Hauterivian; e.g., Cecca *et al*., 1994; Baudin *et al*., 1999; Baudin, 2005) and a phase of enhanced phosphorus input during the Early Barremian (Bodin *et al*., 2006). Using improved biostratigraphy and sedimentology of the Altmann Mb, this study aims at linking the initiation, unfolding and termination of the Altmann Mb drowning event to these major palaeoceanographic events.

B.2.2. Geological setting

The studied sections are located in the Helvetic nappes of Switzerland, situated in the northern part of the Alps and representing the northern Tethyan margin. This domain was thrusted, overthrusted and folded in a northward direction during Alpine orogenesis (Fig. B.2.1). With regards to its age, almost the entire Hauterivian is represented in this tectonic unit by the Kieselkalk Fm (Fig. B.2.2), which is divided into three members; the Lower Kieselkalk, the Lidernen and the Upper Kieselkalk Mbs (Funk, 1969). The Kieselkalk Fm overlays the Gemsmättli Mb (early Late Valanginian to earliest Hauterivian; Kuhn, 1996). The latest Hauterivian to early Late Barremian correspond to the Drusberg formation, which is divided into a lower part (the Altmann Mb) and an upper part (the Drusberg Mb) (cf. Bollinger, 1988; Funk *et al*., 1993). During the Late Barremian – Early Aptian, the Helvetic platform is represented by the Schrattenkalk Fm, which is the equivalent of the Urgonian limestone facies described in many other locations in the world (e.g., Arnaud *et al*., 1998; Lehmann *et al*., 1999). Gemsmättli, Lidernen and Altmann Mbs represent three successive phases of incipient Helvetic platform drowning (D1, D2 and D3 respectively, in Föllmi *et al*., 1994; See also Kuhn, 1996 and van de Schootbrugge, 2001).

The Helvetic carbonate platform morphology can be defined as a ramp (*sensu* Burchette & Wright, 1992). During the Berriasian, the situation was close to a distally steepened carbonate ramp (Kuhn, 1996). Rapid subsidence together with a second order

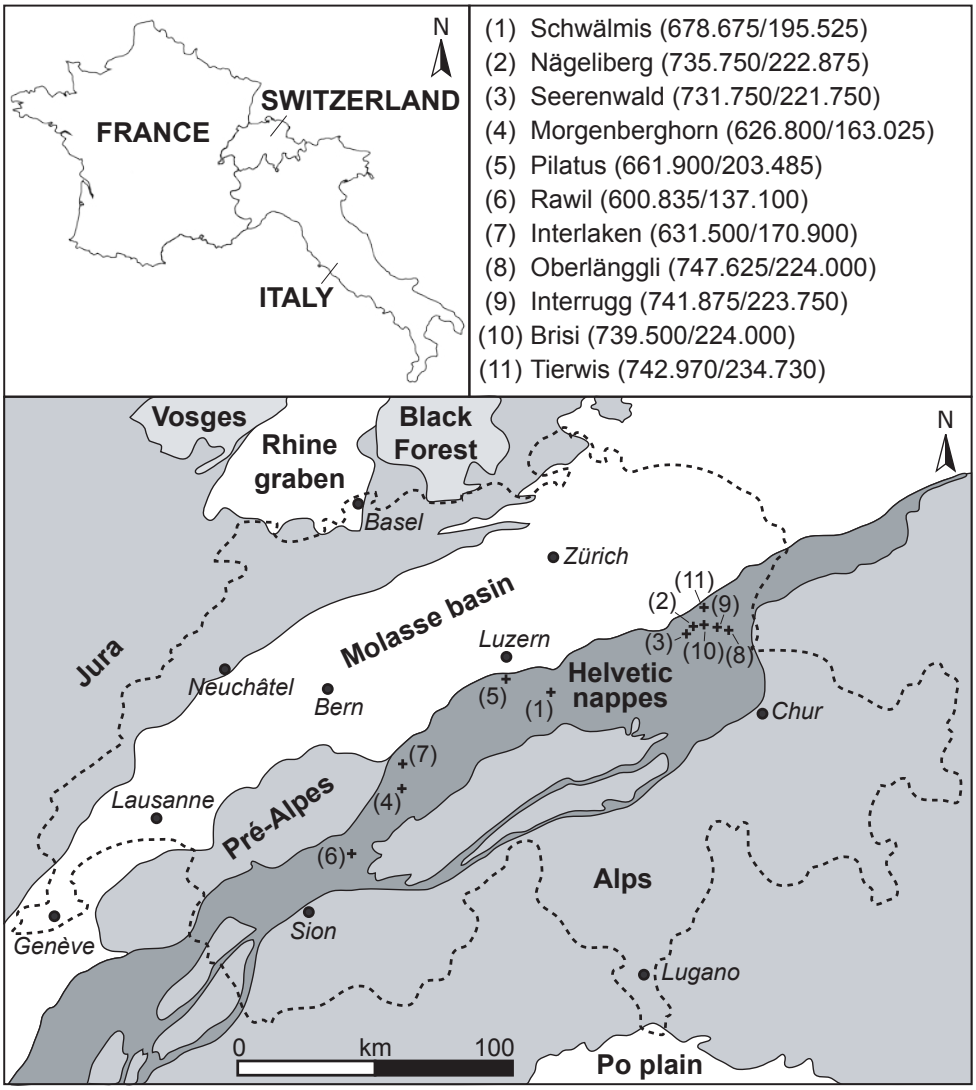

Fig. B.2.1: Location of the studied sections and their geographical coordinates, expressed in the Swiss orthogonal coordinate system. The Helvetic realm is shown in dark grey.

sea-level rise during the Early Valanginian resulted in a homoclinal ramp morphology (Kuhn, 1996) until the Late Barremian and the installation of the Urgonian facies, which signaled the return to a distally steepened carbonate ramp morphology. These changes in platform morphology were accompanied by changes of the sediment-producing benthic community, from a photozoan mode (sensu James, 1997; oligotrophic conditions) during the late Tithonian to Berriasian to a heterozoan mode (sensu James, 1997; meso-eutrophic conditions) from the Early Valanginian to the Early Barremian. During the Late Barremian, the installation of the Urgonian platform (Schrattenkalk Fm) underlines the return of photozoans (Föllmi *et al*., 1994). During the Early Cretaceous, reef-related organisms such as corals, stromatoporoids and rudists characterize photozoan assemblages whereas crinoids, bryozoans, abundant sponges and the absence of reef-related organisms mark heterozoan assemblages. The condensed sediments associated with drowning deposits are characterized by the dominance of siliciclastic particles, glaucony and phosphates (e.g., Föllmi *et al*., 1994; van de Schootbrugge, 2001).

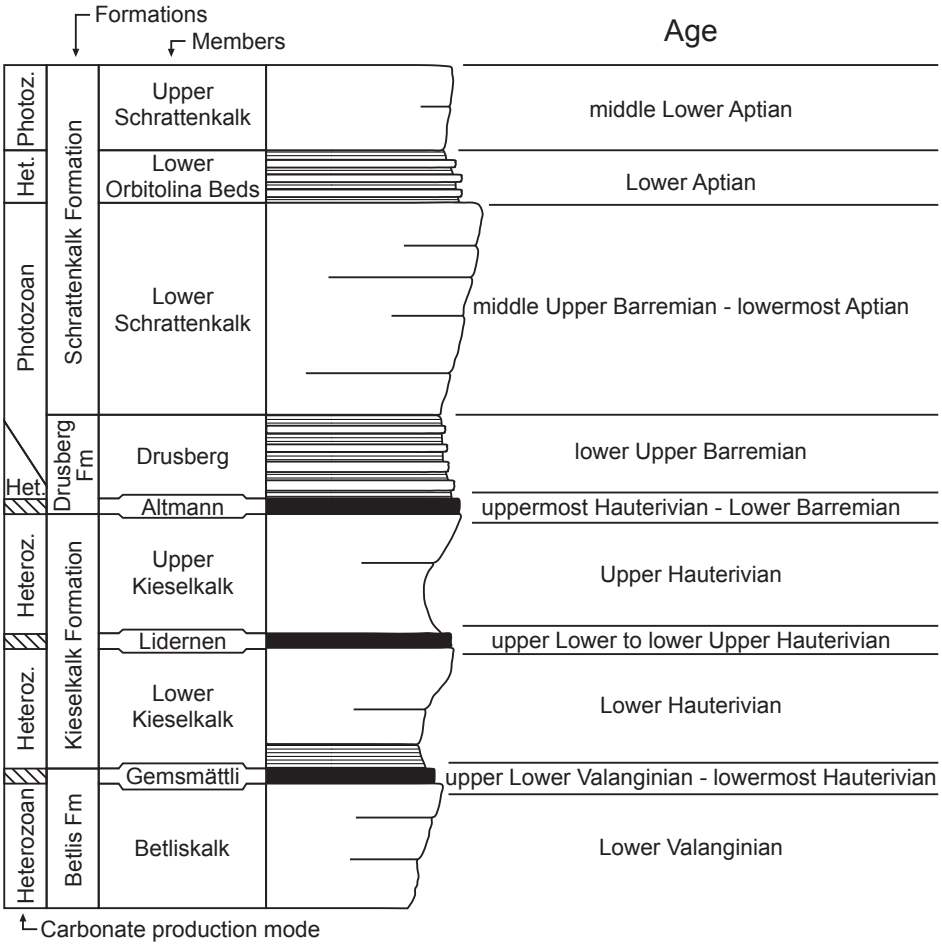

Fig. B.2.2: Synthetic log of Helvetic platform deposits of Valanginian to Early Aptian age.

B.2.3. Materials and methods

Eleven sections are documented (Schwalmis, Nägeliberg, Seerenwald, Morgenberghorn, Pilatus, Rawil, Interlaken, Oberlänggli, Interrugg, Brisi and Tierwis section). The majority of the studied sections is situated in the eastern part of Switzerland (Fig. B.2.1), in the Säntis – Churfirsten – Alvier massif, where the good quality and continuity of the outcrops allow to trace a proximal to distal transect along the northern Tethyan margin. These sections were sampled bed by bed, in order to identify high-frequency microfacies variations along the sedimentary succession. Coupled with stacking-pattern observations, these observations allow sequence-stratigraphic interpretations of the studied section.

To provide a high-resolution biostratigraphy for the Altmann Mb, a large number of ammonites were investigated, including newly collected ammonites as well as previous findings (e.g., Fichter, 1934; Briegel, 1972; Rick, 1985; Wyssling, 1986; and many others…) that are stored in the Museums of Natural History of St. Gallen (Switzerland) and Dornbirn (Austria), and at the ETH Zürich. A total of 211 ammonites were identified. 108 of them provide accurate ages and are listed in Table B.2.1 (see also Fig. B.2.3). The stratigraphic position of the newly collected ammonites was precisely documented within each section in order to allow precise correlations. Combined with sequential stratigraphic interpretations, this allows to establish a markedly improved ammonite biostratigraphy of the Altmann Mb.

Location	Sample	Number
This study		
Tierwis section		
Abrytusites sp.	1	Sa 16a
Balearites sp. gr. mortilleti	1	Sa 16a
Emericiceras gr. koechlini	1	Sa 33
Emericiceras sp.	1	Sa 33
Paraspiticeras gr. percevali	2	Sa 16a
Parathurmannia sp.	1	Sa 16a
Plesiospitidiscus sp.?	1	Sa 16a
Subtorcapella sp.?	2	Sa 38
Torcapella gr. davydovi	1	Sa 33
Torcapella sp.?	2	Sa 36-38
Oberlänggli section		
Barremites sp. juv.	1	Ob 2
Parathurmannia cf. catulloi	1	Ob 2
Interlaken		
Barremites sp.	1	int 2
Dornbirn museum		
Avramidiscus aff. gastaldianus	1	P 11691
Avramidiscus cf. gastaldianus	1	P 6345
Avramidiscus intermedius	1	P 9392
Avramidiscus seunesi	2	P 11675
Balearites aff. mortilleti	1	P9385
Kotetishvilia aff. armenica ??	1	P 9345
Kotetishvilia aff. nicklesi	1	P 9346
Kotetishvilia compressissima	1	P 9370
Metahoplites cf. fallax	2	P 11649
Metahoplites cf. nodosus	1	P 9338
Metahoplites gr. fallax	3	P 9340
Metahoplites nodosus	1	P 11693
Nicklesia pulchella	1	P 11714
Parasaynoceras aff. perezianus	1	P 6332
Torcapella cf. fabrei	1	P 1615
? Metahoplites rarecostatus ?	1	P 11703
St. Gallen museum		
Avramidiscus seunesi	1	52.4
Kotetishvilia cf. compressissima	1	52.2
Pseudothurmanniform fragments	1	51.2
Torcapella sp.?	1	55.2

Location	Sample	Number
ETH Zürich		
Acrioceras sp.	4	F 7102
Anahamulina davidsoni	1	W 2273
Astieridiscus sp.	1	R1
Avramidiscus aff. intermedius	1	F 71007
Avramidiscus aff. kiliani	2	W 4876
Avramidiscus aff. querolensis	1	F 71006
Avramidiscus cf. druentiacus	1	W 4741
Avramidiscus gr. intermedius	2	F 7102.4
Avramidiscus sp.	2	F 71042
Balearites aff. catulloi	1	F 71055
Balearites sp. ?	1	F 71010
Costidiscus sp.	1	W 4518
Davidiceras sp.	1	W 5123
Dissimilites sp. ?	1	W 4955
Hamulina astieri	1	J 1078
Honnoratia sp.	4	F 71008
Karsteniceras aff. beyrichii	1	J 1043
Kotetishvilia cf. compressissima	2	J 1102
Leptoceratoides cf. annulatum	1	C 1042
Leptoceratoides sp.	1	W 5969
Metahoplites aff. fallax	1	J 1044
Metahoplites aff. nicklesi	2	W 4561
Metahoplites cf. fallax	1	J 1101
Metahoplites fallax	2	W 4916.1
Metahoplites gr. fallax	1	W 4860.1
Nickesia aff. nodosa	1	W 5263
Nicklesia cf. didayi	1	J 1039.3
Nicklesia pulchella	2	J 1039.4
Nicklesia pulchella morphotype tardif	2	J 1039.1
Paracrioceras sp.	3	J 1068
Parasaynoceras aff. perezianus	1	F 71005
Parasaynoceras sp.	2	W 4919
Pseudothurmannia aff. catulloi	2	F 71011
Pseudothurmannia aff. ohmi	1	W3 5135
Pseudothurmannia sp. s.l.	1	W 5028
Silesites gr. vulpes	1	W 4232
Taveraidiscus sp.	4	F 71035
Teschenites sp. ?	1	J 1011
Torcapella cf. fabrei	1	W 4971
Torcapella gr. davydovi	7	W 4221
Torcapella gr. fabrei	1	F 71019

Table B.2.1: List of identified ammonites from the Altmann Mb.

Fig. B.2.3 (opposite page): Examples of well-preserved representative ammonites from the Altmann Mb. A-D: After the study of Wyssling, 1986, re-identified, Vorarlberg region, Austria (stored in the Museum of Natural history of Dornbirn, Austria); E-F: Newly collected ammonites from the Tierwis section (all the newly collected ammonites are stored at the Geological Institute of Neuchâtel). A: *Balearites aff. mortilleti*, specimen n° P9385. B: *Kotetishvilia aff. nicklesi*, specimen n° P9346. C: *Metahoplites nodosus*, specimen n° P11693. D: *Avramidiscus cf. gastaldianus*, specimen n° P6345. E: *Torcapella gr. davydovi*, bed Sa 33. F: *Emericiceras sp.*, bed Sa 33. G: *Balearites sp. gr. mortilleti*, bed Sa 16a.

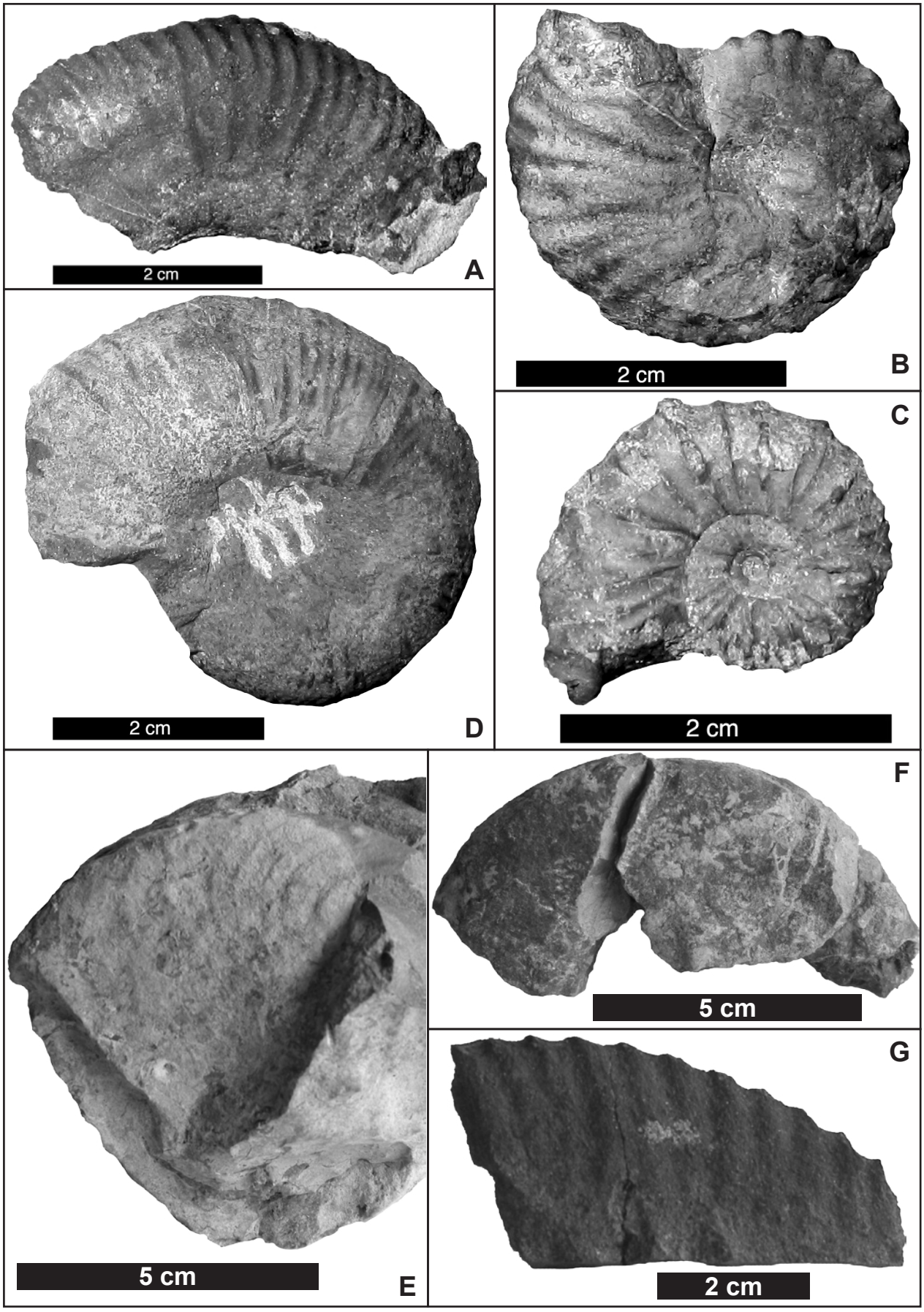
2 cm
A
2 cm
B
C
2 cm
D
2 cm
5 cm
E
F
5 cm
G
2 cm

B.2.4. Biostratigraphy

The outcome of the here established improved ammonite biostratigraphy (Fig. B.2.4) suggests that the time documented in the Altmann Mb spans from the latest Hauterivian (*P. seitzi* biozone) to the latest Early Barremian (*C. darsi* biozone). This new age determination is different from the previous ones by which a middle Early Barremian age for the end of the Altmann Mb was assumed (e.g., Funk *et al.*, 1993; Föllmi *et al.*, 1994). Moreover, the distribution of these ammonites in time and space suggests that the biostratigraphic ages for the lower and upper limits of the Altmann Mb are synchronous (i.e. within the same ammonite zone) for the entire studied area. Following cyclo-stratigraphic interpretations of late Hauterivian – Barremian successions from the Vocontian trough (Bodin *et al.*, 2006), a duration of approximately 3 Myr is estimated for the time preserved in the Altmann Mb. The reduced thickness of the majority of the sections of the Altmann Mb (see below) implies that these sections are highly condensed, and the average sedimentation rate is approximately 1 m/Myr. In comparison, for the Upper Kieselkalk Mb at the Pilatus locality, an average sedimentation rate of 50 m/Myr is estimated (e.g., Funk, 1969; Van de Schootbrugge, 2001). This difference is related to the phase of carbonate platform drowning documented by the Altmann Mb and the associated slowdown or stop of the benthic carbonate production.

B.2.5. Microfacies

Ten different microfacies types have been recognized in the Upper Hauterivian – Lower Barremian deposits of the Helvetic realm (Upper Kieselkalk, Altmann and Drusberg Mbs). The microfacies HF0 to HF6 are adapted from previous studies focusing on Lower Cretaceous Western Tethyan carbonate platforms (e.g., Arnaud-Vanneau, 1980; Schenk, 1992; Wissler *et al.*, 2003) because of the meso-eutrophic conditions prevailing on the Helvetic platform during the Hauterivian to Early Barremian. These microfacies are placed on a palinspastic transect through the northern Tethyan Helvetic homoclinal ramp (Figs. B.2.5-6) using the carbonate ramp depositional system description from Burchette and Wright (1992). The microfacies HFa, HFb and HFc are specific for the glauconitic- and phosphatic-rich horizons and the gravity-flow deposits within the Altmann Mb, hence a precise localization is not feasible.

B.2.5.1. HF0 (marls; marls - micrite)

The rocks corresponding to this facies are finely laminated and composed of radiolaria, calcispheres, rare sponge spicules and rare beds with sparse bivalve fragments, as well as of large amounts of very small and unidentifiable bioclasts. If the conditions of preservation are good, this facies contains a macro-fauna including ammonites, belemnites or fish teeth.

Interpretation: According to the presence of pelagic fauna, this facies is thought to represent a distal shelf deposit (hemi-pelagic facies).

B.2.5.2. HF1 (mudstone or wackestone; spicule-rich biomicrite)

The rocks corresponding to this facies are limestones and marly limestones. It is composed of numerous sponge spicules, in addition to some very small echinoderm fragments, peloids, benthic foraminifera and rare ostracods. Sporadic fish teeth are present.

Interpretation: This facies may represent the outer ramp deposits below the storm-weather wave base (hemi-pelagic facies), as testified by the presence of numerous sponge spicules.

Fig. B.2.4 (opposite page): A. Stratigraphic range of the most significant ammonites identified in the Altmann Mb sections. Ammonite biostratigraphy zonation *sensu* Vermeulen (2005). Stratigraphic sequences after Hardenbol *et al.* (1998), modified by Arnaud (2005) for the latest Hauterivian – Barremian. Dating of the Lidernen Mb after van de Schootbrugge (2001). B. Correlation of the ammonite zonation of Vermeulen (2002, 2005) for the late Hauterivian with the current standard zonation (e.g., Hoedemaeker et al., 2003).

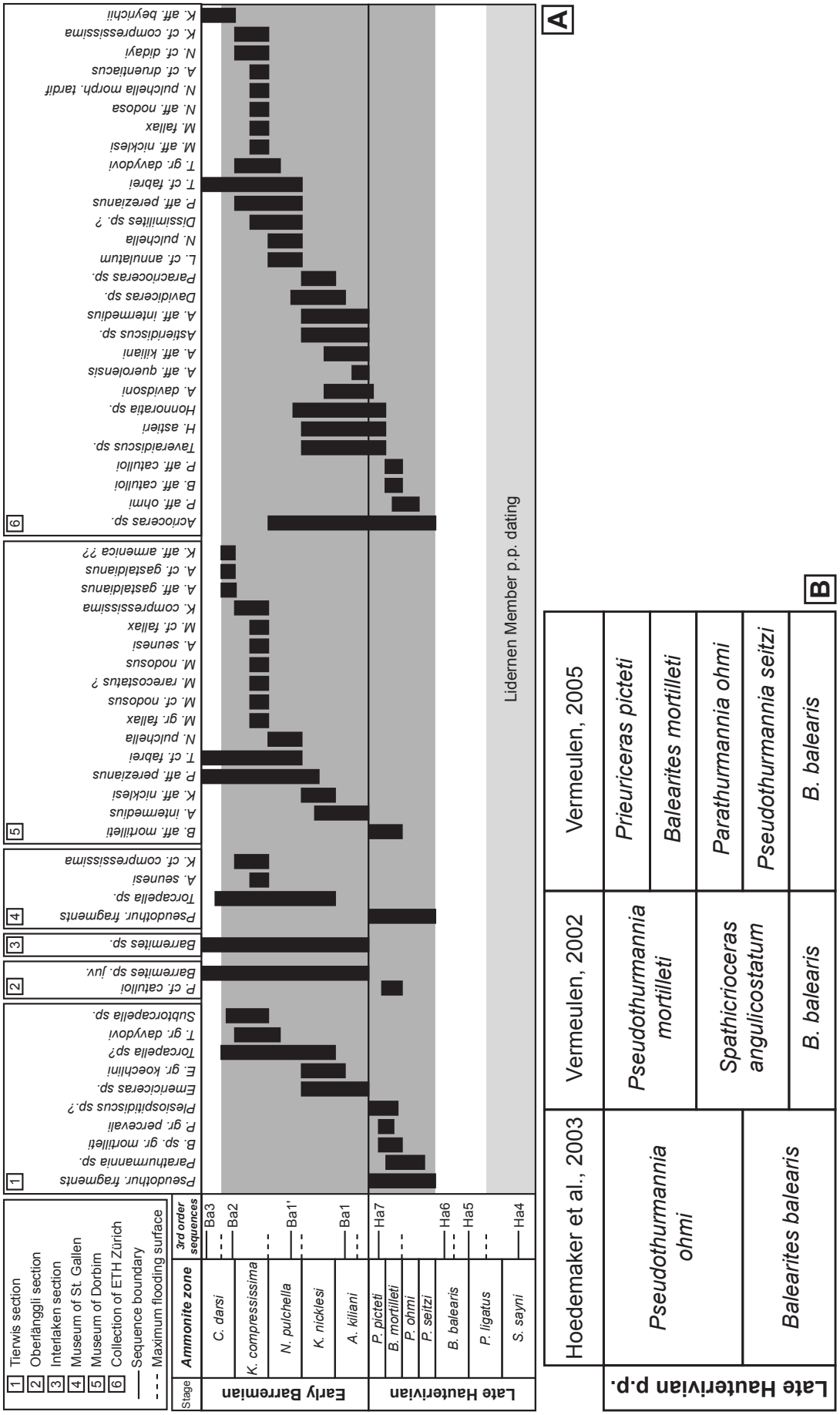
1 Tierwis section
2 Oberlänggli section
3 Interlaken section
4 Museum of St. Gallen
5 Museum of Dorbim
6 Collection of ETH Zürich
Sequence boundary
Maximum flooding surface
Stage
Ammonite zone
3rd order sequences
Early Barremian
Late Hauterivian
C. darsi
K. compressissima
N. pulchella
K. nicklesi
A. kiliani
P. picteti
B. mortilleti
P. ohmi
P. seitzi
B. balearis
P. ligatus
S. sayni
Ba3
Ba2
Ba1'
Ba1
Ha7
Ha6
Ha5
Ha4
Lidernen Member p.p. dating
A
B
Hoedemaker et al., 2003
Vermeulen, 2002
Vermeulen, 2005
Late Hauterivian p.p.
Pseudothurmannia ohmi
Balearites balearis
Pseudothurmannia mortilleti
Spathicrioceras angulicostatum
B. balearis
Prieuriceras picteti
Balearites mortilleti
Parathurmannia ohmi
Pseudothurmannia seitzi
B. balearis

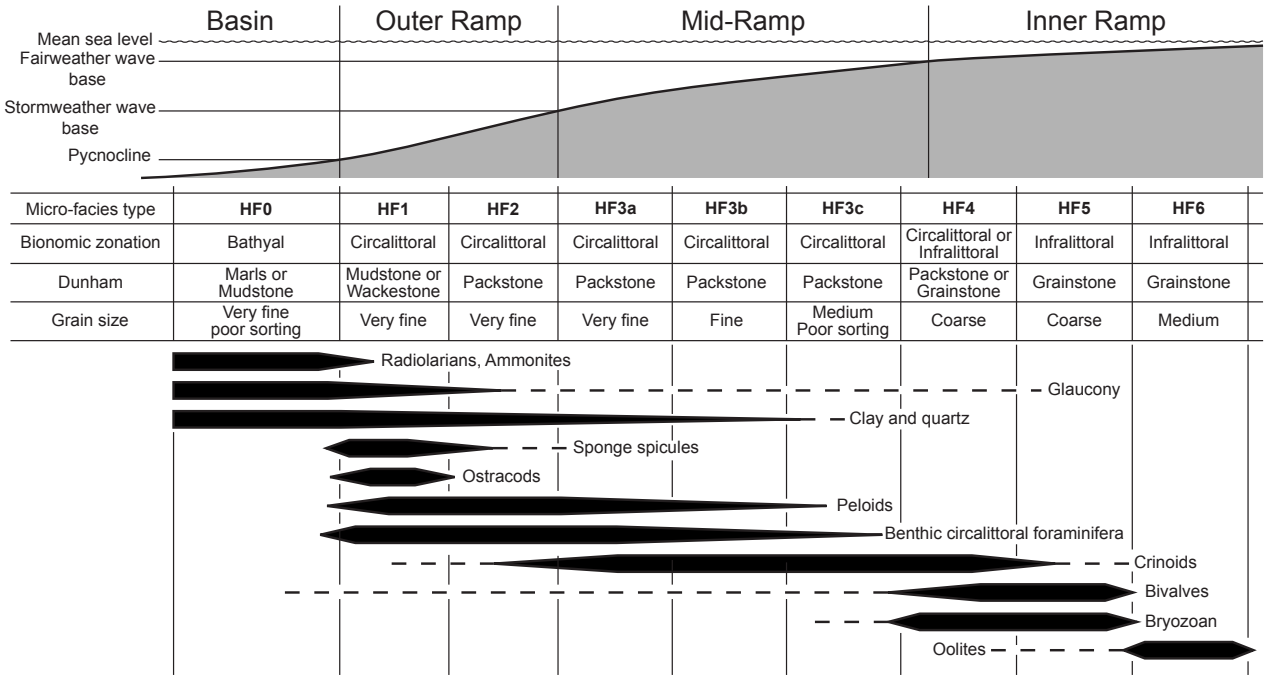

Fig. B.2.5: Distribution of the principal facies types in a schematic transect through the Helvetic ramp during the Hauterivian – Early Barremian. Bionomic zonation after the classification of Pérès (1961).

B.2.5.3. HF2 (packstone; biopelmicrite)

The rocks corresponding to this facies are limestones and marly limestones. It is composed of large quantities of very small echinoderm fragments, rare sponge spicules, bivalve fragments, peloids, benthic foraminifera and quartz grains.

Interpretation: This facies may represent the upper part of the outer ramp deposits, affected by very rare storm events, as testified by the presence of very small fragments, which were likely derived from shallower regions.

B.2.5.4. HF3 (packstone; crinoid-rich biopelmicrite)

The lithology of this facies is typical for the Helvetic Kieselkalk Fm, i.e. crinoidal limestone or marly limestone (some chert nodules may also occur). It is mainly composed of angular crinoid fragments, small quartz grains, sparse bivalve fragments, benthic foraminifera and peloids. It is divided into three sub-facies: HF3a, 3b and 3c, taking into account the mean size of the crinoid grains, from very fine to medium grained.

Interpretation: The sorting of the mean size of crinoid grains may reflect redistribution of these grains during storm events. The absence of sparitic cement may, however, reflect the lack of permanent hydrodynamic currents. This facies may thus represent a middle ramp deposit, above the storm wave base and below the fair-weather wave base.

B.2.5.5. HF4 (packstone or grainstone; crinoïdal and bryozoan biomicrite or biosparite)

This facies is typical for the "Kieselkalk – Echinodermenbreccie" Mb (Funk, 1969) and is expressed in relatively thick (up to 2-meters-thick) limestone beds, which are sometime cross-stratified. This facies is coarsely grained, poorly sorted, and composed of angular echinodermal and bivalve fragments, bryozoans, gastropods, peloids and rare ooids. Sparitic cements are observed.

Interpretation: The presence of sparitic cement in this facies hints to a deposition under quasi-permanent hydrodynamic currents. This facies is thus attributed to the transition between the upper middle and the lower inner ramp.

B.2.5.6. HF5 (grainstone; coarse biosparite with rounded grains)

This facies presents the same allochem assemblage as the previous one, with the main difference being that all the grains are well rounded. Some grains present traces of incipient ooid formation (superficial ooid).

Interpretation: According to the presence of rounded grains and sparitic cement, which suggests deposition under permanent agitation, this facies may have been deposited on the inner ramp, under permanent hydrodynamic currents, above the fair-weather wave base.

B.2.5.7. HF6 (grainstone; oosparite or oobiosparite)

This facies was never observed in the Hauterivian – Early Barremian of the Helvetic realm. Only indirect clues for oolithic bars are present (i.e. oolithes dispersed in MF4 and MF5 facies). During the Hauterivian, the presence of oolithic bars is, however, observed in the deposits of the Jura Mountains (Pierre Jaune de Neuchâtel Fm; e.g., Blanc-Aletru, 1995; see Fig. B.2.1 for localization), which represent the upper part of the Helvetic ramp.

Interpretation: According to the presence of oolithes and sparitic cement, this facies may be representative of the inner ramp.

B.2.5.8. HFa (glauconitic-rich sandstone)

The lithology of this facies is characteristic for the highly reduced sections of the Altmann Mb (less than 2m thick). It is composed of coarse rounded quartz grains, mature glaucony grains, some phosphate and calcite grains, as well as authigenic pyrite grains. The matrix corresponds to micritic or phosphatized ooze. In the field, oblique stratifications are sometimes recognized.

Interpretation: The presence of numerous mature glauconitic grains, as well as phosphate and pyrite, may point to a highly condensed or an allochthonous deposit derived from a condensed deposit.

B.2.5.9. HFb (wackestone or packstone; biomicrite)

The lithology of this facies is recognized in deposits occurring within Altmann Mb sections with phosphatized hardground at their base or with phosphatic nodules. It has the same characteristic as the micro-facies HFa. Quartz grains are, however, rare and smaller and glaucony grains (if present) are well rounded. The sorting is relatively good and many coarse crinoid grains are present. In addition, bryozoans, brachiopods and bivalve fragments, as well as small benthic foraminifera and phosphate grains are observed. The matrix is often phosphatized.

Interpretation: Well-rounded glaucony grains may indicate their parautochtonous origin (e.g., Pasquini *et al*., 2004). Due to the presence of oblique stratification, as well as an erosive base below the bed presenting this microfacies, theses rocks are interpreted as gravity flow deposits.

B.2.5.10. HFc (phosphatized hardground)

The macroscopic aspect of this facies differs between different sections. Similarities include the presence of macrofauna (ammonites, belemnites, bivalves, brachiopods, sponges…), as well as the presence of burrows, encrusting organisms and sometimes burrow infills below the hardground. The matrix is always composed of completely or partially phosphatized ooze. Phosphate grains, glaucony and lithoclasts are frequent, as well as grains or rock fragments reworking.

Interpretation: Hardground surfaces are subaquatic features. The formation of such discontinuity surfaces can be related to the lowering of the effective wave base exposing the sea floor to wave action (e.g., Immenhauser *et al*., 2000).

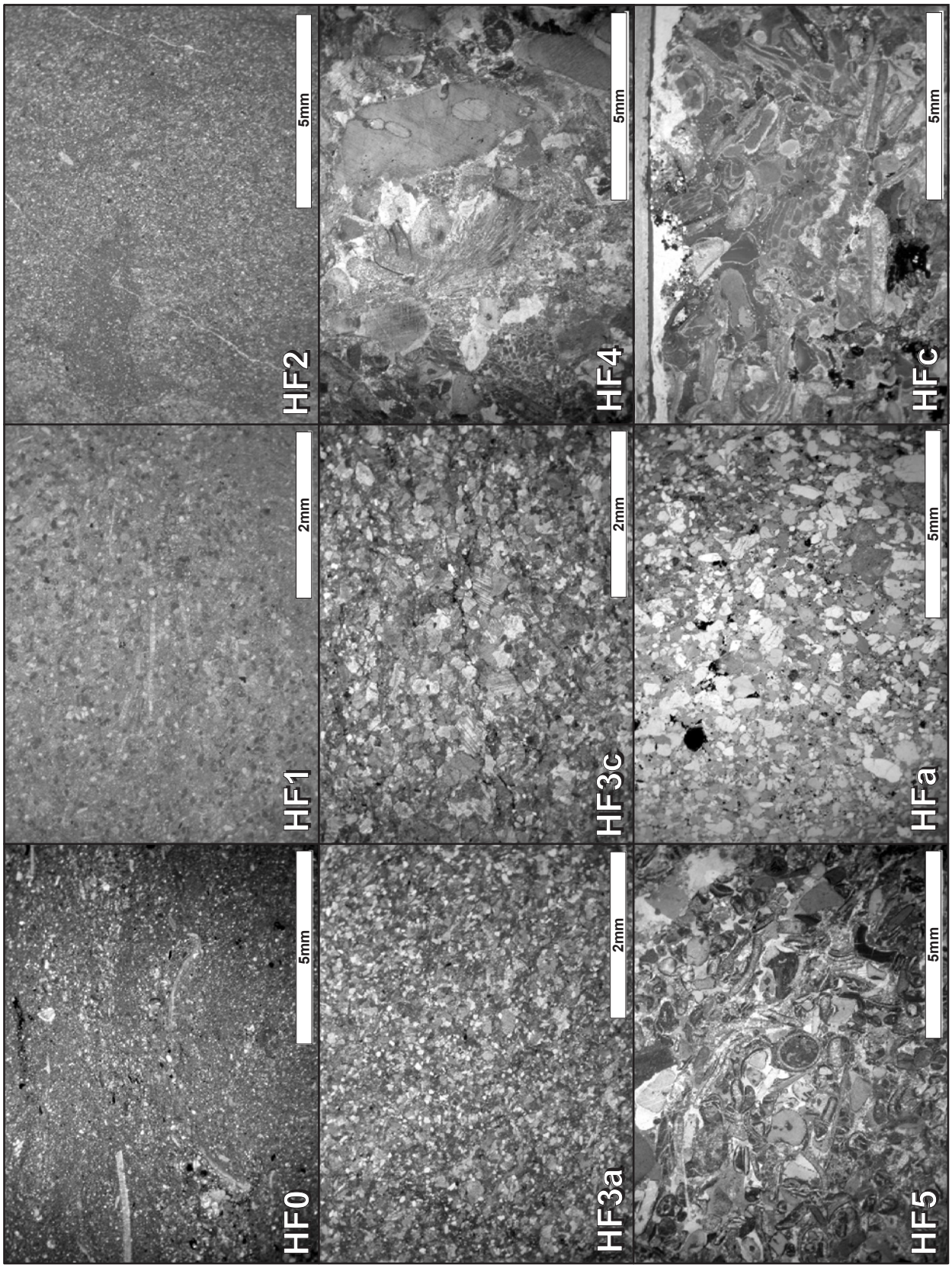

Fig. B.2.6: Photomicrographs of micro-facies HF0-5 and HFa-c. See the text for details. HF0: Sample Sa38. HF1: Sample Sa40. HF2: Sample Sa23. HF3a: Sample Sa30a. HF3c: Sample Sa7. HF4: Sample Pil145. HF5: Sample Pil143. HFa: Sample Schwa1. HFc: Sample Pi1 (note the marine phreatic cement and the phosphatized matrix occurring in the top of this thin-section. Note that this is also the top of the basal hardground in this photomicrograph). Samples Pil145 and Pil143 are taken from the top of the Upper Kieselkalk Mb in the Pilatus section (after van de Schootbrugge, 2001).

B.2.6. Macroscopic sedimentological aspects

The Altmann Mb is easily distinguished in the field due to its high content of glauconitic grains and the presence of phosphatic particles and crusts (Funk, 1969). The distinct lithological differences between the dark colored, sandy crinoidal limestones of the subjacent Kieselkalk Fm and the grey colored hemipelagic marl – limestone alternations of the superjacent Drusberg Mb are characteristic properties that assist in the identification of the Altmann Mb. The sections of the Altmann Mb studied here are subdivided into four main types according to their thickness and lithologic pattern.

B.2.6.1. Highly reduced sections or hiatus

Reduced sections and hiatus represent the majority of the Altmann Mb sections. This highly reduced type of section is characterized by the following field aspects: a total thickness < 2 meters, occasionally with an erosive base (e.g., the Schwalmis and the Nägeliberg sections; Fig. B.2.7). In some beds, oblique stratifications are observed, depending on the exposure conditions. Glaucony-rich sandstone and rare phosphatized grains characterize the facies of these beds. No datable ammonites have been found in these sections, even if some of the dispersed phosphate grains, due to their bean-shaped aspect, could be attributed to altered and phosphatized ammonite clasts. The Seerenwald section (Fig. B.2.7) is no more accessible today, and was drawn after the precise descriptions of Heim (1910-1916). In most outcrops situated in proximal settings, the Altmann Mb is not present between the Kieselkalk Fm and the Drusberg Mb, and only an erosive surface is observed (e.g., at the Morgenberghorn section; Fig. B.2.7).

B.2.6.2. Sections with a phosphatized hardground at their base

This type of section of the Altmann Mb is characterized by a thickness varying between 1 and 8 meters and by a same stacking pattern, even if some local differences exist. At the base, a phosphatized hardground rich in macrofossils is present (e.g., Pilatus, Rawil, Interlaken and Oberlänggli sections; Fig. B.2.8). The thickness of the phosphatized crust associated to the hardground varies from 2 to 15 cm. Below the hardground, burrows are observed in all sections except the one measured at the Oberlänggli locality. Above this basal horizon, a succession of alternating limestone and marls follows. In the studied sections, the Altmann Mb always ends in a marly interval, which is locally rich in fish teeth and glaucony. In the Pilatus and Oberlänggli sections, a glauconitic-rich bed occurs just below the uppermost marl interval.

B.2.6.3. Sections with phosphatic nodules

Sections with phosphatic nodules are found in the Interrugg and the Brisi localities (Fig. B.2.9). This type of section is characterized by the following field aspects: an erosive base, the presence of phosphate nodules and an obliquely stratified glaucony-rich bed (up to 60 cm thick at the Brisi locality) occurring just below an uppermost marly interval. In the Interrugg section, the poor outcrop conditions do not allow to log a complete section.

B.2.6.4. Expanded sections

Expanded Altmann Mb sections are found in the Tierwis (Fig. B.2.10), Altmann-Sattel and Fluebrig localities (e.g., Funk, 1969; Rick, 1985). The Altmann-Sattel section is the Altmann Mb type section whereas the Tierwis section is the paratype section of the Altmann Mb (Funk, 1969). At Tierwis, the Altmann Mb is approximately 35 m thick and consists of crinoidal limestones intercalated with two marly intervals; a thin and darkly colored one near the base (ca. 6 m above the Kieselkalk – Altmann boundary) and a thick second one, with intercalated layers rich in fish teeth at the top of the Altmann Mb.

The lowermost four meters of the Altmann Mb section present all the characteristics of the

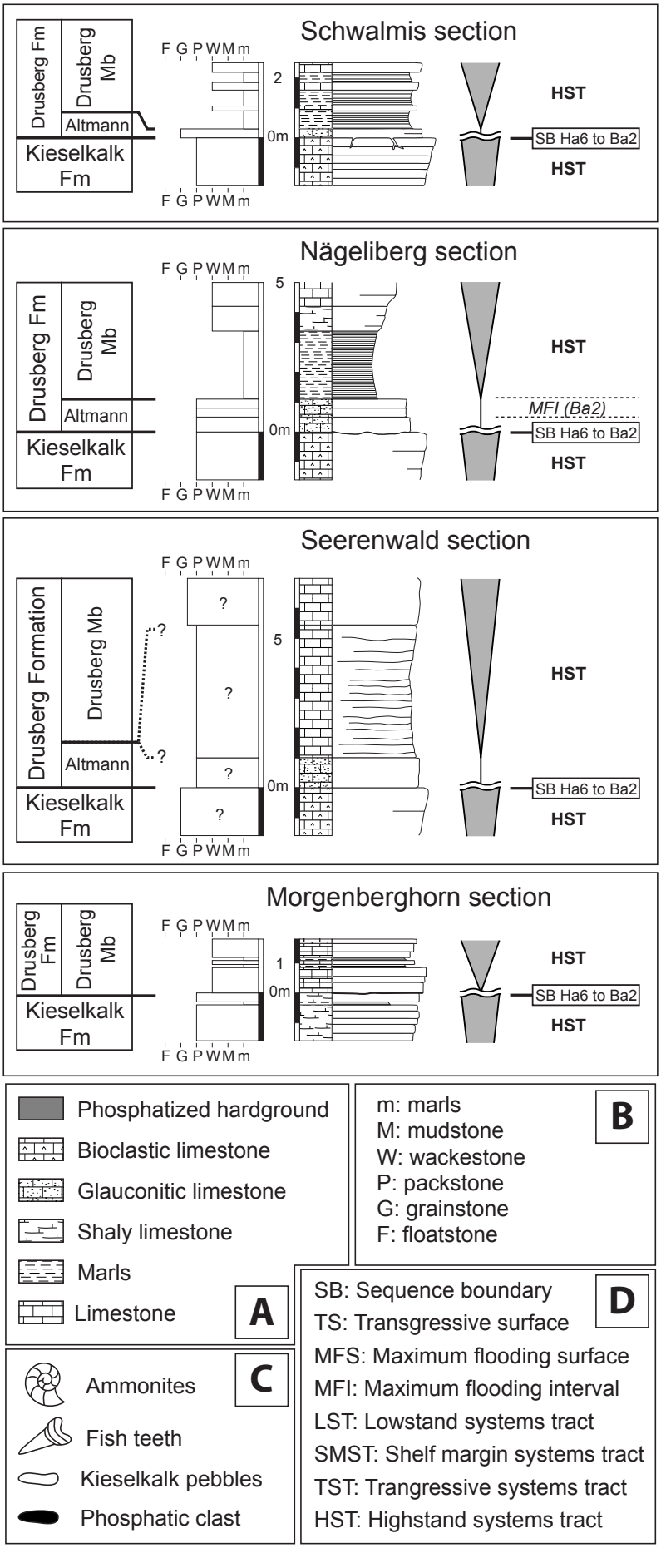

Fig. B.2.7: Highly reduced sections or hiati. The Seerenwald section is drawn after the description of Heim (1910-1916). A: lithology; B: Dunham classification; C: Key to fossils or nodules. D: sequence-stratigraphic terminology.

"Kieselkalk – Echinodermenbreccie" facies and were first attributed to the Kieselkalk Fm according to Funk (1969). The discovery of an erosive surface below these beds and the presence of a relatively high amount of glaucony within the limestone (contrary to the Pilatus section, which is the type section for the Kieselkalk Fm) suggest that these beds belong to the Altmann Mb. At their top, an horizon with ferric concretions and glauconitic crusts is observed (Funk, 1969).

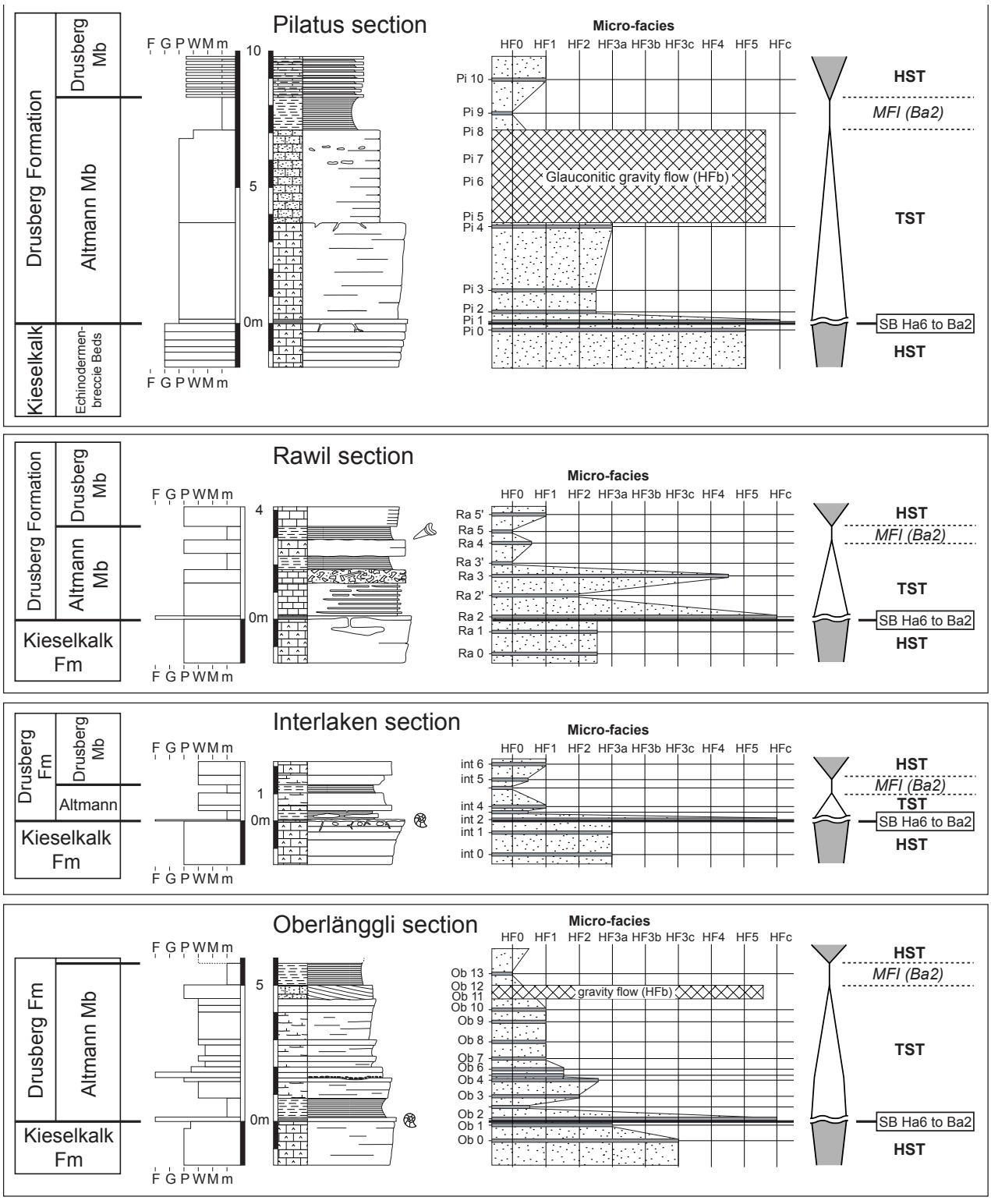

Fig. B.2.8: Sections with a phosphatized hardground at the base. See Fig. B.2.7 for key to abbreviations and symbols.

The middle part of the section is constituted by a thick crinoidal thickening-upward limestone succession (ca. 25 m) capped by Thalassinoides, Ophiomorpha and Skolithos burrows belonging to the *Cruziana – Glossifungites* ichnofacies (e.g., Pemberton, 1998; Malpas *et al*., 2005). A 3-meters-thick glauconitic-rich zone follows, presenting *Cruziana – Glossifungites* ichnofacies in the first meter. This zone precedes ca. 3 m of marly crinoidal limestone capped by a hardground surface. The latter is rich in macrofossils such as ammonites, oysters, sponges, belemnites and incrusting organisms, and presents many reworked rock fragments (with phosphatized outlines), burrows and traces of silicification (see Fig. B.2.11).

The Drusberg Mb is separated from the Altmann Mb by a 1-meters-thick marly interval. The lower part of the Drusberg Mb is characterized by a thickening-upward limestone – marl alternation whereas a thinning-upward marl-dominated deposit characterizes the upper part of the Drusberg Mb.

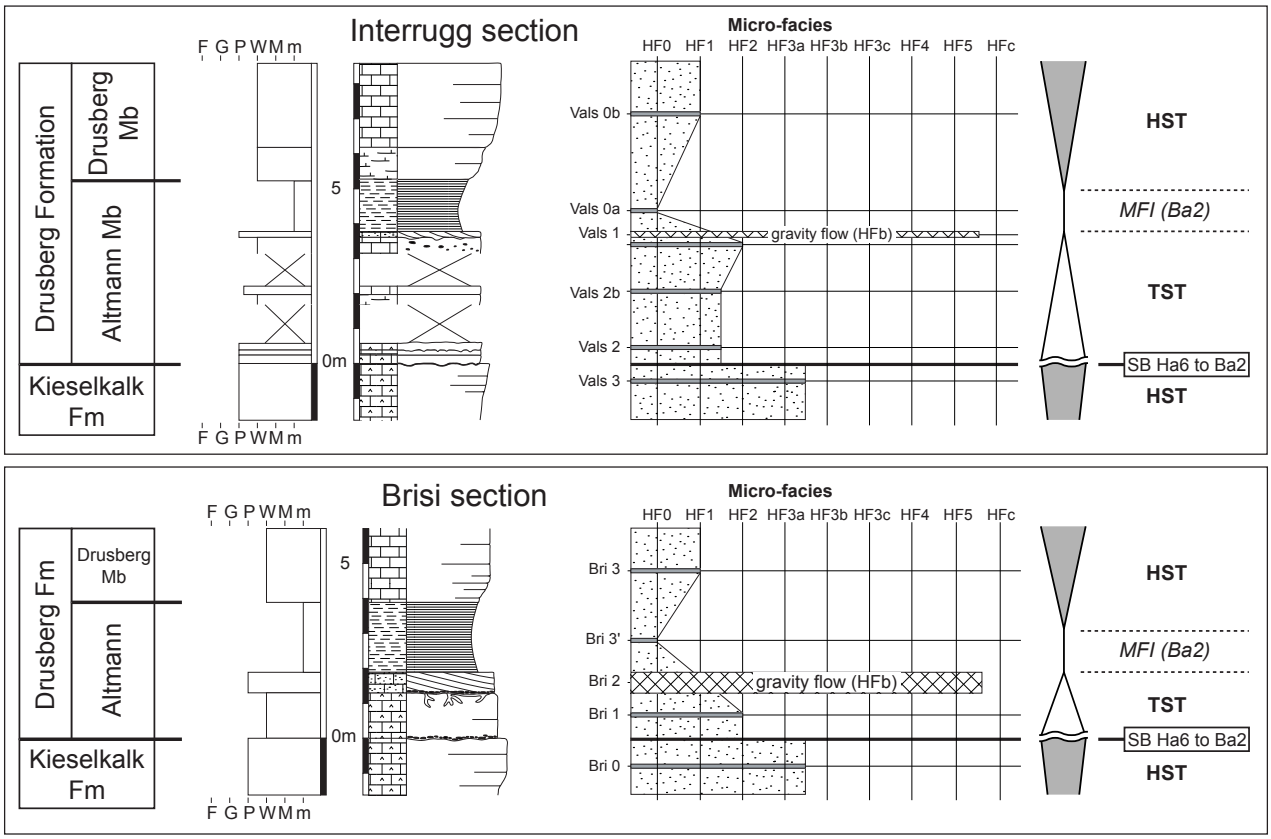

Fig. B.2.9: Sections with phosphatic nodules. See Fig. B.2.7 for key to abbreviations and symbols.

B.2.6.5. Ammonite biostratigraphy in the Altmann Member

Newly collected ammonites come from the basal hardground of the Interlaken and Oberlänggli sections (Fig. B.2.8), and in different levels of the Tierwis section (Fig B.2.10). The ammonites from the two first sections are phosphatized and belong to the *B. mortilleti* biozone and to the Early Barremian (Fig. B.2.4), indicating significant periods involved in the condensation or reworking associated with the basal hardground. In the Tierwis section, the bed Sa 16b (Fig. B.2.10), which is particularly rich in ammonites, is dated as belonging to the *B. mortilleti* biozone by *Parathurmannia sp*., *Balearites sp. gr. mortilleti*, *Paraspiticeras gr. percevali* and *Plesiospitidiscus sp*. The hardground (bed Sa 33) yields ammonites from the *A. kiliani*

Fig. B.2.10 (opposite page): Tierwis section. See Fig. B.2.7 for key to abbreviations and symbols.

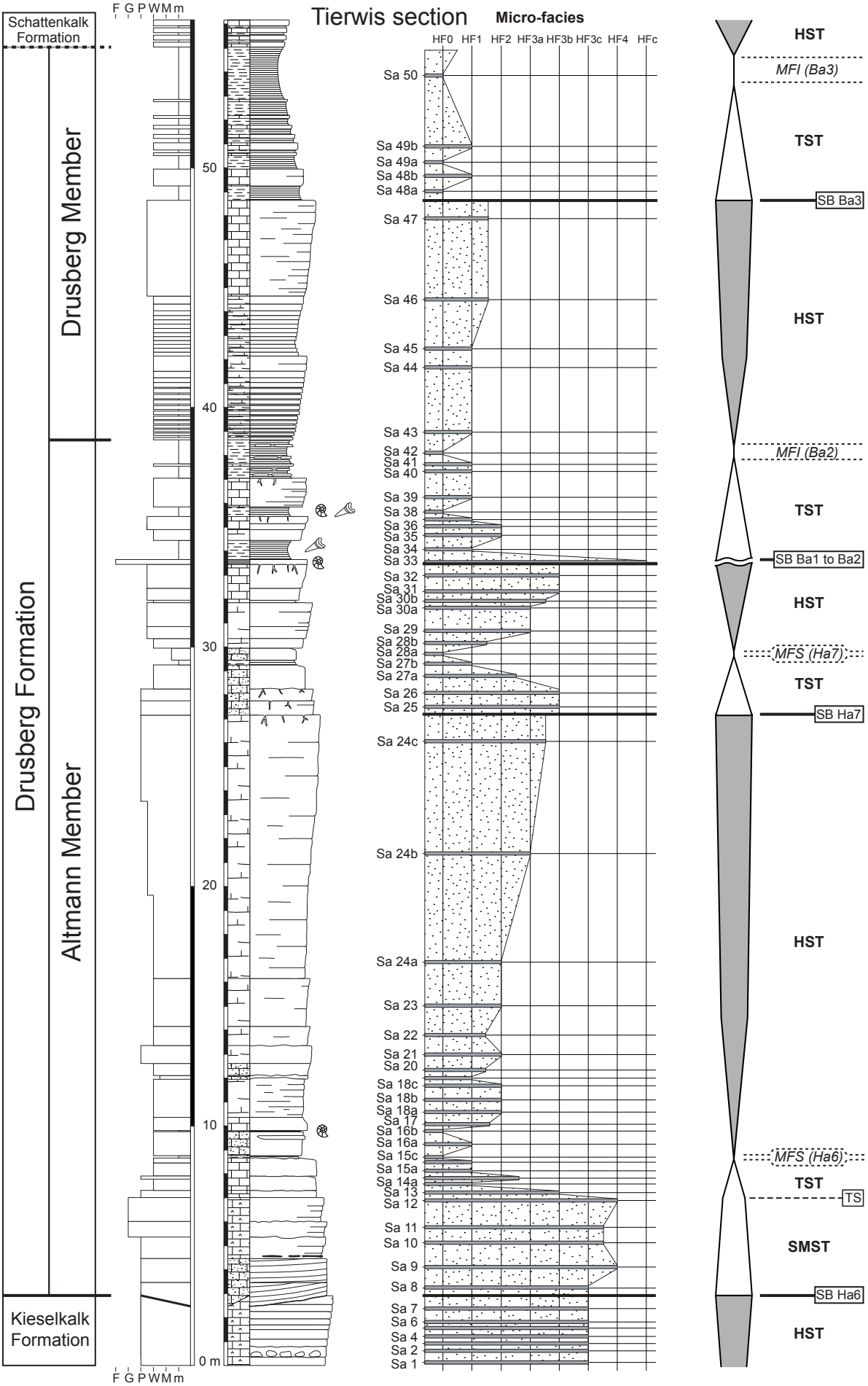
Schattenkalk Formation
Drusberg Formation
Drusberg Member
Altmann Member
Kieselkalk Formation
F G P W M m
0 m
10
20
30
40
50
Tierwis section
Micro-facies
HF0 HF1 HF2 HF3a HF3b HF3c HF4 HFc
Sa 50
Sa 49b
Sa 49a
Sa 48b
Sa 48a
Sa 47
Sa 46
Sa 45
Sa 44
Sa 43
Sa 42
Sa 41
Sa 40
Sa 39
Sa 38
Sa 36
Sa 35
Sa 34
Sa 33
Sa 32
Sa 31
Sa 30b
Sa 30a
Sa 29
Sa 28b
Sa 28a
Sa 27b
Sa 27a
Sa 26
Sa 25
Sa 24c
Sa 24b
Sa 24a
Sa 23
Sa 22
Sa 21
Sa 20
Sa 18c
Sa 18b
Sa 18a
Sa 17
Sa 16b
Sa 16a
Sa 15c
Sa 15a
Sa 14a
Sa 13
Sa 12
Sa 11
Sa 10
Sa 9
Sa 8
Sa 7
Sa 6
Sa 4
Sa 2
Sa 1
HST
MFI (Ba3)
TST
SB Ba3
HST
MFI (Ba2)
TST
SB Ba1 to Ba2
HST
MFS (Ha7)
TST
SB Ha7
HST
MFS (Ha6)
TST
TS
SMST
SB Ha6
HST

to the *K. compressissima* biozones (Table B.2.1) indicating again an extended period of condensation or reworking associated to this hardground. In the upper part of the section, ammonites were found in the beds Sa 36 to Sa 38. They belong to the *K. compressissima* to *C. darsi* biozones (Table B.2.1).

B.2.7. Sequence-stratigraphic interpretation

The analysis of the micro-facies temporal evolution and the stacking pattern leads to a sequence stratigraphic interpretation of the studied sections (Figs. B.2.7-10).

In highly reduced Altmann Mb sections, sequential interpretation of the thin glaucony-rich beds is rather difficult. However, the condensed pattern of these section, as well as the high amount of glaucony, point to a deposit associated with a maximum flooding surface (MFS). In addition, the shallowing-upward stacking of the overlying Drusberg Beds (which are attributed to highstand deposits) supports this interpretation. Due to its shallowing- and thickening-upward pattern, the underlying Upper Kieselkalk Mb is attributed to a highstand deposit. No transgressive systems tract (TST) could be identified in these sections.

In sections with a phosphatized hardground or with phosphatic nodules at their base, an identified trend toward deeper facies as well as a thinning-upward stacking pattern is observed. These beds represent thus a TST. This latter overlies the Upper Kieselkalk Mb, attributed to a highstand systems tract (HST) deposit, without a recognizable sea-level fall or lowstand deposits in between. Following Schlager (1999), this SB can thus be qualified as a type 3 sequence boundary. Due to the presence of Late Hauterivian and Early Barremian ammonites in the phosphate crust of the basal hardground, this latter may be interpreted as the result of a long-period of condensation. In the Oberlänggli section, which is the most distal section studied, as indicated by microfacies variations, the first 1.5 meters consist of shallowing-upward sediments and are overlain by a phosphatic lag. These beds are interpreted as representing a first shallowing-upward parasequence associated to the TST.

In the Altmann Mb of the Tierwis section, the preserved succession is more complete, with three main sequences recorded. The Altmann Mb begins with four meters of aggrading "Echinodermenbreccie – like" limestone overlying an erosive surface. This erosive surface, which lacks any indication of emersion, may be the expression of a type 2 SB. The following deposits are thus attributed to shelf margin systems tract (SMST) deposits. This succession is capped by a thin interval of glaucony-rich marly limestone. The strong shift toward deeper facies, as well as the high content of glaucony of these deposits, is characteristic of the TST (e.g., Chamley, 1989; Amorosi & Centineo, 1997). Between these two systems tracts, the horizon with ferric concretions and glauconitic crusts may thus be attributed to the TS. The MFS is represented by a thin dark-colored marl interval. The following HST is represented by thick shallowing- and thickening-upward marl-limestone succession.

This first main sequence is followed by a thinner second sequence. Here, no lowstand deposits are identified. The TST is thin (ca. 3m), and is marked by an enrichment in glaucony content and a shift to deeper facies. The SB is expressed as a firmground, rich in *Cruziana – Glossifungites* burrows, which may underline pauses in sedimentation (e.g., Pemberton, 1998) and may be transgressively modified during subsequent relative sea-level rise (e.g., MacEachern *et al.*, 1999). The HST is ca. 3.5 meters thick, and presents one shallowing-upward sequence.

The following phosphatized hardground (bed Sa 33, Fig. B.2.10) represents a SB, above which a ca. 4 m thick TST occurs. The Altmann Mb ends within a marly interval, corresponding to a MFS. The overlying lower part of the Drusberg Mb shows two shallowing-upward deposits, attributed to the following HST.

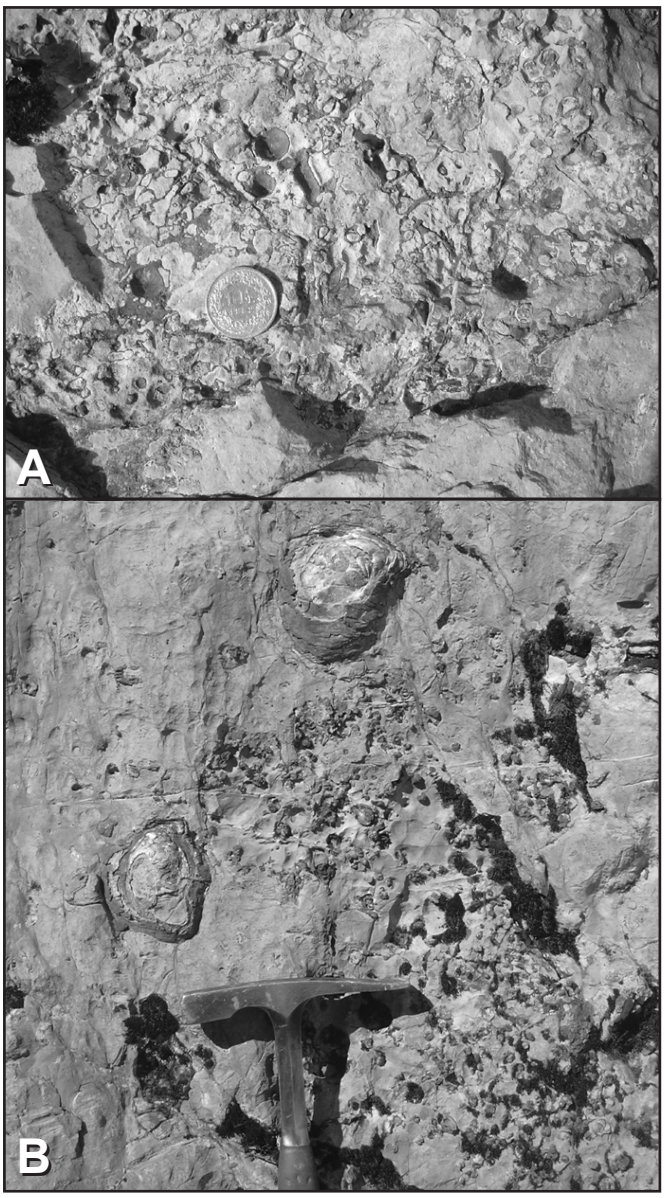

Fig. B.2.11: Details of features at the top of the phosphatized hardground (bed Sa33, Tierwis section). A: Phosphatized burrows; B: Oysters, burrows and phosphatized nodules.

These interpretations, coupled with sequential stratigraphic interpretations of chronostratigraphically calibrated, fossiliferous basinal sections (Haq *et al.*, 1987; Hardenbol *et al.*, 1998; modified by Arnaud (2005) for the late Hauterivian – Barremian of the Angles section, Vocontian trough, France; Fig. B.2.4), allow to date the identified sequences. Thus, in the Tierwis section, the Altmann Mb begins with the Ha6 sequence. The dark-colored marly interval of the MFS is thus contemporaneous with the Faraoni level documented so far only from basin sections (Cecca *et al.*, 1994; Baudin *et al.*, 1999). By extrapolation, the second sequence may correspond to the Ha7 sequence, even if ammonite biostratigraphy dating within these beds is lacking to confirm this hypothesis. According to the presence of *Emericiceras gr. Koechlini* and *Torcapella gr. Davydovi* in the phosphatized hardground (bed Sa 33), this latter represents a time interval associated to the Ba1 and Ba1' sequences. The presence of *Subtorcapella sp.* (bed Sa 38) in the third sequence indicates that this TST deposit is dated from the *K. compressissima – C. darsi* biozone interval. In basinal sections from the Vocontian Trough, only one TST is noted during this time interval: the Ba2 TST, dated from the base of the *C. darsi* biozone. The *Torcapella sp.* found in the bed Sa 36-38, which belongs to the *K. compressissima* biozone, may thus be reworked from the underlying hardground. As a result,

this confirms that Ba1 and Ba1' sequences are condensed and/or lacking in the phosphatized hardground of this section.

In sections with a phosphatized hardground or with phosphatic nodules at their base (Figs. B.2.8-9), the temporal resolution is less good

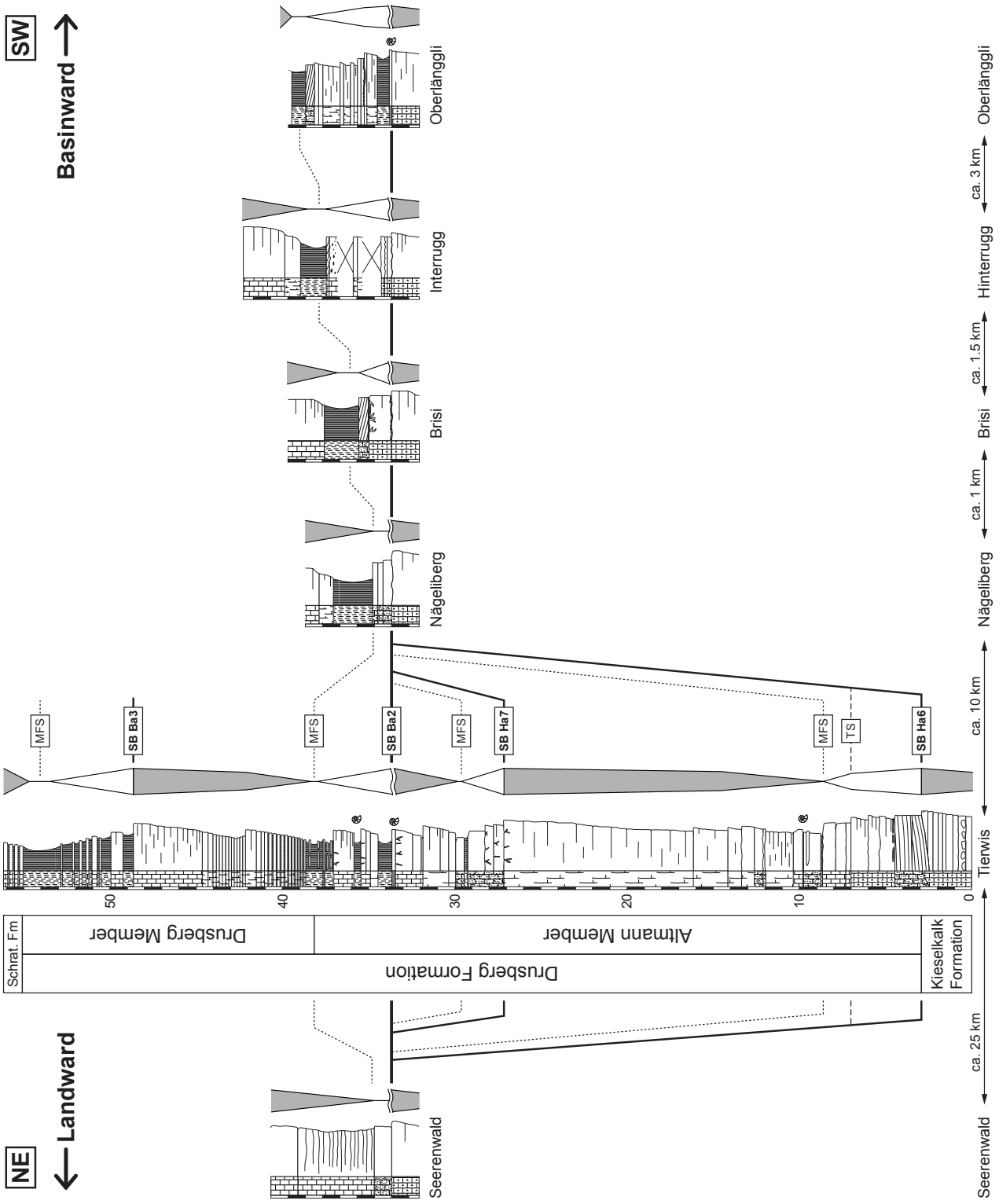

Fig. B.2.12: Palinspastic transect along the Säntis-Churfirsten-Alvier massif with a proposed sequential correlation of sections. Note the decrease in the thickness of the Altmann Mb from basinward to landward positions (except for the Tierwis section; see text for discussion).

due to the absence of numerous fossil findings. However, the presence of *Barremites sp*. in the phosphatized hardground argues in favor of a Barremian age for the overlaying TST deposit. Owing to the general trends in ammonite biostratigraphy in the Altmann Mb, as well as the fact that this TST is overlain by the Drusberg Mb without any evidence of a major hiatus, this TST may thus correspond to the Ba2 TST. Consequently, the sequences Ha6 to Ba1 are lacking in these sections and/or condensed within the basal phosphatized hardground. A notable point is the fact that the Ba2 sequence lacks evidence for a LST deposit in all studied sections, as well as in the basinal section of Angles (e.g., Arnaud, 2005; Bodin *et al*., 2006). This is compatible with the here-proposed hypothesis that the highly-condensed basal phosphatized hardground is representative of a type 3 SB.

In Fig. B.2.12, a palinspastic transect along the Säntis-Churfirsten-Alvier massif is shown. With the exception of the Tierwis section, a small decrease in thickness of the Altmann Mb is observed toward proximal sections. This thickness decrease is related to the progressive landward disappearance of parasequences. In this transect, the important thickness of the Tierwis section, which is due to the preservation of the sequences Ha6 and Ha7, may be related to a locally, rapidly subsiding area, or the infill of an incised (sub-marine?) valley. No direct clues for both hypothesis were, however, found in the field. The observation of a synsedimentary normal fault at the top of the Altmann Mb of the Fluebrig section may argue in favor of the first hypothesis.

B.2.8. Depositional model

The depositional history of the Altmann Mb begins with the sequence Ha6 (Fig. B.2.13). In the Säntis massif, a local depression (probably initiated by normal faults) led to the record of a thin SMST, followed by a very thin TST and a thick HST. The thin transgressive deposits reflect slower rates of sediment production that may be associated to the reduction of carbonate growth potential. Thus, the beginning of the "drowning episode" may correspond to the TS Ha6. During maximum flooding, the Helvetic ramp is drowned and ca. 1-m-thick, dark glauconitic-rich marls and marly limestone are deposited during the *B. mortilleti* biozone. According to cyclostratigraphic interpretations of Late Hauterivian – Barremian successions from the Vocontian trough (Bodin *et al*., 2006), a duration of approximately 300 kyr is likely to be condensed in this interval. During the HST, the important thickness of deposits indicates renewed carbonate production and the end of the first drowning phase in the Säntis massif. The sequence Ha7 is recorded only in the Säntis massif and is characterized by a thin TST followed by a thin HST.

The absence of Upper Hauterivian – lowermost Barremian deposits in other part of the Helvetic ramp, as well as the finding of a well-preserved phosphatized ammonite dated from the Late Hauterivian (*Parathurmannia cf. catulloi*) of the Oberlänggli section, may point to erosion, sediment starvation and/or winnowing and phosphatization along the other parts of the platform associated with this first drowning step. Following previous sea-level reconstructions (e.g., Ruffell, 1991; Hardenbol *et al*., 1998), this first drowning phase is coeval with a second order sea-level rise (Ha6 third order MFS). The observation that at the Säntis locality the carbonate platform has not been drowned during the entire Ha6 and Ha7 sequences, but only during the Ha6 TST and MFS interval, could be related to the peculiar paleogeographical setting of this locality. Indeed, the sediments preserved at this locality were likely to be deposited within a tectonically-induced depression, that could have protected this part of the platform from winnowing currents.

The Helvetic platform preserved no major deposits during the time interval corresponding to sequences Ba1 and Ba1'. In the middle and outer ramp, the platform experienced the development of a phosphatized hardground,

which is indicative of important winnowing and sediment starvation (e.g., Föllmi, 1996; Trappe, 1998). The excellent preservation of phosphatized fossils such as ammonites or sponges may point to the effect of rapid burial and consequent phosphogenesis (Föllmi, 1996). In places where no phosphatized hardground is present, an erosive surface has been observed. This feature might point to bottom current erosion and reworking. In other parts of the European continent, the Early Barremian corresponds to a second order sea-level lowstand (Ruffel, 1991; Arnaud, 2005). This may imply that winnowing and phosphogenesis along the northern Tethyan realm might have take place during a long sea-level lowstand period. Hardground formation during sea-level lowstand can be related to the lowering of the effective wave base exposing the sea floor to wave action (e.g., Immenhauser *et al.*, 2000).

A second drowning phase took place during the Ba2 sequence. According to the overall backstepping pattern of the platform recorded within the Ba2 and Ba3 sequences, the SB Ba2, which is qualified as a type 3 SB, may thus be related to the TS of this Barremian second order sea-level cycle. The presence of phosphatized nodules in the TST might highlight ongoing phosphogenesis during the transgressive phase. Reworking of sediments is recorded by glauconitic-rich gravity-flow deposits in a majority of the studied sections. The deposit of a thick marly interval related to the MFS BA2, which marks the top of the Altmann Mb and which is associated to pelagic facies (HF0), documents the second drowning of the Helvetic platform. During the Ba2 HST, a great part of the Helvetic platform experienced the deposition of outer-ramp hemi-pelagic facies (HF1). This might indicate a strong decrease of the platform-growth area associated to the second drowning episode (backstepping of the platform). Following Tucker and Wright (1990; p. 57), this episode can be defined as an incipient drowning stage.

Whereas sea-level change plays an important role in the Late Hauterivian – Early Barremian drowning of the Helvetic platform, it alone cannot explain the drowning of the carbonate platform. Indeed, the growth rates of carbonate platforms can easily exceed the fastest sea-level rise (e.g., Schlager, 1981; Hallock & Schlager, 1986; Mallarino *et al.*, 2002). One solution to resolve this apparent paradox is to reduce the growth potential of the carbonate platform through environmental stress, such as the reduction of water transparency, temperature or nutrient excess (Hallock & Schlager, 1981). Bodin *et al.* (2006) have observed significantly high phosphorus levels in the western Tethys during the latest Hauterivian – Early Barremian. This observation might be best explained by high nutrient input correlated with the observed carbonate platform-drowning episode. On the other hand, this drowning might also have a non-negligible effect on the carbon-isotope variations of Tethyan basin sections. Indeed, following Godet *et al.* (2006), the high oceanic DIC resulting from this drowning may explain the rather stable trend of the ∂13C curve during the latest Hauterivian – Early Barremian.

The close relationship between the timing of the onset of the Altmann Mb drowning event and the Faraoni oceanic anoxic event point to a connection between these two events. Indeed, in basinal sections, the bottom water anoxia associated to the Faraoni level led to decreased phosphorus preservation in sediments and a positive feedback that led to a rise in nutrient levels in sea water (Bodin *et al.*, 2006). This mechanism may have highly reduced the growth potential of the carbonate platform through environmental stress by nutrient excess, and induced the first step of this drowning event. During the Early Barremian, winnowing, associated to a second order sea-level lowstand and also to high nutrient level in the ocean (Bodin *et al.*, 2006), may have induced the formation of a phosphatized hardground and the complete stop of platform growth. During the latest Early Barremian (*C. darsi* zone), the following second order sea-level transgression, which is also associated to high nutrient levels, led to the end of the hardground formation and to a second drowning step. The overall decrease

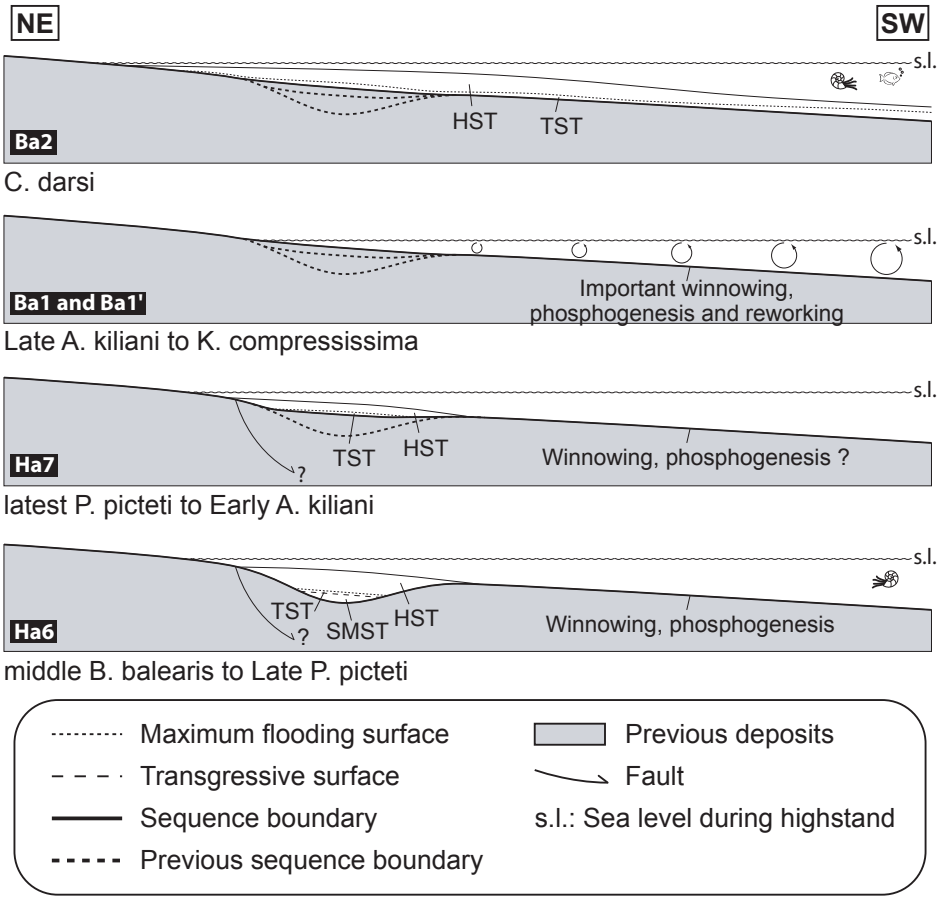

Fig. B.2.13: Depositional model for the Altmann Mb in four successive time steps (see text for details).

in nutrient levels during the Late Barremian marks the end of the slowdown and demise of carbonate platform growth and the progressive return of a photozoan association (i.e. the Schrattenkalk Fm).

B.2.9. Conclusions

(1) Ammonite biostratigraphy shows that the Altmann Mb spans the time interval from the *P. seitzi* (latest Hauterivian) to the *C. darsi* ammonite zone (latest Early Barremian). Coupled with a detailed sequence stratigraphic interpretation of basin sections, these age data indicate that the Altmann Mb begins at the Sb Ha6 and ends within the MFS Ba2.

(2) The majority of the Altmann Mb sections records only the upper part of the Hauterivian – Barremian transition drowning event. Only some sections, mainly located in the Säntis massif, recorded evidence of a more detailed depositional history of the Altmann Mb.

(3) This may be the result of a twofold drowning. A first drowning phase is recorded in the Tierwis section (representative of the Säntis massif) and documents the Ha6 transgression, leading to the deposition of glaucony-rich black marls during the TST-MFS. These deposits are contemporaneous to the Faraoni event black-shales in basin sections (e.g., Cecca *et al.*, 1994; Baudin *et al.*, 1999; Baudin, 2005). In the other platform areas, reworking, winnowing and phosphogenesis recorded this first drowning stage. A second phase is contemporaneous to the Ba2 transgression and is associated to a following pronounced backstepping of the carbonate factory. With the exception of the Tierwis section, the sequences Ha6, Ha7, Ba1 and Ba1' are either condensed in a phosphatized hardground or lacking. This observation is best explained by strong winnowing and bottom current-induced reworking along the northern Tethyan ramp. The Altmann Mb drowning episode ended with the Ba2 highstand and the beginning of the Drusberg Mb deposition.

(4) There is a strong coupling of this drowning event with a palaeoceanographic changes within the western Tethyan realm: the onset of the drowning episode is linked to the Faraoni oceanic anoxic event (latest Hauterivian) by platform eutrophication. During the Early Barremian, the high nutrient levels in the northern Tethys, associated with current-induced winnowing, preclude carbonate platform growth until the beginning of the Late Barremian and the progressive return of photozoans in association with a significant decrease in seawater nutrient levels (Bodin *et al*., 2006).

B.2.10. Acknowledgments

The authors acknowledge Hans-Peter Funk, Urs Oberli, Ueli Briegel, Hubert Arnaud, Guillaume Cailleau, Christophe Dupraz, Laureline Scherler, Laure Pelletier and Charles Robert-Charrue for their help in the field and/ or constructive discussions, and also André Villard for the preparation of thin-sections. We thank the Museums of Natural History of St. Gallen and Dornbirn, and the ETH Zürich, for providing Altmann Mb ammonites from their collections. Critical reviews by Miguel Company and Adrian Immenhauser were much appreciated and helped to considerably improve this manuscript. Financial support from the Swiss National Science Foundation (project 2100-067807/1 and 200020-105206/1) is gratefully acknowledged.

B.2.11. References

Amorosi, A. & Centineo, M.C. 1997: Glaucony from the Eocene of the Isle of Wight (southern UK): implications for basin analysis and sequence-stratigraphic interpretation. Journal of Geological Society of London 154, 887-896.

Arnaud, H. 2005: Sequence stratigraphy interpretation. In: Adatte, T. *et al.* (eds.): The Hauterivian - Lower Aptian sequence stratigraphy from Jura platform to Vocontian basin: a multidisciplinary approach. Géologie Alpine, Série Spéciale "Colloques et Excursions" N°7, 174-179.

Arnaud, H., Arnaud-Vanneau, A., Blanc-Aletru, M.C., Adatte, T., Argot, M., Delanoy, G., Thieuloy, J.-P., Vermeulen, J., Virgone, A., Virlouvet, B. & Wermeille S. 1998: Répartition stratigraphique des orbitolinidés de la plate-forme urgonienne subalpine et jurassienne (SE de la France). Géologie Alpine 74, 3-89.

Arnaud-Vanneau, A. 1980: Micropaléontologie, paléoécologie et sédimentologie d'une plate-forme carbonatée de la marge passive de la Téthys; L'Urgonien du Vercors septentrional et de la Chartreuse (Alpes occidentales). Géologie Alpine, Mémoire Hors-Série, N°11, v. 3.

Baudin, F., Bulot, L.G., Cecca, F., Coccioni, R., Gardin, S. & Renard, M. 1999: Un équivalent du «Niveau Faraoni» dans le bassin du Sud-Est de la France, indice possible d'un événement anoxique fini-hauterivien étendu à la Téthys méditerranéenne. Bulletin de la Société Géologique de France 170, 487-498.

Baudin, F. 2005: A Late Hauterivian short-lived anoxic event in the Mediterranean Tethys: the «Faraoni Event». Comptes Rendus Geoscience 337, 1532-1540.

Blanc-Aletru, M.C. 1995: Importance des discontinuités dans l'enregistrement sédimentaire de l'urgonien jurassien: micropaléontologie, sédimentologie, minéralogie et stratigraphie séquentielle. Géologie Alpine. Mémoire Hors-Série 24, 299 p.

Bodin, S., Godet, A., Föllmi, K. B., Vermeulen, J., Arnaud, H., Strasser, A., Fiet, N. & Adatte, T. 2006: The Late Hauterivian Faraoni oceanic anoxic event in the western Tethys: Evidence from phosphorus burial rates. Palaeogeography, Palaeoclimatology, Palaeoecology 235, 245-264.

Bollinger, D. 1988: Die Entwicklung des distalen osthelvetischen Schelfs im Barremian und Früh-Aptian [unpublished PhD thesis].

ETH Zürich, Zürich, Switzerland, 136 p.

Briegel, U. 1972: Geologie der östlichen Alviergruppe (Helvetische Decken der Ostschweiz) unter besonderer Berücksichtigung der Drusberg- und Schrattenkalkformation (Unterkreide). Eclogae Geologicae Helvetiae 65, 425-483.

Burchette, T.P. & Wright, V.P. 1992: Carbonate ramp depositional systems. Sedimentary Geology 79, 3-57.

Cecca, F., Marini, A., Pallini, G., Baudin, F. & Begouen, V. 1994: A guide-level of the uppermost Hauterivian (Lower Cretaceous) in the pelagic succession of Umbria-Marche Apennines (Central Italy): the Faraoni Level. Riv. Ital. Paleontol. Stratigr. 99, 551-568.

Chamley, H. 1989: Clay Sedimentology: Berlin, Springer-Verlag, 623 p.

Fichter, H.J. 1934: Geologie der Bauen-Brisen-Kette am Vierwaldstaettersee und die zyklische Gliederung der Kreide und des Malm der helvetischen Decken: Bretträge zur Geologischen Karte, 128 p.

Föllmi, K.B. 1989: Evolution of the Mid-Cretaceous Triad. Platform Carbonates, Phosphatic Sediments, and Pelagic Carbonates along the Northern Tethys margin. Lecture Notes in Earth Sciences 23, Springer-Verlag, 153 p.

Föllmi, K.B. 1996: The phosphorus cycle, phosphogenesis and marine phosphate-rich deposits. Earth-Science Reviews 40, 55-124.

Föllmi, K.B., Weissert, H., Bisping, M. & Funk, H. 1994: Phosphogenesis, carbon-isotope stratigraphy, and carbonate-platform evolution along the Lower Cretaceous northern Tethyan margin. Geological Society of America Bulletin 106, 729-746.

Funk, H. 1969: Typusprofile der helvetischen Kieselkalk Formation und der Altmann Schichten. Eclogae geologicae Helvetiae 62, 191-203.

Funk, H. 1971: Zur stratigraphie und lithologie des Helvetischen Kieselkalkes und der Altmannschichten im der Säntis-Churfirsten-Gruppe (Nordostschweiz). Eclogae geologicae Helvetiae 64, 345-433.

Funk, H., Föllmi, K.B. & Mohr, H. 1993: Evolution of the Tithonian-Aptian carbonate platform along the northern Tethyan margin, eastern Helvetic Alps: In: Simo J.A.T., Scott R.W. & Masse J.-P. (Eds.): Cretaceous carbonates platforms. AAPG Memoir, American Association of Petroleum Geologists. Tulsa, OK, United States, 387-407.

Godet, A., Bodin, S., Föllmi, K.B., Vermeulen, J., Gardin, S., Fiet, N., Adatte, T., Berner, Z., Stüben, D. & Van de Schootbrugge, B. 2006: Evolution of the marine stable carbon-isotope record during the early Cretaceous: A focus on the late Hauterivian and Barremian in the Tethyan realm. Earth and Planetary Science Letters 242, 254-271.

Goldschmid, K. 1927: Geologie der Morgenberghorn-Schwalmerengruppe bei Interlaken. Mitt. Nat. Ges. Bern, 195-268.

Hallock, P. & Schlager, W. 1986: Nutrient excess and the demise of coral reefs and carbonate platforms. Palaios 1, 389-398.

Hantke, R. 1961: Tektonik der helvetschen Kalkalpen zwischen Obwalden und dem St. Galler Rheintal: Mitteilungen aus dem Geologischen Institut der Eidg. Techn. Hochschule und der Universität Zürich, Serie B, v. 16, 212 p.

Haq, B.U., Hardenbol, J. & Vail, P.R. 1987: Chronology of fluctuating sea levels since the Triassic. Science 235, 1156-1167.

Hardenbol, J., Thierry, J., Farley, M.B., de Graciansky, P.-C. & Vail, P.R. 1998: Mesozoic and Cenozoic Sequence Chronostratigraphic Framework of European Basins. In: de Graciansky, P.-C., Hardenbol, J., Jacquin, T. & Vail, P.R. (eds.): Mesozoic and Cenozoic Sequence Stratigraphy of European Basins. Special Publication - Society for Sedimentary Geology 60, 3-13.

Heim, A. 1910-1916: Monographie der Churfirsten-Mattstock-Gruppe: Beiträge zur Geologischen Karte der Schweiz 50: Bern, 662 p.

Hoedemaeker, P.J., Reboulet, S., Aguirre-Urreta, M.B., Alsen, P., Aoutem, M., Atrops, F., Barragan, R., Company, M., Gonzalez, C., Klein, J., Lukeneder, A., Ploch, I., Raisossadat, N., Rawson, P.F., Ropolo, P., Vasicek, Z., Vermeulen, J. & Wippich, M.G.E. 2003: Report on the 1st International Workshop of the IUGS Lower Cretaceous Ammonite Working Group, the 'Kilian Group' (Lyon, 11 July 2002). Cretaceous Research 24, 89-94.

Immenhauser, A., Schlager, W., Burns, S.J., Scott, R.W., Geel, T., Lehmann, J., van der Gaast, S. & Bolder-Schrijver, L.J.A. 2000: Origin and correlation of disconformity surfaces and marker beds, Nahr Umr Formation, northern Oman. In: Alsharhan, A.S. & Scott, R.W. (Eds.): Middle East models of Jurassic/Cretaceous carbonate systems. Special Publication - Society for Sedimentary Geology 69, 209-225.

James, N.P. 1997: The cool-water carbonate depositional realm. In: James N.P. & Clarke J.A.D. (Eds): Cool water carbonates. Society for Sedimentary Geology 56, 1-22.

Kuhn, O. 1996: Der Einfluss von Verwitterung auf die Paläozeanographie zu Beginn des Kreide-Treibhausklimas (Valanginian und Hauterivian) in der West-Tethys [unpublished PhD thesis]. Universität Zürich, Zürich, 380 p.

Lehmann, C., Osleger, D.A., Montanez, I.P., Sliter, W.V., Arnaud-Vanneau, A. & Banner, J. 1999: Evolution of Cupido and Coahuila carbonate platforms, Early Cretaceous, northeastern Mexico. Geological Society of America Bulletin 111, 1010-1029.

MacEachern, J.A., Zaitlin, B.A. & Pemberton, S.G. 1999: A sharp-based sandstone of the Viking Formation, Joffre Field, Alberta, Canada: criteria for regnition of transgressively incised shoreface complexes. Journal of Sedimentary Research 69, 876-892.

Mallarino, G., Goldstein, R.H. & Di Stefano, P. 2002: New approach for quantifying water depth applied to the enigma of drowning of carbonate platforms. Geology 30, 783-786.

Malpas, J.A., Gawthorpe, R.L., Pollard, J.E. & Sharp, I.R. 2005: Ichnofabric analysis of the shallow marine Nukhul Formation (Miocene), Suez Rift, Egypt: implications for depositional processes and sequence stratigraphic evolution. Palaeogeography Palaeoclimatology Palaeoecology 215, 239-264.

Pasquini, C., Lualdi, A. & Vercesi, P. 2004: Depositional dynamics of glaucony-rich deposits in the Lower Cretaceous of the Nice arc, southeast France. Cretaceous Research 25, 179-189.

Pemberton, S.G. 1998: Stratigraphic applications of the Glossifungites ichnofacies: Delineating discontinuities in the rock record. American Association of Petroleum Geologists Bulletin 82, 2155.

Pérès, J.M. 1961: La vie benthique. In: Océanographie biologique et biologie marine, T1. 541 p., Presses Universitaires de France, Vendôme.

Rick, B. 1985: Geologie des Fluhbrig (Kt. Sz): unter besonderer beruecksichzigung der Altmannschichten und der «Gault»-formation [unpublished master thesis], Zürich, 83 p.

Ruffell, A. 1991: Sea-level events during the Early Cretaceous in western Europe. Cretaceous Research 12, 527-551.

Schenk, K. 1992: Die Drusberg- und Schrattenkalk-Formation (Unterkreide) im Helvetikum des Berner Oberlandes. Inauguraldissertation der Philosophisch-naturwissenschaftlichen Fakultät: Universität Bern, Bern, 169 p.

Schlager, W. 1981: The paradox of drowned reefs and carbonates platforms. Geological Society of America Bulletin 92, 197-211.

Schlager, W. 1999: Type 3 sequence boundaries. In: Harris, P.M., Saller, A.H. & Simo,

J.A.T. (Eds.): Advances in carbonate sequence stratigraphy: Application to reservoirs, outcrops and models. SEPM Spec. Pub. 63, 35-45.

Trappe, J. 1998: Phanerozoic Phosphorite Depositional Systems: a dynamic model for a sedimentary resource system: Lecture Notes in Earth Sciences 76, Springer, 316 p.

Tucker, M.E. & Wright, J.D. 1990: Carbonate sedimentology. 482 p., Blackwell Science, Oxford.

Van de Schootbrugge, B. 2001: Influence of paleo-environmental changes during the Hauterivian (Early Cretaceous) on carbonate deposition along the northern margin of the Tethys: Evidence from geochimical records (C, O, and Sr-isotopes, P, Fe, Mn) [unpublished PhD thesis]: Université de Neuchâtel, Institut de Géologie, Neuchâtel (Switzerland), 268 p.

Vermeulen, J. 2002. Etude stratigraphique et paléontologique de la famille des Pulchelliidae (ammonoidea, Ammonitina, Endemoceratacеae). Géologie Alpine, Memoire H.S. n°42, 333 pp, Grenoble, France.

Vermeulen, J. 2005: Boundaries, ammonite fauna and main subdivisions of the stratotype of the Barremian. In: Adatte, T. *et al*. (eds.): The Hauterivian - Lower Aptian sequence stratigraphy from Jura platform to Vocontian basin: a multidisciplinary approach. Géologie Alpine, Série Spéciale «Colloques et Excursions» N°7, 147-173.

Weissert, H., Lini, A., Föllmi, K.B. & Kuhn, O. 1998: Correlation of Early Cretaceous carbon isotope stratigraphy and platform drowning events: a possible link? Palaeogeography, Palaeoclimatology, Palaeoecology 137, 189-203.

Wissler, L., Funk, H. & Weissert, H. 2003: Response of Early Cretaceous carbonate platforms to changes in atmospheric carbon dioxide levels. Palaeogeography, Palaeoclimatology, Palaeoecology 200, 187-205.

Wyssling, G.W. 1986: Der frühkretazische helvetische Schelf in Vorarlberg und im Allgäu - Stratigraphie, Sedimentologie und Paläogeographie. Jb. Geol. Bund. 129, 161-265.

B.3.

New data on the age of the installation of Urgonian-type carbonates along the northern Tethyan margin: Biostratigraphy of the Chopf Member (Helvetic Alps, eastern Switzerland)

Données nouvelles sur la datation de l'installation des calcaires Urgonien le long de la marge nord-téthysienne: Biostratigraphie du Membre du Chopf (nappes Helvétiques, Suisse orientale)

Stéphane Bodin [1], Jean Vermeulen [2], Alexis Godet [1] & Karl B. Föllmi [1]

[1] Institut de Géologie et d'Hydrogéologie, Université de Neuchâtel, Rue Emile Argand 11, Case postale 158, 2009 Neuchâtel, Switzerland

[2] Grand Rue, 04330 Barrême, France

Keywords: Helvetic platform; Switzerland; Drusberg Formation; Urgonian limestone; Late Barremian; carbon isotope curve

Mots-clés: Plateforme helvétique ; Suisse ; Formation du Drusberg ; Calcaire Urgonien ; Barrémien supérieur ; courbe isotopique du carbone

Published in: Comptes Rendus Geoscience **338** (2006), 727-733

Abstract

The Chopf Member is a glauconitic, phosphate-bearing succession that occurs in the distal part of the Helvetic Alps (eastern Switzerland). The recent discovery of age-diagnostic ammonites within this horizon allows for its attribution to the lower part of the Gerhardtia sartousiana zone (middle late Barremian). This new age corresponds to a maximal age for the onset of the Schrattenkalk Fm in this area, and is coeval with the onset of the Urgonian facies in other parts of the western Tethyan realm. This new age allows also for a more precise dating of late Barremian $\partial^{13}C$ curves.

Résumé

Le Membre du Chopf correspond à un horizon glauconieux déposé dans la partie distale de la plate-forme helvétique. La découverte récente d'ammonites permet de dater précisément cet horizon de la partie inférieure de la zone à Gerhardtia sartousiana (Barrémien supérieur moyen). Cette nouvelle datation permet de donner un âge maximal à la Formation du Schrattenkalk dans cette région. Cet âge est cohérent avec ceux qui sont obtenus dans les autres parties de la Téthys occidentale pour l'installation des faciès urgoniens. Cette nouvelle datation permet aussi d'apporter des précisions sur la calibration des courbes du $\partial^{13}C$ du Barrémien supérieur.

B.3.1. Version française abrégée

B.3.1.1. Introduction

Les nappes Helvétiques affleurent dans la partie nord des Alpes suisses (Fig. B.3.1) et documentent les restes de la marge nord Téthysienne. Dans ces unités tectoniques, des carbonates de plate-forme alternent avec des sédiments phosphatés et glauconieux (e.g. [9-10]). Dans cette note, de nouvelles ammonites appartenant à un de ces intervalles glauconieux (le Membre du Chopf) sont figurées; elles sont attribuées au Barrémien supérieur moyen. Cette importante découverte permet non seulement de dater l'installation des faciès urgoniens (Formation du Schrattenkalk) dans cette partie de la Téthys, mais aussi de discuter la calibration des courbes téthysiennes de référence du $\partial^{13}C$.

B.3.1.2. Cadre géographique et géologique

Le Barrémien du domaine Helvétique est composé de deux formations : la Formation (Fm) du Drusberg et la Fm du Schrattenkalk (Fig. B.3.2). En domaine proximal, la Fm du Drusberg peut être divisée en deux membres (Mb) : le Mb d'Altmann et le Mb du Drusberg (e.g., [7-8]). En domaine distal (région de l'Alvier), Briegel [5] adjoint deux autres membres à la Fm du Drusberg : le Mb du Chopf et le Mb d'Hurst. D'après cet auteur, l'âge de ces deux derniers membres serait Barrémien moyen, sans plus de précision.

B.3.1.3. Sedimentologie et biostratigraphie

Le Mb du Chopf a été étudié au lieu dit du « Barbielergrat » (voir Briegel [5] pour une localisation précise), où son épaisseur atteint environ 2 m ; il affleure sous forme de quatre bancs calcaires intercalés entre les marnes du Mb du Drusberg et du Mb d'Hurst (Fig. B.3.3). La glauconie est présente dans les deux premiers bancs et abondante dans le troisième. Des traces de phosphatogenèse peuvent être également discernées dans les trois derniers bancs. À la base du troisième banc, la présence de nombreux nodules phosphatés et de nombreuses bélemnites est à noter.

Parmi ces nodules, quatre ammonites phosphatées ont été trouvées (Fig. B.3.3). Deux d'entre elles se sont avérées être des Hemihoplitidae sp., tandis que les deux autres sont identifiées comme étant une Ezeiceras aff. janus et une Hemihoplites sp. aff. limentinus (Fig. B.3.4). Cet assemblage d'ammonites est typique de la partie terminale de la zone à Heinzia sayni et de la première moitié de

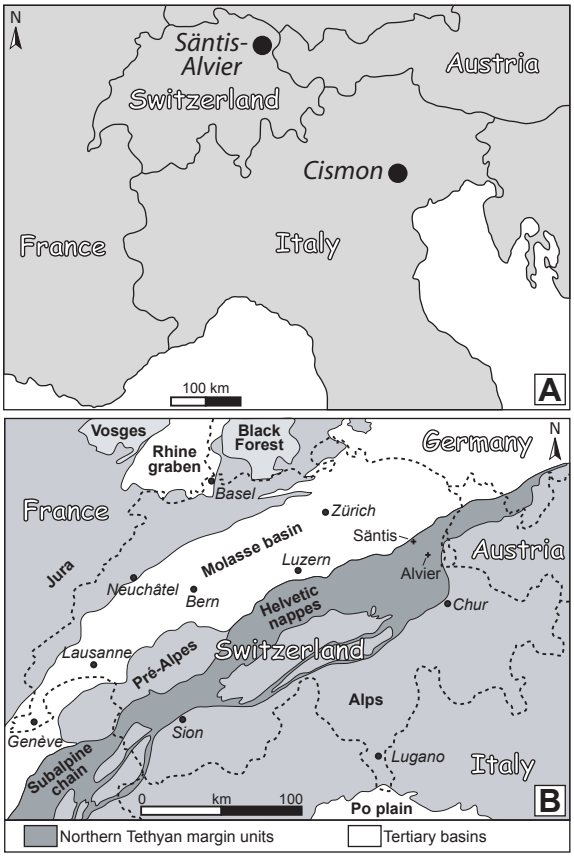

Fig. B.3.1. Location of the different mentioned sections. (A) Location of the Cismon APTICORE drilling and the Säntis and Alvier regions (modified after [14]). For a precise location of Cismon, see [6]. (B) Tectonic map of Switzerland with the location of the Helvetic realm (dark grey colored) and the Säntis and Alvier regions. For precise location, see [5, 7].

Fig. B.3.1. Localisation des différentes coupes mentionnées. (A) Localisation du forage de Cismon APTICORE et des régions du Säntis et de l'Alvier (modifié d'après [14]). Pour une localisation précise de Cismon, se reporter à [6]. (B) Carte tectonique de la Suisse avec l'emplacement du domaine Helvétique (gris foncé), ainsi que des régions du Säntis et de l'Alvier. Pour une localisation précise, se reporter à [5, 7].

la zone à Gerhardtia sartousiana (Barrémien supérieur moyen; [12-13]).

B.3.1.4. Discussion

Cette nouvelle datation du Mb du Chopf permet de discuter quelques aspects importants de la sédimentologie du Barrémien tardif dans les nappes Helvétiques, ainsi que d'affiner la corrélation basée sur l'évolution du $\partial^{13}C$ entre cette région et les sections barrémiennes de références (e,g, Cismon Apticore ; [6]), précédemment proposée par Wissler et al. [14].

La présence relativement élevée de glauconie et la trace de phosphatogenèse dans le Mb du Chopf témoignent en faveur d'une sédimentation condensée, caractéristique des surfaces d'inondations maximales (SIM) de troisième ordre. Dans le domaine Téthysien, une SIM majeure est localisée dans la zone à G. sartousiana (e.g. [1-2]), la SIM Ba3. Par conséquent, cet horizon condensé semble être synchrone avec la SIM Ba3.

De plus, Bodin et al. [3] ont observé que la SIM Ba3 correspond à la transition entre la Fm du Drusberg et celle du Schrattenkalk en domaine plus proximal (coupe de Tierwis, région du Säntis). Ainsi, le membre du Chopf doit correspondre en temps à la limite Drusberg – Schrattenkalk en domaine proximal. Par conséquent, en situation distale, l'installation du Mb du Schrattenkalk, qui est séparé du Mb du Drusberg par le Mb d'Hurst, doit être plus jeune qu'en situation proximale. Cette observation souligne la progradation de la plate-forme urgonienne durant le Barrémien supérieur dans le domaine Helvétique (Fig. B.3.5 ; e.g., [4]). Il est également important de noter que cet âge est cohérent avec l'installation des faciès urgoniens dans les autres parties de la Téthys occidentale, et particulièrement dans le Vercors (e.g. [2]).

Par ailleurs, Wissler et al. [14] ont publié une courbe haute résolution du $\partial^{13}C$ pour cette région, montrant deux excursions positives durant le Barrémien supérieur, le Mb du Chopf étant situé exactement au milieu de ces deux excursions (Fig. B.3.6). En considérant cette

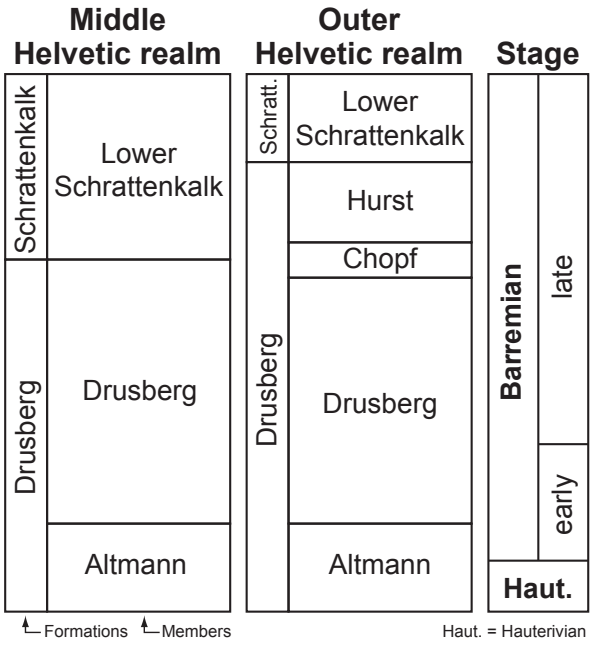

Fig. B.3.2. Barremian Formations and Members from the middle and outer Helvetic shelf.
Fig. B.3.2. Formations et Membres du Barrémien du domaine Helvétique proximal et distal.

nouvelle datation, il apparaît que la première excursion est plus âgée que la zone à G. sartousiana. D'après la datation du sommet du Mb de l'Altmann par Bodin et al. [3] et la conséquente datation de la base du Mb du Drusberg (zone à C. darsi), cette première excursion est datée de la partie inférieure du Barrémien supérieur (zone à H. uhligi – H. sayni).

B.3.1.5. Conclusions

Le Mb du Chopf est daté de la zone à Gerhardtia sartousiana (Barrémien supérieur moyen) et correspond à la surface d'inondation maximale Ba3. Il en résulte que la Fm du Schrattenkalk, équivalente de la Fm Urgonienne dans les autres parties du domaine Téthysien, est plus jeune que la zone à G. sartousiana dans la partie distale de la plate-forme Helvétique. Cependant, dans les parties internes, l'installation de ces faciès est datée, par corrélation en stratigraphie séquentielle, de cette même zone à G. sartousiana. Cette dichotomie souligne donc la progradation de la marge distale de la plate-forme Helvétique durant le Barrémien supérieur.

B.3.2. Introduction

The Helvetic fold- and thrust belt is situated in the northern part of the central European Alps (Fig. B.3.1) and includes a sedimentary succession which documents the evolution of the northern Tethyan margin during the Mesozoic and early Tertiary. The lower Cretaceous comprised in this tectonic zone is composed of an alternation of photozoan and heterozoan platform carbonates and highly condensed phosphatized and glauconitic sediments (e.g., [9-10]). These latter sediments are associated with repetitive drowning episodes, which interfered with the growth of the northern Tethyan carbonate platform. In this paper, we report the discovery of ammonites from one of these glauconitic beds (the Chopf Member), which date from the middle late Barremian. This new age date allows us to attribute a maximal age to the installation of the Schrattenkalk Formation (Fm), which is the equivalent of the Urgonian-type carbonates known from other parts of the Tethyan realm (e.g., [2, 12]). Finally, this new age date helps also to refine the dating of $\partial^{13}C$ references curves from the Tethyan realm.

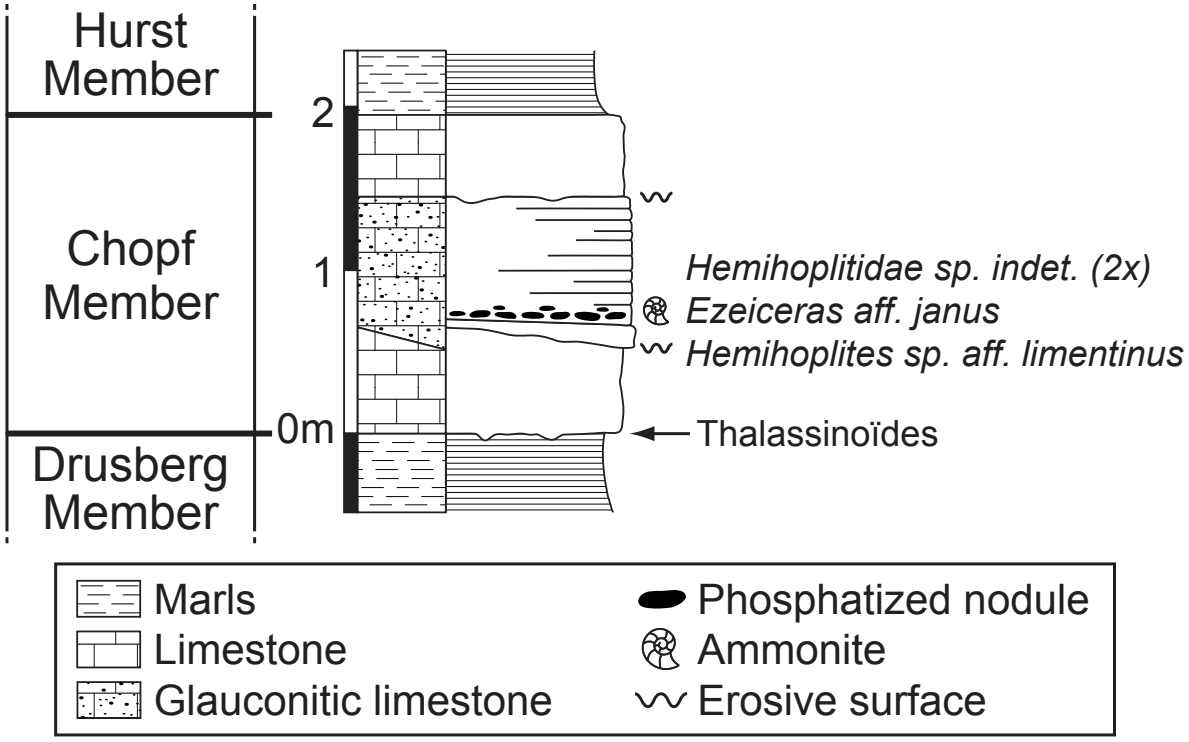

Fig. B.3.3. Sedimentary log of the Chopf Mb at the Barbielergrat locality.
Fig. B.3.3. Colonne sédimentaire du Mb du Chopf au lieu dit du Barbielergrat.

B.3.3. Geographical and geological setting

In the Helvetic realm, the Barremian stage is characterized by the deposition of two distinct formations: the Drusberg Fm and the Schrattenkalk Fm (Fig. B.3.2). In proximal settings, the Drusberg Fm is divided into two members (Mb): the Altmann Mb and the Drusberg Mb (e.g., [7-8]). In the distal part of the Helvetic platform, and particularly in the Alvier region, Briegel [5] divided the Drusberg Mb into four members by adding two further members to the top of the Drusberg Mb: the Chopf Mb and the Hurst Mb (Fig. B.3.2). The Chopf Mb represents a thin and glauconite-rich interval, for which no equivalent exists in the more internal part of the helvetic shelf, whereas the Hurst Mb consists of a marly succession which Briegel [5] considered as a distal equivalent of the lower part of the Schrattenkalk Fm. According to this author, these two latter members are dated as «middle» Barremian, without any further precision.

B.3.4. Sedimentology and biostratigraphy

The Chopf Mb was logged and sampled at Barbielergrat, 1 km NE of Alvier, eastern Switzerland (swiss coordinates: 750.650/ 220.075; [5, 14]). At this locality, this member is composed of four principal beds and reaches a total thickness of approximately 2m; it is under- and overlain by marly beds corresponding to the Drusberg Mb and the Hurst Mb, respectively (Fig. B.3.3). The base of the Chopf Mb is well-defined and marked by the presence of up to 10 cm thick Thalassinoides burrows. The basal bed is composed of a spicule-rich limestone, whereas the three following beds are characterized by carbonate rich in intraclasts, echinodermal debris, and isolated phosphatized particles. Glaucony is present in the first two beds, and abundant in the third bed. At the base of the third bed, both phosphatized pebbles and fossils, as well as numerous belemnites, are abundant.

Among theses nodules, four well-preserved phosphatized ammonites have been found (Fig. B.3.3). Two of them are identified as Hemihoplitidae sp., whereas the two others are identified as Ezeiceras aff. janus and Hemihoplites sp. aff. limentinus (Fig. B.3.4). This assemblage allows the attribution of the Chopf Mb to the middle late Barremian; more precisely, from the latest Heinzia Sayni and the first half of the Gerhardtia sartousiana zones (e.g., [12-13]).

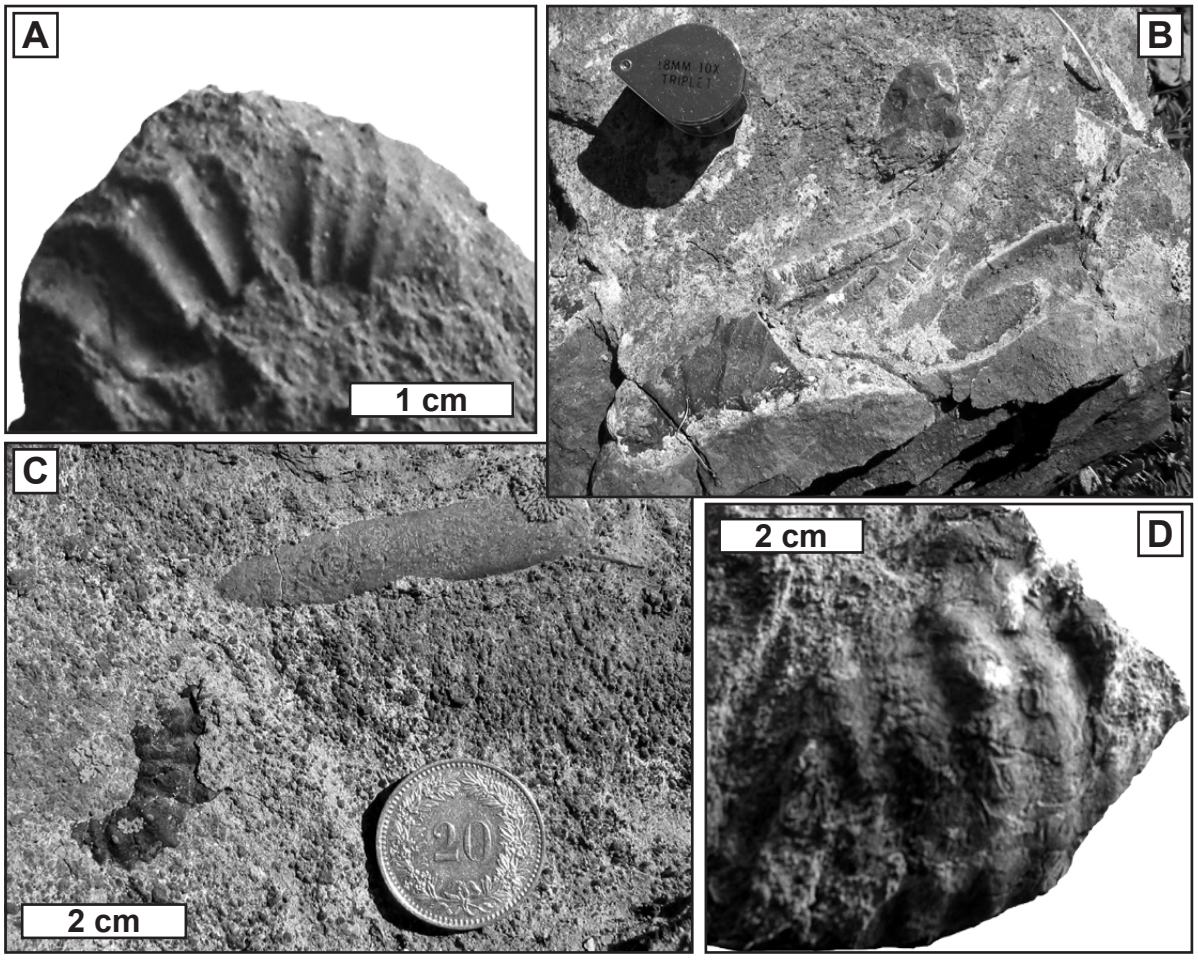

Fig. B.3.4. Photographs of the ammonites of the Chopf Mb. (A) and (B) Hemihoplitidae sp. (C) Ezeiceras aff. janus. (D) Hemihoplites sp. aff. limentinus.
Fig. B.3.4. Photographies des ammonites dans le Mb du Chopf. (A) et (B) Hemihoplitidae sp. (C) Ezeiceras aff. janus. (D) Hemihoplites sp. aff. limentinus.

B.3.5. Discussion

The newly obtained age of the Chopf Mb allows us to discuss the chronostratigraphic evolution of late Barremian sediments distribution in the Helvetic realm, and also to refine correlations between $\partial^{13}C$ reference curves for this particular section, published by Wissler et al. [14], and other settings in the Tethyan realm.

The presence of glaucony and phosphate within the Chopf Mb relates its origin to a period of condensation during high sea-level, even if subsequent sediment reworking and transport by gravity flow can not be excluded. This horizon may therefore correspond to a maximum flooding surface (mfs) deposit. In the western Tethyan realm, the presence of a major mfs has been identified in sediments corresponding in age to the middle of the G. sartousiana zone (the Ba3 mfs; [1-2]). Hence, we propose that this horizon corresponds in time to the Ba3 mfs.

Bodin et al. [3] have observed that the transition between the Drusberg Fm and the Schrattenkalk Fm in more proximal areas of the Helvetic shelf (Tierwis section, Säntis region) corresponds equally to the Ba3 mfs. Indeed, they dated the boundary between the Altmann Mb and Drusberg Mb as middle C. darsi zone and associated it to a mfs (mfs Ba2). The sediments of the Drusberg Mb are characterized by a regressive trend followed by a transgressive trend, which are attributed to the Ba2 highstand and the Ba3 transgressive systems tract, respectively. On top of the Drusberg Fm, the basal part of the Lower Schrattenkalk Mb is characterized by a regressive trend that can be associated with the Ba3 highstand systems tract. The Drusberg – Schrattenkalk boundary may thus correspond to the Ba3 mfs.

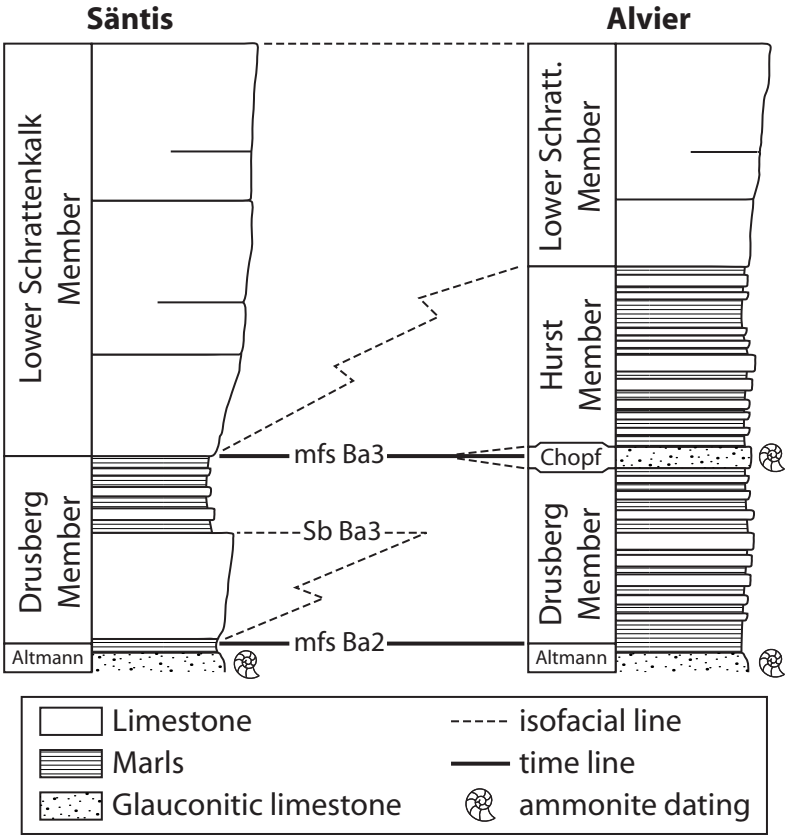

Fig. B.3.5. Synthetic sedimentary columns from the Säntis and the Alvier regions showing the diachronous onset of the Lower Schrattenkalk Mb and the subsequent progradation of the Helvetic margin during the late Barremian.
Fig. B.3.5. Colonnes sédimentaires synthétiques des régions du Säntis et de l'Alvier. On peut y voir l'installation diachronique du Mb inférieur du Schrattenkalk et la conséquente progradation de la marge Helvétique durant le Barrémien supérieur.

The Chopf Mb may therefore represent a distal time-equivalent of the sediments associated with the transition between the Drusberg Fm and Schrattenkalk Fm of more proximal areas. Hence, in distal areas of the Helvetic shelf, the onset of the Lower Schrattenkalk Mb - separated from the Chopf Mb by the Hurst Mb - is therefore younger than in more proximal areas, which is related to the time-transgressive progradation of the "Urgonian" platform during the latest Barremian in the Helvetic realm (Fig. B.3.5; e.g., [4]).

The maximal age obtained here for the onset of the Schrattenkalk Fm is in good agreement with the onset of the Urgonian facies in other parts of the western Tethyan realm, and especially in the Vercors area (e.g., [2]). This underlines the close relationships of the sedimentary history between the areas of the northern Tethyan margin, which now are part of France and Switzerland.

Wissler et al. [14] published a high-resolution $\partial^{13}C$ curve for the Alvier region, showing two positive shifts for the late Barremian. The Chopf Mb is situated exactly in the middle of these two positive shifts (Fig. B.3.6). With the new precise age date for the Chopf Mb, it appears that the first positive shift is older than the G. sartousiana zone. According to the new age dates for the lower and upper boundaries of the Altmann Mb by Bodin et al. [3] and the corresponding maximal age for the base of the Drusberg Mb (C. darsi zone), this first shift may be dated as early late Barremian (H. uhligi – H. sayni zone).

In the Italian Cismon APTICORE drilling, the late Barremian is also characterized by two positive shifts [6]. In the case these two shifts

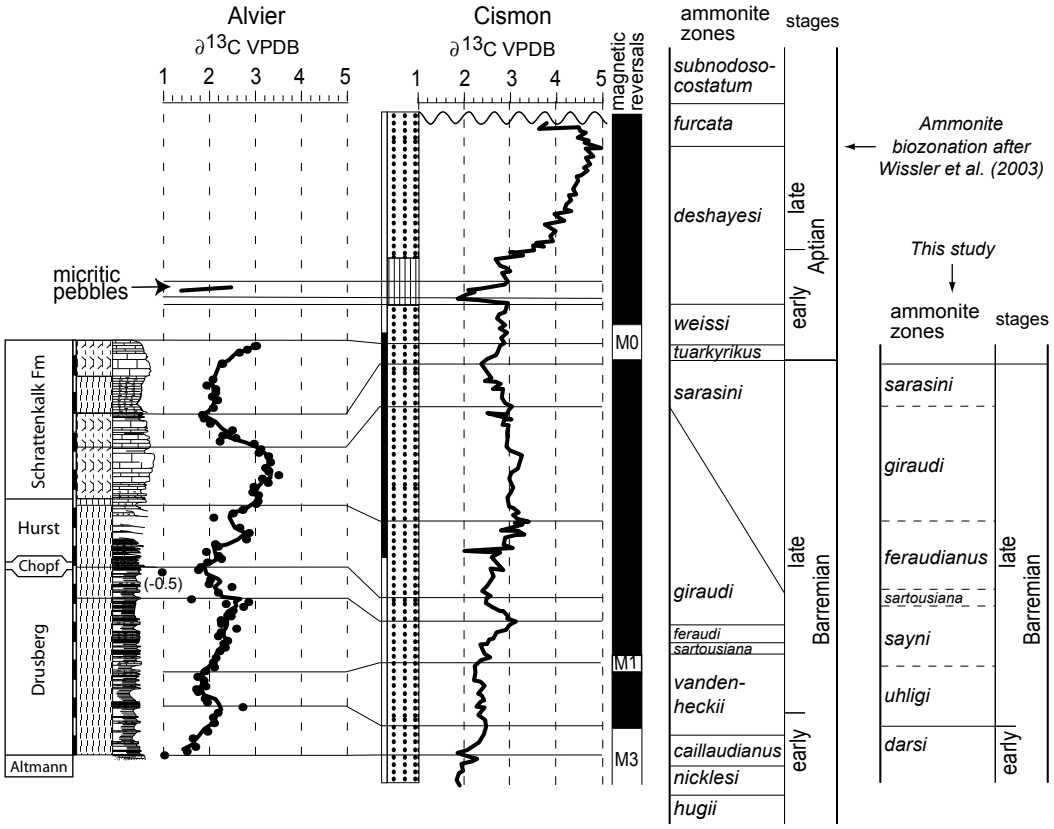

Fig. B.3.6. Carbon isotope correlation between the Alvier region and the Cismon APTICORE drilling (figure modified from [14], after the results of [6, 14]), and proposition of a new biostratigraphic framework after the results from [11] and this study.

Fig. B.3.6. Corrélation des courbes isotopiques du carbone entre la région d'Alvier et le forage de Cismon APTICORE (figure modifiée d'après [14], d'après les résultats de [6, 14]), ainsi que la proposition d'un nouvelle zonation biostratigraphique résultant des travaux de cette note et de [11].

are correlated with the two excursions observed by Wissler et al. [14] in the Alvier region (Fig. B.3.6), the older shift in Cismon - where precise ammonite stratigraphy is lacking - would also correspond to the early late Barremian.

B.3.6. Conclusions

The glaucony-rich and phosphate-bearing Chopf Mb (Helvetic zone, eastern Switzerland) is dated from the Gerhardtia sartousiana ammonite zone (middle late Barremian) and its formation may be linked to the maximum flooding surface Ba3. This new age date indicates that the overlying Schrattenkalk Fm - equivalent of Urgonian carbonates in other parts of the Tethyan realm - is younger than the G. sartousiana zone in distal parts of the Helvetic shelf. In inner parts of the shelf, using sequence-stratigraphic arguments, the onset of the Schrattenkalk Fm dates as G. sartousiana zone. This dichotomy underlines the progradation of the distal Helvetic platform margin during the late Barremian.

B.3.7. Acknowledgments

The authors acknowledge Urs Oberli and Ueli Briegel for their help in the field and André Villard (Uni Neuchâtel) for the preparation of thin-sections. We thank two anonymous reviewers for their constructive criticism of the manuscript. Financial support from the Swiss National Science Foundation Project 2100-067807/1 and 200020-105206/1 is gratefully acknowledged.

B.3.8. References

[1] H. Arnaud, Sequence stratigraphy interpretation, in: T. Adatte, A. Arnaud-Vanneau, H. Arnaud et al. (Eds.), The Hauterivian - Lower Aptian sequence stratigraphy from Jura platform to Vocontian basin: a multidisciplinary approach: Géologie Alpine, Série Spéciale «Colloques et Excursions» n°7, 2005, pp. 174-179.

[2] H. Arnaud, A. Arnaud-Vanneau, M. C. Blanc-Aletru, T. Adatte, M. Argot, G. Delanoy, J.-P. Thieuloy, J. Vermeulen, A. Virgone, B. Virlouvet, S. Wermeille, Répartition stratigraphique des orbitolinidés de la plate-forme urgonienne subalpine et jurassienne (SE de la France). Géologie Alpine 74 (1998) 3-89.

[3] S. Bodin, A. Godet, J. Vermeulen, P. Linder, K. B. Föllmi, Biostratigraphy, sedimentology and sequence stratigraphy of the latest Hauterivian - early Barremian drowning episode of the Northern Tethyan margin (Altmann Member, Helvetic nappes, Switzerland), Eclogae Geologicae Helvetiae 99 (2006) 157-174.

[4] D. Bollinger, Die Entwicklung des distalen osthelvetischen schelfs im Barremian und Früh-Aptian. Drusberg-, Mittagspitz- und Schrattenkalk-Fm im Vorarlberg und Allgäu. Mitteilungen aus dem Geologischen Institut der Eidg. Technischen Hochschule und der Universität Zürich, Neue Folge Nr. 259a, 1988, 159 pp.

[5] U. Briegel, Geologie der östlichen Alviergruppe (Helvetische Decken der Ostschweiz) unter besonderer Berücksichtigung der Drusberg- und Schrattenkalkformation (Unterkreide), Eclogae Geologicae Helvetiae 65(2) (1972) 425-483.

[6] E. Erba, J. E. T. Channell, M. Claps, C. E. Jones, R. L. Larson, B. Opdyke, I. Premoli-Silva, A. Riva, G. Salvini, S. Torriceli, Integrated stratigraphy of the Cismon APTICORE (Southern Alps, Italy): A «reference section» for the Barremian-Aptian interval at low latitudes, Journal of Foraminiferal Research 29(4) (1999) 371-391.

[7] H. Funk, Typusprofile der helvetischen Kieselkalk Formation und der Altmann Schichten, Eclogae geologicae Helvetiae 62(1) (1969) 191-203.

[8] H. Funk, Zur Stratigraphie und Lithologie

des Helvetischen Kieselkalkes und der Altmannschichten im der Säntis-Churfirsten-Gruppe (Nordostschweiz), Eclogae geologicae Helvetiae 64(2) (1971) 345-433.

[9] H. Funk, K. B. Föllmi, H. Mohr, Evolution of the Tithonian-Aptian carbonate platform along the northern Tethyan margin, eastern Helvetic Alps, in: Simo J.A.T., Scott R.W., Masse J.-P. (Ed.), Cretaceous carbonates platforms, American Association of Petroleum Geologists. Tulsa, OK, United States, 1993, pp. 387-407.

[10] K. B. Föllmi, H. Weissert, M. Bisping, H. Funk, Phosphogenesis, carbon-isotope stratigraphy, and carbonate-platform evolution along the Lower Cretaceous northern Tethyan margin, Geological Society of America Bulletin 106 (1994) 729-746.

[11] A. Godet, S. Bodin, K. B. Föllmi, J. Vermeulen, S. Gardin, N. Fiet, T. Adatte, Z. Berner, D. Stüben, B. Van de Schootbrugge, Evolution of the marine stable carbon-isotope record during the early Cretaceous: A focus on the late Hauterivian and Barremian in the Tethyan realm, Earth and Planetary Science Letters 242 (2006) 254-271.

[12] J. Vermeulen, Etude stratigraphique et paléontologique de la famille des Pulchelliidae (ammonoidea, Ammonitina, Endemoceratacea), Grenoble, Géologie Alpine, Mémoire H.S. n° 42, France, 2002, 333 pp.

[13] J. Vermeulen, Boundaries, ammonite fauna and main subdivisions of the stratotype of the Barremian, in: T. Adatte, A. Arnaud-Vanneau, H. Arnaud et al (Eds.), The Hauterivian - Lower Aptian sequence stratigraphy from Jura platform to Vocontian basin: a multidisciplinary approach: Géologie Alpine, Série Spéciale «Colloques et Excursions» n°7, 2005, pp. 147-173.

[14] L. Wissler, H. Funk, H. Weissert, Response of Early Cretaceous carbonate platforms to changes in atmospheric carbon dioxide levels, Palaeogeography, Palaeoclimatology, Palaeoecology 200(1-4) (2003) 187-205.

B.4.

Correlation between the Helvetic and the Jura realms during the Hauterivian – Early Aptian: a common northern Tethyan margin history?

Keywords: Urgonian limestone; Ammonites; Northern Tethyan margin; Barremian

B.4.1. Introduction

This chapter includes a description of an attempt to correlate the Helvetic and the Jura realms using the biostratigraphic and chemiostratigraphic results obtained in the Jura realm by A. Godet. In order to observe if the changes monitored in the Helvetic realm can be traced in other depositional settings, a literature review is proposed to demonstrate that, at least along the northern Tethyan realm, the same changes occur.

During the Mesozoic, the Jura realm was located northwest to the Helvetic realm. Cretaceous deposits are only present in the western part of the Jura Mountains. Due to the alpine orogeny and concomittant unroofing of the Alps with northwards shedding of the associated erosional products, the Tertiary molasse basin is presently separating these two tectonic units. It is as such difficult to establish the exact relationship between the two areas during the Early Cretaceous. Two hypotheses can be formulated (Fig. B.4.1): On one hand, the Jura realm can be considered as the proximal prolongation of the western Helvetic realm. On the other hand, it can also be hypothesized that the Helvetic and the Jura realm were separated by a topographic high, which is now buried under the molasse infill. In this case, the Jura realm would represent the inner part of the Paris basin.

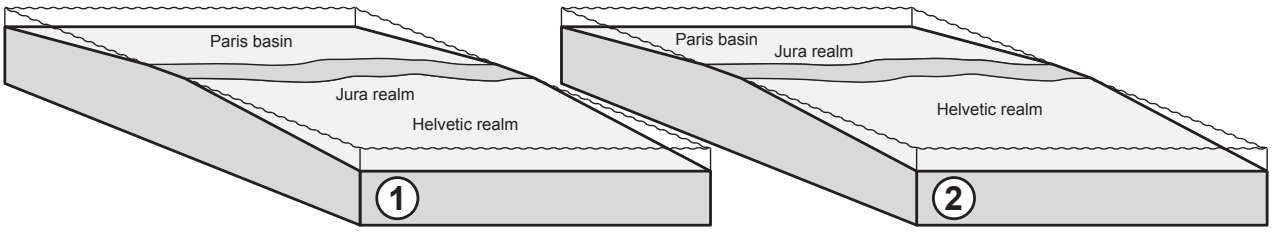

Fig. B.4.1. Palaeogeographic position of the Helvetic and Jura realm during the Hauterivian – Early Aptian. *Hypothesis 1*: the Jura realm represents the inner part of the Helvetic ramp. *Hypothesis 2*: the Jura realm in located at the southwestern margin of the Paris basin.

B.4.2. Lithostratigraphy

B.4.2.1. The Helvetic realm

Hauterivian – Lower Aptian sedimentary rocks in the Helvetic realm consist of nine members that are grouped into four formations (Fig. B.4.2). The lowermost member discussed here is the Gemsmättli Member (Mb), which ended within the earliest Hauterivian. It is followed by the Kieselkalk Formation (Fm), which is divided in three parts: the Lower Kieselkalk Mb, the Lidernen Mb and the Upper Kieselkalk Mb (Funk, 1969). The superjacent Drusberg Fm is divided into the Altmann Mb

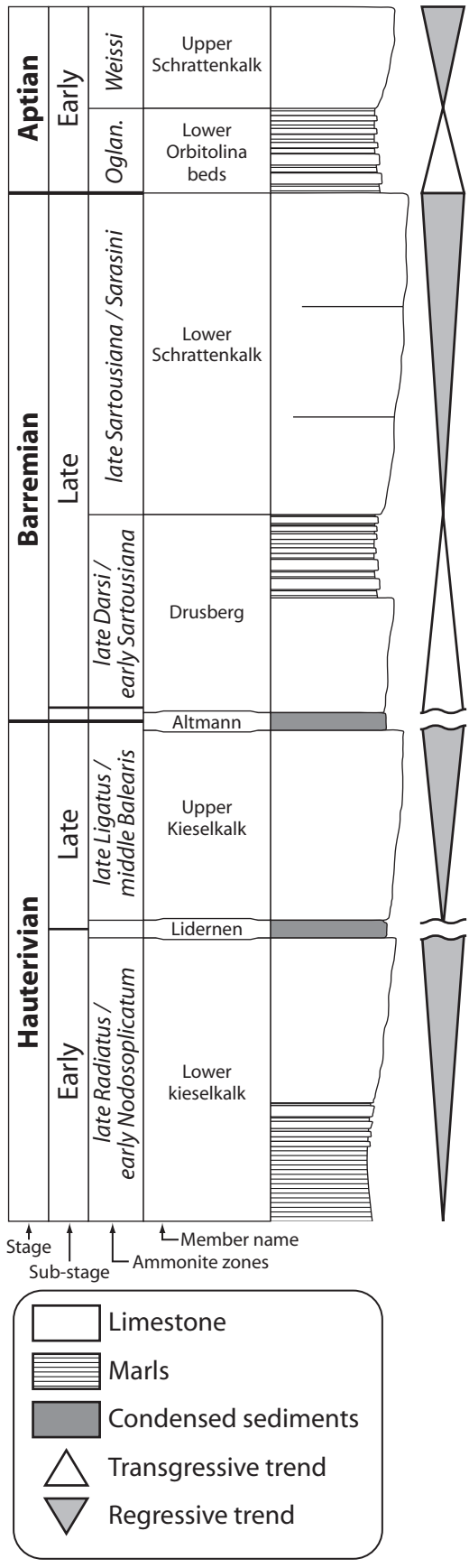

Fig. B.4.2. Synthetic sedimentary column of the Helvetic realm and corresponding age of the different Members and Formations.

and the Drusberg Mb. The youngest formation to be discussed here is the Schrattenkalk Fm, which is divided into the Lower Schrattenkalk Mb, the Lower Orbitolina Beds and the Upper Schrattenkalk Mb. In the distal part of the Helvetic realm, the top of the Drusberg Fm is capped by a condensed horizon: the Chopf Mb.

Gemsmättli, Lidernen and Altmann Mbs are associated with drowning episodes (Föllmi et al., 1994) and are characterized by high amounts of glauconite and phosphate-rich nodules or crusts. Lower and Upper Kieselkalk Mbs are representative of the heterozoan-dominated carbonate platform, whereas the Lower and Upper Schrattenkalk Mbs are representative of the photozoan-dominated carbonate platform. A shallowing-upward trend is recognized in both Lower and Uppern Schrattenkalk Mbs (Bollinger, 1988). Finally, the Drusberg and Lower Orbitolina Mbs can be classified in the heterozoan-photozoan transition field (sensu Halfar et al., 2004). A shallowing-upward trend is recognized both in the Lower and Upper Kieselkalk Mbs (Funk et al., 1993). The Lower Kieselkalk Mb starts with a marly interval that passes progressively into echinoderm-rich limestone.

B.4.2.2. The Jura realm

Eight members characterize the Hauterivian – Lower Aptian sedimentary rock succession in the western Swiss Jura (Fig. B.4.3). They are called, from base to top: the Marnes bleues, the Zone marno-calcaire, the Lower Pierre Jaune, the Marnes d'Uttins, the Upper Pierre Jaune, the Urgonien Jaune, the Marnes de la Russille and the Urgonien Blanc Mbs.

The Marnes bleues, the Zone marno-calcaire, the Lower Pierre Jaune, the Upper Pierre Jaune and the Urgonien Jaune are characteristic of heterozoan-dominated carbonate platform deposits, whereas the Marnes de la Rusille and the Urgonian Blanc Mb are representative of photozoan-dominated carbonate platform. The Marnes bleues, Zone marno-calcaire and Lower Pierre Jaune Mbs can

be grouped into one shallowing-upward unit. In the Marne d'Uttins Mb, Godet et al. (in prep.) have recognized the presence of a glauconitic hardground with traces of phosphatization. These same authors have also observed a glauconite-enriched interval at the base of the Urgonien Jaune Mb, which is associated with and followed by numerous erosive surfaces and reworked sediment intervals.

B.4.3. Discussion

B.4.3.1. Dating of the Helvetic realm Members

Hauterivian – Early Aptian deposits in the Helvetic realm have been relatively well dated by ammonite biostratigraphy (Heim, 1910-1916; Fichter, 1934; Wyssling, 1986; Kuhn, 1996; Van de Schootbrugge, 2001; Bodin et al., 2006a, 2006b; Linder et al., submitted). The earliest Hauterivian (*Radiatus* zone) is represented by the youngest part of the Gemsmättli Member (Kuhn, 1996). Most of the Hauterivian is recorded in the Kieselkalk Formation (Fm). Van de Schootbrugge (2001) dated the Lidernen Mb from the top of the *Nodosoplicatum* zone to the basal part of the *Ligatus* zone (Fig. B.4.2).

The overlying Drusberg Fm is dated thanks to ammonite findings in the Altmann Mb and Chopf Mb (Bodin et al., 2006a, 2006b). The Altmann Mb spans from the latest *Balearis* zone to the Early *Darsi* zone. The Chopf Mb which follows on top of the Drusberg Fm in distal parts of the Helvetic shelf, is dated from the *Sartousiana* zone.

Bodin et al. (2006a) dated the base of Schrattenkalk Fm in proximal settings by means of a sequence stratigraphic interpretation based on the identification of the maximum flooding interval Ba3 (*Sartousiana* zone, middle Late Barremian). Linder et al. (submitted) have dated the demise of the Schrattenkalk Fm to the earliest Aptian (*Deshayesi* zone).

All Hauterivian – Early Aptian members from the Helvetic realm have thus been precisely dated by ammonite biostratigraphy with the exception of the Lower Orbitolina Beds. However, due to the fact that the helvetic

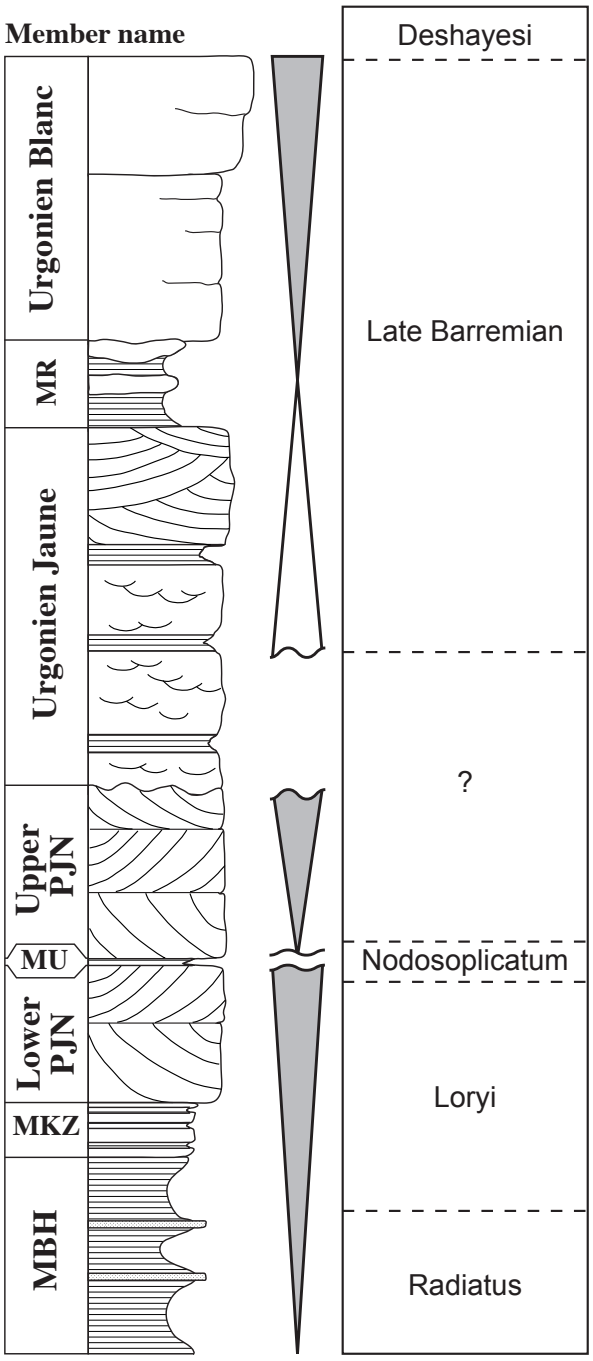

Fig. B.4.3. Synthetic sedimentary column of the Jura realm (modified from Godet et al., in prep.) and corresponding age of the different Members.

Schrattenkalk Formation is correlatable with the Urgonian Formation in the Vercors area of eastern France and that the ages of both formations are comparable (*e.g.,* Arnaud et al., 1998), the earliest Aptian age (*Oglanlensis* – Early *Weissi* zone) proposed for the «Couches inférieures à Orbitolina» in the Vercors can be also assumed for the Lower Orbitolina Beds of the helvetic realm.

B.4.3.2. Dating of the Jura realm Members

Hauterivian – Early Aptian deposits of the Jura realm have been the subject of numerous studies (*e.g.,* Renz & jung, 1978; Remane et al., 1989). Thanks to the study of Blanc-Aletru (1995) and Godet et al. (submitted; in prep.), a good biostratigraphic scheme can now be proposed for the whole Hauterivian – Early Aptian deposits in the western Swiss Jura (Fig. B.4.3).

The lower part of the lithostratigraphic succession is relatively well constrained due to abundant ammonites (Busnardo & Thieuloy, 1989). As such, the Marne Bleue Mb belongs to the *Radiatus* and earliest *Loryi* ammonite zones. Both the marno-calcaire and Lower Pierre Jaune Mbs belongs to the *Loryi* zone. The Marnes d'Uttins Mb provides the last well-conserved and identifiable ammonites from this lithostratigraphic succession. They allow dating this Member from the *Nodosoplicatum* zone (Busnardo & Thieuloy, 1989). No precise dating can be emitted for the Upper Pierre Jaune Mb.

Thanks to orbitolinids, Blanc-Aletru (1995) dated the upper part of the Urgonien Jaune and the Urgonien Blanc Mbs as belonging to the Late Barremian. This dating is confirmed by chemiostratigraphic studies of Godet et al. (submitted; in prep.). The first glauconitic horizon of the Urgonien Jaune Mb, which is situated below the two dated horizons, has for the moment not delivered any biostratigraphic useful fossils. The age of the boundary between the Upper Pierre Jaune Mb and the Urgonien Jaune Mb is thus impossible to date precisely. Sediments overlying the Urgonien Blanc Mb delivered an ammonite assemblage which was described by Renz & Jung (1978). As such, the demise of the Urgonien Blanc Mb is dated as older than or equal to the *Deshayesi* zone.

B.4.3.3. Correlation

According to these age dates, the similarity in facies, the correlation of glauconite-enriched horizons, and the correlatable trends in sequence-stratigraphic patterns, a common depositional history between the Helvetic and the Jura realm can thus be recognized (Fig. B.4.4). Moreover, the correlation between these two realms also helps to propose a dating of the horizons in the Jura realm which are poor in biostratigraphic fossils.

Firstly, due to its dating, its shallowing-upward trend and the fact that it corresponds to a heterozoan carbonate factory platform, the triad Marnes bleues – Zone Marno-calcaire – Lower Pierre Jaune may correspond to the Lower Kieselkalk Mb. However, it can be observed that the onset of the Marne bleue Mb is dated as *Radiatus* zone, whereas the basal marly part of the Lower Kieselkalk Mb may correspond to the *Loryi* zone. This time lag could be related to the absence of winnowing and phosphatization in the Jura realm contrary to the Helvetic realm during the earliest Hauterivian. However, the presence of a glauconite-enriched level in the upper part of the Marnes bleues and a glauconitic hardground in the Zone marno-calcaire can also be considered as proximal equivalents of the top of the Gemsmättli Member.

The basal part of the Lidernen Mb can be correlated to the Marnes d'Uttins Mb, thanks to ammonite dating and traces of phosphatization. However, the lack of early Late Hauterivian ammonites in the Marnes d'Uttins Mb, as well as the lack of dating of the Upper Pierre Jaune Mb, leaves some uncertainties. Two hypotheses can be formulated: On one hand, if the entire Marnes d'Uttins Mb corresponds to the Lidernen Mb, the Upper Pierre Jaune Mb may thus correspond to the Upper Kieselkalk Mb.

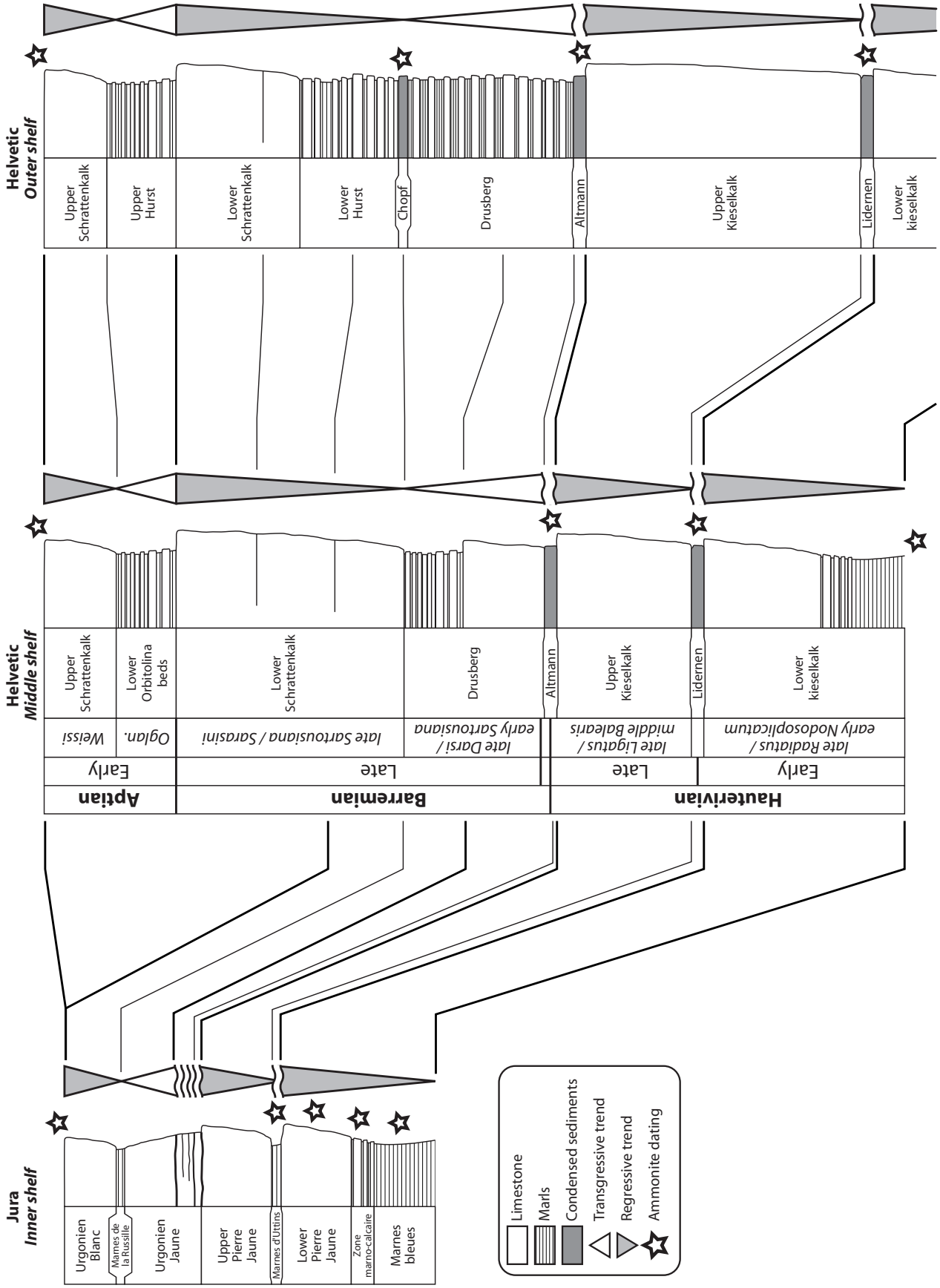

Fig. B.4.4. Members and Formations correlation between the Helvetic and the Jura realms during the Hauterivian – Early Aptian.

The presence of a well-developed hardground at the base of the Marnes d'Uttins Mb is an indication of the long duration involved in its formation and the similarities between the upper Pierre Jaune and Kieselkalk are rather compelling evidence for their correlation. In this case, the Jura record would mirror the Helvetic realm deposit. On the other hand, if the Marnes d'Uttins Mb is restricted to the *Nodosoplicatum* zone and if the Upper Pierre Jaune Mb belongs to the early Late Hauterivian, a decoupling of the Jura record from the Helvetic realm may thus be hypothesized. In this case, platform growth would thus have started earlier in the Jura realm than in the Helvetic realm. This hypothesis would thus argue in favor of a topographic high that has separated the Jura and Helvetic realms.

Biostratigraphical and chemiostratigraphical age dates of the Urgonien Jaune Mb indicates that a whole part of this member is correlated to the Drusberg Fm and the Lower Schrattenkalk Mb. Because of the relatively small thickness of these deposits, it also indicates that the erosive surfaces recognized in the basal part of the Urgonien Jaune Mb (Godet et al., submitted) represent significant time lags. Due to the high amount of glaucony in the basal part of the Urgonien Jaune Mb, which lack age dating, a correlation with a part or the entire Altmann Mb can be formulated. This correlation needs however further dating to be tested. In this case, an important part of the Barremian is missing or condensed above the basal glauconitic layer of the Urgonien Jaune Mb. This feature can be linked to the overall second-order sea-level lowstand that is reported along the northern Tethyan margin during that time (*e.g.,* Arnaud, 2005)

The deepening-upward trend of the upper part of the Urgonien Jaune Mb, coupled with biostratigraphic and chemiostratigraphic results, indicate that it is correlated with the Drusberg Mb in the Helvetic realm. The Urgonien Blanc Mb corresponds to the basal part of the Lower Schrattenkalk Mb. This latter was drowned during the *Deshayesi* zone in both realms.

B.4.3.4. Globalization.

The changes between photozoan and heterozoan dominated carbonate production can be traced, at least, through the entire northern Tethyan realm. Indeed, heterozoan-dominated platform during the Hauterivian – Early Barremian are also recorded in the Chartreuse and Vercors area (Blanc, 1996; Arnaud et al., 1998). Heterozoan platform seems also to dominate the sedimentary record in Northern Oman during the Hauterivian – Early Barremian (*e.g,* Hillgärtner et al., 2003). The reinstallation of the photozoan association during the Late Barremian (Urgonian-type carbonate) seems to be a worldwide event in tropical and subtropical area of the Tethyan margins (*e.g.,* Garcia-Hernandez, 1979, for SE Spain; Michalik, 1994, for Western Carpathians; Blanc-Aletru, 1995, for Jura mountains; Ivanov et al., 1997 and Peybernès et al., 2000, for Bulgaria; Arnaud et al., 1998, for SE France; Lehmann et al., 1999, 2000, for Northeastern Mexico; Arnaud et al., 2000, for Venezuela; Bernaus et al., 2003, for Spanish Pyrenees; Hillgärtner et al., 2003, for Northern Oman).

The major drowning event of the Early Aptian, which lead to the demise of the Urgonian platform and which is correlated with a major perturbation of the carbon cycle (Weissert et al., 1998), can be traced worldwide (*e.g.,* Masse, 1993). On the other hand, the drowning events of the middle Hauterivian and latest Hauterivian – Early Barremian are more difficult to be traced beyond the Helvetic and the Jura realms because no phosphatization traces have been recognized so far. Latest Hauterivian carbonate platform deposits are however absent in the Chartreuse and Vercors area.

B.4.4. Conclusions

Large parts of the northern Tethyan margin have experienced changes in the carbonate production factory changes which are coeval to those documented in the Helvetic realm. Thus, the development of an heterozoan-dominated

platform during the Hauterivian seems to be recorded all along the northern Tethyan margin, whereas the development of photozoan-dominated platform took place during the Late Barremian – Earliest Aptian in the same area.

The Jura realm record is very similar with the Helvetic one. In particular, the similarity of the Pierre Jaune and the Kieselkalk Fms is convincing evidence that environmental conditions common to both areas have driven their depositional history. It is possible that the base of the Altmann Mb (corresponding to the latest Hauterivian) is expressed in the first glauconitic layer of the Urgonien Jaune Mb. The lack of Early Barremian deposits in the Jura realm is to be linked to a second-order sea-level lowstand.

The upper part of the Urgonien Jaune Mb is correlated to the Drusberg Mb in the Helvetic realm. The Urgonien Blanc Mb corresponds to the basal part of the Lower Schrattenkalk Mb.

B.4.5. References

Arnaud, H. 2005. The South-East France Basin (SFB) and its Mesozoic evolution. In: The Hauterivian - Lower Aptian sequence stratigraphy from Jura platform to Vocontian basin: a multidisciplinary approach (Eds T. Adatte et al.), Géologie Alpine, Série Spéciale «Colloques et Excursions» n°7, pp. 5-28.

Arnaud, H., Arnaud-Vanneau, A., Blanc-Aletru, M.C., Adatte, T., Argot, M., Delanoy, G., Thieuloy, J.-P., Vermeulen, J., Virgone, A., Virlouvet, B. and Wermeille, S. 1998. Répartition stratigraphique des orbitolinidés de la plate-forme urgonienne subalpine et jurassienne (SE de la France). Géologie Alpine, 74: 3-89.

Arnaud, H., Arnaud-Vanneau, A., Bulot, L.G., Beck, C., MacSotay, O., Stephan, J.-F. and Vivas, V. 2000. Le Crétacé inférieur du Venezuela oriental: stratigraphie séquentielle des carbonates sur la transversale Casanay-Maturin (Etats de Anzoategui, Monagas et Sucre). Géologie Alpine, 76: 3-81.

Bernaus, J.M., Arnaud-Vanneau, A. and Caus, E. 2003. Carbonate platform sequence stratigraphy in a rapidly subsiding area: the Late Barremian-Early Aptian of the Organya basin, Spanish Pyrenees. Sedimentary Geology, 159: 177-201.

Blanc, E. 1996. Transect plate-forme - basin dans les séries carbonatées du Berriasien supérieur et du Valanginien inférieur (domaine jurassien et nord-vocontien): chronostratigraphie et transfert des sédiments. Géologie Alpine, Memoire H.S. n° 25, Grenoble, France, 312 pp.

Blanc-Aletru, M.C. 1995. Importance des discontinuités dans l'enregistrement sédimentaire de l'urgonien jurassien: micropaléontologie, sédimentologie, minéralogie et stratigraphie séquentielle. Géologie Alpine, Memoire H.S. n°24, Grenoble, France, 299 pp.

Bodin, S., Godet, A., Vermeulen, J., Linder, P. and Föllmi, K.B. 2006a. Biostratigraphy, sedimentology and sequence stratigraphy of the latest Hauterivian - early Barremian drowning episode of the Northern Tethyan margin (Altmann Member, Helvetic nappes, Switzerland). Eclogae geologicae Helvetiae 99, 157-174.

Bodin, S., Vermeulen, J., Godet, A. and Föllmi, K.B. 2006b. New data on the age of the installation of Urgonian-type carbonates along the northern Tethyan margin: Biostratigraphy of the Chopf Member (Helvetic Alps, eastern Switzerland). Comptes Rendus Geoscience, 338: 727-733.

Bollinger, D. 1988. Die Entwicklung des distalen osthelvetischen schelfs im Barremian und Früh-Aptian. Drusberg-, Mittagspitz- und Schrattenkalk-Fm im Vorarlberg und Allgäu. Mitteilungen aus dem Geologischen Institut der Eidg. Technischen Hochschule und der Universität Zürich, Neue Folge Nr. 259a, 159 pp.

Fichter, H.J. 1934. Geologie der Bauen-Brisen-

Kette am Vierwaldstaettersee und die zyklische Gliederung der Kreide und des Malm der helvetischen Decken. Bretträge zur Geologischen Karte, 128 pp.

Funk, H. 1969. Typusprofile der helvetischen Kieselkalk Formation und der Altmann Schichten. Eclogae geologicae Helvetiae, 62: 191-203.

Funk, H., Föllmi, K.B. and Mohr, H. 1993. Evolution of the Tithonian-Aptian carbonate platform along the northern Tethyan margin, eastern Helvetic Alps. In: Cretaceous carbonates platforms (Eds Simo J.A.T., Scott R.W. and Masse J.-P.), AAPG Memoir, 56, pp. 387-407. American Association of Petroleum Geologists. Tulsa, OK, United States.

Föllmi, K.B., Weissert, H., Bisping, M. and Funk, H. 1994. Phosphogenesis, carbon-isotope stratigraphy, and carbonate-platform evolution along the Lower Cretaceous northern Tethyan margin. Geological Society of America Bulletin, 106: 729-746.

Garcia-Hernandez, M. 1979. Les faciès urgoniens pendant la sédimentation barrémo-albienne dans les Sierras de Cazorla et du Segura (zone prébétique, S-E- de l'Espagne). Mém. Spéc. Géobios, 3: 57-69.

Godet, A., Bodin, S., Adatte, T. and Föllmi, K.B. submitted. Clay mineral assemblages along the Northern Tethyan margin during the Late Hauterivian - Early Aptian: Interactions between climate change and carbonate platform evolution. Cretaceous Research.

Godet, A., Bodin, S., Stille, P., Adatte, T., Van de Schootbrugge, B., Matera, V. and Föllmi, K.B. in prep. Strontium-isotopes stratigraphy of the Urgonian Formation from the Western Swiss Jura: implication for the evolution of the Early Cretaceous northern Tethyan carbonate platforms.

Halfar, J., Godinez-Orta, L., Mutti, M., Valdez-Holguin, J.E. and Borges, J.M. 2004. Nutrient and temperature controls on modern carbonate production: An example from the Gulf of California, Mexico. Geology, 32: 213-216.

Heim, A. 1910-1916. Monographie der Churfirsten-Mattstock-Gruppe. Beiträge zur Geologischen Karte der Schweiz, 50, Bern, 662 pp.

Hillgärtner, H., van Buchem, F.S.P., Gaumet, F., Razin, P., Pittet, B., Grötsch, J. and Droste, H. 2003. The Barremian-Aptian evolution of the eastern arabian carbonate platform margin (northern Oman). Journal of Sedimentary Research, 73: 756-773.

Ivanov, M., Peybernes, B., Nikolov, T., Ciszak, R., Stoykova, K. and Minkovska, V. 1997. Attempt of sequence correlations during Barremian - Aptian times within a system platform-basin-platform along a Danube-Gabrovo cross-section (Central Northern Bulgaria). Comptes Rendus de l'Academie des Sciences - Series IIA - Earth and Planetary Science, 325: 967-972.

Kuhn, O. 1996. Der Einfluss von Verwitterung auf die Paläozeanographie zu Beginn des Kreide-Treibhausklimas (Valanginian und Hauterivian) in der West-Tethys, Universität Zürich, Zürich, 380 pp.

Lehmann, C., Osleger, D.A., Montanez, I.P., Sliter, W.V., Arnaud-Vanneau, A. and Banner, J. 1999. Evolution of Cupido and Coahuila carbonate platforms, Early Cretaceous, northeastern Mexico. GSA Bulletin, 111: 1010-1029.

Linder, P., Gigandet, J., Hüsser, J.-L., Gainon, F. and Föllmi, K.B. submitted. The Early Aptian Grünten Member: Description of a new lithostratigraphic unit of the helvetic Garschella Formation. Eclogae geologicae Helvetiae.

Masse, J.-P. 1993. Valanginian-Early Aptian Carbonate Platforms from Provence, Southeastern France. In: Cretaceous carbonates platforms (Eds Simo J.A.T., Scott R.W. and Masse J.-P.), AAPG Memoir, 56, pp. 363-374. American Association of Petroleum Geologists.

Tulsa, OK, United States.

Michalik, J. 1994. Lower Cretaceous carbonate platform facies, Western Carpathians. Palaeogeography, Palaeoclimatology, Palaeoecology, 111: 263-277.

Peybernes, B., Ivanov, M., Nikolov, T., Ciszak, R. and Stoykova, K. 2000. Séquence de dépôt à l'articulation plate-forme urgonienne-bassin (intervalle Barrémien-Albien) dans le Prébalkan occidental (Bulgarie du Nord-Ouest). Comptes Rendus de l'Academie des Sciences - Series IIA - Earth and Planetary Science, 330: 547-553.

Remane, J., Busnardo, R. and Charollais, J. 1989. Révision de l'etage Hauterivien (région-type et environs, Jura Franco-Suisse). Mémoires de la Société neuchâteloise des Sciences naturelles, 11, Neuchâtel, Switzerland, 322 pp.

Renz, O. and Jung, P. 1978. Aptian to Maastrichtian in the Swiss Jura Mountains. Eclogae geologicae Helvetiae, 71: 1-18.

Van de Schootbrugge, B. 2001. Influence of paleo-environmental changes during the Hauterivian (Early Cretaceous) on carbonate deposition along the northern margin of the Tethys: Evidence from geochimical records (C, O, and Sr-isotopes, P, Fe, Mn). Thèse de Doctorat ès Sciences, spécialité Géologie, Université de Neuchâtel, Institut de Géologie, Neuchâtel (Switzerland), 268 pp.

Weissert, H., Lini, A., Föllmi, K.B. and Kuhn, O. 1998. Correlation of Early Cretaceous carbon isotope stratigraphy and platform drowning events: a possible link? Palaeogeography, Palaeoclimatology, Palaeoecology, 137: 189-203.

Wyssling, G.W. 1986. Der frühkretazische helvetische Schelf in Vorarlberg und im Allgäu - Stratigraphie, Sedimentologie und Paläogeographie. Jb. Geol. Bund., 129: 161-265.

Chapter C.

The pelagic record

Prof. Hubert Arnaud showing the mfs Ha7 (bed AN 79, Angles section, France)

"On fait la science avec des faits, comme on fait une maison avec des pierres : mais une accumulation de faits n'est pas plus une science qu'un tas de pierre n'est une maison"

Henri Poincaré

C.1.

Introduction

In order to better understand temporal changes in shallow-water carbonate factory of the northern Tethyan margin accompanied by a drowning episode during the Late Hauterivian – Barremian, the geochemical record in coeval pelagic sections was investigated. The results of these analyses may help to improve our understanding the palaeoceanographic changes which occurred during the studied time interval.

Four pelagic sections were studied: the Fiume-Bosso and Gorgo a Cerbara sections in Italy (Umbria-Marche basin); the Veveyse de Châtel – St. Denis section in Switzerland (Ultrahelvetic realm); the Angles section in France (Vocontian trough). These sections are well dated and present the advantage to cover a large part of the western Tethyan realm.

Studied geochemical proxies are redox-sensitive trace metals, phosphorus, and carbon and oxygen stable isotopes. They give information about the evolution of the bottom water redox state, palaeoproductivity, palaeotemperatures and the carbon cycle. Three published papers resulted from these studies.

Foreword to "Enrichment of redox-sensitive trace metals (U, V, Mo, As) associated with the late Hauterivian Faraoni oceanic anoxic event"

The main goal of this paper, published in *International Journal of Earth Sciences* (former *Geologische Rundschau*), is to characterize the redox state of the Faraoni level. This organic-rich level is dated from the latest Hauterivian and has many sedimentological features similar to the deposits of other Oceanic Anoxic Events. This paper aims at confirming the anoxic character of the episode leading to the depostion of the Faraoni level.

Foreword to "The late Hauterivian Faraoni oceanic anoxic event in the western Tethys: Evidence from phosphorus burial rates"

The reconstruction of Phosphorus burial rates provides a powerful tool to trace the evolution of palaeoproductivity pattern. Therefore, the main goals of this paper, published in *Palaeogeography, Palaeoclimatology, Palaeoecology*, are:

(1) To explain the unfolding of the Faraoni event.

(2) To understand the effect of nutrient level variations on changes in the carbonate platform factory and platform drowning during the Late Hauterivian – Barremian.

Foreword to "Evolution of the marine stable carbon-isotope record during the early Cretaceous: A focus on the late Hauterivian and Barremian in the Tethyan realm"

The main goals of this paper, published in *Earth and Planetary Science Letters* (with Alexis Godet as the first author), are:

(1) To characterize sea-surface water density (temperature and/or salinity) variations in the western Tethyan realm

(2) To understand the late Hauterivian – Barremian carbon cycle and its link to changes in the carbonate platform factory and platform drowning.

Foreword to "Links between palaeoceanographic changes and platform carbonate factory modes during the Early Cretaceous: a multi-proxy approach"

This paper, which will be submitted to *Earth and Planetary Science Letters*, proposes an integrated approach to carbonate platform factory changes and drowning. It uses a compilation of previously published data as well as a new elementary and isotopic dataset performed on belemnites.

The main goal of this paper is to decipher the mechanisms responsible for carbonate platform factory changes and drowning during the Early Cretaceous.

C.2.

Enrichment of redox-sensitive trace metals (U, V, Mo, As) associated with the late Hauterivian Faraoni oceanic anoxic event

Stéphane Bodin[a], Alexis Godet[a], Virginie Matera[a], Philipp Steinmann[a], Jean Vermeulen[b], Silvia Gardin[c], Thierry Adatte[a], Rodolfo Coccioni[d], Karl B. Föllmi[a]

[a] Institut de Géologie, Université de Neuchâtel, Rue Emile Argand 11, CP 158, 2009 Neuchâtel, Switzerland

[b] Grand Rue, 04330 Barrême, France

[c] CNRS-UMR 5143 "Paléodiversité et Paléoenvironnement", case 104, Université Paris 6, 4 Place Jussieu, 75252 Paris Cedex 05, France

[d] Istituto di Geologia e Centro di Geobiologia dell'Università, Campus Scientifico, Località Crocicchia, 61029 Urbino, Italy

Keywords: Hauterivian, Barremian, Chemostratigraphy, Western Tethys, Trace metals.

Published in: International Journal of Earth Sciences (in press; DOI 10.1007/s00531-006-0091-9)

Abstract

The Faraoni Level is a short-lived oxygen-deficient event that took place during the latest Hauterivian. In order to improve our understanding of the palaeoenvironmental conditions that occurred during this event, we have analysed the contents of several redox-sensitive trace elements (U, V, Mo, As, Co, Cd, Cu, Zn, Ni, Pb, Cr) from bulk limestone samples of late Hauterivian – early Barremian age from three reference sections. U, V, Mo and As show consistent and significant enrichments during the Faraoni event whereas the other redox-sensitive trace elements analysed here are not systematically enriched. In order to explain this discrepant behaviour, we propose that the Faraoni Level was deposited during a period of anoxic conditions near the sediment-water interface. The distinctive peaks in U, V, Mo and As contents are traceable throughout the three studied sections and represent a good correlation tool which helps to identify the Faraoni Level and its equivalents in the western Tethyan realm and outside of the Tethys. For example, a peak in U contents in upper Hauterivian sediments of the northwestern Pacific realm (ODP leg 185, site 1149) may well be an expression of the Faraoni event in this particular basin.

C.2.1. Introduction

Since the first description by Cecca et al. (1994) of an organic-rich guide level – the so-called Faraoni Level – in upper Hauterivian (late *Spathicrioceras angulicostatum* ammonite zone) pelagic carbonates of the Umbria-Marche Basin (Italy), it has been shown that correlatable organic-rich levels occur throughout the western Tethyan realm. Equivalents of the Faraoni Level have been identified on the Trento Plateau in Italy (Cecca et al. 1996; Coccioni et al. 1998), in the Vocontian Trough in France (Baudin et al. 1999), and in the Swiss Préalpes (Busnardo et al. 2003). It is for this reason that Baudin et al. (2002) associated this level with a short-lived oxygen-deficient event in the western Tethyan realm. And following Baudin (2005), the Faraoni Level and its equivalent can be qualified as an anoxic event (compare this reference for a detailed biostratigraphic definition of this event). With the Valanginian event (Erba et al. 2004), the Faraoni event is one of the first palaeoceanographic events which led to major change in the carbon cycle during the early Cretaceous.

The environmental circumstances leading to this short-lived oxygen-deficient event in the late Hauterivian are still not clear. In contrast to the anoxic events in the Valanginian, the early Aptian, and near the Cenomanian/Turonian boundary (e.g. Schlanger and Jenkyns 1976; Schlanger et al. 1987; Lini et al. 1992; Jones and Jenkyns 2001; Sanfourche and Baudin 2001), the Faraoni Level is not accompanied by a major carbon isotope excursion towards more positive values, but rather by a small long-term increase culminating around the Faraoni event (Föllmi et al. 1994; Erba et al. 1999; van de Schootbrugge et al. 2000; Company et al. 2005; Godet et al. 2006). Furthermore, no major volcanic episode has, of yet, been identified for the late Hauterivian. This means that the classical model postulated for the origin of oceanic anoxic events in general, i.e. increased volcanism leading to an increase in atmospheric CO_2, climate warming, increased weathering and nutrient availability, higher productivity and consequently higher preservation rates of organic matter (e.g. Jenkyns 1999; Jenkyns 2003) can not be applied in this case.

The Faraoni event corresponds in time to the onset of drowning episode D3 during the evolution of a carbonate platform system located along the northern Tethyan margin (Föllmi et al. 1994). But, in contrast to the Valanginian and the Aptian – Albian drowning episodes (D1, D4 and D5), the drowning episode D3 - not being mirrored by a distinct positive excursion in carbon isotopes, is also in need of an alternative explanation (van de Schootbrugge et al. 2000, 2003). It is therefore important to identify the palaeoenvironmental conditions leading to the Faraoni event, whilst also respecting the coeval drowning event on the northern Tethyan carbonate platform, which may have been linked to this anoxic event.

We investigated three (hemi-) pelagic key sections representing a north-south transect through the western Tethys and including micritic carbonates and marls of the Hauterivian—Barremian transition with regards to their redox-sensitive trace-element concentrations. The studied trace elements are uranium (U), vanadium (V), molybdenum (Mo), arsenic (As), cobalt (Co), cadmium (Cd), cupper (Cu), zinc (Zn), nickel (Ni), lead (Pb) and chromium (Cr). Their behaviour around the Faraoni Level is quite distinct and helps us to improve our understanding of redox conditions and changes therein in this basin during the Faraoni event.

In this paper, the term “Faraoni Level” and “Faraoni Level equivalent” refers to the interval composed of organic-rich sediments and the intervening carbonate beds that are associated with the Faraoni oceanic anoxic event. The term “Faraoni Level” is used when the lithological characteristics are the same as in the type area (e.g., Cecca et al., 1994), whereas the term “Faraoni Level equivalent” is used when the lithology is different from that of the type area (i.e., lacking a distinct enrichment in organic matter). The redox classification of sedimentary environments used here is adapted from Algeo

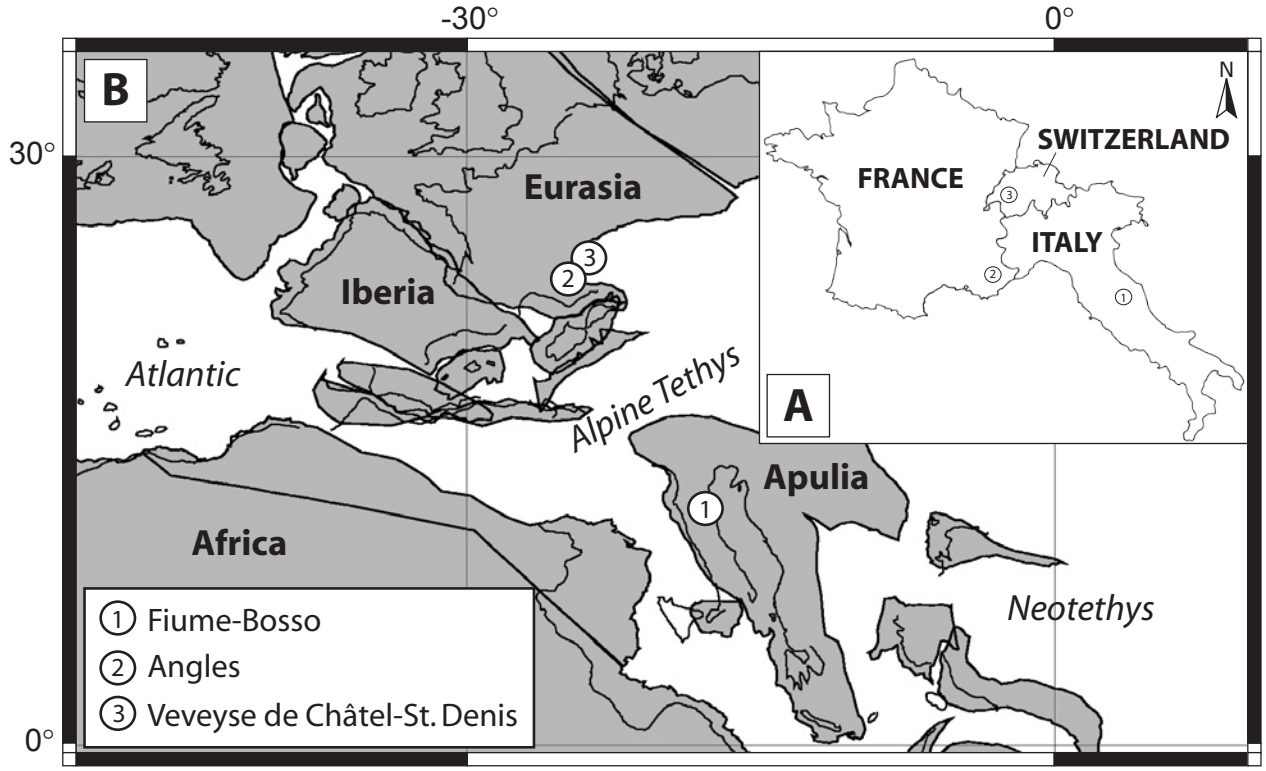

Fig. C.2.1 – A. Actual location of the three studied sections. B. Paleogeographic position of the three studied sections at the Hauterivian – Barremian boundary. Palaeomap modified from Hay *et al.* (1999). Modified from Bodin et al. (2006).

and Maynard (2004) and references therein. Thus, oxic, suboxic and anoxic environments are characterized by >2.0, 2.0-0.2, and <0.2 ml O_2 l^{-1} H_2O respectively. Anoxia and euxinia are distinguished by the absence or presence of free H_2S in the water column respectively.

C.2.2. Studied sections and palaeogeographic setting

The studied sections were chosen according to the following criteria: (1) presence of the Faraoni Level or its equivalent; (2) good age control based on biostratigraphy (ammonites, nannofossils); (3) presence of pelagic carbonates and (4); representative of different areas of the western Tethys (Fig. C.2.1).

The first studied section is the Fiume-Bosso section, located between Urbino and Gubbio, near Cagli (central Italy; see also Cecca et al. 1994). This section represents the type section for the Faraoni Level (Cecca et al. 1994). The lithology consists of pelagic limestone and chert, which locally includes thin organic-rich marl layers and laminae, characteristic of the Maiolica Formation. The Faraoni Level is composed by a succession of three laminated black-shale layers and intervening calcareous beds.

The Veveyse de Châtel-St. Denis (VCD) is the second studied section. It is situated in the canton of Fribourg, along the Veveyse river, in western Switzerland (see Busnardo et al. (2003) for a detailed geographic description). Its lithology consists of a succession of alternating pelagic marls and marly limestones, which are rich in macrofossils. The equivalent of the Faraoni Level (identified by ammonite dating) is represented by the "couches à poissons" (an alternation of more or less organic-rich shale and marly limestone, rich in fish fossils) (Busnardo et al. 2003).

The third studied section is along the «route d'Angles», near Barrême in southeastern France, and is situated in the Vocontian Trough (see Busnardo 1965, for a detailed

geographic description). Its lithology consists of a fossiliferous, hemi-pelagic succession of regularly alternating marlstone and limestone. Ammonite dating indicates that the Faraoni Level equivalent is situated around the bed AN 53. Black shale has not been distinguished within this interval, which is characterized by an alternation of limestone and laminated shale. In the sedimentary interval attributed to the *P. mortilleti* zone, no marls were sampled due to poor outcrop quality.

During the late Hauterivian, the Angles and the VCD sections were situated along the northern Tethyan margin. The VCD section is part of the Ultrahelvetic realm, which is considered as the deeper offshore prolongation of the Vocontian Trough to the northeast (Trümpy 1960). The Fiume-Bosso section, which is the deepest section, was situated in the southern part of the Tethys, in the Umbria-Marche Basin, remote from any continent.

C.2.3. Methods

ICP-MS analyses were performed on bulk rock samples from limestone and marlstone for all three sections. The limestone samples were sawed in order to eliminate altered parts and rock veins. Then, powders were obtained for both limestone and marls using a mechanic agate crusher. A portion of approximately 250 mg was transferred into a digestion vessel (PTFE) and 10 ml of concentrated nitric acid (suprapur, Merck) were added. The sample was digested in a microwave oven (MSL-Ethos plus, Milestone) using the heating program recommended by the EPA 3051 method. After cooling, the resulting solution was filtered (0.45 μm) and diluted to 100 ml with ultrapure water. For the limestone, dissolution percentages determined after filtration were about 91% of initial sample weight in the Angles section, 83% in the VCD section, and 98% in the Fiume-Bosso section. Moreover, no correlation was observed between the concentration of the different analysed samples and the dissolution percentage obtained during digestion procedure (e.g., U in Fig. C.2.2). This shows that the studied elements are present in the soluble authigenic phase and are not due to partial leaching of the detrital insoluble fraction.

In the marls, the dissolution percentages were close to 50%. Mineralogical analyses indicate that clay and quartz grains constitute the insoluble part of the rock. No trace of carbonate is found, allowing us to postulate that the entire authigenic portion of the rock is dissolved with this method.

A second dilution (1/20) was then performed prior to analysis. To correct for matrix-induced ion signal variation and instrumental drift, rhodium was used as the internal standard. The element concentrations of the acid digests were determined by ICP-MS (ELAN 6100, Perkin Elmer) using a semi-quantitative mode (Totalquant). Totalquant (TQ) is a simple, rapid and accurate panoramic method based on full mass-spectra scan methods and was successfully applied to the analysis of various biological and environmental samples (Jitaru et al. 2003) like, for instance, in sediments (Bayon et al. 1998). TQ enables spectral interpretation of a full mass spectrum by comparison with an internal response table which includes assignment of

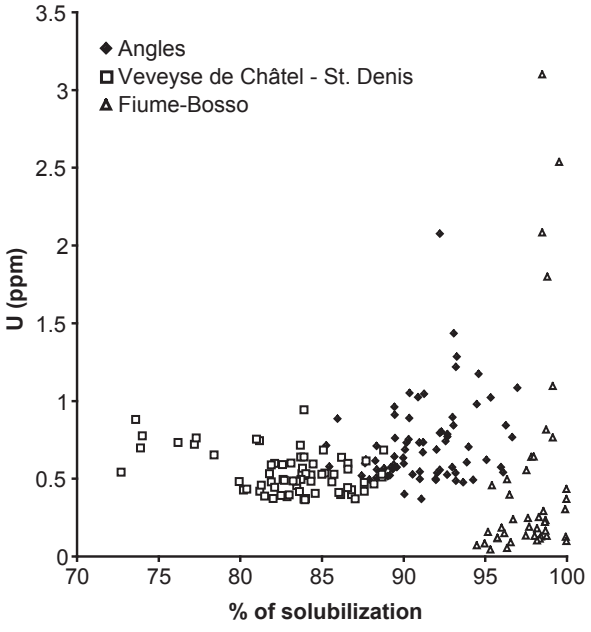

Fig. C.2.2 – U (ppm) versus percentage of dissolution in the three studied sections. No correlation is observed. See text for discussion.

element intensities based on internal response factors and an interpretation of interferences based on implemented algorithms for numerical calculation of interference corrections. The response table is usually updated before analysis by determination of a blank and one standard solution. Two Certified Reference Materials (CRM) (NIST-1640 natural water, LKSD-1 lake sediment from Canadian Centre for Mineral and Energy Technology – CANMET – Canada) were measured to evaluate the accuracy which is achieved in panoramic analysis with the Elan 6100. Here we present the results obtained for the four principal trace elements discussed in this study (V, Mo, As, and U). The mean recovery rates were determined for V, Mo, and As (no certified concentration values for U are available for the two CRM) and were, for the NIST-1640 CRM (N=11) 101% for V; 99% for Mo, and 101% for As, and Relative Standard Deviation (RSD) was better than ± 9% for V; ± 6% for Mo and ± 7% for As; for the LKSD-1 CRM (N=12 digestions) mean recovery rates were 90% for V; 89% for Mo, and 110% for As (for this CRM, recovery rates are based on certified concentration values obtained by partial extraction using concentrated HNO_3 and HCl whereas we used concentrated HNO_3 digestion); analytical precision (RSD) was about ± 8% for V; ± 9% for Mo, and ± 12% for As.

Furthermore, multiple digestions (N=10) of a sample corresponding to the Faraoni Level of the Angles section (bed AN 53-2) were analyzed. The RSD of these analyses were about ± 15% for V; ± 12% for Mo; ± 12% for As and ± 3% for U. A detection limit lower than 1 μg/kg was observed for the four trace elements studied.

The content and the type of organic matter were determined using Rock-Eval pyrolysis (Rock-Eval 6; Behar et al. 2001). The parameters TOC (total organic carbon in weight %) was obtained using the standard temperature cycle. Two standards (an in-house standard and the «IFP 160000» standard from the Institut Français du Pétrole, Paris, France) were passed at the beginning and at the end of a batch of approximately 15 samples.

C.2.4. Results

C.2.4.1. Redox-sensitive trace elements

The data for U, V, Mo, As, Co, Cd, Cu, Zn, Ni, Pb and Cr are shown in Tables C.2.1 and C.2.2 for limestone and marl for the three sections.

C.2.4.1.1. The Fiume-Bosso section

In limestone samples, the data obtained for U, V, Mo, and As contents show comparable variations, with a consistently low background level, contrasted by a maximum in concentrations in and close to the Faraoni Level (Fig. C.2.3, Table C.2.1). The average values for the background level correspond to approximately 0.2, 0.9, 0.03 and 0.3 ppm and the maximum values to approximately 3.1, 11.6, 0.5 and 3.0 ppm, for the U, V, Mo, and As contents, respectively.

The data obtained in the marlstones show equally a clear enrichment of U, V, Mo, and As around the Faraoni Level (Table C.2.2). The maximum values reach 15.4 ppm for U, 345.9 ppm for V, 61.8 ppm for Mo, and 177.4 ppm for As, whereas background level are equal to approximately 2.9, 54.1, 2.3, and 13.2 ppm respectively.

Despite a small negative shift in the upper part of the section, the global trend of Co in limestone samples seems to be more or less constant (Table C.2.1), fluctuating around 1.8 ppm. The Faraoni Level is marked by a short negative shift towards 0.9 ppm. In the shale, the Co curve shows a small positive shift within the Faraoni Level. A maximum of 106.6 ppm is present just above the Faraoni Level (Table C.2.2) whereas the background level values correspond to approximately 50 ppm.

For the other elements, only Cd and Zn show a small positive shift in limestone levels within the Faraoni Level. In the upper part of the section, a positive shift (up to 66.1 ppm) of Zn is remarked. In the Faraoni shale samples, a positive shift of Cd, Cu, Zn, Ni is present,

Fiume-Bosso		Sample	U	V	Mo	As	Co	Cd	Cu	Zn	Ni	Pb	Cr
late Hauterivian	no ammonite zonation	FB 59	0.15	0.81		0.39	2.61	0.06	2.61	8.96	13.30	0.90	1.81
		FB 65	0.05	0.58		0.25	1.51	0.14	3.69	7.21	12.31	1.27	2.13
		FB 71	0.09	0.64		0.23	3.02	0.12	5.20	7.43	12.24	1.48	2.38
		FB 79		0.63		0.16	0.99	0.09	2.26	6.01	12.10	1.02	2.09
		FB 89	0.07	0.71		0.08	1.43	0.14	5.06	9.05	13.76	0.89	2.18
		FB 94	0.11	0.79		0.09	1.87	0.26	3.11	10.22	13.58	1.23	2.36
		FB 99	0.08	0.80		0.17	2.06	0.35	4.22	19.28	14.69	5.07	3.19
		FB 104	0.18	1.25	0.03	0.31	2.26	0.10	6.74	20.41	16.34	2.00	1.85
		FB 109	0.64	1.10	0.01	0.16	1.70	0.07	3.91	4.64	15.09	6.63	1.62
		FB 115	0.12	0.91		0.33	1.92	0.14	3.48	8.91	15.30		1.83
		FB 123	0.15	0.93	0.10	0.12	2.28	0.21	5.24	31.52	15.04		1.70
	angulicos.	FB 128a	0.19	0.91	0.03	0.22	1.64	0.28	2.92	17.02	13.45	2.87	3.10
		FB 134a	0.24	1.08	0.16	0.51	2.07	0.08	5.70	17.88	15.64	1.53	1.77
		FB 136	0.23	0.73	0.03	0.46	1.48	0.10	4.78	24.86	13.74	0.91	1.95
		FB 139	0.39	1.08		0.21	1.23	0.16	2.56	5.23	11.14	1.80	2.01
	catulloi	FB 371	0.55	2.04	0.09	0.18	1.08	0.09	2.64	8.95	10.37		1.99
		FB 373a	0.49	4.60	0.42	0.50	1.36	0.37	1.56	22.37	12.40		1.62
		FB 373d	0.76	5.21	0.55	0.29	0.96	0.27	1.68	9.14	11.67		1.97
		FB 375	2.53	11.61	0.31	0.42	0.94	0.19	1.84	16.43	10.12		2.44
		FB 378	3.10	10.36	0.32	0.23	0.92	0.29	3.27	7.42	11.36		2.16
		FB 380a	1.09	7.74	0.29	0.31	0.89	0.04		13.40	13.22		2.18
		FB 380b	1.80	7.35	0.40	0.27	0.79	0.18		28.41	10.03		1.97
		FB 382a	2.08	6.96	0.15	0.32	1.01	0.09	1.36	7.07	11.37		2.29
		FB 382c	0.81	2.78	0.20	3.73	2.25	0.14		26.70	11.24		1.70
		FB 385	0.64	3.01	0.14	3.37	1.49	0.09	2.16	8.69	11.87		1.84
		FB 387b	0.37	2.08	0.14	0.39	1.79	0.17	3.54	9.88	11.96		3.19
		FB 391	0.24	0.84	0.03	0.29	2.35	0.26	3.01	8.32	11.93		1.79
		FB 396b	0.43	0.82	0.08	0.44	2.02	0.08	1.92	7.97	11.82		1.49
		FB 402b	0.12	0.63	0.12	0.20	1.37	0.14	2.12	20.70	12.44		
		FB 410	0.22	1.13	0.16	0.43	2.33	0.13	2.65	10.22	15.59	0.98	
early Barremian	no ammonite zonation	FB 417	0.13	0.89		0.24	1.05	0.11	1.48	5.95	12.97		
		FB 424	0.09	0.65	0.05	0.19	1.37	0.16	2.65	5.80	12.72		
		FB 430a	0.30	0.89		0.26	1.51	0.25	2.32	9.71	13.31	0.83	
		FB 433	0.11	1.00	0.01	0.22	0.97	0.12	1.88	6.88	11.71		
		FB 440a	0.13	1.73	0.02	0.28	1.93	0.18	3.58	12.15	15.39	1.03	1.60
		FB 448b	0.18	0.86	0.01	0.12	1.11	0.11	2.01	6.24	12.77		
		FB 451a	0.25	0.89	0.04	0.35	1.35	0.10	2.26	5.09	12.06		
		FB 454b	0.13	0.85	0.03	0.12		0.13	2.14	7.02	12.78		
		FB 459b	0.11	0.68		0.13	1.21	0.13	2.46	5.20	11.97		
		FB 464a	0.14	1.09	0.03	0.37	1.04	0.10	1.93	9.53	7.96		
		FB 469	0.16	0.93	0.04	0.32	1.25	0.10	2.72	6.54	12.49		
		FB 473b	0.29	0.85		0.21	1.14	0.06	1.85	5.73	13.86		
		FB 480a	0.13	0.85	0.10	0.24	1.27	0.10	2.88	17.81	12.31		1.96
		FB 487	0.10	0.85	0.04	0.29	1.86	0.23	3.18	3.34	17.36		
		FB 494b	0.23	1.08	0.04	0.24	1.22	0.09	1.71	41.15	16.10		
		FB 499a	0.45	1.82	0.17	1.76	1.45	0.11	2.84	66.11	15.79	2.32	1.42

VCD		Sample	U	V	Mo	As	Co	Cd	Cu	Zn	Ni	Pb	Cr
late Hauterivian	sayni	VCD 1A	0.64	8.74	0.27	1.38	2.28		7.55	26.45	11.68	2.22	7.73
		VCD 3A	0.52	6.28	0.02	0.45	2.08	0.02	7.44	23.04	16.91		6.58
		VCD 4A	0.59	4.92	0.25	0.56	1.79	0.03	8.04	14.88	18.34		4.97
		VCD 6A	0.43	5.02		0.25	1.99		7.26	19.28	17.01		5.01
		VCD 9A	0.42	4.36	0.10	0.13	1.37		6.41	12.55	14.31		5.11
		VCD 13A	0.72	6.27	0.33	0.46	1.91	0.01	7.98	15.41	17.41		6.14
		VCD 15A	0.54	6.17	0.08	0.64	2.06		7.40	12.24	16.34		4.59
		VCD 18A	0.77	6.40	0.19	0.46	1.29		7.08	15.07	14.44		4.85
		VCD 21A	0.76	5.82	0.34	0.66	1.76	0.03	9.08	17.76	16.73		6.02
		VCD 24A	0.48	5.79	0.41	0.70	1.64		6.70	13.81	16.87		5.56
		VCD 27A	0.65	8.14	0.21	1.24	1.92	0.04	6.92	19.41	13.19	4.67	5.97
		VCD 29A	0.43	6.98	0.15	0.91	2.12	0.08	9.10	31.52	14.93	2.84	5.92
	ligatus	SDII 1	0.48	6.60	0.29	1.21	2.16	0.07	7.63	20.81	14.79	3.49	5.12
		SDII 3	0.59	4.09	0.24	0.88	1.77	0.03	6.29	23.44	12.49	2.53	2.88
		SDII 5	0.52	5.17	0.07	0.82	1.51	0.05	5.43	21.42	20.02	4.22	4.50
		SDII 6	0.52	4.95	0.15	0.37	1.28	0.04	5.76	17.89	11.12	2.34	4.07
		SDII 7c	0.45	5.57	0.18	0.36	1.44	0.08	4.70	21.01	11.31	2.27	3.62
		SDII 10	0.53	6.33	0.19	0.85	1.93	0.03	8.60	23.37	15.30	5.20	4.51
		SDII 11	0.48	7.77	0.47	0.66	2.25	0.02	6.69	22.48	14.73		5.72
		SDII 13a	0.40	6.06	0.31	0.67	1.79	0.04	6.33	20.49	12.03	5.22	3.97
		SDII 14	0.51	4.33	0.15	0.55	1.76		6.25	15.62	12.48		2.43
		SDII 15	0.53	5.89		0.79	2.12		6.01	15.90	13.55		4.14
	balearis	SDII 16b	0.59	6.38		0.56	1.77		45.52	29.02	12.91		3.53
		SDII 18	0.54	5.26	0.26	0.67	1.93		5.45	17.30	12.72		4.04
		SDII 19	0.38	5.66	0.04	0.76	2.43	0.28	6.72	93.62	14.17	6.48	3.42
		SDII 21	0.68	4.92	0.14	0.47	1.64		4.05	17.02	12.65		4.36
		SDII 23	0.71	4.76		0.47	1.96		5.12	16.02	13.27		3.78
		SDII 25	0.57	5.54	0.02	0.62	1.37		9.60	14.59	11.24	1.87	3.76
		SDII 27	0.40	4.72		0.51	1.68		7.00	19.06	9.74	1.96	4.03
		SDII 28	0.53	5.32	0.06	1.53	3.94		10.82	31.10	19.45	4.59	4.16
		SDII 30	0.48	4.64		0.32	1.89		6.18	28.28	10.29	1.81	3.75
		SDII 33	0.74	7.73	0.12	0.95	2.79	0.07	11.08	37.47	16.66	3.37	8.04
		SDII 34	0.53	5.25		0.88	3.06		5.57	13.85	13.84	2.69	4.61
		SDII 36	0.53	4.46	0.01	1.28	2.60		5.38	27.48	13.70	3.48	2.30
		SDII 40	0.61	6.17		0.70	1.47		6.60	22.08	10.30	1.49	5.37
		VCDII 51A	0.42	4.33	0.10	0.61	2.40	0.09	6.76	22.40	10.58	2.24	4.39
		SDII 42	0.47	5.82		0.60	1.69		5.42	16.23	10.90	2.10	4.11
	angulicostata	VCDII 50A	0.64	4.96		0.47	1.35	0.03	6.25	13.85	9.02	1.34	3.57
		SDII 43	0.64	7.88	0.21	0.53	1.26	0.11	9.11	22.73	11.26	2.24	6.28
		VCDII 49A	0.60	6.28		1.01	3.11	0.14	7.24	38.48	13.49	1.64	4.93
		VCDII 48A	0.60	8.57		1.00	2.66	0.17	7.31	47.85	12.39	2.68	6.31
		VCDII 46A	0.75	5.33		0.45	1.71	0.03	7.64	24.44	10.43	1.25	3.61
		VCDII 44A	0.56	5.88		0.58	1.00		4.70	12.86	8.48		3.79
		VCDII 42A	0.53	5.15		0.54	1.86	0.05	5.89	13.90	8.57	0.89	4.19
		VCDII 40A	0.73	8.04	0.26	1.14	2.32	0.07	7.46	16.68	11.50	1.47	6.77
		SDII 51	0.49	6.52		0.44	0.99		7.19	19.08	10.36	1.47	5.11
		VCDII 37A	0.60	5.06		0.48	1.39		3.93	13.15	8.45	0.86	3.95
		VCDII 35A	0.39	4.82	0.01	0.44	1.32	0.02	4.59	13.49	7.57	1.16	3.06
		VCDII 33A	0.40	4.83		0.57	1.77		5.47	14.92	8.82	1.51	3.25
		VCDII 30A	0.39	4.39		0.48	1.11		4.59	10.09	13.62	0.96	3.33
		VCDII 27A	0.37	5.02		0.68	1.85		3.90	22.87	9.85	0.89	2.66
		VCDII 25A	0.70	8.50	0.04	1.03	3.63		10.99	36.43	16.85	2.43	8.37
		VCDII 22A	0.88	6.95	0.01	1.20	2.84	0.12	9.23	47.93	14.57	3.26	4.65

Table C.2.1

VCD		Sample	U	V	Mo	As	Co	Cd	Cu	Zn	Ni	Pb	Cr
late Hauterivian	angulicostata	VCDII 19A	0.59	7.16		1.15	2.34		7.02	21.65	14.25	2.73	5.43
		VCDII 16A	0.94	11.69	1.22	2.54	1.51		5.44	13.43	11.39	1.13	3.60
		VCDII12A	0.68	6.79	0.75	1.13	1.66	0.05	5.27	13.92	6.94	1.19	3.28
		VCDII10A	0.53	3.96		0.73	1.45	0.02	5.45	14.87	7.66	1.59	2.40
		VCDII8A	0.46	4.48		0.51	1.57	0.03	6.46	17.02	7.54	1.28	3.81
		SD 42	0.44	6.50		0.75	1.88	0.05	5.53	20.46	12.37	4.58	5.72
		VCDII6A	0.41	4.14		0.74	1.63		4.41	15.89	8.05	1.44	2.15
		SD 38	0.48	6.45	0.31	0.89	1.62	0.04	5.81	17.32	11.00	1.47	3.83
		SD 36	0.43	5.24		0.38	1.22	0.03	6.02	20.50	11.61		2.94
		SD 32	0.41	5.88		0.51	1.12	0.05	4.66	16.93	12.01	1.30	4.07
		SD 29	0.37	5.39	0.07	0.88	1.91		5.25	17.39	10.62	2.20	4.09
		SD 27	0.49	1.88			1.24	0.01	5.65	15.35	12.01	2.43	
		SD 24	0.50	1.79			2.02		5.72	18.61	11.17	1.30	
Barremian	hugii	SD 21	0.36	2.17			0.97		5.69	7.73	11.63	1.61	
		SD 19	0.44	2.69			1.25		5.97	11.26	11.74	1.92	
		SD 16	0.37	2.54			1.42		5.60	16.38	18.00	2.43	
		SD 12	0.49	2.67			1.22		7.72	12.33	11.73	1.44	
		SD 8	0.37	1.96			1.99		6.60	18.12	10.74	1.56	
		SD 5	0.42	4.14		0.05	2.36		5.82	14.32	12.02	1.84	
		SD 1	0.46	5.18		0.30	2.61		6.08	25.27	14.83	3.05	

Angles		Sample	U	V	Mo	As	Co	Cd	Cu	Zn	Ni	Pb	Cr
late Hauterivian	balearis	AN 2	0.57	7.78	0.60	0.82	1.04	0.02	5.54	16.12	13.14	1.52	6.69
		AN 4	0.50	4.88	0.26	0.65	1.36	0.02	4.47	17.42	12.63	2.00	3.87
		AN 6	0.60	5.04	0.20	0.77	1.49	0.03	4.68	21.93	13.41	2.35	3.68
		AN 8	0.71	5.03	0.33	0.44	1.01	0.06	5.91	35.59	12.25	1.25	4.79
		AN 10	0.88	4.87	0.14	0.77	1.79	0.02	5.79	15.46	13.57	1.54	4.44
		AN 13	0.64	3.64	0.11	0.29	0.97	0.01	3.72	13.18	11.18		3.29
		AN 15.1	0.57	2.62	0.19	0.39	1.23	0.03	3.58	11.36	11.29	1.05	2.75
		AN 16	0.52	2.75	0.14	0.36	1.28		3.64	7.65	11.24	1.28	2.33
		AN 18	0.55	3.89	0.40	0.45	1.32	0.05	4.88	30.37	11.16		3.70
		AN 20	0.49	3.43	0.45	0.25	0.80	0.04	3.11	17.93	8.95	0.91	3.41
		AN 23	0.91	4.13	0.16	0.41	1.36	0.07	6.66	17.79	12.45	1.48	3.61
		AN 26	0.76	2.92	0.18	0.30	0.83		4.32	14.90	9.81	0.98	3.79
		AN 27.2	0.62	4.64	0.25	0.66	1.15	0.11	6.85	26.72	11.30	1.91	4.43
		AN 29	0.55	2.70	0.44	0.73	1.11	0.03	3.35	13.45	10.79	1.55	2.63
		AN 31	0.67	3.04	0.17	0.61	1.17	0.02	4.61	20.26	11.28	1.24	3.18
		AN 33	0.47	2.71	0.11	0.40	1.06		3.42	6.85	10.55	1.16	3.11
		AN 35	1.02	4.02	0.13	0.50	1.05	0.09	5.49	16.32	11.66	1.62	2.99
	angulicostatum	AN 38	0.48	2.45	1.02	1.49	5.15	0.39	5.92	75.44	24.32	6.24	2.39
		AN 40	0.63	4.15	0.57	0.61	0.98	0.20	4.40	23.53	10.43	1.99	3.30
		AN 43	0.73	3.97	0.24	0.57	1.25	0.09	5.67	18.99	11.65	1.93	3.81
		AN 46	0.49	2.85	0.06	0.35	1.08	0.04	3.60	15.65	11.06	0.96	2.90
		AN 49.1	0.73	4.18	0.10	0.43	1.13	0.11	3.93	48.61	10.54	1.13	3.00
		AN 50	0.49	3.45	0.36	0.35	0.77	0.06	3.22	14.54	9.72	1.21	2.65
		AN 51	1.05	4.62	0.59	0.74	1.16	0.08	5.34	26.19	12.53	1.58	3.48
		AN 52	1.43	8.93	4.87	4.80	2.36	2.12	6.41	420.80	26.63	5.73	2.14
		AN 53.2	1.28	7.43	4.61	3.45	1.42	0.05	3.83	13.13	23.69	4.81	1.99
	mortilleti	AN 55	2.07	4.75	0.14	0.20	0.71	0.03	3.16	25.79	8.58	1.02	2.35
		AN 62.1	0.78	4.79	0.44	0.64	1.03		3.52	17.13	10.21	1.08	2.45
		AN 65.1	0.98	4.38	0.16	0.54	1.56		3.93	12.59	11.89	2.06	1.87
		AN 68	0.79	4.61	0.20	0.46	0.98	0.06	4.69	24.61	10.37	1.03	3.13
early Barremian		AN 71	0.89	4.22	0.06	0.47	0.99		3.70	15.91	10.74	1.22	2.40
	kiliani	AN 72	1.17	4.61		0.31	1.05	0.12	4.14	23.89	11.19	1.91	2.22
		AN 75	0.53	3.57	0.05	0.38	1.03	0.02	3.44	16.25	10.10	1.15	2.76
		AN 78	0.54	5.00	0.17	0.62	2.17	0.04	4.18	29.54	11.93	1.57	3.40
		AN 81	0.73	5.30	0.04	0.50	1.30	0.08	4.84	33.86	10.64	1.51	2.83
		AN 84	0.52	4.88	0.18	0.42	1.28	0.04	3.50	26.82	11.05	1.35	2.44
		AN 87	0.59	7.34	0.61	0.88	1.57	0.04	5.15	17.40	12.42	2.05	5.31
		AN 89	0.56	5.17	0.21	0.61	1.25	0.03	3.89	14.02	9.25	1.26	3.48
		AN 90	0.56	4.98	0.29	0.86	1.79		4.52	18.55	13.17	2.06	3.59
		AN 92	0.40	4.08	0.20	0.58	1.34	0.04	4.55	12.24	11.60	2.37	3.18
		AN 93	0.37	3.59	0.03	0.46	1.25	0.02	3.62	16.10	11.02	1.36	3.52
	nicklesi	AN 95	0.51	3.95	0.21	0.87	1.47	0.06	5.80	17.18	10.65	1.74	3.31
		AN 97	0.49	3.13	0.07	0.42	1.11	0.06	3.85	15.57	11.56	1.26	2.64
		AN 98	0.53	3.49	0.21	0.75	1.50	0.11	11.51	29.09	10.91	1.40	2.71
		AN 101	0.71	4.92	0.23	0.92	1.33	0.04	6.11	23.13	12.82	2.21	3.65
		AN 103	0.57	6.88	0.65	1.02	2.01	0.06	6.03	30.35	12.74	2.42	4.53
		AN 104	0.52	5.15	0.37	1.10	1.30	0.06	6.05	24.55	11.33	2.22	4.06
		AN 105	0.52	4.47	0.63	1.22	1.49	0.05	6.94	33.44	11.80	2.28	3.79
	pulchella	AN 108	0.89	5.81	0.71	1.08	1.49	0.08	6.21	37.61	11.22	2.20	3.37
		AN 109.4	0.49	4.14	0.69	1.14	1.72	0.02	5.75	29.79	11.49	2.08	3.04
		AN 110.1b	0.68	5.48	1.11	1.36	1.73	0.04	5.34	52.45	13.14	2.66	3.08
		AN 110.3c	0.62	3.99	0.33	0.67	1.38	0.08	4.04	47.02	10.42	0.91	2.64
		AN 110.4	1.04	5.03	0.47	1.07	1.09	0.07	5.29	21.30	11.21	1.77	2.88
		AN 111.2	0.80	5.36	0.12	0.87	0.88	0.05	4.58	20.12	8.83	1.50	2.58
		AN 111.5	1.22	7.64	0.72	1.12	1.20	0.09	5.10	65.66	10.84	1.86	3.26
		AN 112.2	0.74	6.66	0.17	0.55	1.33	0.07	4.41	23.15	10.43	1.24	2.52
	compressissima	AN 112.7	0.59	5.55	0.42	0.63	1.04	0.08	4.12	150.20	10.55	1.83	2.41
		AN 114.2	0.68	4.61	0.41	0.88	0.93	0.04	4.68	24.82	10.13	1.43	1.80
		AN 115	0.77	6.43	0.62	1.21	1.05	0.03	5.45	24.46	13.81	9.36	2.57
		AN 117	0.60	4.16	0.30	0.74	1.27	0.05	5.44	24.94	10.40	1.36	1.87
		AN 119	0.57	3.10	0.23	0.34	1.00	1.25	4.83	80.29	10.27		1.55
		AN 121	0.54	3.38	0.12	0.32	1.34	0.06	3.29	18.69	10.94	0.99	1.86
		AN 123	0.57	4.26	0.27	0.53	1.38	0.08	4.57	30.62	11.74	1.10	2.53
	darsi	AN 125	0.96	6.99	0.73	1.06	1.95	0.05	7.09	41.84	14.53	1.94	3.81
		AN 127	1.02	4.27	0.32	0.36	0.76	0.03	5.15	18.56	8.52		1.98
		AN 128	0.76	3.24	0.34	0.42	0.84	0.07	4.39	14.86	9.74		1.69
		AN 129	0.75	4.25	1.70	2.58	1.76	0.09	6.48	23.92	12.89	1.88	2.28
		AN 131	0.84	8.34	0.73	0.95	1.25	0.03	7.52	21.95	13.50	1.47	1.90
		AN 133	0.84	3.10	0.39	1.08	1.00	0.10	6.30	21.42	12.97	1.45	2.01
		AN 136.2	0.61	4.88	0.47	1.94	2.27	0.07	8.46	29.82	14.45	3.71	2.89
		AN 138	0.70	3.41	0.57	1.10	0.97	0.21	6.72	44.43	11.66	1.36	1.17
		AN 139d	1.08	3.54	0.16	0.63	0.94	0.17	4.86	26.74	11.87	1.95	3.74

Table C.2.1 (continued) – Redox-sensitive trace elements analyses in limestones for the three studied sections (expressed in ppm). The dark grey band indicates the Faraoni Level or its equivalent. No value is indicated when below the limit of detection.

Fiume-Bosso		Sample	U	V	Mo	As	Co	Cd	Cu	Zn	Ni	Pb	Cr
late Hauterivian	angu.	FB 133	2.01	69.51	2.96	15.55	39.00	1.62	93.32	287.33	136.27	39.08	38.66
		Fb 138	3.97	27.74	1.00	19.77	41.14	1.20	139.33	235.05	99.30	26.68	33.83
		FB 372	9.47	84.72	1.90	14.29	58.25	3.38	214.15	528.47	223.99	50.01	53.08
	catulloi	FB 374	12.83	345.94	61.83	177.42	84.54	10.48	270.70	1068.19	533.54	49.22	66.55
		FB 377	6.29	68.15	15.97	8.13	9.42	4.32	23.68	220.95	99.15	4.49	8.79
		FB 379	15.40	306.71	19.28	28.51	67.00	4.23	273.71	701.05	428.86	33.57	71.43
		FB 381b	9.92	151.09	28.26	33.44	29.64	5.06	61.67	313.80	268.18	14.52	22.21
		FB 384	12.04	169.53	5.48	40.58	106.59	3.83	211.07	612.52	277.61	51.44	66.48
		FB 397	2.85	20.43	0.30	8.25	67.51	0.90	164.07	248.47	143.25	34.58	33.69

VCD		Sample	U	V	Mo	As	Co	Cd	Cu	Zn	Ni	Pb	Cr
late Hauterivian	angulicostata	VCDII 10b	1.38	12.59	0.45	1.89	4.14	0.13	14.62	50.26	19.43	2.25	12.93
		VCDII 11b	1.29	8.27	0.29	1.87	3.84	0.21	13.77	49.12	21.39	3.79	8.43
		VCDII 14b	0.82	5.47	0.57	1.95	3.00	0.05	10.19	20.06	19.01	1.90	7.22
		VCDII 17b	3.27	15.21	1.59	6.74	3.46	0.60	15.77	53.27	23.53	3.95	8.34
		VCDII 18b	1.26	11.67	0.12	2.37	4.93	0.05	16.14	51.92	27.56	4.30	13.63
		VCDII 20b	1.45	11.60		3.44	7.42	0.20	18.30	86.81	37.34	9.23	11.95
		VCDII 25b	1.08	8.15		1.85	5.13	0.43	19.39	112.65	28.29	4.37	9.33
		VCDII 26b	1.05	8.56		2.68	4.41	0.13	15.84	56.10	23.71	5.68	9.18
		VCDII 27b	1.31	11.47	0.21	1.94	4.38	0.07	20.00	49.23	28.48	3.75	13.25
		VCDII 28b	1.06	13.37	0.15	2.16	5.01	0.16	16.50	61.06	21.64	4.25	12.78
		VCDII 29b	0.91	7.75	0.06	1.47	3.00	0.13	14.43	36.53	20.36	3.41	7.89
		VCDII 30b	1.03	6.84	0.03	1.44	4.01	0.07	17.12	41.84	22.74	3.64	8.05
		VCDII 31b	1.17	6.99	0.19	2.09	5.13	0.06	15.28	36.51	26.18	5.04	8.26
		VCDII 32b	1.24	9.64	0.03	1.52	4.43	0.17	19.81	47.95	28.04	3.25	13.09
		VCDII 33b	1.50	11.92	0.17	2.30	4.63	0.10	24.18	65.32	34.76	6.90	13.59

Angles		Sample	U	V	Mo	As	Co	Cd	Cu	Zn	Ni	Pb	Cr
late Hauterivian	angulicostatum	AN37b	1.92	21.45	0.57	2.86	5.76	0.56	42.80	100.62	50.60	12.67	26.37
		AN38b	1.59	14.64	0.44	3.13	5.71	0.38	38.98	81.97	38.78	13.09	16.89
		AN39b	1.62	16.99	1.15	4.12	6.64	1.28	36.73	167.87	42.80	14.17	16.63
		AN40b	2.17	16.34	0.71	3.86	6.89	0.56	44.88	139.18	42.11	22.05	16.67
		AN41b	2.56	22.10	0.73	4.47	8.67	0.84	58.35	205.46	55.25	20.63	23.53
		AN42b	2.28	15.30	0.16	2.99	5.63	0.58	39.87	110.99	42.70	10.33	17.90
		AN43b	1.59	12.39	0.27	1.73	3.39	0.35	24.57	74.26	29.27	7.90	12.99
		AN44b	1.58	12.78	0.28	2.41	3.88	0.34	28.36	72.99	27.64	10.51	14.37
		AN45b	2.32	31.12	0.57	4.80	13.38	0.32	57.41	111.72	55.01	16.73	30.66
		AN46b	2.15	12.78	0.25	3.45	7.80	0.39	48.73	103.01	68.49	9.22	15.47
		AN48b	1.85	18.98	0.37	3.35	6.26	0.49	44.40	114.71	37.86	10.54	21.80
		AN51b	3.54	19.23	2.97	2.06	1.82	0.06	8.39	31.71	33.60	3.61	8.42
		AN52b	3.73	27.35	1.78	4.71	4.19	0.45	19.08	91.12	51.41	7.13	17.08
		AN53.1b	2.98	18.84	3.30	1.52	1.69	0.06	10.16	19.16	38.32	3.13	7.90
Barr.	kilian.	AN72b	1.59	10.45	0.37	3.20	3.72	0.22	25.72	136.80	24.11	7.30	8.84
		AN73b	1.61	10.84	0.31	2.94	6.00	0.50	22.91	138.40	32.25	7.44	10.76
		AN75b	1.48	13.92	0.19	3.39	5.66	0.29	26.22	128.48	33.94	8.73	14.48

Table C.2.2 – Redox-sensitive trace-element analyses in marlstones for the three studied sections (expressed in ppm). The dark grey band indicates the Faraoni Level or its equivalent. No value is indicated for values below the limit of detection.

with very high maximum values (10.5, 273.7, 1068.2, and 533.5 ppm respectively). On the other hand, it appears that Pb and Cr record a negative shift.

C.2.4.1.2. The Veveyse de Châtel-St. Denis section

In this section, the data obtained in limestone samples for U, V, Mo, and As contents show a behaviour similar to that of the Fiume-Bosso section, with the difference that peaks are less pronounced in comparison to the background level (Fig. C.2.4, Table C.2.1). We also note that the background levels are generally higher in the lower part of the section, below the "couches à poissons" (Faraoni Level equivalent), with the exception of Mo, which shows an interval of increased values only in the first 40 m of the measured section. Interestingly, U and V present a double peak in contents around the level of the "couches à poissons", with the higher peak representing the "couches à poissons" itself. The average values of the background levels correspond to approximately 0.5, 5.4, 0.09. and 0.8 ppm and the maximum values are approximately 0.9, 11.7, 1.2, and 2.5 ppm, for U, V, Mo and As contents, respectively. The data obtained in the marls show equally a clear enrichment of U, V, Mo, and As around the Faraoni Level (Table C.2.2).

Co contents in limestone show a small overall decrease from the bottom to the top of the section, with a mean value of about 1.7 ppm. A peak is distinguished 5 m below the equivalent of the Faraoni Level, reaching 3.6

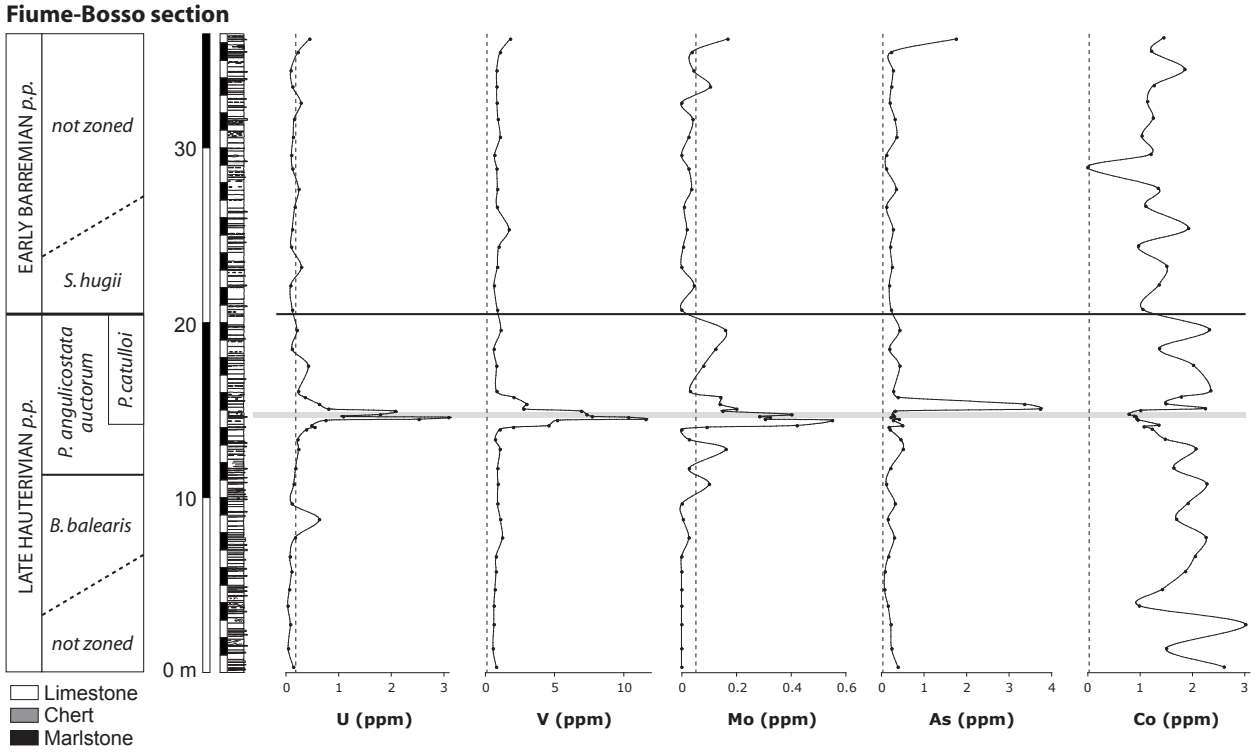

Fig. C.2.3 – Redox sensitive trace elements distributions for the Fiume-Bosso section. The grey band indicates the position of the Faraoni Level and the dashed line the limit of quantification for each element.

ppm. In the marls, a peak reaching 7.4 ppm is distinguished 3 m below the Faraoni Level.

In this section, the Cu, Zn, Ni, and Pb show a small positive shift in the limestone 5 m below the Faraoni Level equivalent. They correspond to the peaks of U, V, and Co. Cu and Zn show equally a peak approximately 40 m below the Faraoni Level, at the beginning of the *B. balearis* zone. On the other hand, in the marls, only Cd is enriched within the Faraoni Level equivalent, whereas enrichment of Cd, Zn, Ni and Pb characterizes again the beds situated 5 m below this level.

C.2.4.1.3. The Angles section

In the limestone samples, the trends in U, V, Mo, and As contents are comparable to the other two sections, with peak values at the level of the Faraoni Level equivalent (Fig. C.2.5, Table C.2.1). Whereas the background levels are low and rather constant for U, Mo, and As, V contents show a more variable evolution, with a series of positive excursions above the Faraoni Level equivalent. The average values for the background levels are at about 0.7, 4.5, 0.2, and 0.6 ppm and the maximum values correspond to approximately 2.1, 8.9, 4.9, and 6.3 ppm, for U, V, Mo, and As contents, respectively. The data obtained in the marl samples show equally a clear enrichment of U, V, Mo, and As around the Faraoni Level equivalent (Table C.2.2).

The overall trend in Co contents in limestone is more or less constant, with average values oscillating around 1.3 ppm. A peak with a value of 5.1 ppm is distinguished approximately 6 m below the equivalent of the Faraoni Level (bed AN 38). In the same bed, a small peak is present in the Mo and the As curves. Within the equivalent of the Faraoni Level, a small peak of Co reaching 2.4 ppm is distinguished. The data obtained in the marls show equally a clear enrichment of U, V, Mo, and As around the Faraoni Level equivalent (Table C.2.2). In the marl samples, a remarkable peak in Co contents characterizing the Faraoni Level equivalent has not been observed. A maximum of 13.4 ppm is seen within bed AN 45b.

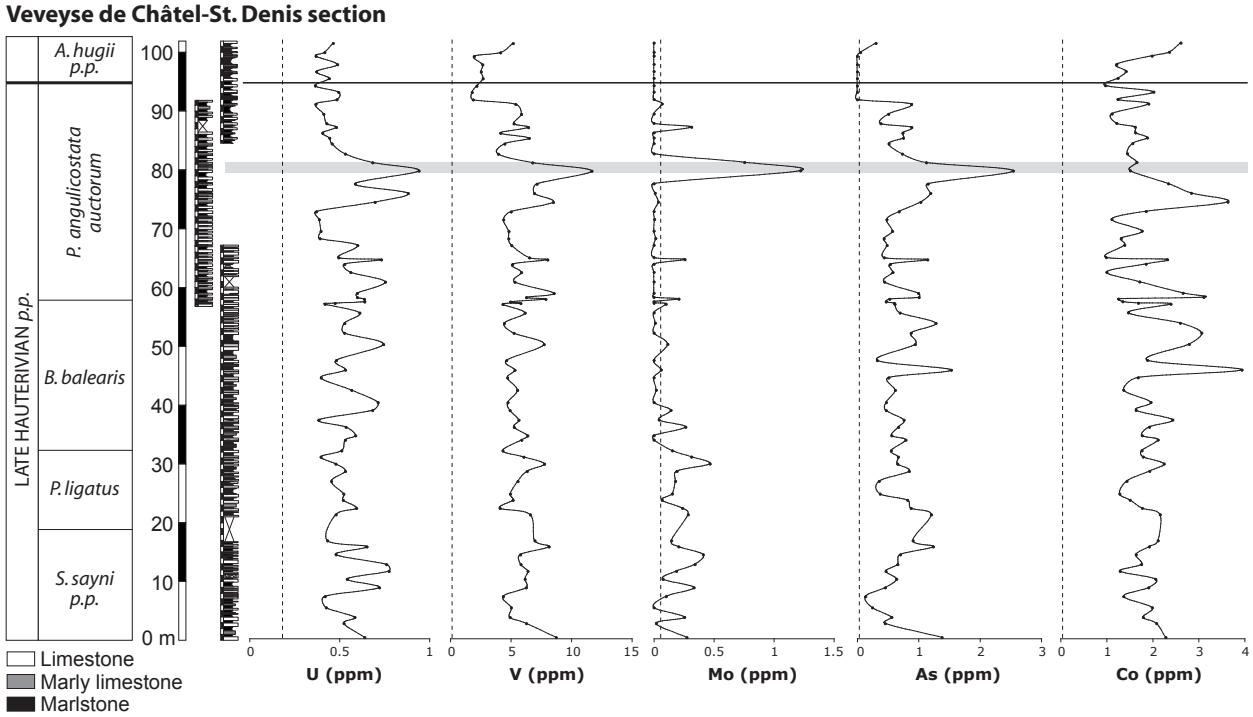

Fig. C.2.4 – Redox sensitive trace elements distributions for the Veveyse de Châtel-St. Denis section. The grey band indicates the position of the "couche à poissons" (Faraoni Level equivalent) and the dashed line the limit of quantification for each element.

In this section, a clear peak of Cd, Zn, Ni, and Pb occurs within the limestone beds of the Faraoni Level equivalent. Moreover, a peak of Ni and Pb marks bed AN 38. On the other hand, no significant peak of these elements has been found in the Faraoni Level equivalent marls. We notice, however, that all these elements are more concentrated in the marls below the Faraoni equivalent than above.

C.2.4.2. Total organic carbon (TOC)

In the limestone samples, measured TOC values are not higher than 0.1%. We will therefore restrict our discussion to the results obtained in the marl samples (see Fig. C.2.6). In the Fiume-Bosso section, a maximum TOC value of 14.8% has been measured in the thin marl level interval just below the Faraoni Level. Within the Faraoni Level, the average value of TOC is close to 3.25%. These values are not significantly different from those obtained in marl samples above and below the Faraoni Level.

In the VCD section, no major variations have been measured (Fig. C.2.6). The average value is close to 0.5% and the Faraoni Level equivalent TOC value is equal to 0.31%. In the Angles section, no major variation has been observed as well. The TOC values are however higher and reach 2.63 %. TOC values in the Faraoni Level equivalent are close to 1.25%.

C.2.5. Discussion

C.2.5.1. Comparison between the three sections

Trends in U, V, Mo, and As contents are all characterized by pronounced positive peaks marking the Faraoni Level and its equivalent, and are very distinct relative to the measured intervals below and above this level, representing the upper Hauterivian and the lower Barremian. This positive peak is present in both limestone and marl samples, despite differing background level values. For the trends in Co, Cd, Cu,

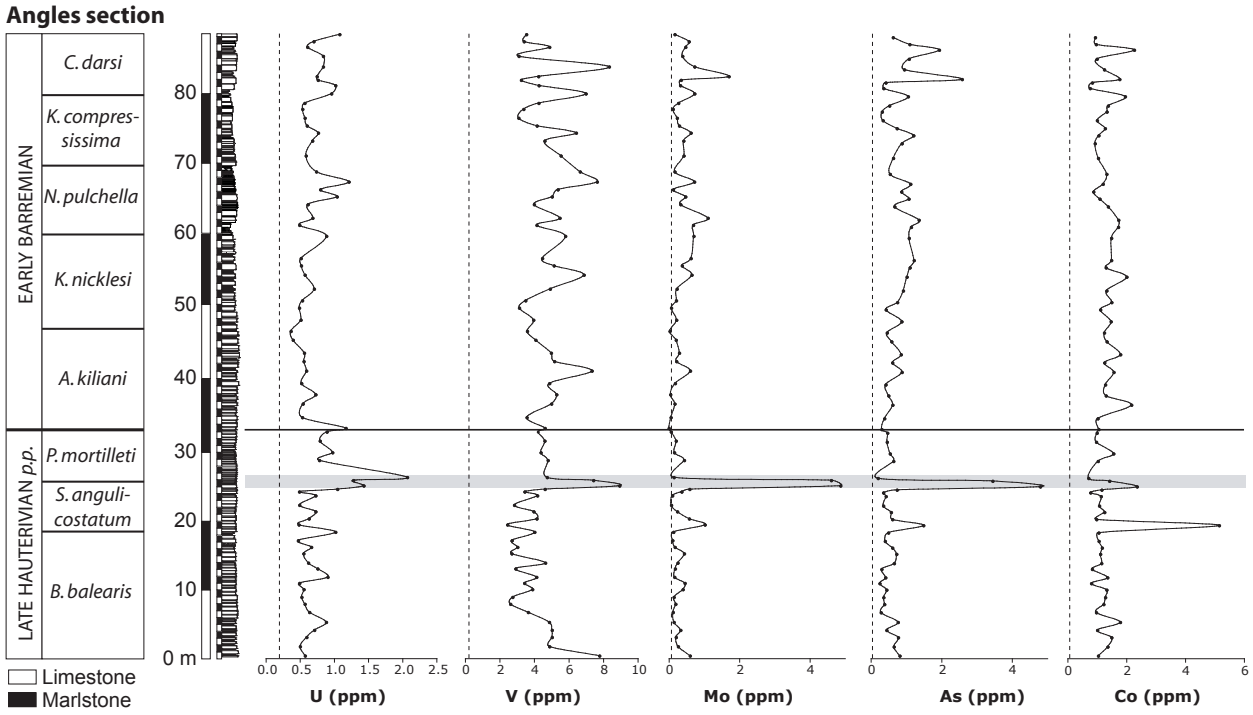

Fig. C.2.5 – Redox sensitive trace elements distributions for the Angles section. The grey band indicates the position of the Faraoni Level equivalent and the dashed line the limit of quantification for each element.

Zn, Ni, Pb, and Cr contents, no significant overall variations are observed and no specific enrichments are recorded for the Faraoni Level and its equivalent apart from local variations.

C.2.5.2. Behaviour of U, V, Mo, Co, and As

Enrichments in U, V, and Mo are well known for numerous black shales of the Phanerozoic (e.g., Brumsack and Gieskes 1983; Brumsack 1989; Coveney et al. 1991; Sun and Püttmann 1997; Nijenhuis et al. 1999; Warning and Brumsack 2000; Yarincik et al. 2000; Mangini et al. 2001; Tribovillard et al. 2004; Wilde et al. 2004; Brumsack, 2006). U and V enrichments are usually associated to anoxic to euxinic bottom-water conditions during the time of deposition (e.g., Hastings et al. 1996; Morford and Emerson 1999; Mangini et al. 2001). Under mildly reducing and anoxic conditions, U and V may be removed from the ocean by the formation of organo-metal ligands in humic acids; by crystalline precipitation (UO_2 and V_2O_3 or $V(OH)_3$), and V may also be removed by surface-adsorption processes (Algeo and Maynard 2004). For Mo, Algeo and Maynard (2004) propose adsorption onto humic substances as a main possible mechanism to transfer this element from the water column into the sediment, and under euxinic conditions, by a rapid uptake by authigenic/syngenetic sulfides.

Overall, the solubility of these three elements decreases in the reduced state, and their precipitation and enrichment in sediments is favoured during periods of anoxia (e.g. Yarincik et al. 2000; Mangini et al. 2001; Algeo and Maynard 2004).

Co shows a more complex behaviour in the three sections studied here. This element should behave similar to U, V and Mo, and indeed, in oxygen-depleted waters, Co forms an insoluble sulfide (CoS) that is trapped in sediments (Algeo and Maynard 2004). These sulfides are taken up in solid solution by authigenic Fe sulfides (Huerta-Diaz and Morse 1992). But, because of the slow kinetics of this uptake, significant Co enrichment in the sedimentary environment is limited to euxinic conditions (Sun and Püttmann 1997; Algeo and Maynard 2004).

Sedimentary enrichments in As are less well documented from the geological record. As is usually mobile under slightly reducing conditions through the reductive dissolution of the As bearing phases (Fe (hydr)oxides). Furthemore, Bostick and Fendorf (2003) detailed the mechanisms of As uptake in more anoxic environments and demonstrated the surface precipitation of As on iron sulphide minerals. This hypothesis is supported by Huerta-Diaz and Morse (1992) who noted a close link between As and pyrite in sediments underneath anoxic water. Hence, the presence of abundant marcasite nodules within the Faraoni Level in central Italy (Cecca et al. 1994) is compatible with the enrichment in As.

An increased input of trace metals in the ocean in association with large igneous province (LIP) activity has been forwarded as an alternative explanation for trace-metal enrichment in mid-Cretaceous organic-rich sediments, which were formed during oceanic anoxic events (e.g., Sinton and Duncan 1997; Larson and Erba 1999; Leckie et al. 2002; Erba 2004; Snow et al. 2005). For the late Hauterivian, however, there is no evidence for LIP volcanism so far (e.g., Larson 1991; Courtillot and Renne 2003), although a certain degree of volcanic activity has been documented at Rio Grande, documenting the end of the Paraná continental flood basalts (Stewart et al. 1996). The volume of lava emitted during this episode is one order of magnitude lower compared to other LIP's. Moreover, Brumsack (2006) pointed out that trace-metal enrichment (with the exception of extreme enrichment of Ag, Cu, Ni, V and Zn) in sediments associated with the Cenomanian – Turonian boundary oceanic anoxic event may be explained by seawater as the mere source for these elements (see also Arthur et al. 1988; Piper 1994; Böning et al. 2004). The trace-metal enrichments calculated for the Faraoni event (Table C.2.3) are on the same order of magnitude as those calculated for present-day coastal upwelling zones and anoxic basins (e.g., Brumsack, 2006). We therefore exclude volcanic activity as a major source of trace-metal enrichment during the Faraoni event.

C.2.5.3. Redox conditions during the Faraoni event

The behaviour of the redox-sensitive elements, measured in and around the Faraoni Level and its equivalents, allows us to precise the redox conditions that were present during the Faraoni event. The enrichment of U, V, Mo, and As are interpreted as a signature of anoxic and euxinic conditions (Algeo and Maynard 2004). The conservative behaviour of Co during the Faraoni event with regards to its background level is characteristic of dysoxic to anoxic facies according to these authors. The Faraoni Level is therefore clearly the expression of an anoxic event (with eventually locally weakly euxinic conditions such as is indicated at Angles with regard to a small increase of the Co content). The fact that the other redox-sensitive trace elements studied here are not systematically enriched within the Faraoni Level underlines the limit of our comprehension of this system. Partial diagenetic remobilization or differences in sediment uptake processes may be evoked to explain the non-systematic presence of enrichments in the other studied trace elements. Such remobilization processes are thus thought to be responsible of the slight shift of Mo and As peak within the Angles section. Further investigations are however needed to resolve this problem.

Using total sulphur versus TOC plots, Baudin et al. (2002) argued for dysoxic rather than for truly anoxic conditions for the Faraoni Level. This observation together with the conservative behaviour of Co may hint at the possibility that the anoxic conditions were not so strong and closer to the dysoxia/anoxia threshold that to the anoxia/euxinic threshold (O_2 close to 0.2 ml/l of H_20), with the exception of the section at Angles, where conditions may have been more severe.

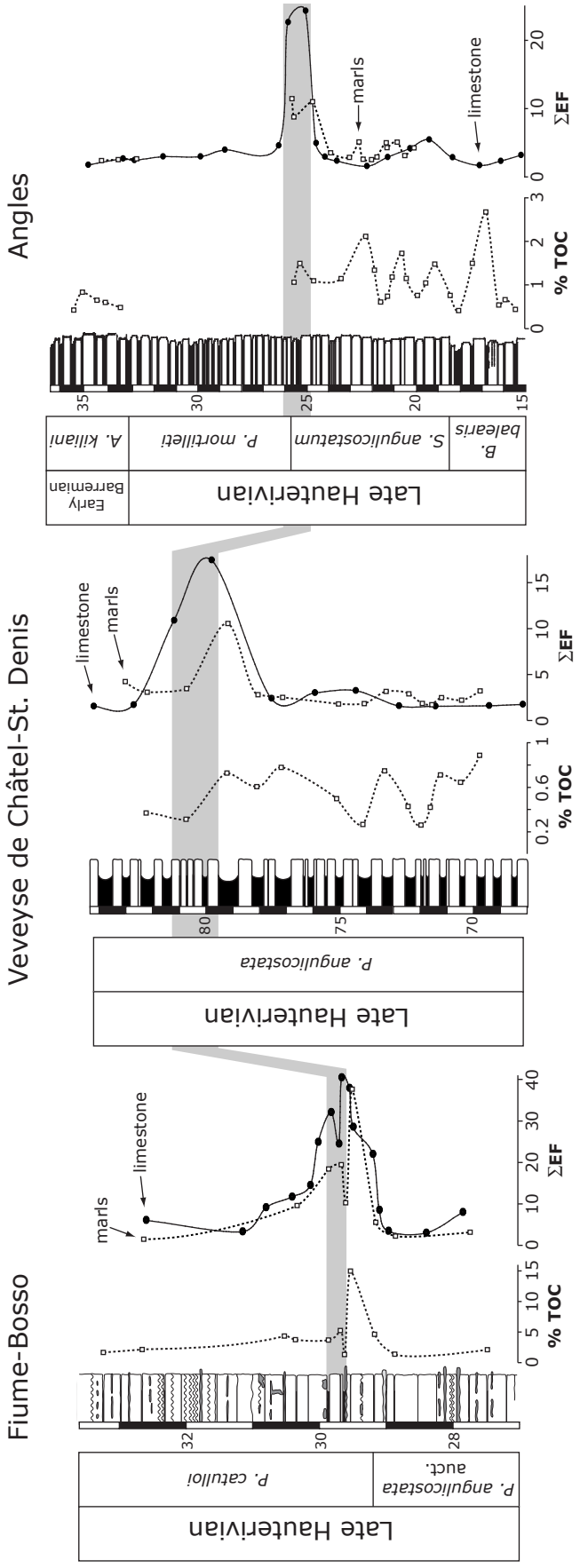

Fig. C.2.6 – Correlation of the Faraoni Level for the three different sections. For each section, the TOC analyses in marls as well as the Trace Element Index (∑EF) in both limestone and marls are figured. See text for ∑EF calculation details. The lithologic legend for each section is the same as in previous figures.

C.2.5.4. Local oxygen-deficient conditions below the Faraoni Level

In the Angles and the VCD sections, isolated maxima in trace-metal contents are recognized, notably below the Faraoni Level equivalent. In the VCD section, U, V, Zn, Ni, and Co contents show a peak 5 m below the Faraoni equivalent. In the Angles section, Mo, As, Ni, Pb, and Co contents show a peak 6 m below the Faraoni Level equivalent. These peaks are not correlated in time between the two sections and could have resulted from local changes in bottom-water oxygen conditions, resulting in local anoxia or euxinia.

C.2.5.5. Enrichment factors

For each separated lithology (i.e. limestones or marls), enrichment factors (EFs) were calculated for U, V, Mo, and As according to the following equation (see Table C.2.3 and Fig. C.2.6):

$$EFs = [Me]_{peak} / [Me]_{background}$$

In this equation, $[Me]_{background}$ represents the average value of the background level of the different curves and $[Me]_{peak}$ is the maximum value of the different peaks. The EFs thus obtained are coherent with those obtained by Morford and Emerson (1999) (for U, V, and Mo, and based on references therein) for anoxic conditions, representing another clue for anoxic conditions during the Faraoni event.

In order to compare the different sections, an enrichment factor index (∑EF) is calculated by adding the EFs of U, V, and Mo (see Fig. C.2.6). A clear peak is thus obtained for the three sections for both lithologies, underlining the higher uptake of U, V, and Mo in the sediment during the Faraoni event.

A remarkable feature of the Faraoni Level is the alternation between limestones and laminated shales, which is interpreted, in a first approximation, as the results of variations in oxygen content (see Westphal et al. 2004 for a review). The higher values of redox-sensitive trace elements in the Faraoni shales compared with the Faraoni limestones seem to confirm this hypothesis. However, if we look at the enrichment factors index (∑EF) calculated for both marls and limestones (Fig. C.2.6), such a dichotomy is not found. The variation of these indices is more or less the same within the same section. On the contrary, it seems that

(ppm)	Background level average	Maximum value of the peak	Enrichment factors
Fiume-Bosso			
U	0.17	3.1	**18.24**
V	0.9	11.6	**12.89**
Mo	0.03	0.55	**18.33**
As	0.3	3	**10.00**
Veveyse			
U	0.53	0.94	**1.77**
V	5.411	11.7	**2.16**
Mo	0.09	1.22	**13.56**
As	0.75	2.54	**3.39**
Angles			
U	0.69	2.1	**3.04**
V	4.55	8.9	**1.96**
Mo	0.24	4.87	**20.29**
As	0.65	4.8	**7.38**

Table C.2.3 – Background level values, maximum value of the peak and enrichment factors of U, V, Mo, and As for the three studied sections (see text for calculation details).

the limestones are a little bit more enriched in redox-sensitive trace elements than the marls during the Faraoni event compared to "normal" conditions. The higher redox-sensitive trace element content of the marlstones (compared to the limestones) is thus not induced by difference of synsedimentary redox conditions between marlstones and limestones (as already shown by Westphal et al. 2004), but is rather the result of synsedimentary condensation or early diagenetic processes. This underlines the importance of the lithology effect on analyses and the need to consider "mono-lithologic" analyses when discussing temporal variations.

In Fig. C.2.6, where the TOC is plotted versus the ∑EF, we remark that TOC is only clearly enriched in the Faraoni Level of the Fiume-Bosso section, whereas ∑EF shows a positive shift in all three sections. This allows us to postulate that the enrichment of redox-sensitive trace elements is a more conservative tracer of anoxic conditions than TOC contents. This latter may be more easily removed during diagenetic processes.

C.2.5.6. Chemostratigraphic tools

The distinct enrichment of the redox-sensitive elements U, V, Mo and As in the sedimentary environment during the Faraoni event appears to be unique for the examined time interval of the Late Hauterivian – Early Barremian and is therefore useful as a tracer of the Faraoni event within the Tethyan realm.

Outside the Tethyan realm, a distinct enrichment in U contents occurs in sediments of the Late Hauterivian of the Izu-Mariana margin, northwestern Pacific, in ODP hole 1149b, (ODP leg 185; Plank et al. 2000, upper part of the lithologic unit IV, interval 185-1149B-19R-1, see Fig. F27 and F72). This peak is associated with a layer containing elevated quantities of euhedral barite, along with dolomite rhombs and phosphatic fish remains. Plank et al. (2000) argue that this peculiar mineral assemblage indicates an episode of enhanced organic-matter accumulation, which they correlate with the Faraoni event. According to the data presented here, the enrichment in U represents a further strong argument in favour of this assumption. This suggests that the Faraoni event was not restricted to the western Tethyan realm, but may also be recorded in sediments of the northwestern Pacific. Further investigations - especially in sediments of the southern hemisphere - are required to confirm the global character of this event.

In the Fiume-Bosso section, the enrichment in U, V, and Mo contents began slightly before and ended slightly after the Faraoni Level s.s. This may indicate that the Faraoni anoxic event may have started slightly earlier and lasted longer than the time associated with the formation of the Faraoni Level itself. This would signify that the organic-rich facies of the Faraoni Level in the Italian sections does not reflect the entire period of oxygen depletion, but rather the time of important organic matter preservation and/or accumulation during the culmination of this event. This may be taken into account when tracing the equivalent of the Faraoni Level by using trace-metal enrichment in sections were ammonites are absent or extremely rare. The here described trace-metal enrichments trace the Faraoni anoxic event rather than the Faraoni Level itself.

C.2.5.7. Initiating factors of the Faraoni event

As recognized by Baudin et al. (2002) and Baudin (2005), the Faraoni Level and its equivalent can be qualified as an anoxic event. An important difference between the Faraoni event and other Cretaceous OAE's consists, however, in the fact that the anoxic event is not mirrored by a major shift in the carbon isotope record (e.g., Erba et al. 1999; van de Schootbrugge et al. 2000; Company et al. 2005; Godet et al. 2006), but only by a small positive excursion (0.5‰). Godet et al. (2006) explain this attenuated signal by a buffering effect on the carbon-isotope record exerted by the large size of the oceanic dissolved inorganic carbon reservoir. Furthermore, the classical scenario invoking an episode of intensified volcanism

and reinforced greenhouse conditions (e.g., Jenkyns 1999, 2003) is difficult to apply to this peculiar event. As previously said, there is no evidence for large igneous province (LIP) volcanism during the late Hauterivian so far, even if a certain degree of volcanism has been documented in Rio Grande. This volcanic activity is however one order of magnitude lower than that associated with LIP (e.g., Larson 1991; Courtillot and Renne 2003). We therefore consider the Rio Grande volcanism as not responsible for the Faraoni event, even if slightly stronger greenhouse conditions may have been induced by this volcanic episode.

As discussed by Baudin et al. (2002), the Faraoni Level corresponds to the maximum flooding surface (mfs) of the Ha6 sequence (Haq et al. 1987; Hardenbol et al. 1998). For the VCD section, Busnardo et al. (2003) attributed the "couches à poissons" to the transgressive surface (ts) of the Ha6 sequence, but A. Strasser (Fribourg, personal communication) correlates the same horizon also to the mfs of the Ha6 sequence (see also Bodin et al. 2006). The Ha6 mfs corresponds to the maximum of a second-order transgression (Haq et al. 1987; Hardenbol et al. 1998), which led to the connection of the Tethyan and the Boreal realms, as is suggested by belemnite migration patterns observed by Mutterlose and Bornemann (2000) and the presence of boreal nannoplankton in the Angles section around the Faraoni Level (Godet et al. 2006). This second-order transgression may have lead to the flooding of large epicontinental areas. Bodin et al. (2006) pointed out the role of this mechanism as the main trigger for the onset of anoxic conditions during the Faraoni anoxic event, by increased nutrient delivery, and the related increase in primary productivity (see also Company et al. 2005). Baudin et al. (2002) also proposed increased primary productivity as the prime factor leading to the origin of the Faraoni event along the line of the scenario proposed here.

C.2.6. Conclusions

Redox-sensitive trace elemental analysis is a fruitful method to better understand and constrain anoxic events. Indeed, the multi-element analysis discussed here provides additional insight into the oxygenation conditions during the Faraoni anoxic event and serves as a promising correlation tool, especially if biostratigraphic information is lacking.

By comparing the behaviour of the redox-sensitive trace elements with the specific enrichments in U, V, and Mo contents, the Faraoni Level appears to be the expression of anoxic conditions at least near the sediment-water interface. This interpretation is supported by the enrichment of As, which is largely controlled by its sorption onto sulfide minerals in anoxic environments (Bostick and Fendorf 2003). The lack of systematic enrichment of Cd, Cu, Zn, Ni, Pb, and Cr may be related to diagenetic removal or unknown synsedimentary differences in uptake processes.

In the sections analysed, the distinct enrichments in U, V, and Mo are a feature characteristic of the Faraoni Level, and are unique with regards to the time interval of the late Hauterivian and the early Barremian. We therefore propose to use this feature to correlate the Faraoni Level throughout the entire Tethys, and especially in sections where organic-rich intervals are lacking such as in the section of Angles, and to search for expressions of the Faraoni event also in other basins. For example, a distinct enrichment in U in sediments of late Hauterivian age in the northwestern Pacific may well be correlated with the Faraoni event (Plank et al. 2000, see Fig F27 and F72).

According to the general behaviour of the redox-sensitive trace elements in the three analyzed sections, the Faraoni Level may be the expression of a climax situation during a longer period of steadily increasing anoxia induced by a second-order sea level rise. The mobilization of nutrients during this sea level rise may have played an important role in the onset of the Faraoni event.

C.2.7. Acknowledgements

We thank B. van de Schootbrugge, H. Mort, P. Linder, and C. Rambeau for their help in the field, J. Charollais, H. Mort, and F. Baudin for stimulating discussions, T. Monnier for help in the laboratory work and the team of the "Reserve Géologique de Haute-Provence" for providing the authorization for field work and sampling in this region. We also thank E. Erba and J. Hölemann for constructive criticism of the manuscript. Financial support from the Swiss National Science Foundation is gratefully acknowledged (projects 2100-067807/1 and 200020-105206/1).

C.2.8. References

Algeo TJ, Maynard JB (2004) Trace-element behavior and redox facies in core shales of Upper Pennsylvanian Kansas-type cyclothems. Chemical Geology 206: 289-318

Arthur MA, Jenkyns HC, Brumsack H-J, Schlanger SO (1988) Stratigraphy, geochemistry, and paleoceanography of organic carbon-rich Cretaceous sequences. In: Ginsburg RN, Beaudoin B (eds). Cretaceous resources, events and rhythms: Background and plans for research, Kluwer Academic Publishers, Digne, France, Proc. of ARW, pp. 75-119

Baudin F, Bulot LG, Cecca F, Coccioni R, Gardin S, Renard M (1999) Un équivalent du «Niveau Faraoni» dans le bassin du Sud-Est de la France, indice possible d'un événement anoxique fini-hauterivien étendu à la Téthys méditerranéenne. Bulletin de la Société Géologique de France 170: 487-498

Baudin F, Cecca F, Galeotti S, Coccioni R (2002) Palaeoenvironmental controls of the distribution of organic matter within a Corg-rich marker bed (Faraoni Level, uppermost Hauterivian, central Italy). Eclogae geologicae Helvetiae 95: 1-13

Baudin F (2005) A Late Hauterivian short-lived anoxic event in the Mediterranean Tethys: the "Faraoni Event". Comptes Rendus Geosciences 337: 1532-1540

Bayon MM, Alonso JIG, Medel AS (1998) Enhanced semiquantitative multi-analysis of trace elements in environmental samples using inductively coupled plasma mass spectrometry. Journal of Analytical Atomic Spectrometry 13: 277-282

Behar F, Beaumont V, Penteado HLD (2001) Rock-Eval 6 technology: Performances and developments. Oil and Gas Science and Technology 56: 111-134

Bodin S, Godet A, Föllmi KB, Vermeulen J, Arnaud H, Strasser A, Fiet N, Adatte T (2006) The Late Hauterivian Faraoni oceanic anoxic event in the western Tethys: Evidence from phosphorus burial rates. Palaeogeography, Palaeoclimatology, Palaeoecology 235: 245-264

Böning P, Brumsack H-J, Bottcher ME, Schnetger B, Kriete C, Kallmeyer J, Borchers SL (2004) Geochemistry of Peruvian near-surface sediments. Geochimica et Cosmochimica Acta 68: 4429-4451

Bostick BC, Fendorf S (2003) Arsenite sorption on troilite (FeS) and pyrite (FeS2). Geochimica et Cosmochimica Acta 67: 909-921

Brumsack H-J (1989) Geochemistry of recent TOC-rich sediments from the Gulf of California and the Black Sea. Geol. Rundsch. 78: 851-882

Brumsack H-J (2006) The trace metal content of recent organic carbon-rich sediments: Implications for Cretaceous black shale formation. Palaeogeography, Palaeoclimatology, Palaeoecology 232: 344-361

Brumsack H-J, Gieskes JM (1983) Interstitial water trace-element chemestry of laminated sediments of the Gulf of California (Mexico). Marine Chemistry 14: 89-106

Busnardo R (1965) Le stratotype du Barrémien. Mémoires du Bureau de Recherche Géologiques et Minières. 34: 101-116

Busnardo R, Charollais J, Weidmann M, Clavel B (2003) Le Crétacé inférieur de la Veveyse de Châtel (Ultrahelvétique des Préalpes externes; canton de Fribourg, Suisse). Revue Paléobiol., Genève 22: 1-174

Cecca F, Galeotti S, Coccioni R, Erba E (1996) The equivalent of the «Faraoni Level» (uppermost Hauterivian, Lower Cretaceous) recorded in the eastern part of Trento Plateau (Venetian southern Alps, Italy). Riv. Ital. Paleontol. Stratigr. 102: 417-424

Cecca F, Marini A, Pallini G, Baudin F, Begouen V (1994) A guide-level of the uppermost Hauterivian (Lower Cretaceous) in the pelagic succession of Umbria-Marche Apennines (Central Italy): the Faraoni Level. Riv. Ital. Paleontol. Stratigr. 99: 551-568

Coccioni R, Baudin F, Cecca F, Chiari M, Galeotti S, Gardin S, Salvini G (1998) Integrated stratigraphic, palaeontological, and geochemical analysis of the uppermost Hauterivian Faraoni Level in the Fiume Bosso section, Umbria-Marche Apennines, Italy. Cretaceous Research 19: 1-23

Company M, Aguado R, Sandoval J, Tavera JM, Jiménez de Cisneros C, Vera JA (2005) Biotic changes linked to a minor anoxic event (Faraoni Level, latest Hauterivian, Early Cretaceous). Palaeogeography, Palaeoclimatology, Palaeoecology 224: 186-199

Courtillot VE, Renne PR (2003) On the ages of flood basalt events. Comptes Rendus Geosciences 335: 113-140

Coveney JRM, Lynn Watney W, Maples CG (1991) Contrasting depositional models for Pennsylvanian black shale discerned from molybdenum abundances. Geology 19: 147-150

Erba E (2004) Calcareous nannofossils and Mesozoic oceanic anoxic events. Marine Micropaleontology 52: 85-106

Erba E, Bartolini A, Larson RL (2004) Valanginian Weissert oceanic anoxic event. Geology 32: 149-152

Erba E, Channell JET, Claps M, Jones CE, Larson RL, Opdyke B, Premoli-Silva I, Riva A, Salvini G, torriceli S (1999) Integrated stratigraphy of the Cismon APTICORE (Southern Alps, Italy): A "reference section" for the Barremian-Aptian interval at low latitudes. Journal of Foraminiferal Research 29: 371-391

Föllmi KB, Weissert H, Bisping M, Funk H (1994) Phosphogenesis, carbon-isotope stratigraphy, and carbonate-platform evolution along the Lower Cretaceous northern Tethyan margin. Geological Society of America Bulletin 106: 729-746

Godet A, Bodin S, Föllmi KB, Vermeulen J, Gardin S, Fiet N, Adatte T, Berner Z, Stüben D, van de Schootbrugge B (2006) Evolution of the marine stable carbon-isotope record during the early Cretaceous: a focus on the late Hauterivian and Barremian in the Tethyan realm. Earth and Planetary Science Letters 242: 254-271

Haq BU, Hardenbol J, Vail PR (1987) Chronology of fluctuating sea levels since the Triassic. Science 235: 1156-1167

Hardenbol J, Thierry J, Farley MB, de Graciansky P-C, Vail PR (1998) Mesozoic and Cenozoic Sequence Chronostratigraphic Framework of European Basins. In: de Graciansky P-C, Hardenbol J, Jacquin T and Vail PR (eds), Mesozoic and Cenozoic Sequence Stratigraphy of European Basins. Special Publication Society for Sedimentary Geology, pp. 3-13

Hastings DW, Emerson SR, Mix AC (1996) Vanadium in foraminiferal calcite as a tracer for changes in the areal extend of reducing sediments. Paleoceanography 11: 665-678

Hay WW, DeConto R, Wold CN, Wilson KM, Voigt S, Schulz M, Wold-Rossby A, Dullo W-C, Ronov AB, Balukhovsky AN, Soeding E (1999) Alternative global Cretaceous paleogeography. In: Barrera

E, Johnson C (eds), The Evolution of Cretaceous Ocean/Climate Systems. Geological Society of America Special Paper, pp. 332

Huerta-Diaz MA, Morse JW (1992) Pyritization of trace metals in anoxic marine sediments. Geochimica et Cosmochimica Acta 56: 2681-2702

Jenkyns HC (1999) Mesozoic anoxic events and palaeoclimate. Zentralblatt Geologie und Paläontologie 1 Heft 7-9: 943-949

Jenkyns HC (2003) Evidence for rapid climate change in the Mesozoic-Palaeogene greenhouse world. Philosophical Transactions of the Royal Society, London, A 361: 1885-1916

Jitaru P, Tirez K, De Brucker N (2003) Panoramic analysis for monitoring trace metals in natural waters by ICP-MS. Atomic Spectroscopy 24: 1-10

Jones CE, Jenkyns HC (2001) Seawater strontium isotopes, oceanic anoxic events, and seafloor hydrothermal activity in the Jurassic and Cretaceous. American Journal of Science 301: 112-149

Larson RL (1991) Latest pulse of Earth: Evidence for a mid-Cretaceous superplume. Geology 19: 547-550

Larson RL, Erba E (1999) Onset of the mid-Cretaceous greenhouse in the Barremian-Aptian: Igneous events and the biological, sedimentary and geochemical responses. Paleoceanography 14: 663-678

Leckie RM, Bralower TJ, Cashman R (2002) Oceanic anoxic events and plankton evolution: Biotic response to tectonic forcing during the mid-Cretaceous. Paleoceanography 17: PA000623

Lini A, Weissert H, Erba E (1992) The Valanginian carbon isotope event; a first episode of greenhouse climate conditions during the Cretaceous. Terra Nova 4: 374-384

Mangini A, Jung M, Laukenmann S (2001) What do we learn from peaks of uranium and of manganese in deep sea sediments? Marine Geology 177: 63-78

Morford JL, Emerson SR (1999) The geochemistry of redox sensitive trace metals in sediments. Geochimica et Cosmochimica Acta 63: 1735-1750

Mutterlose J, Bornemann A (2000) Distribution and facies patterns of Lower Cretaceous sediments in northern Germany: a review. Cretaceous Research 21: 733-759.

Nijenhuis IA, Bosch H-J, Sinninghe Damste JS, Brumsack H-J, De Lange GJ (1999) Organic matter and trace element rich sapropels and black shales: a geochemical comparison. Earth and Planetary Science Letters 169: 277-290.

Plank T, Ludden JN, Escutia C, et al. (2000) Proceeding of the Ocean Drilling Program, Initial Reports, 185 [Online], Available from World Wide Web: <http://www-odp.tamu.edu/publications/185_IR/185ir.htm>

Piper DZ (1994) Seawater as the source of minor elements in black shales, phosphorites and other sedimentary rocks. Chemical Geology 114: 95-114

Sanfourche J, Baudin F (2001) La genèse des évènements anoxiques de la période moyenne du Crétacé. Examen de l'hypothèse du meromictisme océanique. Annale de la Société Géologique du Nord 8: 107-119

Schlanger SO, Arthur MA, Jenkyns HC, Scholle PA (1987) The Cenomanian-Turonian oceanic anoxic event, I. Stratigraphy and distribution of organic-rich beds and the marine ^{13}C excursion. In: Brooks J, Fleet AJ (eds), Marine Petroleum Sources Rocks. Geological Society, London, Special Publications, pp. 371-399

Schlanger SO, Jenkyns HC (1976) Cretaceous oceanic anoxic events: causes and consequences. Geologie en Mijnbouw 55: 179-184

Sinton CW, Duncan RA (1997) Potential links between ocean plateau volcanism and global ocean anoxia at the Cenomanian-Turonian boundary. Economic Geology 92: 836-842

Snow LJ, Duncan RA, Bralower TJ (2005) Trace element abundances in the Rock Canyon

Anticline, Pueblo, Colorado, marine sedimentary section and their relationship to Caribbean plateau construction and oxygen anoxic event 2. Paleoceanography 20: PA3005

Stewart K, Turner S, Kelley S, Hawkesworth C, Kirstein L, Mantovani M (1996) 3-D, ^{40}Ar-^{39}Ar geochronology in the Paraná continental flood basalt province. Earth and Planetary Science Letters 143: 95-109

Sun Y, Püttmann W (1997) Metal accumulation during and after deposition of the Kupferschiefer from the Sangerhausen Basin, Germany. Applied Geochemistry 12: 577-592

Tribovillard N, Riboulleau A, Lyons T, Baudin F (2004) Enhanced trapping of molybdenum by sulfurized marine organic matter of marine origin in Mesozoic limestones and shales. Chemical Geology 213: 385-401

Trümpy R (1960) Paleotectonic evolution of the Central and Western Alps. Bulletin of the Geological Society of America 71: 843-908

Van de Schootbrugge B, Föllmi KB, Bulot LG, Burns SJ (2000) Paleoceanographic changes during the early Cretaceous (Valanginian-Hauterivian): evidence from oxygen and carbon stable isotopes. Earth and Planetary Science Letters 181: 15-31

Van de Schootbrugge B, Kuhn O, Adatte T, Steinmann P, Föllmi KB (2003) Decoupling of P- and Corg-burial following Early Cretaceous (Valanginian-Hauterivian) platform drowning along the NW Tethyan margin. Palaeogeography, Palaeoclimatology, Palaeoecology 199: 315-331

Warning B, Brumsack H-J (2000) Trace metal signatures of eastern Mediterranean sapropels. Palaeogeography, Palaeoclimatology, Palaeoecology, 158: 293-309.

Westphal H, Munnecke A, Pross J, Herrle JO (2004) Multiproxy approach to understanding the origin of Cretaceous pelagic limestone-marl alternations (DSDP site 391, Blake-Bahama Basin). Sedimentology 51: 109-126

Wilde P, Lyons TW, Quinby-Hunt MS (2004) Organic carbon proxies in black shales: molybdenum. Chemical Geology 206: 167-176

Yarincik KM, Murray RW, Lyons TW, Peterson LC, Haug GH (2000) Oxygenation history of bottom waters in the Cariaco Basin, Venezuela, over the past 578,000 years: Results from redox-sensitive metals (Mo, V, Mn, and Fe). Paleoceanography 15: 593-604

C.3.

The late Hauterivian Faraoni oceanic anoxic event in the western Tethys: Evidence from phosphorus burial rates

Stéphane Bodin [a], Alexis Godet [a], Karl B. Föllmi [a], Jean Vermeulen [b], Hubert Arnaud [c], André Strasser [d], Nicolas Fiet [e], Thierry Adatte [a]

[a] Institut de Géologie, Université de Neuchâtel, Rue Emile Argand 11, 2007 Neuchâtel, Switzerland

[b] Grand Rue, 04330 Barrême, France

[c] Laboratoire de Géodynamique des Chaînes Alpines, Maison des Géosciences, 38041 Grenoble Cedex, France

[d] Department of Geosciences, Geology-Palaeontology, Perolles, CH-1700 Fribourg, Switzerland

[e] UMR 8148 – I.D.E.S., Bât. 504, University of Paris XI Orsay, 91405 Orsay Cedex, France

Keywords: Faraoni anoxic event; Hauterivian; Barremian; Tethys; phosphorus accumulation rate; platform drowning

Published in: Palaeogeography, Palaeoclimatology, Palaeoecology **235** (2006), 245-264

Abstract

In uppermost Hauterivian sediments of the western Tethys, a short-lived anoxic event (Faraoni event) is documented both in form of an interval enriched in organic matter (pelagic realm) as well as a condensed interval enriched in glauconite and phosphate (shelf realm). This latter interval represents the onset of a drowning episode on the Helvetic carbonate platform along the northern tethyan margin, which lasted throughout the early Barremian. This drowning episode marks a turning point in the way the platform carbonate factory functioned: during the Hauterivian, carbonate production was dominated by heterozoans, whereas during the late Barremian a photozoan assemblage developed that is preserved in the so-called Urgonian limestone. The late Hauterivian Faraoni oceanic anoxic event is of particular interest, because it is not accompagnied by a major positive shift in $\partial^{13}C$, unlike other oceanic anoxic events during the Cretaceous (Valanginian, early Aptian, Cenomanian-Turonian boundary).

We have analyzed four (hemi-)pelagic sections with regards to their phosphorus content in order to better understand the palaeoceanographic conditions related to this anoxic event and the associated changes in the shallow-water carbonate factory. The sections are located in Angles (SE France), Fiume-Bosso and Gorgo a Cerbara (central Italy), and Veveyse de Châtel-St. Denis (west Switzerland). We calculated phosphorus mass accumulation rates by using a cyclostratigraphic approach in order to obtain an adequate age model. We observe a comparable and correlatable long-term trend for the four sections, which suggests that the phosphorus mass accumulation rates and temporal changes therein are representative for the western tethyan pelagic realm. The Faraoni event is marked by a minimum in phosphorus accumulation and a positive shift in the C_{org}/P_{tot} ratios, which is interpreted as a reflection of the decreased capacity of storing and preserving phosphorus in oxygen-depleted sediments. Moreover, the onset in the decrease in phosphorus accumulation coincides with a sea level rise, while the Faraoni level itself corresponds to a maximum flooding interval. This phase of sea-level rise may have been important in the establishment of marine connections between the boreal and tethyan realms, and as such in the exchange of nutrient-enriched waters. The model for the origin of the Faraoni oceanic anoxic event proposed here incorporates these aspects together with a positive feedback loop generated by phosphorus regeneration, and a negative feedback loop related to changes in the ocean oxygen cycle.

The subsequent long-term changes in phosphorus burial rates during the Barremian suggest that the Faraoni event marks the onset of a long period of environmental instability with regards to platform growth, leading to periodic phases of eutrophication and drowning of the northern tethyan carbonate platform. This environmental crisis ended during the late Barremian with the onset of the deposition of the Urgonian limestone under oligotrophic conditions.

C.3.1. Introduction

The early Cretaceous is characterized by marked environmental and palaeoceanographic changes, which are documented by episodic oceanic anoxic events, repeated platform drowning phases, and pronounced excursions in the stable carbon (C) isotope record (e.g., Lini *et al.*, 1992; Föllmi *et al.*, 1994; Weissert *et al.*, 1998; Herrle, 2002). One of the less well-understood events of this period is the so-called Faraoni event (Baudin *et al.*, 1999; Cecca *et al.*, 1994), which is a short-lived oceanic event that occurred during the latest Hauterivian. In comparison to the other anoxic events, the Faraoni event is a rather atypical event for which the environmental circumstances are still not clear: in contrast to the anoxic events during the Valanginian, the early Aptian, and near the Cenomanian-Turonian boundary (e.g., Schlanger and Jenkyns, 1976; Schlanger *et al.*, 1987; Weissert, 1989; Lini *et al.*, 1992; Jones and Jenkyns, 2001; Weissert and Erba, 2004), the Faraoni level is not accompanied by a major carbon isotope excursion towards more positive values but instead by a minor long-term increase (Föllmi *et al.*, 1994; Erba *et al.*, 1999; Van de Schootbrugge *et al.*, 2000). Furthermore, no major volcanic episode has, of yet, been identified for the late Hauterivian. This means that the classical model postulated for the origin of oceanic anoxic events in general, (i.e., increased volcanism leading to an increase in atmospheric CO_2, climate warming, increased weathering and nutrient availability, higher productivity and consequently higher preservation rates of organic matter (e.g., Jenkyns, 1999, 2003)) can not be applied in this case.

The Faraoni event marks the onset of a long-lasting drowning episode on the Helvetic carbonate platform of the northern tethyan margin (D3 in Föllmi *et al.*, 1994), which is documented by a hiatus or by the presence of condensed glauconite and phosphate-rich sediments – the so-called Altmann Beds (Funk, 1969). This drowning episode is associated with a fundamental change in the carbonate factory of this platform system: during the Hauterivian, carbonate production occurred mainly by heterozoan assemblages, which are documented – for example - by the Kieselkalk Formation (Funk, 1969; Föllmi *et al.*, 1994), whereas during the late Barremian, photozoan assemblages dominated and their debris accumulated in the widespread "Urgonian" limestone (= Schrattenkalk Formation in the Helvetic realm).

For this period and for the early Cretaceous in general, only a limited amount of data has been obtained with regards to its phosphorus (P) record (Föllmi, 1995, 1996; van de Schootbrugge *et al.*, 2003). P is an important and often limiting biophile element (Broecker and Peng, 1982; Ingall and Jahnke, 1994; Tyrrell, 1999), which is closely linked to the Carbon (C) cycle through two interfaces: (1) biogeochemical weathering, during which atmospheric CO_2 is transformed into HCO_3^- and P is mobilized; and (2) photosynthesis, which is often limited by P and by which CO_2 is transformed into organic C (e.g., Föllmi *et al.*, 2004). A reconstruction of changes in the P cycle during this critical period may, for these reasons, help to improve our understanding of the mechanisms leading to the Faraoni anoxic event and the associated platform drowning episode.

Four pelagic or hemi-pelagic sections located in Angles (SE France), Fiume-Bosso (central Italy), Gorgo a Cerbara (central Italy) and Veveyse de Châtel-St. Denis (west Switzerland) were analyzed. By monitoring the P record in these key sections and integrating sequence stratigraphy and cyclostratigraphy, we are able to reconstruct a general trend in P accumulation for the western Tethyan realm during the late Hauterivian and Barremian. In using the C_{org}/P_{org} and C_{org}/P_{tot} ratios, we also show that a decrease in the capacity of storing and preserving P in the sedimentary reservoir during the unfolding of the Faraoni event may have helped to sustain this anoxic event.

C.3.2. Geological setting

Four pelagic or hemi-pelagic sections in different basins within the western Tethys were selected. These sections are well dated and include the Faraoni level or its equivalent. The first studied section is the Fiume-Bosso section, located between Urbino and Gubbio, near Cagli (central Italy, Fig. C.3.1; see also Cecca *et al*., 1994). It represents the type section for the Faraoni level (Cecca *et al.*, 1994). The lithology is characteristic of the Maiolica Formation and consists of a succession of pelagic limestone beds containing abundant cherts, and locally intercalated thin organic-rich marl layers and/or laminae. The section of Gorgo a Cerbara is situated in the same area and its lithology is similar to the one of the Fiume-Bosso section. It is situated approximately 4 km east of Piobbico city along the Candigliano River (Fig. C.3.1; see Cecca *et al.*, 1995). This type section for the Barremian/Aptian boundary is complementary to the Fiume-Bosso section and covers the whole Barremian.

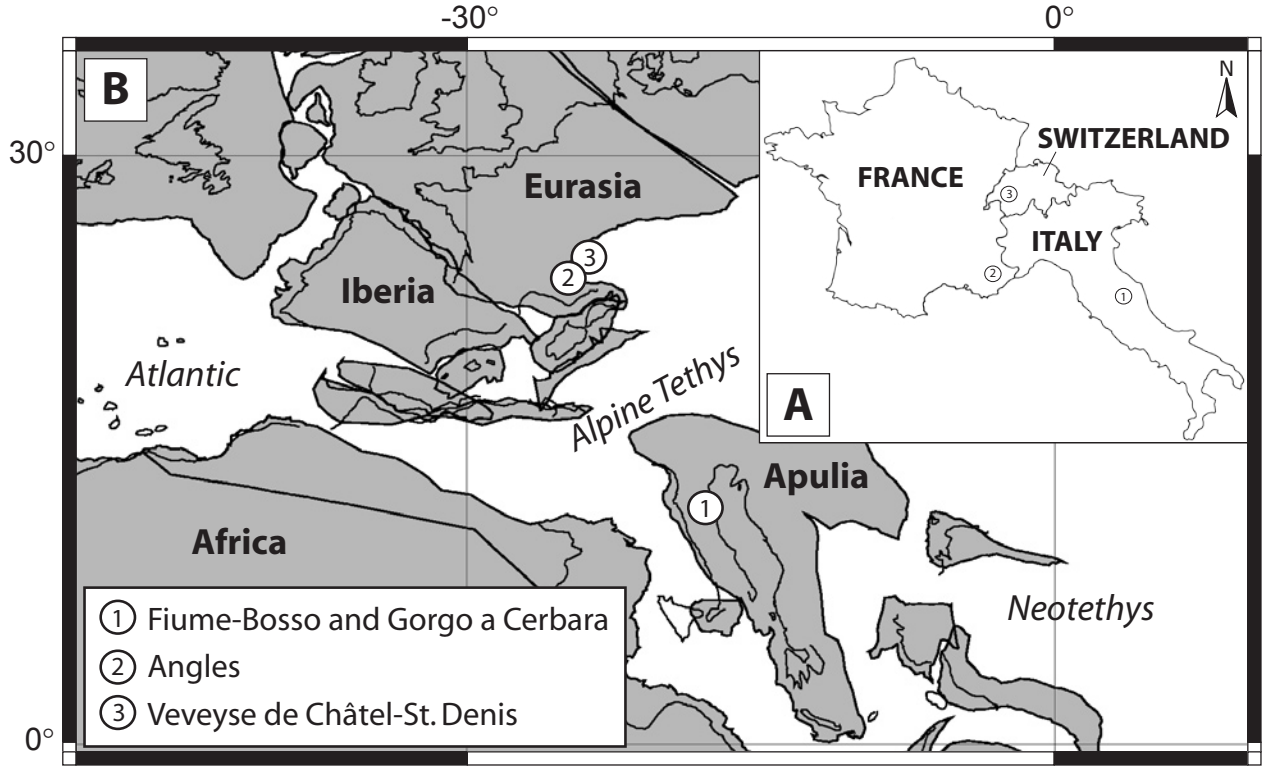

Fig. C.3.1: A. Localization of the four studied sections. B. Palaeogeographic map at the Hauterivian-Barremian transition (127 Myr B.P.) showing the localization of the four sections (modified from Hay *et al.*, 1999).

The section of the Veveyse de Châtel-St. Denis (VCD) is the third studied section. It is situated in the canton of Fribourg, along the Veveyse river, in western Switzerland (see Busnardo *et al*., 2003, for a detailed geographic description). Its lithology consists of a succession of alternating pelagic marl and marly limestone, which are rich in macrofossils.

The fourth studied section outcrops along the "Route d'Angles", near St. André-Les-Alpes, in the Vocontian basin (S-E of France, see Busnardo (1965) for a detailed geographic description). Its lithology consists of a fossiliferous, hemi-pelagic succession of regularly alternating marl and limestone.

The palaeogeographic location of these four sections is shown in Fig. C.3.1. During the early Cretaceous, the Angles and the VCD sections were situated along the northern tethyan margin. The VCD section is part of the Ultrahelvetic realm, which is considered as the deeper offshore prolongation of the Vocontian basin to the northeast (Trümpy, 1960). The Fiume-Bosso and the Gorgo a Cerbara sections

were located in the southern part of the tethyan realm, remote from any continent, and were surrounded by carbonate shelves. The four sections represent a N-S transect across the western Tethys.

C.3.3. Methods

C.3.3.1. Phosphorus analyses

Total phosphorus analyses were performed on bulk rock samples from the limestone intervals for all four sections. The samples were sawed in order to eliminate the altered parts and the veins of the rock. Then, powders were obtained using an agate crusher. Around 100 mg of powder were mixed with 1 ml of $MgNO_3$ and left to dry in an oven at 45°C for 2 hours. The samples were then ashed in a furnace at 550°C during two hours. After cooling, 10 ml of 1N HCl were added and placed under constant shaking for 14 hours. The solutions were filtrated with a 63µm filter, diluted ten times, and analyzed using the ascorbic acid method of Eaton *et al.* (1995). For this process, the solution was mixed with ammonium molybdate and potassium antimonyl tartrate, which in an acid medium react with orthophosphate to form phosphomolybdic acid. This acid is reduced with ascorbic acid to form an intense blue color. The intensity of the blue color is determined with a photospectrometer (Perkin Elmer UV/Vis Photospectrometer Lambda 10). The concentration of PO_4 in mg/L is obtained by calibration with known standard solutions. Individual samples were measured three times and precision was better than 5%. Replicate analyses of samples have a precision better than 10% in the case of low P concentration (such as in samples of the Fiume-Bosso and Gorgo a Cerbara sections) and better than 7% in the two other sections.

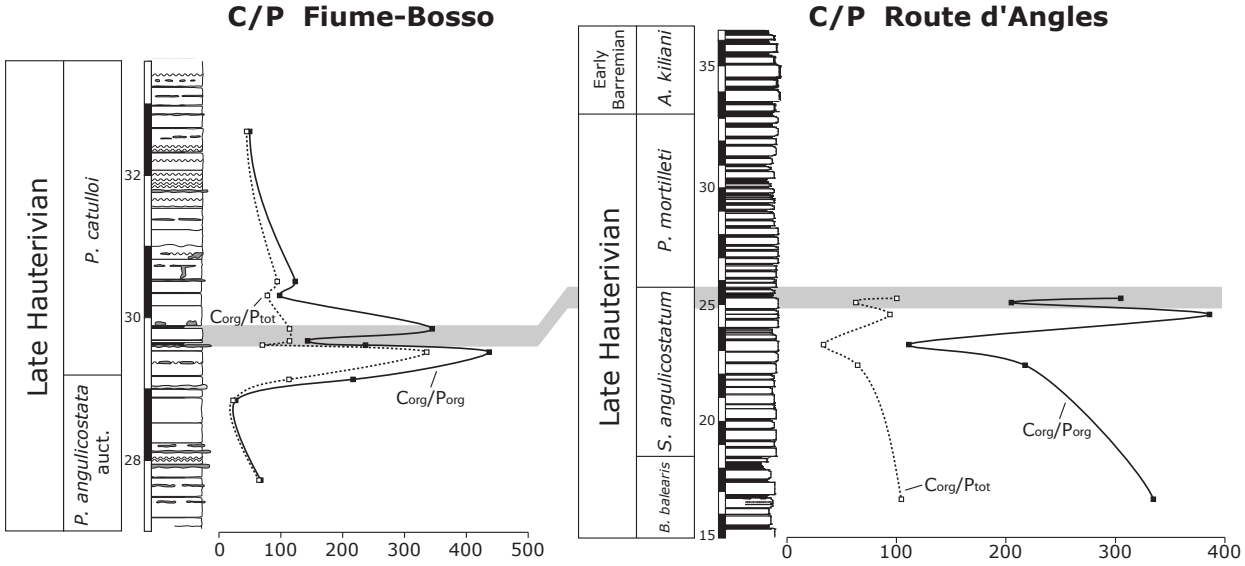

Fig. C.3.2: C/P_{org} and C/P_{tot} ratios (expressed in mol/mol) in the Fiume-Bosso and Angles sections. The grey band traces the Faraoni level.

Total P content in marls was determined using the same method as for the limestone. P content of the organic matter was determined by using a sequential extraction technique, adapted from the SEDEX method developed by Ruttenberg (1992) and modified by Anderson and Delaney (2000). As for total phosphorus, the solutions were diluted ten times, colorated using the ascorbic acid method of Eaton *et al.* (1995) and analyzed with a photospectrometer (Perkin Elmer UV/Vis Photospectrometer Lambda 10).

C_{org}/P_{org} and C_{org}/P_{tot} ratios were determined in the marls within and around the Faraoni level for three sections (Fiume-Bosso, Angles and

Ech	TOC [%]	[P_{org}] (ppm)	[P_{tot}] (ppm)	C_{org} (mmol/g)	P_{org} (mmol/g)	P_{tot} (mmol/g)	C_{org}/P_{org}	C_{org}/P_{tot}
Fiume-Bosso								
FB 133	2.11	786.7	809.0	1.760	0.0254	0.0261	69.3	67.4
FB 138	1.12	1001.1	1280.2	0.931	0.0323	0.0413	28.8	22.5
FB 372	4.51	540.5	1011.8	3.752	0.0174	0.0327	215.0	114.9
FB 374	14.81	871.0	1130.2	12.329	0.0281	0.0365	438.5	337.9
FB 377	1.12	120.8	404.4	0.931	0.0039	0.0131	238.6	71.3
FB 379	4.99	897.6	1091.0	4.152	0.0290	0.0352	143.3	117.9
FB 381b	3.65	274.3	813.8	3.037	0.0089	0.0263	343.0	115.6
FB 384	3.69	954.8	1195.6	3.073	0.0308	0.0386	99.7	79.6
FB 386	4.25	902.6	1163.7	3.537	0.0291	0.0376	121.4	94.2
FB 397	2.02	1014.7	1094.5	1.679	0.0328	0.0353	51.3	47.5
Angles								
AN32b	2.63	202.8	668.7	2.191	0.0065	0.0216	334.6	101.5
AN46b	2.13	251.3	894.1	1.769	0.0081	0.0289	218.1	61.3
AN48b	1.11	256.9	942.4	0.926	0.0083	0.0304	111.6	30.4
AN51b	1.09	72.8	311.6	0.908	0.0024	0.0101	386.3	90.3
AN52b	1.49	186.5	645.2	1.244	0.0060	0.0208	206.6	59.7
AN53.1b	1.09	92.0	289.7	0.906	0.0030	0.0094	304.9	96.9
Veveyse								
VCDII 11B	0.37	127.2	263.0	0.305	0.0041	0.0085	74.2	35.9
VCDII 14B	0.31	103.5	258.4	0.258	0.0033	0.0083	77.2	30.9
VCDII 17B	0.73	154.4	380.4	0.604	0.0050	0.0123	121.1	49.2
VCDII 18B	0.61	159.2	410.4	0.505	0.0051	0.0132	98.3	38.1
VCDII 20B	0.78	146.0	315.3	0.645	0.0047	0.0102	137.0	63.4

Table C.3.1: TOC (%), P_{org} (ppm), P_{tot} (ppm) and calculated C/P_{org} and C/P_{tot} ratios for the marls samples of the Fiume-Bosso, Angles and VCD sections around the Faraoni level.

VCD). The C concentration was obtained by Rock-Eval pyrolysis (Behar *et al*., 2001) using the standard temperature cycle. Two standards (an in-house standard and the «IFP 160000» standard from the Institut Français du Pétrole, Paris, France) were analyzed at the beginning and at the end of a batch of ca. 15 samples. C/P is expressed in mol/mol unit (Fig. C.3.2). The results for TOC and phosphorus are shown in Table C.3.1.

C.3.3.2. Age model

In order to avoid problems of condensation and to better compare the different sections, we decided to calculate phosphorus accumulation rates (PAR). The PAR is expressed in mg of P per cm^2 per kyr. This is a multiplication of the concentration in P (mg/g), the density (g/cm^3), and the sedimentation rate (cm/kyr). As all the samples are pelagic or hemi-pelagic mudstones, the density was assumed to be constant and equal to 2.5 g/cm^3 for all analyzed samples.

An age model was obtained for the four sections by a cyclostratigraphic approach (Table C.3.2). For the Angles section, following the study of Giraud *et al*. (1995) in the late Hauterivian (*angulicostata* zone) sediment of Vergons, we considered that each limestone-marl couplet represents a duration of 20 kyr. We estimated as such an average sedimentation rate for the successions of sediments that correspond to the time envelopes of complete ammonite zones (Vermeulen, 2002). It appears that in the Angles section, the *sartousiana* and the *feraudianus* zones are not complete due to the presence of hiati and/or condensed sediments (Delanoy, 1997; Vermeulen, 2002; see also Wissler *et al*., 2002). For the sediments attributed to these two ammonite zones, we decided to use the time envelopes for the corresponding sedimentary intervals from the Saut-du-Loup section, which is situated in the same area (close to Barrême) and appears to be more complete (Vermeulen, 1980). For the Fiume-Bosso and the Gorgo a Cerbara sections, we followed the method described in Fiet and Gorin (2000) to discriminate 100-kyr bundles in Barremian carbonate-dominated pelagic deposits of central Italy, and then determine sedimentation rates based on the eccentricity bundles. Finally, in the VCD section, the same method as for the Angles section was applied.

Angles

Ammonite Zone	20 kyr bundles	Duration
B. balearis *(at least)*	35	700000
S. angulicostatum	21	420000
P. mortilleti	24	480000
A. kiliani	25	500000
K. nicklesi	20	400000
N. pulchella	20	400000
K. compressissima	20	400000
C. darsi	17	340000
H. uhligi	12	240000
H. sayni	28	560000
G. sartousiana	20	400000
H. feraudianus	23	460000
I. giraudi	16	320000
M. sarasini	25	500000
D. oglanlensis *(at least)*	20	400000
late Hauterivian *(at least)*	80	1600000
Lower Barremian	102	2040000
Upper Barremian	124	2480000
Lowermost Aptian *(at least)*	20	400000
Barremian	226	4520000
Begining of Faraoni level to H/B boundary	25	500000

Fiume-Bosso

Ammonite Zone	100 kyr bundles	Duration
B. balearis *(at least)*	8	800000
P. angulicostata auct.	8	800000
P. catulloi (subzone)	5.5	550000
S. hugii *(at least)*	3	300000
Begining of Faraoni level to H/B boundary	5	500000

Veveyse de Châtel-St. Denis

Ammonite Zone	20 kyr bundles	Duration
S. sayni *(at least)*	34	680000
P. ligatus	25	500000
B. balearis	36	720000
P. angulicostata auct.	52	1040000
T. hugii *(at least)*	12	240000
Begining of Faraoni level to H/B boundary	21	420000

Gorgo a Cerbara

Magneto-chron	100 kyr bundles	Duration
M-4 *(at least)*	6	600000
M-3	17.5	1750000
M-2	6	600000
M-1	3.5	350000
M-1n	22	2200000
M-0	3.3	330000
late Hauterivian *(at least)*	5	500000
Lower Barremian	16	1600000
Upper Barremian	33.3	3330000
Lowermost Aptian *(at least)*	4	400000
Barremian	49.3	4930000
Begining of Faraoni level to H/B boundary	5	500000

Table C.3.2: Calculated duration of the different ammonite or magnetochron zones within the four sections. The values obtained for the first and the last ammonite zone or magnetochron for each section is a minimum value.

The ammonite zones have been defined by Busnardo *et al*. (2003) and their limits are dated approximately by Hardenbol *et al*. (1998). By counting the limestone-marl alternations between these limits, an average time span of 20 kyr is suggested for one limestone-marls couplet. Occasionally it is observed that five couplets group into bundles, which would then correspond to 100 kyr. These frequencies imply that sedimentation was controlled by orbital cycles in the Milankovitch frequency band.

We find a duration of 500 kyr for the interval between the base/onset of the Faraoni level and the Hauterivian-Barremian boundary in three sections (Fiume-Bosso, Gorgo a Cerbara and Angles). In the VCD section, the calculated duration is equal to 420 kyr. This slight difference reflects the limits of the cyclo-stratigraphy approach. In the Angles section, the duration of the Barremian is estimated to be equal to 4.52 Myr (with the integration of the duration of the *sartousiana* and *feraudianus* zones from the Saut-du-Loup section). This duration is in relative good agreement with those obtained by Fiet and Gorin (2000) for the Barremian of the Gorgo a Cerbara section (5.11 ± 0.34 Myr) and the estimation of the age of the Barremian proposed by Gradstein *et al*. (2004) (between 130 ±1.5 and 125 ±1.0 Myr B.P.). However, a discrepancy exists with the study of Wissler *et al*. (2004), who found a duration of 4 Myr between the top of Chron M3 and the base of Chron M0, which is not in good agreement with our estimation of 3.15 Myr for the same time interval at Gorgo a Cerbara.

C.3.4. Results

C.3.4.1. The Fiume-Bosso section

The PAR values vary between 0.09 and 0.44 mg/cm^2/kyr (Fig. C.3.3). In the lower part of the section (below the *angulicostatum* auctorum zone), the long-term trend appears more or less constant (approximately 0.21 mg/cm^2/kyr) despite high-frequency fluctuations. Then, within the *angulicostatum* auctorum zone, the values begin to decrease and reach a minimum (0.13 mg/cm^2/kyr) around the Faraoni level. Above the Faraoni level, the values increase and reach a maximum in the sediments approximately 10 meters above the Faraoni level. In the upper part of the section we observe again a decrease in the PAR trend.

The C_{org}/P_{org} ratios measured in marly intervals within and around the Faraoni level show two closely spaced excursions toward values between 300 and 450 near and within the Faraoni level whereas background values vary between 50 and 100 (Fig. C.3.2). The C_{org}/P_{tot} ratios show approximately the same behaviour as the C_{org}/P_{org} ratios but with lower absolute values. Near or within the Faraoni level, values are higher than 114 (with the exception of one sample) whereas the other samples have values between 20 and 100.

C.3.4.2. The Veveyse de Châtel-St. Denis section

The VCD section displays the highest PAR values of this work (Fig. C.3.4). They vary between 0.98 and 3.48 mg/cm^2/kyr, with a mean value of 1.82 mg/cm^2/kyr. In the lower part of the section (*sayni* zone), a first decrease in PAR is observed, with values reaching a minimum at the *sayni-ligatus* boundary. A strong increase follows and PAR values reach a maximum within the *balearis* zone. The sediments attributed to the late *balearis* – early *angulicostata auct*. zones are marked by generally low PAR values and a decreasing trend. A short positive shift is distinguished in the middle of the *angulicostata auct*. zone. We note that the sediments considered to represent the equivalent of the Faraoni level are marked by a negative shift in PAR. Finally, the upper part of the section shows an increase in PAR values.

Fig. C.3.3: (opposite page) Fiume-Bosso PAR values. The trend curve is calculated using a five point moving average formula. Biostratigraphy after Coccioni *et al.* (1998).

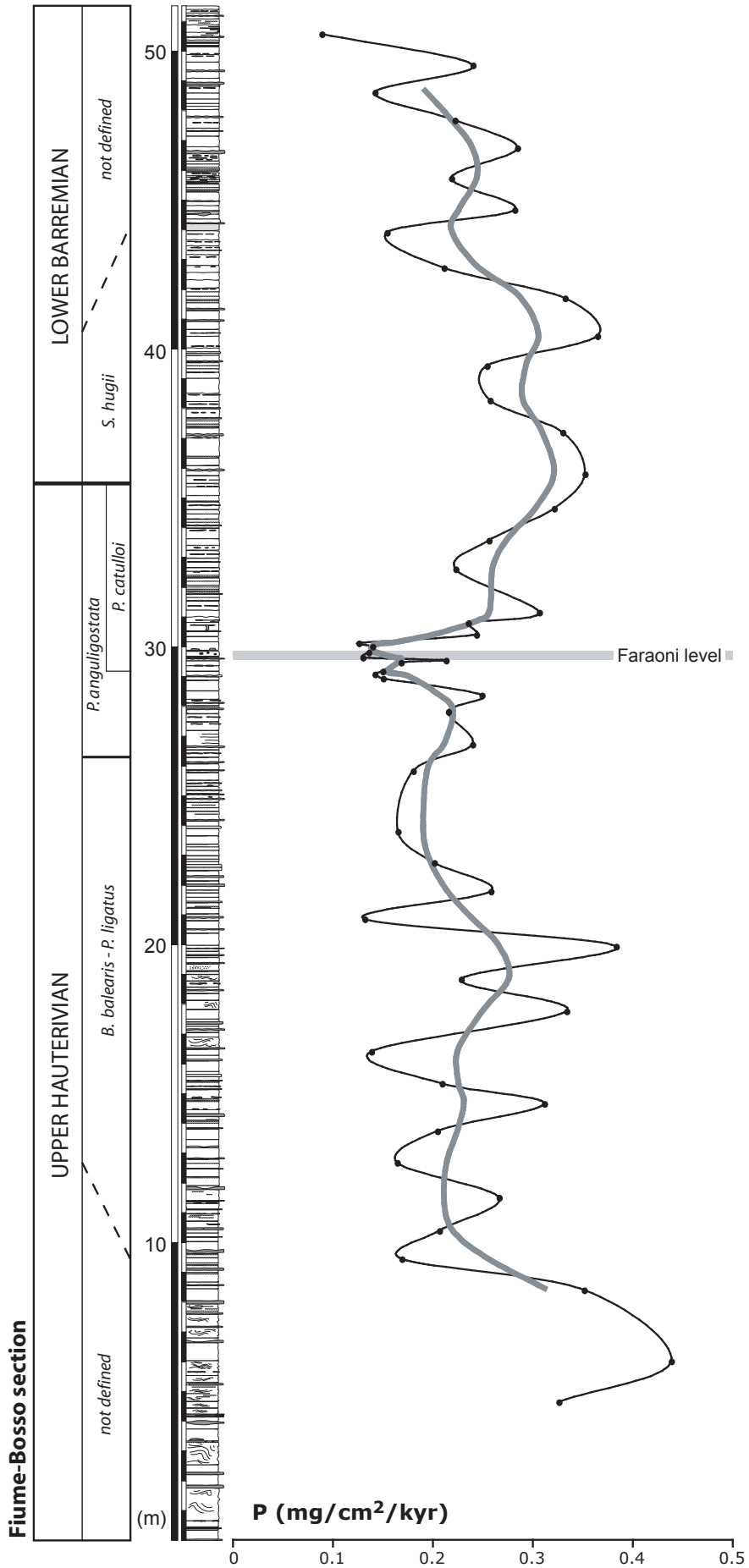
Fiume-Bosso section
UPPER HAUTERIVIAN
LOWER BARREMIAN
not defined
B. balearis - P. ligatus
P.anguligostata
P. catulloi
S. hugii
not defined
(m)
50
40
30
20
10
Faraoni level
P (mg/cm2/kyr)
0
0.1
0.2
0.3
0.4
0.5

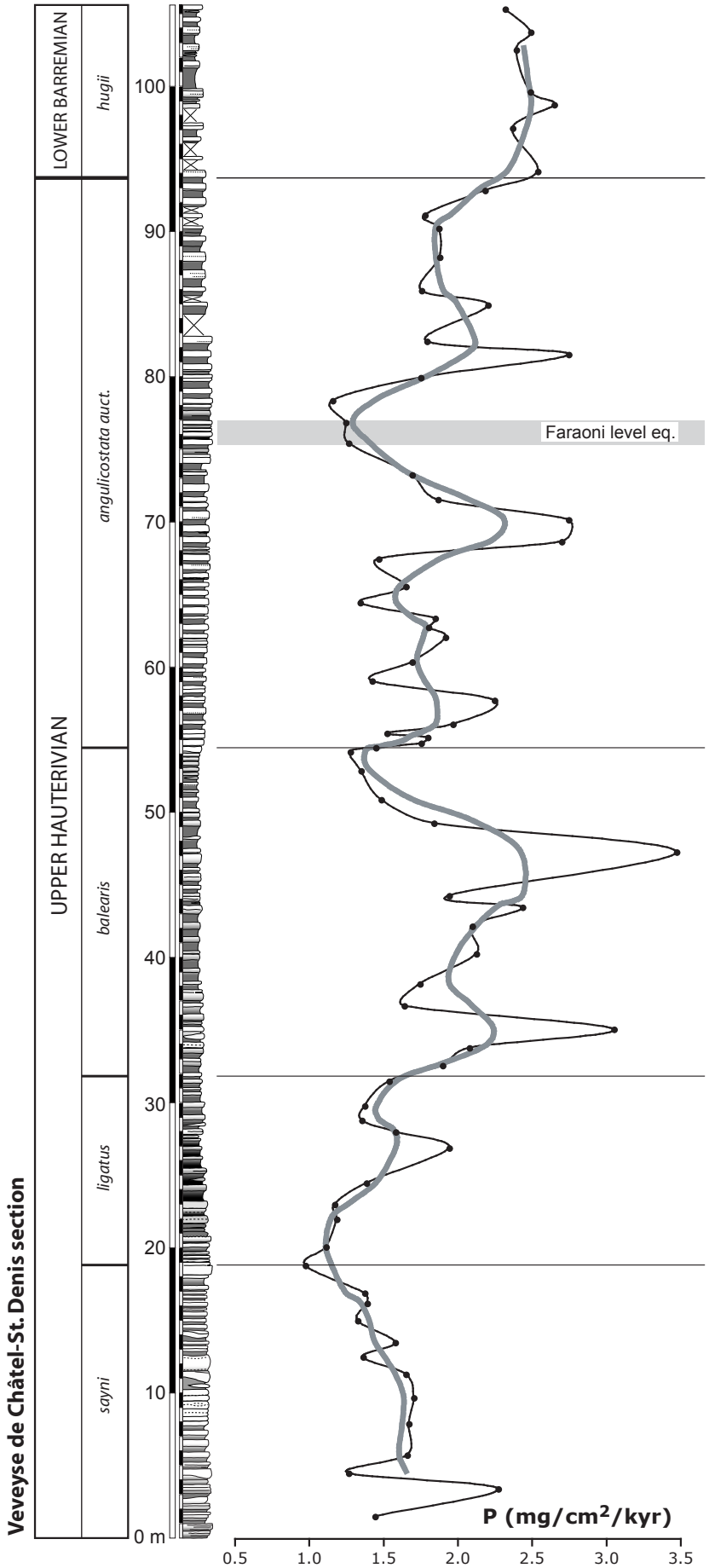

Fig. C.3.4: Veveyse PAR values. The trend curve is calculated using a five point moving average formula. Biostratigraphy modified after Busnardo *et al.* (2003).

The C/P ratios are very low, with an average value close to 100 for the C_{org}/P_{org} ratios and close to 45 for the C_{org}/P_{tot} ratios. No specific trend is distinguished.

C.3.4.3. The Angles section

The sediment succession of the Angles section studied here represents the time interval between the *balearis* zone (late Hauterivian) and the *oglanlensis* zone (earliest Aptian). This specific section yielded the most contrasted PAR curve (Fig. C.3.5). PAR values vary between 0.57 and 1.96 mg/cm^2/kyr, with an average value of 1.08 mg/cm^2/kyr. After a more or less constant trend in sediments attributed to the *balearis* zone (mean value of 1.28 mg/cm^2/kyr), a first decrease is observed in sediments of the *angulicostatum* zone (Vermeulen, 2002), and a minimum in PAR values is reached within the Faraoni level (0.57 mg/cm^2/kyr). Higher up in the section, the trend in PAR values increases again up to the sediments of the latest *nicklesi* zone. A small positive shift is observed in sediments of the middle *kiliani* zone. In sediments from the *pulchella* to the *darsi* zones, the values are firstly rapidly decreasing, and then more or less constant with a positive shift in sediments dating from the beginning of the *compressissima* zone. In the following, the PAR values are increasing up to the end of the *darsi* zone. Finally, in the sediments near the top of the section dated as late Barremian – earliest Aptian, the long-term trend appears more or less constant (around 0.98 mg/cm^2/kyr) despite some high-frequency fluctuations (especially in sediments of the *sartousiana – feraudianus* zones).

The C_{org}/P_{org} ratios are clearly enriched around the Faraoni level (with a twofold peak and a maximum value of 386). Approximately 8m below the Faraoni level, a further peak near 330 is distinguished (Fig. C.3.2). The same behaviour is seen for the C_{org}/P_{tot} ratios, but with a maximum value of 102 for the enriched samples.

C.3.4.4. The Gorgo a Cerbara section

The PAR values vary between 0.08 and 0.77 mg/cm^2/kyr (Fig. C.3.6). Sediments belonging to the early Barremian and the early-late Barremian boundary transition are characterized by two strong positive shifts (the values exceed 0.60 mg/cm^2/kyr in both shifts). In sediments attributed to the late Barremian, a slightly diminishing trend of around 0.30 mg/cm^2/kyr is distinguished, along with higher frequency fluctuations.

C.3.5. Discussion

C.3.5.1. Phosphorus accumulation

The flux of dissolved, bio-available, P into the ocean is mainly controlled by continental runoff and atmospheric transport (Föllmi, 1996; Delaney, 1998; Benitez-Nelson, 2000; Compton *et al.*, 2000). The removal of bio-available P from the ocean reservoir is given by the difference between the rate of P sedimentation and its return flux from the sedimentary reservoir. The transfer of bio-available P into the sedimentary reservoir occurs either by sedimentation of organic matter bound P, P adsorbed on clay particles and Fe- and Mn-oxyhydroxides, P in fish debris, or by direct (microbial?) precipitation of dissolved inorganic P (e.g., Ruttenberg, 1993; Filippelli and Delaney, 1996; Föllmi, 1996). Early diagenetic regeneration of P and its removal from the sediments is an important process (Broecker and Peng, 1982; Colman and Holland, 2000; Tamburini *et al.*, 2002, 2003; but see also Anderson et al., 2001). The efficiency of P storage in the sedimentary reservoir is redox dependent and P regeneration becomes more important in oxygen-depleted bottom waters (Ingall and Jahnke, 1994; Van Cappellen and Ingall, 1996; Colman and Holland, 2000; Emeis *et al.*, 2000). The redox-sensitive capacity of P storage in the sedimentary reservoir may result in a

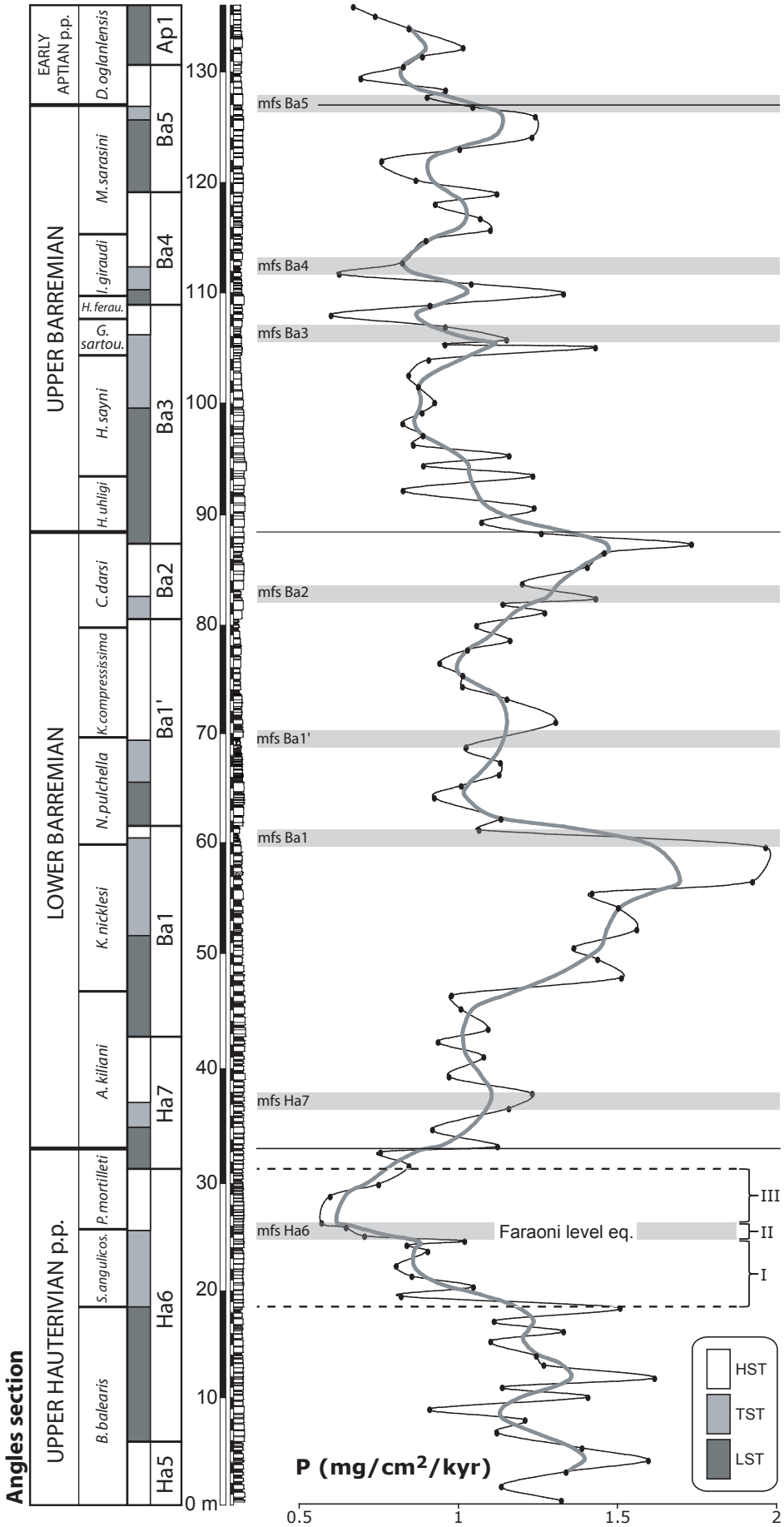

Fig. C.3.5: Angles PAR values. The trend curve is calculated using a five point moving average formula. Biostratigraphy after Vermeulen (2002). I, II and III refers to the model stages developed in Fig. C.3.7.

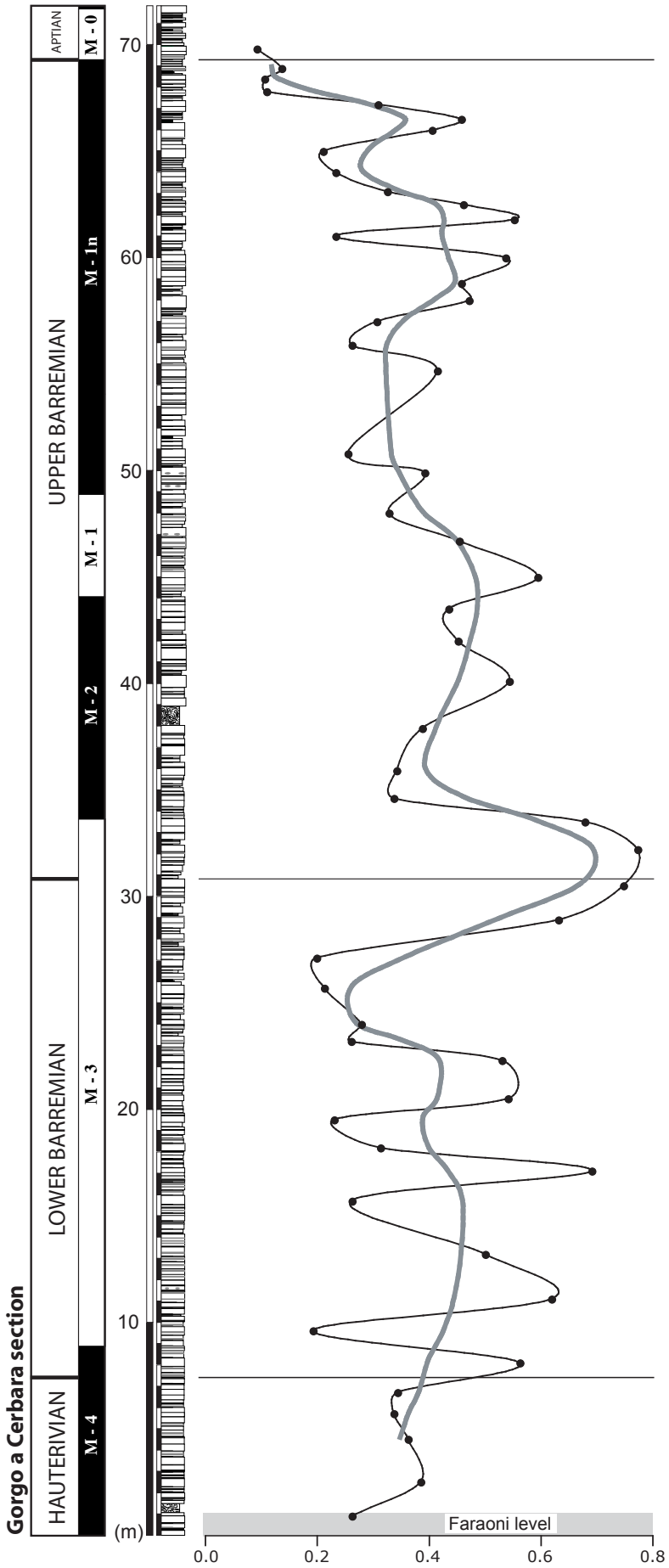

Fig. C.3.6: Gorgo a Cerbara PAR values. The trend curve is calculated using a five point moving average formula. Modified after Fiet and Gorin, 2000.

positive feedback mechanism between water-column anoxia, enhanced benthic phosphorus regeneration, and increased marine productivity (Ingall and Jahnke, 1994, 1997; Van Cappellen and Ingall, 1996; Colman and Holland, 2000).

The rate of P accumulation integrated over larger areas and time scales exceeding the actual residence time of P (approximately 10 kyr; Ruttenberg, 1993; Filippelli and Delaney, 1996; Colman and Holland, 2000) is therefore driven by two main processes: (1) the combined river and atmospheric input of P, which is linked to the rates of continental weathering, erosion, and runoff; and (2) the degree of bottom-water oxygenation. As such, an increase in PAR indicates either an increase in the intensity of continental weathering and erosion rate, for example induced by a more humid climate and/or an increase in bottom-water oxygenation. On the other hand, a decrease in PAR indicates either a decrease in continental weathering rates, related for example to a change to a drier climate, or a spread of dysaerobic to anoxic bottom-waters, or the combined effect of both processes.

C.3.5.2. The C/P molar ratio

In the Fiume-Bosso and Angles sections, the marls associated with the Faraoni level are marked by an increase of the C_{org}/P_{org} molar ratio in preserved organic matter to values of maximal 400. The marls in and around the equivalent of the Faraoni level of the VCD section yielded very low TOC values (< 0.5%) and an interpretable C/P molar ratio could not be obtained. The measured C_{org}/P_{org} molar ratios deviate from the Redfield ratio (106:1; Redfield, 1958), which implies that the preserved organic matter is depleted in phosphorus relative to carbon. Ingall *et al*. (1993), Ingall and Jahnke (1994, 1997), Van Cappellen and Ingall (1996), and Slomp *et al*. (2004) associated increased C_{org}/P_{org} molar ratios in organic matter with the degradation of organic matter and the relative loss of organic phosphorus under the influence of water column anoxia, which would concur with the overall minimal values in P accumulation rates during the Faraoni anoxic event. Interestingly, a twofold spike in C_{org}/P_{org} molar ratio is present in both sections, which may suggest that the unfolding of anoxic conditions may not have been uniform, but stepwise, with an intermittent return to more normal conditions. Within the Faraoni level, the C_{org}/P_{tot} molar ratio appears to trace well the lower spike in the twofold spike in the C_{org}/P_{org} ratio; the upper spike is less markedly traced.

Following Anderson *et al*. (2001), it appears that the $C_{org}/P_{reactive}$ molar ratio ($P_{reactive} = P_{oxide\text{-}associated} + P_{authigenic} + P_{org}$) is a more robust measure of the degree of P lost to the ocean than C_{org}/P_{org} molar ratio, due to the possible diagenetic transfer of organic phosphorus into an authigenic phase. In ancient marine sedimentary rocks, the chemical distinction between the $P_{authigenic}$ and $P_{detritic}$ phases is, however, difficult (e.g., Filippelli and Delaney, 1995) and we decided, therefore, to analyze P_{tot} and to calculate the C_{org}/P_{tot} ratio ($P_{tot} = P_{reactive} + P_{detritic}$). Silt- and sand-sized detrital material is quasi absent in the here analyzed (hemi-)pelagic sections and the presence of detrital phosphate seems minimal but cannot be totally excluded. The here presented C_{org}/P_{tot} ratio is therefore a minimal value and the ratio approaching the effective quantity of organic phosphorus that was transferred into an authigenic phase and remained as such within the marly bed lies somewhere between the C_{org}/P_{tot} and C_{org}/P_{org} molar ratios.

At Fiume Bosso, pre- and post Faraoni sediments show C_{org}/P_{tot} and C_{org}/P_{org} molar ratios which are almost identical and mostly substantial lower than the Redfield ratio, whereas the organic-rich Faraoni sediment have higher C_{org}/P_{tot} and C_{org}/P_{org} molar ratios. The low and almost identical pre- and post-Faraoni C_{org}/P_{tot} and C_{org}/P_{org} molar ratios suggest that practically all P is conserved as P_{org} and that the organic matter is depleted in C_{org} relative to P_{org}, most likely by bacterial degradation (e.g., Reimers *et al.,* 1990). The Faraoni sediment show systematically lower C_{org}/P_{tot} than C_{org}/P_{org} ratios, which are all slightly to markedly higher

than the Redfield ratio, with the exception of one sample (Fig. C.3.2). This suggests that during early diagenesis of the organic-rich sediments of the Faraoni level, P_{org} was preferentially mobilized (relative to C_{org}) and a transfer of P_{org} took place both into an authigenic phase as well as out of the organic-rich layer, most likely back into the bottom water. This systematic stratigraphic change in C_{org}/P_{tot} and C_{org}/P_{org} molar ratios in and around the Faraoni sediments suggests that under normal conditions, a preferential loss of C_{org} relative to P_{org} took place, whereas under more anoxic conditions during the deposition of the Faraoni level, a preferential loss of P_{org} relative to C_{org} is observed, which is related both to a transfer of P_{org} into an authigenic phase, as well as out of the initial layer back into the seawater.

For the Angles section, the C_{org}/P_{tot} molar ratios are systematically lower than the C_{org}/P_{org} molar ratios, both within the sediments of the Faraoni equivalent, as well as around this level. This may indicate that in all analyzed marl samples, P_{tot} is a composite of P_{org} and $P_{authigenic+detritic}$. The C_{org}/P_{org} molar ratios are all higher than the Redfield ratio, whereas the C_{org}/P_{tot} molar ratios are lower or near the Redfield ratio. This may signify that systematically a transfer took place of P_{org} into an authigenic P phase, whereas – in contrast to the Fiume Bosso section – a diagenetic transfer of P back to the seawater is less likely. In addition, due to the paleogeographic position of Angles close to the European continent, a more significant influx of $P_{detritic}$ than at Fiume-Bosso can not be excluded. Moreover, in the Angles section, TOC values are generally low (mean value close to 1.5%) and the Faraoni level is not as much enriched as could be expected from a basinal record (cf. Fiume-Bosso results, Table C.3.1). This may hint at the possibility of late-stage diagenetic alteration of organic matter coupled with the preferential loss of C_{org}. These two mechanisms could thus also be responsible of the negative shift of the Angles C_{org}/P_{tot} molar ratios relative to the C_{org}/P_{org} molar ratios.

C.3.5.3. Comparison of the PAR curves between the four sections

The PAR of the Fiume-Bosso and the Gorgo a Cerbara sections are characterized by low average values whereas the VCD section shows PAR values which are about eight times higher than those of the Fiume-Bosso and Gorgo a Cerbara sections. This difference in absolute PAR values is likely related to the different paleogeographic positions of the sections. The paleogeographical location of the Fiume-Bosso and Gorgo a Cerbara sections is remote from any continental source, and the low PAR, which are comparable to the PAR values from the ODP and DSPD compilation from Föllmi (1995), indicate generally low detrital influx rates. Moreover, the values of the VCD section, which are high also compared to those of the Angles section, indicate that along the northwestern tethyan margin the Ultrahelvetic realm received more detrital material than the Vocontian Basin during the time period studied. In the field, the more marly facies of the Ultrahelvetic carbonates supports this observation.

The good overall correlation between the PAR trend calculated for the four sections, as well as with the PAR trend given by Föllmi (1995) and van de Schootbrugge *et al.* (2003), suggests that the evolution in PAR during the late Hauterivian and the Barremian is similar over wide areas within the western Tethys (Fig. C.3.7). PAR values show a first minimum close to the *sayni – ligatus* zone boundary, which was already described by van de Schootbrugge *et al.* (2003) for the Tethyan realm. In the absence of known anoxia events during this time, this may be explained by low nutrient influx rates into the Tethyan realm during the early late Hauterivian. PAR values show subsequently a general increase until the *balearis* zone, which is followed by a general decrease towards the Faraoni level. In the Fiume-Bosso, Angles and VCD sections, the Faraoni level itself is marked by a minimum in PAR values. In sediments above the Faraoni level, PAR values increase again in all four sections. The early Barremian is thus

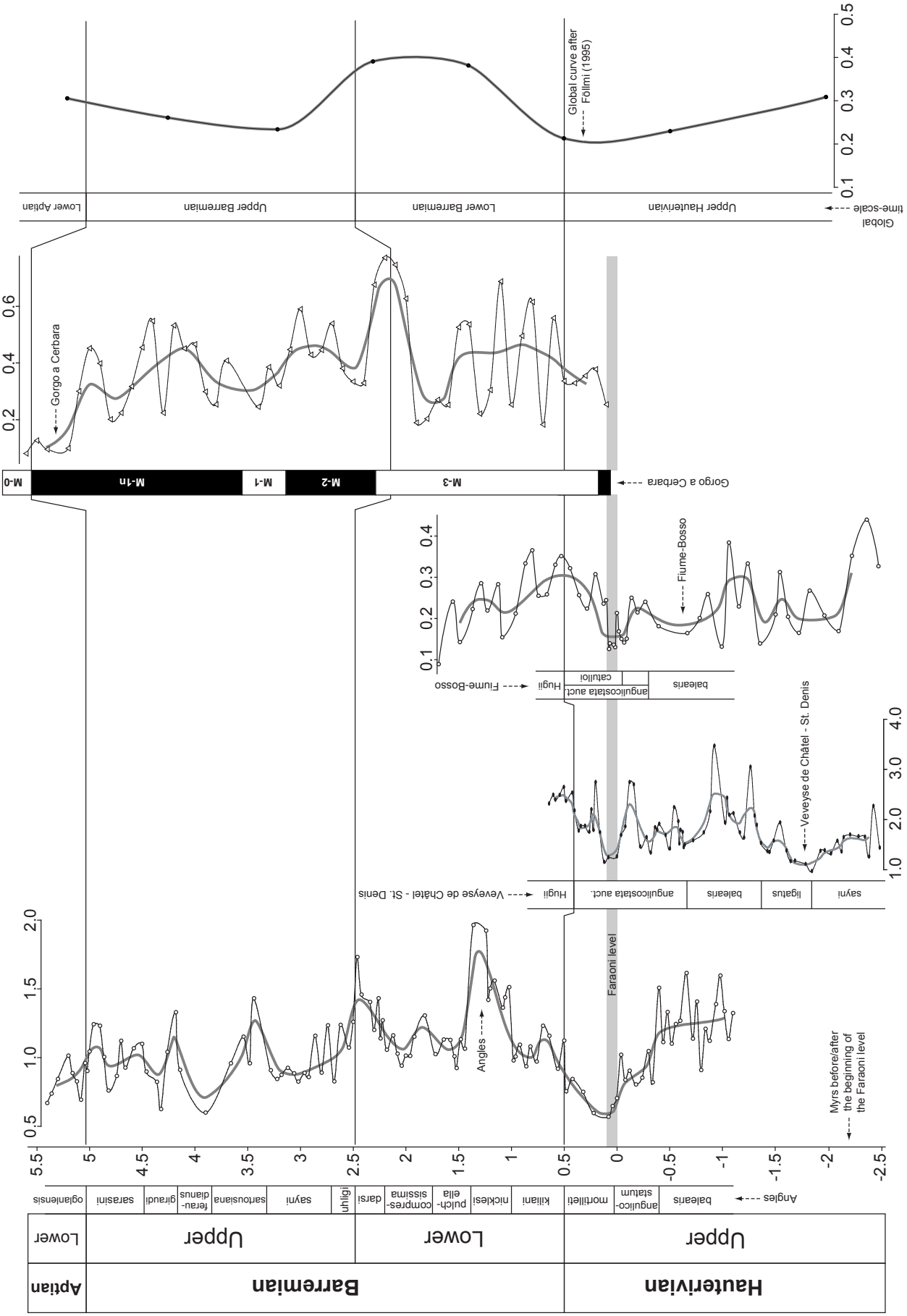
Hauterivian
Barremian
Aptian
Upper
Lower
Upper
Lower
balearis
angulicostata
statum
mortilleti
kiliani
nicklesi
pulchella
compressissima
darsi
uhligi
sayni
sartousiana
feraudianus
giraudi
sarasini
oglanlensis
Angles
Myrs before/after the beginning of the Faraoni level
Faraoni level
Angles
Veveyse de Châtel - St. Denis
sayni
ligatus
balearis
angulicostata auct.
Hugii
Veveyse de Châtel - St. Denis
Flume-Bosso
balearis
angulicostata auct.
Hugii
catulloi
Flume-Bosso
Gorgo a Cerbara
M-0
M-1n
M-1
M-2
M-3
Gorgo a Cerbara
Gorgo a Cerbara
Global curve after Föllmi (1995)
Global time-scale
Upper Hauterivian
Lower Barremian
Upper Barremian
Lower Aptian

characterized by relative high values in the four studied sections as well as in the global curve of Föllmi (1995). Following Bréhéret (1994) and Erba *et al.* (1999), the early Barremian in the western tethyan realm is characterized by the deposition of black shales that appear contemporaneous with the positive peaks in PAR. Finally, in the late Barremian, PAR values are more or less constant (with a slight decrease), even if the global curve of Föllmi (1995) shows a slight increase (Fig. C.3.7). In the Italian sections, extreme fluctuations are observed during the late Hauterivian and the early Barremian. Moreover, in these sections, many thin and isolated black-shale horizons are found during this time interval, arguing for local and short-lived anoxic conditions during the late Hauterivian – early Barremian within the Umbria-Marche basin.

C.3.5.4. The Faraoni oceanic anoxic event

The latest Hauterivian minimum in PAR values observed in the Fiume-Bosso, Angles and VCD sections coincides with the Faraoni level, which may hint at a causal relationship between late Hauterivian PAR behaviour and the Faraoni anoxic event. If this is the case, then the decrease in PAR values during the late Hauterivian may well be the consequence of a progressive loss of oxygen in oceanic bottom waters, with the Faraoni anoxic event as a result of the culminating effect of the loss of oxygen, which may have started in the late *balearis* zone. This could also explain the presence of the pronounced negative shift in the VCD section during the *angulicostata auct.* zone below the Faraoni level. Eventual anoxic conditions may have developed earlier than in shallower regions, which were bathed in oxygen-depleted bottom waters only later, due, for example, to the progressive vertical expansion of an oxygen minimum zone. The minimum in PAR is probably related to a general diminution both in the capacity of transferring P into the sedimentary reservoir as well as in the capacity of preserving P within the sedimentary reservoir, as is indicated by the C/P molar ratios in Fiume Bosso – both in dependency of oxygen contents in the bottom waters.

For the Angles section, a detailed study of the trends in stacking patterns has been made, which was used for a sequence-stratigraphic interpretation (Fig. C.3.5). This allows us to compare the PAR curve with the inferred sequence-stratigraphic trends. It appears that almost every maximum in PAR values is related to a maximum flooding surface (mfs), except for of the Faraoni level and the mfs Ba4, which are characterized by a minimum in PAR values. Interestingly, the sea-level lowstands are not characterized by high PAR values. These observations correlate well with the observations of Föllmi (1995) who noted a positive correlation between sea level and phosphorus burial during greenhouse climates. A clear difference in the nutrient cycle between greenhouse and icehouse conditions is thus underlined in the Barremian sediments of the Angles section. Below the Faraoni level, the onset of the PAR decrease coincides with the transgressive surface (ts) of Ha6 and the minimum in PAR values with the mfs Ha6.

This relationship suggests the presence of a link between the Faraoni anoxic event and the late Hauterivian phase of sea-level rise (Ha6), which represent an important transgression during the late Hauterivian and early Barremian (Haq *et al.*, 1987; Hardenbol *et al.*, 1998). During this transgression, straits connecting the tethyan and boreal realms were opened and/or became broader and deeper, as is suggested by belemnite migration patterns observed by Mutterlose and Bornemann (2000) and the presence of boreal nannoplancton in the Angles section around the Faraoni level (Silvia Gardin, pers. comm.). This may have led to the increased influx of colder

Fig. C.3.7 (opposite page): Correlation of the PAR values from the four studied sections and the global curve established by Föllmi (1995). The absolute PAR values being different for the four sections, the curves are not to scale to better compare the different variations of the PAR values. The absolute ages, in regard to the beginning of the Faraoni level, were obtained using cyclo-stratigraphic interpretations (see text for explanation).

and eventually more nutrient-rich waters into the Tethys, as was also proposed for the middle Hauterivian transgression (van de Schootbrugge *et al*., 2003).

During greenhouse conditions, a link between sea-level change and nutrient influx has already been noted by different authors (e.g., Jenkyns *et al*., 1994; Föllmi, 1995; Hilbrecht *et al*., 1996; Gale *et al*., 2000; Jarvis *et al*., 2002; van de Schootbrugge *et al*., 2003), and different mechanisms have been proposed:

(1) Jarvis *et al*. (2002) invoked reworking of sediments and soils by flooding of land areas to explain the increase in nutrient fluxes during transgression. The peculiar palaeogeography of the Cretaceous world, characterized by the presence of extensive shallow epicontinental seas during high sea level, may have favoured this process.

(2) An additional mechanism may have been provided by intensified sea surface-water evaporation due to the enhanced surface of epicontinental seas: intensified evaporation may have lead to increased wind velocities (e.g., Iruthayaraj and Morachan, 1978), which may have resulted in stronger coastal upwelling and in increased availabity of nutrients during sea-level rise

(3) A third mechanism which relates sea-level with nutrient supply is climate: Transgression, climate warming, and enhanced evaporation may accelerate the global water cycle and intensify precipitation on the continent, which again favours biogeochemical weathering and the release of biophile elements (e.g., Föllmi, 1996).

(4) A positive feedback between water-column anoxia, enhanced benthic phosphorus regeneration, and marine productivity during transgressions should also be taken into account (Ingall and Jahnke, 1994, 1997). This mechanism, however, appears to be balanced by the phosphorus-oxygen negative feedback loop described by Holland (1994) and Lenton and Watson (2000). In this model, the amount of phosphorus dissolved in the water is influenced by changes in the levels of dissolved oxygen in the water column. The decrease of the burial of organic and iron-bound phosphorus under oxygen-depleted conditions in ocean bottom waters tends to increase the ocean nutrient inventory and provide negative feedback against declining oxygen by increasing the population of oxygen-producing organisms.

In taking into account the observed link between the minima in the PAR record accompanying the oceanic anoxic Faraoni event, we propose the following model (Fig. C.3.8):

(1) The third-order sea-level rise during the late Hauterivian (Ha6 transgression: Haq *et al*., 1987; Hardenbol *et al*., 1998) led to a combination of the above-mentioned mechanisms (i.e., reworking of sediments and soils on flooded land areas, stronger evaporation rates, stronger winds and stronger upwelling, stronger biogeochemical weathering), which - together with enhanced tethyan-boreal connection and the influx of colder and eventually nutrient-rich waters - resulted in increased nutrient input into the Tethys. The resulting increase in primary productivity and corresponding export production induced a decrease in oceanic oxygen levels and the expansion of the oxygen minimum zone. The spreading of oxygen-depleted ocean bottom waters may have resulted in enhanced P regeneration from the sediments, which also contributed to a further fertilisation of the ocean. During this time interval, true anoxic conditions were not reached on a global scale and short-lived anoxic conditions were only locally present. During the late Hauterivian sea-level rise, the phosphorus-oxygen negative feedback loop described by Holland (1994) and Lenton and Watson (2000) may have been overwhelmed by the coupled positive feedback mechanism leading to higher nutrient concentrations, and may have been too weak to balance the decrease in oceanic oxygen levels.

(2) During the period of most rapid sea-level rise (mfs Ha6), these coupled mechanisms reached their climax and resulted in the

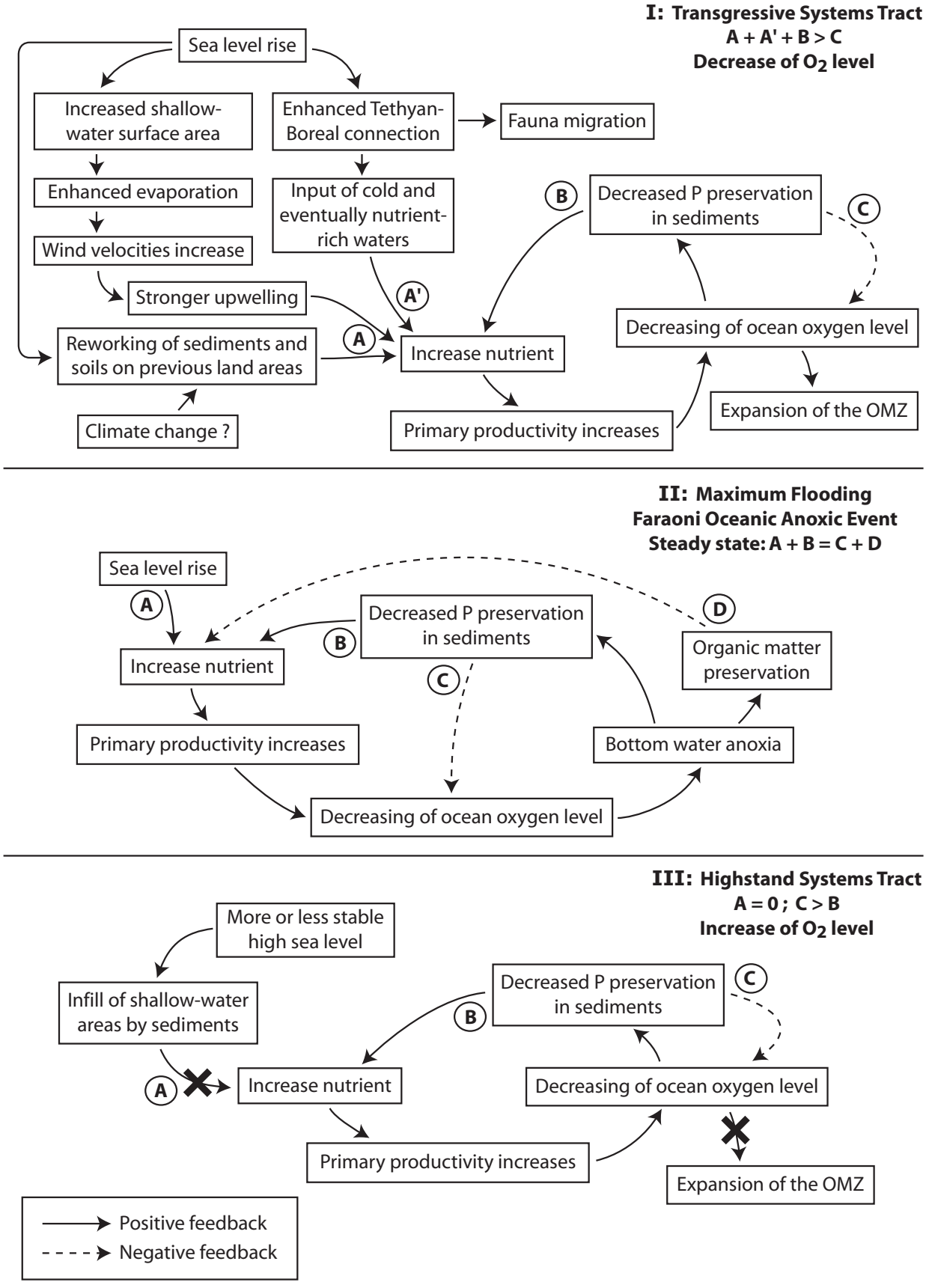

Fig. C.3.8: Three step (transgressive systems tract, maximum flooding, highstand systems tract) box model of the unfolding of the Faraoni event. See text for explanation.

Faraoni oceanic anoxic event. This event may be considered as the result of a steady-state situation, in which the positive feedback mechanisms leading to increased nutrient availability are balanced by the negative feedback mechanisms (phosphorus-oxygen negative feedback coupled with organic matter preservation). The limestone–black shale alternation, which is characteristic of the Faraoni level in the four investigated sections and elsewhere may then be explained by high-frequency oscillations superimposed on this steady-state situation.

(3) During subsequent sea-level highstand (highstand systems track of Ha6), the rapid filling of shallow-water areas by sediments may have diminished the importance of the tethyan-boreal connection, and the associated nutrient influx. Also the other mechanisms leading to nutrient mobilisation may have become less efficient, due, for example, to less intense biochemical weathering in a transport-limited weathering system (Stallard and Edmond, 1983), or to a progressively diminishing return flux of P from the sediments. As such the phosphorus-oxygen negative feedback mechanism may have become stronger than the positive feedback mechanisms leading to enhanced P availability. This then may have resulted in an increase in oceanic oxygen levels, the diminution of the OMZ and thus the termination of the oceanic anoxic conditions.

In this model, the Faraoni level is considered as the turning point during the evolution of this oceanic oxygen depletion event. Indeed, the increased transfer of organic matter into the sedimentary reservoir should be considered as the response of the Earth system by which it counteracts the decrease of oceanic oxygen levels.

C.3.5.5. The attenuated $\delta^{13}C$ signature during the late Hauterivian and early Barremian

One of the remarkable features of the Faraoni oceanic anoxic event is its poor expression in the $\partial^{13}C$ record. The $\partial^{13}C$ record of the late Hauterivian is characterized by a long-term steady increase of approximately 1‰ which culminates in a maximum near the Hauterivian-Barremian boundary, followed by a small decrease in the earliest Barremian (van de Schootbrugge *et al.*, 2000; Godet *et al.*, in press). Unlike the oceanic anoxic events of the Valanginian, early Aptian and latest Cenomanian, the Faraoni anoxic event is not related to a well-expressed positive excursion in $\partial^{13}C$. The accumulation of organic-rich sediments accompanied by an episode of carbonate platform drowning is an expression of important changes in the carbon cycle, which normally would find an expression in the $\partial^{13}C$ record. Either the Faraoni anoxic event is the result of regional, rather than global environmental change, limited to the Tethyan realm, and the changes in the carbon household within this realm were not sufficiently important to influence global $\partial^{13}C$ signatures, or a buffering mechanism capable to attenuate the $\partial^{13}C$ record played a role. This buffering mechanism maybe related to different mechanisms, such as the enhanced productivity of shallow-water carbonates outside the western tethyan realm or the increased size of the oceanic dissolved inorganic carbon reservoir (e.g., van de Schootbrugge *et al.*, 2003; Bartley and Kah, 2004).

C.3.5.6. The carbonate platform drowning episode during the latest Hauterivian and early Barremian: consequence of the Faraoni event?

The Faraoni oceanic anoxic event is contemporaneous with the onset of a platform drowning event along the northern tethyan margin that started during the latest Hauterivian and ended near the boundary between the early and late Barremian (D3 in Föllmi *et al.*, 1994). Interestingly, the time covered by this drowning episode is mirrored by contrasted variations in PAR in the Western Tethys, i.e. by a negative shift associated with the late Hauterivian Faraoni event and by two major positive shifts during the early Barremian.

These two latter peaks in PAR may reflect an increase of nutrient input induced by change towards probably more humid climate in the western tethyan realm. These climate changes and related changes in nutrient input came after the Faraoni oceanic anoxic event and may have prolonged the drowning episode, which onset is related to the environmental changes during the Faraoni event. Subsequently, during the late Barremian, platform growth took up again leading to the deposition of the "Urgonian" limestone was promoted to a large extend by photozoans. The unfolding of this important phase in the evolution of helvetic platform growth may have been related to an overall decrease in P availability as is documented by our P-accumulation curve.

C.3.6. Conclusions

Monitoring phosphorus accumulation in pelagic and hemi-pelagic sediments of the western Tethys during the late Hauterivian and Barremian allows us to better understand the associated palaeoceanographic changes, and especially the unfolding of the late Hauterivian Faraoni oceanic anoxic event. Our results correlate well with those previously obtained by van de Schootbrugge *et al*. (2003) for the late Hauterivian. Good correlation is also seen with the DSDP-ODP based curve of Föllmi (1995).

Based on the general evolution of the PAR curve and its correlation with inferred sea-level variations, we propose a new model for the origin of the Faraoni event, which incorporates increased nutrient mobilization on the continent and an improved tethyan-boreal connection, which is linked to a positive feedback loop generated by a decrease in the capacity of phosphorus preservation in the sedimentary reservoir, and a negative feedback loop related to changes in the ocean oxygen cycle.

Moreover, the Faraoni event is linked to the onset of an important platform drowning event along the northern tethyan margin. An extended increase in nutrient input during the early Barremian may have extended the drowning episode well into the Barremian.

Finally, during the late Barremian, the recorded low PAR values are in agreement with the worldwide development of the Urgonian facies, reflecting oligotrophic conditions on the shelf.

C.3.7. Acknowledgments

The authors acknowledge Rodolfo Coccioni, Pascal Linder, Haydon Mort, Claire Rambeau, Virginie Matera and Philipp Steinmann for their help in the field and/or stimulating discussions. Special thanks go to the team of the "Reserve Géologique de Haute-Provence" for providing an authorization for fieldwork. We thank Helmut Weissert and an anonymous reviewer for their critical reviews. Financial support from the Swiss National Science Foundation Project 2100-067807/1 and 200020-105206/1 is gratefully acknowledged.

C.3.8. References

Anderson, L.D., Delaney, M.L., 2000. Sequential extraction and analysis of phosphorus in marine sediments: Streamlining of the SEDEX procedure. Limnology and Oceanography 45 (2), 509-515.

Anderson, L.D., Delaney, M.L., Faul, K.L., 2001. Carbon to phosphorus ratios in sediments: Implications for nutrient cycling. Global Biogeochemical Cycles 15 (1), 65-79.

Bartley, J.K., Kah, L.C., 2004. Marine carbon reservoir, Corg - Ccarb coupling, and the evolution of the Proterozoic carbon cycle. Geology 32 (2), 129-132.

Baudin, F., Bulot, L.G., Cecca, F., Coccioni, R., Gardin, S., Renard, M., 1999. Un équivalent du «Niveau Faraoni» dans le bassin du Sud-Est de la France, indice possible d'un événement anoxique fini-hauterivien étendu à la Téthys méditerranéenne. Bulletin de la Société Géologique de France 170 (4), 487-498.

Behar, F., Beaumont, V., Penteado, H.L.D., 2001. Rock-Eval 6 technology: Performances

and developments. Oil and Gas Science and Technology 56 (2), 111-134.

Benitez-Nelson, C.R., 2000. The biogeochemical cycling of phosphorus in marine systems. Earth-Science Reviews 51 (1-4), 109-135.

Bréhéret, J.-G., 1994. The Mid-Cretaceous organic-rich sediments from the Vocontian zone of the French Southeast basin. In Mascle, A. (Ed.), Hydrocarbon and Petroleum Geology of France, Special Publication of the European Association of Petroleum Geoscientists, 4, p. 295-320.

Broecker, W.S., Peng, T.-H., 1982. Tracers in the sea, Lamont-Doherty Geological Observatory, Columbia University, Palisades, New-York, Eldigio Press, 690 pp.

Busnardo, R., 1965. Le stratotype du Barrémien. Mémoires du Bureau de Recherche Géologiques et Minières 34, 101-116.

Busnardo, R., Charollais, J., Weidmann, M., Clavel, B., 2003. Le Crétacé inférieur de la Veveyse de Châtel (Ultrahelvétique des Préalpes externes; canton de Fribourg, Suisse). Revue Paléobiology., Genève 22 (1), 1-174.

Cecca, F., Faraoni, P., Marini, A., Pallini, G., 1995. Field-trip across the representative sections for the Upper Hauterivian - Barremian ammonite biostratigraphy in the Maiolica exposed at Monte Nerone, Monte Petrano and Monte Catria (Umbria-Marche, Apennines). Memorie Descrittive della Carta Geologica d'Italia 51, 187-211.

Cecca, F., Marini, A., Pallini, G., Baudin, F., Begouen, V., 1994. A guide-level of the uppermost Hauterivian (Lower Cretaceous) in the pelagic succession of Umbria-Marche Apennines (Central Italy): the Faraoni Level. Riv. Ital. Paleontol. Stratigr. 99, 551-568.

Coccioni, R., Baudin, F., Cecca, F., Chiari, M., Galeotti, S., Gardin, S., Salvini, G., 1998. Integrated stratigraphic, palaeontological, and geochemical analysis of the uppermost Hauterivian Faraoni Level in the Fiume Bosso section, Umbria-Marche Apennines, Italy. Cretaceous Research 19 (1), 1-23.

Colman, A. S., Holland, H. D., 2000. The global diagenetic flux of phosphorus from marine sediments to the oceans; redox sensitivity and the control of atmospheric oxygen levels. In Glenn, C.R., Prévôt-Lucas, L., Lucas, J. (Eds.), Marine authigenesis; from global to microbial, SEPM Special Publication n° 66, pp. 53-75.

Compton, J., Mallinson, D., Glenn, C. R., Filippelli, G. M., Föllmi, K. B., Shields, G., Zanin, Y., 2000. Variations in the global phosphorus cycle. In Glenn, C.R., Prévôt-Lucas, L., Lucas, J. (Eds.), Marine authigenesis; from global to microbial, SEPM Special Publication n° 66, pp. 21-33.

Delaney, M. L., 1998. Phosphorus accumulation in marine sediments and the oceanic phosphorus cycle. Global Biogeochemical Cycles 12 (4), 563-572.

Delanoy, G., 1997. Biostratigraphie des faunes d'ammonites à la limite Barrémien-Aptien dans la région d'Angles-Barrême-Castellane. Annales du Muséum d'Histoire Naturelle de Nice (Nice), tome XII, 1-270.

Eaton, A.D., Clesceri, L.S., Greenberg, A. E., 1995. Standard methods for the examination of water and wastewater. 19th edition.

Emeis, K.-C., Struck, U., Leipe, T., Pollehne, F., Kunzendorf, H., Christiansen, C., 2000. Changes in the C, N, P burial rates in some Baltic Sea sediments over the last 150 years - relevance to P regeneration rates and the phosphorus cycle. Marine Geology 167, 43-59.

Erba, E., Channell, J.E.T., Claps, M., Jones, C.E., Larson, R.L., Opdyke, B., Premoli-Silva, I., Riva, A., Salvini, G., Torriceli, S., 1999. Integrated stratigraphy of the Cismon APTICORE (Southern Alps, Italy): A «reference section» for the Barremian-Aptian interval at low

latitudes. Journal of Foraminiferal Research 29 (4), 371-391.

Fiet, N., Gorin, G., 2000. Lithological expression of Milankovitch cyclicity in carbonate-dominated, pelagic, Barremian deposits in central Italy. Cretaceous Research 21 (4), 457-467.

Filippelli, G.M., Delaney, L.M., 1996. Phosphorus geochemistry of equatorial Pacific sediments. Geochimica et Cosmochimica Acta 60 (9), 1479-1495.

Filippelli, G.M., Delaney, M.L., 1995. Phosphorus geochemestry, diagenesis, and mass balances of the Miocene Monterey Formation at Shell Beach, California. U.S. Geological Survey Bulletin, G1-G11.

Föllmi, K.B., 1995. 160 m.y. record of marine sedimentary phosphorus burial: Coupling of climate and continental weathering under greenhouse and icehouse conditions. Geology 23, 859-862.

Föllmi, K.B. 1996. The phosphorus cycle, phosphogenesis and marine phosphate-rich deposits. Earth-Science Reviews 40 (1-2), 55-124.

Föllmi, K.B., Tamburini, F., Hosein, R., Van de Schootbrugge, B., Arn, K., Rambeau, C., 2004. Phosphorus, a servant faithful to Gaia? Biosphere remediation rather than regulation. In Schneider, S.H., Miller, J.R., Crist, E., Boston, P.J. (Eds.), Scientist Debate Gaia: The Next Century, pp. 79-92.

Föllmi, K.B., Weissert, H., Bisping, M., Funk, H., 1994. Phosphogenesis, carbon-isotope stratigraphy, and carbonate-platform evolution along the Lower Cretaceous northern Tethyan margin. Geological Society of America Bulletin 106 (6), 729-746.

Funk, H., 1969. Typusprofile der helvetischen Kieselkalk Formation und der Altmann Schichten. Eclogae geologicae Helvetiae 62 (1), 191-203.

Gale, A.S., Smith, A.B., Monks, N.E.A., Young, J.A., Howard, A., Wray, D.S., Huggett, J.M., 2000. Marine biodiversity through the late Cenomanian - Early Turonian: palaeoceanographic controls and sequence stratigraphic biases. Journal of Geological Society of London 157, 745-757.

Giraud, F., Beaufort, L., Cotillon, P., 1995. Contrôle astronomique de la sédimentation carbonatée dans le Crétacé inférieur du Bassin vocontien (SE France). Bulletin de la Société Géologique de France 166 (4), 409-421.

Godet, A., Bodin, S., Föllmi, K.B., Vermeulen, J., Gardin, S., Fiet, N., Adatte, T., Berner, Z., Stüben, D., van de Schootbrugge, B., 2006. Evolution of marine stable carbon-isotope record during the early Cretaceous: A focus on the late Hauterivian and Barremian in the Tethyan realm. Earth and Planetary Science Letters, In press.

Gradstein, F.M., Ogg, J.G., Smith, A.G., Bleeker, W., Lourens, L.J., 2004. A new Geologic Time Scale with special reference to Precambrian and Neogene. Episodes 27 (2), 83-100.

Haq, B.U., Hardenbol, J., Vail, P.R., 1987. Chronology of fluctuating sea levels since the Triassic. Science 235, 1156-1167.

Hardenbol, J., Thierry, J., Farley, M.B., de Graciansky, P.-C., Vail, P. R., 1998. Mesozoic and Cenozoic Sequence Chronostratigraphic Framework of European Basins. In de Graciansky, P.-C., Hardenbol, J., Jacquin, T., Vail, P. R. (Eds.), Mesozoic and Cenozoic Sequence Stratigraphy of European Basins. Special Publication Society for Sedimentary Geology, 3-13.

Hay, W.W., DeConto, R., Wold, C.N., Wilson, K.M., Voigt, S., Schulz, M., Wold-Rossby, A., Dullo, W.-C., Ronov, A.B., Balukhovsky, A.N., Soeding, E., 1999. Alternative global Cretaceous paleogeography. In Barrera, E., Johnson, C. (Eds.), The Evolution of Cretaceous Ocean/Climate Systems. Geological Society of America Special Paper, p. 332.

Herrle, J.O., 2002. Paleoceanographic and paleoclimatic implications on Mid-Cretaceous black shale formation in the

Vocontian basin and the Atlantic: Evidence from calcareous nannofossils and stable isotopes. Mikropaläontologische Mitteilungen 27, 1-113.

Hilbrecht, H., Frieg, C., Troger, K.-A., Voigt, S., Voigt, T., 1996. Shallow water facies during the Cenomanian-Turonian anoxic event: bio-events, isotopes, and sea level in southern Germany. Cretaceous Research 17, 229-253.

Holland, H.D., 1994. The phosphate-oxygen connection. Eos Trans. AGU 75 (3) (Ocean Sci. Meet. Suppl.: 96).

Ingall, E., Jahnke, R., 1994. Evidence for enhanced phosphorus regeneration from marine sediments overlain by oxygen depleted waters. Geochimica et Cosmochimica Acta 58 (11), 2571-2575.

Ingall, E.D., Bustin, R.M., Van Cappellen, P., 1993. Influence of water column anoxia on the burial and preservation of carbon and phosphorus in marine shales. Geochimica et Cosmochimica Acta 57 (2), 303-316.

Ingall, E.D., Jahnke, R., 1997. Influence of water-column anoxia on the elemental fractionation of carbon and phosphorus during sediment diagenesis. Marine Geology 139, 219-229.

Iruthayaraj, M.R., Morachan, Y.B., 1978. Relationship between evaporation from different evaporimeters and meteorological parameters. Agricultural Meteorology 19 (2-3), 93-100.

Jarvis, I., Mabrouk, A., Moody, R.T.J., de Cabrera, S., 2002. Late Cretaceous (Campanian) carbon isotope events, sea-level change and correlation of the Tethyan and Boreal realms. Palaeogeography, Palaeoclimatology, Palaeoecology 188 (3-4), 215-248.

Jenkyns, H.C., 1999. Mesozoic anoxic events and palaeoclimate. Zentralblatt Geologie und Paläontologie 1 (Heft 7-9), 943-949.

Jenkyns, H.C., 2003. Evidence for rapid climate change in the Mesozoic-Palaeogene greenhouse world. Philosophical Transactions of the Royal Society, London, A 361, 1885-1916.

Jenkyns, H.C., Gale, A.S., Corfield, R.M., 1994. Carbon- and oxygen-isotope stratigraphy of the English Chalk and Italian Scaglia and its palaeoclimatic significance. Geological Magazine 131, 1-34.

Jones, C.E., Jenkyns, H. C., 2001. Seawater strontium isotopes, oceanic anoxic events, and seafloor hydrothermal activity in the Jurassic and Cretaceous. American Journal of Science 301, 112-149.

Lenton, T.M., Watson, A.J., 2000. Redfield revisited: 2. What regulates the oxygen content of the atmosphere? Global Biogeochemical Cycles 14 (1), 249-268.

Lini, A., Weissert, H., Erba, E., 1992. The Valanginian carbon isotope event; a first episode of greenhouse climate conditions during the Cretaceous. Terra Nova 4 (3), 374-384.

Mutterlose, J., Bornemann, A., 2000. Distribution and facies patterns of Lower Cretaceous sediments in northern Germany: a review. Cretaceous Research 21 (6), 733-759.

Redfield, A.C., 1958. The biological control of chemical factors in the environment. American Scientist 46, 205-222.

Reimers, C., Kastner, M., Garrison, R.E., 1990. The role of bacterial mats in phosphate mineralization with particuliar reference to the Monterey Formation. In Burnett, W.C., Riggs, S.R. (Eds.), Phophate Deposits of the World, Vol. 3, Neogene to Modern Phosphorites, Cambridge University Press, p. 300-311.

Ruttenberg, K.C., 1992. Development of a sequential extraction method for different forms of phosphorus in marine sediments. Limnology Oceanography 37 (7), 1460-1482.

Ruttenberg, K.C., 1993. Reassessment of the oceanic residence time of phosphorus. Chemical Geology 107 (3-4), 405-409.

Schlanger, S.O., Arthur, M.A., Jenkyns, H.C., Scholle, P.A., 1987. The Cenomanian-Turonian oceanic anoxic event: I. Stratigraphy and distribution of organic-rich beds and the marine 13C excursion.

In Brooks, J., Fleet, A.J. (Eds.), Marine Petroleum Sources Rocks, Geological Society, London, Special Publications, 371-399.

Schlanger, S.O., Jenkyns, H.C., 1976. Cretaceous oceanic anoxic events: causes and consequences. Geologie en Mijnbouw 55, 179-184.

Slomp, C.P., Thomson, J., de Lange, G.J., 2004. Controls on phosphorus regeneration and burial during formation of eastern Mediterranean sapropels. Marine Geology 203 (1-2), 141-159.

Stallard, R.F., Edmond, J.M., 1983. Geochemestry of the Amazon: 2. The influence of geology and weathering environment on the dissolved load. Journal of Geophysical Research 88, 9671-9688.

Tamburini, F., Föllmi, K.B., Adatte, T., Bernasconi, S.M., and Steinmann, P., 2003. Sedimentary phosphorus record from the Oman margin: New evidence of high productivity during glacial periods. Paleoceanography 18 (1), PA 1015.

Tamburini, F., Huon, S., Steinmann, P., Grousset, F.E., Adatte, T., Föllmi, K.B., 2002. Dysaerobic conditions during Heinrich events 4 and 5: Evidence from phosphorus distribution in a North Atlantic deep-sea core. Geochimica et Cosmochimica Acta 66 (23), 4069-4083.

Trümpy, R., 1960. Paleotectonic evolution of the Central and Western Alps. Bulletin of the Geological Society of America 71, 843-908.

Tyrrell, T., 1999. The relative influences of nitrogen and phosphorus on oceanic primary production. Nature 400, 525-531.

Van Cappellen, P., Ingall, E.D., 1996. Redox stabilization of the atmosphere and oceans by phosphorus-limited marine productivity. Science 271, 493-496.

Van de Schootbrugge, B., Föllmi, K.B., Bulot, L.G., Burns, S.J., 2000. Paleoceanographic changes during the early Cretaceous (Valanginian-Hauterivian): evidence from oxygen and carbon stable isotopes. Earth and Planetary Science Letters 181, 15-31.

Van de Schootbrugge, B., Kuhn, O., Adatte, T., Steinmann, P., Föllmi, K.B., 2003. Decoupling of P- and Corg-burial following Early Cretaceous (Valanginian-Hauterivian) platform drowning along the NW Tethyan margin. Palaeogeography, Palaeoclimatology, Palaeoecology 199 (3-4), 315-331.

Vermeulen, J., 1980. Etude de la famille des Pulchelliidae, révision de trois espèces types du Barrémien du Sud-Est de la France, Thèse de Doctorat de Spécialité, Nice, 101 pp.

Vermeulen, J., 2002. Etude stratigraphique et paléontologique de la famille des Pulchelliidae (ammonoidea, Ammonitina, Endemoceratacea). Géologie alpine, Grenoble, France, 333 pp.

Weissert, H., 1989. C-isotope stratigraphy, a monitor of paleoenvironmental change: a case study from the Early Cretaceous. Surveys in Geophysics 10, 1-61.

Weissert, H., Erba, E., 2004. Volcanism, CO2 and palaeoclimate; a Late Jurassic-Early Cretaceous carbon and oxygen isotope record. Journal of the Geological Society of London 161 (4), 695-702.

Weissert, H., Lini, A., Föllmi, K.B., Kuhn, O., 1998. Correlation of Early Cretaceous carbon isotope stratigraphy and platform drowning events: a possible link? Palaeogeography, Palaeoclimatology, Palaeoecology 137, 189-203.

Wissler, L., Weissert, H., Buonocunto, F. P., Ferreri, V., and D'Argenio, B., 2004. Calibration of the Early Cretaceous time scale: a combined chemostratigraphic and cyclostratigraphic approach to the Barremian-Aptian interval, Campania Apennines and Southern Alps (Italy). In D'Argenio, B., Fischer, A.G., Premoli-Silva, I., Weissert, H., Ferreri, V. (Eds.), Cyclostratigraphy: Approach and case histories, SEPM Special Publication No. 81, 123-133.

Wissler, L., Weissert, H., Masse, J.-P., and Bulot, L.G., 2002. Chemostratigraphic correlation of Barremian and lower Aptian ammonite zones and magnetic reversals. International Journal of Earth sciences (Geol. Rundsch.) 91, 272-279.

C.4.

Evolution of the marine stable carbon-isotope record during the early Cretaceous: A focus on the late Hauterivian and Barremian in the Tethyan realm

Alexis Godet [1], Stéphane Bodin [1], Karl B. Föllmi [1], Jean Vermeulen [2], Silvia Gardin [3], Nicolas Fiet [4], Thierry Adatte [1], Zsolt Berner [5], Doris Stüben [5], Bas van de Schootbrugge [6]

[1] Institut de Géologie, Université de Neuchâtel, rue Emile Argand 11, 2007 Neuchâtel, Switzerland.

[2] Grand Rue, 04330 Barrême, France.

3 CNRS-UMR 5143 «Paléobiodiversité et Paléoenvironnement», case 104, Université Paris 6, 4 Place Jussieu, 75252 Paris Cedex 05, France.

[4] UMR 8148 – I.D.E.S., Bât. 504, University of Paris XI Orsay, 91405 Orsay Cedex, France

[5] Institut für Mineralogie und Geochemie, Universität Karlsruhe, 76131 Karlsruhe, Germany

[6] Institut für Geologie und Paläontologie, J.W. Goethe Universität, 60054 Frankfurt am Main, Germany

Keywords: Hauterivian; Barremian; Tethys; oceanic anoxic Faraoni event; carbon and oxygen isotopes; paleoceanography.

Published in: Earth and Planetary Science Letters **242** (2006), 254-271

Abstract

In order to improve our understanding of the relationships between the late Hauterivian oceanic anoxic Faraoni event, contemporaneous platform drowning along the northern Tethyan margin and global environmental change in general, we established high-resolution $\delta^{13}C$ and $\delta^{18}O$ curves for the late Hauterivian and the entire Barremian stage. These data were obtained from whole-rock carbonate samples from the Veveyse de Châtel St. Denis section (Switzerland), the Fiume-Bosso section and the nearby Gorgo a Cerbara section (central Italy), and the Angles section (Barremian stratotype, France).

We observe an increase of 0.3‰ in mean $\delta^{13}C$ values within sediments from the middle Hauterivian Subsaynella sayni ammonite zone to the Hauterivian-Barremian boundary; $\delta^{13}C$ values remain essentially stable during the early Barremian. During the latest early Barremian and most of the late Barremian, $\delta^{13}C$ values increase slowly (until the Imerites giraudi zone) and the latest Barremian is characterized by a negative trend in $\delta^{13}C$ values, with minimal values at the Barremian-Aptian boundary. During the earliest Aptian, $\delta^{13}C$ mean values start to rise again and attain +2.25‰.

We interpret the evolution of the $\delta^{13}C$ record as resulting from the interaction between changes in the carbon cycle in the Tethyan basin and the adjacent platforms and continents. In particular, changes towards warmer and more humid conditions on the continent and coeval phases of platform drowning along the northern Tethyan margin may have contributed to enhance the oceanic dissolved inorganic carbon (DIC) reservoir which may have pushed the $\delta^{13}C$ record towards more negative values and exerted a general attenuation on the $\delta^{13}C$ record. From this may have come the general change from a heterozoan to a photozoan carbonate platform community, which influenced the evolution in $\delta^{13}C$ values by increasing the export of aragonite and diminishing export of dissolved organic carbon into the basins.

C.4.1. Introduction

Correlated stratigraphic records of stable carbon isotopes measured in marine whole-rock carbonates or on isolated marine carbonate shells and skeletons provide very valuable insight into temporal changes in the global carbon cycle and in paleo-environmental conditions in general. The Cretaceous carbon cycle was perturbed by a series of short-lived oceanic anoxic events (OAEs) and contemporaneous phases of carbonate platform destruction, which are marked in the carbon isotope records of bulk carbonate ($\delta^{13}C_{carb}$) and organic matter ($\delta^{13}C_{org}$) record (e.g. [1-9]; compare also [10-12]). An exception to these observed links between environmental change and corresponding variations in the $\delta^{13}C$ record seems to be exemplified by the Faraoni anoxic event, a black-shale interval recovered in Tethyan (hemi-) pelagic sections of latest Hauterivian age [13, 14] and which is coeval to the onset of a major platform drowning episode along the northern Tethyan margin [3]. This event does not appear to be associated with an abrupt change in $\delta^{13}C$ values but rather with a long-term increase in the $\delta^{13}C$ record (e.g. [15]).

We investigated four hemipelagic to pelagic sections in the Tethyan realm (Angles (SE France), Fiume-Bosso (central Italy), Gorgo a Cerbara (central Italy) and Veveyse de Châtel-St. Denis (west Switzerland)), in order to more precisely constrain the $\delta^{13}C$ and $\delta^{18}O$ record around the Faraoni anoxic event and during the associated platform drowning event, which itself extends well into the early Barremian. We associate the obtained trends with changes in the oceanic carbon cycle, which was influenced by a number of mechanisms, amongst which we count the paleo-ecology of Tethyan carbonate platforms and their influence on the isotope signature of inorganic carbon species. In particular, we suggest that the change between photozoan and heterozoan dominated carbonate-platform ecosystem [3] may influence the isotope signature of the adjacent open ocean.

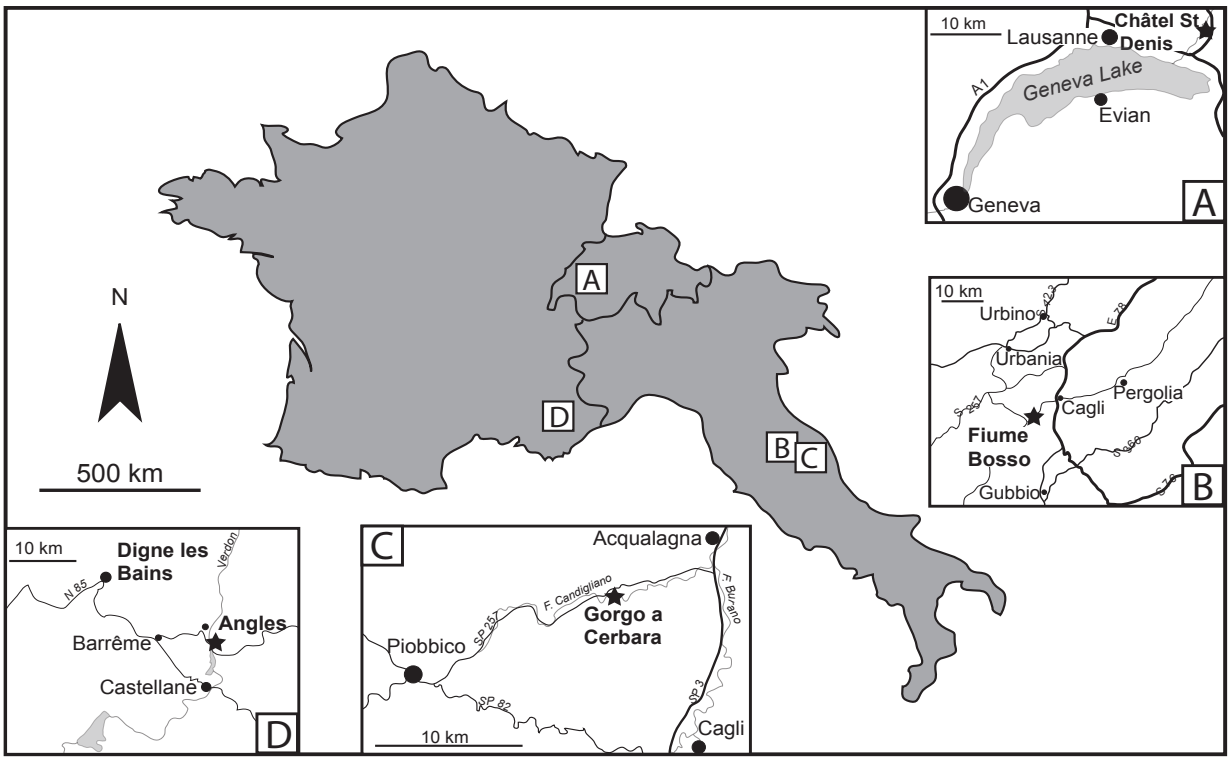

Fig. C.4.1: location of the different studied sections.

C.4.2. Geological setting

C.4.2.1. The sections of Fiume Bosso and Gorgo a Cerbara

The lower Cretaceous sedimentary succession of the Umbria Marche basin (Italy) is composed of the Maiolica (late Tithonian to early Aptian) and the Marne a Fucoidi (early Aptian to late Albian) formations [16].

The section of Fiume Bosso (FB) is located between Urbino and Gubbio, near Cagli (central Italy, Fig. C.4.1; see also [13]). It represents the type section for the Faraoni level [13]. The section is composed of white to grey limestone of the Maiolica Formation which is regularly intercalated with siliceous lenses and layers and contains rare marly and shaly, organic-rich intervals; it was deposited in a pelagic environment near the central zone of the Tethys (paleo-latitude ≈ 17°N for the middle Cretaceous after [17]). The magnetostratigraphy and ammonite biostratigraphy of this section were provided by Channel et al. [18] and by Cecca et al. [13], respectively. Coccioni et al. [16] employed an accurate age model for the middle part of the measured section, where they recognized the Pseudothurmannia angulicostata auct., Pseudothurmannia catulloi and Spitidiscus hugii ammonite zones (Fig. C.4.2).

The section of Gorgo a Cerbara (GC) is located approximately 4 km east of Piobbico, along the Candigliano River (Fig. C.4.1; cf. [19]). This outcrop represents the type locality for the Barremian-Aptian boundary (e.g. [20]) and consists of a lithology which is comparable to that of the FB section. As the GC section covers the entire Barremian stage (e.g. [21]), it complements the FB section upward.

C.4.2.2. The section of the Veveyse de Châtel-Saint-Denis

The section at Veveyse de Châtel-Saint-Denis (VCD) is located in the canton of Fribourg, Switzerland (Fig. C.4.1) and is part of the tectonic unit "Ecaille de Riondonnaire" (Ultrahelvetic realm, northern Tethyan shelf margin [22, 23]).

The measured VCD section consists of bioturbated limestones alternating with marls, and covers the time interval from the late Hauterivian (S. sayni zone) to the early Barremian (Avramidiscus hugii zone; [23]). This section lacks chert and the amount of marls is higher, in comparison with the FB and GC sections.

C.4.2.3. The section of Angles

The section at route d'Angles (RA) is located in the Alpes de Haute Provence region of France (Fig. C.4.1) and represents the stratotype of the Barremian stage [24]. The sediments of this hemipelagic section were deposited in the Vocontian Trough (e.g. [14]).

For this section, we used the bio-stratigraphical scheme of Vermeulen [25], who developed an ammonite zonation from the Balearites balearis zone (late Hauterivian) up to the Martellites sarasini zone (late Barremian); the upper part of the section (early Aptian) is not yet completely prospected, but is thought to belong to the Deshayesites oglalensis zone. Lithologically, the Angles section is composed of poorly bioturbated grey limestones alternating with dark marls.

C.4.3. Methods

We measured all sections in detail sampling each separate limestone bed and, where appropriate, the marl and black-shale levels. The carbonate samples were sawn in order to eliminate weathered surfaces and recrystallized areas or veins. Rock powder was obtained by using a mechanic agate crusher.

The samples of the FB, VCD, and RA sections were analyzed at the stable isotope laboratory of the Department of Mineralogy and Geochemistry at the University of Karlsruhe, Germany, using an Optima (Micromass, UK) ratio mass spectrometer equipped with an online carbonate preparation line (MultiCarb)

with separate vials for each sample. Subsequent replicate sample analyses for $\delta^{13}C$ were within 0.05 to 0.06‰ and for $\delta^{18}O$ ranged from 0.06 to 0.12‰. Carbonates samples from the GC section were analyzed at the Stable Isotope Laboratory of Hydrology (UMR 8148-IDES, University of Paris Sud, Orsay, France), using a VG SIRA 10 triple collector instrument. The powdered carbonate samples were reacted with anhydrous orthophosphoric acid at 25 °C [26]. Using internal carbonate standards, the reference material NBS 19 as well as replicate analyses of samples, the reproducibility of C and O analyses was better than ± 0.05 ‰ and ± 0.08 ‰ respectively.

C.4.4. Note on the ammonite biostratigraphy used

During the last ten years, the ammonite zonation of the early Cretaceous has become more and more precise, due to the prospecting of several key sections such as the outcrops at Rio Argos (Spain) or Angles (France), and the correlation of the obtained biozonations (e.g. [27, 28]). As a consequence, the ammonite zonation currently proposed by the Kilian Group [28] is not identical with the biostratigraphy published for the FB, VCD and RA sections: the Pseudothurmannia mortilleti zone used by Vermeulen [25] in the latest Hauterivian does not exist in the biostratigraphy of the FB section [16], but corresponds to the upper part of the P. angulicostata auct. zone used at FB.

In table C.4.1, we propose a correlation between the different biostratigraphical schemes used for the VCD, FB and RA sections. For the VCD section, we use the zonation of Hoedemaeker and Rawson [27] instead of scheme adopted by Busnardo et al. [23], in order to facilitate the comparison between all studied sections.

Stages	Coccioni *et al.*, 1998	Hoedemaeker & Rawson, 2000	Vermeulen, 2002	Nannofossils events (Angles section, this work)
Aptian *p.p*			*D. oglalensis*	└ *Assipetra* spp. bloom
Late Barremian			*M. sarasini*	└ FO *R. irregularis*
			I. giraudi	
			H. feraudianus	
			G. sartousiana	
			H. sayni	└ FO *F. oblonga*
			H. uhligi	
Early Barremian			*C. darsi*	
			K. compressissima	
			N. pulchella	
		K. nicklesi	*K. nicklesi*	┐ LO *C. oblongata*
	S. hugii	*A. hugii*	*A. kiliani*	
Late Hauterivian	*P. angulicostata* auct.	*P. angulicostata* auct.	*P. mortilleti*	
			S. angulicostatum	┐ LO *L. bollii*
	B. balearis	*B. balearis*	*B. balearis*	
	P. ligatus	*P. ligatus*		
	S. sayni	*S. sayni*		

Table C.4.1: Synthesis of the different ammonite biostratigraphies used in the Fiume Bosso, Veveyse de Châtel Saint Denis and Angles sections ([16, 23, 25], respectively). Nannofossils bioevents from Angles are also reported (S. Gardin, this work).

C.4.5. Results

C.4.5.1. The sections of Fiume Bosso and Gorgo a Cerbara

The carbon isotope curve obtained for the FB section (Fig. C.4.2) shows a rather regular behavior for the lower part of the measured section, with $\delta^{13}C$ mean values increasing from 1.7 up to 2.15‰ (P. catulloi zone). The Faraoni level itself is characterized by a positive shift of approximately 0.15‰. In the upper part of the measured section, $\delta^{13}C$ mean values range between 1.8‰ and 1.9‰.

The $\delta^{18}O$ curve displays variations with a similar frequency, and with a range of mean values from –2.45 to –2.15‰.

The $\delta^{13}C$ record in sediments of the GC section displays a slight increase from approximately 2.2 to 2.7‰ (Fig. C.4.3). The general trend towards more positive values is superimposed by two negative excursions in sediments corresponding to the middle of the CM3 and to the interval around the Barremian – Aptian boundary.

The $\delta^{18}O$ curve shows a slight decrease from the base of the section up to sediments corresponding to the end of the CM3; in the following, the $\delta^{18}O$ record evolves slowly towards heavier values.

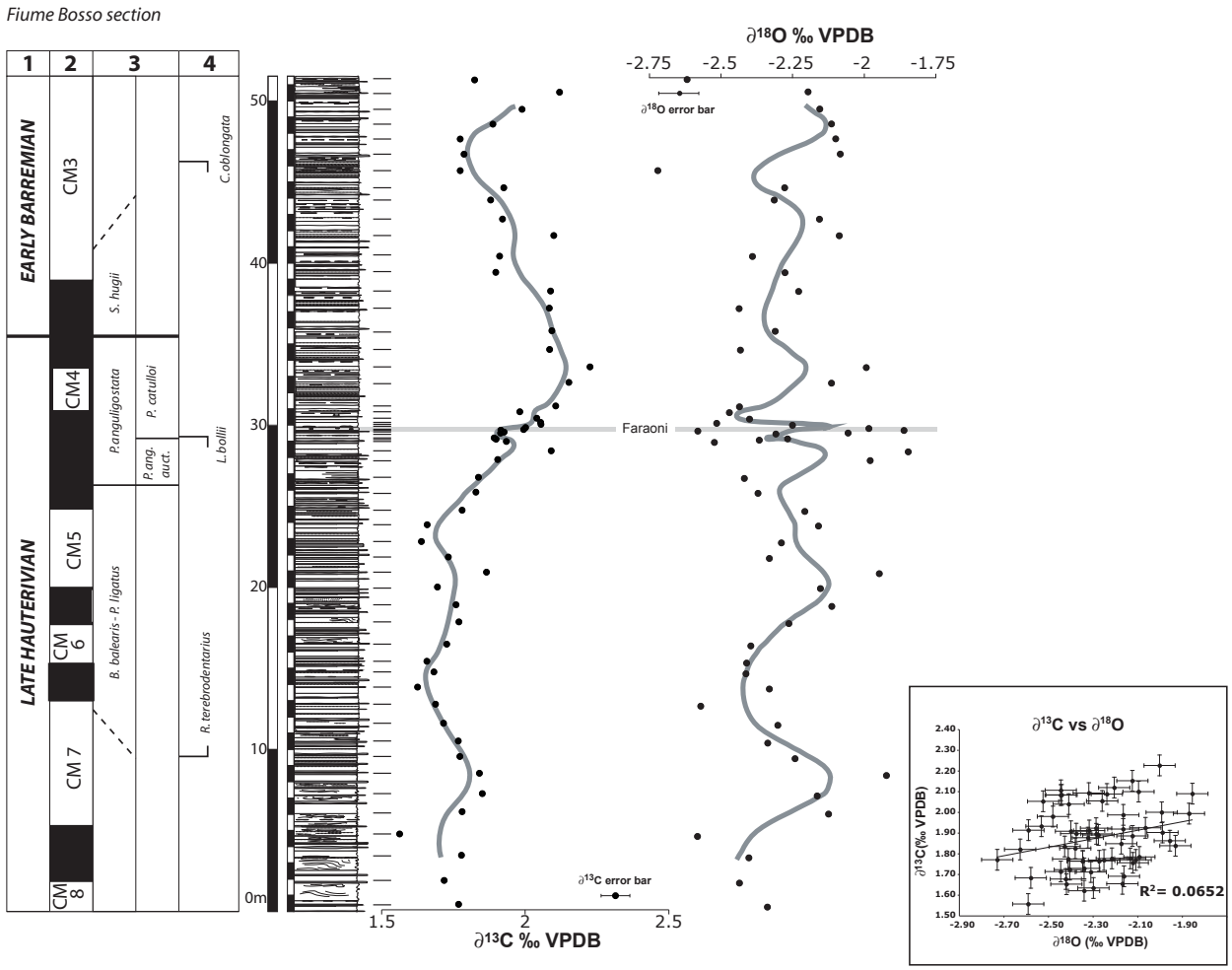

Fig. C.4.2: $\delta^{13}C$ and $\delta^{18}O$ curves obtained from whole-rock carbonate samples (n = 59) of the Fiume Bosso section. 1: stages; 2: magnetostratigraphy from Channell et al. [18]; 3: ammonite zonation after Coccioni et al. [16]; 4: nannofossil bioevents this work. The grey line represents the five point moving average curve.

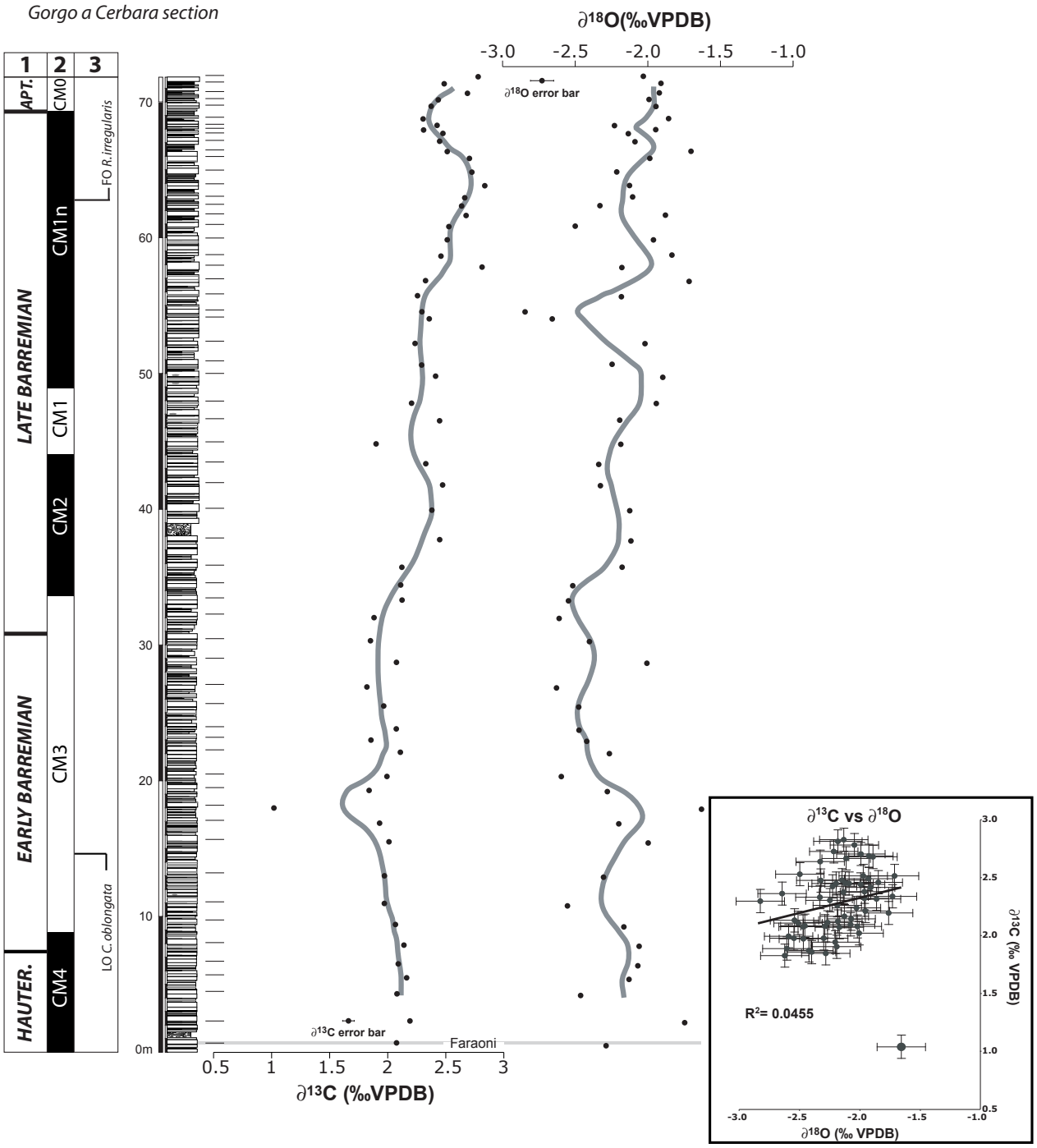

Fig. C.4.3: $\delta^{13}C$ and $\delta^{18}O$ curves obtained from whole-rock carbonate samples (n = 60) of the Gorgo a Cerbara section. 1: stages; 2: magnetostratigraphy after Lowrie and Alvarez [29], Erba [30] and Channell et al. [18], as reported in Fiet and Gorin [21]; 3: bioevents after Cecca et al. [31]. The grey line represents the five point moving average curve.

C.4.5.2. The section of the Veveyse de Châtel-Saint-Denis

In the lower part of the measured section (S. sayni zone up to the base of the Pseudothurmannia angulicostata zone), a slow and steady increase from 0.85 to 1.15‰ characterizes the main trend of the curve (Fig. C.4.4). In the overlying sediments of the P. angulicostata zone, the positive gradient in $\delta^{13}C$ curve becomes steeper, with a positive shift of about 0.5‰ in sediments in the vicinity of the "Couche à Poissons", which is considered as an equivalent of the Faraoni level [23]. The $\delta^{13}C$

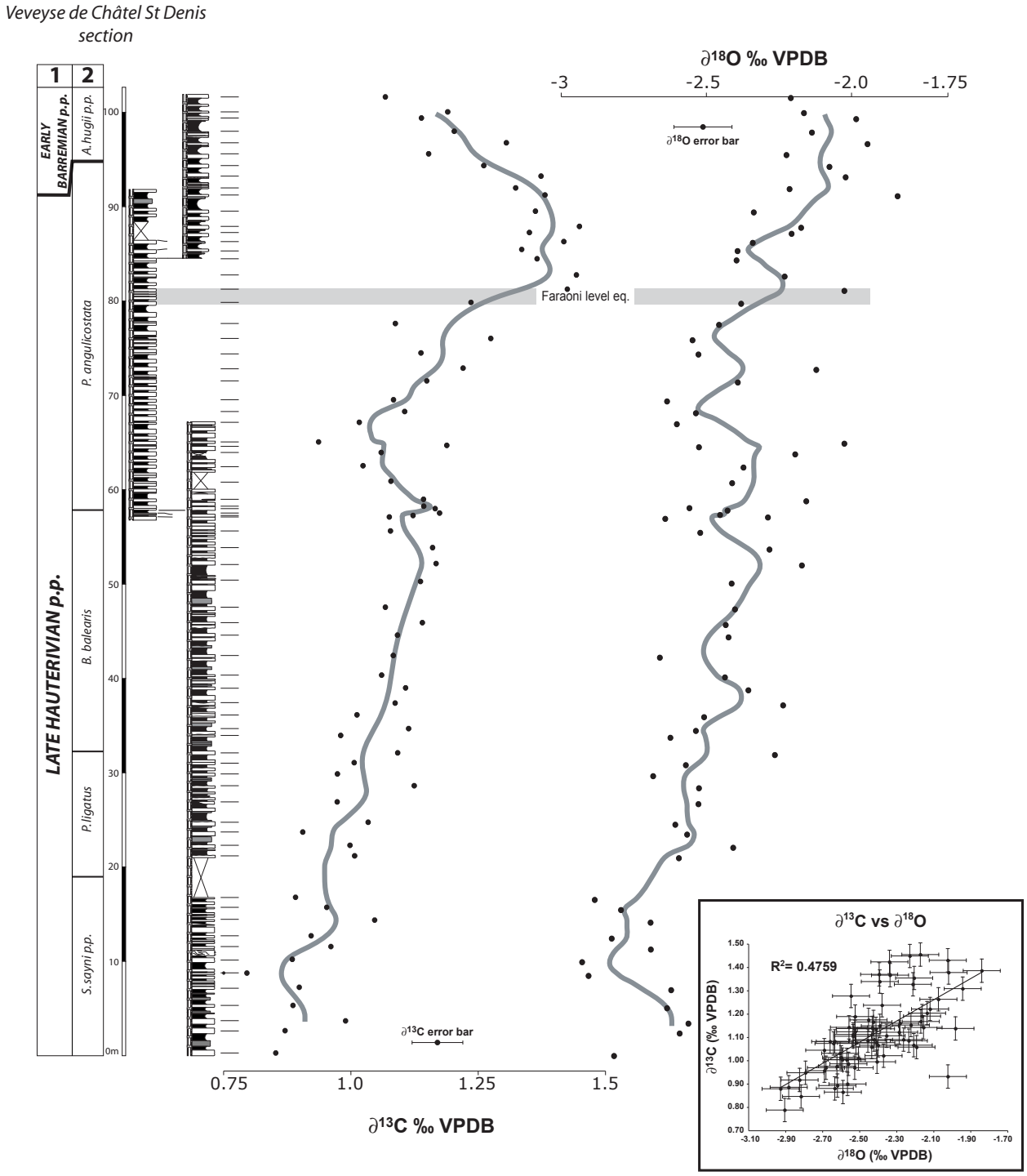

Fig. C.4.4: $\delta^{13}C$ and $\delta^{18}O$ curves obtained from whole-rock carbonate samples (n = 41) of the Veveyse de Châtel Saint Denis section. 1: stages; 2: ammonite zonation modified after Busnardo et al. [23]. The grey line represents the five point moving average curve.

curve reaches a maximum of approximately 1.35‰ in sediments just below the Hauterivian-Barremian boundary. In the uppermost part of the measured section the $\delta^{13}C$ curve shows a slight decreasing trend with values diminishing from 1.35 to 1.05‰.

The $\delta^{18}O$ curve is characterized by a general trend toward heavier values, from approximately –2.7‰ to –2.1‰, which seems to be superimposed by a shorter interval in sediments of the early P. angulicostata zone, where the trend in $\delta^{18}O$ is stable or even directed towards lighter values.

C.4.5.3. The section of Angles

The $\delta^{13}C$ curve displays a slight increase for sediments belonging to the B. balearis and Spathicrioceras angulicostatum zones (from 1 to 1.4‰; Fig. C.4.5); the data corresponding to the Faraoni equivalent display an acceleration of the general increase before a stabilization of the signal. After a decrease of 0.2‰ in the P. mortilleti and the A. kiliani zones, the $\delta^{13}C$ curve displays an irregular evolution from the K. nicklesi to K. compressissima zone. Sediments attributed to the C. darsi zone show an increase in $\delta^{13}C$ values from 1.3 to 1.8‰, whereas sediments from the Holcodiscus uhligi to Gerhardtia sartousiana zones display a more stable albeit a slightly increasing set of values. The $\delta^{13}C$ curve shows an increase for sediments of the Hemihoplites feraudianus zone, followed by a decrease from 2.25 to 1.75‰ for sediments belonging to the I. giraudi and M. sarasini zones. The $\delta^{13}C$ trend increases again to 2.25‰ in sediments of the D. oglanlensis zone, thereby marking a minimum precisely at the Barremian – Aptian boundary.

The evolution of the $\delta^{18}O$ curve is more variable, with a double negative peak from –3 to –4.15‰ near the base of the measured section. Then, the $\delta^{18}O$ record slowly increases in sediments belonging to the latest Hauterivian and remains rather stable for sediments in the remainder of the Hauterivian and the lower part of the early Barremian. In sediments from the N. pulchella to the H. sayni zone, the $\delta^{18}O$ trend is negative, with a minimal value of about –4.15‰ reached in sediments of the H. sayni zone. The subsequent positive trend in $\delta^{18}O$ values lasts until the base of the I. giraudi zone, where the $\delta^{18}O$ curve reaches a value of –2.75‰. The uppermost part of the $\delta^{18}O$ curve displays a decrease toward the lowest values of the measured section (–4.18‰).

C.4.6. Discussion

C.4.6.1. Stable isotopes and diagenesis

$\delta^{18}O$-$\delta^{13}C$ cross plots reveal a lack of correlation between the trends in oxygen and carbon isotopes for all sections (R^2 = 0.0652, 0.0686, 0.4759, and 0.041 for the FB, GC, VCD and RA sections, respectively; Fig. C.4.2 - C.4.5); the good correlation between the $\delta^{18}O$ and the $\delta^{13}C$ record at VCD may reflect the comparable evolution of both proxies during the late Hauterivian, as previously described by van de Schootbrugge [15]. Moreover, the results obtained are coherent with values for open marine carbonates from previous studies (e.g., [9, 15]; Fig. 8 in Weissert [1]). We assume therefore that for the four studied sections, diagenetic transformations had little impact on the carbon isotopic system.

The oxygen isotope record of the RA section, however, appears to be affected by slight diagenetic change: the $\delta^{18}O$ values are systematically lighter by approximately 1-1.2‰ in comparison with the other sections analyzed here or even to the Hauterivian part of the Vergons section [15]. This is consistent with the burial history of the RA section, which is part of the Digne thrust system and has been exposed to higher burial temperatures during alpine deformation (e.g., [15]). Thus, paleotemperatures can not be deduced from the absolute $\delta^{18}O$ values of RA, whereas trends in $\delta^{18}O$ may be used for correlation, as diagenesis did not totally reset the isotopic system as shown by the value of R^2 at RA and by the preservation of the clay mineral assemblage [32].

The $\delta^{18}O$ records for the Italian and Swiss sections show rather high and probably only mildly altered oxygen isotopic values, which is again consistent with their tectonic history. We will refrain from an indepth discussion of the trends discerned and only mention the long-term trend in $\delta^{18}O$ values.

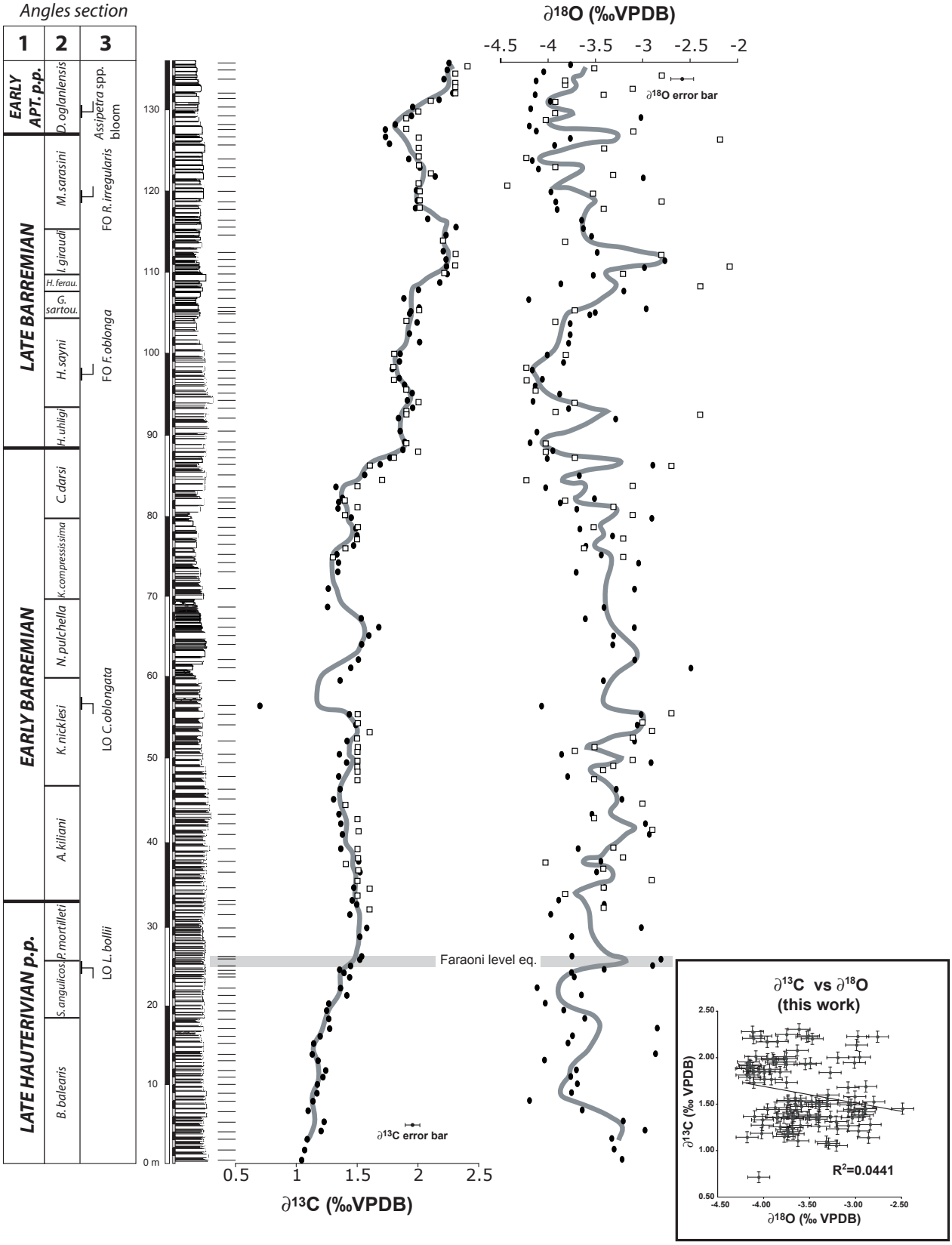

Fig. C.4.5: $\delta^{13}C$ and $\delta^{18}O$ curves obtained from whole-rock carbonate samples (black circles: this study, n = 116; white square: data from Wissler et al [35]) of the Angles section. 1: stages; 2: ammonites zone after Vermeulen [25]; 3: nannofossils bioevents (this work). The grey line represents the five point moving average curve. Note the complementarity of the data of [35] and of this study.

C.4.6.2. Evolution of the $\delta^{13}C$ record during the late Hauterivian and Barremian

The integration of geochemical, biostratigraphic and magnetostratigraphic data allows us to correlate and to describe general trends in the evolution of the $\delta^{13}C$ record for the time span between the S. sayni and the D. oglanlensis. In Fig. C.4.6, several time lines support our correlation between the Umbria-Marche basin, the Ultrahelvetic realm, and the Vocontian trough: (1) the top of the B. balearis ammonite zone between the VCD, FB, and RA sections; (2) the Faraoni level, which is considered to result from a synchronous anoxic event; this level is well approximated by the LO of nannofossil L. bollii at FB, RA, GC and Cismon; (3) the Hauterivian-Barremian boundary which is defined by means of ammonites in the VCD, RA, and FB sections; (4) the early / late Barremian boundary which is defined by ammonites at RA and by magnetostratigraphy, ammonites and nannofossils at GC and Cismon; and (5) the Barremian-Aptian boundary, which is defined by magnetostratigraphy and nannofossil biostratigraphy (FO of R. irregularis) in the GC section and the Cismon core, and by ammonite and nannofossil biostratigraphy in the RA section.

The trend in $\delta^{13}C$ values for the late Hauterivian appears to be marked by a stable long-term trend towards slightly higher values, which becomes more accentuated during the P. angulicostata zone. A maximum in $\delta^{13}C$ values for the late Hauterivian is reached in the upper P. angulicostata zone (VCD section), just above the Faraoni level. This implies that this level is placed within the slope of a positive increase in $\delta^{13}C$, with an amplitude of 0.5-0.8‰. This positive shift was already observed in the Vergons section, near the RA section [14, 15], and is thought to be characteristic of the Faraoni level. The short-lived negative excursion observed within the organic-rich Faraoni level of the FB section (Fig. C.4.2), which exhibits TOC values of up to 25% [16], is interpreted here to reflect a local, early diagenetic signal due to the mineralization of organic carbon during bacterial sulfate reduction (e.g. [34]).

The evolution of the $\delta^{13}C$ record during the early Barremian is illustrated by a trend toward more negative values in the A. kiliani zone (RA section), which is followed by an irregular long-term trend with no discernible gradient. The top of the early Barremian (C. darsi zone) is again marked by a positive gradient of about 0.4% (RA section).

The $\delta^{13}C$ record during the late Barremian shows an irregular long-term trend towards more positive values followed by a negative gradient. The Barremian-Aptian boundary is marked by a minimum in $\delta^{13}C$ values in both the RA and GC sections.

We also compared our results with the $\delta^{13}C$ record established for the Cismon Apticore (Fig. C.4.6; [33]) and from this correlation it appears that the identification of the early – late Barremian boundary in the RA, GC and Cismon sections is not coherent. At RA, this boundary is defined by ammonites, and corresponds to the end of a positive shift of the $\delta^{13}C$, whereas at GC this boundary is located in the upper part of the CM3 chron [18], just below the beginning of a positive shift, which seems comparable to the positive shift observed at RA. At Cismon, the location of the early-late Barremian boundary with respect to the positive shift of the $\delta^{13}C$ curve is identical to RA; however a discrepancy occurs between the magnetostratigraphic records from GC and Cismon, as the early-late Barremian boundary is located several meters above the boundary between the CM3 and CM2 magnetozones at Cismon.

The correlation of the RA and GC sections with the Cismon record shows a further discrepancy: Wissler et al. [35] already called into question the continuity of the record at RA and, in particular, proposed the presence of a significant hiatus in sediments attributed to the I. giraudi zone, and inferred the absence of up to 50% of the entire Barremian stage in the stratotype of the Barremian. In the RA

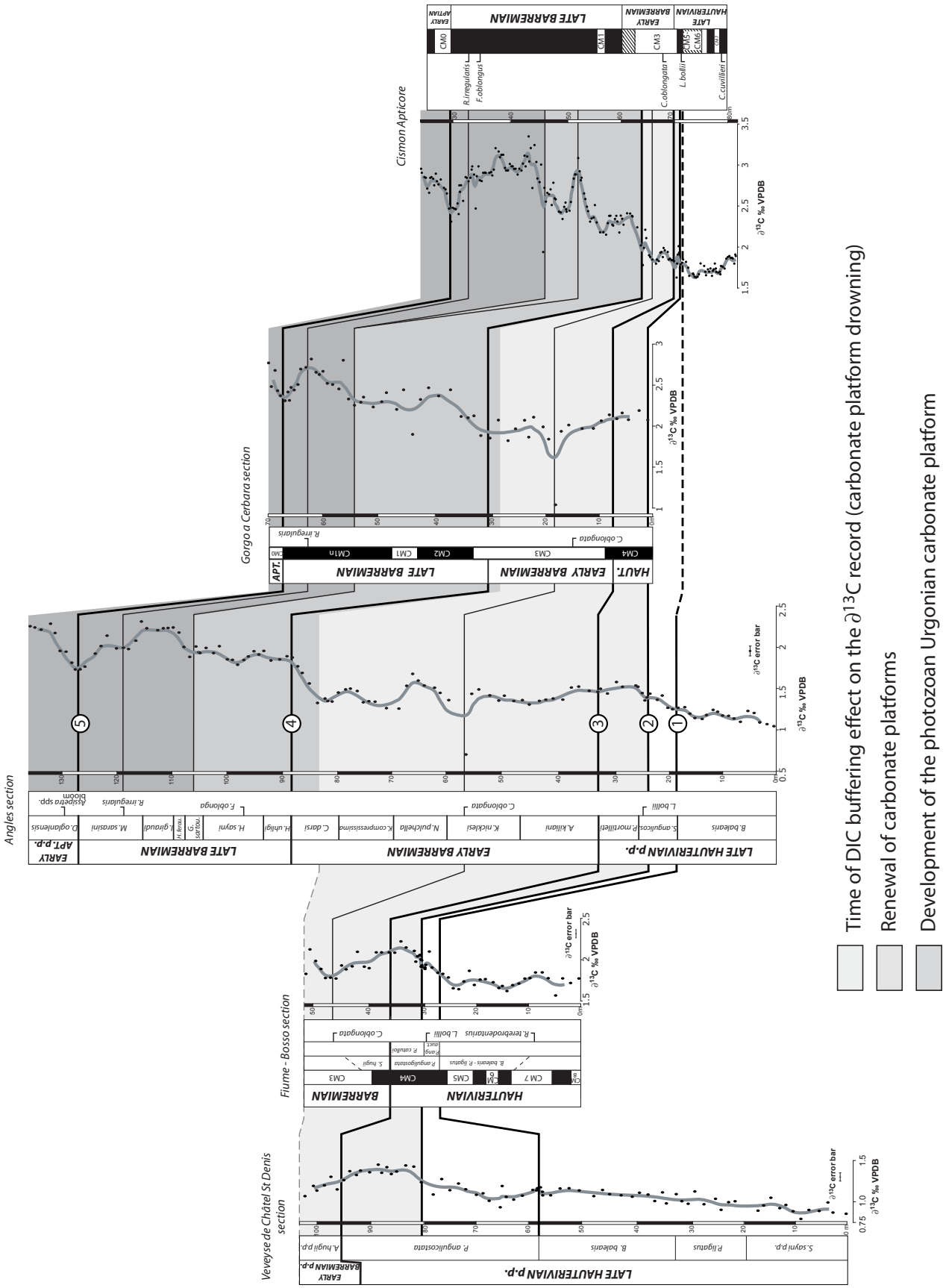

Fig. C.4.6: Correlation of the Veveyse de Châtel Saint Denis, Fiume Bosso, Angles, Gorgo a Cerbara and Cismon Apticore $\delta^{13}C$ curves (magnetostratigraphy and nannofossil bioevents of Cismon apticore from Erba et al. [33]). Numbers on the time-lines refer to the numbering used in the text.

section, the I. giraudi zone is characterized by a positive shift ($\Delta\delta^{13}C = 0.35‰$), which is also easily recognizable at GC and Cismon with amplitudes of 0.28 and 0.45‰, respectively. On the other hand, just below the above-mentioned positive shift, the $\delta^{13}C$ curve at Cismon displays a negative excursion, which is not recorded at RA. Based on these observations, it seems that either condensation or omission may have occurred in sediments belonging to the G. sartousiana or the H. feraudianus zones of the RA section. These phenomena may be linked to the maximum flooding surface of the B3 sequence, which is expressed by a glauconitic level within the G. sartousiana zone, or to the sequence boundary B4, a major sequence boundary in south-eastern France located in the H. feraudianus zone [36].

Alternatively, normal (syn-sedimentary?) faults led to the formation of a decametric graben in the H. sayni zone of the Angles section. It is therefore possible that a hiatus, coinciding with the first positive excursion of the Cismon section, is present within this zone. Further investigations are needed to solve this question.

C.4.6.3. Evolution of the $\delta^{18}O$ record during the late Hauterivian and Barremian

In Fig. C.4.7, the correlation of the $\delta^{18}O$ curves from the RA, VCD, and GC sections allows to define major trends in the evolution of the $\delta^{18}O$ during the late Hauterivian and the Barremian. We do not consider the FB section because it covers a relatively short time-period, and does not add essential information with regards to the long-term trend in $\delta^{18}O$ values. The late Hauterivian and a part of the early Barremian (until the K. nicklesi zone; data from the VCD and the RA sections) are characterized by an increase of approximately 1.1‰. The later is followed by a decreasing trend which lasted until the base of the H. sayni zone, with values reaching – 4.1‰ at Angles. The beginning of the late Barremian is characterized by a positive trend ($\Delta\delta^{18}O = 1.1‰$) with a maximum located near the base of the I. giraudi zone (RA section). Finally, the $\delta^{18}O$ record shows a decreasing trend for the latest Barremian and the earliest Aptian.

The increasing trend during the late Hauterivian may be linked to the installation of a marine passage between the boreal and the tethyan realms. Indeed, Mutterlose and Bornemann [37] described the arrival of tethyan faunas in lower Cretaceous sediments from northern Germany, in particular in the latest Hauterivian. This implies that a connection came into place between the Tethys and the boreal region during the late Hauterivian (Fig. 20 in [37]), which through the exchange of water masses may have led to relatively high $\delta^{18}O$ values observed in the late Hauterivian – early Barremian. This hypothesis is also supported by the presence of boreal nannofossil species at Angles in sediments of the P. mortilleti and A. kiliani zones. Alternatively, the $\delta^{18}O$ trend may reflect an increased salinity which would be in agreement with the enhanced evaporation and the subsequent increased continental weathering deduced from the kaolinite evolution during the latest Hauterivian and the early Barremian [32].

The return to more negative values in sediments from the N. pulchella to the H. sayni zones at RA (i.e., middle of CM3 to the base of CM2 at GC) may indicate the end of the interaction between boreal and tethyan water masses, and consequently the return to warmer oceanic temperatures; this would be in agreement with a short-term eustatic minimum [38].

Finally, the $\delta^{18}O$ curve forms a maximum which is located in the I. giraudi zone (RA section). This appears to be synchronous with a short-term eustatic maximum that would have led to the arrival of cooler water in the Tethys and a corresponding positive shift of the $\delta^{18}O$ curve. However, boreal nannofloras were not detected in this interval and therefore the trend towards higher values may also be due to climate cooling, in the absence of water-mass exchange between the Tethyan and the boreal realms.

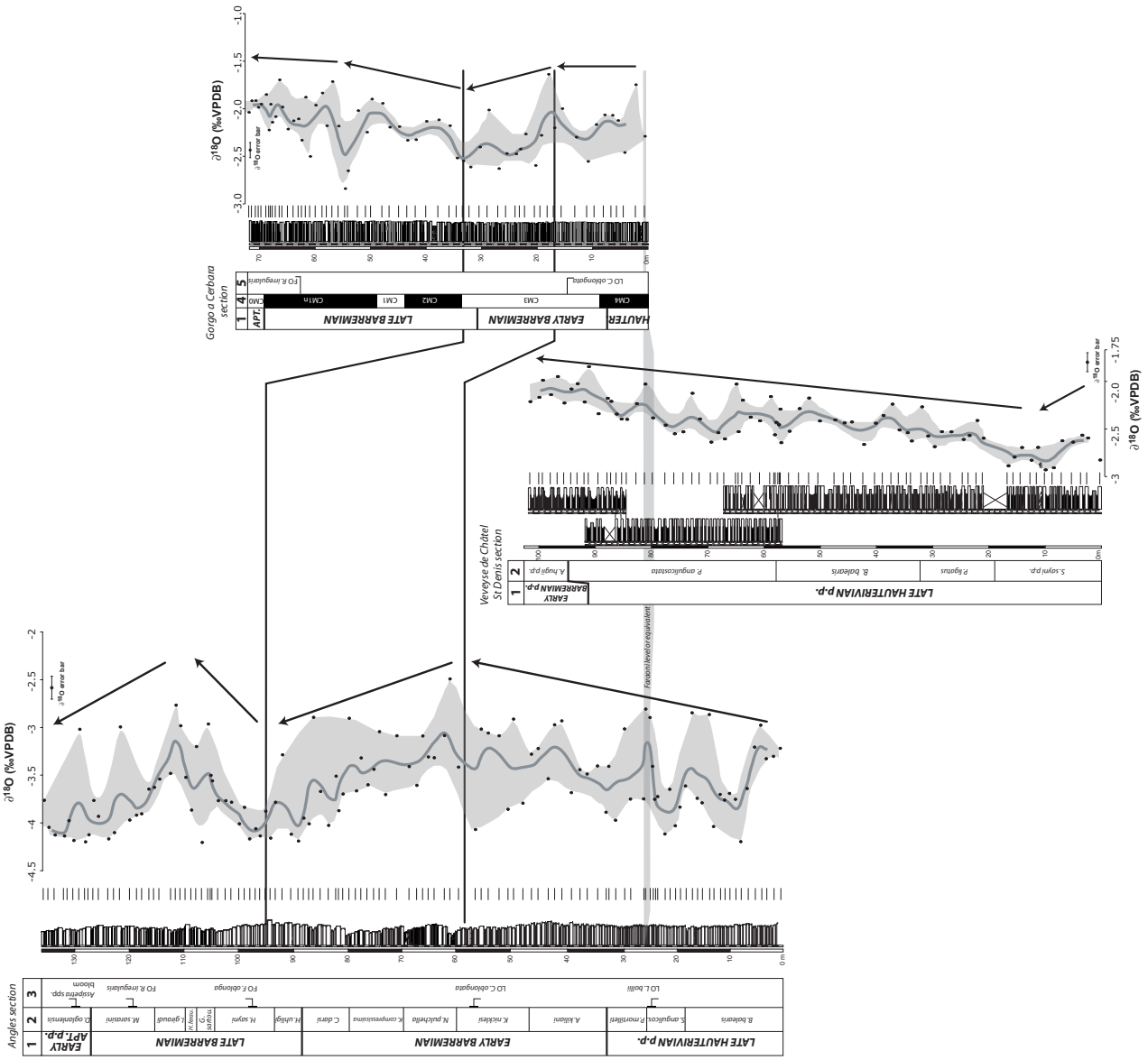

Fig. C.4.7: Correlation of the $\delta^{18}O$ curves from the Angles, Veveyse de Châtel Saint Denis and Gorgo a Cerbara sections. 1: stages; 2: ammonite zonations of the RA [25] and VCD (modified after [23]) sections; 3: nannofossils bioevents (this work); 4: magnetostratigraphy of GC [18, 21, 29, 30]; 5: nannofossils bioevents of the CG section [31]. The dark grey lines represent the five points moving average curves. The light grey areas represent the scattering of the minima and maxima values.

These observed trends are in agreement with the trends of the $\delta^{18}O$ curve obtained from belemnites by Podlaha et al. [39], van de Schootbrugge et al. [15] or by Veizer et al. [6], who observed the heaviest $\delta^{18}O$ values of the entire early Cretaceous during the Hauterivian, whereas the Barremian is characterized by an initial warming phase followed by a cooling phase. Moreover, the trend we observe is coherent with published early Cretaceous $\delta^{18}O$ curve [9]. This thermal evolution during the Barremian is also reported from fish tooth enamels analysis by Pucéat et al. [40], although the low-resolution of their study - probably due to the scarcity of fish teeth in sediments - does not allow a precise correlation between their results and the curves presented therein. Finally, the shift toward more negative values recorded at Angles from the I. giraudi zone to the top of the section, may correspond to the lower part of the negative shift recorded by rudists in the latest Barremian-earliest Aptian [41].

C.4.6.4. Possible mechanisms driving the evolution of the $\delta^{13}C$ values during the late Hauterivian and Barremian

In a classical sense, the evolution of the carbonate $\delta^{13}C$ record is interpreted as an approximation of the ratio between carbonate carbon and organic carbon burial fluxes in marine environments and their associated changes (e.g., [1, 5, 42]). External factors such as the release of methane from clathrate dissociation in slope environments (e.g., [43, 44]), atmosphere-ocean exchange of CO2 (including volcanic activity; e.g., [9]), and the influx of terrestrial organic matter may also influence this record as well (e.g., [45]).

A new approach in the interpretation of marine carbonate $\delta^{13}C$ records is given by a linkage in the style and intensity of shallow-water carbonate production and the rate of export of shallow-water carbonates into the basin environment, levels of dissolved inorganic carbon (DIC) in open oceans, and the $\delta^{13}C$ record (e.g., [46, 47]).

The latest Hauterivian is characterized by an increase in the $\delta^{13}C$ record ($\Delta\delta^{13}C$ = 0.5 – 1‰), which reaches a maximum just before the Hauterivian-Barremian boundary. The Faraoni level and its equivalents are localized in the middle of this positive gradient. Even if the $\delta^{13}C$ excursion does not have the same amplitude as the excursions associated with the oceanic anoxic events during the Valanginian, Aptian, and late Cenomanian (e.g. [2, 48, 49], respectively), the trend towards more positive values could still be explained by a shift in the burial ratio of organic carbon and carbonate carbon, as is suggested by the Faraoni anoxic event and the coeval onset in platform demise along the northern Tethyan margin. It remains, however, to be seen in how far this event has had an impact on the global carbon cycle. The Faraoni level is mainly known from the western Tethyan realm [14, 50]. Recently, a possible equivalent was described from the northwestern Pacific realm [51], which would imply that the extent of this event is more important than previously assumed. If indeed the Faraoni oceanic anoxic event is implied in this small positive shift in $\delta^{13}C$ values, an explanation for the attenuated isotope signature needs to be found. In following Bartley and Kah [46] we suggest that the attenuating effect may have been related to the increased size of the oceanic DIC reservoir.

Two principal processes may have enhanced the DIC reservoir during the late Hauterivian: (1) clay mineral studies in sections of late Hauterivian and Barremian age of the northern and the southern Tethyan margin in western Europe show systematic increases in kaolinite contents in the late Hauterivian, which may indicate a change of the climate towards warmer and more humid conditions for this time period [32, 52, 53]. Such climate conditions are favorable for increasing rates of DIC mobilization via biogeochemical weathering and throughput of DIC into the ocean by enhanced river transport [54]. During the late Hauterivian, the threefold evolution of ammonite fauna linked to sea-level fluctuations [55] may reflect the enhanced and facilitated export of DIC; (2) a widespread platform drowning event that started during the latest Hauterivian along the northern Tethyan margin may also have contributed to an increase in the oceanic DIC reservoir through the decrease in shallow-water carbonate production – a potential sink of DIC- and a corresponding increase in ocean alkalinity (e.g., [56]). The increased oceanic DIC reservoir may have been sustained throughout most of the early Barremian, paralleled by persisting drowning conditions on the northern Tethyan platform, and this may explain the rather steady evolution in the $\delta^{13}C$ record throughout the early Barremian.

The positive shift in the $\delta^{13}C$ record close to the early–late Barremian transition ($\Delta\delta^{13}C$ = 0.5-0.7‰) is more difficult to be explained in terms of changes in the burial ratio of organic and carbonate carbon, since to our knowledge no major change in organic carbon output has been documented from this time interval. We propose to link this shift to an important change in the shallow-water platform carbonate factory,

which is documented from the northern Tethyan margin and elsewhere: the platform drowning episode that started in the latest Hauterivian and ended near the early-late Barremian boundary (S. Bodin, pers. com.) marks the transition between carbonate production dominated by heterozoans ("green water" or foramol facies, [3, 57]) and photozoans ("blue water" or chlorozoan facies). This transition is documented by the widespread installation of the so-called «Urgonian» facies in France and Switzerland, which is, for example, also documented from the Cupido and Coahuila carbonate platforms of northeastern Mexico, where peritidal shelf-lagoonal carbonate deposits are formed during the late Barremian and Aptian ([58, 59]; see also [60]), and from the Jebel Akhdar in northeastern Oman where the installation and subsequent progradation of shallow-water carbonate platforms is observed during the Barremian [61, 62].

The principal carbonate mineral produced by heterozoan assemblages, which – in the helvetic realm - are dominated by crinoidal remains, is calcite, whereas photozoan assemblages also produced aragonite during the early Cretaceous (corals and associated rudists, green algae, etc.; e.g., [63, 64]). Aragonite tends to be enriched in ^{13}C relative to calcite and $\delta^{13}C_{aragonite}$ may reach values of up to 5‰ (e.g., [47, 65]). If produced by green algae, aragonite consists of a fine-grained material that is readily transported and exported into adjacent basins, where it is either dissolved in the water column or integrated into peri-platform sediments (e.g., [47, 66]). The increased export of meta-stable, ^{13}C-enriched particulate inorganic carbon (PIC) in the form of aragonite with the renewal of photozoan assemblages may have influenced the $\delta^{13}C$ record from the early-late Barremian transition, in particular through the installation of the Urgonian-type platforms in the G. sartousiana zone. This is coherent with the Phosphorus Mass Accumulation Rate evolution during this period [67]: the onset of photozoans may be coeval with oligotrophic conditions, which is in agreement with Mutti and Hallock [57]. Moreover, the arrival of photozoan carbonate platforms around the Tethys in the middle late Barremian may have led to a decrease in the oceanic DIC reservoir implicitly diminishing the DIC buffering effect. This we relate to the possible reduction in the throughput of DIC via the platform because of its transformation and storage by carbonate-producing organisms and because of the rather closed architecture of the platform, which is usually rimmed towards the basin by patch reefs and/or oolithic shoals. Consequently, the oceanic C-system would have become more sensitive to paleoceanographic and / or paleoecological perturbations, in particular to the export of material that holds a more positive $\delta^{13}C$ signature.

The negative excursion in $\delta^{13}C$ values of approximately 0.5‰ at the Barremian-Aptian boundary is in our view related to a widespread decrease in kaolinite and an increase of detrital input in general registered along the northern Tethyan margin and elsewhere, and a corresponding temporary disappearance of the Urgonian facies (e.g., [52, 68]). The corresponding increase in continentally derived DIC and decrease in shallow-water carbonate production may have contributed to this negative excursion. The involvement of increased methane release from slope environments cannot be excluded either (e.g., [7, 43]), even though direct evidence is lacking.

C.4.6.5. Quantification of the carbonate platform exportation and its influence on the pelagic record

In order to quantify the impact of the export of aragonite and/or calcite from the platform to the basin, we calculated theoretical $\delta^{13}C$ values that would result from an increasing input of platform-derived calcite or aragonite into the pelagic environment.

Concerning the platform, we estimated the volume of carbonates produced by using the surface covered by neritic carbonates during the early Aptian [69], and assuming a sedimentation rate of 5 $cm.ky^{-1}$ ([3, 62]). Using paleomaps of the Tethyan realm, Philip [69] estimated that the deposition of neritic carbonates was

mainly limited to intertropical seas, and that they covered an area of approximately 4.63 × 10^6 km^2 in the early Aptian. Presently, reefs are estimated to represent an area of only 247,000 km^2 [70]. The importance of late early Cretaceous shallow-water carbonate production relative to today points to a potentially significant influence on the oceanic carbon-cycle during the early Cretaceous. In this estimation we used a $\delta^{13}C_{calcite}$ value of 1‰ and a $\delta^{13}C_{aragonite}$ value of 5‰ [47].

For the pelagic production, we estimated the area covered by the Tethys as the average of the late Tithonian and early Aptian areas [71, 72]. Then, the volume of carbonate produced per ky and per km^2 was estimated from the sedimentation rate recorded during the late Barremian in the RA section, assuming that $CaCO_3$ represents on average, approximately 73% of the total pelagic sedimentation [73].

For both parts of the model we quantify both the quantity of ^{12}C and ^{13}C produced, then we calculate a theoretical $\delta^{13}C$ (noted $\delta^{13}C_{theo}$) that takes into account the influence of the platforms. So the variable parameters are the rate of export (ø) under particulate or dissolved form, and the $\delta^{13}C$ that would be recorded in the basin without any influence from the platforms ($\delta^{13}C_{ini}$).

The results (Fig. C.4.8) show that during time of aragonite production, the $\delta^{13}C$ increases; even with a ø of 20% and with a $\delta^{13}C_{ini}$ of 2‰, the $\delta^{13}C_{theo}$ reaches a value of 2.20‰. Such a shift is recorded in RA sediments attributed to the G. sartousiana zone, which corresponds to the onset of the Urgonian platform. In comparison, storms can remove up to 50 % of present-day reefs [74].

In contrast, the $\delta^{13}C_{theo}$ values decrease in the theoretical case that platform carbonate is mainly produced as calcite. With a $\delta^{13}C_{ini}$ value of 2‰ and a ø of 30%, the $\delta^{13}C_{theo}$ value corresponds to 1.90‰. This suggests that photozoan carbonate factories such as the Urgonian platforms and their potential to produce and export aragonite into the pelagic realm may have had a considerable effect on the pelagic $\delta^{13}C$ signal, whereas shallow-water carbonate production in the heterozoan mode would be less influential.

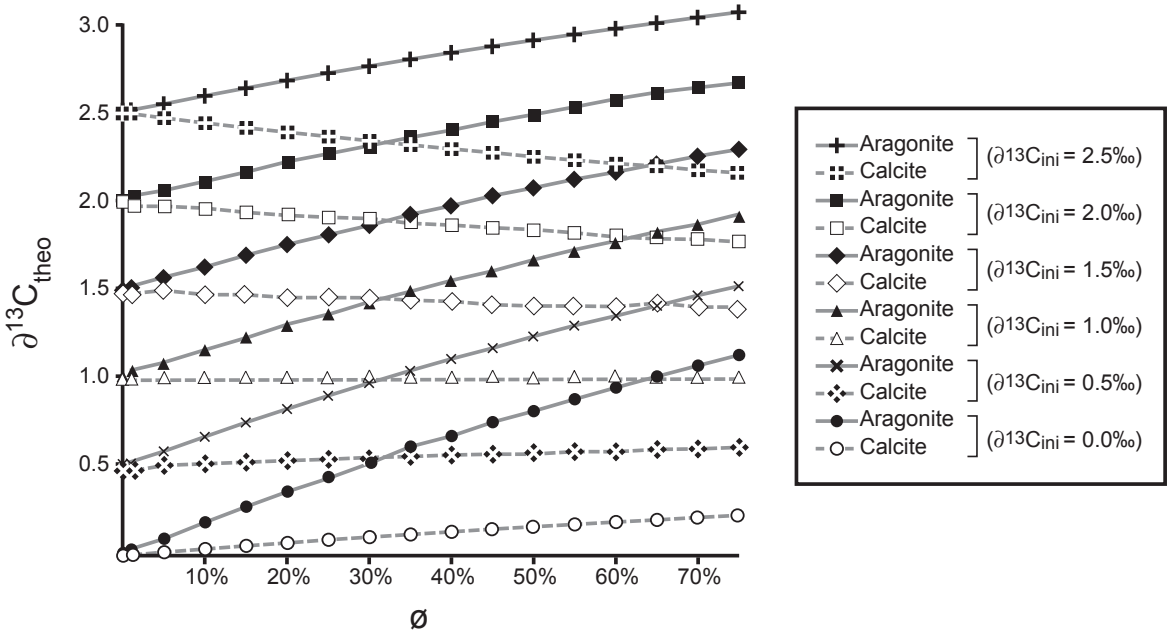

Fig. C.4.8: Predicted $\delta^{13}C$ values recorded in pelagic settings ($\delta^{13}C_{theo}$), as a function of the exportation rate (ø), of the $\delta^{13}C$ in the basin without platform influence ($\delta^{13}C_{ini}$) and of the mineralogy of the exported material ($\delta^{13}C_{calcite}$ = 1‰; $\delta^{13}C_{aragonite}$ = 5‰, after Swart and Eberli [47]).

C.4.7. Conclusions

The carbon and oxygen stable isotope records of selected sections representative for the northern and southern Tethyan margins give a consistent image of environmental change during the late Hauterivian and Barremian. The late Hauterivian is characterized by a long-term increase in the $\delta^{13}C$ record, which becomes accentuated during the latest part of this stage. This trend is explained here in a classical sense, with a shift in the burial ratio of organic and inorganic carbon in favor of organic carbon, which culminated in the widespread deposition of organic-rich sediments during the Faraoni oceanic anoxic event during the latest Hauterivian. This anoxic event is coeval with the onset of a platform drowning episode along the northern Tethyan margin, which lasted until the latest early Barremian. This was also a period of relative climate stability albeit with a tendency towards warmer conditions as is shown by the $\delta^{18}O$ record. The general stability of the $\delta^{13}C$ record during the early Barremian is explained by a buffering effect of the increased oceanic DIC reservoir, which is sustained by increased continental DIC input and diminished carbonate sedimentation rates along the northern Tethyan margin.

Near the transition from the early to the late Barremian, a shift toward more positive values is seen in the $\delta^{13}C$ record, which is explained here by the installation of widespread photozoan-type shallow-water carbonates of the so-called Urgonian platforms. This type of carbonate production likely favored the production of aragonite, which may have been a source of heavy $\delta^{13}C$ material in the adjacent basins, once exported into those realms.

The negative excursion in $\delta^{13}C$ values at the Barremian-Aptian boundary is explained by a widespread decrease in the production of photozoan carbonates and an increase in detritus, which both may have contributed to an increase in the transfer of DIC towards the ocean.

C.4.8. Acknowledgments

We acknowledge the Swiss National Science Foundation (projects 2100-067807/1 and 200020-105206/1) for its financial support and the “Réserve Géologique de Haute Provence” for its permission to sample the RA section. The authors would like to thank Rodolfo Coccioni (University of Urbino, Italy) and Jean Charollais (University of Geneva, Switzerland) for their advice and help in the field, and Elisabetta Erba (University of Milan, Italy) for providing the Cismon Apticore isotope data. We are also grateful to Haydon Mort, Pascal Linder, and Claire Rambeau (University of Neuchâtel, Switzerland) for their assistance during the sampling of the different sections, and to Gesine Preuss (University of Karlsruhe, Germany) for her technical support during the isotope analytical work. The quality of the English was improved by Haydon Mort, and this manuscript benefited from the constructive comments of three anonymous reviewers.

C.4.9. References

[1] H. Weissert, C-Isotope stratigraphy, a monitor of paleoenvironmental change: a case study from the Early Cretaceous, Surveys in Geophysics 10 (1989), 1-61.

[2] A. Lini, H. Weissert, E. Erba, The Valanginian carbon isotope event: a first episode of greenhouse climate conditions during the Cretaceous, Terra Nova 4 (1992), 374-384.

[3] K.B. Föllmi, H. Weissert, M. Bisping, H. Funk, Phosphogenesis, carbon-isotope stratigraphy, and carbonate-platform evolution along the Lower Cretaceous northern Tethyan margin, Geological Society of America Bulletin 106 (1994), 729-746.

[4] H.C. Jenkyns, A.S. Gale, P.M. Corfield, Carbon and oxygen isotope stratigraphy of english chalk and Italian Scaglia and its palaeoclimatic significance, Geol. Mag. 131 (1994), 1-34.

[5] H. Weissert, A. Lini, K.B. Föllmi, O. Kuhn, Correlation of Early Cretaceous carbon isotope stratigraphy and platform drowning events: a possible link?, Palaeogeography, Palaeoclimatology, Palaeoecology 137 (1998), 189-203.

[6] J. Veizer, D. Ala, K. Azmy, P. Bruckschen, D. Buhl, F. Bruhn, G.A.F. Carden, A. Diener, S. Ebneth, Y. Godderis, $^{87}Sr/^{86}Sr$, $d^{13}C$ and $d^{18}O$ evolution of Phanerozoic seawater, Chemical Geology 161 (1999), 59-88.

[7] H.C. Jenkyns, Evidence for rapid climate change in the Mesozoic-Paleogene greehouse world, Phil. Trans. R. Soc. Lond. 361 (2003), 1885-1916.

[8] E. Erba, A. Bartolini, R.L. Larson, Valanginian Weissert oceanic anoxic event, Geology 32 (2004), 149-152.

[9] H. Weissert, E. Erba, Volcanism, CO2 and paleaoclimate: a Late Jurassic-Early Cretaceous carbon and oxygen isotope record, Journal of the Geological Society, London 161 (2004), 695-702.

[10] S.O. Schlanger, H.C. Jenkyns, Cretaceous oceanic anoxic events: causes and consequences, Geologie en Mijnbouw 55 (1976), 179-184.

[11] H.C. Jenkyns, Cretaceous anoxic events: from continents to oceans, Journal of the Geological Society, London 137 (1980), 171-188.

[12] C.E. Jones, H.C. Jenkyns, Seawater strontium isotopes, oceanic anoxic events, and seafloor hydrothermal activity in the Jurassic and Cretaceous, American Journal of Science 301 (2001), 112-149.

[13] F. Cecca, A. Marini, G. Pallini, F. Baudin, V. Begouen, A guide-level of the uppermost Hauterivian (lower Cretaceous) in the pelagic succession of Umbria-Marche Apennines (central Italy): the Faraoni level, Riv. It. Paleont. Strat. 99 (1994), 551-568.

[14] F. Baudin, L.G. Bulot, F. Cecca, R. Coccioni, S. Gardin, M. Renard, Un équivalent du «Niveau Faraoni» dans le Bassin du Sud-Est de la France, indice possible d'un événement anoxique fini-hauterivien étendu à la Téthys méditerranéenne, Bull. Soc. géol. France 170 (1999), 487-498.

[15] B. van de Schootbrugge, K.B. Föllmi, L.G. Bulot, S..J. Burns, Paleoceanographic changes during the early Cretaceous (Valanginian-Hauterivian): evidence from oxygen and carbon stable isotopes, Earth and Planetary Science Letters 181 (2000), 15-31.

[16] R. Coccioni, F. Baudin, F. Cecca, M. Chiari, S. Galeotti, S. Gardin, G. Salvini, Integrated stratigraphic, palaeontological, and geochemical analysis of the uppermost Hauterivian Faraoni Level in the Fiume Bosso section, Umbria-Marche Apeninnes, Italy, Cretaceous Research 19 (1998), 1-23.

[17] C.R. Scotese, L.M. Gahagan, R.L. Larson, Plate tectonic reconstructions of the Cretaceous and Cenozoic ocean basins, Tectonophysics 155 (1988), 27-48.

[18] J.E.T. Channell, F. Cecca, E. Erba, Correlations of Hauterivian and Barremian (Early Cretaceous) stage boundaries to polarity chrons, Earth and Planetary Science Letters 134 (1995), 125-140.

[19] F. Cecca, G. Pallini, E. Erba, I. Premoli-Silva, R. Coccioni, Hauterivian-Barremian chronostratigraphy based on ammonites, nannofossils, planktonic foraminifera and magnetic chrons from the Mediterranean domain, Cretaceous Research 15 (1994), 457-467.

[20] R. Coccioni, E. Erba, I. Premoli Silva, Barremian-Aptian calcareous plankton biostratigraphy from the Gorgo Cerbara section (Marche, central Italy) and implications for plankton evolution, Cretaceous Research 13 (1992), 517-537.

[21] N. Fiet, G. Gorin, Lithological expression of Milankovitch cyclicity in carbonate-dominated, pelagic, Barremian deposits in central Italy, Cretaceous Research 21 (2000), 457-467.

[22] R. Trümpy, Paleotectonic evolution of the central and western Alps, Bulletin of the

Geological Society of America 71 (1960), 846-908.

[23] R. Busnardo, J. Charollais, M. Weidmann, B. Clavel, Le Crétacé inférieur de la Veveyse de Châtel (Ultrahelvétique des Préalpes externes ; canton de Fribourg, Suisse), Revue Paléobiol., Genève 22 (2003), 1-174.

[24] R. Busnardo, Le stratotype du Barrémien. I.- Lithologie et macrofaune, Mém. Bur. Rech. Géol. Min. 34 (1965), 101-116.

[25] J. Vermeulen, Etude stratigraphique et paléontologique de la famille des Pulchelliidae (Ammonoidea, Ammonitina, Endomocerataceae), Géologie Alpine Mémoire H.S. N°42 (2002), 3-333.

[26] J.M. Mc Crea, On the isotope chemistry of carbonates and a paleotemperature scale, J. Chem. Phys. 18 (1950), 849-857.

[27] P.J. Hoedemaeker, P.F. Rawson, Report on the 5th International Workshop of the Lower Cretaceous Cephalopod Team (Vienna, 5 September 2000), Cretaceous Research 21 (2000), 857-860.

[28] P.J. Hoedemaeker, S. Reboulet, M.B. Aguirre-Urreta, P. Alsen, M. Aoutem, F. Atrops, R. Barragan, M. Company, C. Gonzalez, J. Klein, Report on the 1st International Workshop of the IUGS Lower Cretaceous Ammonite Working Group, the 'Kilian Group' (Lyon, 11 July 2002), Cretaceous Research 24 (2003), 89-94.

[29] W. Lowrie, W. Alvarez, Lower Cretaceous magnetic stratigraphy in Umbrian pelagic limestone sections, Earth and Planetary Science Letters 71 (1984), 315-328.

[30] E. Erba, The Aptian stage, Bulletin de l'Institut Royal des Sciences Naturelles de Belgique 66-Supplement (1996), 31-43.

[31] F. Cecca, P. Faraoni, A. Marini, G. Pallini, Field-trip across the representative sections for the Upper Hauterivian-Barremian ammonite biostratigraphy in the Maiolica exposed at Monte Nerone, Monte Petrano and Monte Catria (Umbria-Marche, Apennines), Memorie Descrittive della Carta Geologica d'Italia 51 (1995), 187-211.

[32] S. Bodin, A. Godet, T. Adatte, K.B. Föllmi, Palaeoceanographic and palaeoclimatic changes of the northern tethyan realm during the Hauterivian-Barremian: New insight from the Angles section (SE France), Géologie Alpine Série Spéciale «Colloques et Excursions» N°7(2005).

[33] E. Erba, J.E.T. Channell, M. Claps, C.E. Jones, R.L. Larson, B. Opdyke, I. Premoli-Silva, A. Riva, G. Salvini, S. Torriceli, Integrated stratigraphy of the Cismon APTICORE (Southern Alps, Italy): A «reference section» for the Barremian-Aptian interval at low latitudes., Journal of Foraminiferal Research 29 (1999), 371-391.

[34] R. Raiswell, Q.J. Fisher, Rates of carbonate cementation associated with sulphate reduction in DSDP/ODP sediments: implcations for the formation of concretions, Chemical Geology 211 (2004), 71-85.

[35] L. Wissler, H. Weissert, J.-P. Masse, L.G. Bulot, Chemostratigraphic correlation of Barremian and lower Aptian ammonite zones and magnetic reversals, Int. J. Earth Sci. (Geol. Rundsch.) 91 (2002), 272-279.

[36] H. Arnaud, A. Arnaud-Vanneau, M.C. Blanc-Aletru, T. Adatte, M. Argot, G. Delanoy, J.-P. Thieuloy, J. Vermeulen, A. Virgone, B. Virlouvet. S. Wermeille, Répartition stratigraphique des orbitolinidés de la plate-forme urgonienne subalpine et jurassienne (SE de la France), Géologie Alpine 74 (1998), 3-89.

[37] J. Mutterlose, A. Bornemann, Distribution and facies patterns of Lower Cretaceous sediments in northern Germany: a review, Cretaceous Research 21 (2000), 733-759.

[38] B.U. Haq, J. Hardenbol, P.R. Vail, The chronology of fluctuating sea level since the Triassic, Science 235 (1987), 1156-1167.

[39] O.G. Podlaha, J. Mutterlose, J. Veizer, Preservation of $d^{18}O$ and $d^{13}C$ in belemnite

rostra from the Jurassic / early Cretaceous successions, American Journal of Science 298 (1998), 324-347.

[40] E. Pucéat, C. Lécuyer, S.M.F. Sheppard, G. Dromart, S. Reboulet, P. Grandjean, Thermal evolution of Cretaceous Tethyan marine waters inferred from oxygen isotope composition of fish tooth enamels, Paleoceanography 18(2003) 1029, doi: 1010.1029/2002PA000823.

[41] T. Steuber, M. Rauch, J.-P. Masse, J. Graaf, M. Malkoč, Low-latitude seasonnality of Cretaceous temperatures in warm and cold episodes, Nature 437(2005) 1341-1344.

[42] P.A. Scholle, M.A. Arthur, Carbon Isotope Fluctuations in Cretaceous Pelagic Limestones: Potential Stratigraphic and Petroleum Exploration Tool, The American Association of Petroleum Geologists Bulletin 64 (1980), 67-87.

[43] G.R. Dickens, J.R. O'Neil, D.K. Rea, R.M. Oven, Dissociation of oceanic methane hydrate as a cause of the carbon isotope ecxcursion at the end of the Paleocene, Paleoceanography 10 (1995), 965-971.

[44] G.R. Dickens, T. Fewless, E. Thomas, T.J. Bralower, Excess barite accumulation during the Paleocene-Eocene Thermal Maximum: Massive input of dissolved barium from seafloor gas hydrate reservoirs, in: S.L. Wing, P.D. Gingerich, B. Schmitz and E. Thomas, eds., Causes and Consequences of Globally Warm climates in the Early Paleogene Special Paper 369, Geological Society of America, pp. 11-23, 2002.

[45] T.E. Cerlings, Y. Wang, J. Quade, Expansion of C4 ecosystems as an indicator of global ecological change in the late Miocene, Nature 361 (1993), 344-345.

[46] J.K. Bartley, L.C. Kah, Marine carbon reservoir, Corg - Ccarb coupling, and the evolution of the Proterozoic carbon cycle, Geology 32 (2004), 129-132.

[47] P.K. Swart, G. Eberli, The Nature of the $d^{13}C$ of Periplatform Sediments: Implications for stratigraphy and the global carbon cycle, Sedimentary Geology, in press

[48] J.O. Herrle, P. Kößler, O. Friedrich, H. Erlenkeuser, C. Hemleben, High-resolution carbon isotope records of the Aptian to Lower Albian from SE France and the Mazagan Plateau (DSDP Site 545): a stratigraphic tool for paleoceanographic and paleobiologic reconstruction, Earth and Planetary Science Letters 218 (2004), 149-161.

[49] G. Keller, Z. Berner, T. Adatte, D. Stueben, Cenomanian-Turonian and $d^{13}C$, and $d^{18}O$, sea level and salinity variations at Pueblo, Colorado, Palaeogeography, Palaeoclimatology, Palaeoecology 211 (2004), 19-43.

[50] F. Baudin, F. Cecca, S. Galeotti, R. Coccioni, Palaeoenvironmental controls of the distribution of organic matter within a Corg-rich marker bed (Faraoni level, uppermost Hauterivian, central Italy), Eclogae geol. Helv. 95 (2002), 1-13.

[51] T. Plank, J.N. Ludden, C. Escutia et al., Proceeding of the Ocean Drilling Program, Initial Reports, 185 [Online], in: Available from World Wide Web: <http://www-odp.tamu.edu/publications/185_IR/185ir.htm>, 2000.

[52] A.H. Ruffell, D.J. Batten, The Barremian-Aptian arid phase in western Europe, Palaeogeography, Palaeoclimatology, Palaeoecology 80 (1990), 197-212.

[53] J.-F. Deconinck, D. Bernouilli, Clay mineral assemblages of Mesozoic pelagic and flysch sediments of the Lombardian Basin (Southern Alps): implications for palaeotectonics, paleoclimate and diagenesis, Geologische Rundschau 80 (1991), 1-17.

[54] C. Holmden, R.A. Creaser, K. Muehlenbachs, S.A. Leslie, S.M. Bergström, Isotopic evidence for geochemical decoupling between ancient epeiric seas and bordering oceans:

Implications for secular curves, Geology 26 (1998), 567-570.

[55] M. Company, R. Aguado, J. Sandoval, J.M. Tavera, C.J. de Cisneros, J.A. Vera, Biotic changes linked to a minor anoxic event (Faraoni Level latest Hauterivian, Early Cretaceous), Palaeogeography, Palaeoclimatology, Palaeoecology 224(2005) 186-199.

[56] B. van de Schootbrugge, O. Kuhn, T. Adatte, P. Steinmann, K. Follmi, Decoupling of P- and Corg-burial following Early Cretaceous (Valanginian-Hauterivian) platform drowning along the NW Tethyan margin, Palaeogeography, Palaeoclimatology, Palaeoecology 199 (2003), 315-331.

[57] M. Mutti, P. Hallock, Carbonate systems along nutrient and temperature gradients: some sedimentological and geochemical constraints, Int. J. Earth Sci. (Geol. Rundsch.) 92 (2003), 465-475.

[58] T.J. Bralower, E. CoBabe, B. Clement, W.V. Sliter, C.L. Osburn, J. Longoria, The record of global change in mid-Cretaceous (Barremian-Albian) sections from the Sierra Madre, northeastern Mexico, Journal of Foraminiferal Research 29 (1999), 418-137.

[59] C. Lehman, D.A. Osleger, I.P. Montanez, A. Arnaud-Vanneau, J. Banner, Evolution of Cupido and Coahuila carbonate platforms, Early Cretaceous, northeastern Mexico, GSA Bulletin 111 (1999), 1010-1029.

[60] D.V. Ager, The Nature of the Stratigraphical Record, New York, 1981, 177 pp., John Wiley and Sons.

[61] J.-P. Masse, J. Borgomano, S.A. Maskiry, Stratigraphy and tectonosedimentary evolution of a late Aptian-Albian carbonate margin: the northeastern Jebel Akhdar (Sultanate of Oman), Sedimentary Geology 113 (1997), 269-280.

[62] H. Hillgärtner, F.S.P. Van Buchem, F. Gaumet, P. Razin, B. Pittet, J. Grötsch, H. Droste, The Barremian-Aptian evolution of the eastern Arabian carbonate platform margin (northern Oman), Journal of Sedimentary Research 73 (2003), 756-773.

[63] T. Steuber, Plate tectonic control on the evolution of Cretaceous platform-carbonate production, Geology 30 (2002), 259-262.

[64] S.M. Stanley, L.A. Hardie, Secular oscillations in the carbonate mineralogy of reef-building and sediment-producing organisms driven by tectonically forced shifts in seawater chemistry, Palaeogeography, Palaeoclimatology, Palaeoecology 144 (1998), 3-19.

[65] C.S. Romanek, E.L. Grossman, J.W. Morse, Carbon isotopic fractionation in synthetic aragonite and calcite: Effects of temperature and precipitation rate, Geochimica et Cosmochimica Acta 56 (1992), 419-430.

[66] A.W. Droxler, W. Schlager, C.C. Whallon, Quaternary aragonite cycles and oxygen isotope record in Bahamian carbonate ooze, Geology 11 (1983), 235-239.

[67] S. Bodin, A. Godet, J. Vermeulen, H. Arnaud, A. Strasser, N. Fiet, T. Adatte, K.B. Föllmi, The late Hauterivian Faraoni oceanic anoxic event in the western Tethys: Evidence from phosphorus burial rates, Palaeogeography, Palaeoclimatology, Palaeoecology 235 (2006), 245-264.

[68] H. Weissert, Siliciclastics in the early Cretaceous Tethys and north Atlantic oceans: documents of periodis greenhouse climate conditions, Mem. Soc. Geol. It. 44 (1990), 59-69.

[69] J. Philip, Peri-Tethyan neritic carbonate areas: distribution through time and driving factors, Palaeogeography, Palaeoclimatology, Palaeoecology 196 (2003), 19-37.

[70] L. Burke, D. Bryant, J.W. McManus, M. Spalding, Reefs at Risk: A Map-Based Indicator of Potential Threats to the World's Coral Reefs, in: World Resources Institute, pp. 3-11, Washington D.C., 1998.

[71] E. Fourcade, J. Azema, F. Cecca, J.

Dercourt, R. Guiraud, M. Sandulescu, L.E. Ricou, B. Vrielynck, N. Cottereau, M. Petzold, Late Tithonian Palaeoenvironments (138 to 135 Ma), in: J. Dercourt, L.E. Ricou and B. Vrielynck, eds., Atlas Tethys Palaeoenvironmental Maps, Gauthier-Villars, Paris, pp. Maps. BEICIP-FRANLAB, Rueil-Malmaison, 1993.

[72] J.-P. Masse, Y. Bellion, J. Benkhelil, J. Dercourt, R. Guiraud, L.E. Ricou, Lower Aptian Palaeoenvironments (114 to 112 Ma), in: J. Dercourt, L.E. Ricou and B. Vrielynck, eds., Atlas Tethys Palaeoenvironmental Maps, Gauthier-Villars, Paris, pp. Maps. BEICIP-FRANLAB, Rueil-Malmaison, 1993.

[73] A. Munnecke, H. Westphal, M. Elrick, J.J.G. Reijmer, The mineralogical composition of precursor sediments of calcareous rhythmites: a new approach, Int. J. Earth Sci. (Geol. Rundsch.) 90 (2001), 795-812.

[74] J.A. Kleypas, R.W. Buddemeir, J.-P. Gattuso, The future of coral reefs in an age of global change, Int. J. Earth Sci. (Geol. Rundsch.) 90 (2001), 426-437 DOI 10.1007/s005310000125.

C.5.

Links between palaeoceanographic changes and platform carbonate factory modes during the Early Cretaceous: a multi-proxy approach

Stéphane Bodin[1]*, Nicolas Fiet[2], Alexis Godet[1], Virginie Matera[1], Arnaud Clément[3], Nico M.M. Janssen[4], & Karl B. Föllmi[1]

[1] Institut de Géologie et d'Hydrogéologie, Université de Neuchâtel, Rue Emile Argand 11, CP 158, 2009 Neuchâtel, Switzerland

[2] UMR 8148 – I.D.E.S., Bât. 504, University of Paris XI Orsay, 91405 Orsay Cedex, France

[3] 5b rue de Camargue, la Cigalière, 05000 Gap, France

[4] Geertekerkhof 14bis, 3511XC Utrecht, The Netherlands

Keywords: Carbonate platform drowning; belemnites; phosphorus burial rates; seawater temperature.

In preparation for: Earth and Planetary Science Letters

Abstract

As a function of palaeoceanographic and palaeoclimatic change, carbonate platforms are submitted to changes in the carbonate-producing factory that may go as far as a strong reduction in production leading to platform drowning. The mechanisms implied in changes between photozoan and heterozoan carbonate-producing biota as well as in carbonate platform drowning are increasingly well understood today, but key aspects are still in need of better interpretations, such as the reconstruction of conditions which are implied in the switch between heterozoan production and platform drowning.

For this purpose, we have investigated the Early Cretaceous time period in the northwestern Tethyan realm, and especially the Berriasian-Barremian interval, which represents a case study for carbonate platform factory changes and drowning. During the Berriasian and the Late Barremian, the northern Tethyan carbonate platform developed in a photozoan mode. During the Valanginian to Early Barremian, the same platform functioned in a heterozoan mode and was submitted to repeated drowning events. Palaeoceanographic and palaeoclimatic changes associated with these events were inferred from complementary geochemical and mineralogical data such as $\delta^{13}C$ and $\delta^{18}O$ records which were obtained from belemnite rostra and compared to corresponding whole-rock records, and phosphorus burial rates and clay mineralogy gathered from recent publications.

These data confirm that changes in nutrient input are the main driving factor for carbonate factory changes during Early Cretaceous. Photozoan carbonate-producing biota were associated with low nutrient input (oligotrophic conditions), whereas heterozoan carbonate-producing biota were linked to higher nutrient input (meso- to eutrophic conditions). Moreover, they suggest that the drowning events occurred during time of high nutrient levels coupled with palaeoceanographic changes such as intensified upwelling and Tethyan-Boreal water-mass exchange, leading to current reorganization along the northern Tethyan margin. These changes may have precluded benthic carbonate growth and promoted phosphogenesis through winnowing processes.

C.5.1. Introduction

Carbonate platform drowning is defined as an event during which rates of relative sea-level rise exceeds rates of benthic carbonate accumulation, leading to a halt in benthic carbonate production and the onset in deposition of pelagic sediments or to a period of non-deposition, which is mainly recorded by the formation of thin crusts consisting of ferromanganese oxide, phosphate, and/or glauconite (e.g., Schlager, 1981). An important paradox appears with regards to this definition. The growth potential of carbonate platforms largely exceeds the rate of long-term sea-level rise, and carbonate platform drowning is theoretically impossible if only sea-level change is implied. Environmental stress and a corresponding reduction in benthic growth, as well as rapid pulses of relative sea level rise, were therefore invoked as an additional or even alternative factors involved in platform drowning (Schlager, 1981). Hallock and Schlager (1986) proposed that an excess in nutrient availability may provoke environmental stress. They argued that coral reefs are mostly adapted to nutrient-deficient environments and an increase in nutrient input may be harmful for these organisms because of the decrease of water transparency and the increase of fast-growing bio-erosive organisms (Hallock, 1988; Hallock et al., 1988; Wood, 1993; see also Caplan et al., 1996).

On the other hand, changes in nutrient input are also held to be responsible for changes in types of carbonate platform factory (*e.g.,* Föllmi et al., 1994; Mutti and Hallock, 2003; Halfar et al., 2004). Indeed, following the studies of Lees and Buller (1972), Carannante et al. (1988), and James (1997), two main carbonate factories are distinguished nowadays: photozoan and heterozoan carbonate-producing biotic ecosystems. During the Early Cretaceous, hermatypic corals, stromatoporoids, and rudists dominate photozoan carbonate assemblages whereas light-independent biota such as crinoids, bryozoans, and siliceous sponges dominate heterozoan carbonate assemblages. Carbonate factory changes between photozoan and heterozoan carbonate-producing biota are controlled both by nutrient availability as well as sea-surface temperature (*e.g.,* Hallock and Schlager, 1986; Carannante et al., 1988; Hallock et al., 1988; Mutti and Hallock, 2003; Halfar et al., 2004). Following these authors, the presence of photozoan carbonate assemblages is a sign of oligotrophic warm-water conditions, whereas the presence of heterozoan carbonate assemblages reflects either cool-water or meso-eutrophic warm-water conditions (see also Samankassou, 2002; Wilson & Vecsei, 2005).

In order to better understand the different parameters that control both carbonate factory changes and drowning, we have investigated Berriasian to Barremian carbonate platform outcrops from the former northern Tethyan margin, which are presently preserved in the Helvetic nappes of Switzerland (Fig. C.5.1) and their time-equivalent basin sections, which represent the Vocontian Through and are presently outcropping in SE France. During the Early Cretaceous, major palaeoceanographic changes occurred on a global scale and especially within the Western Tethyan realm. On the northern Tethyan shelf these changes are mirrored by carbonate factory changes and carbonate platform drowning (Fig. C.5.2; Föllmi et al., 1994; Weissert et al., 1998). During the Berriasian, photozoan organisms dominated the carbonate factory (Fig. C.5.3). During the Valanginian – Early Barremian, the carbonate factory switched into a heterozoan mode and was interrupted by several drowning events. Finally, during the Late Barremian, carbonate production started again in a photozoan mode (Funk et al., 1993; Föllmi et al., 1994; Kuhn, 1996; Van de Schootbrugge, 2001; Bodin et al., 2006b).

The Berriasian – Barremian stages provide thus a time interval of great interest with regards to carbonate factory changes and drowning. Indeed, based on the recent collection of detailed geochemical records ($\delta^{13}C$, $\delta^{18}O$, phosphorus burial rates, clay mineralogy) of basin sections as well as new $\delta^{13}C$, $\delta^{18}O$, Mg/

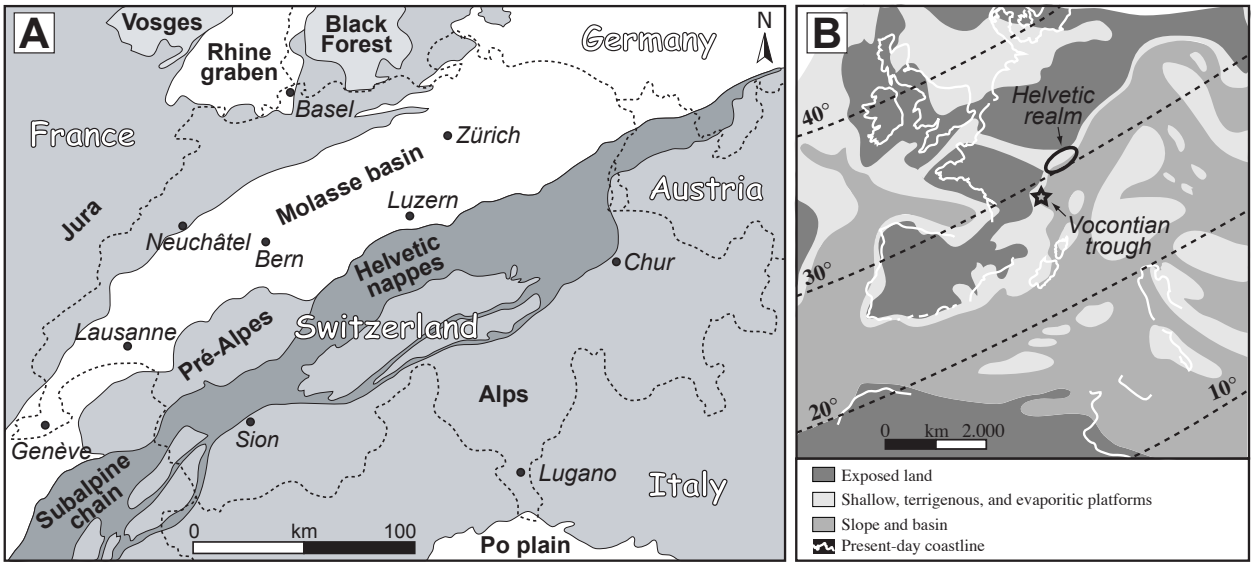

Fig. C.5.1: A. Tectonic map of Switzerland with the location of the Helvetic nappes (dark grey colored) and their French equivalent (subalpine chain). After Bodin et al., 2006b. B. Early Aptian palaeomap of the western Tethyan realm showing the original location of the Helvetic realm and Vocontian trough (after Masse, 1993b).

Ca and Sr/Ca data obtained on belemnites, and thanks to high precision biostratigraphic dating of the Berriasian – Barremian Helvetic outcrops (Föllmi et al., 1994, 2006; Kuhn, 1996; Van de Schootbrugge, 2001; Bodin et al., 2006b), we are able to reconstruct palaeoceanographic and palaeoclimatic change within the western Tethyan realm and correlate this with changes in the carbonate factory and drowning along the northern Tethyan realm. This allows us to decipher the different mechanisms that may have driven these events and to better understand the links between the carbonate factory and paleoceanographic change.

C.5.2. Geological settings

C.5.2.1. Early Cretaceous platform stratigraphy in the Helvetic zone

The Helvetic tectonic unit is situated in the northern part of the Alps and represents the northern Tethyan margin, which was thrusted, overthrusted and folded in a northward direction during Alpine orogenesis (Fig. C.5.1). The Zemenstein and Oehrlikalk Formations represent Berriasian rocks in the Helvetic realm (Fig. C.5.2). The Oehlikalk Formation (Fm) is divided into two parts: Lower and Upper Oerlikalk Members (e.g., Mohr, 1992; Funk et al., 1993; Föllmi et al., 1994; Föllmi et al., 2006). The Early Valanginian experienced the deposition of the Betliskalk Fm. It is divided into two members that are separated by the Büls Member (Mb). The latter represent a first phase of condensation in the distal part of the Helvetic platform (e.g., Kuhn, 1996). This formation is overlaid by the Gemsmättli Mb (early Late Valanginian to earliest Hauterivian). Almost the whole Hauterivian is represented in the Helvetic realm by the Kieselkalk Fm, which can be divided into three members (Lower Kieselkalk, Lidernen and Upper Kieselkalk Members) following Funk (1969). The latest Hauterivian to middle Barremian correspond to the Drusberg Fm, which is divided into a lower part (the Altmann Mb, latest Hauterivian to latest Early Barremian) and an upper part (the Drusberg Mb) (Funk et al., 1993; Bodin et al., 2006b). Büls, Gemsmättli, Lidernen and Altmann Mb represent four successive phases of platform drowning (*e.g.,* Föllmi et al., 1994; See also Kuhn, 1996, Van de Schootbrugge, 2001).

The Schrattenkalk Fm characterizes the middle Late Barremian – earliest Aptian in the Helvetic realm. This formation is the equivalent

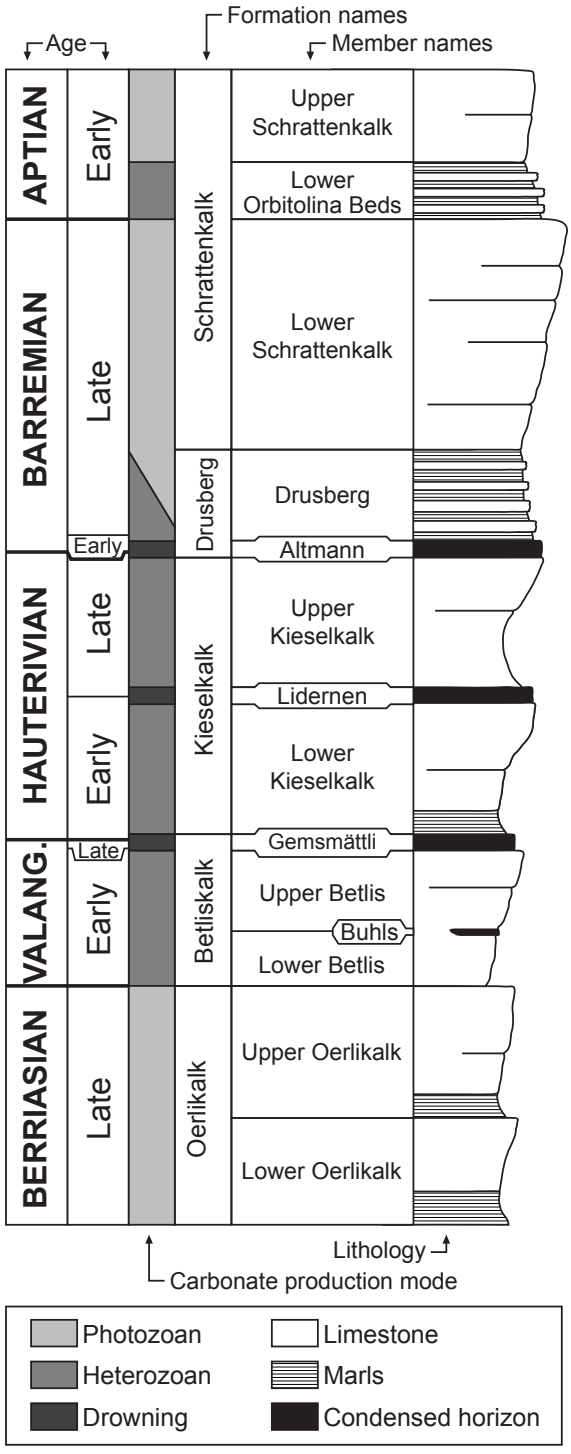

Fig. C.5.2: Synthetic sedimentary column of the stratigraphic formations in the Helvetic realm, showing the carbonate factory production modes and drowning episodes, from the Late Berriasian to the earliest Aptian.

of the "Urgonian" limestone. Its installation is dated in non-distal settings by sequence stratigraphic correlation (Bodin et al., 2006b) and may correspond to the mfs Ba3 (middle of the *G. sartousiana* ammonite zone). This date is in agreement with the installation of the "Urgonian" platform is other part of the western Tethyan realm (e.g., Arnaud et al., 1998). In distal settings, this installation occurred during the latest Barremian (Briegel, 1972; Bodin et al., 2006c), which may reflect the progradation of the "Urgonian" facies during the latest Barremian – earliest Aptian.

C.5.2.2. Helvetic carbonate platform factories

Both Betliskalk and Kieselkalk Fms are mainly composed of echinoderm-rich siliceous limestone with sponge spicules and bryozoans. This assemblage is typical for Early Cretaceous heterozoan carbonates (Fig. C.5.3; Föllmi et al., 1994). On the other hand, the macrofauna preserved in the Oerlikalk and Schrattenkalk Fms are mainly composed of hermatypic corals, stromatoporoids and rudists which is representative for Early Cretaceous photozoan carbonates. The lack of carbonate factory markers within the Drusberg Mb makes its classification more difficult. Indeed, in proximal parts of the Helvetic shelf, it is composed of reworked ooids, benthic foramifera and dasycladacea (*e.g.,* Bollinger, 1988). In distal parts, it is mainly composed of an alternation of spiculitic limestone and marl. During the Early Cretaceous, sponge spicules are present in both carbonate factories and are deposited in outer-ramp setting, below the photic zone (cf. Arnaud-Vanneau, 1980; Bodin et al., 2006b; but see also Gammon et al., 2000). On the other hand, dasycladacea are preferentially associated with photozoan carbonates. The Drusberg Mb may thus be classified as a heterozoan-photozoan transition carbonate deposit (*sensu* Halfar et al., 2004).

The presence of phosphatized hardgrounds and nodular beds, and glaucony-rich sediments, or of a hiatus often coupled with important erosion characterizes the different phases of platform drowning (Funk et al., 1993). Such phases are recognized in the Büls, Gemsmättli, Lidernen and Altmann Mbs, and also higher up in the stratigraphic column, on top of the Schrattenkalk Formation (Garschella Fm; e.g., Föllmi et al., 2006).

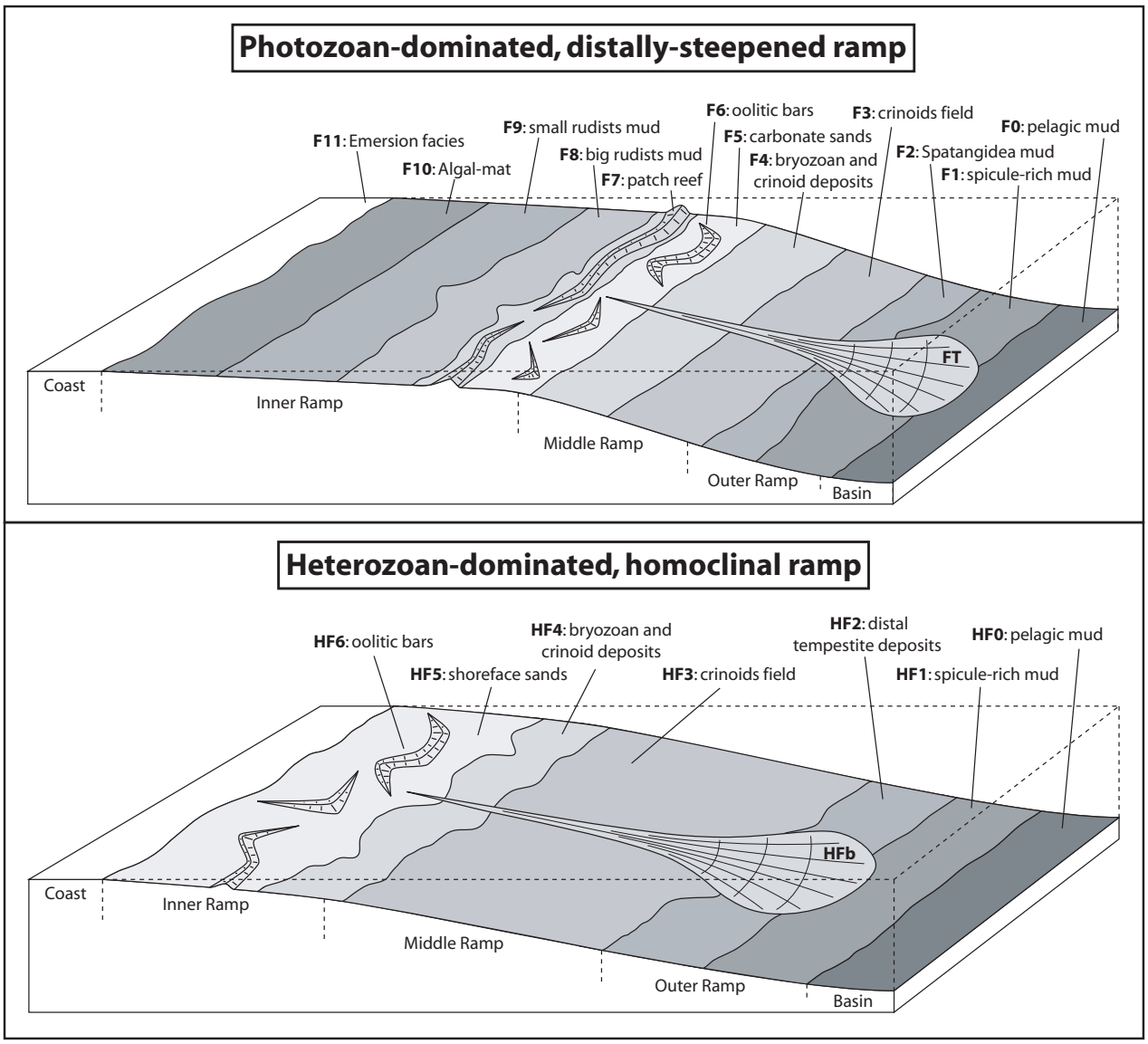

Fig. C.5.3: Schematic 3D model of photozoan- and heterozoan-dominated carbonate platform factories. Drawn after Arnaud-Vanneau (1980) and Bodin et al. (2006b). Note the landward settling of the crinoidal ecosystem in a heterozoan-dominated carbonate platform compared to a photozoan-dominated one.

C.5.2.3. Vocontian trough sections

Most of the geochemical results used here are derived from previously published studies on hemi-pelagic sections outcropping in the Vocontian trough. This basin is located in the southeast of France. During the Early Cretaceous it was surrounded by the northern Tethyan carbonate platform and opened to the Tethys ocean in an eastward direction (Masse, 1993a). Hemi-pelagic sections of the Vocontian basin are composed of marl – limestone alternations and dated by ammonite biostratigraphy (*e.g.*, Vermeulen, 2002; Duchamp-Alphonse et al., 2006).

C.5.3. Methods

70 belemnites were collected in the Vocontian Trough from sections covering the latest Hauterivian to Barremian time interval. Most of them were found in the Angles section, which is the Barremian stratotype section situated near St. André-les-Alpes (see Bodin et al., 2006a, for a more precise location). In addition, eight belemnites were collected in the Saut-du-Loup, Combe Lambert and Clos-de-Barral sections in order to complete our sampling from ammonite biozones poor in belemnites in the Angles section (see Delanoy,

1997, a for a precise location of these sections).

Belemnites were cleaned in an ultrasonic bath, followed by 1 minute cleaning in a 10% HCl solution. In the following, they were dried and crushed in small pieces of approximately 1 mm which were also cleaned within a sieve with a 10 % HCl solution and ultrapure water. After being dried, non-opaque pieces, showing growth bands, were selected by hand picking. Final powders were obtained by hand crushing.

$\delta^{18}O$ and $\delta^{13}C$ ratios from belemnites were analyzed at the Stable Isotope Laboratory of the Hydrology department (UMR 8148-IDES), University of Paris Sud (Orsay, France), using a VG SIRA 10 triple collector instrument. The powdered carbonate samples were reacted with anhydrous orthophosphoric acid at 25 °C. Using internal carbonate standards, the reference material NBS 19 as well as replicate analyses of samples, the reproducibility of C and O analyses was better than ± 0.05 ‰ and ± 0.08 ‰ respectively. In order to compare belemnite and bulk-rock results, a mean $\delta^{13}C$ and $\delta^{18}O$ value was calculated for each ammonite zone.

Mg, Sr, Mn, Fe and Ca concentrations in belemnites were analyzed using the ICP-MS equipment of the Geological Institute, University of Neuchâtel. A portion of approximately 25 mg was transferred into an Eppendorf tube and 10 ml 0.6 M nitric acid (suprapur, Merck) was added. A second dilution (1/10) was then performed prior to analysis. The element concentrations of the acid digests were determined by ICP-MS (ELAN 6100, Perkin Elmer). See Bodin et al. (in press) for a more detailed analytical procedure.

Other data ($\delta^{13}C$, $\delta^{18}O$, phosphorus burial rates, clay mineralogy) were gathered from recently published papers dealing with western Tethyan Early Cretaceous palaeoceanography and palaeoclimatology (*e.g.,* Föllmi, 1995; Van de Schootbrugge et al., 2000, 2003; Schnyder et al., 2005; Bodin et al., 2006a; Duchamp-Alphonse et al., 2006; Godet et al., 2006).

C.5.4. Results

C.5.4.1. Carbon isotopes

The here obtained belemnite carbon isotope ($\delta^{13}C_{bel}$) results show a twofold division (Table C.5.1 and Fig. C.5.4). From the *B. balearis* to the *H. sayni* zone, the $\delta^{13}C_{bel}$ values are relatively stable and vary between 0 and 0.5 ‰. Then, a positive shift occurred in the *H. feraudianus* zone and values rise to approximately 1.6 ‰ and decrease onward to reach a level of approximately 0.7 ‰ in the *M. sarasini* zone. The $\delta^{13}C_{bel}$ value in the *H. feraudianus* zone is the maximum value recorded in belemnites for the entire Valanginian – Barremian interval. There is a very good continuity of $\delta^{13}C_{bel}$ values between the results of Van de Schootbrugge et al. (2000) and the ones presented here.

The compilation of belemnite and bulk-rock data from the Valanginian to the Barremian (after these results and Van de Schootbrugge et al., 2000; Duchamp-Alphonse et al., 2006; Godet et al., 2006) shows comparable long-term $\delta^{13}C$ trends. Belemnite carbon isotope values are however always lower than bulk-rock ones. During the Valanginian, the maximal values reached after the positive shift are however shifted by an ammonite zone.

$\Delta\delta^{13}C$ values, which correspond to the absolute difference between $\delta^{13}C_{bulk}$ and $\delta^{13}C_{bel}$ values, show a well-contrasted trend during the Valanginian – Barremian interval. A first important positive shift, reaching 2.5 ‰, is recorded in the *B. campylotoxus* zone. It is followed by a negative shift reaching approximately 0.4 ‰ in the *C. trinodosum* zone. Less pronounced positive shifts are also recorded around the *T. callidiscus*, in the *P. ligatus,* in the *S. angulicostatum*, in the *N. pulchella* and around the *H. sayni* zones. The *H. Feraudianus* zone is characterized by a distinct negative shift reaching approximately 0.5 ‰.

Stage	Sample N°	Specimen type	Ammonite zone	∂^{13}C VPDB (‰)	∂^{18}O VPDB (‰)	Mg (ppm)	Mn (ppm)	Fe (ppm)	Ca (%)	Sr (ppm)	Mg/Ca (mmol/mol)	Sr/Ca (mmol/mol)
Hauterivian	AN 1b	*Hibolithes sp.*	*B. balearis*	0.04	-0.26	3379	1.40	343	39.58	1317	14.07	1.52
Hauterivian	AN 2b	*Hibolithes sp.*	*B. balearis*	0.28	-0.42	3647	1.29	350	40.02	1386	15.03	1.58
Hauterivian	AN 7b	*Hibolithes sp.*	*B. balearis*	0.42	-0.40	3301	1.15	310	39.01	1387	13.96	1.63
Hauterivian	AN 18b	*Hibolithes sp.*	*B. balearis*	0.06	-0.02	2830	0.82	305	37.94	1319	12.30	1.59
Hauterivian	AN 22b	*Hibolithes sp.*	*B. balearis*	0.39	-0.39	2930	1.72	310	36.28	1266	13.32	1.60
Hauterivian	AN 37b	*Hibolithes sp.*	*S. angulicostatum*	0.37	-0.56	3379	10.66	322	36.79	1101	15.15	1.37
Hauterivian	AN 41 b	*Hibolithes gr. subfusiformis*	*S. angulicostatum*	0.12	-0.15	3151	1.93	212	35.82	1283	14.51	1.64
Hauterivian	AN 43b	*Hibolithes gr. subfusiformis*	*S. angulicostatum*	0.32	-0.24	3018	0.89	142	36.65	1386	13.58	1.73
Hauterivian	AN 43b bis	*Hibolithes gr. subfusiformis*	*S. angulicostatum*	-0.42	-0.20	3076	7.42	306	36.15	1195	14.03	1.51
Hauterivian	AN 53.2b	*Hibolithes gr. subfusiformis*	*S. angulicostatum*	0.09	-0.03	3213	2.15	150	37.87	1334	13.99	1.61
Hauterivian	AN 54.1b	*Hibolithes sp.*	*P. mortilleti*	0.09	0.08	3304	1.64	189	35.83	1358	15.21	1.73
Hauterivian	AN 54.2b	*Hibolithes sp.*	*P. mortilleti*	0.80	-0.23	3298	17.13	187	32.24	1058	16.86	1.50
Hauterivian	AN 71b	*Hibolithes sp.*	*P. mortilleti*	0.18	-0.48	3459	2.26	177	39.00	1348	14.63	1.58
Barremian	AN 73b	*Hibolithes sp.*	*A. kiliani*	0.52	-0.04	2379	1.19	297	37.15	1217	10.56	1.50
Barremian	AN 74b	*Hibolithes sp.*	*A. kiliani*	0.40	-0.28	3451	1.99	217	38.93	1410	14.62	1.66
Barremian	AN 75b	*Hibolithes gr. jaculiformis*	*A. kiliani*	0.40	-0.21	2877	0.89	184	33.78	1246	14.04	1.69
Barremian	AN 76b	*Hibolithes sp.*	*A. kiliani*	0.46	-0.75	3493	4.31	316	36.48	1249	15.79	1.57
Barremian	AN 77b	*Hibolithes sp.*	*A. kiliani*	0.54	-0.23	3231	0.96	283	35.31	1286	15.09	1.67
Barremian	AN 77.2b	*Hibolithes sp.*	*A. kiliani*	0.38	-0.22	3270	6.85	196	38.22	1262	14.11	1.51
Barremian	AN 78b	*Hibolithes sp.*	*A. kiliani*	0.35	-0.44	4025	1.84	175	40.53	1440	16.38	1.63
Barremian	AN 79b	*Hibolithes sp.*	*A. kiliani*	0.28	-0.50	3387	1.83	190	40.38	1339	13.83	1.52
Barremian	AN 80b	*Hibolithes sp.*	*A. kiliani*	0.31	-0.29	3391	1.36	155	38.62	1332	14.48	1.58
Barremian	AN 84b	*Hibolithes sp.*	*A. kiliani*	-0.04	-0.33	3209	1.27	167	38.66	1327	13.69	1.57
Barremian	AN 85b	*Hibolithes sp.*	*A. kiliani*	0.41	-0.51	3870	1.65	179	39.23	1412	16.27	1.65
Barremian	AN 87b	*Hibolithes sp.*	*A. kiliani*	0.02	-0.63	3334	3.88	201	39.02	1446	14.09	1.70
Barremian	AN 88b	*Hibolithes sp.*	*A. kiliani*	0.50	-0.55	3762	6.85	230	39.03	1410	15.89	1.65
Barremian	AN 89b	*Hibolithes sp.*	*A. kiliani*	0.18	-0.39	2490	8.71	197	38.79	1215	10.59	1.43
Barremian	AN 92b	*Hibolithes sp.*	*A. kiliani*	0.43	-0.34	3807	9.20	183	37.59	1392	16.70	1.69
Barremian	AN 94b	*Hibolithes sp.*	*K. nicklesi*	0.70	-0.50	3539	2.01	119	37.88	1308	15.41	1.58
Barremian	AN 102b	*Hibolithes sp.*	*K. nicklesi*	0.46	-0.68	2526	1.87	241	40.40	1217	10.31	1.38
Barremian	AN 103b	*Hibolithes sp.*	*K. nicklesi*	0.60	-0.44	3239	1.54	249	41.46	1492	12.88	1.65
Barremian	AN 103 b2	*Hibolithes sp.*	*K. nicklesi*	0.10	-0.53	3788	1.45	177	38.08	1485	16.40	1.78
Barremian	AN 104b	*Hibolithes sp.*	*K. nicklesi*	0.52	-0.78	3301	1.49	222	38.68	1371	14.07	1.62
Barremian	AN 110.1b	*"Mesohibolites" sp.*	*N. pulchella*	0.38	-0.70	3147	1.77	189	37.16	1255	13.96	1.54
Barremian	AN 110.4b	*Hibolithes gr. jaculiformis*	*N. pulchella*	0.55	-0.40	4023	1.53	150	35.38	1199	18.75	1.55
Barremian	AN 111.1b	Unspecified	*N. pulchella*	-0.34	-1.28	4082	22.54	230	40.36	1409	16.68	1.60
Barremian	AN 111.4b	*"Mesohibolites" sp.*	*N. pulchella*	0.69	-0.52	3042	1.82	202	32.54	1068	15.42	1.50
Barremian	AN 112	Unspecified	*N. pulchella*	0.17	-1.64	4233	6.08	252	40.68	1340	17.16	1.51
Barremian	AN 112.7b	*"Mesohibolites" sp.*	*K. compressissima*	0.53	-0.35	2963	10.20	257	35.93	1239	13.60	1.58
Barremian	AN 119b	Unspecified	*K. compressissima*	0.61	-2.68	3257	26.36	304	41.18	1308	13.04	1.45
Barremian	AN 121b	*"Mesohibolithes" sp.*	*K. compressissima*	-0.31	-0.71	4144	23.58	237	40.64	1395	16.82	1.57
Barremian	AN 125	*Duvalia sp. ?*	*C. darsi*	-0.29	-0.34	3287	10.53	226	43.36	1304	12.50	1.38
Barremian	AN 125b	Unspecified	*C. darsi*	0.65	-0.26	4203	1.40	236	41.50	1404	16.70	1.55
Barremian	AN 136b	*"Mesohibolithes" sp.*	*C. darsi*	-0.08	-0.31	4208	3.09	218	41.75	1415	16.62	1.55
Barremian	AN 139.1	*Mesohibolitidae indet.*	*C. darsi*	0.11	-0.60	3023	3.92	286	33.94	1401	14.69	1.89
Barremian	AN 143b	*"Mesohibolithes" gr. minaret*	*H. uhligi*	1.96	-2.41	2354	83.03	1105	38.44	1005	10.10	1.20
Barremian	AN 144b	*Duvalia sp. ?*	*H. uhligi*	0.31	-0.19	4943	2.11	170	42.14	1498	19.34	1.63
Barremian	AN 151.3b	*Mesohibolithes sp.*	*H. sayni*	0.37	-0.54	3608	7.52	260	39.65	1290	15.00	1.49
Barremian	AN 155.2b	*Mesohibolithes sp.*	*H. sayni*	-0.55	-0.85	4047	19.77	356	40.43	1283	16.50	1.45
Barremian	AN 158	Unspecified	*H. sayni*	0.44	-0.27	3386	3.62	209	37.02	1185	15.08	1.46
Barremian	AN 158b	*Mesohibolithes sp.*	*H. sayni*	1.07	-0.62	3348	2.85	254	40.39	1344	13.67	1.52
Barremian	AN 160.3b	*Mesohibolithes sp.*	*G. sartousiana*	0.53	-0.59	4340	27.08	191	39.49	1213	18.12	1.40
Barremian	AN 161.1b	*Mesohibolithes sp.*	*G. sartousiana*	0.61	-0.70	3737	7.92	178	40.00	1408	15.41	1.61
Barremian	AN 161.2b	*Mesohibolithes sp.*	*G. sartousiana*	1.23	-0.26	3139	2.65	185	40.35	1258	12.83	1.43
Barremian	AN 161.3b	*Mesohibolithes sp.*	*G. sartousiana*	0.17	-0.53	3512	3.51	162	40.76	1319	14.21	1.48
Barremian	AN 161.3b	Unspecified	*G. sartousiana*	1.24	-0.24	3407	0.78	220	43.10	1434	13.03	1.52
Barremian	AN 162b	*Mesohibolithes sp.*	*G. sartousiana*	0.44	-0.32	3337	4.23	170	40.32	1341	13.65	1.52
Barremian	AN 165b	*Mesohibolithes sp.*	*H. feraudianus*	1.69	-0.41	3486	0.77	145	39.40	1402	14.59	1.63
Barremian	AN 165b bis	*Mesohibolithes sp.*	*H. feraudianus*	1.66	-0.51	3413	2.57	241	40.44	1445	13.91	1.63
Barremian	AN 165b ter	*Mesohibolithes sp.*	*H. feraudianus*	1.32	-0.62	4294	31.41	308	43.12	1591	16.42	1.69
Barremian	AN 172.2b	*Neohibolithes sp.*	*I. giraudi*	0.72	0.02	1879	2.53	271	41.03	1191	7.55	1.33
Barremian	AN 173b	*Neohibolithes sp.*	*I. giraudi*	1.29	-0.58	2378	49.73	519	43.71	1232	8.97	1.29
Barremian	AN 185b	*Mesohibolites sp. (imm.)*	*M. sarasini*	1.52	-1.80	2133	1.92	269	34.44	1072	10.21	1.42
Aptian	AN 202	*Mesohibolites sp.*	*D. oglanlensis*	-0.19	-0.67	2764	1.84	177	33.50	1129	13.61	1.54
Barremian	SDL 362b	*Neohibolithes sp.*	*I. giraudi*	1.28	-0.23	2006	2.50	233	41.77	1236	7.92	1.35
Barremian	SDL 365	*Mesohibolites sp.*	*I. giraudi*	1.97	-1.83	2504	13.63	355	36.34	1086	11.36	1.37
Barremian	SDL 366b	*Mesohibolithes sp.*	*I. giraudi*	1.24	-0.31	3492	15.82	263	41.78	1351	13.79	1.48
Barremian	SDL 373b	*Mesohibolithes sp.*	*M. sarasini*	-0.11	-0.65	3419	2.01	250	41.58	1432	13.56	1.58
Aptian	COM 109b	*Mesohibolithes sp.*	*D. weissi*	0.93	-0.74	4144	16.39	274	39.96	1448	17.10	1.66
Barremian	CB 134.4b	*"Mesohibolithes" sp.*	*N. pulchella*	-0.10	-0.49	3682	1.36	189	40.69	1414	14.92	1.59

Table C.5.1: Isotopic and chemical data for belemnites from the latest Hauterivian- Barremian strata of the Vocontian trough. Most of these belemnites were collected in the Angles section. The sample number corresponds to the official bed numbering from this section (refer to Vermeulen, 2002). The grey band highlights belemnites that are considered to be diagenetically altered and were therefore not used in the discussion (see text for more details).

C.5.4.2. Oxygen isotopes

With regards to their oxygen isotope values ($\delta^{18}O_{bel}$), the belemnites from this study (Table C.5.1 and Fig. C.5.5) show a stable trend of around -0.3 ‰ during the latest Hauterivian, which is followed by a progressive decrease and a minimum of -1.25 ‰ during the *K. compressissima* zone. From the *C. darsi* to the *I. giraudi* zone $\delta^{18}O_{bel}$ values are again increasing and center around -0.75 ‰. A second negative

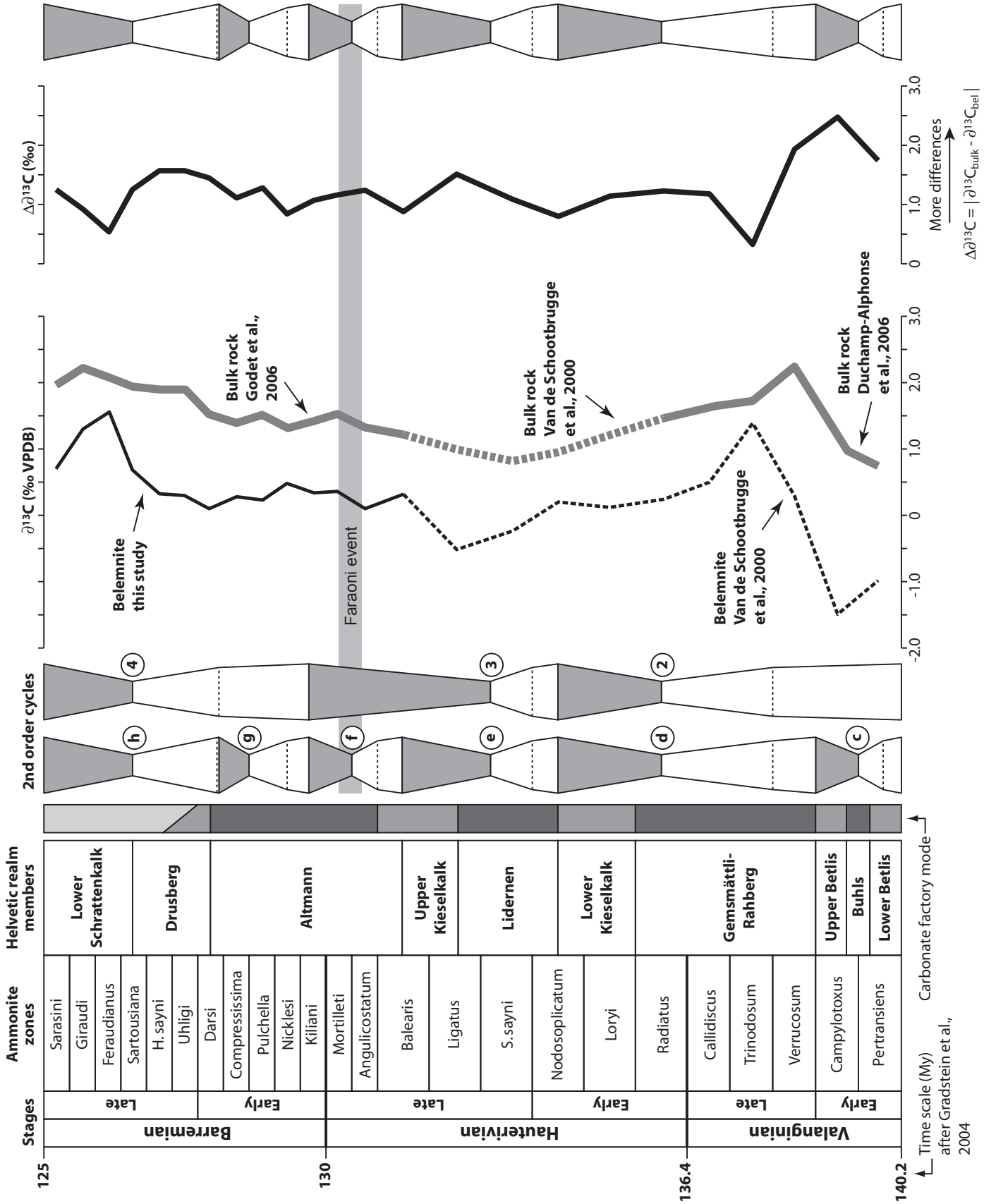

Fig. C.5.4: Bulk-rock and belemnite carbon isotope evolution from the Valanginian to the Barremian. The $\Delta\delta^{13}C$ index is the absolute difference between $\delta^{13}C_{bulk}$ and $\delta^{13}C_{bel}$. Second-order sea-level cycles are also shown as well as the position of the Faraoni event. See Fig. C.5.7 for legend.

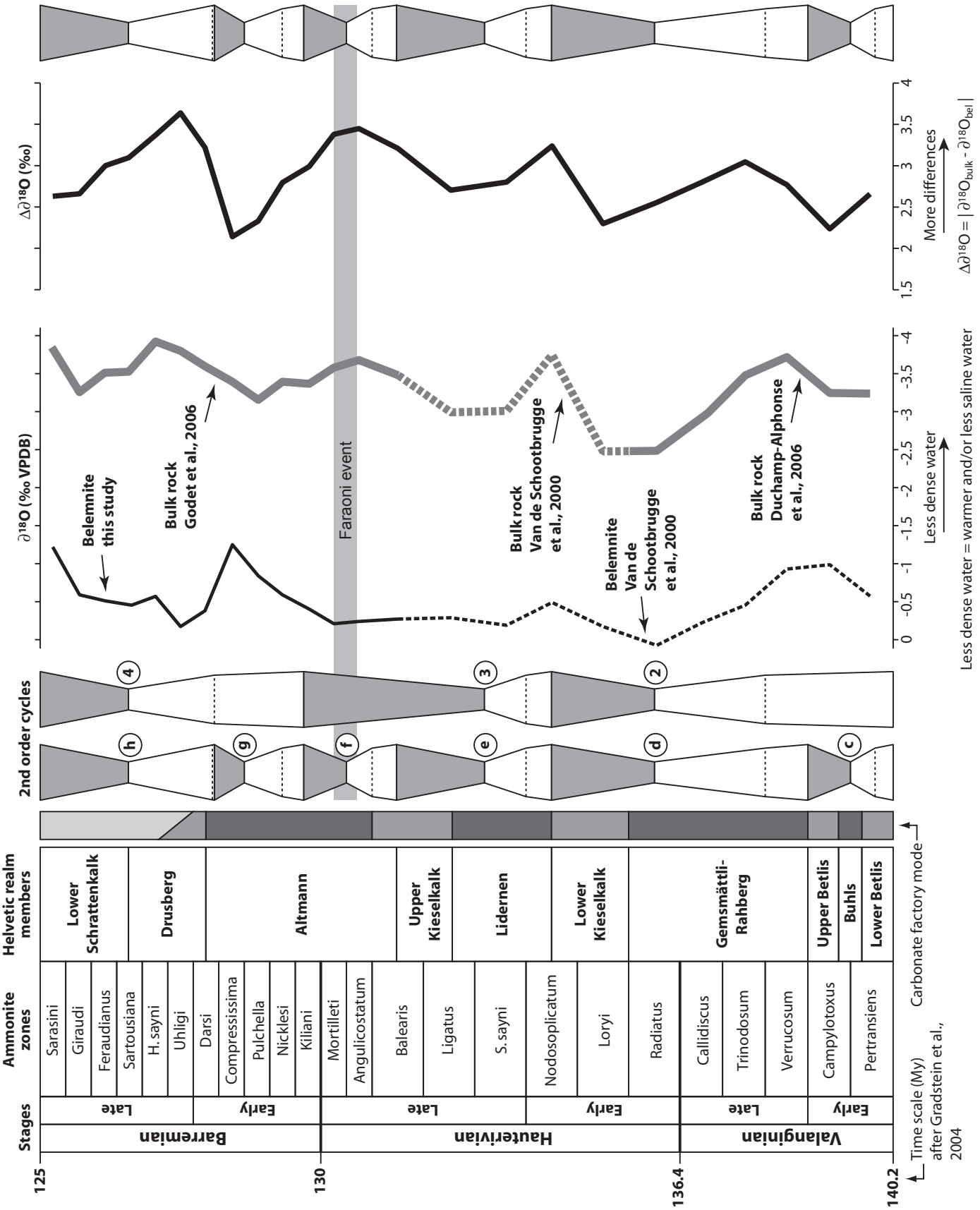

Fig. C.5.5: Bulk-rock and belemnite oxygen isotope evolution from the Valanginian to the Barremian. The $\Delta\delta^{18}O$ index is the absolute difference between $\delta^{18}O_{bulk}$ and $\delta^{18}O_{bel}$. Second-order sea-level cycles are also shown as well as the position of the Faraoni event. See Fig. C.5.7 for legend.

shift is documented during *M. sarasini* zone (-1.2 ‰). As for the $\delta^{13}C$ results, there is a very good continuity of $\delta^{18}O_{bel}$ values between the results of Van de Schootbrugge et al. (2000) and our own. McArthur et al. (2004) also noted a negative shift in the $\delta^{18}O_{bel}$ record of the late Early Barremian of Speeton. As shown in Fig. C.5.6, no correlation is observed between $\delta^{18}O$ and $\delta^{13}C$ in belemnite from *Hibolites* and *Mesohibolites* genera.

A compilation of $\delta^{18}O$ belemnite and bulk-rock records based on the data from Van de Schootbrugge et al. (2000), Duchamp-Alphonse et al. (2006), Godet et al. (2006), and our own data shows a good correlation for the Valanginian – Hauterivian. During the Early Barremian, there is a decoupling between the $\delta^{18}O_{bel}$ and $\delta^{18}O_{bulk}$records: the $\delta^{18}O_{bel}$ negative shift is mirrored by a positive $\delta^{18}O_{bulk}$ shift. Correlation between both records seems to improve again from the *H. sayni* zone onward.

$\Delta\delta^{18}O$ values, which correspond to the absolute difference between $\delta^{18}O_{bulk}$ and $\delta^{18}O_{bel}$ values, show a very contrasted trend during the Valanginian – Barremian interval. Minimum values are recorded around the *B. campylotoxus*,

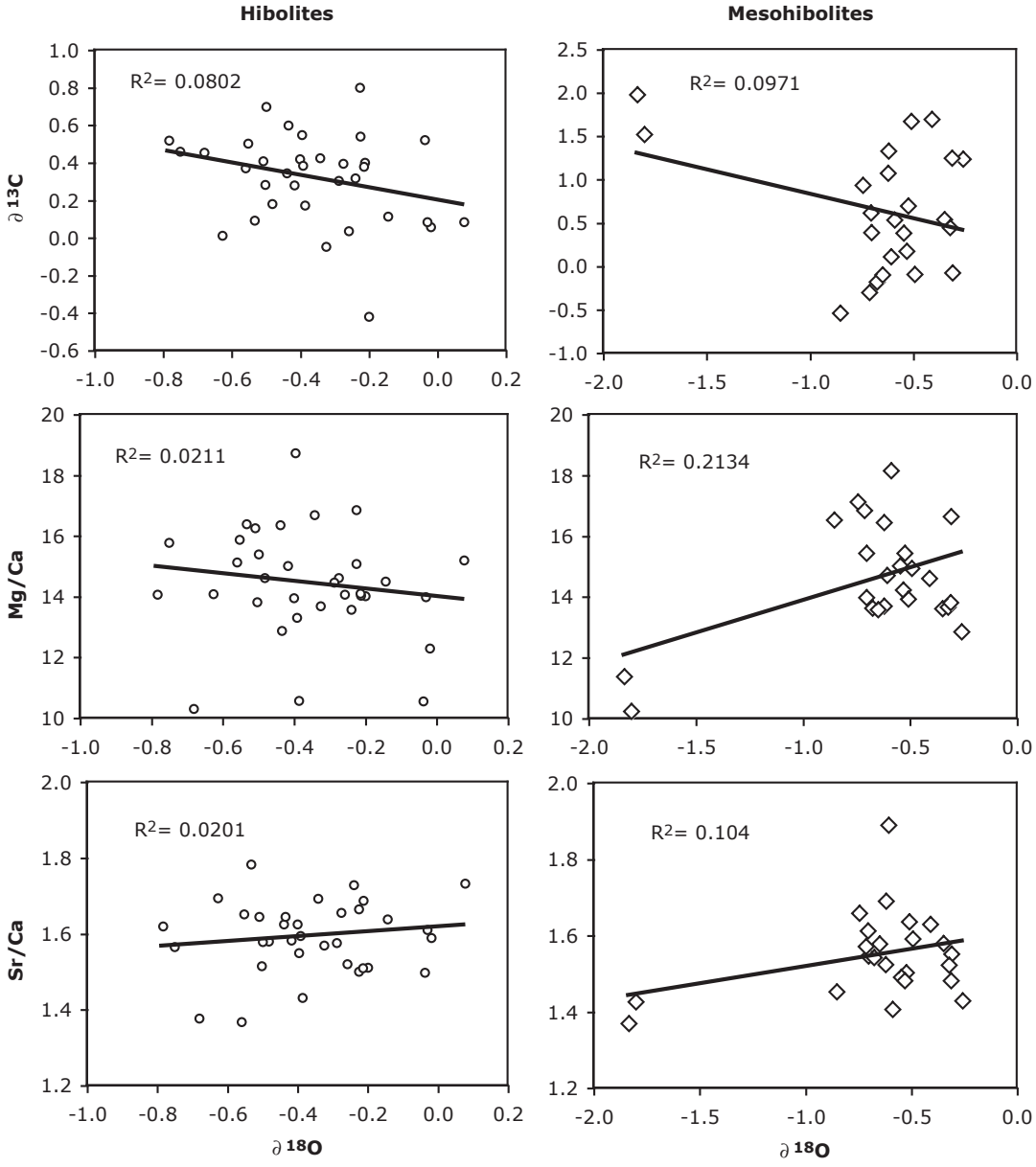

Fig. C.5.6: Relation of $\delta^{13}C$, Mg/Ca and Sr/Ca to $\delta^{18}O$ in the belemnite genera *Hibolites* and *Mesohibolites*. No correlation can be observed. See text for discussion.

C. loryi, *P. ligatus*, *K. compressissima* and *M. sarasini* zones. Maximum values are recorded in the *C. trinodosum*, *L. nodosoplicatum*, *S. angulicostatum* and *H. uhligi* zones.

C.5.4.3. Mn, Fe, Mg, Sr and Ca

Chemical data from belemnites are listed in Table C.5.1. Mn results show values between 0.77 and 83.05 ppm with an average value of 7.82 ppm. Fe results are comprised between 119 and 1105 ppm with an average value of 247 ppm. Two samples (AN 143b and AN 173b) show high values above 50 ppm for the Mn and 500 ppm for Fe.

Mg values are comprised between 1878 and 4943 ppm with an average value of 3351 ppm. Sr values vary between 1005 and 1591 ppm with an average value of 1315 ppm. These values are in good agreement with those from Van de Schootbrugge et al. (2000) who studied Valanginian-Hauterivian belemnite in the Vocontian trough.

Cross plots of Mg/Ca and Sr/Ca ratios to $\delta^{18}O$ values show a very poor correlation for both *Hibolites* and *Mesohibolites* genera (Fig. C.5.6). Due to the few number of belemnites from the *Duvalia* and *Neohibolites* genera, we were not able to test these correlations for these genera.

C.5.5. Discussion

C.5.5.1. Belemnite preservation

According to previous publications on Early Cretaceous belemnite stratigraphy (Ditchfield, 1997; Podlaha et al., 1998; Van de Schootbrugge et al., 2000; McArthur et al., 2004, and references therein), the following criteria have been proposed to check sample preservation: visually well-preserved belemnites, isotopic and element composition that replicate well, low concentration of Fe and Mn, concentration of Sr and Mg typical of well-preserved belemnites, no covariance between oxygen and carbon isotope values, carbon isotopes values lighter and oxygen isotopes heavier than the bulk rock values. Cut-off values for Fe and Mn are rather arbitrary and vary depending on the author (*e.g.,* Ditchfield, 1997). We decided to set the limit for Fe and Mn at 500 ppm and 50 ppm, respectively. Belemnite samples with higher concentrations (AN 143b and AN 173b) were excluded from our discussion and considered as diagenetically altered.

All other here-used belemnite samples match all criteria listed here, so we assume that they have retained their original isotopic and elemental compositions. Moreover, the fact that our results match well with those obtained by Van de Schootbrugge et al. (2000) for latest Hauterivian belemnites from the Vocontian Trough, as well as the fact that we are able to correlate the here observed trends with the trend described in McArthur et al. (2004) for the Boreal realm, is another hint for their good reliability.

C.5.5.2. Bulk-rock diagenesis

Following Godet et al. (in press), the clay minerals in the Angles section show that this region has suffered from minor diagenetic impact. This can also be seen in the slight negative offset in the $\delta^{18}O$ values from this region compared to other Vocontian sections situated further away from the "nappes de Dignes" (Van de Schootbrugge et al., 2000). However, Godet et al. (2006) have showed that this slight diagenetic effect was not sufficient enough to reset the trends in the original $\delta^{18}O$ record and that the long-term trend is conserved and comparable to others regions. Moreover, except for the Early Barremian (see the following for a discussion on this point), the trend observed in bulk rock and belemnite oxygen isotopes is the same and differs only in exact value and amplitude. This may also indicate that the bulk rock $\delta^{18}O$ signal is related to palaeoceanographic conditions and was not reset during diagenesis.

C.5.5.3. Influence of palaeogeography on the carbonate factory

Following palaeogeographic reconstructions of the Early Cretaceous (Masse et al., 1993b; Hay et al., 1999), the Helvetic realm was situated approximately at paleolatitude 40°N (*e.g.,* Funk et al., 1993; Föllmi et al., 1994). This position was close to the actual northern limit of warm-water reef growth (*e.g.,* James, 1997), and this may have contributed to render this carbonate platform very sensitive to palaeoceanographic changes. Moreover, it was also situated close to the Polish Trough and thus sensitive to Tethyan – Boreal water-mass exchanges (Van de Schootbrugge et al., 2001).

The here described changes between photozoan and heterozoan dominated carbonate production can be traced, at least, along the entire northern Tethyan margin and may thus reflect supra-regional changes. Indeed, the transition from photozoan to heterozoan associations at the Berriasian – Valanginian boundary is also recorded in the Jura, Chartreuse and Vercors area (Blanc, 1996). The reinstallation of the photozoan association during the Late Barremian (Urgonian-type carbonate) seems to be a worldwide event in tropical and subtropical areas of the Northern Tethyan margin (*e.g.,* Garcia-Hernandez, 1979, for SE Spain; Michalik, 1994, for the western Carpathians; Blanc-Aletru, 1995, for the Jura mountains; Ivanov et al., 1997 and Peybernès et al., 2000, for Bulgaria; Arnaud et al., 1998, for SE France; Lehmann et al., 1999, 2000, for northeastern Mexico; Arnaud et al., 2000, for Venezuela; Bernaus et al., 2003, for the Spanish Pyrenees). The same Hauterivian - Barremian carbonate factory changes can also be observed along the southern Tethyan margin (*e.g.,* Hillgärtner et al., 2003, for northern Oman).

The major drowning events of the Valanginian and Early Aptian, that are correlated with major perturbations in the carbon cycle (Weissert et al., 1998), can be traced worldwide (*e.g.,* Masse, 1993a). They may thus be linked to strong palaeoceanographic perturbations. On the other hand, the drowning events of the middle Hauterivian and latest Hauterivian – Early Barremian are more difficult to be traced out of the northern Tethyan margin and may thus be linked rather to unfavorable palaeoceanographic conditions enhanced by the peculiar palaeogeographic position.

In regions closer to the equatorial belt such as Spain or the Vercors, some occurrences of isolated and sporadic oligotrophic patch reefs have been noted within Hauterivian and Early Barremian heterozoan-dominated carbonate platforms (Götz et al., 2005; Arnaud, 2005). Such occurrences have never been reported from the Helvetic heterozoan-dominated platform. From our point of view, this may be due to palaeoceanographic and climatic conditions in southern settings which were more favorable than in the Helvetic realm. In addition to the general palaeoceanographic conditions in the Tethys, the palaeogeographic position of the Helvetic realm may have played an important role.

C.5.5.4. Palaeoceanographic and palaeoclimatic changes

C.5.5.4.1. Changes in nutrient level

Global nutrient levels in past oceans can be approximated by phosphorus burial rates, in the case oceans did not become too anoxic. Using the data sets of Föllmi (1995), Van de Schootbrugge et al. (2003) and Bodin et al. (2006a), we are able to constrain nutrient inputs in the western Tethyan realm during the Early Cretaceous (Fig. C.5.7). From the Berriasian to Barremian stages, three periods can be distinguished with the help of phosphorus burial rates: the Berriasian, the Valanginian to Early Barremian and the Late Barremian periods. Indeed, during the Valanginian – Early Barremian, phosphorus burial rates are relatively high - with the exception of the latest Hauterivian, whereas they are relatively low during the Berriasian and the Late Barremian. During the latest Hauterivian, the PAR curve shows a negative shift that reach a minimum

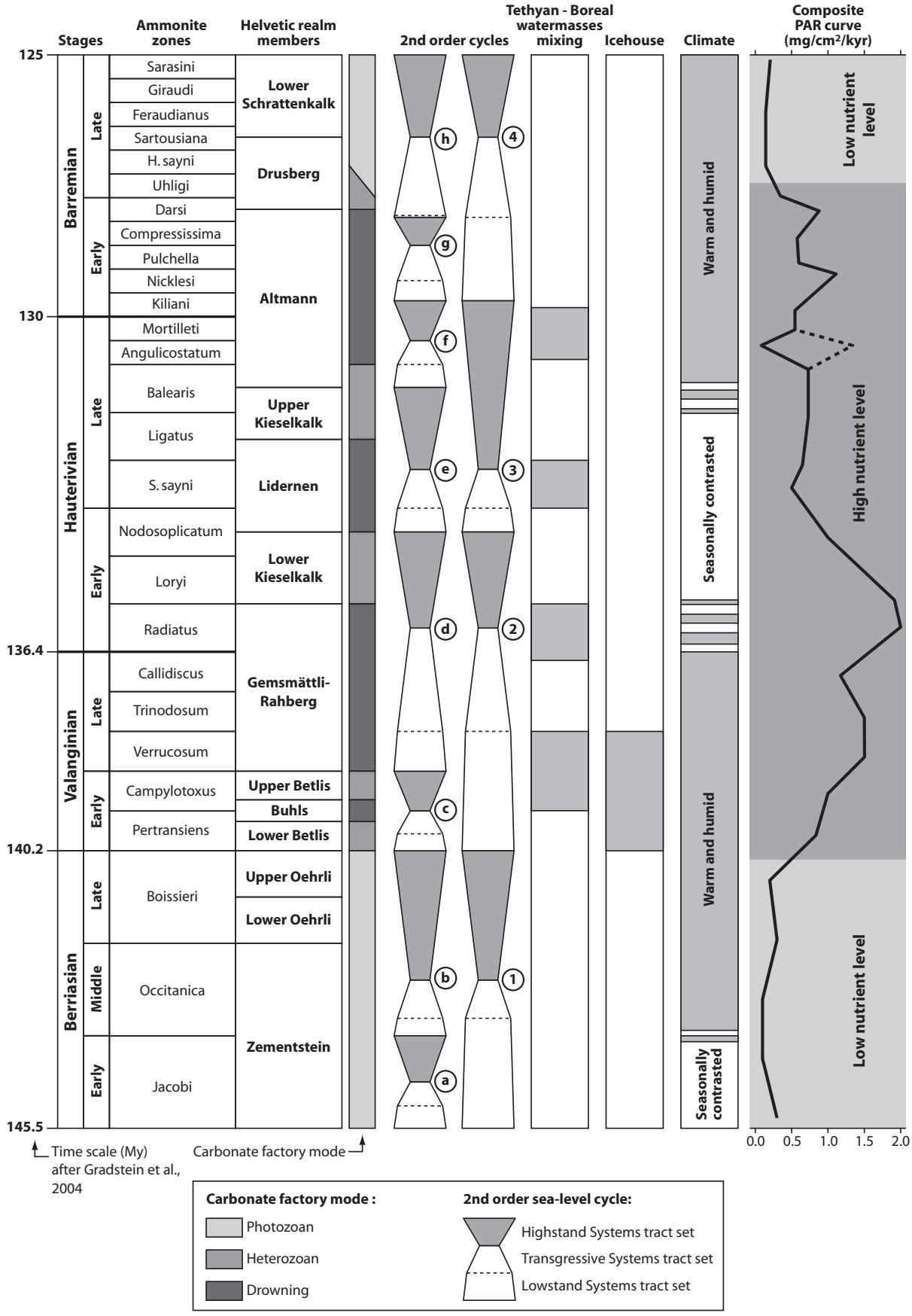

Fig. C.5.7: Variations in the carbonate platform factory and drowning episodes plotted against second-order sea-level cycle, Tethyan-Boreal water-mass mixing, icehouse and greenhouse modes, northern Tethyan climate change and a synthetic curve of phosphorus accumulation during the Berriasian – Barremian interval.

within the Faraoni level. Following Bodin et al. (2006a), this may not be linked to a decrease of phosphorus input during this time, but rather to the onset of the anoxic event recorded in the Faraoni level, leading to weakened phosphorus preservation in ocean sediments.

Consequently, a switch between low nutrient to high nutrient levels in the ocean is associated with the Berriasian – Valanginian transition, whereas the inverse occurs at the Early – Late Barremian transition. Interestingly, these changes can be traced on the Northern Tethyan margin. Thus, periods of low nutrient levels in the ocean were associated with the development of the photozoan carbonate factory, whereas the period of high nutrient levels is mirrored by a heterozoan carbonate factory and a series of drowning events. This confirms previous works (*e.g.*, Halfar et al., 2004) suggesting nutrient control on the carbonate platform factory as an additional factor to sea-surface temperature.

During the time of heterozoan carbonate platform production and drowning events (Valanginian to Early Barremian), no direct correlation between nutrient level and carbonate platform drowning has been observed. Carbonate platform drowning events do not seem to be linked to higher nutrient level than the deposition of heterozoan carbonate. Other additional driving mechanisms may thus have been implied in carbonate platform drowning.

C.5.5.4.2. Sea level changes

Berriasian – Barremian sea-level changes in the European realm have been the matter of numerous studies (*e.g.,* Rawson & Riley, 1982; Ruffell, 1991; Jacquin et al., 1998; Mutterlose & Bornemann, 2000; Ford & Golonka, 2003; Arnaud, 2005). The here-proposed stacking pattern of sea-level cycles (Fig. C.5.7) results from the compilation of data from Arnaud-Vanneau & Arnaud (1991), Hoedemaeker (1995), Mutterlose & Bornemann (2000), Arnaud (2005) and Föllmi et al. (2006). All these studies (except Hoedemaeker, 1995) have focused on the Helvetic platform or regions close to it. A common history of sea-level changes can be recognized. The identified sea-level cycles are also close to the one proposed by Ogg et al. (2004) for the Early Cretaceous. In Fig. C.5.7, these cycles are representative of second-order cycles, in the sense that they group, at least, two third-order cycles. These second-order cycles are however different from the second-order cycles defined by Hardenbol et al. (1998). They correspond to the "variations of average sea level" defined by Arnaud-Vanneau & Arnaud (1991; cf. Hoedemaeker, 1995 or Schlager, 2004, for a discussion on this subject). Eight cycles have been recognized during the Berriasian – Barremian (noted "a" to "h"). Cycles a-b, c-d, e-f and g-h can also be grouped into supra-cycles 1, 2, 3 and 4, respectively.

Although Cretaceous sea-level variations cannot be directly implied in carbonate platform drowning by simply submerging the platform below the photic zone (*e.g.,* Schlager, 1981, 1991), they may play a role because all the four drowning events reported here are centered on times of sea-level transgression and maximum flooding intervals. The condensation associated to some drowning events is however starting earlier during time of sea-level lowstand It can thus be suggested that sea-level variations are accompanied by palaeoceanographic changes such as changes in oceanic circulation pattern (*e.g.,* Poulsen et al., 1998) or sea column parameters that lead to carbonate platform drowning during transgression.

This is however not the case when the platform experienced the growth of the photozoan community. Indeed, the onset of the development of photozoan platforms is not affected by sea-level change. For example, the onset of the Urgonian platform ("Schrattenkalk formation") during the Late Barremian is coeval with a second order maximum flooding interval. On the contrary, the development of the Urgonian platform may thus have been favored by the creation of important accommodation space. This corresponds to the concept of constructive or destructive transgressions developed by Föllmi et al. (1994). Thus, even if sea-level variations are accompanied

by palaeoceanographic changes, the overall oceanic low nutrient content during times of photozoan platforms development dominates oceanographic parameters.

For the Gemsmättli and Lidernen drowning events, ammonite dating indicates that the onset of the condensation is coeval with a second-order sea-level lowstand (Kuhn, 1996; Van de Schootbrugge, 2001). For these events, it can be hypothesized that sea-level lowstand may have contributed to weaken the carbonate factory and thus favored drowning event during the subsequent sea-level rise (*e.g.,* Schlager, 1991).

C.5.5.4.3. Tethyan – Boreal water-mass exchanges

Due to the close location of the Northern Tethyan margin to the Boreal realm, the opening of pathways between these two realms may have played an important role in the functioning of the shallow-water carbonate factory (Van de Schootbrugge, 2001). In order to trace such connections, the simultaneous occurrence of Tethyan organisms within the Boreal realm and Boreal organisms within the Tethyan realm was used. To our point of view, such events may best be explained by pathway opening between the two realms.

Occurrences of Tethyan organisms in the boreal realm were described by Hoedemaeker (1995) and Mutterlose & Bornemann (2000). Four periods have recorded such migrations: the early to Late Valanginian transition, the Valanginian-Hauterivian transition, the mid-Hauterivian and the latest Hauterivian. Occurrences of boreal organisms in the Tethyan realm were described, for example, by Van de Schootbrugge (2001), Godet et al. (2006), Bodin et al. (2006a) and Duchamp (2006) in the Vocontian trough. These Boreal incursions into the Tethyan realm correspond in time to the Tethyan ones into the Boreal realm. Four episodes of water-masses mixing are thus identified during the Berriasian-Barremian (Fig. C.5.7). These four events are related to periods of maximum flooding and sea-level highstand (c, d, e and f cycle), which confirms the crucial role of sea level in the opening of marine pathways. Not every sea-level highstand (cycles a, b, g and h) is however mirrored by such water-masses exchanges. Peculiar conditions may thus be implied to preclude migrations of Tethyan and Boreal fauna and flora. Thus, during the Berriasian and the Late Barremian, the rapid growth of the photozoan-dominated carbonate platform along the northern Tethyan margin could have been a determining factor to prevent water-mass exchange by rapid infill of Boreal-Tethyan pathways. Moreover, the cycle "g" during the Early Barremian belongs to the lowstand of the cycle n°4. The sea-level was thus perhaps not sufficiently high during this cycle to allow for pathway opening.

Interestingly, the four Boreal-Tethyan water-mass exchanges are also correlated to the four drowning events. A link between the two phenomena may thus be considered. On one hand, the opening of the pathway between the Boreal and Tethyan realm may have lead to a cold-water influx along the northern Tethyan margin. It can thus be proposed that carbonate factory hypothermia may have been responsible of the Helvetic realm drowning events. This explanation is however not satisfying because heterozoan systems can grow in cold conditions (*e.g.,* James, 1997). On the other hand, the influx of Boreal cold water through the Polish furrow may also have been responsible of circulation pattern changes in the western Tethyan realm, which would have been harmful for carbonate platform growth. It may also have contributed to a supplementary nutrient input into the Tethyan realm.

C.5.5.4.4. Climate change

Climate change during the Early Cretaceous can be characterized by the relative amount of the different clay minerals in the bulk carbonate rocks. Following numerous studies, climate change along the northern Tethyan margin is relatively well constrained (Fig. C.5.7). During the Early Berriasian, a seasonally contrasted climate, typical of today's intertropical climate was observed by Schnyder et al. (2005). A

shift to tropical warm and humid climate took place during the Middle Berriasian and ended during the earliest Hauterivian (Schnyder et al., 2005; Duchamp-Alphonse, 2006). The middle Hauterivian was characterized by the return of a seasonally contrasted climate. During the latest Hauterivian (Balearis zone), Godet et al. (in press) noted the return of a warm and humid climate, which persisted through the whole Barremian.

Compared to the evolution of the carbonate platform along the northern Tethyan margin, no direct link between these climatic changes and carbonate factory changes or drowning can be seen. This is however not surprising because nowadays, photozoan carbonate factories develop in both tropical and inter-tropical climatic settings.

C.5.5.4.5. Changes in water density

The values of $\delta^{18}O$ in seawater are a function of water density, which depends on water temperature and salinity. Thus, the most depleted $\delta^{18}O$ values are representative of the least dense water (*i.e.* warmer/less saline) while heavier $\delta^{18}O$ values represent more dense water. In the Vocontian Trough, carbonate bulk rocks are mostly composed of nannoplankton remains and exported platform carbonates (*e.g.*, Reboulet et al., 2003). The here recorded $\delta^{18}O$ signal of carbonate bulk rock may thus be related to near sea-surface water density values. On the other hand, belemnites are though to be nektobenthic animals and may thus have inhabited deeper water settings. This can be seen in the $\delta^{18}O$ values from belemnites that are systematically heavier and thus representative of denser water (see also Van de Schootbrugge et al., 2000, for a discussion on this subject). The $\Delta\delta^{18}O$ index, which is the absolute difference between $\delta^{18}O_{bulk}$ and $\delta^{18}O_{bel}$ can thus be used to trace the difference of sea-water density between the surface and deeper settings. The closer the values are to zero, the less difference there is.

With the exception of the cycle “f” (latest Hauterivian), $\Delta\delta^{18}O$ variations are remarkably well correlated to sea-level changes during the Valanginian – Barremian (Fig. C.5.5). Sea-level transgressions and early highstands are characterized by less difference between water masses, whereas the opposite is observed for sea-level lowstands. During the cycle “f”, no significant changes can be observed.

For cycles c, d, e and h, the smaller difference between water masses is mirrored by increased water density as indicated by bulk rock $\delta^{18}O$. This situation is likely related to enhanced upwelling along the northern Tethyan margin during sea-level transgression and early highstand stage. In the opposite situation, sea-level lowstands are characterized by weakened upwelling and less dense surface water leading to water masses stratification.

Cycles f and g however did not correspond to this situation. Within the cycle “f”, which is associated to the Faraoni oceanic anoxic event, the maximum flooding interval is characterized by less dense surface water and a pronounced difference between water masses. Within the cycle “g”, even if the maximum flooding interval is characterized by a very weak water masses difference, it can not be associated to enhanced upwelling because the $\delta^{18}O_{bel}$ signal indicates that the deeper waters are associated to less dense water, which is incompatible with an upwelling scenario. To our point of view, the peculiar behavior of water masses during cycles f and g was linked to the Faraoni event and its aftermath. See chapter C.5.5.5.2 for a detailed discussion on this event.

No significant correlation can be observed between sea-surface density variations and carbonate-platform factory changes. Sea-surface temperature and salinity changes may thus not have been responsible of such changes, which indirectly confirms the role of nutrient level as the main driving factor of carbonate-platform factory along the northern Tethyan margin during the Early Cretaceous.

Mg, Sr and Ca belemnite content were analyzed in order to trace palaeotemperature evolution and complete the oxygen isotope results. McArthur et al. (2004) however showed that these ratios in *Hibolites* are not temperature

dependant. The here-obtained results lead us to the same conclusions because there is no co-variation between the Mg/Ca and Sr/Ca ratios to the $\delta^{18}O$ values (Fig. C.5.6). Furthermore, this conclusion can also be extended to the *Mesohibolites* genera which also lacks good correlation.

C.5.5.4.6. Changes in carbon cycle

In a classical view, the bulk-rock $\delta^{13}C$ signal is used to trace phytoplankton productivity. Indeed, the higher the phytoplankton productivity is, the more ^{13}C enriched will be the surface waters and thus the calcareous shells of planktonic organisms that compose the bulk carbonate rock. As a result, the higher the phytoplankton productivity will be, the higher will be the $\delta^{13}C$ difference between the surface and deeper water (Broecker & Peng, 1982; Fisher & Arthur, 2002). This difference can be traced with the $\Delta\delta^{13}C$ index, which is the absolute difference between $\delta^{13}C_{bulk}$ and $\delta^{13}C_{bel}$.

However, following Godet et al. (2006) and Föllmi et al. (2006), it appears that the $\delta^{13}C$ signal in the Vocontian trough is influenced by carbonate platform shedding. Indeed, during time of heterozoan-dominated platform growth, the export of low $\delta^{13}C$ calcite and dissolved inorganic carbon (DIC) lead to the buffering of the seawater $\delta^{13}C$ signal. During time of photozoan-dominated platform growth, the export of high $\delta^{13}C$ aragonite and DIC causes a significant rise of seawater $\delta^{13}C$. The use of the $\delta^{13}C$ curve as well as the $\Delta\delta^{13}C$ index to trace phytoplankton productivity may thus be impaired, especially during time of photozoan-dominated platform growth.

With the exception of the cycle "h" (latest Barremian), $\Delta\delta^{13}C$ variations are remarkably well correlated to sea-level changes during the Valanginian – Barremian (Fig. C.5.4). Sea-level lowstands are characterized by less phytoplankton productivity, whereas the opposite is observed for sea-level highstands, especially around the maximum flooding interval. During the cycle "h", the maximum flooding interval is characterized by a negative shift of $\Delta\delta^{13}C$ values. This period corresponds to the onset of the Schrattenkalk Fm (photozoan-dominated carbonate platform) and an impact of platform shedding could thus be implied to explain this peculiar $\Delta\delta^{13}C$ signal. Indeed, the important positive shift of $\delta^{13}C_{bel}$ may thus be related to the export of aragonite into the Vocontian trough. This may have disturbed the $\delta^{13}C$ record as a phytoplankton productivity signal and caused the negative shift of the $\Delta\delta^{13}C$ index.

A potential link between phytoplankton productivity and carbonate-platform factory changes is difficult to observe because of the carbonate shedding effect on the $\delta^{13}C$ signal. Nevertheless, the enhanced phytoplankton productivity around maximum flooding intervals may have contributed to weaken carbonate platform productivity, and thus have played a role in drowning episodes, for example by blooms of bioeroding organisms (*e.g.*, Hallock, 1988).

C.5.5.5. The Valanginian and Late Hauterivian events

Two periods of major perturbation in the carbon cycle are reported from the Berriasian – Barremian: the Valanginian Weissert event and the latest Hauterivian Faraoni event. Along the lines of this study, new observations and interpretations can be proposed for these events.

C.5.5.5.1. A fresh look at the Valanginian Weissert event

The most notable feature of the Valanginian is the positive $\delta^{13}C$ shift recorded both in marine and terrestrial materials (Lini et al., 1992; Van de Schootbrugge et al., 2000; Erba et al., 2004; Gröcke et al., 2005). Erba et al. (2004) proposed that this event is an equivalent of an oceanic anoxic event. However, the lack of significant organic-carbon burial, which is one of the major criteria for defining oceanic anoxic event, makes this event somewhat mysterious.

Following the high-resolution $\delta^{13}C$ record from the Vocontian Trough (Hennig et al.,

1999; Duchamp-Alphonse et al., 2006), the carbon-isotope excursion starts in the latest Early Valanginian (*B. campylotoxus* zone) and reaches a maximum in the earliest Late Valanginian (S. *verrucosum* zone) followed by a slightly decreasing plateau during the latest Valanginian. These results on ammonite-calibrated sections show thus clearly that the positive excursion is centered on the Early-Late Valanginian boundary (Fig. C.5.4). Minor black-shale levels are also reported in Italian sections during this time interval (Lini et al., 1992).

Of peculiar interest is the relationship between this event and the icehouse mode described during the Valanginian (*e.g.,* Kemper, 1987). Erba et al. (2004) and Weissert and Erba (2004) suggested that a cooling episode post-dates the Valanginian event. They linked this cooling to pCO_2 drop by atmospheric CO_2 consumption from basalt weathering and organic matter burial. The presence of a positive $\delta^{18}O$ excursion, in both bulk carbonate rocks and belemnite, reaching a maximum around the Valanginian – Hauterivian boundary, was used as another hint for this post-event cooling scenario. Gröcke et al. (2005), however, were not able to observe a significant drop of pCO_2 over the Valanginian event. Interesting is also the fact that in its founder paper of the Valanginian Icehouse, Kemper (1987) described glendonite occurrences only within the Early Valanginian and the earliest Late Valanginian (Fig. C.5.7). If such glendonite occurrences are related to an icehouse mode, it may follow that the Valanginian event took place during icehouse conditions, and may as such not be related to a first episode of greenhouse conditions during the Cretaceous (*e.g.,* Lini et al., 1992). This is also confirmed by sea-level variations during the Valanginian (sea-level cycle n°2; cf. Fig. C.5.7). Indeed, the Early Valanginian is characterized by a second-order sea-level lowstand, followed by a sea-level rise that reaches its paroxysm during the earliest Hauterivian (*A. radiatus* zone). This sea-level cycle is recognized worldwide (*e.g.,* Hardenbol et al., 1998, and many others) and may thus be of eustatic origin, and may confirm the presence of polar ice-cap during the Early – earliest Late Valanginian followed by the reinstallation of Greenhouse conditions during the latest Valanginian.

The Valanginian-Hauterivian transition cooling recorded along the northern Tethyan margin (Fig. C.5.5) is thus not related to a global cooling, but rather to peculiar palaeogeographic settings. Indeed, as recorded by the $\Delta\delta^{18}O$ signal, this period is characterized by enhanced upwelling. This is confirmed by the absence of sea-surface water cooling during the Valanginian in the Pacific (Erba et al., 2004).

During the late Early Valanginian, at the beginning of the $\delta^{13}C$ positive excursion, the $\Delta\delta^{13}C$ curve shows the highest values recorded during the Valanginian – Barremian. This is related to strongly enhanced surface phytoplankton productivity (*e.g.,* Broecker & Peng, 1982; Fisher & Arthur, 2002). The onset of this event is also mirrored by a strong shift of nutrient input into the ocean as recorded by phosphorus accumulation rates (Fig. C.5.7). The Valanginian event is thus perhaps the result of icehouse conditions, leading to enhanced nutrient input through enhanced ice-sheet weathering and a resulting increased surface phytoplankton productivity. Further investigations are however needed to test this model.

C.5.5.5.2. The Faraoni event and its aftermath

According to the reconstruction of phosphorus burial rates around the Faraoni Level, Bodin et al. (2006a) have proposed a model in which reworking of nutrients from previous land area, together with an enhanced Tethyan-Boreal connection and stronger upwelling, may have lead to increased nutrient content in sea waters. Following the here-presented new oxygen-isotope belemnite data, it appears that enhanced upwelling did not occur during the latest Hauterivian. Indeed, both bulk rock and belemnite $\delta^{18}O$ curves indicate that the Faraoni event is characterized by less dense seawater (Fig. C.5.5). Moreover, contrary to the other sea-level highstands, the $\Delta\delta^{18}O$ curve does not show any shift characteristic of seawater

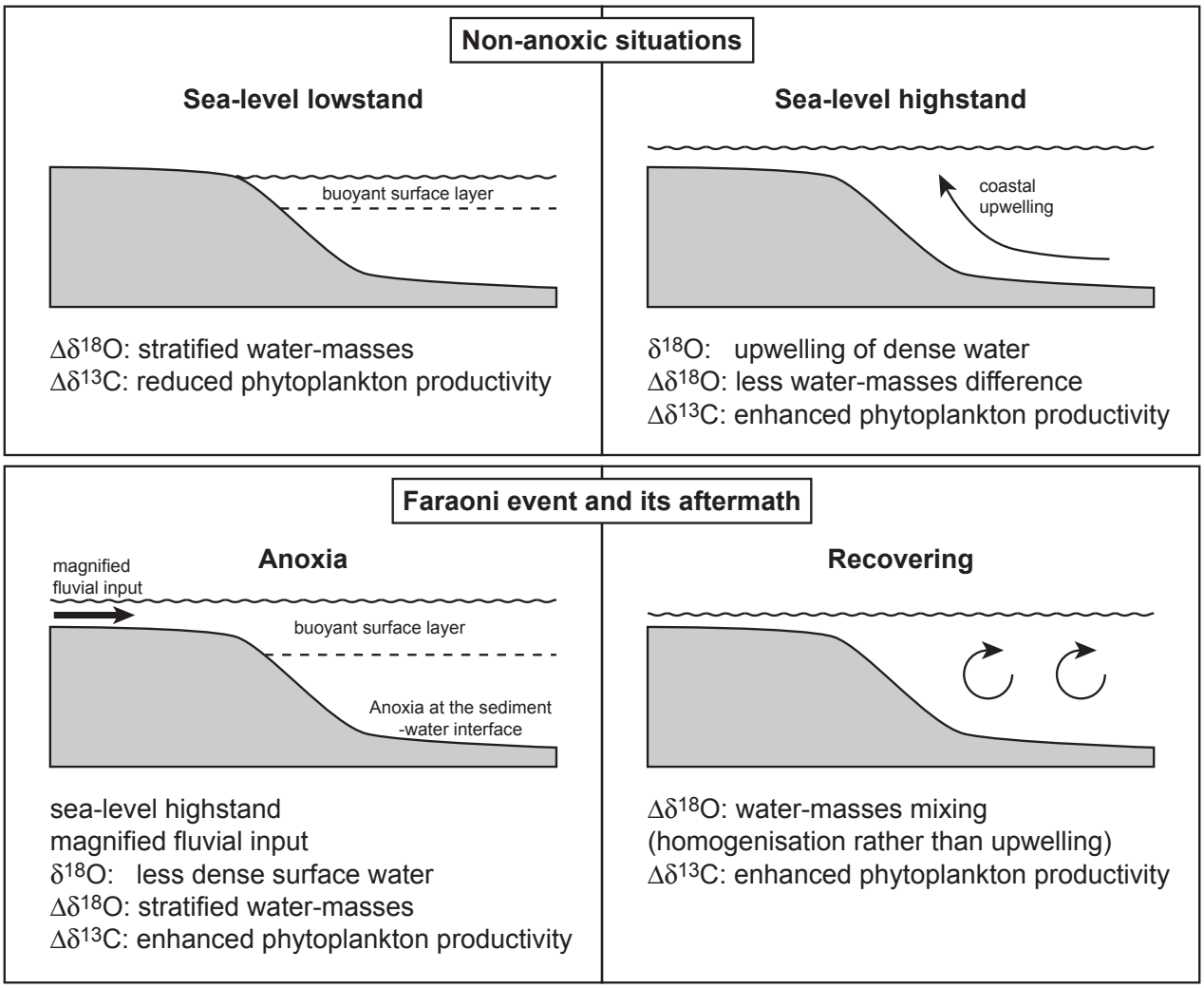

Fig. C.5.8: Synthetic model resuming palaeoceanographic change during the Early Cretaceous as deduced from this study.

mixing. This shows that upwelling may not have been responsible for the Faraoni event, but on the contrary, that the water masses were stratified during that time, with a buoyant, less dense, surface layer.

Of peculiar interest is the fact that, just prior to the Faraoni Level, in the *B. balearis* zone, a major climate shift to humid and warm conditions is reported along the northern Tethyan margin (Godet et al., in press). The onset of this type of climate may have increased fluvial inputs into the Tethys. Following the model of Meyers (2006), magnified fluvial input may be responsible of the development of stratified water masses that allows an expanded and intensified oxygen minimum zone intruding into the photic zone and favoring enhanced primary production. This mechanism, coupled with enhanced nutrient reworking from previous land area, the input of eventually nutrient-rich cold water from the Boreal realm, and a positive feedback by intensified phosphorus recycling, may thus be able to explain the Faraoni oceanic anoxic event.

Following this scenario, it is possible to give an explanation for the Early Barremian event occurring during the maximum flooding interval of the cycle "g". This event is characterized by an important negative shift of $\delta^{18}O_{bel}$ values, more positive $\delta^{18}O_{bulk}$ values and less important $\Delta\delta^{18}O$ values. As previously discussed, it cannot be linked to enhanced upwelling. This feature can however be associated to important water mixing over a large part of the water column, which leads to reduced deep-water density and increased surface water density. This peculiar

event can be explained if one takes into account the previous Faraoni event. Indeed, it can be hypothesized that the Early Barremian event is the result of the mixing of the important buoyant surface layer responsible for the Faraoni event with deeper water layers. Thus, during sea-level cycle "g", the renewed transgression may have disturbed the buoyant surface layer and induced water-column mixing. This mixing may also have induced enhanced surface productivity as reported by the $\Delta\delta^{13}C$ record. The enhanced deposition of organic matter reported in the Tethyan realm during the Early Barremian (Bréhéret, 1994; Erba et al., 1999; Bersezio et al., 2002) my thus be related to this event. If this hypothesis is correct, the Faraoni event may not only have disturbed the latest Hauterivian carbon cycle, but may also have influenced the carbon cycle during the Early Barremian.

C.5.5.6. Carbonate platform drowning events

Berriasian - Barremian carbonate platform drowning events reported along the northern Tethyan margin are challenging our knowledge because they do not fit the platform eutrophication hypothesis (*e.g.,* Drzewiecki & Simo, 1997). In this peculiar setting, there is no nutrient level threshold separating the times of carbonate growth and drowning episodes. This is linked to the fact that a heterozoan-dominated carbonate platform replaced the photozoan-dominated one during times of high-nutrient levels. Indeed, along the northern Tethyan margin ramp, during times of high nutrient levels, the disappearance of reef-related organisms such as corals and rudists allowed the crinoid-dominated ecosystem to extend over a large part of the ramp (*e.g.,* Bodin et al., 2006b), which allowed the carbonate platform to continue to growth under high nutrient levels. An additional factor to high nutrient level may thus be evoked to explain the repeated demise of the heterozoan-dominated carbonate platform.

As previously discussed, carbonate-platform drowning events are centered on sea-level maximum flooding intervals and coeval with enhanced Tethyan-Boreal realm connections. Around maximum flooding intervals, except for the latest Hauterivian, enhanced upwelling is also reported. Such palaeoceanographic changes may have played a role because it can be hypothesized that they lead to changes in current pattern (*e.g.,* Poulsen et al., 1998). Hallock et al. (1988) and John & Mutti (2005) have already suggested that strong benthic currents were the main controlling factor of heterozoan carbonate systems demise through sea-sediment interface sweeping. Föllmi (1989), Van de Schootbrugge (2001) and Bodin et al. (2006b) have noted that winnowing processes in relation to the presence of an E-W directed current were important to carbonate-platform drowning deposits in the Helvetic realm. All these observations lead to the conclusion that the reorganization of current patterns during maximum flooding intervals may have been a crucial factor in triggering drowning episodes. Moreover, some carbonate platform demise episodes have begun during a sea-level lowstand, which may have contributed to weaken the carbonate factory and thus favored drowning event during the subsequent sea-level rise (*e.g.,* Schlager, 1991). Finally, the Altmann Member drowning episode onset is also coeval with an oceanic anoxic event (the Faraoni event), which could have lead to platform suffocation as suggested by the occurrence of a dark shaly layer coeval with the Faraoni event in the Helvetic realm (Bodin et al., 2006b).

C.5.6. Conclusions

An integrated approach of palaeoceanographic and palaeoclimatic proxies is a fruitful method to better understand palaeoenvironmental changes and their links to carbonate platform factory changes and drowning. The comparison of bulk-rock and belemnite stable isotope records and sea-level change during the Early Cretaceous suggests that periods of maximum flooding and early highstands during second-order sea-level change were characterized by enhanced upwelling and

phytoplankton productivity, whereas periods of sea-level lowstands were characterized by sea-water stratification and lower phytoplankton productivity (Fig. C.5.8).

This was however not the case during the Faraoni oceanic anoxic event (latest Hauterivian) and its aftermath (Early Barremian). In this peculiar setting (Fig. C.5.8), the period of second-order maximum flooding was characterized by sea-water stratification, probably initiated by the onset of tropical climate on land and the resulting magnified fluvial input into the ocean, which may finally have been responsible of bottom water anoxia. This strongly stratified ocean became better mixed again during the following sea-level cycle, which may have favored the deposition of the numerous organic-matter enriched horizons reported in the Tethyan realm from the Early Barremian.

Switches between photozoan and heterozoan-dominated carbonate platform ecosystems along the northern Tethyan margin during the Early Cretaceous were driven by overall nutrient levels in sea-water. Sea-surface temperature and salinity changes were rather not responsible of such changes. Early Cretaceous carbonate platform drowning events were linked to the occurrence of strong bottom currents during second-order sea-level maximum flooding intervals. These episodes were probably also favored by general weakening of the carbonate platform factory during sea-level lowstands or by suffocation associated with oceanic anoxic events.

C.5.7. Acknowledgments

We thank Thierry Adatte for stimulating discussions, Jean Vermeulen and Jaap Klein for their help on the field, Bas Van de Schootbrugge for advices on the procedure of belemnite preparation and Tiffany Monnier for help in the laboratory work. Financial support from the Swiss National Science Foundation (project 2100-067807/1 and 200020-105206/1) is gratefully acknowledged.

C.5.8. References

Arnaud, H. 2005. The South-East France Basin (SFB) and its Mesozoic evolution. In: The Hauterivian - Lower Aptian sequence stratigraphy from Jura platform to Vocontian basin: a multidisciplinary approach (Eds T. Adatte et al.), Géologie Alpine, Série Spéciale «Colloques et Excursions» n°7, pp. 5-28.

Arnaud, H., Arnaud-Vanneau, A., Blanc-Aletru, M.C., Adatte, T., Argot, M., Delanoy, G., Thieuloy, J.-P., Vermeulen, J., Virgone, A., Virlouvet, B. and Wermeille, S. 1998. Répartition stratigraphique des orbitolinidés de la plate-forme urgonienne subalpine et jurassienne (SE de la France). Géologie Alpine, 74: 3-89.

Arnaud, H., Arnaud-Vanneau, A., Bulot, L.G., Beck, C., MacSotay, O., Stephan, J.-F. and Vivas, V. 2000. Le Crétacé inférieur du Venezuela oriental: stratigraphie séquentielle des carbonates sur la transversale Casanay-Maturin (Etats de Anzoategui, Monagas et Sucre). Géologie Alpine, 76: 3-81.

Arnaud-Vanneau, A. 1980. Micropaléontologie, paléoécologie et sédimentologie d'une plate-forme carbonatée de la marge passive de la Téthys; L'Urgonien du Vercors septentrional et de la Chartreuse (Alpes occidentales). Géologie Alpine, Mémoire Hors-Série, 11.

Arnaud-Vanneau, A. and Arnaud, H. 1991. Sédimentation et variations relatives du niveau de la mer sur les plates-formes carbonatées du Berriasien-Valanginien inférieur et du Barrémien dans les massifs subalpins septentrionaux et le Jura (Sud-Est de la France). Bull. Soc. Geol. France, Huitième série, 162: 535-545.

Bernaus, J.M., Arnaud-Vanneau, A. and Caus, E. 2003. Carbonate platform sequence stratigraphy in a rapidly subsiding area: the Late Barremian-Early Aptian of the Organya basin, Spanish Pyrenees. Sedimentary Geology, 159: 177-201.

Bersezio, R., Erba, E., Gorza, M. and Riva,

A. 2002. Berriasian-Aptian black shales of the Maiolica formation (Lombardian Basin, Southern Alps, Northern Italy): local to global events. Palaeogeography, Palaeoclimatology, Palaeoecology, 180: 253-275.

Blanc, E. 1996. Transect plate-forme - basin dans les séries carbonatées du Berriasien supérieur et du Valanginien inférieur (domaine jurassien et nord-vocontien): chronostratigraphie et transfert des sédiments. Géologie Alpine, Memoire H.S. n° 25, Grenoble, France, 312 pp.

Blanc-Aletru, M.C. 1995. Importance des discontinuités dans l'enregistrement sédimentaire de l'urgonien jurassien: micropaléontologie, sédimentologie, minéralogie et stratigraphie séquentielle. Géologie Alpine, Memoire H.S. n°24, Grenoble, France, 299 pp.

Bodin, S., Godet, A., Föllmi, K.B., Vermeulen, J., Arnaud, H., Strasser, A., Fiet, N. and Adatte, T. 2006a. The Late Hauterivian Faraoni oceanic anoxic event in the western Tethys: Evidence from phosphorus burial rates. Palaeogeography, Palaeoclimatology, Palaeoecology, 235: 245-264.

Bodin, S., Godet, A., Matera, V., Steinmann, P., Vermeulen, J., Gardin, S., Adatte, T., Coccioni, R. and Föllmi, K.B. in press. Enrichment of redox-sensitive trace metals (U, V, Mo, As) associated with the late Hauterivian Faraoni oceanic anoxic event. International Journal of Earth Sciences (Geol. Rundsch.).

Bodin, S., Godet, A., Vermeulen, J., Linder, P. and Föllmi, K.B. 2006b. Biostratigraphy, sedimentology and sequence stratigraphy of the latest Hauterivian - Early Barremian drowning episode of the Northern Tethyan margin (Altmann Member, Helvetic nappes, Switzerland). Eclogae geologicae Helvetiae 99, 157-174.

Bodin, S., Vermeulen, J., Godet, A. and Föllmi, K.B. 2006c. New data on the age of the installation of Urgonian-type carbonates along the northern Tethyan margin: Biostratigraphy of the Chopf Member (Helvetic Alps, eastern Switzerland). Comptes Rendus Geoscience, 338: 727-733.

Bollinger, D. 1988. Die entwicklung des distalen osthelvetischen schelfs im Barrenian und Früh-Aptian. Drusberg-, Mittagsspitz- und Schrattenkalk-Fm im Voralpberg und Allgäu. Mitteilungen aus dem Geologischen Intitut der Eidg. Technischen Hochschule und der Universität Zürich, Neue Folge Nr. 259a, 159 pp.

Briegel, U. 1972. Geologie der östlichen Alviergruppe (Helvetische Decken der Ostschweiz) unter besonderer Berücksichtigung der Drusberg- und Schrattenkalkformation (Unterkreide). Eclogae Geologicae Helvetiae, 65: 425-483.

Broecker, W.S. and Peng, T.-H. 1982. Tracers in the sea. Lamont-Doherty Geological Observatory, Columbia University, Palisades, New-York, Eldigio Press, 690 pp.

Bréhéret, J.-G. 1994. The Mid-Cretaceous organic-rich sediments from the Vocontian zone of the French Southeast basin. In: Hydrocarbon and Petroleum Geology of France (Ed A. Mascle), Special Publication of the European Association of Petroleum Geoscientists, 4, 4, pp. 295-320.

Caplan, M.L., Bustin, R.M. and Grimm, K.A. 1996. Demise of a Devonian-Carboniferous carbonate ramp by eutrophication. Geology, 24: 715-718.

Carannante, G., Esteban, M., Milliman, J.D. and Simone, L. 1988. Carbonate lithofacies as paleolatitude indicators: problems and limitations. Sedimentary Geology, 60: 333-346.

Delanoy, G. 1997. Biostratigraphie des faunes d'ammonites à la limite Barrémien-Aptien dans la région d'Angles-Barrême-Castellane. Etude particulière de la famille des Heteroceratina Spath, 1922 (Ancyloceratina, Ammonoidea). Annales

du Muséum d'Histoire Naturelle de Nice (Nice), tome XII: 1-270.

Ditchfield, P.W. 1997. High northern palaeolatitude Jurassic-Cretaceous palaeotemperature variation: new data from Kong Karls Land, Svalbard. Palaeogeography, Palaeoclimatology, Palaeoecology, 130: 163-175.

Drzewiecki, P.A. and Simo, J.A.T. 1997. Carbonate platform drowning and oceanic anoxic events on a Mid-Cretaceous carbonate platform, South-Central Pyrenees, Spain. Journal of Sedimentary Research, 67: 698-714.

Duchamp-Alphonse, S., Gardin, S., Fiet, N., Bartolini, A., Blamart, D. and Pagel, M. 2006. Fertilization of the northwestern Tethys (Vocontian basin, SE France) during the Valanginian carbon isotope perturbation: Evidence from calcareous nannofossils and trace element data. Palaeogeography, Palaeoclimatology, Palaeoecology.

Erba, E., Bartolini, A. and Larson, R.L. 2004. Valanginian Weissert oceanic anoxic event. Geology, 32: 149-152.

Erba, E., Channell, J.E.T., Claps, M., Jones, C.E., Larson, R.L., Opdyke, B., Premoli-Silva, I., Riva, A., Salvini, G. and Torriceli, S. 1999. Integrated stratigraphy of the Cismon APTICORE (Southern Alps, Italy): A «reference section» for the Barremian-Aptian interval at low latitudes. Journal of Foraminiferal Research, 29: 371-391.

Fisher, C.G. and Arthur, M.A. 2002. Water mass characteristics in the Cenomanian US Western Interior seaway as indicated by stable isotopes of calcareous organisms. Palaeogeography, Palaeoclimatology, Palaeoecology, 188: 189-213.

Ford, D. and Golonka, J. 2003. Phanerozoic paleogeography, paleoenvironment and lithofacies maps of the circum-Atlantic margins. Marine and Petroleum Geology, 20: 249-285.

Funk, H. 1969. Typusprofile der helvetischen Kieselkalk Formation und der Altmann Schichten. Eclogae geologicae Helvetiae, 62: 191-203.

Funk, H., Föllmi, K.B. and Mohr, H. 1993. Evolution of the Tithonian-Aptian carbonate platform along the northern Tethyan margin, eastern Helvetic Alps. In: Cretaceous carbonates platforms (Eds Simo J.A.T., Scott R.W. and Masse J.-P.), AAPG Memoir, 56, pp. 387-407. American Association of Petroleum Geologists. Tulsa, OK, United States.

Föllmi, K.B. 1989. Evolution of the Mid-Cretaceous Triad. Platform Carbonates, Phosphatic Sediments, and Pelagic Carbonates along the Northern Tethys margin. Lecture Notes in Earth Sciences, 23. Springer-Verlag, 153 pp.

Föllmi, K.B. 1995. 160 m.y. record of marine sedimentary phosphorus burial: Coupling of climate and continental weathering under greenhouse and icehouse conditions. Geology, 23: 859-862.

Föllmi, K.B., Godet, A., Bodin, S. and Linder, P. 2006. Interaction between environmental change and shallow-water carbonate build-up along the northern Tethyan margin and their impact on the early Cretaceous carbon-isotope record. Paleoceanography, 21, PA4211.

Föllmi, K.B., Weissert, H., Bisping, M. and Funk, H. 1994. Phosphogenesis, carbon-isotope stratigraphy, and carbonate-platform evolution along the Lower Cretaceous northern Tethyan margin. Geological Society of America Bulletin, 106: 729-746.

Gammon, P.R., James, N.P. and Pisera, A. 2000. Eocene spiculites and spongolites in southwestern Australia: not deep, not polar, but shallow and warm. Geology, 28: 855-858.

Garcia-Hernandez, M. 1979. Les faciès urgoniens pendant la sédimentation barrémo-albienne dans les Sierras de Cazorla et du Segura (zone prébétique, S-E- de l'Espagne). Mém. Spéc. Géobios, 3: 57-69.

Godet, A., Bodin, S., Adatte, T. and Föllmi,

K.B. in press. Clay mineral assemblages along the Northern Tethyan margin during the Late Hauterivian - Early Aptian: Interactions between climate change and carbonate platform evolution. Cretaceous Research.

Godet, A., Bodin, S., Föllmi, K.B., Vermeulen, J., Gardin, S., Fiet, N., Adatte, T., Berner, Z., Stüben, D. and Van de Schootbrugge, B. 2006. Evolution of the marine stable carbon-isotope record during the early Cretaceous: A focus on the late Hauterivian and Barremian in the Tethyan realm. Earth and Planetary Science Letters, 242: 254-271.

Gröcke, D.R., Price, G.D., Robinson, S.A., Baraboshkin, E.Y., Mutterlose, J. and Ruffell, A.H. 2005. The Upper Valanginian (Early Cretaceous) positive carbon-isotope event recorded in terrestrial plants. Earth and Planetary Science Letters, 240: 495-509.

Götz, S., Löser, H. and Schmid, D.U. 2005. Reef development on a deepening platform: two Early Cretaceous coralgal patch reefs (Cati, Llacova Formation, eastern Spain) compared. Cretaceous Research, 26: 864-881.

Halfar, J., Godinez-Orta, L., Mutti, M., Valdez-Holguin, J.E. and Borges, J.M. 2004. Nutrient and temperature controls on modern carbonate production: An example from the Gulf of California, Mexico. Geology, 32: 213-216.

Hallock, P. 1988. The role of nutrient availability in bioerosion: Consequences to carbonate buildups. Palaeogeography, Palaeoclimatology, Palaeoecology, 63: 275-291.

Hallock, P., Hine, A.C., Vargo, G.A., Elrod, J.A. and Jaap, W.C. 1988. Platforms of the Nicaraguan Rise: Examples of the sensitivity of carbonate sedimentation to excess trophic resources. Geology, 16: 1104-1107.

Hallock, P. and Schlager, W. 1986. Nutrient excess and the demise of coral reefs and carbonate platforms. Palaios, 1: 389-398.

Hardenbol, J., Thierry, J., Farley, M.B., Jacquin, T., de Graciansky, P.-C. and Vail, P.R. 1998. Mesozoic and Cenozoic Sequence Chronostratigraphic Framework of European Basins. In: Mesozoic and Cenozoic Sequence Stratigraphy of European Basins. (Eds P.-C. de Graciansky, J. Hardenbol, T. Jacquin and P.R. Vail), Special Publication Society for Sedimentary Geology, 60, pp. 3-13.

Hay, W.W., DeConto, R., Wold, C.N., Wilson, K.M., Voigt, S., Schulz, M., Wold-Rossby, A., Dullo, W.-C., Ronov, A.B., Balukhovsky, A.N. and Soeding, E. 1999. Alternative global Cretaceous paleogeography. In: The Evolution of Cretaceous Ocean/Climate Systems (Eds E. Barrera and C. Johnson), Geological Society of America Special Paper, pp. 332.

Hennig, S., Weissert, H. and Bulot, L.G. 1999. C-isotope stratigraphy, a calibration tool betwen ammonite- and magnetostratigraphy: the Valanginian-Hauterivian transition. Geol. Carpath., 50: 91-96.

Hillgärtner, H., van Buchem, F.S.P., Gaumet, F., Razin, P., Pittet, B., Grötsch, J. and Droste, H. 2003. The Barremian-Aptian evolution of the eastern arabian carbonate platform margin (northern Oman). Journal of Sedimentary Research, 73: 756-773.

Hoedemaeker, P.J. 1995. Ammonite evidence for long-term sea-level fluctuations between the 2nd and 3rd order in the lowest Cretaceous. Cretaceous Research, 16: 231-241.

Ivanov, M., Peybernes, B., Nikolov, T., Ciszak, R., Stoykova, K. and Minkovska, V. 1997. Attempt of sequence correlations during Barremian - Aptian times within a system platform-basin-platform along a Danube-Gabrovo cross-section (Central Northern Bulgaria). Comptes Rendus de l'Academie des Sciences - Series IIA - Earth and Planetary Science, 325: 967-972.

Jacquin, T., Rusciadelli, G., Amedro, F., de

Graciansky, P.-C. and Magniez-Jannin, F. 1998. The North Atlantic cycle: an overview on 2nd-order transgressive/ regressive facies xycles in the Lower Cretaceous of Western Europe. In: Mesozoic and Cenozoic Sequence Stratigraphy of European Basins (Eds P.-C. de Graciansky, J. Hardenbol, T. Jacquin and P.R. Vail), Special Publication Society for Sedimentary Geology, 60, pp. 397-409.

James, N.P. 1997. The cool-water carbonate depositional realm. In: Cool water carbonates (Eds N.P. James and J.A.D. Clarke), 56, pp. 1-22. Society for Sedimentary Geology, Spec. Pub.

Kemper, E. 1987. Das klima der Kreide-zeit. Geologisches Jahrbuch, Reihe A, 96: 5-185.

Kuhn, O. 1996. Der Einfluss von Verwitterung auf die Paläozeanographie zu Beginn des Kreide-Treibhausklimas (Valanginian und Hauterivian) in der West-Tethys., Ph.D. thesis, Universität Zürich, Zürich, 380 pp.

Lehmann, C., Osleger, D.A. and Montanez, I.P. 2000. Sequence stratigraphy of lower Cretaceous (Barremian-Albian) carbonate platforms of northeastern Mexico: regional and global correlations. Journal of Sedimentary Research, 70: 373-391.

Lehmann, C., Osleger, D.A., Montanez, I.P., Sliter, W.V., Arnaud-Vanneau, A. and Banner, J. 1999. Evolution of Cupido and Coahuila carbonate platforms, Early Cretaceous, northeastern Mexico. GSA Bulletin, 111: 1010-1029.

Lini, A., Weissert, H. and Erba, E. 1992. The Valanginian carbon isotope event: a first episode of greenhouse climate conditions during the Cretaceous. Terra Nova, 4: 374-384.

Masse, J.-P. 1993a. Valanginian-Early Aptian Carbonate Platforms from Provence, Southeastern France. In: Cretaceous carbonates platforms (Eds Simo J.A.T., Scott R.W. and Masse J.-P.), AAPG Memoir, 56, pp. 363-374. American Association of Petroleum Geologists. Tulsa, OK, United States.

Masse, J.P., Bellion, Y., Benkhelil, J., Ricou, L.E., Dercourt, J. and Guiraud, R. 1993b. Early Aptian (114 to 111 Ma). In: Atlas, Tethys, Palaeoenvironmental Maps (Eds J. Dercourt, L.E. Ricou and B. Vrielynck). BEICIP-FRANLAB, Rueil-Malmaison.

McArthur, J.M., Mutterlose, J., Price, G.D., Rawson, P.F., Ruffell, A. and Thirlwall, M.F. 2004. Belemnites of Valanginian, Hauterivian and Barremian age: Sr-isotope stratigraphy, composition (87Sr/ 86Sr, ∂13C, ∂18O, Na, Sr, Mg), and palaeo-oceanography. Palaeogeography, Palaeoclimatology, Palaeoecology, 202: 253-272.

Meyers, P.A. 2006. Paleoceanographic and paleoclimatic similarities between Mediterranean sapropels and Cretaceous black shales. Palaeogeography, Palaeoclimatology, Palaeoecology, 235: 305-320.

Michalik, J. 1994. Lower Cretaceous carbonate platform facies, Western Carpathians. Palaeogeography, Palaeoclimatology, Palaeoecology, 111: 263-277.

Mohr, H. 1992. Der helvetische Schelf der Ostschweiz am Übergang vom späten Jura zur frühen Kreide, Ph.D. thesis, ETH Zürich, Zürich, Switzerland, 221p.

Mutterlose, J. and Bornemann, A. 2000. Distribution and facies patterns of Lower Cretaceous sediments in northern Germany: a review. Cretaceous Research, 21: 733-759.

Mutti, M. and Hallock, P. 2003. Carbonate systems along nutrient and temperature gradients: some sedimentological and geochemical constraints. International Journal of Earth Sciences (Geol. Rundsch.), 92: 465-475.

Ogg, J.G., Agterberg, F.P. and Gradstein, F.M. 2004. The Cretaceous Period. In: A geologic time scale 2004 (Eds F.M. Gradstein, J.G. Ogg and A.G. Smith), pp. 344-383. Cambridge University Press.

Peybernes, B., Ivanov, M., Nikolov, T., Ciszak,

R. and Stoykova, K. 2000. Séquence de dépôt à l'articulation plate-forme urgonienne-bassin (intervalle Barrémien-Albien) dans le Prébalkan occidental (Bulgarie du Nord-Ouest). Comptes Rendus de l'Academie des Sciences - Series IIA - Earth and Planetary Science, 330: 547-553.

Podlaha, O.G., Mutterlose, J. and Veizer, J. 1998. Preservation of ∂18O and ∂13C in belemnite rostra from the Jurassic/ Early Cretaceous successions. American Journal of Science, 298: 324-347.

Poulsen, C.J., Seidov, D., Barron, E.J. and Peterson, W.H. 1998. The impact of paleogeographic evolution on the surface oceanic circulation and the marine environment within the mid-Cretaceous Tethys. Paleoceanography, 13: 546-559.

Rawson, P.F. and Riley, L.A. 1982. Latest Jurassic - Early Cretaceous events and the «Late Cimmerian unconformity» in North Sea area. American Association of Petroleum Geologists Bulletin, 66: 2628-2648.

Reboulet, S., Mattioli, E., Pittet, B., Baudin, F., Olivero, D. and Proux, O. 2003. Ammonoid and nannoplankton abundance in Valanginian (early Cretaceous) limestone-marl successions from the southeast France Basin: carbonate dilution or productivity? Palaeogeography, Palaeoclimatology, Palaeoecology, 201: 113-139.

Ruffell, A. 1991. Sea-level events during the Early Cretaceous in western Europe. Cretaceous Research, 12: 527-551.

Samankassou, E. 2002. Cool-water carbonates in a paleoequatorial shallow-water environment: The paradox of the Auernig cyclic sediments (Upper Pennsylvanian, Carnic Alps, Austria-Italy) and its implications. Geology, 30: 655-658.

Schlager, W. 1981. The paradox of drowned reefs and carbonates platforms. Geological Society of America Bulletin, 92: 197-211.

Schlager, W. 1991. Depositional bias and environmental change--important factors in sequence stratigraphy. Sedimentary Geology, 70: 109-130.

Schlager, W. 2004. Fractal nature of stratigraphic sequences. Geology, 32: 185-188.

Schnyder, J., Gorin, G., Soussi, M., Baudin, F. and Deconinck, J.-F. 2005. Enregistrement de la variation climatique au passage Jurassique/Crétacé sur la marge sud de la Téthys: minéralogie des argiles at palynofaciès de la coupe du Jebel Meloussi (Tunisie centrale, formation Sidi Kralif). Bull. Soc. Geol. France, 176: 171-182.

Van de Schootbrugge, B. 2001. Influence of paleo-environmental changes during the Hauterivian (Early Cretaceous) on carbonate deposition along the northern margin of the Tethys: Evidence from geochimical records (C, O, and Sr-isotopes, P, Fe, Mn). Thèse de Doctorat ès Sciences, spécialité Géologie, Université de Neuchâtel, Institut de Géologie, Neuchâtel (Switzerland), 268 pp.

Van de Schootbrugge, B., Föllmi, K.B., Bulot, L.G. and Burns, S.J. 2000. Paleoceanographic changes during the early Cretaceous (Valanginian-Hauterivian): evidence from oxygen and carbon stable isotopes. Earth and Planetary Science Letters, 181: 15-31.

Van de Schootbrugge, B., Kuhn, O., Adatte, T., Steinmann, P. and Föllmi, K.B. 2003. Decoupling of P- and Corg-burial following Early Cretaceous (Valanginian-Hauterivian) platform drowning along the NW Tethyan margin. Palaeogeography, Palaeoclimatology, Palaeoecology, 199: 315-331.

Vermeulen, J. 2002. Etude stratigraphique et paléontologique de la famille des Pulchelliidae (ammonoidea, Ammonitina, Endemoceratacea). Géologie Alpine, Grenoble, France, Memoire H.S. n°42, 333 pp.

Weissert, H. and Erba, E. 2004. Volcanism, CO2 and palaeoclimate; a Late Jurassic-Early Cretaceous carbon and oxygen isotope

record. Journal of the Geological Society of London, 161: 695-702.

Weissert, H., Lini, A., Föllmi, K.B. and Kuhn, O. 1998. Correlation of Early Cretaceous carbon isotope stratigraphy and platform drowning events: a possible link? Palaeogeography, Palaeoclimatology, Palaeoecology, 137: 189-203.

Wilson, M.E.J. and Vecsei, A. 2005. The apparent paradox of abundant foramol facies in low latitudes: their environmental significance and effect on platform development. Earth-Science Reviews, 69: 133-168.

Wood, R. 1993. Nutrients, Predation and the History of Reef-Building. Palaios, 8: 526-543.

Chapter D.

General conclusions

Brisi (Churfirsten, ct. St. Gallen, Switzerland)

"Avec tout ce que je sais, on pourrait faire un livre... Il est vrai qu'avec tout ce que je ne sais pas, on pourrait faire une bibliothèque"

Sacha Guitry, extrait de la pièce *Le KWTZ*

D.1.

Main conclusions

The chapter "general conclusions" includes a summary of the most important findings of this PhD thesis and an outline of some of the remaining questions and problems. Please refer to each individual chapter for more extensive conclusions on each point.

D.1.1. The Helvetic realm

Thanks to new ammonite age dates, a precise biostratigraphic scheme is postulated for the Late Hauterivian – Barremian deposits in the Helvetic realm. Thus the deposition of the Altmann Member spans from the latest Hauterivian (*P. seitzi* ammonite zone) to the latest Early Barremian (*C. darsi* ammonite zone). The Chopf Member was deposited during the middle Late Barremian (*G. sartousiana* ammonite zone). Coupled with sequence stratigraphy interpretations, it is inferred that the onset of the Altmann Member is coeval with the Ha6 sequence boundary and its end with the maximum flooding interval Ba2. The Chopf Member was deposited during the maximum flooding interval Ba3. These new results allow also to date the intercalated sediments of the Drusberg Member, as well as to give a maximal age for the onset of the Schrattenkalk Formation. Thus, the Drusberg Member is representative of the Ba2 highstand and Ba3 transgressive intervals. The onset of the Schrattenkalk Formation is diachronous and is the result of the progradation of the Urgonian facies during the latest Barremian. Indeed, in the Helvetic ramp inner part, it corresponds to the maximum flooding interval Ba3 whereas in outer part the oldest Schrattenkalk sediments were deposited during the latest Barremian.

The Altmann Member drowning event is the result of a twofold drowning phase. A first drowning phase occurred during the latest Hauterivian and its onset is linked to the Faraoni oceanic anoxic event. A second phase is contemporaneous to the Ba2 transgression and is associated with a pronounced backstepping of the carbonate factory. In many sections, the first drowning phase is associated to a highly condensed phosphatized horizon at the base of the Altmann Member.

D.1.2. Palaeoenvironmental changes

D.1.2.1. Early Cretaceous palaeoceanography

There is a strong impact of relative sea level change on palaeoceanographic parameters such as sea-surface water density and phytoplankton productivity. During non-oceanic anoxic events, sea-level highstands are associated with enhanced upwelling and phytoplankton productivity, whereas sea-level lowstands are rather associated to stratified water masses and lesser phytoplankton productivity.

In term of global oceanic nutrient level, the Berriasian – Barremian interval can be divided into three periods: the Berriasian and the Late Barremian, characterized by low nutrient levels, and the Valanginian to Early Barremian, associated to high nutrient levels.

The interpretation of carbon isotopes as a pelagic palaeoproductivity proxy in basinal sections close to carbonate platform must be handled with care. Indeed, it appears that in these areas, there is a non-negligible influence of carbonate platform shedding on the carbon isotope signal. Thus, the development of photozoan-dominated carbonate platform increases the $\partial^{13}C$ signal in basinal sections,

whereas the development of heterozoan-dominated carbonate platform buffers this signal on a relatively low level of values.

D.1.2.2. The Faraoni event

The Faraoni Level is characterized by the enrichment of redox-sensitive trace metals (U, V, Mo and As) and a positive shift in C/P ratios. This feature is indicative of deposition in an oxygen-depleted environment, and allows to postulate that the Faraoni Level is the result of an Oceanic Anoxic Event (OAE). Even if many other organic-carbon-rich levels are recorded from the latest Hauterivian – Early Barremian, no other OAE could be reported during this time interval using these two proxies.

The following model is proposed to explain the Faraoni OAE: During sea-level transgression, the reworking of nutrients from previously exposed land, together with the progressive influx of cold (and eventually nutrient-rich) boreal water and the magnified fluvial input, lead to the eutrophication and stratification of surface-water masses. The increased nutrient recycling associated with phosphorus regeneration from the oxygen-depleted sea-sediment interface helped to sustain and enhance the eutrophication of seawater. The Faraoni AOE is the result of the climax of these phenomena. The deposition of organic matter within the Faraoni Level, together with an enhanced phosphorus-oxygen negative feedback mechanism, leads to the overall decrease of nutrients level in the ocean and to the end of the OAE.

During the Early Barremian, in the aftermath of the Faraoni Level, water masses became better mixed as the consequence of a second-order sea-level rise. This may have enhanced surface productivity and lead to the deposition of organic carbon-rich levels in non-anoxic settings.

D.1.2.3. Interactions with the northern Tethyan margin carbonate factory

Changes in the carbonate factory during the late Hauterivian and Barremian were driven by the overall nutrient content in seawaters. During times of oligotrophic conditions, photozoan carbonate systems dominated the neritic realm whereas during times of meso-eutrophic conditions, heterozoan carbonate systems developed.

Carbonate platform drowning events were linked to changes in ocean current flow pattern during times of sea-level highstand, together with high seawater nutrient levels. These changes have favored the winnowing of sediments covering the platform surface and the deposition of phosphate-rich layers, and precluded the continuation of carbonate platform growth along the northern Tethyan margin.

D.2.

Outlook

Some questions still remain open at the end of this PhD thesis. The results obtained here also calls for further studies. In the Helvetic realm, three points may be considered:

- Firstly, it would be interesting to obtain a complete 3rd order sequence stratigraphy scheme, as for the Altmann Member, for the remainder of the Early Cretaceous deposits. This would help to still better correlate the Helvetic realm with basinal sections as well as with other northern Tethyan margin realm such as the Vercors.
- Moreover, carbon and oxygen isotope stratigraphy would also be of great help in the expanded section of the Altmann Member at Tierwis, because it may allow to confirm the location of sequence boundaries and to decipher emersion episodes.
- Finally, due to the fact that the exact nature of the local depression during the latest Hauterivian in the Säntis region could not be determined, it would be also interesting to study this point in more detail. Is it related to an incised valley or to more rapid local subsidence?

Even if a wide range of palaeoenvironmental changes during the Late Hauterivian – Barremian are better constrained now for the western Tethyan realm, additional and complementary research can be envisaged.

- In order to better understand the Faraoni event, a first crucial step would be to trace it with the help of redox-sensitive trace elements out of the Eurasian realm, and especially into South America or Australia. This may help to decipher if this event is only related to regional conditions or if it is the result of a global phenomenon.
- Benthic foraminifera from the Vocontian trough could be analyzed in the same way as belemnites in order to obtain a bottom-water signal. This would allow to complement the here-obtained results.
- Similar kind of studies may be applied to other time periods in order to see if the here-proposed model for carbonate platform factory changes and drowning can always be applied, or if each case is different.
- The results presented here could also be challenged by General Circulation Models to better constrain the oceanic circulation pattern in the western Tethyan realm.

Appendix 1.

Other manuscripts

The Gorgo a Cerbara section in winter (Italy)

E.1.

Interactions between environmental change and shallow-water carbonate build-up along the northern Tethyan margin and their impact on the early Cretaceous carbon-isotope record

Karl B. Föllmi, Alexis Godet, Stéphane Bodin, and Pascal Linder

Geological Institute, University of Neuchâtel, CH-2007 Neuchâtel, Switzerland

Keywords: Helvetic realm; Photozoan; Heterozoan; Carbonate platform drowning; Calcite; Aragonite

Published in: Paleoceanography **21** (2006), PA4211, doi: 10.1029/2006PA001313

Abstract

The evolution of the early Cretaceous, northern Tethyan carbonate platform was not only influenced by changes in sea level, detrital influx, and surface-water temperature, but also by changes in trophic levels. We distinguish between phases of carbonate production dominated by oligotrophic photozoan communities and by mesotrophic and eventually colder water heterozoan communities. Superimposed on this bimodal trend in platform evolution were phases of platform demise for which we provide improved age control based on ammonite biostratigraphy. The initial phase of these episodes of platform demise corresponds in time to episodes of oceanic anoxic events (OAE's) and environmental change in general.

Based on a comparison between the temporal changes in an early Cretaceous, ammonite-calibrated, $\delta^{13}C$ record from southeastern France and coeval changes in the platform record, we suggest that the history of carbon fractionation along the northern Tethyan margin was not only influenced by changes in the oceanic carbon cycle such as in the rate of production and preservation of organic and carbonate carbon, and in the size of the oceanic dissolved inorganic carbon (DIC) reservoir, but also by the above-mentioned changes in the ecology and geometry of the adjacent carbonate platform. Phases of photozoan carbonate production induced positive trends in the hemipelagic carbonate $\delta^{13}C$ record. Phases of heterozoan carbonate production pushed the $\delta^{13}C$ system towards more negative values. Platform drowning episodes implied an initial increase in $\delta^{13}C$ values, followed by longer-term decrease in $\delta^{13}C$ values.

E.1.1. Introduction

Shallow-water carbonate successions of early Cretaceous age are widespread in the western Carpathians, the Alps, southeastern France, the Pyrenees, and the Betic Cordillera [e.g., Garcia-Hernandez, 1979; Pascal, 1982; Arnaud-Vanneau and Arnaud, 1990; Masse, 1993; Funk et al., 1993; Michalík, 1994; Föllmi et al., 1994; Bernaus et al., 2003]. They embody the remains of an extensive shallow-water carbonate platform, which developed along the northern Tethyan margin along a distance of over 2500 km [e.g., Golonka, 2004]. The central European portion of the platform is presently locked up in the northern, Helvetic Alps, which extend from southeastern Germany and western Austria through Switzerland to eastern France (Fig. E.1.1). The structural architecture of the Helvetic nappe and thrust belt allows for the palinspastic reconstruction of proximal-distal transects across the former platform for distances surpassing 80 km (Fig. E.1.2), and the early Cretaceous platform sediments preserved therein provide, therefore, excellent insight into the spatial and temporal evolution of this platform. Furthermore, the presence of ammonites in marker horizons within the Helvetic succession is the key to excellent time control.

Of special interest is the observation that the Helvetic platform succession does not only document the influence of regional environmental change such as relative sea-level fluctuations, variations in ambient sea-surface water temperature, and the type and intensity of detrital influx, but also the impact of global paleoceanographic and paleoenvironmental change, such as modifications in the carbon and phosphorus cycles in association with global oceanic anoxic events [Föllmi et al., 1994; Weissert et al., 1998; Wissler et al., 2003; van de Schootbrugge et al., 2003; Bodin et al., 2006a]. One important indicator of the paleoceanographic influence on the evolution of this carbonate platform system is the near-coincidence in timing of the phases of platform demise with episodes of major paleoceanographic change

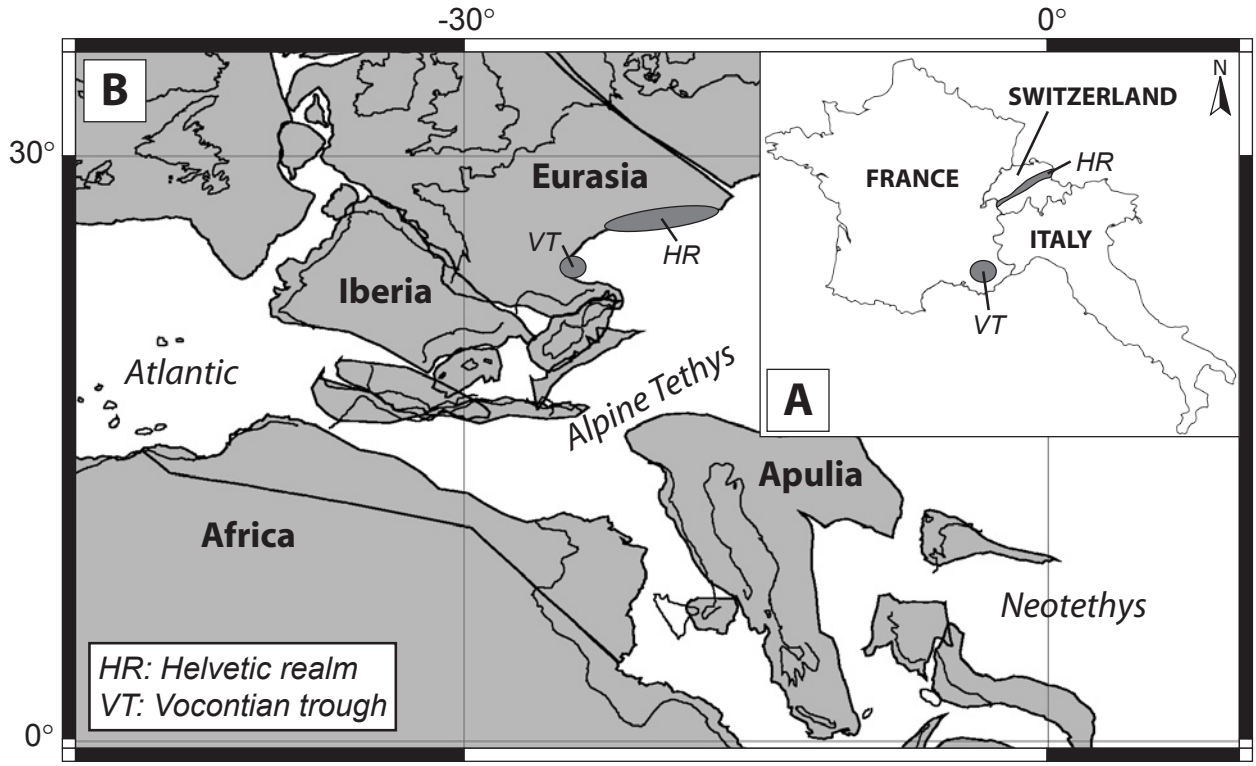

Figure E.1.1. A. Geographic location of the studied areas. B. Paleogeographic map of the northern Tethyan margin during the late Hauterivian – early Barremian showing the position of the studied areas (modified from *Bodin et al.*, 2006a).

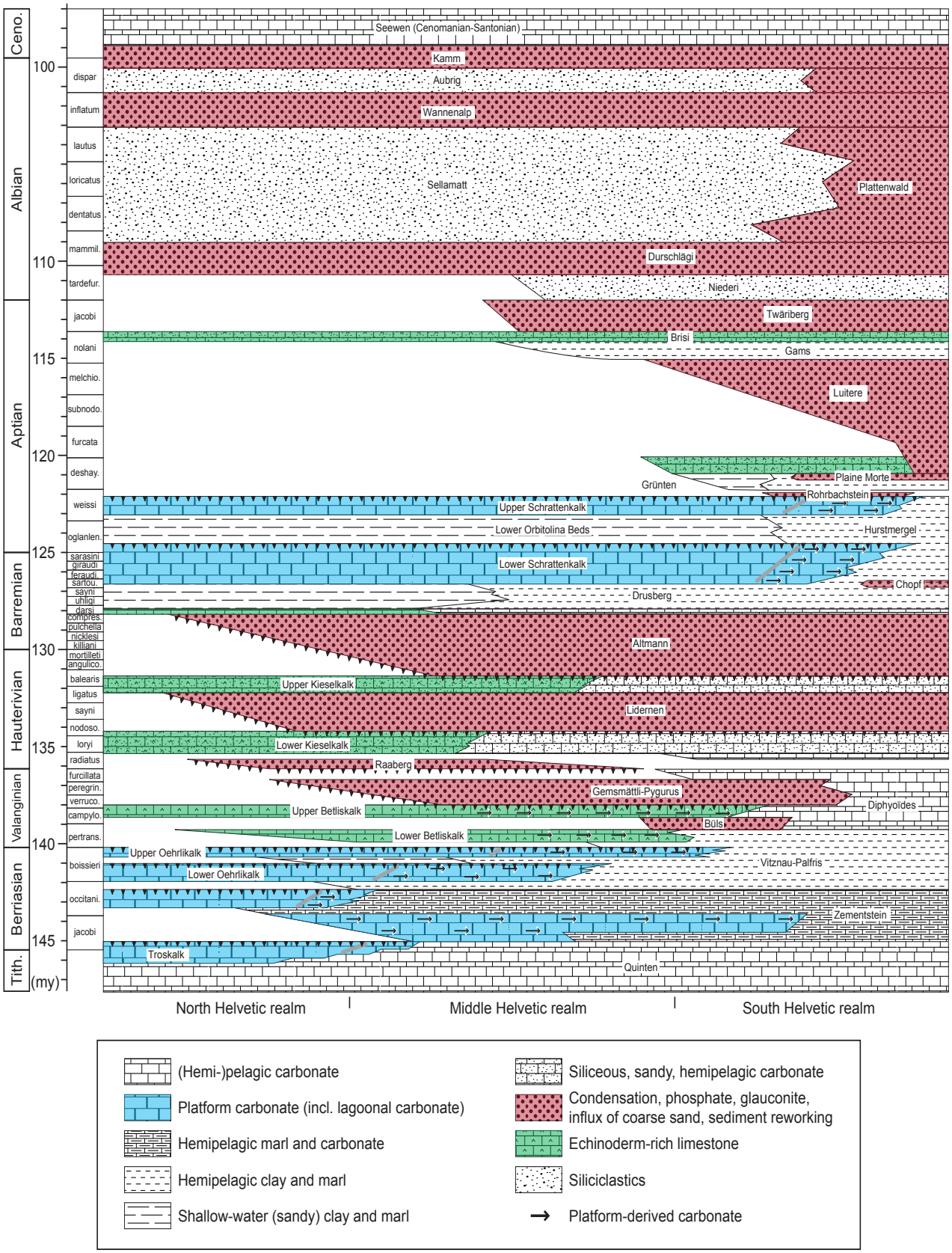

Figure E.1.2. Time-space diagram showing the temporal evolution of the distal portion of the northern Tethyan carbonate platform during the early Cretaceous, based on occurrences in the Helvetic Alps of central and eastern Switzerland (modified from *Föllmi et al.*, 1994). Time scale after *Gradstein et al.* [2004].

during the Valanginian, Hauterivian, Aptian, and Albian [Schlanger and Jenkyns, 1976; Arthur and Schlanger, 1979; Jenkyns, 1980; Weissert et al., 1979; Weissert, 1981; Schlager, 1981; Hallock and Schlager, 1986; Erbacher et al., 2001; Leckie et al., 2002; Höfling and Scott, 2002; Erba et al., 2004].

The changes in carbonate-platform growth and the phases of platform demise in association with the global anoxic events had a probable, but poorly quantifiable influence on the marine carbon cycle and associated $\delta^{13}C$ record, in that carbonate-carbon burial may have generally been diminished in neritic domains, whereas organic-carbon burial may have been increased in general [e.g., Weissert et al., 1998; Weissert and Erba, 2004]. Triggering mechanisms for these events proposed so far include modifications in the global output rate of primordial CO_2 by episodes of intense volcanic activity, and eventually by the increased release of methane [e.g., Jenkyns, 2003; but compare also Heimhofer et al., 2004].

With this contribution, we give an update on the temporal record of the northern Tethyan carbonate platform exposed in the Helvetic Alps and provide improved time control on the episodes of platform demise by ammonite biostratigraphy, thereby using new data obtained from recently published and ongoing Ph.D. thesises [Kuhn, 1996; van de Schootbrugge, 2001; Linder et al., submitted; Bodin et al., 2006b, 2006c]. We also present a new, high-resolution compilation of $\delta^{13}C$ records for the early Cretaceous, which has been derived from hemipelagic sections invariably belonging to the Vocontian basin (southeastern France) and its immediate surroundings (Figs. E.1.1 and E.1.3). The here presented record is obtained from a single region, thereby precluding the potentially blurring effect related to the accumulation of records from different basins with different environmental and depositional histories. Furthermore, it is derived from a marginal epicontinental basin indented into the northern Tethyan margin, bordered to the north, west, and south by the northern Tethyan carbonate platform [e.g., Bréhéret, 1997]. Its proximity to this platform is, for this reason, ideal for a study of the potential interactions between the northern Tethyan platform and the adjacent basin in terms of the carbon cycle. A further important advantage of this record is its calibration by ammonite biostratigraphy, which facilitates its correlation with the record from the early Cretaceous northern Tethyan shelf environment.

We also propose a novel interpretation of the changes in the here presented $\delta^{13}C$ record, which we view not only as the consequence of ocean-wide changes in the ratio of Ccarb to Corg burial flux rates, and changes in continental output of DIC and oceanic DIC reservoir size, but also as the result of changes in the ecology and geometry of the adjacent shallow-water carbonate platform. We thereby follow up on earlier publications, in which a close link between the Tethyan whole-rock $\delta^{13}C$ record and the evolution of the northern Tethyan carbonate platform was already suggested [Föllmi et al., 1994; Weissert et al., 1998; Godet et al., 2006].

E.1.2. Methodology

The sediments of the Helvetic platform have been investigated by a combination of traditional fieldwork consisting of detailed logging and sampling of key sections, the analysis of sedimentological features and determination of biostratigraphically significant fossils (mostly ammonites), and different types of geochemical and mineralogical laboratory analyses (stable carbon and oxygen isotopes, organic matter contents, XRD, XRF, etc.). The data discussed here are extracted from a selection of publications which resulted from a long tradition of research in the Helvetic zone [e.g., Heim, 1910-1916; Fichter, 1934], and are also based on the results of more recent and still ongoing research projects at the ETH Zürich, and the Universities of Berne, Geneva, and Neuchâtel.[e.g., Mohr, 1992; Kuhn, 1996; van de Schootbrugge, 2001].

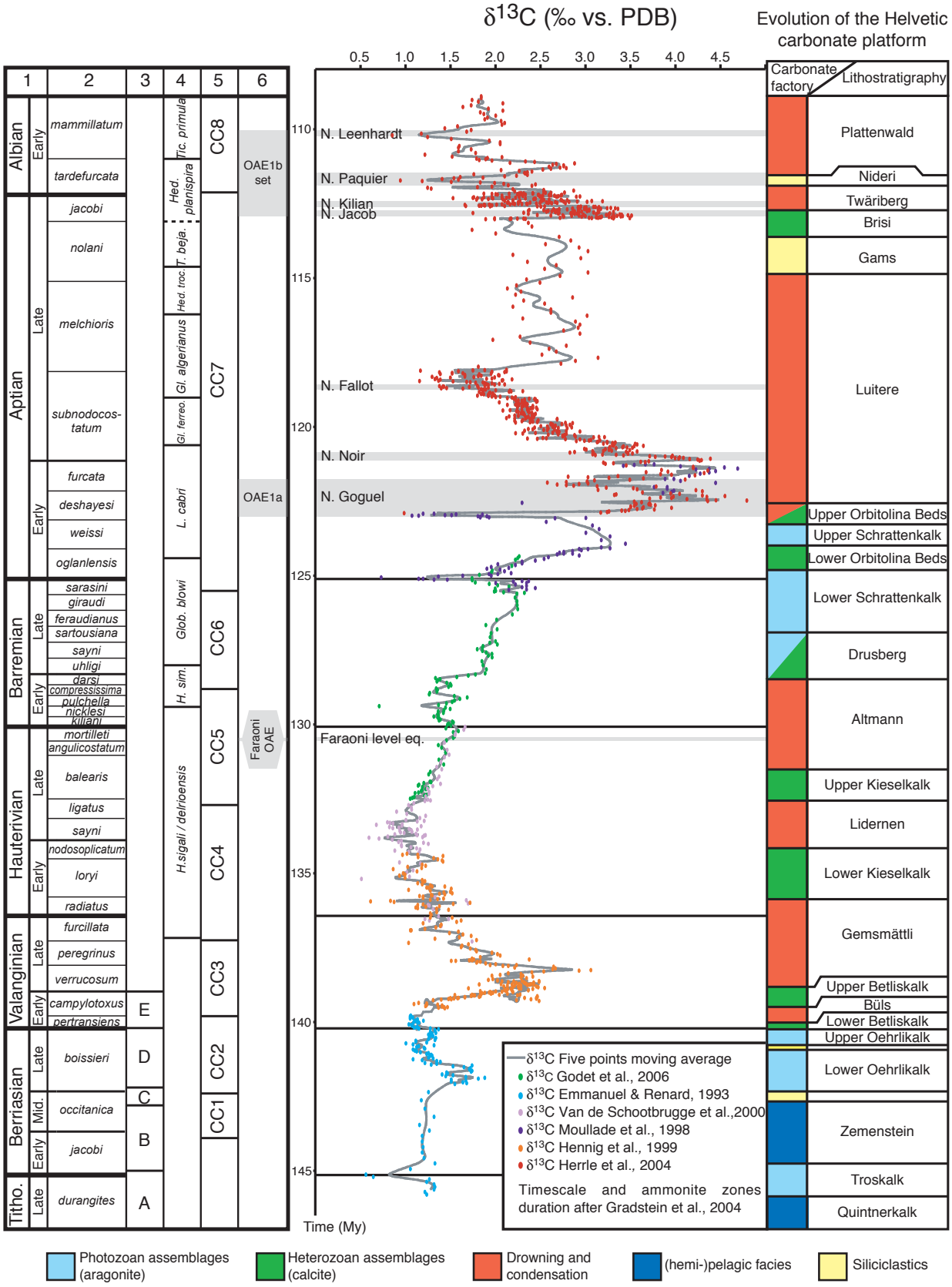

Figure E.1.3. Whole-rock carbonate $\delta^{13}C$ record from southeastern France. The general trends in the evolution of the northern Tethyan carbonate platform are from Figure 2. On the left side of the figure, the numbers on the top of columns refer to 1: stages and sub-stages; 2: ammonite zones; 3: calpionellid zones; 4: planktonic foraminifera zones; 5: calcareous nannoplankton zones; 6: Oceanic Anoxic Events (all according to *Gradstein et al.*, 2004). Shown is also the timing of the occurrence of organic-rich layers resulting from oceanic anoxic events in the Vocontian basin [after *Bréhéret*, 1997; *Herrle et al.*, 2004; *Bodin et al.*, 2006a].

The here proposed compilation of stable carbon isotopes is based on earlier published work. All data were extracted from whole-rock samples of limestone beds within hemipelagic carbonate and carbonate-marl alternating sections [Emmanuel and Renard, 1993; Moullade et al., 1998; Hennig et al., 1999; van de Schootbrugge et al., 2000; Herrle et al., 2004; Godet et al., 2006]. A small series of stable carbon isotope measurements of early Cretaceous calcite after aragonite were performed for this study at the geochemistry laboratory, University of Orsay-Paris Sud, by using a VG SIRA 10 triple collector instrument and the methods described by Godet et al [2006]. The presence of calcite was confirmed at our laboratory (GEA laboratory, University of Neuchâtel) by using a Scintag 2000 XRD device and the methods described by Adatte et al. [1996].

E.1.3. Evolution of the early Cretaceous northern Tethyan carbonate platform succession in the Helvetic Alps

During the early Cretaceous, the northern Tethyan carbonate platform witnessed a series of profound changes in its carbonate-producing platform ecology, which were superimposed by different episodes of platform demise. The external portion of this platform is well documented and dated by ammonite biostratigraphy in the Helvetic zone of the central European Alps [Wyssling, 1986; Föllmi, 1989b; Mohr, 1992; Kuhn, 1996; van de Schootbrugge, 2001; Bodin et al., 2006b, 2006c], and its distal position determines it as an excellent recorder of the interactions between regional environmental and paleoceanographic change within the Tethyan basin.

Temporal changes in platform paleoecology were essentially between photozoan and heterozoan carbonate-producing communities [Lees and Buller, 1972, Carannante et al., 1988; James, 1997; Mutti and Hallock, 2003]. The preserved photozoan ecosystem includes hermatypic corals, rudists, chaetetids, stromatoporoids, and green algae, whereas the preserved heterozoan community is dominated by sessile crinoids, and includes bryozoans, bivalves, and brachiopods, in addition to variable amounts of siliceous sponge spicules.

Phases of important photozoan carbonate production are discerned for the time periods between the latest Jurassic and the Berriasian-Valanginian boundary (Tros member, Oehrli Formation; Fig. E.1.2), and the late Barremian and early Aptian (sartousiana to weissi zone: the Urgonian Schrattenkalk Formation; Bodin et al., 2006b; Linder et al., submitted). These phases are associated with significant build-up and build-out of the platform by aggradation and progradation (indicated in blue in Fig. E.1.2).

Episodes of carbonate production and distribution by heterozoan communities are documented from the Valanginian (pertransiens to verrucosum zone: Betlis Formation; Fig. E.1.2), the Hauterivian (radiatus to nodosoplicatum zone: lower Kieselkalk member; ligatus to balearis zone: upper Kieselkalk member; Fig. E.1.2), and the Aptian (deshayesi zone: Grünten member; nolani zone: Brisi Beds; Fig. E.1.2). These phases of heterozoan platform production have led to the aggradation and progradation of large volumes of carbonate (indicated in green in Fig. E.1.2). Undecompacted accumulation rates are approximately 50% higher than for those in the photozoan mode [Föllmi et al., 1994].

The construction of the northern Tethyan carbonate platform was interrupted by a series of episodes of platform demise, which each lasted up to several million years (indicated in red in Fig. E.1.2). These episodes are registered by hiatuses and erosion surfaces in proximal parts of the Helvetic succession, and by the presence of centimeter to several meters thick glauconite- and phosphate-rich beds in distal parts, which are either highly condensed or allochthonous. These occurrences suggest that carbonate growth was highly reduced during

these episodes and that the platform was subjected to important erosion instead [Heim 1910-1916, 1924, 1934; Heim and Seitz, 1934; Ganz, 1912; Fichter, 1934; Schaub, 1936, 1948; Haldimann, 1977; Föllmi. 1989a; Föllmi and Delamette, 1991; Föllmi et al., 1994; Kuhn, 1996; van de Schootbrugge, 2001].

Episodes of platform demise are observed and dated for the periods of the early Valanginian to early Hauterivian (pertransiens to campylotoxus zone zone: Büls Bed; verrucosum to radiatus zone: Gemsmättli-Pygurus and Raaberg Beds; Figs. E.1.2 and E.1.4A-B), late early to early late Hauterivian (nodosoplicatum to ligatus zone: Lidernen Bed; Figs. E.1.2 and E.1.4C), latest Hauterivian to latest early Barremian (balearis to darsi zone: Altmann member; Figs. E.1.2 and E.1.4D), middle late Barremian (sartousiana zone: Chopf Bed; Fig. E.1.2), early Aptian to middle late Aptian (deshayesi zone to melchioris zone: Rohrbachstein, Plaine Morte, and Luitere Beds: Figs. E.1.2 and E.1.4E-F), and latest Aptian to earliest Albian (jacobi to tardefurcata zones: Twäriberg Bed; Fig. E.1.2).

The episode of demise associated with the Twäriberg Bed corresponds to the final phase of platform demise in the history of the central European region of the northern Tethyan carbonate platform. Shallow-water carbonates younger than the Brisi Beds are not documented. Additional condensed phosphate- and glauconite-rich beds occur in sediments of Albian and early Cenomanian age, which are greatly reduced in thickness and of siliciclastic and hemipelagic facies (Garschella Formation; Fig. E.1.2; Föllmi and Ouwehand, 1987). These episodes are dated as tardefurcata to mammillatum zone (Durschlägi Bed), inflatum zone (Wannenalp Bed), and dispar zone to middle early Cenomanian (Kamm Bed) (Fig. E.1.2). In the distal part of the Helvetic succession, one single condensed phosphate bed occurs, which bundles these former beds and covers most of the Albian and partly also the early Cenomanian (Plattenwald Bed; Fig. E.1.2).

E.1.4. An ammonite-calibrated $\delta^{13}C$ reference record from southeastern France

In order to compare the temporal changes in style and intensity of platform carbonate production on the northern Tethyan margin with general changes in the carbon cycle of the Tethyan ocean, we compiled a high-resolution $\delta^{13}C$ whole-rock record from hemipelagic successions which were deposited in or near the Vocontian basin. This basin represents a regional depression within the northern Tethyan margin during the Jurassic and Cretaceous, which was bordered by the northern Tethyan carbonate platform (Figs. E.1.1 and E.1.3; e.g., Bréhéret, 1997). The data for this compilation were obtained by our research group for the Hauterivian and Barremian intervals [van de Schootbrugge et al., 2000; Godet et al., 2006], and completed by published records for the Berriasian, Valanginian, and Aptian [Emmanuel and Renard, 1993; Moullade et al., 1998; Hennig et al., 1999; Herrle et al., 2004; compare also Wissler et al., 2002]. A detailed description and interpretation of the short- and long-term trends in the here compiled northern Tethyan $\delta^{13}C$ records is provided in chapter 5.6.

The $\delta^{18}O$ records show significant offsets in the absolute values and trends between different sections and we refrain, therefore, from a specific discussion of these data sets [cf. van de Schootbrugge et al., 2000, for a discussion of this problem].

E.1.5. Discussion and interpretations

E.1.5.1. Correlation between episodes of platform demise and paleoceanographic change

We observe a fairly good correspondence in time between the phases of platform demise and general paleoceanographic change, such as

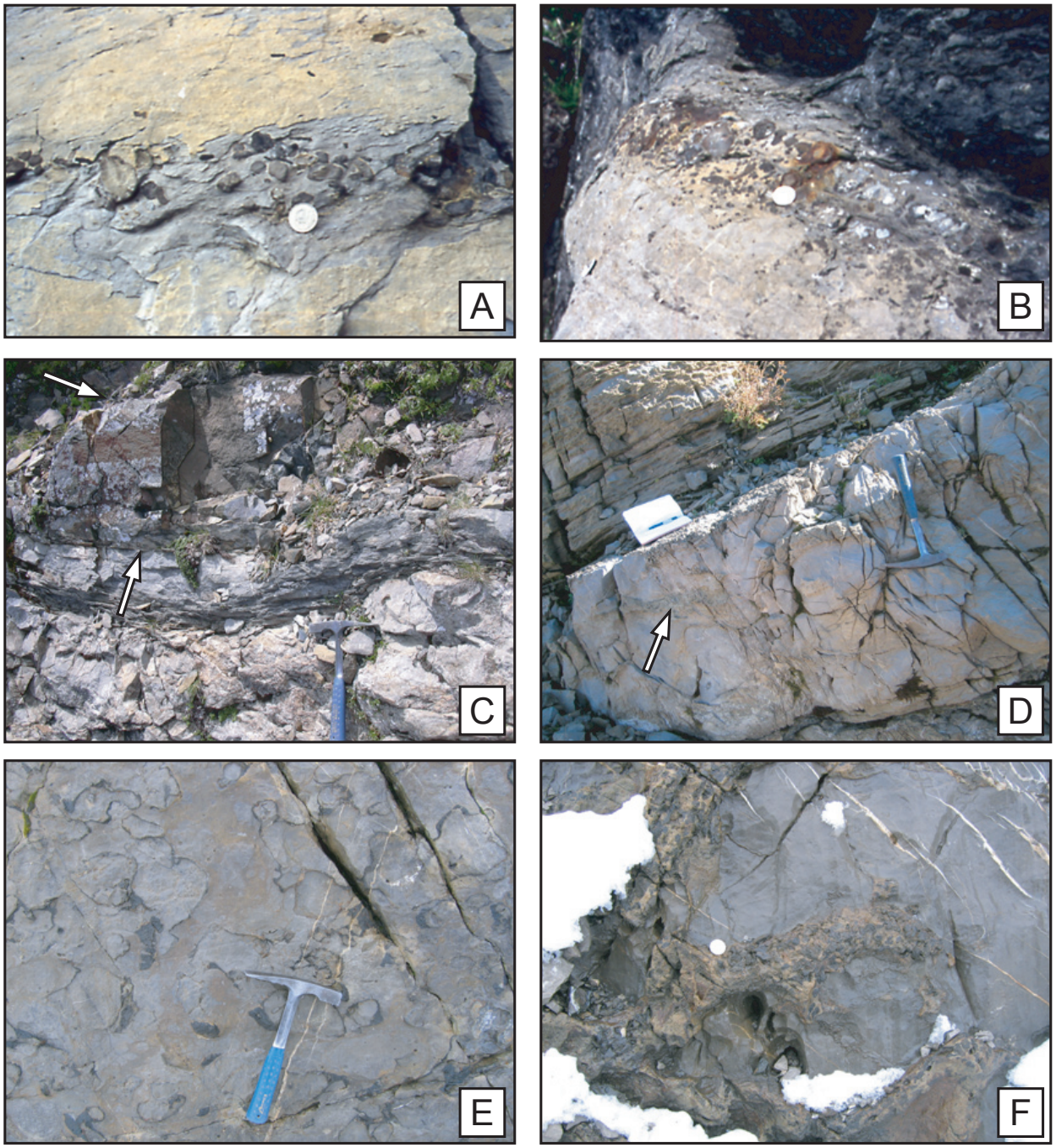

Figure E.1.4. Outcrop photos of phosphate- and glauconite rich beds which formed during the episodes of platform demise along the northern Tethyan margin: A) Büls Bed (*pertransiens* zone; early Valanginian; *Kuhn*, 1996): a thin and probably reworked phosphate nodular layer in hemipelagic limestone of the Palfris and Diphyoides Formations, Büls near Walenstadt, eastern Switzerland; B) Gemsmättli Bed (*verrucosum* to *radiatus* zone; late early Valanginian to early Hauterivian): a nodular phosphatic bed intercalated in heterozoan platform carbonates of the upper Betlis Member and lower Kieselkalk Member, north of Lake Walen, eastern Switzerland; C) Lidernen Bed (*nodosoplicatum* to *ligatus* zone; late early to early late Hauterivian): here developed as a glauconite-rich bed (base and top indicated by arrows) following a marly interval on top of the lower Kieselkalk Member, Pilatus, central Switzerland; D) Altmann Bed (*balearis* to *darsi* zone; late Hauterivian to late early Barremian): a thin layer rich in nodular phosphate which reaches down into the underlying top of the upper Kieselkalk Member by bioturbation (arrow), Rawil, central Switzerland; E) Pleine Morte Bed (*deshayesi* zone; middle early Aptian): shown here in plain view is the surface of this bed, which consists of nodules of heterozoan carbonate of the Grünten Member, which are peripherically phosphatized, Rawil, central Switzerland; F) Luitere Bed (*furcata* to *melchioris* zone; late early to middle late Aptian); a sandy and nodular phosphate rich bed on top of the Grünten Member, with extends locally down into the top layer of the heterozoan Grünten Member through burrow-like structures, Rawil, central Switzerland.

is documented by the occurrence of the oceanic anoxic events (Fig. E.1.5). The oldest episode of platform demise started in the earliest Valanginian (pertransiens zone) and lasted until the earliest Hauterivian (campylotoxus to radiatus zone). The onset of this episode appears to predate the onset of the Valanginian «anoxic» event, which was defined to start at the onset of the Valanginian $\delta^{13}C$ positive excursion dated as campylotoxus zone [Erba et al., 2004; Weissert and Erba, 2004]. The phase of most intense phosphogenesis during this episode of demise took, however, place during the verrucosum zone [Kuhn, 1996], which corresponds exactly to the period of maximum $\delta^{13}C$ values during the Valanginian «anoxic» event.

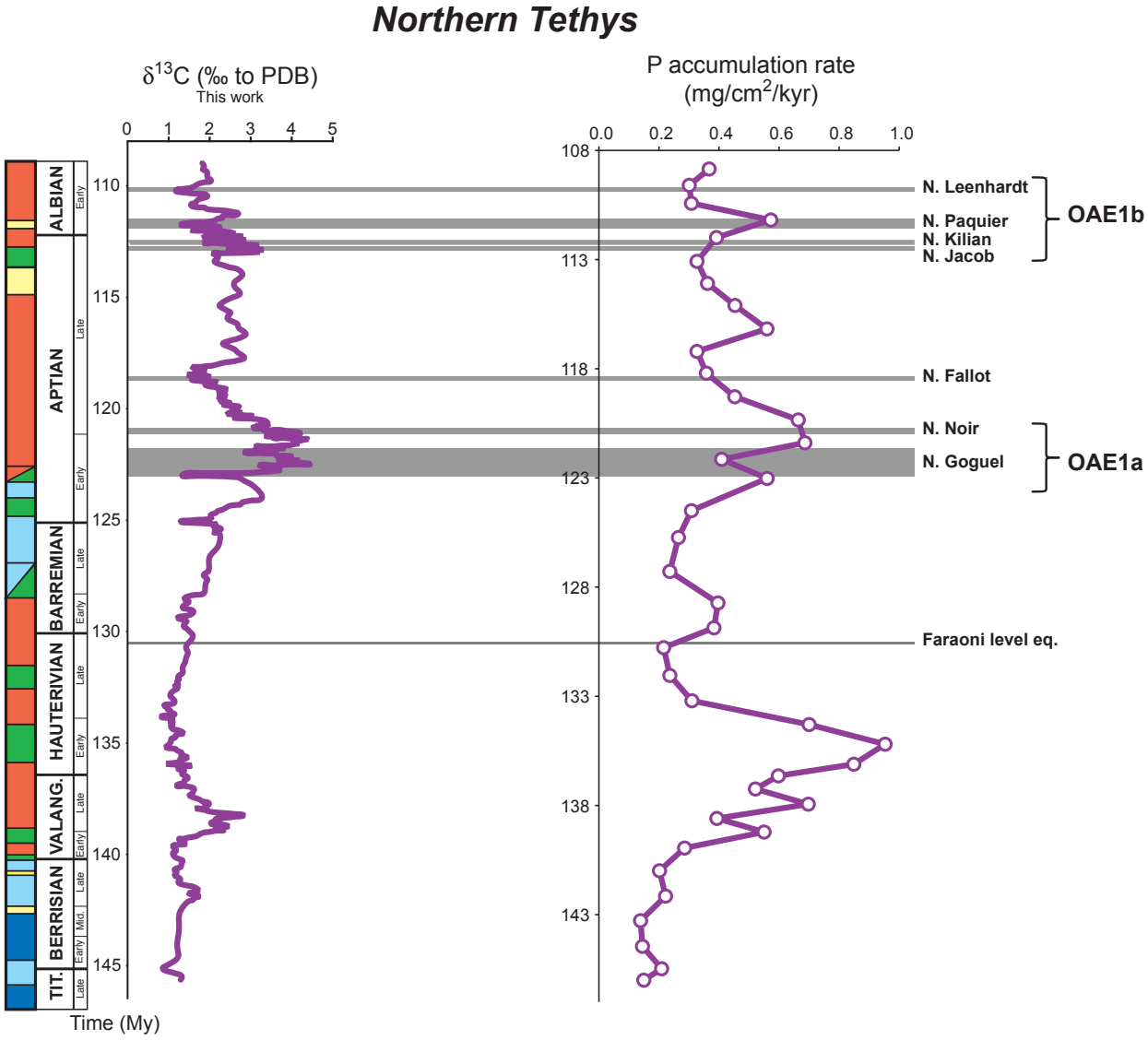

Figure E.1.5. Correlation plot of the general trends in the evolution of the northern Tethyan carbonate platform (from Figure E.1.2; see Figure E.1.3 for the legend), the northern Tethyan $\delta^{13}C$ record (from Figure E.1.3), and the phosphorus accumulation curve [after *Föllmi*, 1995; adapted to the timescale of *Gradstein et al.*, 2004]. Shown is also the occurrence of organic-rich layers resulting from oceanic anoxic events in the Vocontian basin [after *Bréhéret*, 1997; *Herrle et al.*, 2004; *Bodin et al.*, 2006a].

A second episode of platform demise is dated as late early to early late Hauterivian (nodosoplicatum to ligatus zone), and this phase corresponds to a phase of important sea-level change and cold-water inflow into the northern Tethyan realm [e.g., van de Schootbrugge et al. 2003]. A truly anoxic event is, however, not documented from this time period.

The third phase of platform demise started in the latest Hauterivian and lasted until the late early Barremian (balearis to darsi zone). Also here, the onset of the drowning phase appears to predate the Faraoni oceanic anoxic event, but a major phase of condensation, phosphogenesis and glauconite formation appears to coincide with this anoxic event [Bodin et al., 2006c].

Also the onset of the fourth phase of drowning in the history of the northern Tethyan carbonate platform (deshayesi zone to melchioris zone) appears to slightly predate OAE1a, but this event itself is nicely documented by the presence of a phosphate horizon in distal occurrences of the Helvetic platform (Plaine Morte bed, Fig. E.1.2).

The final drowning episode near the Aptian-Albian boundary coincides with OAE 1b, and younger condensed phosphatic beds (tardefurcata to mammillatum zone, inflatum zone, and dispar zone to middle early Cenomanian) all have their equivalent in oceanic anoxic events (OAE 1b upper part, OAE 1c and d; e.g., Leckie et al., 2002).

With the exception of the late early to early late Hauterivian phase of platform demise, all phases of erosion, condensation, phosphogenesis and platform demise appear to have their counterpart in a paleoceanographic anoxic event, and especially the early intervals in each episode appear to coincide with periods of widespread dysaerobic conditions. The time lag between the onset of platform demise and the start of early Cretaceous OAE's was already observed earlier [Föllmi et al., 1994] and it is interpreted here as a lag in the response times of both environments to environmental change: the highly sensitive ecological systems of the northern Tethyan platform appears to have responded rapidly to environmental change, whereas it may have taken up to 1 million year for the establishment of conditions in the deeper basins which allowed for the increased accumulation of organic matter.

E.1.5.2. Changes in trophic levels and changes in platform ecology and morphology

As was already outlined in Föllmi et al. [1994] and Weissert et al. [1998], we conceive changes in trophic levels as one of the important mechanisms driving the changes in style, architecture, and the efficiency of the northern Tethyan platform and linking the platform evolution with overall paleoceanographic change.

During the Valanginian and Aptian, phases of platform demise start in distal portions of the platform and proceed by onlap of drowning-related sedimentary bodies onto the platform (Fig. E.1.2). During the Valanginian, for example, a first pulse of platform demise is registered by the Büls Bed in the distal-most sections, and younger sediment bodies related to consequent drowning episodes expand onto the platform in the form of the Gemsmättli and the Raaberg Beds [Kuhn, 1996]. These highly condensed phosphate-rich beds formed during periods of progressive sea-level rise as part of one or several transgressive system tracts covering major sequence boundaries. In most cases they bundle the effect of a series of successive transgressions into one single and highly condensed bed. The formation of these highly condensed and phosphate-rich beds is related to the influence of deeper-water currents, which arrived onto the platform during times of sea-level rise by upwelling, and which were powerful enough to induce a sedimentary regime dominated by erosion and condensation on top of the platform [Delamette, 1988; Ouwehand, 1988; Föllmi, 1989a; Föllmi and Delamette, 1991]. These currents are thought to have consisted of cooler water, enriched in nutrients and especially phosphate, and eventually also dissolved CO_2. Their arrival on the platform pushed the platform into phases of carbonate production in a heterozoan mode and into the episodes of platform demise. Finally, they arrived from an essentially eastern direction, obliquely onto the platform, whereas the transfer of platform material and water from the platform into the outer shelf and basin

occurred in truly proximal-distal directions, approximately perpendicular to the platform, as is indicated in the orientation of channel structures and the direction of turbidites [Föllmi, 1989a; Föllmi and Delamette, 1991].

An independent confirmation of the importance of trophic levels is the overall good correlation between the record of oceanic phosphorus accumulation and the state of carbonate production on the shelf [Fig. E.1.5; Föllmi, 1995; van de Schootbrugge et al., 2003; Bodin et al., 2006a]. A further indication of a link between platform evolution and trophic levels is the coincidence of major positive excursions in the northern Tethyan $\delta^{13}C$ record during the early Valanginian and early Aptian with periods in which the northern Tethyan carbonate platform shifted into a mixed heterozoan – demise mode (indicated by the green and red zones in Figs. E.1.2, E.1.3, and E.1.5). These phases of major change in the evolution of the northern Tethyan carbonate platform appear to be marked by major transformations in the ocean carbon cycle, which were highly likely induced by a nutrient-driven change in the ratio of carbonate carbon (Ccarb) to organic carbon (Corg) burial (see below; cf. also Immenhauser et al., 2005).

E.1.5.3. Quality and correlation of the northern Tethyan $\delta^{13}C$ record

The here proposed compilation of the northern Tethyan $\delta^{13}C$ record show values typical of early Cretaceous open-marine carbonates [e.g., Jenkyns and Wilson, 1999; Erba et al., 1999]. The stratigraphic continuity of data derived from different sections is an indication of the general quality of the $\delta^{13}C$ signal; the only exception is a jump in absolute values at the base of the late Aptian melchioris zone, which is likely induced by a change in diagenetic conditions between two sections [Herrle et al., 2004; personal communication]. Furthermore, the good correlation of the general trend between the here proposed $\delta^{13}C$ curve and other published curves is also an indication of its quality as a recorder of original paleoceanographic change rather than diagenetic overprint (Fig. E.1.6). The lack of correlation in a $\delta^{18}O$-$\delta^{13}C$ cross plot for all data ($R^2 = 0.0264$) appears to confirm this interpretation [Fig. E.1.7; e.g., Godet et al., 2006].

A comparison between the northern Tethyan $\delta^{13}C$ curve and the $\delta^{13}C$ records of the central Tethyan and the Pacific realms [e.g., Weissert and Channell, 1989; Lini et al., 1992; Adatte et al., 1996; Erbacher et al., 1996; Erba et al., 1999; Jenkyns and Wilson, 1999; Bartolini, 2003] reveals that the long-term trend in the northern Tethyan record fits well with those in the other records, and that especially the two positive excursions during the early Valanginian and early Aptian are well reproduced (Fig. E.1.6). The evolution of the intervals between the major positive excursions is characterized by rather irregular and locally noisy trends, which are, in general, not very well correlated, neither between sections between different oceans nor within the same basin.

We suggest here that whereas the large positive excursions of the early Valanginian and early Aptian are well correlated between the Tethys and the Pacific realms and appear to be a truly global phenomenon, the smaller-scale excursions of the remaining intervals in the early Cretaceous represent most likely a response to local to regional changes in the carbon cycle.

E.1.5.4. Potential mechanisms driving the marine $\delta^{13}C$ record

The (hemi-)pelagic $\delta^{13}C$ record provides an important tracer of reorganization within the marine carbon cycle [e.g., Kump and Arthur, 1999; Veizer et al., 1999], and temporal changes therein are traditionally interpreted as an approximation of changes in the ratio of burial fluxes of Ccarb and Corg [e.g., Scholle and Arthur, 1980; Arthur et al., 1988; Weissert, 1989; Hoefs, 1997; Weissert et al., 1998]. Additional factors of important influence on the marine $\delta^{13}C$ record consist in the quality and flux of externally derived carbon species into the (hemi-)pelagic marine realm, such

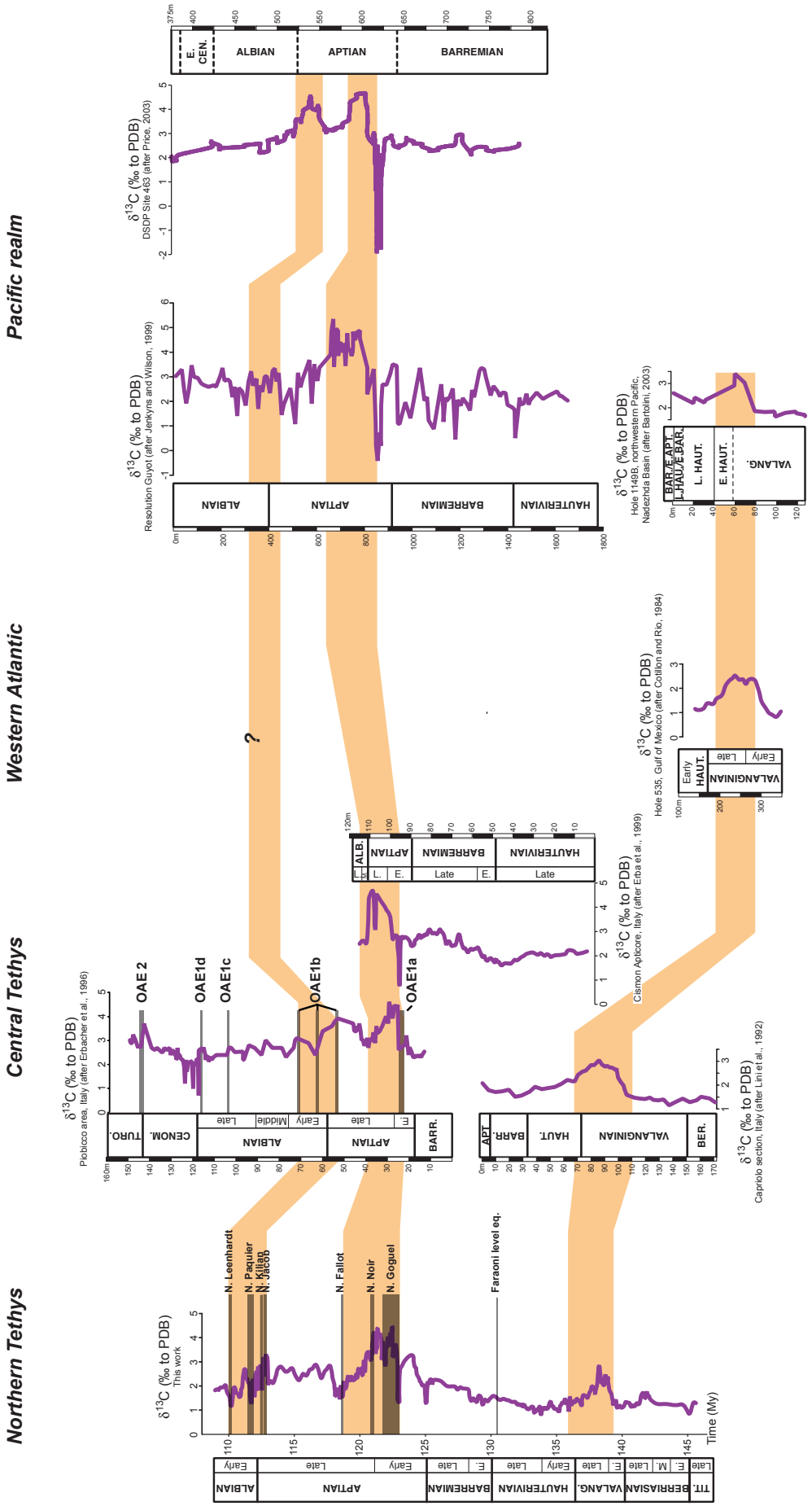

Figure E.1.6. Correlation of the northern Tethyan $\delta^{13}C$ record with $\delta^{13}C$ records from the central Tethys, the western Atlantic, and the Pacific realms [from *Cotillon and Rio*, 1984; *Lini et al.*, 1992; *Adatte et al.*, 1996; *Erbacher et al.*, 1996; *Erba et al.*, 1999; *Jenkyns and Wilson*, 1999; *Bartolini*, 2003; *Price*, 2003]. Note that whereas the northern Tethyan $\delta^{13}C$ record is calibrated against early Cretaceous time (Gradstein et al., 2004), the other records shown here are plotted against their lithostratigraphy. Note also that for the northern Tethyan $\delta^{13}C$ record, the central Tethyan record by *Erba et al.* [1999], and the Pacific record by *Price et al.* [2003] a five-point moving average is shown, whereas for the remaining records, all measured data are shown.

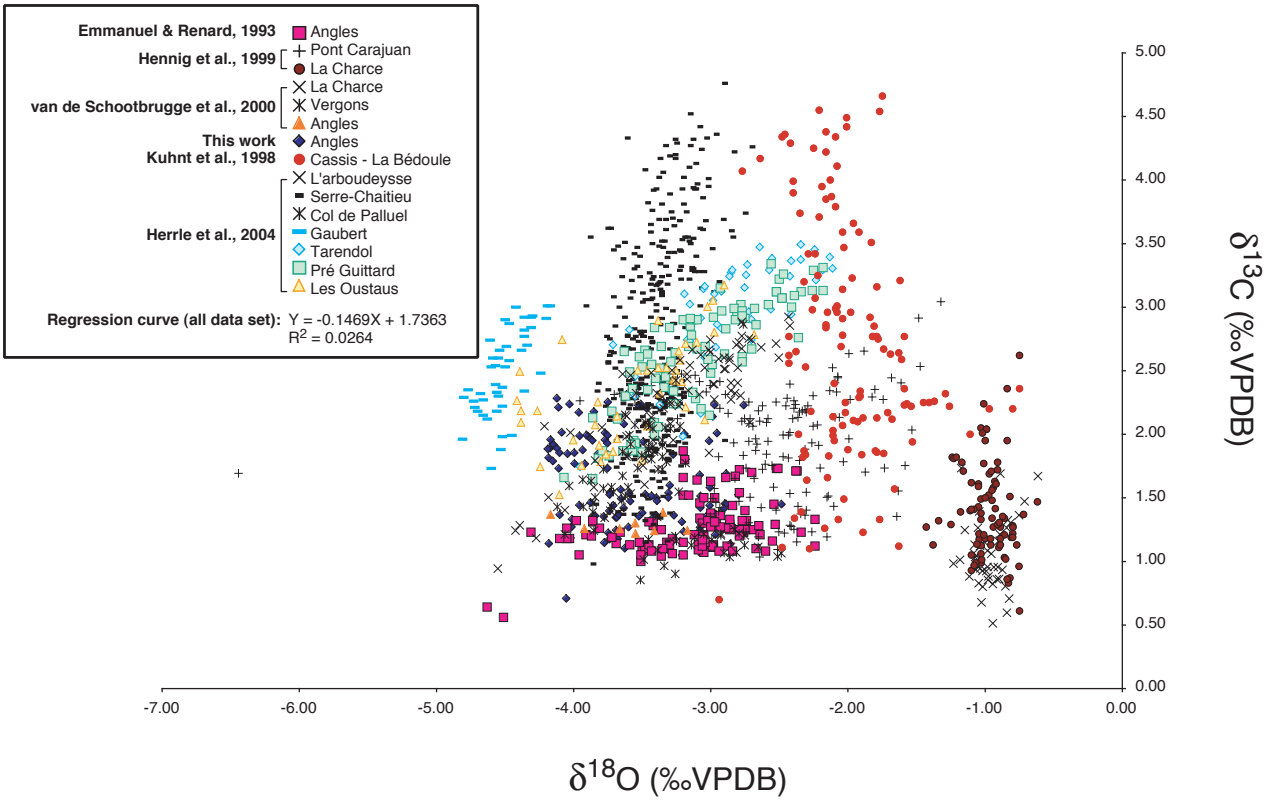

Figure E.1.7. $\delta^{13}C$-$\delta^{18}O$ cross plot of all data used in the $\delta^{13}C$ compilation of Figure E.1.3.

as terrestrial and platform-derived Corg and dissolved inorganic carbon (DIC), atmospheric CO_2, or methane derived from the dissociation of clathrates [Cerlings et al., 1993; Dickens et al., 1995; Kump and Arthur, 1999; Immenhauser et al., 2003; Weissert and Erba, 2004; Swart and Eberli, 2005; Panchuk et al., 2005, 2006]. Furthermore, Bartley and Kah [2004] recently suggested a close relationship between the size of the marine DIC reservoir and the sensitivity of the marine $\delta^{13}C$ system to changes in the carbon cycle.

As we will detail out in the following, a combination of these factors influenced the northern Tethyan early Cretaceous $\delta^{13}C$ record, whereby the precise identification of the relative importance of each factor remains a difficult task. In our interpretation, we especially pay attention to the potential effect of the export of particulate and dissolved inorganic carbon (PIC and DIC) from the northern Tethyan carbonate platform and adjacent European continent, and changes therein, on the here described $\delta^{13}C$ record. We postulate that the smaller temporal shifts in the northern Tethyan $\delta^{13}C$ record, which are not correlated on a wider scale and for which a local or regional cause is to be sought, were influenced by this phenomenon.

There are several reasons for this assumption:

1) Based on a quantification of calcareous nannofossils in the hemipelagic carbonates of the Vocontian basin, Reboulet et al. [2003] were able to show that for the Valanginian sections, hemipelagic carbonate accumulation in this marginal basin was for a large part controlled by the export rate of platform-derived carbonate ooze, rather than by depositional rates of pelagic calcareous plankton [cf. also Colombié and Strasser, 2003, for a similar interpretation of late Jurassic carbonate beds in Vocontian sections]. The influence of shedding of shallow-water carbonate mud into the adjacent basin is also indicated by the important decrease in carbonate accumulation in the Vocontian basin during periods of platform demise, such as during the pertransiens and verrucosum zone (Valanginian; e.g., Reboulet et al., 2003), and the late early to early late Aptian [e.g., Bréhéret, 1997].

2) As will be shown below, the timing and the negative or positive character of the shifts in the northern Tethyan $\delta^{13}C$ record appear to be correlated to changes in the style and intensity in carbonate production on the northern Tethyan platform.

3) A numerical model published by Godet et al. [2006] suggests that the export of platform-derived carbonate and especially aragonite may have an impact on the $\delta^{13}C$ record in adjacent basins

E.1.5.5. Changes in the ecology and geometry of the northern Tethyan carbonate platform and its influence on the northern Tethyan $\delta^{13}C$ record

There are several mechanisms related to the predominant ecosystem and geometry of the early Cretaceous northern Tethyan carbonate platform, which may have influenced the hemipelagic $\delta^{13}C$ record described here (Fig. E.1.8). The northern Tethyan carbonate platform was constituted by photozoan and/or heterozoan ecosystems. The photozoan community included hermatypic corals, rudists, stromatoporoids, chaetitids, and green algae as its main constituents [e.g., Bollinger, 1988; Mohr, 1992; Föllmi et al., 1994]. Of interest here is that these organisms precipitated their hard parts predominantly in aragonite [e.g., Morycowa, 1980; Wefer and Berger, 1991]. This is also true for the early Cretaceous rudists, which had relatively thick aragonite shells covered by a thin calcitic layer [Steuber, 2002]. The participation of photosynthetic organisms in the form of green and zooxanthellic algae was important and the overall high photosynthetic rates in photozoan communities may have increased $\delta^{13}C$ values in skeletal aragonite. Fractionation towards more positive $\delta^{13}C$ values was likely also related to the geometry of the photozoan platform, which was confined by marginal reef build-ups and oolitic shoals [Linder et al., submitted; Godet et al., submitted], thereby promoting carbon recycling within the platform [e.g., Swart and Eberli, 2005; Panchuk et al., 2005, 2006]. Furthermore, in single carbonate systems, aragonite $\delta^{13}C$ values tend generally to be higher than calcite $\delta^{13}C$ values [Romanek et al., 1992]. For instance, Swart and Eberli [2005] reported $\delta^{13}C$ values of maximal +5‰ for aragonite on the present-day Bahamian platform. A preliminary isotopic survey of platform-derived skeletal material which consists of calcitized aragonite appears to confirm the high initial values for early Cretaceous aragonite for samples from the Gargano platform (Italy; sample obtained from Jean-Pierre Masse: $\delta^{13}C$ value = +5‰) and the north Mexican and Texan carbonate platforms [Woo et al., 1993: $\delta^{13}C$ values between 2.3-4.3‰; n=24, mean value = +3.3‰].

The early Cretaceous was characterized by broad epicontinental seas and widespread carbonate platforms [e.g., Philip, 2003] and aragonite production rates may have been significant in photozoan shallow-water communities in generally. The export of this mineral into adjacent basins during, for example, storm events and probably also more generally through the process of platform build-out by the formation of progradational carbonate wedges influenced the northern Tethyan $\delta^{13}C$ signal as a whole either by direct incorporation into pelagic sediments or by dissolution and transfer into the marine DIC reservoir [e.g., Droxler et al., 1983; Swart and Eberli, 2005; Godet et al., 2006]. The potential influence of aragonite shedding on the $\delta^{13}C$ signature in carbonates of the Vocontian basin has been modeled by Godet et al. [2006]. They were able to show that the presence of 20% aragonite in the total depositional rate of carbonate may increase the $\delta^{13}C$ signature by 0.2‰, in the case the initial value is at 2‰, and the initial aragonite $\delta^{13}C$ value is set at 5‰.

In analogy to modern tropical carbonate platforms [Kawahata et al., 1997; Suzuki et al., 2001; Suzuki and Kawahata, 2003, 2004], the confined geometry of photozoan platforms may also have had an effect on the air-sea exchange of CO_2. We assume that most CO_2 derived from respiration of organic matter, precipitation of carbonate, and river influx was directly returned to the atmosphere, rather than transported

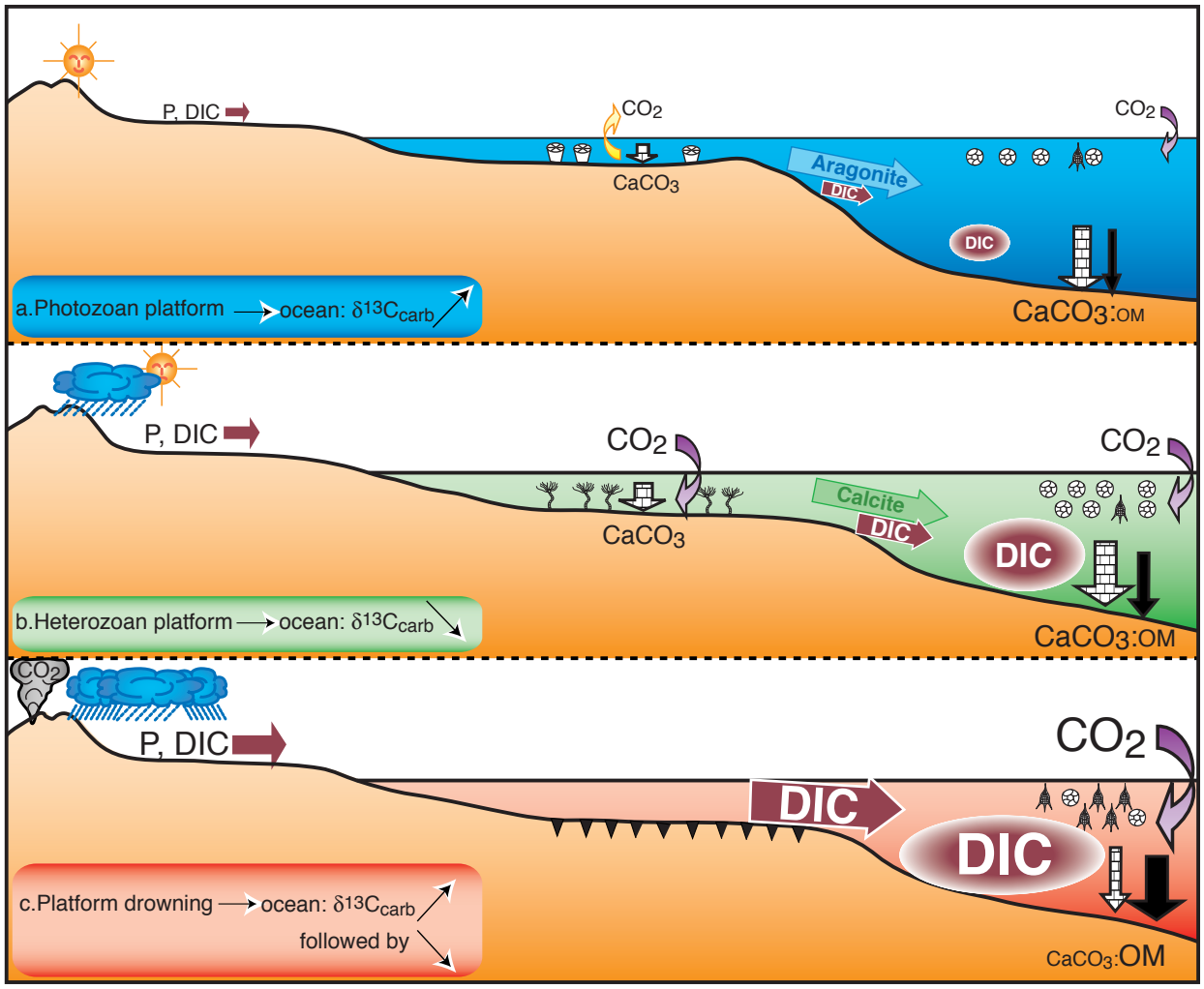

Figure E.1.8. Schematic overview of the potential impact of the different stages in the evolution of the northern Tethyan platform on the oceanic carbon cycle and $\delta^{13}C$ record. Differences in flux rates of DIC into the ocean and burial rates of C_{carb} and C_{org} are indicated by different sizes in arrows and characters.

laterally into deeper waters. This means that photozoan platforms were a likely source of CO_2 to the atmosphere. This also signifies that a non-negligible part of continentally derived DIC was returned to the atmosphere as CO_2 or stored as platform carbonate, rather than transferred into the deep basin. All by all, the dominance of photozoan carbonate platforms may have pushed the oceanic $\delta^{13}C$ system towards more positive values both by increased aragonite exportation and by decreased output of platform-derived DIC and throughput of continentally derived DIC (Fig. E.1.8). The possibility that the early Cretaceous photozoan platform acted as a source of CO_2 to the atmosphere rather than a sink signifies also that this system was less vulnerable towards changes in atmospheric pCO_2 [cf. Wissler et al., 2003; Weissert and Erba, 2004].

Early Cretaceous heterozoan ecosystems consisted predominantly of respiring organisms such as crinoids, thick shelly bivalves, brachiopods, and bryozoans, which precipitated their hard parts mainly in calcite [e.g., Sprinkle and Kier, 1987; Smith et al., 1998; Flügel, 2004]. Early Cretaceous heterozoan platforms consisted of homoclinal or distally steepened ramps with good connections to the adjacent basin [e.g., James, 1997; Linder et al., submitted]. Very few benthic photosynthetic organisms are preserved from the heterozoan assemblages and benthos-related photosynthetic processes may have been less important - at least in comparison to the photozoan carbonate

platform. Due to the specific fractionation pattern of heterozoan organisms and the open-platform architecture, the overall $\delta^{13}C$ signal of precipitated calcite is less positive in comparison to that of aragonite in photozoan platforms [e.g., Wefer and Berger, 1991; Swart and Eberli, 2005]. In addition, the heterozoan mode of platform carbonate production along the early Cretaceous northern Tethyan margin was associated with important detrital input, higher nutrient levels and eventually colder waters [Föllmi et al., 1994]. This implies that phytoplankton productivity was important, thereby favoring the suspension-feeding mode exercised by an important part of the heterozoan community (crinoids, brachiopods, bryozoans). Since almost no organic matter is preserved in the heterozoan carbonate deposits, it is assumed that most of it was efficiently decomposed and reintegrated into the DIC pool, whereas ^{13}C-enriched Ccarb was efficiently buried. This induced a decrease in the $\delta^{13}C$ signal of platform DIC and subsequently also of precipitated calcite [e.g., Immenhauser et al., 2003]. To this comes that the import of terrestrially-derived DIC in association with high detrital flux rates may have reinforced the trend towards a more negative $\delta^{13}C$ signal on top of the heterozoan platform.

Heterozoan platforms may also have acted as a pump of atmospheric CO_2, which was consequently exported into adjacent basins, analogous to the present-day North Sea [Thomas et al., 2004]: the open, ramp-like architecture of heterozoan platforms probably allowed for a better vertical separation of photosynthetic (by planktonic organisms) and respiration processes (by benthic, carbonate-producing organisms) in its external, deeper part. This leads to a corresponding increase of respired CO_2 in subsurface waters, which was ultimately exported into the adjacent basin rather than transferred back to the atmosphere (Fig. E.1.8). The absence of aragonite and the increased export of both calcite as well as platform-derived and continentally-derived DIC likely influenced the marine $\delta^{13}C$ system and induced lower values in open-marine carbonates. The corresponding increase in the marine DIC reservoir may also have attenuated the sensitivity of the open-ocean $\delta^{13}C$ record [Bartley and Kah, 2004].

The repeated phases of platform demise during the early Cretaceous occurred in close relation with oceanic anoxic events (Figs. E.1.3 and E.1.5). Such phases had an important impact on the $\delta^{13}C$ system, in that carbonate production and export were greatly diminished on shelves and also in open-marine systems through the competition with siliceous organisms, whereas Corg production and preservation were enhanced. This situation generates a general shift in the $\delta^{13}C$ record towards more positive values. The greatly reduced output of carbonates and the increased throughput of continentally derived DIC accompanied by an increase in re-mineralized C would automatically have led to an increase in the oceanic DIC reservoir. The environmental conditions leading to oceanic anoxia and platform drowning also induced an increase of this reservoir by increased humidity and weathering on the continent [e.g., Föllmi et al., 1994; Föllmi, 1995; Weissert et al., 1998]. The increase in size of the oceanic DIC reservoir may have also led to a more negative $\delta^{13}C$ signal by its increased recycling into the photic zone [e.g., van de Schootbrugge et al., 2005] and may have also attenuated short-term shifts in the signal [Bartley and Kah, 2004]. Oceanic anoxic events and corresponding platform drowning episodes may therefore first have led to a rather rapid positive excursion in $\delta^{13}C$ followed by a longer term trend towards a more negative $\delta^{13}C$ record, which was less sensitive towards short-term change.

E.1.5.6. Correlation of changes in carbonate platform ecology along the northern Tethyan margin and trends in the northern Tethyan $\delta^{13}C$ record

A direct comparison of the evolution in the northern Tethyan $\delta^{13}C$ record with the changes in platform ecology along the northern Tethyan margin allows us to infer temporal correlations, which are consistent with the above described

influences of platform carbonate production and morphology on basinal $\delta^{13}C$ records. In the Helvetic realm, the minimum in the northern Tethyan $\delta^{13}C$ record at the Jurassic-Cretaceous boundary corresponds to a halt in the growth of a photozoan platform (Tros Member) and the onset of the deposition of marly, hemi-pelagic sediments (Zementstein Formation). The negative excursion as such is interpreted as the result of diminished aragonite shedding and an increase in continental DIC input.

The two positive excursions in the early and late boissieri zone correspond to two phases of platform growth in a photozoan mode (lower and upper Oehrlikalk members), which were interrupted by a phase of detrital input [Mohr, 1992; Mohr and Funk, 1993]. Here, an eventual increase in aragonite shedding and a concomittant decrease in DIC output from the platform may have been influential.

During the early Valanginian, the $\delta^{13}C$ record is first shifted to slightly more negative values and subsequently rapidly toward heavier values. A first maximum in $\delta^{13}C$ values corresponds to the early verrucosum zone. Thereafter, $\delta^{13}C$ values show a slight regression, before they culminate again in the late verrucosum zone. This trend corresponds to the well-known Valanginian positive excursion, which has been established in the Apulian basin and elsewhere [Lini et al., 1992; Föllmi et al., 1994; Hennig et al., 1999; Erba et al., 2004]. A comparison with the Helvetic realm suggests that the slight negative shift at the base of the Valanginian correlates to a change from a photozoan to a heterozoan platform mode (lower Betlis member). The rapid shift toward heavier values during the early Valanginian is coeval with a first platform drowning phase (Büls Beds). The following negative shift corresponds to a return of the platform in a heterozoan mode (upper Betlis member) and the second positive shift is the result of renewed platform drowning (Gemsmättli Bed).

For the remainder of the late Valanginian and the entire Hauterivian, the $\delta^{13}C$ record is remarkably stable with regards to short-term changes and shows only a long-term change towards more negative values. This started in the verrucosum zone and lasted until the late loryi zone and was followed by a long-term increase towards more positive values ending at the Hauterivian-Barremian boundary [van de Schootbrugge et al., 2000]. The drowning phases during the Hauterivian and near the Hauterivian-Barremian boundary are not obvious in the $\delta^{13}C$ record with the possible exception that an eventual increase in organic-carbon burial during the late Hauterivian (culminating in the Faraoni anoxic event) may have pushed the $\delta^{13}C$ record slowly to more positive values. The relative stability of the Hauterivian-early Barremian record is probably related to the increased size of the oceanic DIC reservoir, which induced the trend towards more negative values during the late Valanginian and early Hauterivian and attenuated the sensitivity of the $\delta^{13}C$ signal in general [Godet et al., 2006].

The late Barremian is characterized by a positive shift in $\delta^{13}C$ values, which is correlated with the progressive installation of the photozoan Urgonian platform (Drusberg Member and lower Schrattenkalk Member; Godet et al., 2006; Bodin et al., 2006b). The Barremian-Aptian boundary is marked by a well-defined negative peak in the $\delta^{13}C$ record, which may - amongst others - be related to the increased output of continental detritus and DIC, leading to a corresponding increase in the oceanic DIC reservoir. The minimum of this negative excursion appears close to the onset of a widely documented interruption in photozoan platform growth along the northern Tethyan margin accompanied by an increase in detrital input («lower Orbitolina Beds»).

The Aptian shows a rather unsteady short-term evolution in $\delta^{13}C$, which starts off with an important positive shift during the oglanlensis zone. This shift is well correlated with a significant phase of photozoan carbonate production (upper Schrattenkalk member). This first maximum in $\delta^{13}C$ values during the Aptian is followed by a decrease, which becomes

accelerated near the boundary between the weissi and deshayesi zones and forms a negative spike. This decrease in $\delta^{13}C$ values corresponds to a change to a heterozoan platform mode in the Helvetic zone (Grünten member; Linder et al., submitted), which is followed by the demise of the Urgonian Schrattenkalk platform (Luitere Bed). The negative spike occurs near the base of the Goguel level - an anoxic bed which corresponds to OAE 1a. It was first described by Menegatti et al. [1998] in the Apulian basin and has been interpreted to represent a short period of increased uptake of recycled 12C–enriched carbon and/or increased release of methane [Menegatti et al., 1998; Jenkyns, 2003]. The early Aptian negative spike is followed by a positive excursion towards an early Aptian twofold maximum in $\delta^{13}C$ values, which lasts until the top of the furcata zone. Subsequently, the $\delta^{13}C$ record slowly returns to more negative values, and arrives at a minimum near the top of the subnodosocostatum zone. This trend in $\delta^{13}C$ is paralleled on the Helvetic shelf by a long-lasting drowning episode, and is interpreted to have resulted from increased output of Corg relative to Ccarb during OAE 1a, followed by an increase in the oceanic DIC reservoir, which was due to the prolonged diminution in platform carbonate production paralleled by increased input of continental DIC.

The base of the minimum in the late Aptian $\delta^{13}C$ record near the boundary of the subnodosocostatum and melchioris zones corresponds to a regional anoxic event (Fallot level; Herrle et al., 2004). The subsequent excursion towards more positive $\delta^{13}C$ values is probably artificial and related to different diagenetic conditions in the set of sections measured by Herrle et al. [2004, personal communication]. A final phase of shallow-water carbonate production in a heterozoan mode (Brisi Beds) is documented from the nolani zone, and appears to trace an irregular trend towards more negative values in the $\delta^{13}C$ record. In the latest Aptian and earliest Albian, an ultimate drowning phase occurred on the Helvetic platform which is documented by the Twäriberg Bed. The positive shift in $\delta^{13}C$ values in sediments of the latest Aptian (jacobi zone) appears to register the final demise of the platform. On the Helvetic shelf, the early Albian witnessed a phase of increased detrital input (Nideri beds), followed by a renewed phase of condensation (Plattenwald Bed), which - for its onset - correlates to OAE 1b represented in the Vocontian basin by the Paquier level [e.g., Herrle et al., 2004]. The onset of OAE 1b is paralleled by an increase in $\delta^{13}C$ values of the Vocontian realm, which is followed by a renewed decrease in values.

The good temporal coincidence between changes in the northern Tethyan $\delta^{13}C$ record and changes in platform ecology and morphology opens the possibility to explain almost all minor and major changes in this curve. This was hitherto not possible in using changes in Tethyan paleoceanography as the exclusive driver of carbon isotope fractionation patterns.

E.1.6. Conclusions

The Helvetic zone preserves a distal portion of the early Cretaceous northern Tethyan carbonate platform and its transition into the deeper outer shelf. The succession recovered in the Alps is not only the result of regional environmental conditions on the shelf, but also of global paleoceanographic conditions as is shown by the temporal correspondence between drowning episodes, OAE's, and the here presented early Cretaceous $\delta^{13}C$ reference record of SE France. The link between paleoceanographic changes and coeval modulations in the style and architecture on the platform is provided by the upwelling of deeper and colder waters - rich in nutrients and likely in dissolved CO_2 - onto the platform.

Furthermore, virtually every change in the northern Tethyan $\delta^{13}C$ record makes sense, if correlated with the evolution of the northern Tethyan platform. This indicates that reciprocally, the northern Tethyan platform system exerted an influence on northern Tethyan ocean chemistry. We propose that this occurred by the production and storage of shallow-

water carbonates, and by the existing platform geometry and intensity of photosynthetic activity which both were decisive for the degree of CO_2 return into the atmosphere and/or ocean, and the degree of output of platform-derived DIC and throughput of continental DIC. Furthermore, the changes within the platform ecosystem between photozoan, aragonite-based carbonate production mode and heterozoan, calcite-based carbonate production mode may have also played an important role in the oceanic carbon budget, especially if corresponding carbonates became exported into the adjacent basin. The high-resolution $\delta^{13}C$ record of SE France reflects both the complexity of such changes on the adjacent northern Tethyan platform, as well as coeval changes in paleoceanographic conditions, which episodically culminated in anoxic events, thereby engaging the northern Tethyan carbonate platform in mutual feedback.

E.1.7.Acknowledgements

We are grateful to Thierry Adatte, Bas van de Schootbrugge, Haydon Mort, Annie Arnaud-Vanneau, Hubert Arnaud, Thomas Steuber, Adrian Immenhauser, Helmut Weissert, Hanspeter Funk, Robert Skelton, and Jean-Pierre Masse for insightful discussions and advise. We also thank Jean-Pierre Masse and Elzbietta Morycowa for providing sample material, and Nicolas Fiet for analyzing this material for its stable carbon-isotope contents. We very much appreciated the insightful and highly constructive comments from Karla Panchuk and an anonymous reviewer. We acknowledge the financial support of the Swiss National Fund for this project (projects 2100-067807/1 and 200020-105206/1).

E.1.8.References

Adatte, T., W. Stinnesbeck, and G. Keller (1996), Lithostratigraphic and mineralogic correlations of near K/T boundary sediments in northeastern Mexico: Implications for origin and nature of deposition, in The Cretaceous-Tertiary Event and Other Catastrophes in Earth History, Geol. Soc. Amer. Spec. Paper, vol. 307, edited by G. Ryder, D. Fastovsky, and S. Gartner, pp. 211-226, GSA, Boulder, Colorado.

Adatte, T., W. Stinnesbeck, J. Remane, and H. Hubberten (1996), Paleoceanographic changes at the Jurassic-Cretaceous boundary in the western Tethys, northeastern Mexico, Cret. Research, 17, 671-689.

Arnaud-Vanneau, A., and H. Arnaud (1990), Hauterivian to Lower Aptian carbonate shelf sedimentation and sequence stratigraphy in the Jura and northern subalpine chains, in Carbonate platforms, Internat. Assoc. Sedimentol., Spec. Publ., vol. 9, edited by M. E. Tucker, pp. 203-233, IAS, Blackwell Scient. Publ., Oxford.

Arthur, M. A., and S. O. Schlanger (1979), Cretaceous «Oceanic Anoxic Events» as causal factors in development of reef-reservoired giant oil fields, Amer. Ass. Petrol. Geol. Bull., 63, 870-885.

Arthur, M. A., W. E. Dean, and L. M. Pratt (1988), Geochemical and climatic effects of increased marine organic carbon burial at the Cenomanian/Turonian boundary, Nature, 335, 714-717.

Bartley, J. K., and L. C. Kah (2004), Marine carbon reservoir, Corg-Ccarb coupling, and the evolution of the Proterozoic carbon cycle, Geology, 32, 129-132.

Bartolini, A. (2003), Cretaceous radiolarian biochronology and carbon isotope stratigraphy of ODP Site 1149 (Northwestern Pacific, Nadezhda Basin), Ocean Drill. Program Sci. Results, 185.

Bernaus, J.M., A., Arnaud-Vanneau, and E. Caus (2003), Carbonate platform sequence stratigraphy in a rapidly subsiding area: the late Barremian - early Aptian of the Organyà basin, spanish Pyrenees, Sediment. Geol., 159, 177-201.

Bodin, S., A. Godet, K. B. Föllmi, J.

Vermeulen, H. Arnaud, A. Strasser, N. Fiet, and T. Adatte, (2006a), The late Hauterivian Faraoni oceanic anoxic event in the western Tethys: evidence from phosphorus burial rates, Palaeogeogr., Palaeoclimatol., Palaeoecol., 235, 245-264.

Bodin, S., A. Godet, J. Vemeulen, and K. B. Föllmi (2006b), New data on the age of the installation of Urgonian-type carbonates along the northern Tethyan margin: Biostratigraphy of the Chopf Member (Helvetic Alps, eastern Switzerland), Comptes rendus Geoscience, in press.

Bodin, S., A. Godet, J. Vermeulen, P. Linder, and K. B. Föllmi (2006c), Biostratigraphy, sedimentology and sequence stratigraphy of the latest Hauterivian – early Barremian drowning episode of the northern Tethyan margin (Altmann Member, Helvetic nappes, Switzerland), Eclog. geol. Helv., in press.

Bollinger, D. (1988), Die Entwicklung des distalen osthelvetischen Schelfs im Barremian und Früh-Aptian, Ph.D. thesis, ETH Zürich, Zürich, Switzerland.

Bréhéret, J. G. (1997), L'Aptien et l'Albien de la fosse vocontienne (des bordures au bassin). Evolution de la sédimentation et enseignements sur les événements anoxiques, Soc. Géol. du Nord, 25, 1-164.

Carannante, G., M. Esteban, J. D. Milliman, and L. Simone (1988), Carbonate lithofacies as paleolatitude indicators: problems and limitations, Sedim. Geol., 60, 333-346.

Cerlings, T. E., Y. Wang, and J. Quade (1993), Expansion of C4 ecosystems as an indicator of global ecological change in the late Miocene, Nature, 361, 344-345.

Colombié, C., and A. Strasser (2003), Depositional sequences in the Kimmeridgian of the Voconian Basin (France) controlled by carbonate export from shallow-water platforms, Geobios, 36, 675-683.

Cotillon, P., and M. Rio (1984), Cyclic sedimentation in the Cretaceous of Deep Sea Drilling Project Sites 535 and 540 (Gulf of Mexico), 534 (central Atlantic) and in the Vocontian Basin (France), Deep Sea Drill. Proj. Init.. Reports, 77.

Delamette, M. (1988), L'Evolution du domaine helvétique (entre Bauges et Morcles) de l'Aptien supérieur au Turonien: séries condensées, phosphorites, et circulations océaniques, Publ. Dep. Géol. Paléont., Univ. Genève, 5, 1-316.

Dickens, G. R., J. R. O'Neil, D. K. Rea, and R. M. Owen (1995), Dissociation of oceanic methane hydrate as a cause of the carbon isotope excursion at the end of the Paleocene, Paleoceanography, 10, 965-971.

Droxler, A. W., W. Schlager. and C. C. Whallon (1983), Quaternary aragonite cycles and oxygen isotope record in Bahamian carbonate ooze, Geology, 11, 235-239.

Emmanuel, L., and M. Renard (1993), Carbonate geochemistry (Mn, $\delta^{13}C$, $\delta^{18}O$) of the late Tithonian - Berriasian pelagic limestones of the Vocontian trough (SE France), Bull, Centre Rech. Expl.-Prod. Elf-Aquitaine, 17, 205-221.

Erba, E., A. Bartolini, and R. L. Larson (2004), Valanginian oceanic anoxic event, Geology, 32, 149-152.

Erba, E., J. E. T. Chanell, M. Claps, C. Jones, R. Larson, B. Opdyke, I. Premoli Silva, A. Riva, G. Salvini, and S. Torricelli (1999), Integrated stratigraphy of the Cismon Apticore (southern Alps, Italy): A «reference sections» for the Barremian-Aptian interval at low latitudes, Journ. Foram. Res., 29, 371-391.

Erbacher, J., J. Thurow, and R. Littke (1996), Evolution patterns of radiolaria and organic matter variations: a new approach to identify sea-level changes in mid-Cretaceous pelagic environments, Geology, 24, 499-502.

Erbacher, J., B. T. Huber, R. D. Norris, and M. Markey (2001), Increased thermohaline stratification as a possible cause for an ocean anoxic event in the Cretaceous period, Nature, 409, 325-327.

Fichter, H. J. (1934), Geologie der Bauen-Brisen-Kette, Beitr. Geol. Karte Schweiz, Neue Folge, 69, 1-128.

Flügel, E. (2004), Microfacies of Carbonate Rocks, 976 pp., Springer-Verlag, Berlin.

Föllmi, K. B. (1989a), Evolution of the Mid-Cretaceous triad, Lecture Notes Earth Sci., 23, 1-153.

Föllmi, K. B. (1989b), Beschreibung neugefundener Ammonoidea aus der Vorarlberger Garschella-Formation (Aptian-Albian), Jahrb. Geol. Bundesanstalt, 132, 105-189.

Föllmi, K. B. (1995), 160 m.y. record of marine sedimentary phosphorus burial: Coupling of climate and continental weathering under greenhouse and icehouse conditions, Geology, 23, 859-862.

Föllmi, K. B., and M. Delamette (1991), Comment on: Model simulation of mid-Cretaceous ocean circulation, Science, 251, 94.

Föllmi, K. B., and P. J. Ouwehand (1987), Garschella-Formation und Götzis-Schichten (Aptian-Coniacian): Neue stratigraphische Daten aus dem Helvetikum der Ostschweiz und des Vorarlbergs, Eclog. geol. Helv., 80, 141-191.

Föllmi, K. B., H. Weissert, M. Bisping, and H. Funk (1994), Phosphogenesis, carbon-isotope stratigraphy, and carbonate-platform evolution along the Lower Cretaceous northern Tethyan margin, Geol. Soc. Amer. Bull., 106, 729-746.

Funk, H. P., K. B. Föllmi, and H. Mohr (1993), Evolution of the Tithonian-Aptian carbonate platform along the northern Tethyan margin, eastern Helvetic Alps, in Atlas of Cretaceous Carbonate Platform, Amer. Assoc. Petrol. Geol., Spec. Vol. 56, edited by T. Simo, R. W. Scott, R.W., and J. P. Masse, pp. 387-407, AAPG, Tulsa.

Ganz, E. (1912), Stratigraphie der mittleren Kreide (Gargasien, Albien) der oberen helvetischen Decken in den nördlichen Schweizeralpen, Denkschr. Schweiz. Naturf. Ges., 42/1, 1-148.

Garcia-Hernandez, M. (1979), Les faciès urgoniens pendant la sédimentation barrémo-albienne dans les Sierras de Cazorla et du Segura (zone prébétique, S-E de l'Espagne), Mém. Spéc. Géobios, 3, 57-69.

Godet, A., S. Bodin, K. B. Föllmi, J. Vermeulen, S. Gardin, N. Fiet, T. Adatte, B. Zsolt, D. Stüben, and B. van de Schootbrugge (2006), Evolution of the marine stable carbon-isotope record during the early Cretaceous: a focus on the late Hauterivian and Barremian in the Tethyan realm, Earth Planet. Sci. Letters, 242, 254-271.

Godet, A., S. Bodin, T. Adatte, and K. B. Föllmi (submitted), Clay mineral assemblages along the Northern Tethyan margin during the Late Hauterivian – Early Aptian: Interactions between climate change and carbonate platform evolution, Cret. Research.

Golonka, J. (2004), Plate tectonic evolution of the southern margin of Eurasia in the Mesozoic and Cenozoic, Tectonophysics, 381, 235-273.

Gradstein F. M., J. G. Ogg, A. G. Smith, (2004), A Geologic Time Scale 2004: 500 pp., Cambridge University Press, Cambridge.

Haldimann, P. (1977), Sedimentologische Entwicklung der Schichten an einer Zyklengrenze der helvetischen Unterkreide, Mitt. Geol. Inst. ETH Univ. Zürich, Neue Folge, 219, 1-183.

Hallock, P., and W. Schlager (1986), Nutrient excess and the demise of coral reefs and carbonate platforms, Palaios, 1, 389-398.

Heim, A. (1910-1916), Monographie der Churfirsten-Mattstock-Gruppe, Beitr. Geol. Karte Schweiz, Neue Folge, 20/1-3, 573 p.

Heim, A. (1924), Über submarine Denudation und chemische Sedimente, Geol. Rundschau, 15, 1-47.

Heim, A. (1934), Stratigraphische Kondensation, Eclog. geol. Helv., 27, 372-383.

Heim, A., and O. Seitz (1934), Die mittlere Kreide in den helvetischen Alpen von Rheintal und Vorarlberg und das Problem

der Kondensation, Denkschr. Schweiz. Naturf. Ges. 69/2, 185-310.

Heimhofer, U., P. A. Hochuli, J. O. Herrle, N. Andersen, and H. Weissert (2004), Absence of major vegetation and palaeoatmospheric pCO_2 changes associated with oceanic anoxic event 1a (early Aptian, SE France), Earth Planet. Sci. Letters, 223, 303-318.

Hennig, S., H. Weissert, and L. Bulot (1999), C-isotope stratigraphy, a calibration tool between ammonite- and magnetostratigraphy: the Valanginian-Hauterivian transition, Geol. Carpatica, 50, 91-96.

Herrle, J. O., P., Kößler, O. Friedrich, H. Erlenkeuser, and C. Hemleben (2004), High-resolution carbon isotope records of the Aptian to Lower Albian from SE France and the Mazagan Plateau (DSDP Site 545): a stratigraphic tool for paleoceanographic and paleobiologic reconstruction, Earth Planet. Sci. Letters, 218, 149-161.

Hoefs, J. (1997), Stable Isotope Geochemistry, 201 pp., Springer-Verlag, Berlin.

Höfling, R., and R. W. Scott (2002), Early and mid-Cretaceous buildups, in Phanerozoic Reef Patterns, edited by W. Kiessling, E. Flügel, and J. Golonka, SEPM (Soc. Sedim. Geol.) Spec. Publ., 72, 521-548.

Immenhauser, A., G. Della Porta, J. A. M. Kenter, and J. R. Bahamonde (2003), An alternative model for positive shifts in shallow-marine carbonate $\delta^{13}C$ and $\delta^{18}O$, Sedimentology, 50, 953-959.

Immenhauser, A., H. Hillgärtner, and E. van Bentum (2005), Microbial-foraminiferal episodes in the early Aptian of the southern Tethyan margin: ecological significance and possible relation to oceanic anoxic event 1a, Sedimentology, 52, 77-99.

James, N. P. (1997), The cool-water carbonate depositional realm, in Cool-Water Carbonates, edited by N. P. James, and J. A. D. Clarke, SEPM (Soc. Sedim. Geol.) Spec. Publ., 56, 1-20.

Jenkyns, H. C. (1980), Cretaceous anoxic events: from continents to oceans, Journ. Geol. Soc. London, 137, 171-188.

Jenkyns, H. C. (2003), Evidence for rapid climate change in the Mesozoic-Palaeogene greenhouse world, Phil. Trans. Royal Soc, 361, 1865-1916.

Jenkyns, H. C., and P. A. Wilson (1999), Stratigraphy, paleoceanography, and evolution of Cretaceous Pacific Gyots: Relics from a greenhouse Earth, Amer. Journ. Sci., 299, 341-392.

Kawahata, H., A. Suzuki, and K. Goto (1997), Coral reef ecosystems as a source of atmospheric CO_2: evidence from pCO_2 measurements of surface waters, Coral Reefs, 16, 261-266.

Kuhn, O. (1996), Der Einfluss von Verwitterung auf die Paläozeanographie zu Beginn des Kreide-Treibhausklimas (Valanginian und Hauterivian) in der West-Tethys, Ph.D. thesis, ETH Zürich, Zürich, Switzerland.

Kump, L. R., and M. A. Arthur (1999), Interpreting carbon-isotope excursions: carbonates and organic matter, Chem. Geol., 161, 181-198.

Leckie, R. M., T. J. Bralower, and R. Cashman (2002), Oceanic anoxic events and plankton evolution: biotic response to tectonic forcing during the mid-Cretaceous, Paleoceanography, 17, 10.1029/2001pa000623.

Lees, A., and A. T. Buller (1972), Modern temperate water and warm water shelf carbonate sediments contrasted, Mar. Geol. 13, 1767-1773.

Linder, P., J. Gigandet, J. L. Hüsser, F. Gainon, and K. B. Föllmi (submitted), The early Aptian Grünten member, Eclog. geol. Helv.

Lini, A., H. Weissert, and E. Erba (1992), The Valanginian carbon isotope event: a first episode of greenhouse climate conditions during the Cretaceous, Terra Nova, 4, 374-384.

Masse, J.-P. (1993), Valanginian-early Aptian carbonate platforms from Provence, southeastern France. in Atlas of Cretaceous Carbonate Platform, Amer.

Assoc. Petrol. Geol., Spec. Vol. 56, edited by T. Simo, R. W. Scott, R.W., and J. P. Masse, pp. 363-374, AAPG, Tulsa.

Menegatti, A. P., H. Weissert, R. S. Brown, R. V. Tyson, P. Farrimond, A. Strasser, and M. Caron (1998), High-resolution $\delta^{13}C$ stratigraphy through the early Aptian «Livello Selli» of the Alpine Tethys, Paleoceanography, 13, 530-545.

Michalík, J. (1994), Lower Cretaceous carbonate platform facies, western Carpathians, Palaeogeogr., Palaeoclimatol., Palaeoecol., 111, 263-277.

Mohr, H. (1992), Der helvetische Schelf der Ostschweiz am Übergang vom späten Jura zur frühen Kreide, Ph.D. thesis, ETH Zürich, Zürich, Switzerland.

Mohr, H., and H. Funk, H. (1995), Die Entwicklung der helvetischen Karbonatplattform in der Ostschweiz (Tithonian-Berriasian): eine sequenzstratigraphische Annäherung, Eclog. geol. Helv., 88, 281-320.

Moullade, M., W. Kuhnt, J. A. Bergen, J.-P. Masse, and G. Tronchetti, G. (1998), Correlation of biostratigraphic and stable isotope events in the Aptian historical stratotype of La Bedoule (southeast France), Comptes Rendus Acad. Sci.-Series IIA - Earth Planet. Sci., 327, 693-698.

Mutti, M., and P. Hallock (2003), Carbonate systems along nutrient and temperature gradients: some sedimentological and geochemical constraints, Intern. Journ. Earth Sci. (Geol. Rundsch.) 92, 465-475.

Ouwehand, P. J. (1987), Die Garschella-Formation («Helvetischer Gault», Aptian-Cenomanian) der Churfirsten-Alvier Region (Ostschweiz), Mitt. Geol. Inst. ETH Univ. Zürich, Neue Folge, 275, 1-296.

Panchuk, K. M., C. Holmden, and L. R. Kump (2005), Sensitivity of the epeiric sea carbon isotope record to local-scale carbon cycle processes: Tales from the Mohawkian Sea, Palaeogeogr., Palaeoclimat., Palaeoecol., 228, 320-337.

Panchuk, K. M., C. E. Holmden, and S. A. Leslie (2006), Local controls on carbon cycling in the Ordovician midcontinent region of North America, with implications for carbon isotope secular curves, Journ. Sedim. Res., 76, 200-211.

Pascal, A. (1982), Evolution des systèmes biosédimentaires urgoniens en Espagne du Nord, N. Jb. geol. Paläont. Abh., 165/1, 77-86.

Philip, J. (2003), Peri-Tethyan neritic carbonate areas: distribution through time and driving factors, Palaeogeogr., Palaeoclimat., Palaeoecol., 196, 19-37.

Price, G. D. (2003), New constraints upon isotope variation during the early Cretaceous (Barremian – Cenomanian) from the Pacific Ocean, Geol. Mag., 140, 513-522.

Reboulet, S., E. Mattioli, B. Pittet, F. Baudin, D. Olivero, and O. Proux (2003), Ammonoid and nannoplankton abundance in Valanginian (early Cretaceous) limestone-marl sucessions from the southeast France basin: carbonate dilution or productivity? Palaeogeogr., Palaeoclimat., Palaeoecol., 201, 113-139.

Romanek, C. S., E. L. Grossmann, and J. W. Morse (1992), Carbon isotope fractionation in synthetic aragonite and calcite: effects of temperature and precipitation rate, Geochim. Cosmochim. Acta, 56, 419-430.

Schaub, H. P. (1936), Geologie des Rawilgebietes, Eclog. geol. Helv., 29, 337-407.

Schaub, H. P. (1948), Über Aufarbeitung und Kondensation, Eclog. geol. Helv., 41, 89-94.

Schlager, W. (1981), The paradox of drowned reefs and carbonate platforms, Geol. Soc. Amer. Bull., 92, 197-211.

Schlanger, S. O., and H. C. Jenkyns (1976), Cretaceous oceanic anoxic events: causes and consequences, Geol. Mijnbouw, 55, 179-184.

Scholle, P. A., and M. A. Arthur (1980), Carbon isotope fluctuations in Cretaceous pelagic

limestones: Potential stratigraphic and petroleum exploration tool, Amer. Assoc. Petrol. Geol. Bull., 64, 67-87.

Smith, A. M., C. S. Nelson, and H. G. Spencer (1998), Skeletal carbonate mineralogy of New Zealand bryozoans, Mar. Geol., 151, 27-46.

Sprinkle, J., and P. M. Kier (1987), Phylum Echinodermata, in Fossil Invertrebrates, edited by R. S. Boardman, A. H. Cheetham, and A. J. Rowell, A.J., Blackwell Scientific Publications, Oxford, 550-611.

Steuber, T. (2002), Plate tectonic control on the evolution of Cretaceous platform-carbonate production, Geology, 30, 259-262.

Suzuki, A., and H. Kawahata (2003), Carbon budget of coral reef systems: an overview of observations in fringing reefs, barrier reefs and atolls in the Indo-Pacific regions, Tellus, 55B, 428-444.

Suzuki, A., and H. Kawahata (2004), Reef water CO_2 system and carbon production of coral reefs: topographic control of system-level performance, in Global environmental change in the ocean and on land, edited by M. Shiyomi, et al., Terrapub, p. 229-248.

Suzuki, A., A. Kawahata, T. Ayukai, and K. Goto (2001), The oceanic CO_2 system and carbon budget in the Great Barrier Reef, Australia, Geophys. Res. Lett., 28, 1243-1246.

Swart, P. K., and G. Eberli (2005), The nature of the $\delta^{13}C$ of periplatform sediments: Implications for stratigraphy and the global carbon cycle, Sedim. Geol. 175, 115-129.

Thomas, H., Y. Bozec, K. Elkalay, and H. J. W. de Baar (2004), Enhanced open ocean storage of CO_2 from shelf sea pumping, Science, 304, 1005-1008.

van de Schootbrugge, B. (2001), Influence of paleo-environmental changes during the Hauterivian (early Cretaceous) on carbonate deposition along the northern margin of the Tethys: Evidence from geochemical records (C, O, and Sr-isotopes, P, Fe, Mn), Ph.D. thesis, Univ. Neuchâtel, Neuchâtel, Switzerland,

van de Schootbrugge, B., K. B. Föllmi, L. G. Bulot, and S. J. Burns (2000), Paleoceanographic changes during the early Cretaceous (Valanginian-Hauterivian): evidence from oxygen and carbon stable isotopes, Earth Planet. Sci. Letters, 181, 15-31.

van de Schootbrugge, O. Kuhn, T. Adatte, P. Steinmann, and K. B. Föllmi (2003), Decoupling of P- and Corg-burial following Early Cretaceous (Valanginian-Hauterivian) platform drowning along the NW Tethyan margin, Palaeogeogr., Palaeoclimat., Palaeoecol., 199, 315-331.

van de Schootbrugge, B., J. M., McArthur, T. R. Bailey, Y. Rosenthal, J. D. Wright, and K. G., Miller (2005), Toarcian oceanic anoxic event: An assessment of global causes using belemnite C isotope records, Paleoceanography, 20, PA3008, doi: 10.1029/2004PA001102.

Veizer, J., D. Ala, K. Azmy, P. Bruckschen, D. Buhl, F. Bruhn, G. A. F. Carden, A. Diener, S. Ebneth, Y. Godderis, T. Jasper, C. Korte, F. Pawellek, O. Podlaha, and H. Strauss (1999), $^{87}Sr/^{86}Sr$, $\delta^{13}C$ and $\delta^{18}O$ evolution of Phanerozoic seawater, Chem. Geol., 161, 59-88.

Wefer, G., and W. H. Berger (1991), Isotope paleontology: growth and composition of extant calcareous species, Mar. Geol. 100, 207-248.

Weissert, H. (1981), The environment of deposition of black shales in the early Cretaceous: an ongoing controversy, in The Deep Sea Drilling Project: a decade of progress, edited by J. E., Warme, R. G. Douglas, and E. L. Winterer, Soc. Econ. Paleont. Mineral., Spec. Vol. 32, 547-560.

Weissert, H. (1989), C-Isotope stratigraphy, a monitor of paleoenvironmental change: a case study from the Early Cretaceous, Surveys Geophys., 10, 1-61.

Weissert, H., and J. E. T. Channell (1989),

Tethyan carbonate carbon isotope stratigraphy across the Jurassic-Cretaceous boundary: an indicator of decelerated global carbon cycling? Paleoceanography, 4, 483-494.

Weissert, H., J. A. McKenzie, and P. Hochuli (1979), Cyclic anoxic events in the early Cretaceous Tethys ocean, Geology, 7, 147-151.

Weissert, H., A. Lini, K. B. Föllmi, and O. Kuhn (1998), Correlation of Early Cretaceous carbon isotope stratigraphy and platform drowning events : a possible link ?: Palaeogeogr., Palaeoclimat., Palaeoecol., 137, 189-203.

Weissert, H., and E. Erba (2004), Volcanism, CO_2 and palaeoclimate: a late Jurassic-early Cretaceous carbon and oxygen isotope record, Journ. Geol. Soc. London, 161, 695-702.

Wissler, L., H. Weissert, J.-P. Masse, and L.G. Bulot (2002), Chemostratigraphic correlation of Barremian and lower Aptian ammonite zones and magnetic reversals, Intern. Journ. Earth Sci. (Geol. Rundsch.), 91, 272-279.

Wissler, L. H., H. Funk, and H. Weissert (2003), Response of early Cretaceous carbonate platforms to changes in atmospheric carbon dioxide levels, Palaeogeogr., Palaeoclimat., Palaeoecol., 200, 187-205.

Woo, K. S., T. F. Anderson, and P. A. Sandberg (1993), Diagenesis of skeletal and nonskeletal components of mid-Cretaceous limestones, Journ. Sedim. Petrol., 63, 18-32.

Wyssling, G. W. (1986), Der frühkretazische helvetische Schelf im Vorarlberg und

E.2.

Platform-induced clay-mineral fractionation along a northern Tethyan basin-platform transect: implications for the interpretation of Early Cretaceous climate change (Late Hauterivian-Early Aptian)

Alexis Godet, Stéphane Bodin, Thierry Adatte and Karl B. Föllmi

Institute of Geology, University of Neuchâtel, rue Emile Argand 11, CP 158 2009 Neuchâtel, Switzerland.

Keywords: Kaolinite, smectite, climate change, Early Cretaceous, carbonate platform, Jura mountains, Vocontian Trough, northern Tethyan margin

Submitted to: Cretaceous Research

Abstract

High-resolution clay-mineral analyses were performed on Upper Hauterivian to Lower Aptian sediments along a platform-to-basin transect through the northern Tethyan margin from the Neuchâtel area (Switzerland), to the Vocontian Trough (France) in order to investigate links between climate change, carbonate platform evolution, and fractionation patterns in clay minerals during their transport.

During the Hauterivian, the northern Tethyan carbonate platform developed in a heterozoan mode, and the associated ramp-like topography facilitated the export of detrital material into the adjacent basin, where clay-mineral assemblages are dominated by smectite and kaolinite is almost absent, thereby suggesting dry-seasonal conditions. During the Late Hauterivian Balearites balearis ammonite zone, a change to a more humid climate is documented by the appearance of kaolinite, which reaches up to 30% of the clay fraction in sediments in the Vocontian Trough. This prominent change just preceded the Faraoni Oceanic Anoxic Event and the onset of the demise of the Helvetic Carbonate Platform, which lasted to the late Early Barremian.

From the Late Barremian onwards, the renewed growth of the northern Tethyan carbonate platform in a photozoan mode and the associated development of a marginally confined platform topography segregated or fractionated the clay-mineral assemblages exported into hemipelagic settings: kaolinite particles were preferentially retained in proximal, platform settings, due to their size, relatively high specific weight, and capacity to flocculate in the marine environment. In the inner platform environment preserved in the Swiss Jura, an average of 32% of kaolinite in the clay fraction is observed during the latest Barremian – earliest Aptian, whereas clay-mineral assemblages of coeval sediments from deeper depositional settings are dominated by smectite and show only minor amounts of kaolinite.

This signifies that besides palaeoclimate conditions, the morphology and ecology of the carbonate platform had a significant effect on the distribution and composition of clay assemblages during the late Hauterivian – early Aptian along the northern Tethyan margin.

E.2.1. Introduction

The Early Cretaceous climate was sustained by generally elevated atmospheric pCO_2 (e.g., Berner and Kothavala, 2001), implying reinforced greenhouse conditions, which influenced the water cycle, the intensity of rainfall, and the biogeochemical weathering of continental rocks (e.g., Weissert, 1989; Weissert et al., 1998; Larson and Erba, 1999). The latter may have affected marine biological communities by regulating the input of nutrients in the ocean; episodes of enhanced nutrients transfer to the ocean may have led to increased marine productivity rates and the subsequent generation and preservation of organic-rich sediments under partly anoxic conditions.

An example of such an episode is documented by the Late Hauterivian Faraoni Level, which was first described in the Umbria-Marche basin of Italy (Cecca et al., 1995), and subsequently recovered in sections from other regions of the central and western Tethys (Baudin, 2005). The Faraoni Level displays features similar to other Oceanic Anoxic Events (OAE's; e.g. Schlager and Jenkyns, 1976; Scholle and Arthur, 1980) such as the presence of finely laminated black-shale facies with TOC values of more than 10% in Italian sections. However, unlike other Cretaceous OAE's, the Faraoni Level is not associated with a carbon isotope excursion and only marked by an increase of 0.15‰ in sediments from the western Switzerland and southeastern France (Baudin et al., 1999; Godet et al., 2006); by comparison, the OAE1a (Early Aptian) is associated to a negative spike (amplitude of ca. -1.5‰) followed by a positive excursion (amplitude of ca. +2‰; e.g., Föllmi et al., in press). This is explained by a buffering effect on the marine $\delta^{13}C$ record, through accelerated water cycle and increased delivery of Dissolved Inorganic Carbon (DIC) to the ocean more humid climate conditions (e.g., Bartley and Kah, 2004; Godet et al., 2006).

Climate change during the early Cretaceous has been deduced from the temporal evolution of clay-mineral assemblages (e.g., Ruffell and Batten, 1990; Ruffell et al., 2002). Clay minerals are valid indicators of the intensity of geochemical weathering processes on the continent, because such processes are influenced by climate (humidity, average temperature, seasonality; e.g., Chamley, 1981; Ruffell et al., 2002). Geomorphology is in turn an expression of tectonic and climatic processes. Investigations of clay minerals in Barremian sediments of Western Europe (Spain, England, France, and Germany) have led to the interpretation of a relatively stable dry climate, which were probably interrupted by short-term changes from arid to semi-arid conditions, as is indicated by the occurrence of traces of kaolinite (Ruffell and Batten, 1990). Late Jurassic – Early Cretaceous sediments from the Jura Mountains contain relatively high amounts of kaolinite (up to 30%), except in Hauterivian sediments where smectite represents up to 50% of the clay fraction, which suggests seasonally dry conditions for this stage (Persoz, 1982; Adatte and Rumley, 1989).

Here we show the results of our analysis of clay-mineral assemblages from a selection of sections of Hauterivian and Barremian age along a transect through the northern Tethyan margin, which ranges from the hemipelagic Vocontian Trough to the platform environment preserved in the Jura Mountains. We use this data set to reconstruct the evolution of climate during the Hauterivian and Barremian along the northern Tethyan margin. Then, we propose to deduct the potential effect of this type of environmental change on the continental hydrological cycle and intensity in chemical weathering processes; the related transfer of nutrients and DIC into the ocean will be taken into consideration, as well as the corresponding impact on the marine environment and marine carbon isotope system. We also consider the impact of different carbonate platform morphologies associated with photozoan and heterozoan production modes on the spatial distribution of clay minerals, especially kaolinite.

E.2.2. Geological setting and location of the studied sections

The sections of La Charce, Vergons, Angles (stratotype of the Barremian stage), and Combe-Lambert are located in the region of the Alpes de Haute Provence, southeastern France (Figs. E.2.1, E.2.2, and E.2.3). They represent a hemipelagic environment typical for the Vocontian Trough, and the abundance of ammonites allows for excellent time-calibration (e.g., Bulot et al., 1992; Delanoy, 1997; Vermeulen, 2002). During the Early Cretaceous, the Vocontian Trough constituted an epicontinental basin, which was surrounded by carbonate platforms such as the Bas-Dauphine platform and which was connected to the Ligurian Tethys (e.g., Baudin et al., 1999).

Located in France, approximately 20km southeastward from Geneva (Fig. E.2.1), the section of Cluses (Fig. E.2.4) belongs to the Bornes Massif, which constitutes the northeastern part of the French Subalpine Chains (e.g. Trabold, 1996). In the absence of ammonites in these facies, which is similar to that of the Helvetic ramp, the dating of the Cluses section is mainly based on orbitolinids and echinoids (Trabold, 1996; Wermeille, 1996).

Finally, the Eclépens section is located between Neuchâtel and Lausanne (Switzerland), and belongs to the Western Swiss Jura (Figs. E.2.1 and E.2.5). This region hosts the historical succession of the Hauterivian stage - first described by de Montmollin (1835), which is composed, from the base to the top, by the "Marne à Astiera", the "Marne Bleue d'Hauterive", and the "Pierre Jaune de Neuchâtel" (PJN). Whereas the age of these formations is well-constrained by ammonite biostratigraphy, the overlying "Urgonien Jaune" (UJ) and "Urgonien Blanc" (UB) are lacking ammonites; based on recent nannofossils finding near the base of the UJ, these formations are attributed to the Late Barremian – earliest Aptian (Godet et al., 2005). The study of Blanc-Aletru (1995) on the upper part of the section (UJ and UB) are complementary to the results of this work.

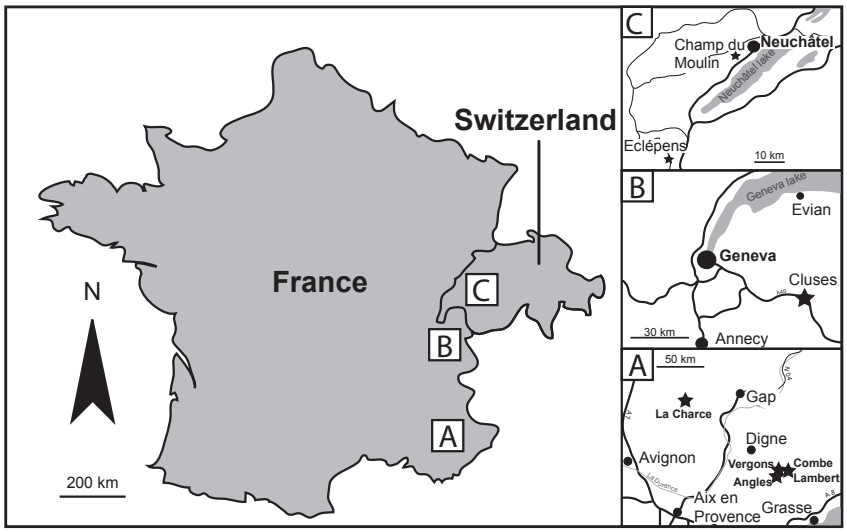

Figure E.2.1: Location of the studied sections.

E.2.3. Methods

E.2.3.1. Rock-Eval analysis

Organic matter analyses were performed using a Rock Eval 6 equipment at the Institute of Geology of the University of Neuchâtel, on a batch of 26 marls around the Faraoni Level equivalent at Angles. Approximately 100 mg of ground and homogenised sample is subjected to a pyrolysis step followed by the complete oxidation of the residual sample (Espitalié et al. (1985), Lafargue et al. (1998) and Behar et al. (2001)). A FID detector measures the

hydrocarbon released during pyrolysis, while CO_2 and CO are detected by infrared absorbance during both steps. In the here applied standard cycle for «whole rock», pyrolysis starts isothermally at 300°C for 3 minutes, after which the sample is heated to 650°C. The oxidation step starts isothermally at 400°C (3 min) and then heats up to 850°C. Organic carbon decomposition results in 4 main peaks: the S1 peak (hydrocarbons released during the isothermal phase), the S2 peak (hydrocarbons produced between 300 and 650°C), the S3 peak (CO_2 from pyrolysis of OM up to 400°C), and the S4 peak (CO_2 released from residual organic matter below ca. 550°C during the oxidation step). Mineral carbon decomposition is recorded by the S3' peak (pyrolysis-CO_2 released above 400°C), and the S5 peak (oxidation-CO_2 released above ca. 550°C).

These peaks are used to calculate the amount of total organic carbon (TOC) and the amount of mineral carbon (MinC). In addition, the so-called hydrogen index (HI = S2/TOC) and oxygen index (OI = S3/TOC) are calculated. The HI and OI indices are proportional to the H/C and O/C ratios of the organic matter, respectively, and can be used for organic matter classification in Van-Krevelen-like diagrams (Espitalié et al., 1985).

Measurements are calibrated using two standards (IFP 160000 and VP143h); the error relative to standard IFP 160000 is approximately 0.77, 0.08, 0.25 and 1.5 % for TOC, MinC, HI and OI, respectively.

E.2.3.2. XRD analysis

X-ray diffraction analyses were performed to identify and quantify the different components of the bulk rock (Angles) and the clay-mineral assemblages (all studied sections). As data for the upper part of Eclépens (Blanc-Aletru, 1995), Cluses (Wermeille, 1996), Vergons and La Charce (van de Schootbrugge, 2001) sections were obtained using the methods described by Kübler (1987) and Adatte et al. (1996), the same procedures were performed on samples from Angles, Combe-Lambert and the lower part of Eclépens. This allowed us to better compare the integrity of the dataset and to avoid discrepancies due to the process of quantification. Moreover, the methods described in these aforementioned papers are accurate enough for bulk rock composed of several different mineral phases, even if the procedures mentioned by Środoń (1980) and Hillier (1989) are known to be precise and have been subsequently used to analyse the bulk-rock composition.

Samples were trimmed to avoid altered material. Subsequently, they were roughly crushed in a "jaw" crusher, and an aliquot of the resulting gravels was crushed using an agate mortar to obtain a fine and homogeneous powder (grain size ≤40μm).

E.2.3.2.1 Bulk-rock analysis

About 800 mg of the powder were pressed (20 bar) in a powder holder, and the bulk-sample was analysed by XRD at the Institute of Geology of the University of Neuchâtel (Scintag XRD 2000 Diffractometer), in order to determine bulk-rock mineralogy using procedures described by Ferrero (1965, 1966), Klug and Alexander (1974), Kübler (1983), and Adatte et al. (1996). This method allows the semi-quantification of the whole-rock mineralogy (obtained by XRD patterns of random powder samples) by using external standards with an error varying between 5 and 10 % for the phyllosilicates and 5 % for grain minerals. The different minerals recognized and quantified are calcite, "phyllosilicates" group, quartz, sodic plagioclase (albite), and potassic feldspar (microcline); the position of the peaks used for their recognition is given in Table E.2.1. Organic matter, poorly crystallised minerals (such as pyrite and goethite), ankerite and dolomite were not quantified due to the low intensity of their respective peak. They constitute the unquantified component of the samples.

E.2.3.2.2. Clay mineral analysis

This procedure is based on the method described by Kübler (1987) and Adatte et al. (1996). Samples are transferred into glass containers with de-ionised water and agitated by air injection; subsequently they are decarbonatized by HCl 10% (1.25N) leaching during 20 min. Dissolution of the samples is promoted by ultrasonic disaggregation (3 minutes per sample). The insoluble residue is washed and centrifuged until a neutral suspension is obtained (pH 7-8). Using the Stokes law, two granulometric fractions are separated (<2μm and 2-16μm). The selected fraction is then pipetted and deposited on a glass plate. A first analysis is performed after air-drying at temperature room, a second one after saturation of the sample with ethylen-glycol, in order to identify swelling minerals, and a third one after heating to 350°C for selected samples. The intensities of the identified minerals are measured for a semi-quantitative estimate of the proportion of clay minerals, which is therefore given in relative percent without correction factors for both fractions.

Mica, kaolinite, chlorite, illite / smectite irregular mixed-layers (R0), and ordered mixed-layers (R1) were identified in the studied sections; the position of the peaks used for their recognition is given in Table E.2.2. Measurements of the amount of smectite and illite layers in the R0 mixed-layers were performed on both limestones and marls, following the procedure of Moore and Reynolds (1997; Table E.2.3). They reveal the presence of two types of R0 minerals. The first one contains more than 80% of smectite layers, and corresponds to an almost pure smectite characterized by a peak at 5.2 °2θ; it will hereafter be called "smectite". The second type is characterized by less than 70-60% of smectite layers and by a peak (001) between 9 and 9.5 °2θ: the term R0 I/S will be used hereafter for such. The R1 mixed-layers are corrensite (chlorite / smectite R1 mixed-layer) or rectorite (illite / smectite R1 mixed-layer). The illite cristallinity index (IC) was measured on several diffractograms of marls and limestones, following the methods described by Kübler (1987), and by Kübler and Goy-Eggenberger (2001).

E.2.4. Results

E.2.4.1. The Angles and Combe-Lambert sections

E.2.4.1.1. XRD analysis

For the Angles section, analyses of whole-rock (n=180) and insoluble-residue (n=170) samples were performed both on marl and limestone samples, whereas in sediments from the Combe-Lambert section, only clay minerals were analysed (n=25).

Calcite content shows no major variations, except for samples belonging to the *Balearites balearis* and *Spathicrioceras angulicostatum* (Late Hauterivian), and to the *Holcodiscus uhligi* and *Heinzia sayni* ammonite zones (early Late Barremian), where significant drops in the calcite content are observed (Fig. E.2.2). The quartz content decreases slightly from the base of the section up to the sedimentary interval attributed to the *Nicklesia pulchella* zone, and then it increases up to the top of the section, which belongs to the Early Aptian. The evolution of phyllosilicates follows that of quartz, with a rapid increase just below the Faraoni Level equivalent (at 24.50m).

From these results, a detrital index (DI), which corresponds to the ratio of the calcite to the quartz and phyllosilicates (in percents), is calculated, assuming that the major part of quartz is of detrital origin, as suggested by the absence of any post-depositional silicification.

High DI values reflect low detrital input. The evolution of the DI can be divided into three parts (Fig. E.2.2; see also Table E.2.1):

I. From the base of the section to the Faraoni Level equivalent (*S. angulicostatum* – *Pseudothurmannnia mortilleti* boundary), DI values are low.

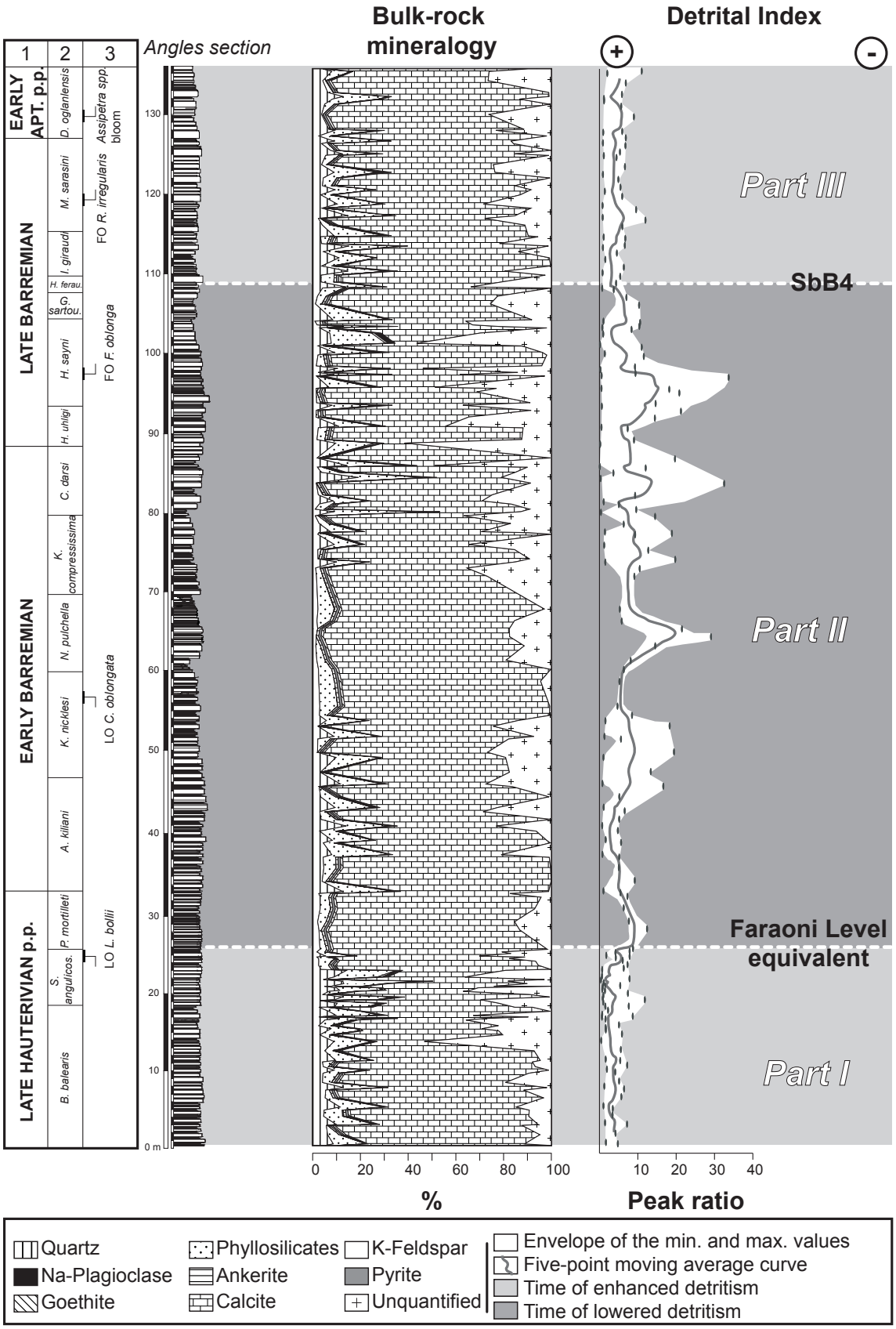

Figure E.2.2: Bulk-rock mineralogy of the Angles section. The detrital index corresponds to the ratio of calcite to quartz and phyllosilicates (in percentage). Numbers on top of the columns (left part of figure) correspond to the 1) stratigraphic stages, 2) ammonite zones and 3) main nannofossils bioevents (after Godet et al., 2006). The sequence boundary B4 (SbB4) is positioned after Arnaud (2005).

Section	Age	Mineral	Peak position (°2θ)	Bulk rock					
				Marls		Limestones		All lithologies	
				Mean value	*Extreme values*	*Mean value*	*Extreme values*	*Mean value*	*Extreme values*
Angles	*Part I*	Calcite	29.43	*51.80*	*19.8 - 78.8*	*82.10*	*68.1 - 91.5*	*66.00*	*19.8 - 91.5*
		Quartz	26.65	*9.50*	*2.5 - 14.4*	*4.30*	*2.6 - 6.5*	*7.10*	*2.5 - 14.4*
		Phyllosilicate	19.80	*16.20*	*7.2 - 32.6*	*3.90*	*0.0 - 8.1*	*10.40*	*0.0 - 32.6*
		K-Feldspars	27.50	*0.70*	*0.0 - 2.2*	*0.00*	*0.0 - 0.3*	*0.40*	*0.0 - 2.2*
		Na-Plagioclases	27.90	*1.00*	*0.0 - 2.1*	*0.10*	*0.0 - 0.6*	*0.60*	*0.0 - 2.1*
		Unquantified	----	*20.70*	*0.4 - 53.2*	*9.60*	*0.1 - 28.5*	*15.50*	*0.1 - 53.2*
		Detrital Index	----	*1.40*	*0.3 - 3.8*	*5.40*	*2.1 - 10.8*	*3.30*	*0.3 - 10.8*
	Part II	Calcite	29.43	*42.20*	*7.4 - 72.7*	*80.90*	*59.9 - 96.9*	*68.70*	*7.4 - 96.9*
		Quartz	26.65	*9.50*	*3.0 - 19.2*	*2.40*	*1.0 - 4.8*	*4.60*	*1.0 - 19.2*
		Phyllosilicate	19.80	*18.80*	*6.9 - 41.3*	*3.00*	*0.0 - 7.7*	*8.00*	*0.0 - 41.3*
		K-Feldspars	27.50	*0.60*	*0.0 - 1.9*	*0.00*	*0.0 - 0.4*	*0.20*	*0.0 - 1.9*
		Na-Plagioclases	27.90	*1.50*	*0.2 - 4.9*	*0.00*	*0.0 - 0.3*	*0.50*	*0.0 - 4.9*
		Unquantified	----	*26.90*	*1.1 - 61.5*	*13.70*	*0.0 - 37.8*	*17.90*	*0.0 - 61.5*
		Detrital Index	----	*1.00*	*0.1 - 2.7*	*6.30*	*1.5 - 30.8*	*4.60*	*0.1 - 30.8*
	Part III	Calcite	29.43	*53.40*	*35.2 - 72.3*	*81.10*	*67.3 - 91.1*	*70.50*	*35.2 - 91.1*
		Quartz	26.65	*11.20*	*8.0 - 15.2*	*4.40*	*2.5 - 7.6*	*7.00*	*2.5 - 15.2*
		Phyllosilicate	19.80	*17.90*	*8.0 - 22.4*	*3.40*	*0.0 - 9.0*	*9.00*	*0.0 - 22.4*
		K-Feldspars	27.50	*0.30*	*0.0 - 1.2*	*0.10*	*0.0 - 0.4*	*0.20*	*0.0 - 1.2*
		Na-Plagioclases	27.90	*0.90*	*0.9 - 2.8*	*0.10*	*0.0 - 0.3*	*0.40*	*0.0 - 2.8*
		Unquantified	----	*15.70*	*0.8 - 33.7*	*11.10*	*0.1 - 28.5*	*12.90*	*0.1 - 33.7*
		Detrital Index	----	*1.30*	*0.6 - 2.6*	*5.50*	*2.1 - 10.7*	*3.90*	*0.6 - 10.7*

Table E.2.1: Synthesis of the results of bulk-rock analysis performed on samples from Angles. All values in percents.

Section	Age	Mineral	Peak position (°2θ)	Clay fraction (< 2 μm)					
				Marls		Limestones		All lithologies	
				Mean value	*Extreme values*	*Mean value*	*Extreme values*	*Mean value*	*Extreme values*
Angles / Combe-Lambert	*Late Hauterivian*	Illite-Micas	8.8 (*001*)	58	30- 81	41	17 - 68	48	17 - 81
		Kaolinite	12.34 (*001*) / 24.9 (*002*)	6	0 - 25	5	0 - 15	5	0 - 25
		"Smectite"	5.2 (*001* on glycolated sample)	6	0 - 38	28	4 - 58	23	0 - 58
		Chlorite	12.34 (*002*) / 25.2 (*004*)	8	0 - 23	18	6 - 38	13	0 - 38
		R0 I/S	9-9.5 (*001*)	11	0 - 19	9	0 - 17	10	0 - 19
	Barremian	Illite-Micas	8.8 (*001*)	51	25 - 73	36	6 - 74	41	6 - 82
		Kaolinite	12.34 (*001*) / 24.9 (*002*)	20	0 - 51	8	0 - 19	11	0 - 51
		"Smectite"	5.2 (*001* on glycolated sample)	12	2 - 25	23	2 - 78	19	0 - 78
		Chlorite	12.34 (*002*) / 25.2 (*004*)	8	0 - 23	25	0 - 61	19	0 - 61
		R0 I/S	9-9.5 (*001*)	10	1 - 25	9	3 - 21	9	1 - 25
	Earliest Aptian	Illite-Micas	8.8 (*001*)	54	29 - 82	29	0 - 63	39	0 - 71
		Kaolinite	12.34 (*001*) / 24.9 (*002*)	9	3 - 52	3	0 - 23	6	0 - 52
		"Smectite"	5.2 (*001* on glycolated sample)	8	0 - 21	42	12 - 76	28	0 - 76
		Chlorite	12.34 (*002*) / 25.2 (*004*)	19	3 - 56	11	0 - 55	15	0 - 56
		R0 I/S	9-9.5 (*001*)	11	3 - 21	14	0 - 26	12	0 - 26
Cluses	*Not attributed*	Illite-Micas	8.8 (*001*)	***No limestone - marl alternation***				94	80 - 100
		Kaolinite	12.34 (*001*) / 24.9 (*002*)					3	0 - 19
		Chlorite	12.34 (*002*) / 25.2 (*004*)					1	0 - 12
		R0 I/S	9-9.5 (*001*)					3	0 - 20
	Barremian	Illite-Micas	8.8 (*001*)					89	23 - 100
		Kaolinite	12.34 (*001*) / 24.9 (*002*)					9	0 - 77
		Chlorite	12.34 (*002*) / 25.2 (*004*)					2	0 - 36
		R0 I/S	9-9.5 (*001*)					1	0 - 12
	Aptian	Illite-Micas	8.8 (*001*)					76	0 - 100
		Kaolinite	12.34 (*001*) / 24.9 (*002*)					20	0 - 100
		Chlorite	12.34 (*002*) / 25.2 (*004*)					3	0 - 45
		R0 I/S	9-9.5 (*001*)					1	0 - 10
Eclépens	*Early Hauterivian*	Illite-Micas	8.8 (*001*)					59	28 - 100
		Kaolinite	12.34 (*001*) / 24.9 (*002*)					3	0 - 15
		"Smectite"	5.2 (*001* on glycolated sample)					25	0 - 60
		Chlorite	12.34 (*002*) / 25.2 (*004*)					2	0 - 8
		R0 I/S	9-9.5 (*001*)					11	0 - 20
	Not attributed	Illite-Micas	8.8 (*001*)					53	22 - 100
		Kaolinite	12.34 (*001*) / 24.9 (*002*)					1.5	0 - 8
		"Smectite"	5.2 (*001* on glycolated sample)					25	0 - 62
		Chlorite	12.34 (*002*) / 25.2 (*004*)					1.5	0 - 6
		R0 I/S	9-9.5 (*001*)					19	0 - 70
	Latest Barremian / Earliest Aptian	Illite-Micas	8.8 (*001*)					31	0 - 100
		Kaolinite	12.34 (*001*) / 24.9 (*002*)					32	0 - 100
		"Smectite"	5.2 (*001* on glycolated sample)					18	0 - 67
		Chlorite	12.34 (*002*) / 25.2 (*004*)					5	0 - 16
		R0 I/S	9-9.5 (*001*)					14	0 - 100

Table E.2.2: Synthesis of the results of insoluble residue (<2μm) analysis performed on samples from Angles, Combe-Lambert, Cluses and Eclépens. All values in relative percents.

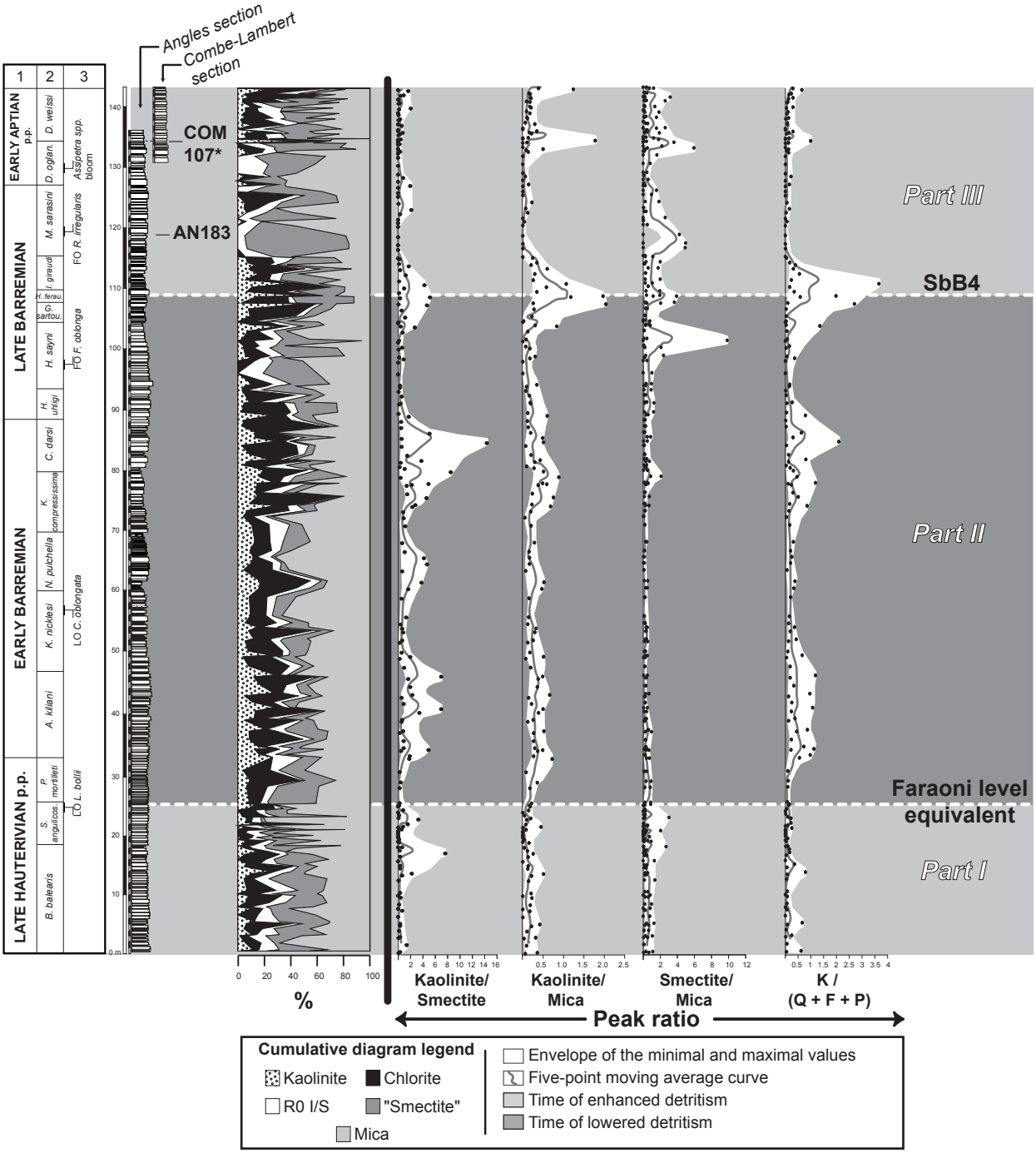

Figure E.2.3: Evolution of the clay-mineral assemblage of the insoluble residue (<2μm fraction) of the Angles and the Combes-Lambert sections. On the right, the curves of the kaolinite/smectite, kaolinite/mica, and kaolinite/(quartz + feldspar + phyllosilicate) ratios point out the dominance of kaolinite during most of the Barremian. Numbers on top of the columns (left part of figure) correspond to the 1) stratigraphic stages, 2) ammonite zones and 3) main nannofossils bioevents (after Godet et al., 2006). Sample numbers refer to the diffractograms C and D displayed in Fig. E.2.6. Abbreviations of the minerals: K = Kaolinite: Q = Quartz; F = potassic feldspar; P = sodic plagioclase.

II. From the Faraoni Level equivalent to the sequence boundary (Sb) B4 (approximately at 109m, in sediments of the *Hemihoplites feraudianus* ammonite zone; after Arnaud, 2005), the DI curve increases sharply.

III. From the SbB4 to the top of the section, the DI decreases to values comparable to those observed in part I.

In the insoluble residue of the <2μm fraction of sediments from the Angles and

the Combe-Lambert sections, mica, kaolinite, "smectite", chlorite, and R0 I/S were identified (Fig. E.2.3; see also Table E.2.2 and Fig. E.2.6 for an example of diffractograms).

The evolution of the kaolinite/mica and kaolinite/smectite ratios points out the predominance of kaolinite relative to smectite and mica in certain intervals (Fig. E.2.3). In particular, the kaolinite content reaches 25% of the total clay-mineral content in selected marly samples of part II of the section, whereas this mineral tends to decrease in content in part III of the section. However, kaolinite remains relatively low in limestone samples, trough the entire section (see Table E.2.2). Contrary to kaolinite, "smectite" is the most abundant mineral in part I and especially in part III of the Angles section, where it reaches a maximum of approximately 80 % in sediments belonging to the *Martelites sarasini* zone. Whereas the evolution of mica is rather monotonous, the chlorite content increases gently from the base to the top, with higher contents in limestones (mean value of 21%) compared to those of marls (mean value of 11%); the repartition of the "smectite" follows the same rule, with higher contents in limestones compared to marls (mean values of 27% and 12%, respectively).

E.2.4.1.2. Rock Eval analysis

A batch of 26 samples of marl belonging to the time span from the *B. balearis* to the *Avramidiscus kiliani* ammonite zone were analysed for their organic geochemistry parameters (Table E.2.4). The TOC values range from 0.35 to 2.63%, with a maximum

Section	Sample	Lithology	Δ2°θ	% smectitic layers	% illitic layers
Angles	AN 2b	marlstone	6.22	61.05	39.07
	AN 6b	marlstone	5.76	76.99	23.11
	AN 10b	marlstone	6.26	59.72	40.40
	AN 15.1b	marlstone	5.93	71.06	29.04
	AN 18b	marlstone	6.93	39.75	60.39
	AN 29b	marlstone	6.69	46.44	53.69
	AN 34b	marlstone	6.51	51.75	48.38
	AN 38b	marlstone	6.51	51.79	48.34
	AN 81b	marlstone	6.15	63.26	36.86
	AN 103b	marlstone	6.21	61.29	38.83
	AN 35	limestone	5.67	80.69	19.40
	AN 49.1	limestone	5.40	91.17	8.92
	AN 156.4	limestone	5.64	81.67	18.43
	AN 156.6	limestone	5.97	69.54	30.56
	AN 181	limestone	5.46	88.79	11.30
	AN 183	limestone	5.70	79.52	20.58
	AN 185	limestone	5.76	77.12	22.98
	AN 190	limestone	5.85	73.81	26.30
	AN 197	limestone	5.37	92.36	7.73
	AN 206	limestone	5.19	100.01	0.07
	Mean values :		*Marlstone*	*58.31*	*41.81*
			Limestone	*83.47*	*16.63*
			All lithologies	**70.89**	**29.22**
Combe-Lambert	COM 108*	marlstone	6.14	63.59	36.52
	COM 122*	marlstone	6.45	53.71	46.42
	COM 104	limestone	6.18	62.37	37.75
	COM 106	limestone	6.03	67.51	32.60
	COM 112	limestone	5.70	79.49	20.61
	COM 122h	limestone	5.94	70.43	29.68
	COM 124	limestone	5.89	72.40	27.70
	Mean values :		*Marlstone*	*58.65*	*41.47*
			Limestone	*70.44*	*29.67*
			All lithologies	**67.07**	**33.04**
Eclépens	ECII 1	limestone	5.57	84.36	15.73
	ECII 3	limestone	5.69	79.67	20.43
	ECII 8	limestone	5.77	76.64	23.46
	ECII52	limestone	6.75	44.75	55.38
	ECII 55	limestone	5.76	77.24	22.86
	ECII 57	limestone	6.00	68.59	31.51
	ECII 60	limestone	6.00	68.61	31.50
	ECII 74	limestone	6.18	62.33	37.78
	ECII 82	limestone	5.70	79.42	20.68
	Mean values :		***All lithologies***	**71.29**	**28.82**

Table E.2.3: Measurements of the content of smectite layers in samples from Angles, Combe-Lambert and Eclépens. All values in percents.

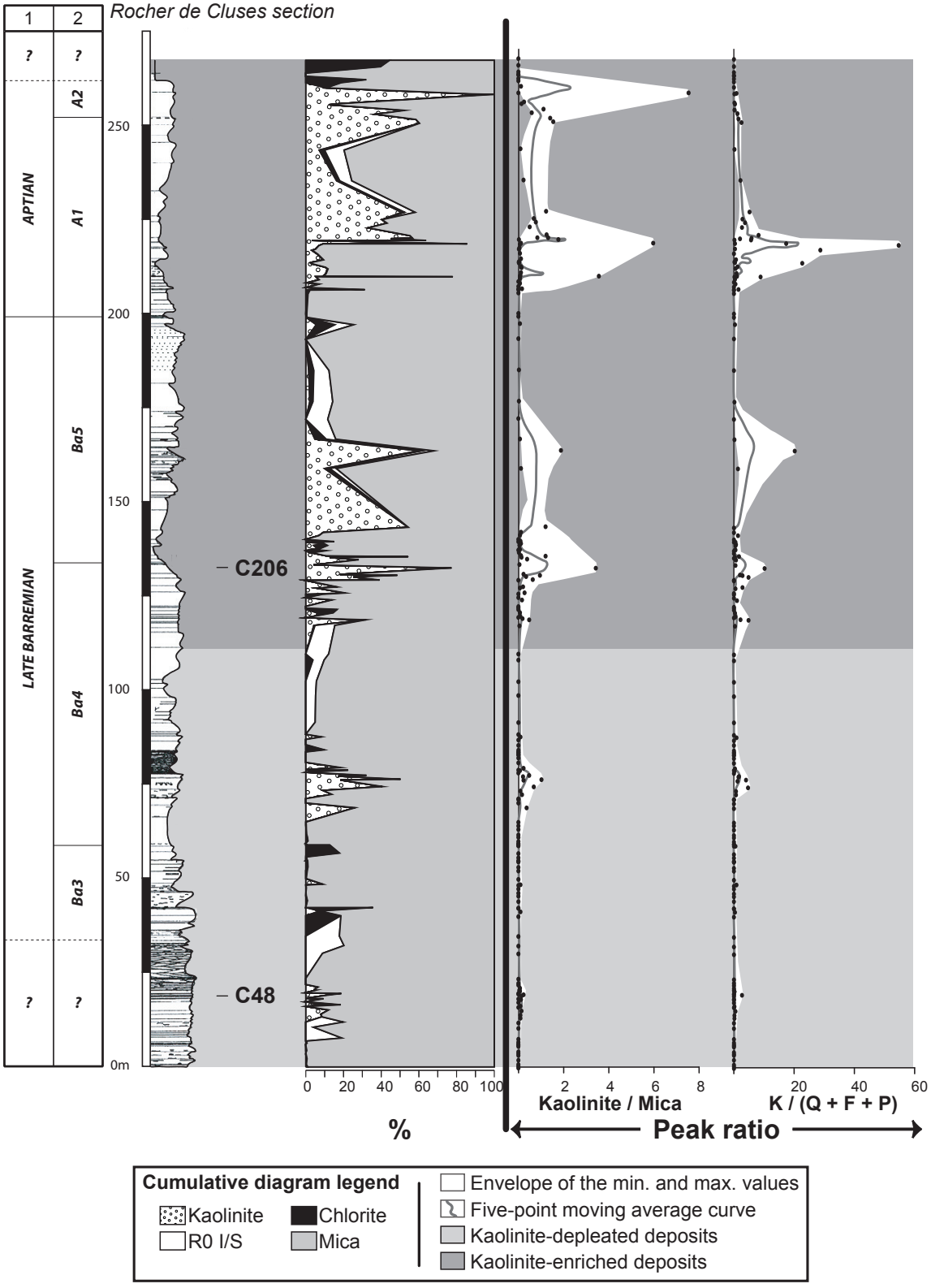

Figure E.2.4: Evolution of the clay-mineral assemblage of the insoluble residue (<2μm fraction) of the Cluses section. On the left part of the figure, the numbers on top of the columns correspond to the 1) stratigraphic stages and 2) depositional sequences (after Wermeille, 1996). On the right, the evolution of the kaolinite/mica and kaolinite/(quartz + feldspar + phyllosilicates) ratios reveals the dominance of kaolinite from the upper part of the Ba4 depositionnal sequence (Late Barremian) to the top of the section (A2 sequence, Early Aptian). Sample numbers refer to the diffractograms E and F displayed in Fig. E.2.6. Abbreviations of the minerals: K = Kaolinite: Q = Quartz; F = potassic feldspar; P = sodic plagioclase.

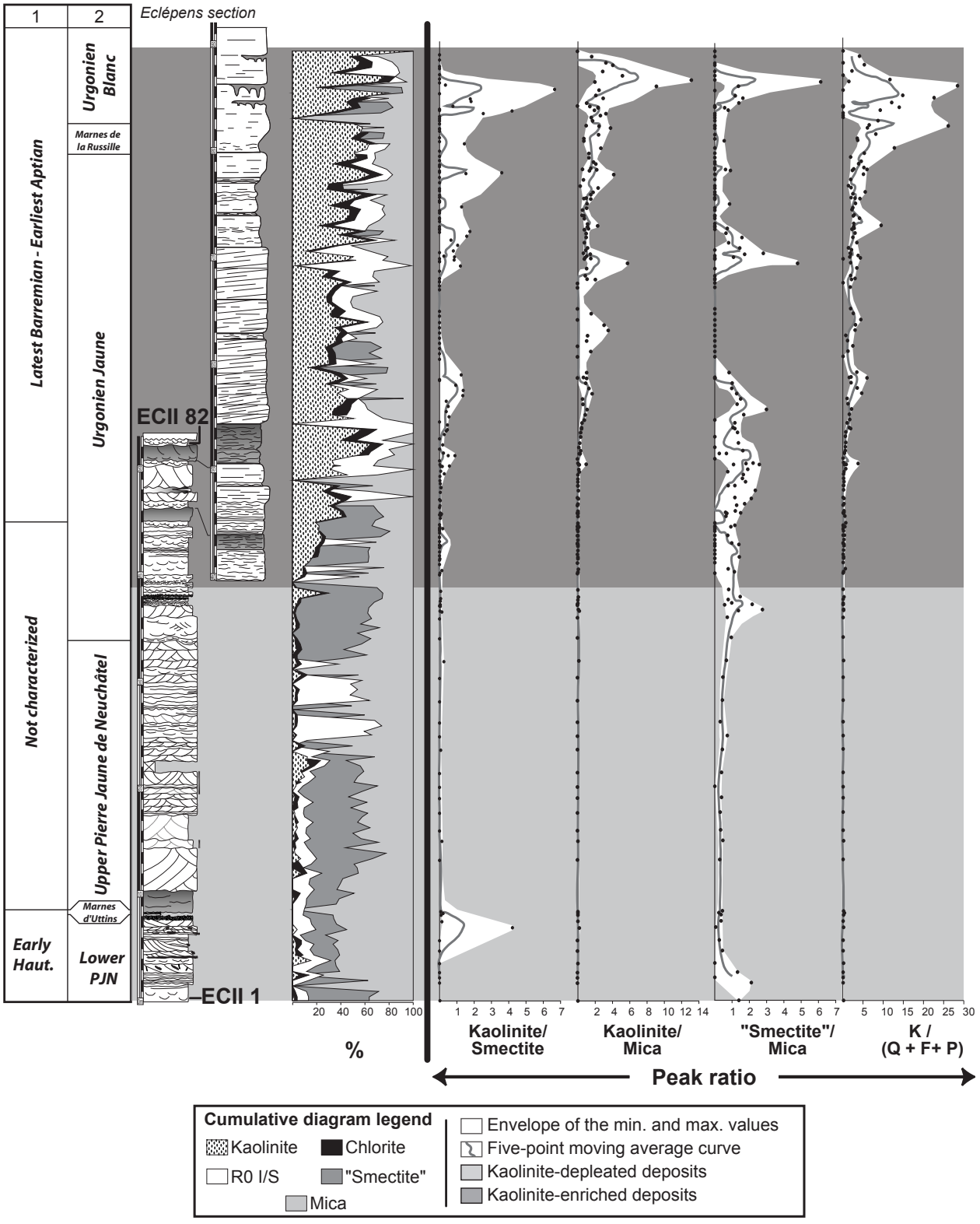

Figure E.2.5: Evolution of the clay-mineral assemblage of the insoluble residue (<2μm fraction) of the Eclépens section. On the left part of the figure, the numbers on top of the columns correspond to the 1) stratigraphic stages (after Godet et al., 2005) and 2) formations. On the right, the curves of kaolinite/smectite, kaolinite/mica, and kaolinite/(quartz + feldspar + phyllosilicate) ratios point out the dominance of the kaolinite throughout the Urgonian limestone, whereas sediments from the Pierre Jaune de Neuchâtel contain almost no kaolinite. Sample numbers refer to the diffractograms A and B displayed in Fig. E.2.6. Abbreviations of the minerals: K = Kaolinite: Q = Quartz; F = potassic feldspar; P = sodic plagioclase.

ID	Depth [m]	Stage	Ammonite Zone	TOC [%]	MINC [%]	HI [mgHC/g TOC]	OI [$mgCO_2$/g TOC]	Tmax [∝C]
AN29b	15.35	Late Hauterivian	*B. balearis*	0.39	8.03	82	137	435
AN30b	15.82	Late Hauterivian	*B. balearis*	0.65	6.74	94	84	437
AN31b	16.12	Late Hauterivian	*B. balearis*	0.47	7.54	93	95	434
AN32b	16.65	Late Hauterivian	*B. balearis*	2.63	3.20	254	35	434
AN33b	17.35	Late Hauterivian	*B. balearis*	1.49	4.76	207	73	438
AN34b	17.94	Late Hauterivian	*B. balearis*	0.35	9.15	70	129	435
AN35b	18.29	Late Hauterivian	*B. balearis*	0.71	7.51	123	113	437
AN37b	19.00	Late Hauterivian	*S. angulicostatum*	1.44	4.79	191	50	438
AN38b	19.47	Late Hauterivian	*S. angulicostatum*	1.08	5.29	101	83	437
AN39b	19.94	Late Hauterivian	*S. angulicostatum*	0.77	5.87	88	88	435
AN40b	20.41	Late Hauterivian	*S. angulicostatum*	1.14	5.06	104	85	437
AN41b	20.59	Late Hauterivian	*S. angulicostatum*	1.73	3.46	130	55	439
AN42b	21.00	Late Hauterivian	*S. angulicostatum*	1.15	4.99	106	65	437
AN43b	21.29	Late Hauterivian	*S. angulicostatum*	0.73	7.24	95	66	439
AN44b	21.59	Late Hauterivian	*S. angulicostatum*	0.65	6.17	80	84	440
AN45b	21.82	Late Hauterivian	*S. angulicostatum*	1.37	1.81	84	63	437
AN46b	22.35	Late Hauterivian	*S. angulicostatum*	2.13	1.89	181	51	436
AN48b	23.29	Late Hauterivian	*S. angulicostatum*	1.11	4.22	109	140	438
AN51b	24.53	Late Hauterivian	*S. angulicostatum*	1.09	10.18	345	42	434
AN52b	25.06	Late Hauterivian	*S. angulicostatum*	1.49	7.97	256	48	434
AN53.1b	25.18	Late Hauterivian	*S. angulicostatum*	1.09	10.16	342	45	434
AN72b	33.87	Early Barremian	*A. kiliani*	0.50	6.42	65	111	437
AN73b	34.43	Early Barremian	*A. kiliani*	0.65	5.42	109	69	435
AN74b	34.74	Early Barremian	*A. kiliani*	0.66	4.78	105	80	432
AN75b	35.37	Early Barremian	*A. kiliani*	0.82	5.19	151	44	437
AN76b	35.68	Early Barremian	*A. kiliani*	0.39	7.60	94	89	435

Table E.2.4: Results of the Rock Eval analyses performed on marls from the *B. balearis* to the *A. kiliani* ammonite zones (Angles section).

reached in the *B. balearis* ammonite zone, under the Faraoni Level equivalent. The HI values are relatively low within the dataset, but an increase in noted around the Faraoni Level equivalent, with a maximum of 345 mgHC/gTOC. Finally, the measured Tmax are somewhat high, with a mean value of 436°C (extreme values of 432 and 440°C).

E.2.4.2. The Cluses section

In contrast to the Angles and Combe-Lambert sections, smectite is absent in the analysed clay-mineral assemblage of this section: only mica, kaolinite, chlorite and mixed-layer clay minerals were identified (n = 194, Fig. E.2.4; see also Table E.2.2 and Fig. E.2.6 for an example of diffractograms). In some samples, the nature of the mixed-layers has been identified: corrensite and rectorite are characterized by peaks at 6.0 and 6.5 °2θ, respectively, and sometimes by a superstructure near 3 °2θ which appears on diffractograms of glycolate-saturated samples. As these minerals are absent in most of the samples, they were not included in the quantification calculation (except for the samples illustrated by their diffractogram in Fig. E.2.6).

In the Cluses section, some narrow intervals are enriched in kaolinite at the base and the top of the depositional sequence Ba4; then, a major episode of enrichment in this mineral is noted from the base of the Ba5 sequence upward, with maximum values reaching more than 50%. Kaolinite contents remains also high in sediments of Aptian age. This trend in kaolinite contents is also well expressed in the curves of the kaolinite/mica and kaolinite/(Qz+Fk+Pl) ratios (Fig. E.2.4; see also Table E.2.2).

E.2.4.3. The Eclépens section

Mica, kaolinite, “smectite”, chlorite, and R0 I/S were identified in the <2μm fraction of sediments from Eclépens (n = 186 in Fig. E.2.5; see also Table E.2.2 and Fig. E.2.6 for an example of diffractograms).

The most characteristic feature of the clay assemblage in this section is the antagonistic behaviour of “smectite” and kaolinite contents: “smectite” contents vary from 50% in the PJN to 0% in the UB, whereas kaolinite is mostly absent in the PJN and only appears in sediments above the boundary between the PJN and the UJ, with values reaching more than 50%.

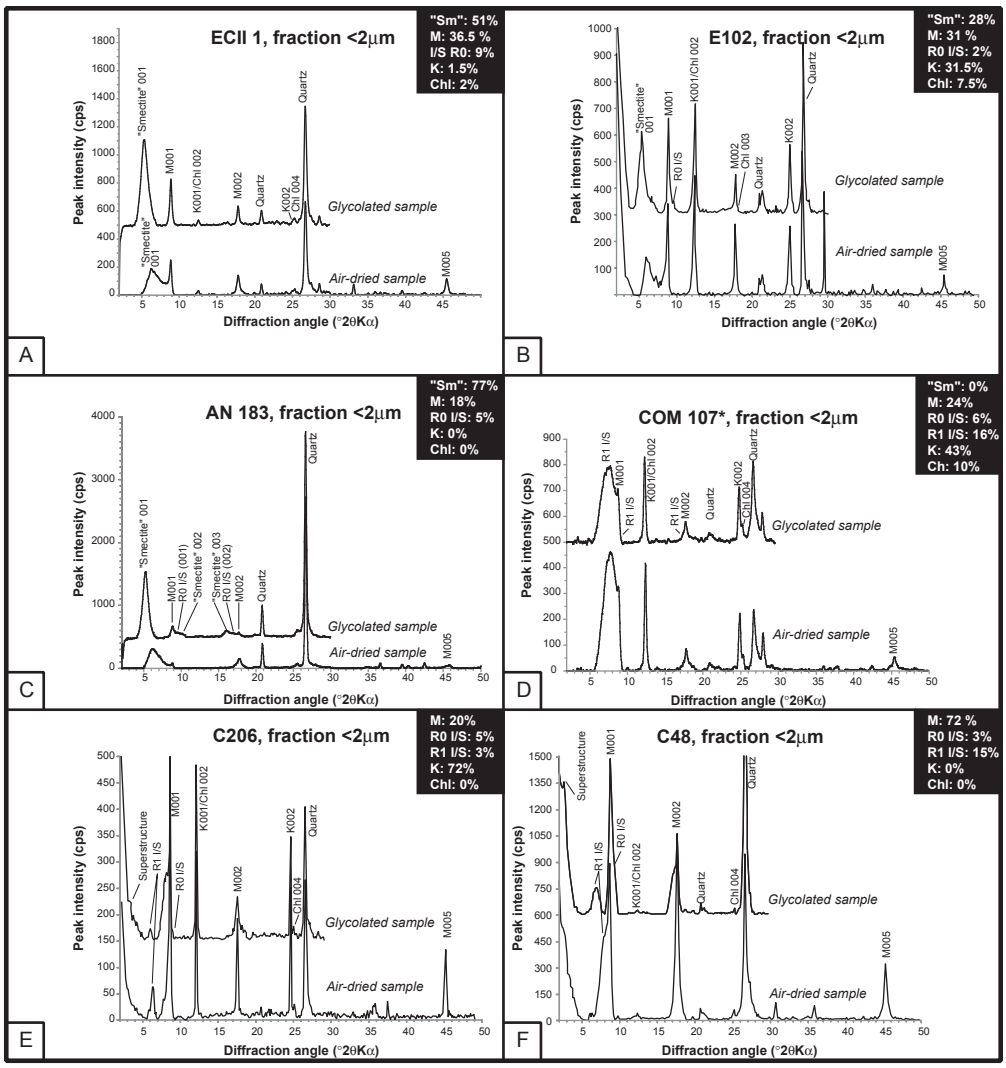

Figure E.2.6: Diffractograms characteristic of the studied sections. A: sample ECII1 (oolitic grainstone), Early Hauterivian, base of the Eclépens section; B: sample E102 (bioclastic packstone), Late Barremian – earliest Aptian, Eclépens section; C: sample AN183 (hemipelagic mudstone), M. sarasini ammonite zone (Late Barremian), Angles; D: sample COM107* (hemipelagic marlstone), boundary between the Deshayesites oglanlensis and D. weissi ammonite zones (Early Aptian), Combe-Lambert; F: sample C45 (bioclastic packstone), base of the Cluses section; E: sample C206 (peloidal grainstone to packstone with large benthic foraminifera), top of the depositional sequence Ba4 (Late Barremian), Cluses. Abbreviations of the minerals: "Sm" = "Smectite"; Sm = Smectite; M = Mica; K = Kaolinite; Chl = Chlorite.

E.2.5. Discussion

E.2.5.1. Reliability of the clay-mineral record

Clay minerals are formed in terrestrial soils, and have the potential to be subsequently eroded and exported to the ocean. Their genesis depends both on the lithological characteristics of the substratum as well as on the prevailing climate. For example, smectite may form in soils exposed to a dry, seasonally well-contrasted climate or it may be also the result of the weathering of basalts (Chamley, 1989). Clay-mineral assemblages may then fractionate during their transport to the ocean - for example due to sea-level change and the shelf morphology, thereby perturbing the original environmental signal. Once deposited in the sedimentary environment clay-mineral compositions may be further modified by diagenetic processes (e.g., Chamley, 1989; Kübler and Jaboyedoff, 2000). The late diagenetic overprint is dependent on the original sediment composition, the degree of burial diagenesis and eventually also its tectonic history. Deconinck and Debrabant

(1985) studied limestones-marls alternations of Berriasian age from the Vergons section (southeastern France), where smectite contained in marl would preferentially transform into illite (and to a lesser extend into chlorite), whereas in limestone smectite would mainly convert into chlorite. Moreover, smectite is very sensitive to high temperatures linked to the burial and / or the tectonic history of the region: Ferry et al. (1983) interpreted the transformation of smectite into chlorite in sediments belonging to the Valanginian of the Vocontian Trough as the result of increasing thermal diagenesis, which may have affected carbonates more strongly than marls. The diagenetic transformation of smectite is also accompanied by the appearance of mixed-layered minerals, such as in Tithonian – Berriasian sediments of the Vergons section and in sediments from the early Cretaceous of the Daluis section (Deconinck and Debrabant, 1985). All these mechanisms fractionating and transforming clay mineral assemblages may led to a misreading of the original climatic signal. This implies that the integrity of the clay-mineral assemblage is to be tested before its interpretation as a signal of the prevailing climate and changes therein.

E.2.5.1.1. Angles and Combe-Lambert

During the Cenozoic, the alpine orogenetic phase led to the formation of thrusts sheets in sediments belonging to the Vocontian Trough, and in particular the formation of the "nappe de Dîgne" had an impact on the thermal evolution of the Hauterivian – Barremian succession in the sections of Angles and Combe-Lambert (e.g., van de Schootbrugge et al., 2000). The associated tectonic overprint of clay-mineral assemblages did not completely obliterate their environmental signal: both the preservation of high contents of "smectites" and kaolinite compared to R0 I/S, as well as the absence of regular mixed-layers indicate low to medium diagenetic overprint. This is coherent with the amount of illite layers within the R0 I/S, which reaches an average value of 30% in the Angles and Combe-Lambert sections (all lithologies). On the other hand, the higher proportion of chlorite preserved in limestones compared to marls may have been the consequence of quite strong diagenetic overprint (e.g., Deconinck and Chamley, 1983; Deconinck, 1987). But, as "smectites" display a similar behaviour, a change from humid to dryer conditions between marls and limestones may have controlled, at least in part, the distribution of both chlorite and "smectites" between the two lithologies. This is in agreement with the content of R0 I/S, which remains the same whatever the lithology. The better preservation of "smectite" in limestones compared to marls may also be a function of the lithology: Burkhard (1988) and Huon et al. (1994) reported the presence of well-crystallised smectite in micrite from the Doldenhorn nappe (Helvetic Alps), which reached temperatures of 300 to 350°C during at least 10 millions years; this suggests that the fine-grained, carbonated lithology constitutes a protection against thermal diagenesis, which is in contradiction with the conclusions of Ferry et al. (1983).

Moreover, the IC values are highly variable, ranging from 0.15 to 0.2 °2θ in limestones, and from 0.35 to 0.4 °2θ in marls, which corresponds to values typical for the diagenetic zones 1 to 3 of Kübler and Jaboyedoff (2000). However, the increase of the IC in marls is certainly due to a higher content of "smectite" and R0 I/S compared to limestones, which may enlarge the peak 001 of the mica. The apparent thickness of this peak may therefore reflect a mixture of detrital illite and of mixed-layers.

On the other hand, Rock-Eval analyses were performed on 26 marl samples belonging to the *B. balearis* (Late Hauterivian) to the *A. kiliani* zones (Early Barremian) of Angles. In Fig. E.2.7, Tmax values reach 440°C (mean value of 436°C), which is consistent with the values obtained in the Vergons section by Baudin et al. (1999), who concluded a low degree of thermal diagenesis for this section. This implies that the sedimentary succession may have reached the beginning of the potential oil window and the zone of transition of the smectite to the R0 I/S (Espitalié et al., 1985; see also Fig. 23 in Kübler, 1997).

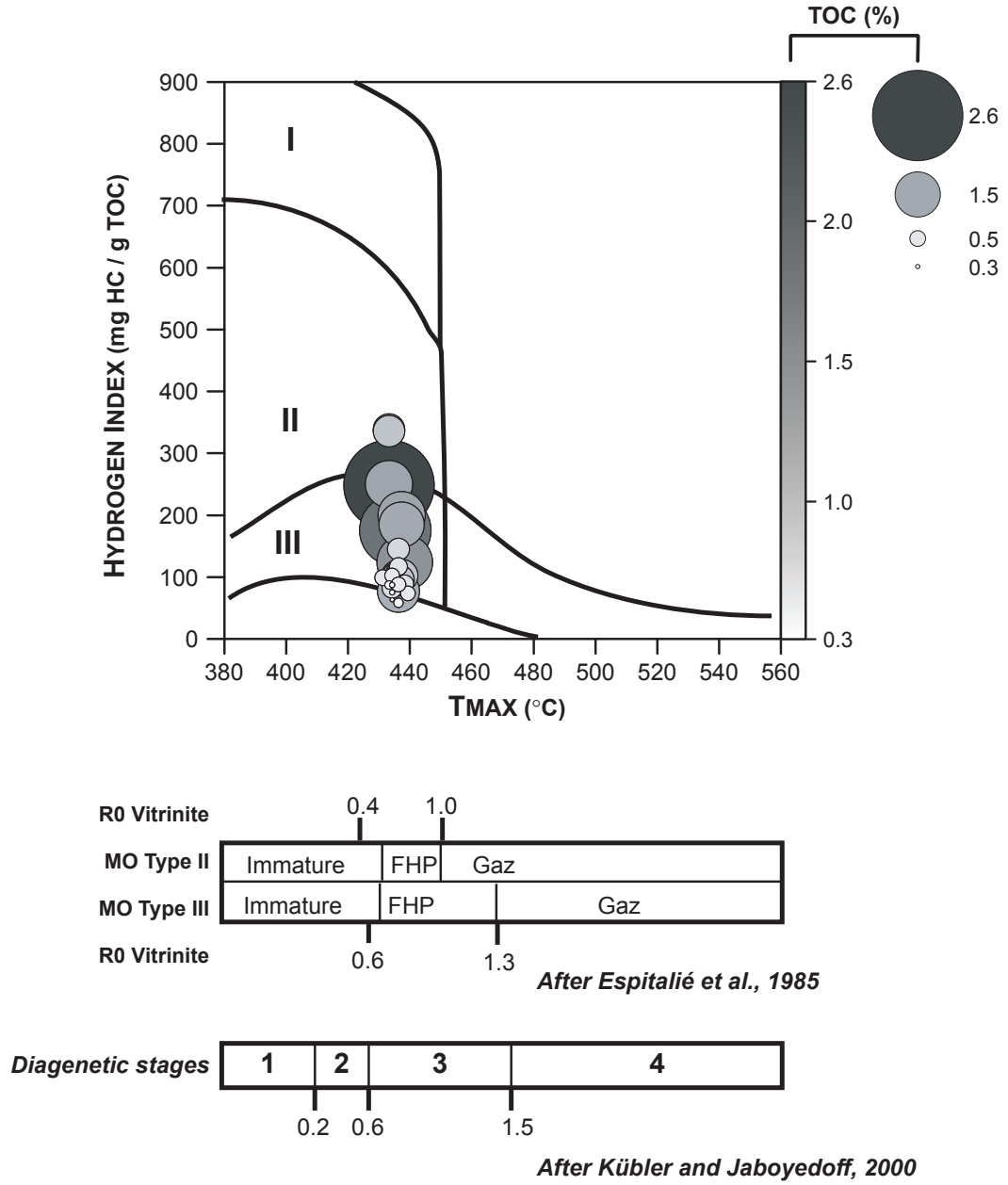

Figure E.2.7: Cross plot of the hydrogen index (HI) versus maximum of temperatures (Tmax) for marls corresponding to the Late Hauterivian – earliest Barremian interval of the Angles section. The shading and sizing of the bubbles corresponds to the total organic carbon (TOC) content. The evolution of kerogens and the correspondence of the diagenetic stages with respect to the reflectance of vitrinite is after Espitalié et al. (1985), and Kübler and Jaboyedoff (2000), respectively.

Finally, a recently published cross plot of $\delta^{13}C$ versus $\delta^{18}O$ measured at Angles (e.g., Wissler et al., 2002; Godet et al., 2006) reveals no clear correlation, and even if $\delta^{18}O$ displays relatively light values (minimum of -4.5‰ in Wissler et al., 2002), the trends observed in the stratigraphic evolution of $\delta^{18}O$ values at Angles can be correlated between the Vocontian Trough, the Ultrahelvetic realm in Switzerland and the Umbria-Marche basin in Italy, which excludes a strong diagenetic overprint at Angles (Godet et al., 2006).

All these parameters constrain the diagenetic overprint at Angles (and by extension at Combe-Lambert) close to the transition between stages 2 and 3 of Kübler and Jaboyedoff (2000). This implies that the main part of the clay-minerals assemblage is well-preserved in this succession, especially the kaolinite may have not suffered from diagenesis.

E.2.5.1.2. Cluses and Eclépens

At Cluses, diagenesis was more pronounced than at Angles and Combe-Lambert, as is suggested by the absence of smectite and the presence of rectorite and corrensite (Wermeille, 1996). However, the preservation of kaolinite suggests that the sedimentary succession underwent diagenetic overprint from the transition between stage 2 and 3 to the middle of the stage 4.

At Eclépens, the mineralogy of the clay fraction is more diversified, and includes some true smectites. This implies that diagenesis had a relatively low impact on the sedimentary succession, as is suggested by the rapid exhumation of the succession after a maximum burial depth of approximately 2500 m (Burkhard and Sommaruga, 1998). Moreover, the IC ranges between 0.25 and 0.3 °2θ (Blanc-Aletru, 1995); this implies that the majority of the mica from Eclépens has a detrital origin. Finally, the relative high content of smectite layers in R0 I/S (average value of approximately 71 %; see Table E.2.3) is another argument to conclude that the intensity of diagenesis did not exceed the middle of the diagenetic stage 2 of Kübler and Jaboyedoff (2000).

E.2.5.2. Climate change during the late Hauterivian – Early Aptian

A correlation based of the stratigraphic evolution of kaolinite is proposed between the Western Swiss Jura, the Subalpine Chains, and the Vocontian Trough, for the time period from the Early Hauterivian to the earliest Aptian (Fig. E.2.8). Kaolinite / smectite and smectite / mica ratios curves are also reported, where appropriate. In southeastern France and in the vicinity of Neuchâtel, clay-mineral assemblages are dominated by smectite during the Hauterivian. The lack of good age control at the base of the Cluses section, as well as diagenetic processes that may have transformed eventually present smectite into mixed-layer minerals, do not allow a firm correlation of this section with the two other domains for this interval.

In general, the dominance of “smectites” from the base of the Hauterivian stage to the *B. balearis* ammonite zone (mean value of 59%; extreme values of smectite for this interval: 20 to 81%), suggests the presence of a dry but seasonally contrasted climate (e.g., Chamley, 1989; Weaver, 1989).

Upwards, the evolution in kaolinite contents follows a threefold division, with low values in part I and III and an increase in part II; the same behaviour is reported for the evolution of the kaolinite / mica and the kaolinite / (quartz + feldspar + plagioclase) ratios. Kaolinite constitutes therefore the main mineral of the clay assemblage in the sections of Angles and Combe-Lambert for most of the Barremian. This conclusion is supported by the clay-mineral evolution from the Cluses section (Fig. E.2.4).

The presence of kaolinite implies warm or humid climates, under which well-drained continental areas may undergo intense biogeochemical weathering leading to the concentration of Al2O3 and the genesis of bauxite and associated kaolinite (e.g., Chamley, 1989; Weaver, 1989; Thiry et al., 1999). In the time interval from the *P. mortilleti* to the *Imerites giraudi* ammonite zones, the development of such soils may have been important on the southern European continent bordering the northern Tethyan margin, due to a shift from a seasonally well contrasted to a warmer and more humid climate during the latest Hauterivian (Fig. E.2.8). The stratigraphically highest peak in kaolinite content is observed in marly sediments near the SbB4 and this may reflect the predominance of humid conditions during the deposition of marls. However, an intensification of humid conditions during the *H. sayni* and the *H. feraudianus* ammonite zones is also suggested by the symmetric shape of this increase around the SbB4.

A comparison with the $\delta^{18}O$ measured on bulk-rock limestone samples from the Angles section (Godet et al., 2006) suggests a possible link between the variations in temperature mirrored by the main trends of the $\delta^{18}O$ curve

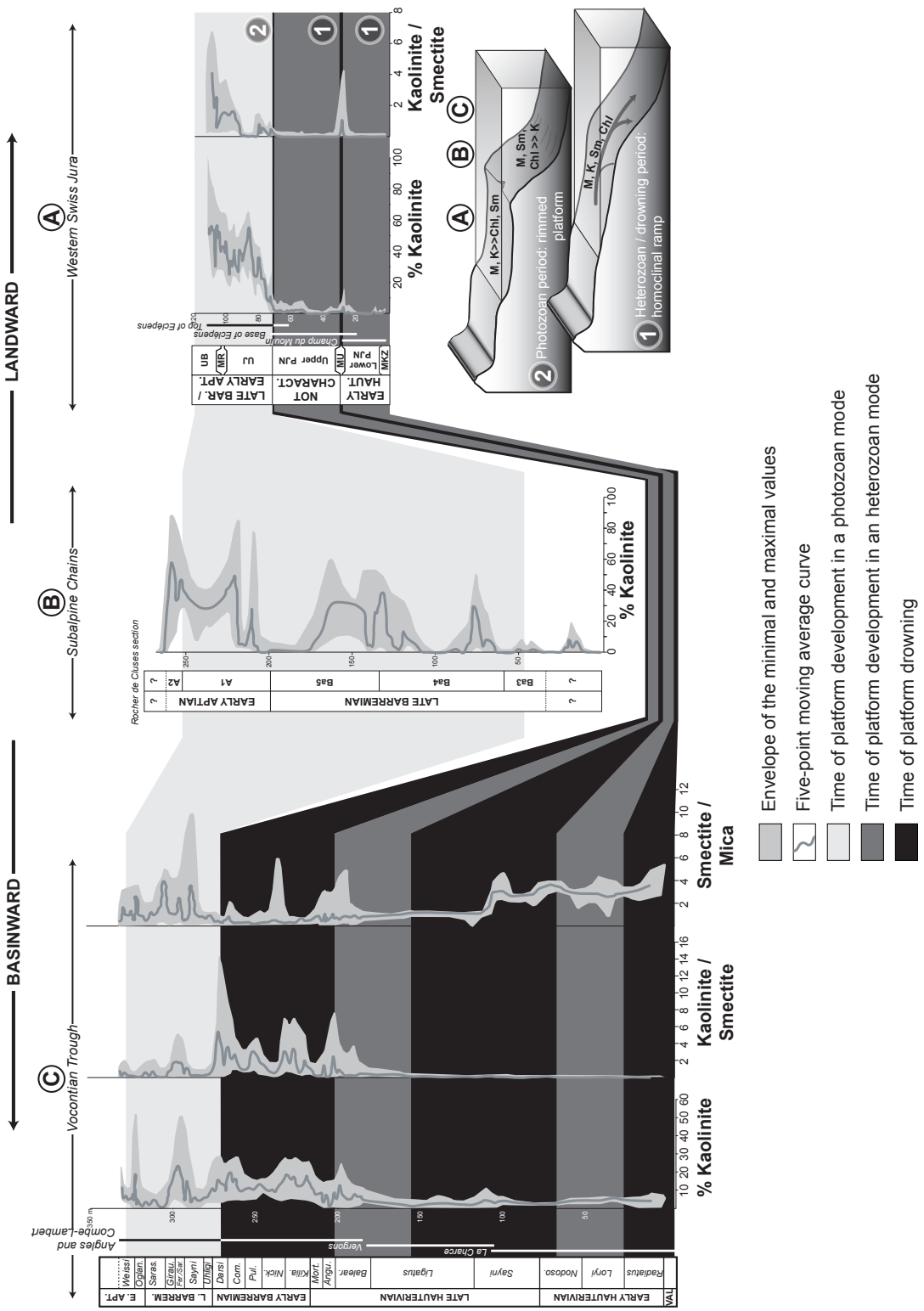

Figure E.2.8: Correlation between the Vocontian Trough (Angles and Combe-Lambert sections), the Subalpine Chains (Cluses section), and the Western Swiss Jura (Champ du Moulin and Eclépens sections), based on the kaolinite evolution. Both the relative abundance of kaolinite, as well as the kaolinite/smectite ratio are used, where appropriate. Bloc diagrams on the right side of the figure illustrate the morphology of the platform and the subsequent differential settling of clay-minerals during times of heterozoan and drowned platform (1), and photozoan platform (2); on the top on these two transects, the letters A, B and C indicate the theoretical position of the three studied regions along the margin. Note that data from Champ du Moulin (after Rumley, 1993; see Fig. E.2.1 for a location) complete the data from Eclépens for the lower PJN. Abbreviations of formations names: MKZ: Mergelkalk zone; MU: Marnes d'Uttins; MR: Marnes de la Russille.

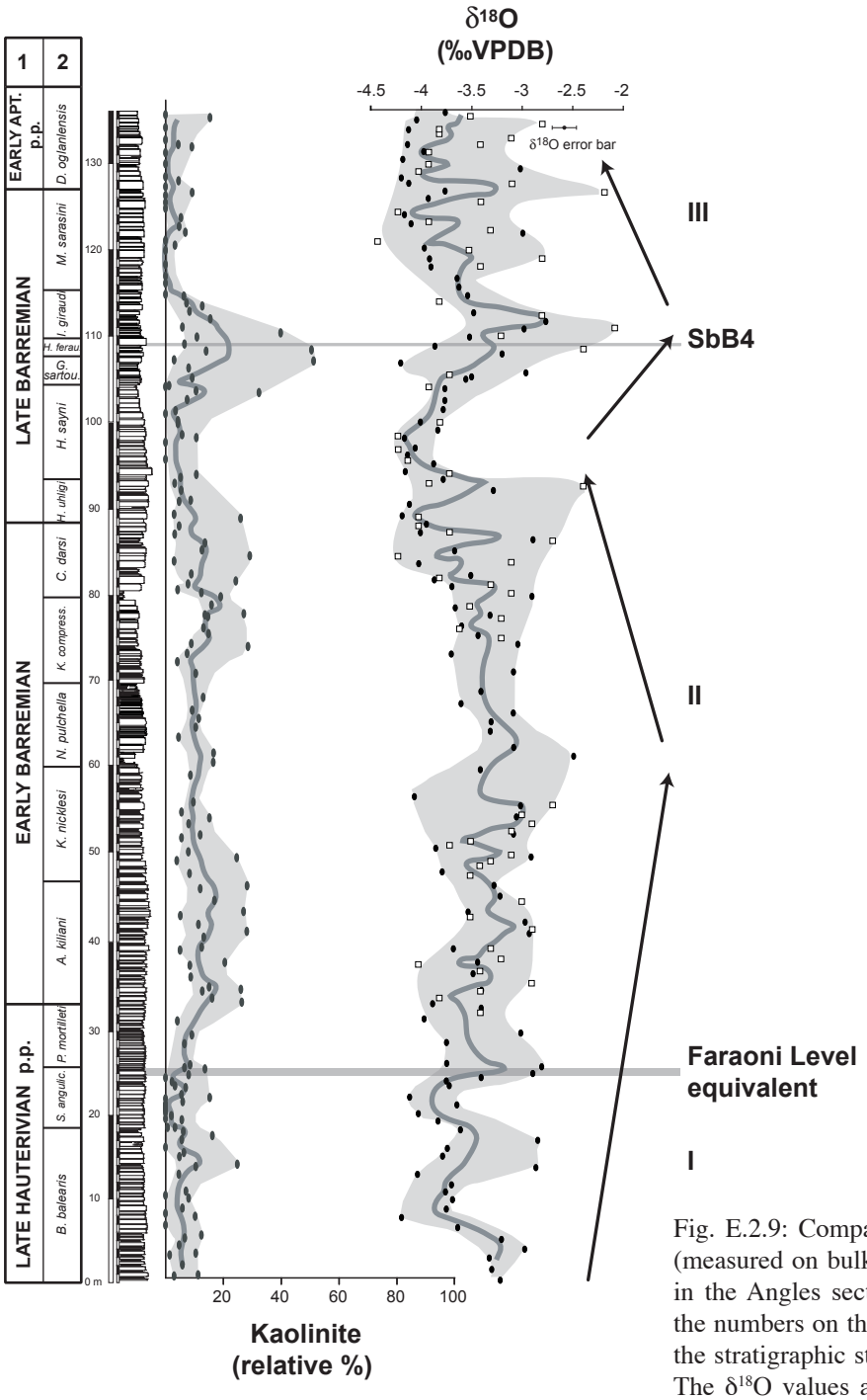

Fig. E.2.9: Comparison of the kaolinite and the $\delta^{18}O$ (measured on bulk-rock limestone samples) evolution in the Angles section. On the left side of the figure, the numbers on the top of the columns corresponds to the stratigraphic stage (1) and the ammonite zone (2). The $\delta^{18}O$ values are after Wissler et al. (2002; white squares), and Godet et al. (2006; black circles).

and the evolution of the kaolinite content (Fig. E.2.9). Effectively, Godet et al. (2006) described a four-fold evolution, with two maxima in $\delta^{18}O$ values at the base of the *N. pulchella* and in particular in the *I. giraudi* ammonite zones. Whereas the first maximum in the $\delta^{18}O$ record corresponds to a period characterized by stable but relatively moderate kaolinite contents, the second maximum follows immediately after the highest values recorded in the kaolinite evolution. The genesis of kaolinite requires a humid and warm climate; in the part II of the Angles section, the augmentation in kaolinite content may mirror an increased continental runoff, which may have constituted a sink for atmospheric CO_2. Subsequently, the greenhouse effect may have decreased and the temperature as well. As a consequence, the $\delta^{18}O$ values may

shift toward more positive values after episodes of high continental runoff, as the one recorded from the end of the *H. sayni* to the *I. giraudi* ammonite zones at Angles. Thereafter, the $\delta^{18}O$ returns to lighter values, reflecting an increase of temperature. Alternatively, the evolution of kaolinite is compatible with the $\delta^{18}O$ record, if the latter reflects salinity rather than temperature; during time of kaolinite dominance, the input of freshwater in the ocean may increase, as kaolinite genesis requires an increased rainfall. Consequently, the salinity of the surface ocean may decrease by dilution and the $\delta^{18}O$ may shift toward more negative values.

E.2.5.3. Kaolinite evolution from the Vocontian Trough to the western Swiss Jura: Evidence for differential settling

The evolution of kaolinite contents along the northern Tethyan margin from the late Early Barremian to the earliest Aptian reveals an ambiguous behaviour of this clay mineral: whereas the latest Barremian - earliest Aptian sedimentary record in the Western Swiss Jura is characterized by high kaolinite contents (Fig. E.2.6 and Table E.2.2), contemporaneous sediments deposited in the Vocontian trough are relatively impoverished in this mineral (Fig. E.2.4 and Table E.2.2). As the kaolinite content displays intermediate values in Aptian sediments from the Cluses section (Table E.2.2), a link between sea-level fluctuation, a change in the morphology of the carbonate platform, and migration of the depo-centre of kaolinite as a function of the distance from the coastline through sea-level change may explain this apparent decrease in kaolinite in distal directions along the northern Tethyan margin.

During the Hauterivian, a heterozoan assemblage dominated the carbonate-producing community along the northern Tethyan margin, whereas during the period between the *C. darsi* ammonite zone (late Early Barremian) and the *Deshayesites weissi* ammonite zone (Early Aptian), this assemblage progressively evolved into a photozoan ecosystem (Föllmi et al., 1994; 2006). In the period between the latest Hauterivian and late Early Barremian (*P. mortilleti* to the *C. darsi* ammonite zone), the Helvetic platform underwent a major drowning phase (Bodin et al., 2006b). An important difference between these two regimes of carbonate production is associated with the platform morphology: the Hauterivian heterozoan platform is interpreted as a ramp structure with a good connection to the ocean, whereas the late Early Barremian to Early Aptian photozoan platform developed a marginal rim consisting of patch reefs and oolitic shoals (e.g., Arnaud-Vanneau, 1980). The heterozoan platform structure was, for this reason, particularly favourable to the bypass of detrital continental material, such as clay minerals and quartz particles, into the open sea. The photozoan platform structure may, on the contrary, have functioned as a barrier for larger detrital particles such as kaolinite, and may have fractioned the clay-mineral assemblage transferred to the ocean in a way that the larger, less reactive kaolinite particles were trapped on the platform (see below).

In the Vocontian Trough, kaolinite is absent in sediments older than the latest Hauterivian (data from van de Schootbrugge, 2001), appears in sediments attributed to the *B. balearis* ammonite zone and reaches more than 30-40% in Early Barremian sediments (Fig. E.2.8). The absence of kaolinite and the dominance of smectite in most of the Hauterivian sediments may reflect a true climatic signal, which is in agreement with the type of carbonate platform that developed at that time, under high nutrient conditions (e.g., van de Schootbrugge et al., 2003; Bodin et al., 2006a). During the latest Hauterivian, the appearance of kaolinite indicates a change from a seasonally contrasted towards a more humid and warm (intertropical) climate that can be linked to an acceleration of the hydrologic cycle, and with that an increase in continental run-off. The related enhanced supply of phosphorus and of Dissolved Inorganic carbon (DIC) to the ocean may have been triggered by intensified biogeochemical weathering, as already suggested by Bodin et al. (2006) and Godet et al. (2006). The latter linked

the very stable evolution of the $\delta^{13}C$ record observed from the base of *the P. mortilleti* to the top of the *C. darsi* ammonite zone to an increase of the oceanic DIC volume in the ocean, which may have buffered the $\delta^{13}C$ signal against paleoceanographic change (see Bartley and Kah (2004) for a detailed explanation of the DIC buffering effect on the $\delta^{13}C$ record). As a consequence of the change towards a warmer and wetter climate during the latest Hauterivian and a corresponding increase in phosphorus input into the ocean, the northern Tethyan carbonate platform drowned (during the period between the *S. angulicostatum* and the *C. darsi* ammonite zones; Arnaud-Vanneau and Arnaud, 1990; Bodin et al., 2006b).

Then, from the *Gerhadtia sartousiana* ammonite zone onward, carbonate production took up again on the platforms of the northern Tethys, and this especially in the Vercors and the Helvetic Alps (Arnaud-Vanneau and Arnaud, 1990; Föllmi et al., 1994; 2006; Bodin et al., 2006c); corals, green algae, stromatoporoids and associated rudists recovered in the platform sediments of this period are typical of a photozoan assemblage (e.g., James, 1997; Mutti and Hallock, 2003). During the time of carbonate production in a photozoan mode, the presence of a barrier or a reef that separated the platform from the basin, as well as the morphology of the platform may have led to a fractionation of clay minerals during its transfer to the ocean. This is related to the size of kaolinite crystals (and consequently its weight) as well as its high capacity to flocculate (Ruffell et al., 2002), which both may have favoured the deposition of this mineral after a relatively brief transport in the ocean (e.g. Gibbs, 1977; Hallam, 1984), and may have led to a decrease of the kaolinite content toward the basin. Moreover, this differential settling of clay particles may have been enhanced by changes in sea-level. During sea-level rise and subsequent sea-level highstand, the shelf area increases and the distance between the continent where kaolinite was formed and the basin becomes more important. Moreover, the diversity and the development of facies susceptible to trap detrital particles are the highest within highstand deposits. This implies that kaolinite may be deposited in proximal shelf settings rather than in hemipelagic environments during periods of high sea-level. This may also explain the difference in the quantity of kaolinite deposited along the northern Tethyan margin during the latest Barremian and earliest Aptian, as this time span corresponds to a long-term maximum in eustatic sea level (Haq et al., 1987; Arnaud, 2005).

This fractionation pattern with regards to the kaolinite distribution in clay-mineral assemblages has already been suggested for the Valanginian-Hauterivian carbonate platform (Adatte and Rumley, 1989), and for the middle Jurassic succession (Bolle et al., 1996) of the Western Swiss Jura. Sediments from a platform developing in a photozoan mode may as a consequence record a faithful climatic signal, whereas in the adjacent hemipelagic setting the preserved clay-mineral assemblage may have been fractionated and the climate signal correspondingly altered. Consequently, looking at the clay-minerals evolution along a platform to basin transect may be more useful than considering only pelagic sections when attempting to trace climate change.

E.2.6. Conclusions

The evolution of clay-mineral assemblages during the Hauterivian, Barremian and earliest Aptian along a platform-basin transect in the northern Tethys highlights the dominance of smectite and the quasi absence of kaolinite in sediments up to the latest Hauterivian. During the latest Hauterivian to the Early Aptian, kaolinite becomes abundant, which may indicate a general change from a seasonally contrasted, temperate climate prevailing during the Hauterivian to a warmer and wetter climate in the period from the latest Hauterivian to the earliest Aptian for the southern European realm adjacent to the Northern Tethys. The increased humidity and enhanced continental runoff may have triggered elevated input of nutrients

and DIC in the ocean. The latter may have contributed to initiate the anoxia characteristic of the Faraoni Level, and also to buffer the $\delta^{13}C$ signal.

The distribution of clay minerals along this transect was not only influenced by climate change, but also by the morphology of the platform and by sea-level change. During the Hauterivian, the ramp-type morphology of the northern Tethyan platform may have favoured a direct transport of clay particles into the basin without major fractionation. From the *B. balearis* to the *C. darsi* ammonite zone, the Helvetic platform underwent a major phase of drowning, which may have also facilitated the transport of clay toward the basin. The re-installation of the carbonate platform in a photozoan mode near the Early - Late Barremian boundary and the development of a marginally rimmed platform topography – together with general sea-level rise - may have fractionated the clay-mineral assemblages during their transport into the basin, with the preferred deposition of kaolinite in proximal settings, and the subsequent depletion of this mineral in distal environments. This highlights the importance of comparing several sections distributed along a proximal – distal transect, in order to better constrain climatic changes by means of clay mineralogy.

E.2.7. Acknowledgements

The authors acknowledge Laureline Scherler and Laurent Chalumeau (University of Neuchâtel) for the preparation of the samples from Angles with regards to the clay-mineral analysis, Philipp Steinmann (University of Neuchâtel) for performing the Rock Eval analyses, and Stéphane Westermann (University of Neuchâtel) for the help in sampling and measuring the Combe-Lambert section. We thank the staff of the Eclépens quarry (Holcim company), for allowing us to sample the Eclépens section. This research is financially supported by the Swiss National Fund (projects n°2100-067807/1 and 200020-105206/1). The reviews of Cédric John, Thomas Pletsch and Alastair Ruffell greatly improved the quality of this manuscript.

E.2.8. References

Adatte, T., Rumley, G., 1989. Sedimentology and mineralogy of the Valanginian and Hauterivian in the stratotypic region (Jura mountains, Switzerland). In: Wiedmann, J. (Ed.), Cretaceous of the Western Tethys: proceedings of the 3rd International Cretaceous Symposium, Tübingen 1987, Stuttgart, E. Schweizerbart'sche Verlagsbuchhandlung (Nägele u. Obermiller), pp 329-351.

Adatte, T., Stinnesbeck, W., Keller, G., 1996. Lithostratigraphic and mineralogic correlations of near K/T boundary sediments in northeastern Mexico: Implications for origin and nature of deposition. In: Ryder, G., Fastovsky, D., Gartner, S. (Eds.), The Cretaceous-Tertiary Event and Other Catastrophes in Earth History, Boulder, Colorado, Geological Society of America Special Paper 307, pp 211-226.

Arnaud, H., 2005. The South-East France Basin (SFB) and Its Mesozoic Evolution. Géologie Alpine Série Spéciale «Colloques et Excursions» N°7, 5-28.

Arnaud-Vanneau, A., 1980. Micropaléontologie, paléoécologie et sédimentologie d'une plate-forme carbonatée de la marge passive de la Téthys: l'Urgonien du Vercors septentrional et de la Chartreuse (Alpes occidentales). Géologie Alpine Grenoble Mém HS 10, 874 p.

Arnaud-Vanneau, A., Arnaud, H., 1990. Hauterivian to Lower Aptian carbonate shelf sedimentation and sequence stratigraphy in the Jura and northern Subalpine chains (southeastern France and Swiss Jura). In: Tucker, M. E., Wilson, J. L., Crevello, P. D., Sarg, J. R., Read, J. F. (Eds.), Carbonate Platforms: Facies, Sequences and Evolution,

Blackwell Scientific Publications, Special Publication of the International Association of Sedimentologists, 9, pp 203-233.

Bartley, J. K., Kah, L. C., 2004. Marine carbon reservoir, Corg - Ccarb coupling, and the evolution of the Proterozoic carbon cycle. Geology 32, 129-132.

Baudin, F., 2005. A Late Hauterivian short-lived anoxic event in the Mediterranean Tethys: the «Faraoni Event». Comptes Rendus de l'Académie des Sciences de Paris.

Baudin, F., Bulot, L. G., Cecca, F., Coccioni, R., Gardin, S., Renard, M., 1999. Un équivalent du «Niveau Faraoni» dans le Bassin du Sud-Est de la France, indice possible d'un événement anoxique fini-hauterivien étendu à la Téthys méditerranéenne. Bull. Soc. géol. France 170, 487-498.

Behar, F., Beaumont, V., De B. Penteado, H. L., 2001. Rock-Eval 6 technology: performances and developments. Oil & Gas Science and Technology - Rev. IFP 56, 111-134.

Berner, R. A., Kothavala, Z., 2001, Geocarb III: a revised model of atmospheric CO_2 over Phanerozoic time. American Journal of Science 301, 182-204.

Blanc-Aletru, M. C., 1995, Importance des discontinuités dans l'enregistrement sédimentaire de l'Urgonien jurassien. Micropaléontologie, Sédimentologie, Minéralogie et Stratigraphie Séquentielle, Géologie Alpine, Ph.D. Thesis Grenoble, Laboratoire de Géologie de l'Université I de Grenoble, p. 299 pp.

Bodin, S., Godet, A., Vermeulen, J., Arnaud, H., Strasser, A., Fiet, N., Adatte, T., Föllmi, K. B., 2006a. The late Hauterivian Faraoni oceanic anoxic event in the western Tethys: Evidence from phosphorus burial rates. Palaeogeography, Palaeoclimatology, Palaeoecology 235, 245-264.

Bodin, S., Godet, A., Vermeulen, J., Linder, P., Föllmi, K. B., 2006b. Biostratigraphy, sedimentology and sequence stratigraphy of the latest Hauterivian - early Barremian drowning episode of the Northern Tethyan margin (Altmann Member, Helvetic Nappes, Switzerland). Eclogae Geologicae Helveticae, in press.

Bodin, S., Vermeulen, J., Godet, A., Föllmi K. B., 2006c. New data on the age of the installation of Urgonian-type carbonates along the northern Tethyan margin: biostratigraphy of the Chopf Member (Helvetic Alps, eastern Switzerland). C.R. Geoscience 338, 727-733

Bolle, M.-P., Adatte, T., Mangold, C., Remane, J., 1996. Microfaciès, minéralogie, stratigraphie du Dogger de la région du Furcil (NE). Bulletin de la Société neuchâteloise des Sciences Naturelles 119, 123-144.

Bulot, L. G., Thieuloy, J.-P., Blanc, E., Klein, J., 1992. Le cadre stratigraphique du Valanginien supérieur et de l'Hauterivien du Sud-Est de la France; définition des biochronozones et caractérisation de nouveaux biohorizons. Géologie Alpine 68, 13-56.

Burkhard, M., 1988. L'Helvétique de la bordure occidentale du massif de l'Aar (évolution tectonique et métamorphique). Eclogae Geologicae Helvetiae 81, 63-114.

Burkhard, M., Sommaruga, A., 1998. Evolution of the western Swiss Molasse basin: structural relations with the Alps and the Jura belt. In: Mascle, A., Puigdefàbregas, C., Luterbacher, H. P., Fernàndez, M. (Eds.), Cenozoic foreland Basins of Western Europe, Geological Society Special Publications, 134, pp 279-298.

Cecca, F., Faraoni, P., Marini, A., Pallini, G., 1995. Field-trip across the representative sections for the Upper Hauterivian-Barremian ammonite biostratigraphy in the Maiolica exposed at Monte Nerone, Monte Petrano and Monte Catria (Umbria-Marche, Apennines). Memorie Descrittive della Carta Geologica d'Italia 51, 187-211.

Chamley, H., 1981. Long-term trends in clay deposition in the ocean. Oceanologica Acta n°SP Proceedings 26th International

Geological Congress, Geology of Oceans Symposium, Paris, July 7-17, 1980, 105-110.

Chamley, H., 1989. Clay sedimentology, Springer Verlag, Berlin, 623 pp.

de Montmollin, A., 1835. Mémoire sur le terrain Crétacé du Jura. Mémoires de la Société des Sciences Naturelles de Neuchâtel tome I, 49-65.

Deconinck, J.-F., 1987. Identification de l'origine détritique ou diagénétique des assemblages argileux: le cas des alternances marne-calcaire du Crétacé inférieur subalpin. Bulletin de la Société Géologique de France (8) t. III, 139-145.

Deconinck, J.-F., Chamley, H., 1983. Héritage et diagenèse des minéraux argileux dans les alternances marno-clacaires du Crétacé inférieur du domaine subalpin. Comptes Rendus de l'Académie des Sciences de Paris 297, 589-594.

Deconinck, J.-F., Debrabant, P., 1985. Diagenèse des argiles dans le domaine subalpin: rôles respectifs de la lithologie, de l'enfouissement et de la surcharge tectonique. Revue de Géologie Dynamique et de Géographie Physique 26, 321-330.

Delanoy, G., 1997. Biostratigraphie des faunes d'Ammonites à la limite Barrémien-Aptien dans la région d'Angles-Barrême-Castellane. Etude particulière de la famille des Heteroceratina Spath, 1922 (Ancyloceratina, Ammonoidea). Annales du Muséum d'Histoire Naturelle de Nice Tome XII, 1-270.

Espitalié, J., Deroo, G., Marquis, F., 1985. La pyrolyse Rock-Eval et ses applications. Revue de l'Institut Français du Pétrole 40, 563-579.

Ferrero, J., 1965. Dosage des principaux minéraux des roches par diffraction de Rayon X. Rapport C.F.P. (Bordeaux), inédit.

Ferrero, J., 1966. Nouvelle méthode empirique pour le dosage des minéraux par diffraction R.X. Rapport C.F.P. (Bordeaux), inédit.

Ferry, S., Cotillon, P., Rio, M., 1983. Diagenèse croissante des argiles dans des niveaux isochrones de l'alternance calcaire-marne valanginienne du bassin vocontien. Zonation géographique. Comptes Rendus de l'Académie des Sciences de Paris Série II 297, 51-56.

Föllmi, K. B., Godet, A., Bodin, S., Linder, P., 2006. Interactions between environmental change and shallow-water carbonate build-up along the northern Tethyan margin and their impact on the early Cretaceous carbon-isotope record. Paleoceanography, In press.

Föllmi, K. B., Weissert, H., Bisping, M., Funk, H., 1994. Phosphogenesis, carbon-isotope stratigraphy, and carbonate-platform evolution along the Lower Cretaceous northern Tethyan margin. Geological Society of America Bulletin 106, 729-746.

Gibbs, R. J., 1977. Clay mineral segregation in the marine environment. Journal of Sedimentary Petrology 47, 237-243.

Godet, A., Blanc-Aletru, M.-C., Bodin, S., Adatte, T., Föllmi, K. B., 2005. The Hauterivian-Barremian of the Western Swiss Jura around Neuchâtel. Géologie Alpine Série Spéciale «Colloques et Excursions» n°7, 79-96.

Godet, A., Bodin, S., Föllmi, K. B., Vermeulen, J., Gardin, S., Fiet, N., Adatte, T., Berner, Z., Stüben, D., van de Schootbrugge, B., 2006. Evolution of the marine stable carbone-isotope record during the early Cretaceous: A focus on the late Hauterivian and Barremian in the Tethyan realm. Earth and Planetary Science Letters 242, 254-271.

Hallam, A., 1984. Continental humid and arid zones during the Jurassic and Cretaceous. Palaeogeography, Palaeoclimatology, Palaeoecology 47, 195-223.

Haq, B. U., Hardenbol, J., Vail, P. R., 1987. The chronology of fluctuating sea level since the Triassic. Science 235, 1156-1167.

Hillier, S., 1989. Clay mineral diagenesis and organic maturity indicators in Devonian lacustrine mudrock from the Orcadian

Basin, Scotland: PhD thesis, University of Southampton, United Kingdom, 298 pp.

Huon, S., Burkhard, M., Hunziker, J.-C., 1994. Mineralogical, K-Ar, stable and Sr isotope systematics of K-white micas during very low-grade metamorphism of limestones (Helvetic nappes, western Switzerland). Chemical Geology (Isotope Geoscience Section) 113, 347-376.

James, N. P., 1997. The cool-water carbonate depositional realm. In: James, N. P., Clarke, J. A. D. (Eds.), Cool-water carbonates, Tulsa, Oklahoma, Society for Sedimentary Geology, SEPM Special Publication N° 56, pp 1-20.

Klug, H. P., Alexander, L., 1974. X-ray Diffraction Procedures for Polycrystalline and Amorphous Materials, John Wiley and Sons, Inc., New York, 992 pp.

Kübler, B., 1983. Dosage quantitatif des minéraux majeurs des roches sédimentaires par diffraction X. Cahiers de l'Institut de Géologie, Université de Neuchâtel, Suisse Série AX n°1.1 and 1.2, 13 p.

Kübler, B., 1987. Cristallinité de l'illite: méthodes normalisées de préparation, méthode normalisée de mesure, méthode automatique normalisée de mesure. Cahiers de l'Institut de Géologie, Université de Neuchâtel, Suisse Série ADX n° 2.

Kübler, B., 1997. Concomitant Alteration of Clay Minerals and Organic Matter During Burial Diagenesis. In: Paquet, H., Clauer, N. (Eds.), Soils and Sediments. Mineralogy and Geochemistry, Springer-Verlag, Berlin, pp 327-362.

Kübler, B., Goy-Eggenberger, D., 2001. La cristallinité de l'illite revisitée: un bilan des connaissances acquises ces trente dernières années. Clay Minerals 36, 143-157.

Kübler, B., Jaboyedoff, M., 2000. Illite Cristallinity. C.R. Ac. Sc. Paris, Sciences de la terre et des planètes / Earth & Planetary Sciences 331, 75-89.

Lafargue, E., Marquis, F., Pillot, D., 1998. Rock-Eval 6 Applications in Hydrocarbon Exploration, Production and Soils Contamination Studies. Oil & Gas Science and Technology 53, 421-437.

Larson, R. L., Erba, E., 1999. Onset of the mid-Cretaceous greenhouse in the Barremian-Aptian: Igneous events and the biological, sedimentary and geochemical responses. Paleoceanography 14, 663-678.

Moore, D. M., Reynolds, R. C. J., 1997. X-Ray diffraction and the Identification and Analysis of Clay Minerals, Oxford University Press, New York, 378 pp. pp.

Mutti, M., Hallock, P., 2003. Carbonate systems along nutrient and temperature gradients: some sedimentological and geochemical constraints. Int. J. Earth Sci. (Geol. Rundsch.) 92, 465-475.

Persoz, F., 1982. Inventaire minéralogique, diagenèse des argiles et minéralostratigraphie des séries jurassiques et crétacées inférieures du Plateau suisse et de la bordure sud-est du Jura entre les lacs d'Annecy et de Constance. Matériaux pour la Carte Géologiaue de la Suisse Nouvelle Série 155, 1-52.

Ruffell, A., Mc Kinley, J., Worden, R., 2002. Comparison of clay mineral stratigraphy to other proxy palaeoclimate indicators in the Mesozoic of NW Europe. Phil. Trans. R. Soc. Lond. 360, 675-693.

Ruffell, A. H., Batten, D. J., 1990. The Barremian-Aptian arid phase in western Europe. Palaeogeography, Palaeoclimatology, Palaeoecology 80, 197-212.

Rumley, G., 1993. Sédimentologie, minéralogie et stratigraphie de l'Hauterivien dans le Jura neuchâtelois et vaudois (Suisse), Université de Neuchâtel, Neuchâtel, 207 pp.

Schlanger, S. O., Jenkyns, H. C., 1976. Cretaceous oceanic anoxic events: causes and consequences. Geologie en Mijnbouw 55, 179-184.

Scholle, P. A., Arthur, M. A., 1980. Carbon Isotope Fluctuations in Cretaceous Pelagic

Limestones: Potential Stratigraphic and Petroleum Exploration Tool. American Association of Petroleum Geologists Bulletin 64, 67-87.

Środoń, J., 1980. Precise identification of illite / smectite interstratification by X-Ray powder diffraction. Clays and Clay Minerals 28, 401-411.

Thiry, M., Simon-Coinçon, S., Schmitt, J.-M., 1999. Paléoaltérations kaoliniques: signification climatique et signature dans la colonne sédimentaire. Comptes Rendus de l'Académie des Sciences de Paris, Sciences de la terre et des planètes 329, 853-863.

Trabold, G. L., 1996. Development of the Urgonian limestones in the Delphino Helvetic Realm (Northern Subalpine Chains, Haute-Savoie, France). Sedimentology, Sequence Stratigraphy and Biostratigraphy. Université de Genève, Publications du Département de Géologie et Paléontologie 20, 1-187.

van de Schootbrugge, B., 2001. Influence of paleo-environmental changes during the Hauterivian (early Cretaceous) on carbonate deposition along the northern margin of the Tethys: Evidence from geochemical records (C, O and Sr-isotopes, P, Fe, Mn): Ph.D. thesis, Université de Neuchâtel, Neuchâtel, 291 pp.

van de Schootbrugge, B., Föllmi, K. B., Bulot, L. G., Burns, S. J., 2000. Paleoceanographic changes during the early Cretaceous (Valanginian-Hauterivian): evidence from oxygen and carbon stable isotopes. Earth and Planetary Science Letters 181, 15-31.

van de Schootbrugge, B., Kuhn, O., Adatte, T., Steinmann, P., Föllmi, K., 2003. Decoupling of P- and Corg-burial following Early Cretaceous (Valanginian-Hauterivian) platform drowning along the NW Tethyan margin. Palaeogeography, Palaeoclimatology, Palaeoecology 199, 315-331.

Vermeulen, J., 2002. Etude stratigraphique et paléontologique de la famille des Pulchelliidae (Ammonoidea, Ammonitina, Endomoceratacea). Géologie Alpine Mémoire H.S. N°42, 333 pp.

Weaver, C. E., 1989. Clays, Muds, and Shales. Developments in Sedimentology, 44, Elsevier Science Publishers B. V., Amsterdam, 819 pp.

Weissert, H., 1989. C-Isotope stratigraphy, a monitor of paleoenvironmental change: a case study from the Early Cretaceous. Surveys in Geophysics 10, 1-61.

Weissert, H., Lini, A., Föllmi, K. B., Kuhn, O., 1998. Correlation of Early Cretaceous carbon isotope stratigraphy and platform drowning events: a possible link? Palaeogeography, Palaeoclimatology, Palaeoecology 137, 189-203.

Wermeille, S., 1996. Etude sédimentologique, minéralogique et micropaléontologique des calcaires urgoniens de la région subalpine (Savoie, France). Coupes du Rocher de Cluses, du Borne et d'Andey: Unpublished diploma thesis, University of Neuchâtel, Neuchâtel, 129 pp.

Wissler, L., Weissert, H., Masse, J.-P., Bulot, L. G., 2002. Chemostratigraphic correlation of Barremian and lower Aptian ammonite zones and magnetic reversals. Int. J. Earth Sci. (Geol. Rundsch.) 91, 272-279.

Appendix 2.

Data

The Tierwis section on the left of the refuge (ct. St. Gallen, Switzerland)

ICP-MS data

Fiume-Bosso section

Stage	Ammonite zone	Sample n°	Li	Be	B	Mg	Al	K	Ca
Late Hauterivian	*B. balearis - P. ligatus*	FB2	1.57	0.07	30.43	2449.70	829.79	183.74	394683.75
		FB5	1.10	0.14	14.58	2462.87	653.24	148.50	401378.19
		FB8	0.65	0.17	4.78	2710.76	498.19	96.07	390501.30
		FB12	1.49	0.12	0.00	2321.52	787.24	216.11	383767.37
		FB15	0.92	0.05	0.00	2594.14	441.05	135.07	378395.13
		FB18	0.75	0.02	0.00	2162.41	517.81	142.38	359922.46
		FB 21	2.06	0.00	2.51	2148.52	604.69	166.52	366975.71
		FB 28	1.08	0.00	0.00	2206.69	285.11	70.43	358276.13
		FB 33	1.30	0.10	0.00	2157.40	337.06	93.15	354330.19
		FB 41	1.50	0.00	0.00	2075.02	313.61	85.21	365147.85
		FB 45	1.61	0.02	0.00	2066.95	363.34	82.54	348174.97
		FB 50	0.94	0.19	0.00	2034.17	269.74	43.13	345598.61
		FB 55	1.97	0.10	0.00	2188.60	582.63	250.55	359868.62
		FB 59	1.68	0.00	0.00	2117.67	464.67	220.19	346429.63
		FB 65	1.45	0.05	0.00	2113.97	464.42	207.17	347576.39
		FB 71	1.42	0.04	0.00	2118.68	443.90	169.54	353901.78
		FB 79	1.39	0.10	0.00	2212.53	529.16	234.94	354071.41
		FB 89	1.28	0.06	0.00	2157.68	519.23	223.55	349903.92
		FB 94	1.67	0.17	0.00	2304.06	647.62	305.03	349358.09
		FB 99	1.56	0.09	0.00	2366.08	594.82	313.76	388269.38
		FB 104	2.03	0.00	0.00	2677.43	674.89	376.26	410965.28
		FB 109	1.49	0.10	0.00	2832.69	468.93	252.83	453255.63
		FB 115	1.63	0.08	0.00	2537.92	545.56	317.48	407852.70
		FB 123	1.69	0.00	0.00	2575.63	531.90	264.14	430087.50
	P. Angulicostata	FB 128a	1.91	0.10	2.60	2687.42	546.47	356.47	437978.22
		FB 134a	1.59	0.08	11.62	2680.53	531.72	301.89	422183.45
		FB 136	1.01	0.03	0.00	2489.60	420.31	194.54	424524.73
		FB 139	1.36	0.03	0.00	2313.19	532.59	255.04	419390.72
		FB 371	1.98	0.04	0.00	2494.22	676.81	307.39	420650.79
	P. catulloi (subzone)	FB 373a	2.41	0.03	2.03	2543.88	795.54	328.31	429618.90
		FB 373d	1.56	0.04	0.00	2626.93	494.92	226.82	453909.12
		FB 375	1.64	0.01	0.00	3032.40	500.76	217.49	445131.85
		FB 378	1.59	0.08	0.00	2714.37	387.42	167.36	427961.08
		FB 380a	1.59	0.06	0.00	2949.82	403.26	173.94	455876.00
		FB 380b	1.28	0.17	0.00	2926.51	335.34	144.71	445279.57
		FB 382a	1.25	0.00	0.00	2587.01	425.77	202.21	429260.23
		FB 382c	0.98	0.08	0.00	2279.78	326.22	113.95	408676.21
		FB 385	1.69	0.03	0.00	2320.20	569.64	258.85	403209.82
		FB 387b	2.45	0.10	0.00	2210.04	782.70	367.92	345134.49
		FB 391	1.59	0.18	0.00	1868.13	466.15	188.08	331339.85
		FB 396b	0.98	0.14	0.00	1942.06	337.10	143.29	335613.25
		FB 402b	1.15	0.00	6.10	2113.11	320.84	156.68	375647.03
		FB 410	1.82	0.00	0.00	2244.36	514.07	187.28	339380.58
Early Barremian	*S. hugii*	FB 417	1.36	0.00	0.00	2117.51	460.32	183.84	357795.57
		FB 424	1.15	0.00	0.00	2109.06	355.21	125.67	359685.38
		FB 430a	1.47	0.00	0.00	2156.01	454.59	198.63	342559.24
		FB 433	1.78	0.00	0.00	2129.95	565.68	223.91	349011.62
		FB 440a	1.98	0.00	0.00	2410.44	789.06	354.60	366826.77
		FB 448b	1.10	0.00	0.00	2121.74	364.23	152.94	352258.36
		FB 451a	1.05	0.00	0.00	2086.59	325.47	115.05	344559.03
		FB 454b	1.24	0.00	0.00	2075.21	389.71	147.90	341671.92
		FB 459b	1.16	0.00	0.00	2091.09	363.83	136.95	344643.73
		FB 464a	0.94	0.00	0.00	1132.14	356.06	161.34	177149.00
		FB 469	1.17	0.00	0.00	2070.25	382.65	149.70	332351.63
		FB 473b	0.77	0.00	0.00	2177.91	293.59	116.26	325441.33
		FB 480a	1.19	0.11	8.45	2178.62	400.51	134.22	371071.90
		FB 487	1.15	0.00	0.00	2265.33	395.13	130.91	406060.87
		FB 494b	1.45	0.07	0.00	2555.70	560.47	205.20	382102.23
		FB 499a	2.62	0.08	1.13	2795.42	690.21	301.10	422405.65

N.B.: All the data presented in this section are expressed in ppm.

Fiume-Bosso section

Sample n°	Sc	Ti	V	Cr	Mn	Fe	Co	Ni	Cu	Zn	Ga
FB2	3.60	183.58	0.75	1.26	279.62	1026.69	1.81	7.66	1.94	8.36	0.18
FB5	1.17	179.80	0.64	1.21	295.16	1020.95	2.00	10.55	1.60	6.54	0.16
FB8	0.51	200.71	0.54	1.02	234.94	1210.50	2.02	10.20	2.38	10.96	0.13
FB12	0.09	180.76	0.75	1.08	253.54	969.84	1.66	9.65	2.50	6.16	0.22
FB15	0.00	195.55	0.51	1.24	316.91	892.86	1.53	10.07	2.05	11.86	0.20
FB18	0.00	161.03	0.58	1.06	227.55	854.20	1.56	8.53	2.35	5.37	0.14
FB 21	0.00	340.44	1.24	0.03	253.62	846.04	1.94	14.36	1.75	1.52	0.25
FB 28	0.03	315.28	0.51	0.00	250.81	620.33	1.27	13.02	0.49	0.00	0.15
FB 33	0.19	349.42	0.68	0.00	272.06	776.52	1.43	13.58	1.08	1.70	0.16
FB 41	0.08	321.52	0.54	0.00	258.05	808.54	1.23	13.54	0.66	7.96	0.16
FB 45	0.00	365.74	0.57	0.00	297.44	770.70	2.32	14.02	1.55	0.59	0.18
FB 50	0.00	337.68	0.55	0.00	285.97	841.53	1.28	14.55	0.00	0.00	0.14
FB 55	0.34	346.18	0.91	2.08	313.07	1008.48	1.76	11.38	2.64	5.29	0.22
FB 59	0.37	332.89	0.81	1.81	494.40	1364.03	2.61	13.30	2.61	8.96	0.23
FB 65	0.31	322.41	0.58	2.13	296.77	984.44	1.51	12.31	3.69	7.21	0.19
FB 71	0.25	359.91	0.64	2.38	334.64	1025.93	3.02	12.24	5.20	7.43	0.20
FB 79	0.38	336.21	0.63	2.09	309.35	937.09	0.99	12.10	2.26	6.01	0.25
FB 89	0.52	298.20	0.71	2.18	320.18	932.59	1.43	13.76	5.06	9.05	0.28
FB 94	0.75	0.00	0.79	2.36	367.32	887.16	1.87	13.58	3.11	10.22	0.29
FB 99	0.92	406.86	0.80	3.19	352.73	1109.04	2.06	14.69	4.22	19.28	0.29
FB 104	0.74	333.08	1.25	1.85	365.27	1559.33	2.26	16.34	6.74	20.41	0.33
FB 109	0.72	372.78	1.10	1.62	353.57	1318.42	1.70	15.09	3.91	4.64	0.23
FB 115	0.50	415.59	0.91	1.83	371.76	1336.98	1.92	15.30	3.48	8.91	0.23
FB 123	0.83	391.43	0.93	1.70	353.23	1251.41	2.28	15.04	5.24	31.52	0.25
FB 128a	0.64	406.02	0.91	3.10	354.15	1245.13	1.64	13.45	2.92	17.02	0.29
FB 134a	0.58	410.46	1.08	1.77	393.38	1345.20	2.07	15.64	5.70	17.88	0.27
FB 136	0.00	348.97	0.73	1.95	316.61	1121.55	1.48	13.74	4.78	24.86	0.20
FB 139	0.15	333.45	1.08	2.01	324.11	1059.27	1.23	11.14	2.56	5.23	0.23
FB 371	0.12	380.33	2.04	1.99	299.39	998.07	1.08	10.37	2.64	8.95	0.26
FB 373a	0.22	313.69	4.60	1.62	357.24	1137.76	1.36	12.40	1.56	22.37	0.32
FB 373d	0.49	361.75	5.21	1.97	271.54	928.14	0.96	11.67	1.68	9.14	0.20
FB 375	0.64	395.67	11.61	2.44	261.79	880.36	0.94	10.12	1.84	16.43	0.22
FB 378	0.63	404.90	10.36	2.16	299.85	864.84	0.92	11.36	3.27	7.42	0.19
FB 380a	0.24	405.42	7.74	2.18	271.19	828.43	0.89	13.22	0.81	13.40	0.20
FB 380b	0.31	407.30	7.35	1.97	265.78	860.81	0.79	10.03	0.64	28.41	0.17
FB 382a	0.03	339.52	6.96	2.29	284.27	883.43	1.01	11.37	1.36	7.07	0.20
FB 382c	0.00	357.51	2.78	1.70	326.96	936.07	2.25	11.24	1.10	26.70	0.16
FB 385	0.07	360.27	3.01	1.84	323.82	982.94	1.49	11.87	2.16	8.69	0.22
FB 387b	0.75	347.60	2.08	3.19	349.82	1069.75	1.79	11.96	3.54	9.88	0.38
FB 391	0.78	315.21	0.84	1.79	280.64	882.03	2.35	11.93	3.01	8.32	0.23
FB 396b	0.27	330.48	0.82	1.49	270.78	1037.02	2.02	11.82	1.92	7.97	0.17
FB 402b	0.21	349.06	0.63	0.39	330.79	786.08	1.37	12.44	2.12	20.70	0.16
FB 410	0.40	346.07	1.13	0.34	262.99	1342.02	2.33	15.59	2.65	10.22	0.25
FB 417	0.61	320.92	0.89	0.58	272.17	847.48	1.05	12.97	1.48	5.95	0.22
FB 424	0.27	329.98	0.65	0.24	293.65	769.28	1.37	12.72	2.65	5.80	0.16
FB 430a	0.42	326.72	0.89	0.24	411.56	1092.59	1.51	13.31	2.32	9.71	0.19
FB 433	0.40	357.29	1.00	0.78	286.82	941.25	0.97	11.71	1.88	6.88	0.22
FB 440a	0.57	356.62	1.73	1.60	261.31	1364.11	1.93	15.39	3.58	12.15	0.34
FB 448b	0.36	369.75	0.86	0.54	216.11	746.72	1.11	12.77	2.01	6.24	0.18
FB 451a	0.39	333.54	0.89	0.65	232.98	741.28	1.35	12.06	2.26	5.09	0.16
FB 454b	0.00	305.49	0.85	0.67	237.45	867.20	0.00	12.78	2.14	7.02	0.16
FB 459b	0.27	319.92	0.68	0.51	218.47	723.06	1.21	11.97	2.46	5.20	0.18
FB 464a	0.12	186.12	1.09	0.35	117.48	707.79	1.04	7.96	1.93	9.53	0.13
FB 469	0.30	314.09	0.93	0.63	207.03	724.62	1.25	12.49	2.72	6.54	0.18
FB 473b	0.39	364.54	0.85	0.28	224.15	696.08	1.14	13.86	1.85	5.73	0.15
FB 480a	0.36	325.40	0.85	1.96	242.64	827.82	1.27	12.31	2.88	17.81	0.20
FB 487	0.37	361.13	0.85	0.77	274.97	973.44	1.86	17.36	3.18	3.34	0.20
FB 494b	0.45	419.16	1.08	0.59	273.17	1245.35	1.22	16.10	1.71	41.15	0.29
FB 499a	0.62	382.78	1.82	1.42	351.34	1402.04	1.45	15.79	2.84	66.11	0.32

Fiume-Bosso section

Sample n°	Ge	As	Se	Rb	Sr	Y	Zr	Nb	Mo	Ru
FB2	0.00	0.41	0.00	0.99	242.90	6.37	0.26	0.00	0.44	0.00
FB5	0.00	1.33	0.00	0.74	241.98	6.15	0.30	0.00	0.33	0.00
FB8	0.00	8.49	0.00	0.65	249.01	6.60	0.24	0.01	0.55	0.00
FB12	0.01	12.79	0.00	1.07	237.01	8.06	0.26	0.00	0.93	0.00
FB15	0.01	13.79	0.00	0.75	239.00	7.13	0.24	0.00	0.49	0.00
FB18	0.00	9.54	0.00	0.69	218.78	6.47	0.37	0.00	0.34	0.00
FB 21	0.00	9.70	0.00	1.44	229.48	5.98	0.00	0.00	0.00	0.00
FB 28	0.02	6.07	0.00	0.77	234.83	5.92	0.00	0.00	0.00	0.00
FB 33	0.02	1.17	0.00	1.06	228.33	6.32	0.00	0.00	0.06	0.00
FB 41	0.01	0.50	0.00	1.15	221.76	7.14	0.00	0.00	0.06	0.00
FB 45	0.02	0.62	0.00	1.18	214.77	7.10	0.00	0.00	0.02	0.00
FB 50	0.03	1.10	0.00	0.69	211.36	5.94	0.00	0.00	0.01	0.00
FB 55	0.01	0.16	0.00	1.24	227.51	6.87	0.31	0.01	0.03	0.00
FB 59	0.00	0.39	0.00	1.22	222.74	6.94	0.22	0.00	0.00	0.00
FB 65	0.01	0.25	0.00	1.37	221.96	7.54	0.21	0.00	0.00	0.00
FB 71	0.00	0.23	0.00	1.20	236.91	7.86	0.21	0.00	0.00	0.03
FB 79	0.02	0.16	0.00	1.35	230.06	8.23	0.23	0.00	0.00	0.03
FB 89	0.01	0.08	0.00	1.35	240.13	8.11	0.22	0.00	0.00	0.00
FB 94	0.00	0.09	0.00	1.69	247.68	7.97	0.23	0.00	0.00	0.03
FB 99	0.04	0.17	2.66	1.75	279.65	10.93	0.44	0.00	0.00	0.00
FB 104	0.04	0.31	0.44	1.93	335.84	11.77	0.20	0.00	0.03	0.00
FB 109	0.04	0.16	0.30	1.15	317.38	10.23	0.17	0.01	0.01	0.00
FB 115	0.05	0.33	0.00	1.64	309.32	9.84	0.22	0.00	0.00	0.00
FB 123	0.03	0.12	8.38	1.49	316.39	11.36	0.15	0.00	0.10	0.00
FB 128a	0.04	0.22	2.10	1.77	316.79	10.36	0.59	0.00	0.03	0.00
FB 134a	0.04	0.51	0.99	1.38	292.46	9.26	0.28	0.01	0.16	0.00
FB 136	0.03	0.46	0.18	1.18	309.47	8.26	0.21	0.00	0.03	0.00
FB 139	0.02	0.21	0.43	1.57	279.69	9.36	0.27	0.00	0.00	0.08
FB 371	0.00	0.18	0.81	1.75	289.52	8.60	0.47	0.00	0.09	0.01
FB 373a	0.03	0.50	0.97	1.73	262.42	7.74	0.43	0.00	0.42	0.05
FB 373d	0.02	0.29	1.33	1.10	314.50	9.12	0.45	0.01	0.55	0.00
FB 375	0.02	0.42	0.52	1.07	310.04	8.01	0.53	0.01	0.31	0.00
FB 378	0.03	0.23	0.00	0.87	343.76	11.61	0.46	0.01	0.32	0.00
FB 380a	0.02	0.31	0.44	1.01	335.20	7.89	0.33	0.00	0.29	0.00
FB 380b	0.02	0.27	0.75	0.77	336.87	8.01	0.26	0.01	0.40	0.00
FB 382a	0.03	0.32	0.42	1.03	301.18	7.68	0.27	0.01	0.15	0.00
FB 382c	0.02	3.73	3.34	0.75	260.36	7.46	0.34	0.01	0.20	0.01
FB 385	0.03	3.37	0.22	1.79	266.94	7.88	0.31	0.01	0.14	0.00
FB 387b	0.02	0.39	0.00	1.97	228.93	8.16	0.44	0.01	0.14	0.00
FB 391	0.02	0.29	0.00	0.97	239.66	7.41	0.26	0.01	0.03	0.01
FB 396b	0.01	0.44	0.00	0.79	226.20	6.04	0.12	0.00	0.08	0.03
FB 402b	0.01	0.20	0.00	1.02	236.36	6.79	0.18	0.00	0.12	0.01
FB 410	0.04	0.43	0.00	1.46	220.18	7.08	0.26	0.00	0.16	0.00
FB 417	0.01	0.24	0.00	1.30	222.77	7.69	0.26	0.00	0.00	0.00
FB 424	0.00	0.19	0.00	0.88	232.34	7.80	0.19	0.00	0.05	0.00
FB 430a	0.01	0.26	0.00	1.07	224.76	6.48	0.25	0.00	0.00	0.00
FB 433	0.01	0.22	0.00	1.42	224.46	7.60	0.30	0.00	0.01	0.00
FB 440a	0.01	0.28	0.00	2.03	239.34	7.04	0.55	0.01	0.02	0.00
FB 448b	0.01	0.12	0.00	0.90	236.17	6.26	0.21	0.00	0.01	0.01
FB 451a	0.01	0.35	0.00	0.75	269.03	6.15	0.18	0.00	0.04	0.00
FB 454b	0.03	0.12	0.00	1.10	228.56	6.75	0.16	0.00	0.03	0.00
FB 459b	0.01	0.13	0.00	0.91	239.41	6.06	0.19	0.00	0.00	0.00
FB 464a	0.00	0.37	0.00	0.99	116.70	3.50	0.14	0.00	0.03	0.00
FB 469	0.00	0.32	0.00	0.96	236.07	5.64	0.22	0.00	0.04	0.00
FB 473b	0.00	0.21	0.00	0.76	248.18	5.78	0.15	0.00	0.00	0.00
FB 480a	0.01	0.24	0.42	1.06	229.73	6.74	0.21	0.00	0.10	0.08
FB 487	0.02	0.29	0.90	1.07	256.01	9.51	0.24	0.01	0.04	0.00
FB 494b	0.07	0.24	0.00	1.57	303.83	8.78	0.01	0.00	0.04	0.00
FB 499a	0.01	1.76	1.05	2.10	324.01	9.46	0.56	0.01	0.17	0.00

Fiume-Bosso section

Sample n°	Pd	Ag	Cd	Ba	Pb	Bi	Th	U
FB2	0.00	0.02	0.08	80.95	1.55	0.01	0.14	0.15
FB5	0.02	0.01	0.12	45.20	1.22	0.02	0.13	0.11
FB8	0.01	0.02	0.16	30.59	1.16	0.01	0.11	0.07
FB12	0.00	0.02	0.05	5.63	0.85	0.01	0.18	0.06
FB15	0.00	0.02	0.33	52.88	1.04	0.01	0.15	0.06
FB18	0.01	0.05	0.09	4.60	1.45	0.00	0.10	0.13
FB 21	0.00	0.00	0.07	4.29	0.00	0.02	0.20	0.05
FB 28	0.00	0.00	0.07	4.73	0.00	0.00	0.15	0.08
FB 33	0.00	0.00	0.06	7.65	0.00	0.00	0.19	0.08
FB 41	0.00	0.00	0.09	60.55	0.00	0.00	0.22	0.05
FB 45	0.01	0.00	0.07	12.19	0.00	0.01	0.23	0.08
FB 50	0.00	0.00	0.01	2.96	0.00	0.00	0.18	0.11
FB 55	0.00	0.00	0.07	4.63	1.18	0.05	0.12	0.09
FB 59	0.01	0.00	0.06	4.16	0.90	0.02	0.15	0.15
FB 65	0.00	0.00	0.14	7.81	1.27	0.03	0.15	0.05
FB 71	0.00	0.00	0.12	4.91	1.48	0.03	0.16	0.09
FB 79	0.00	0.00	0.09	6.39	1.02	0.02	0.17	0.04
FB 89	0.01	0.00	0.14	4.79	0.89	0.02	0.21	0.07
FB 94	0.01	0.00	0.26	5.58	1.23	0.02	0.19	0.11
FB 99	0.00	0.06	0.35	7.36	5.07	0.03	0.24	0.08
FB 104	0.01	0.05	0.10	105.95	2.00	0.04	0.33	0.18
FB 109	0.01	0.03	0.07	6.37	6.63	0.03	0.21	0.64
FB 115	0.01	0.01	0.14	6.14	0.49	0.03	0.23	0.12
FB 123	0.01	0.02	0.21	10.17	0.58	0.05	0.23	0.15
FB 128a	0.02	0.06	0.28	5.50	2.87	0.07	0.22	0.19
FB 134a	0.02	0.05	0.08	26.48	1.53	0.29	0.23	0.24
FB 136	0.02	0.03	0.10	21.34	0.91	0.00	0.17	0.23
FB 139	0.02	0.02	0.16	13.28	1.80	0.00	0.25	0.39
FB 371	0.02	0.07	0.09	50.16	0.00	0.00	0.17	0.55
FB 373a	0.01	0.06	0.37	5.38	0.00	0.07	0.18	0.49
FB 373d	0.02	0.02	0.27	4.24	0.00	0.02	0.15	0.76
FB 375	0.00	0.02	0.19	17.84	0.00	0.01	0.15	2.53
FB 378	0.01	0.03	0.29	3.74	0.00	0.00	0.20	3.10
FB 380a	0.01	0.03	0.04	121.48	0.00	0.00	0.13	1.09
FB 380b	0.02	0.01	0.18	6.25	0.00	0.00	0.13	1.80
FB 382a	0.00	0.01	0.09	3.57	0.00	0.00	0.15	2.08
FB 382c	0.01	0.01	0.14	2.98	0.00	0.00	0.14	0.81
FB 385	0.01	0.01	0.09	7.72	0.00	0.00	0.21	0.64
FB 387b	0.01	0.02	0.17	17.90	0.77	0.02	0.21	0.37
FB 391	0.01	0.00	0.26	4.22	0.77	0.01	0.16	0.24
FB 396b	0.01	0.00	0.08	3.77	0.70	0.01	0.04	0.43
FB 402b	0.00	0.01	0.14	37.56	0.53	0.24	0.19	0.12
FB 410	0.00	0.00	0.13	4.56	0.98	0.05	0.23	0.22
FB 417	0.00	0.00	0.11	5.49	0.65	0.02	0.27	0.13
FB 424	0.00	0.00	0.16	4.18	0.51	0.02	0.15	0.09
FB 430a	0.00	0.00	0.25	5.45	0.83	0.01	0.25	0.30
FB 433	0.00	0.00	0.12	6.15	0.79	0.02	0.27	0.11
FB 440a	0.02	0.01	0.18	7.71	1.03	0.00	0.28	0.13
FB 448b	0.00	0.00	0.11	5.56	0.48	0.00	0.16	0.18
FB 451a	0.00	0.00	0.10	5.10	0.39	0.00	0.15	0.25
FB 454b	0.00	0.00	0.13	7.11	0.62	0.01	0.18	0.13
FB 459b	0.00	0.00	0.13	6.30	0.43	0.00	0.19	0.11
FB 464a	0.01	0.00	0.10	9.84	0.63	0.00	0.19	0.14
FB 469	0.00	0.00	0.10	33.94	0.53	0.00	0.18	0.16
FB 473b	0.00	0.00	0.06	8.92	0.40	0.00	0.16	0.29
FB 480a	0.00	0.00	0.10	157.46	0.48	0.17	0.17	0.13
FB 487	0.03	0.00	0.23	10.18	0.00	0.00	0.15	0.10
FB 494b	0.00	0.01	0.09	544.01	0.00	0.00	0.29	0.23
FB 499a	0.02	0.08	0.11	877.30	2.32	0.05	0.25	0.45

Veveyse de Châtel - St. Denis section

Stage	Ammonite zone	Sample n°	Li	Be	B	Mg	Al	K	Ca
Late Hauterivian	*sayni*	VCD 1A	6.73	1.76	5.47	4999.28	4218.51	0.00	334968.44
		VCD 3A	6.23	0.31	0.00	3055.28	3668.48	846.82	263349.07
		VCD 4A	3.33	0.39	0.00	2960.77	2113.76	510.78	268992.31
		VCD 6A	3.44	0.42	0.00	3301.22	2085.25	482.29	272385.44
		VCD 9A	3.22	0.19	0.00	3054.82	1793.80	444.52	278970.10
		VCD 13A	5.12	0.43	0.00	4015.05	2621.87	703.54	269126.52
		VCD 15A	3.42	0.12	0.00	3805.75	1738.49	473.43	247297.81
		VCD 18A	3.67	0.31	0.00	3491.67	1766.96	482.86	253461.15
		VCD 21A	3.77	0.24	0.00	3693.39	2162.70	528.05	263299.41
		VCD 24A	4.95	0.47	0.00	3388.06	2403.45	647.47	284236.04
		VCD 27A	6.17	0.69	0.00	3873.24	3216.28	0.00	275234.12
		VCD 29A	4.52	0.20	0.00	4089.82	2390.71	0.00	291805.10
	ligatus	SDII 1	4.48	0.00	0.00	4066.68	2445.28	0.00	299480.11
		SDII 3	2.71	0.29	0.00	3031.26	1365.16	0.00	302697.27
		SDII 5	4.13	0.00	0.00	3107.13	2184.58	0.00	315805.22
		SDII 6	3.04	0.14	0.00	2509.60	1859.04	0.00	326632.11
		SDII 7c	4.10	0.00	0.00	2587.59	2077.84	0.00	285714.47
		SDII 10	5.20	0.00	0.00	4513.19	2733.09	0.00	290977.41
		SDII 11	6.66	0.18	0.00	4087.81	3125.75	0.00	314434.90
		SDII 13a	4.99	0.17	0.00	3188.15	2768.64	0.00	308478.01
		SDII 14	3.31	0.17	0.00	2961.60	1612.75	0.00	290523.74
		SDII 15	4.67	0.20	0.00	3439.64	2393.23	0.00	284157.43
	balearis	SDII 16b	3.96	0.00	0.00	3385.93	2357.69	0.00	271529.17
		SDII 18	4.15	0.00	0.00	3576.97	2143.18	0.00	292785.23
		SDII 19	4.32	0.06	0.00	3154.12	2297.67	0.00	271081.53
		SDII 21	4.14	0.05	0.00	2780.01	1941.61	0.00	317058.31
		SDII 23	4.63	0.10	0.00	2655.92	2259.43	0.00	275884.12
		SDII 25	5.99	0.00	0.00	3532.43	3307.62	0.00	289242.75
		SDII 27	3.97	0.14	0.00	3936.76	2761.50	0.00	331835.25
		SDII 28	5.39	0.00	0.00	3933.59	3181.60	0.00	336947.26
		SDII 30	3.93	0.00	0.00	2977.77	2698.89	0.00	329078.76
		SDII 33	6.04	0.14	0.00	4861.89	4061.27	0.00	358659.51
		SDII 34	5.60	0.00	0.00	3850.02	2847.12	0.00	334663.75
		SDII 36	2.61	0.06	0.00	3136.85	1912.49	0.00	322415.79
		SDII 40	3.66	1.25	0.00	2935.30	2401.39	0.00	391856.34
		VCDII 51A	2.48	1.18	0.00	3371.90	1622.93	0.00	406093.54
	angulicostata auct.	SDII 42	3.39	0.00	0.00	3628.04	2093.01	0.00	382520.72
		VCDII 50A	3.23	0.37	0.00	2833.85	1748.70	0.00	330732.86
		SDII 43	5.61	0.00	2.88	2840.99	3922.63	0.00	333216.43
		VCDII 49A	5.67	0.73	0.00	3275.11	3073.07	0.00	391017.49
		VCDII 48A	8.51	0.91	0.00	3899.48	4894.15	0.00	351167.14
		VCDII 46A	4.70	0.41	0.00	2571.74	2765.17	0.00	314244.44
		VCDII 44A	4.22	1.81	0.00	3602.57	2634.06	0.00	364185.93
		VCDII 42A	5.25	1.23	0.00	3481.66	3550.35	0.00	341078.99
		VCDII 40A	6.39	0.61	20.07	5484.08	4063.08	0.00	292859.33
		SDII 51	6.57	0.95	0.00	3513.35	4052.26	0.00	329361.45
		VCDII 37A	3.17	0.00	0.00	3520.70	2400.99	0.00	338424.23
		VCDII 35A	2.51	0.00	0.00	2938.98	1813.70	0.00	335907.12
		VCDII 33A	3.52	0.49	0.00	3144.91	1966.19	0.00	353554.71
		VCDII 30A	1.81	0.00	0.00	3427.15	1657.63	0.00	328097.25
		VCDII 27A	3.80	0.34	0.00	3225.16	2332.03	0.00	319589.07
		VCDII 25A	6.51	0.00	0.00	4393.53	4495.81	0.00	326677.30
		VCDII 22A	5.44	0.00	0.00	5593.27	3296.57	0.00	272253.46
		VCDII 19A	5.96	0.00	0.00	4001.67	4328.22	0.00	326784.57
		VCDII 16A	5.55	0.00	0.00	3921.21	2589.04	0.00	312878.18
		VCDII 12A	3.27	0.01	0.00	4944.65	2385.62	0.00	328818.53
		VCDII 10A	2.81	0.00	0.00	4188.71	1655.01	0.00	302627.90
		VCDII 8A	3.56	0.72	0.00	3688.22	2252.46	0.00	313451.79
		SD 42	6.28	0.23	0.00	3079.92	2986.36	893.20	287091.56
		VCDII 6A	2.53	0.00	0.00	3310.43	1407.43	0.00	283380.05
		SD 38	4.69	0.08	0.00	2595.20	2130.47	448.93	297839.79
		SD 36	4.36	0.15	0.00	2573.73	2190.94	504.18	305090.92
		SD 32	4.81	0.38	0.00	2736.56	2211.30	373.73	300898.79
		SD 29	3.42	0.36	0.00	3874.07	2433.61	0.00	321820.87
		SD 27	4.83	0.44	0.00	2405.98	2630.71	816.43	278825.55
		SD 24	4.42	0.45	0.00	2520.43	2495.25	660.41	280752.32
Early Barremian	*hugii*	SD 21	5.43	0.18	0.00	2926.60	2684.79	758.28	286150.54
		SD 19	5.31	0.23	0.00	2922.60	2868.36	652.68	285787.15
		SD 16	5.41	0.26	0.00	2646.07	2850.83	799.53	276346.75
		SD 12	4.94	0.38	0.00	3403.42	2710.80	714.37	279567.44
		SD 8	5.57	0.39	0.00	3644.98	2650.64	761.11	303107.95
		SD 5	6.51	0.49	0.00	4311.64	3087.62	955.69	296014.22
		SD 1	7.06	0.68	0.00	3195.37	3203.80	1018.09	313835.94

Veveyse de Châtel - St. Denis section

Sample n°	Sc	Ti	V	Cr	Mn	Fe	Co	Ni	Cu	Zn	Ga
VCD 1A	0.59	161.71	8.74	7.73	149.66	6405.17	2.28	11.68	7.55	26.45	0.76
VCD 3A	0.00	74.14	6.28	6.58	150.94	4916.69	2.08	16.91	7.44	23.04	0.77
VCD 4A	0.00	82.76	4.92	4.97	126.40	4074.50	1.79	18.34	8.04	14.88	0.38
VCD 6A	0.00	84.06	5.02	5.01	142.47	4069.19	1.99	17.01	7.26	19.28	0.46
VCD 9A	0.00	84.53	4.36	5.11	127.37	3067.84	1.37	14.31	6.41	12.55	0.43
VCD 13A	0.00	79.09	6.27	6.14	116.25	4231.12	1.91	17.41	7.98	15.41	0.54
VCD 15A	0.00	71.45	6.17	4.59	96.41	3888.22	2.06	16.34	7.40	12.24	0.34
VCD 18A	0.00	77.65	6.40	4.85	85.26	3443.90	1.29	14.44	7.08	15.07	0.39
VCD 21A	0.00	77.54	5.82	6.02	83.66	3909.46	1.76	16.73	9.08	17.76	0.45
VCD 24A	0.00	89.46	5.79	5.56	88.46	3642.65	1.64	16.87	6.70	13.81	0.69
VCD 27A	0.24	85.24	8.14	5.97	95.26	0.00	1.92	13.19	6.92	19.41	0.75
VCD 29A	0.41	89.16	6.98	5.92	104.63	0.00	2.12	14.93	9.10	31.52	0.60
SDII 1	0.36	91.41	6.60	5.12	96.40	0.00	2.16	14.79	7.63	20.81	0.43
SDII 3	0.09	89.57	4.09	2.88	90.09	0.00	1.77	12.49	6.29	23.44	0.31
SDII 5	0.15	90.12	5.17	4.50	96.50	0.00	1.51	20.02	5.43	21.42	0.45
SDII 6	0.26	96.62	4.95	4.07	105.52	0.00	1.28	11.12	5.76	17.89	0.37
SDII 7c	0.06	86.16	5.57	3.62	101.55	0.00	1.44	11.31	4.70	21.01	0.44
SDII 10	0.35	88.75	6.33	4.51	135.29	0.00	1.93	15.30	8.60	23.37	0.59
SDII 11	0.31	99.08	7.77	5.72	143.57	0.00	2.25	14.73	6.69	22.48	0.90
SDII 13a	0.32	93.84	6.06	3.97	142.91	0.00	1.79	12.03	6.33	20.49	0.68
SDII 14	0.08	90.35	4.33	2.43	123.68	0.00	1.76	12.48	6.25	15.62	0.34
SDII 15	0.27	86.45	5.89	4.14	122.14	0.00	2.12	13.55	6.01	15.90	0.52
SDII 16b	0.18	83.83	6.38	3.53	117.53	0.00	1.77	12.91	45.52	29.02	0.46
SDII 18	0.25	88.68	5.26	4.04	134.62	0.00	1.93	12.72	5.45	17.30	0.52
SDII 19	0.26	81.80	5.66	3.42	130.54	0.00	2.43	14.17	6.72	93.62	0.53
SDII 21	0.42	104.07	4.92	4.36	158.21	0.00	1.64	12.65	4.05	17.02	0.43
SDII 23	0.18	87.27	4.76	3.78	126.37	0.00	1.96	13.27	5.12	16.02	0.44
SDII 25	0.20	89.88	5.54	3.76	135.56	0.00	1.37	11.24	9.60	14.59	0.79
SDII 27	0.00	155.09	4.72	4.03	173.60	4329.22	1.68	9.74	7.00	19.06	0.48
SDII 28	0.34	163.12	5.32	4.16	192.70	7464.84	3.94	19.45	10.82	31.10	0.49
SDII 30	0.20	161.51	4.64	3.75	156.18	4461.81	1.89	10.29	6.18	28.28	0.44
SDII 33	1.33	175.30	7.73	8.04	192.78	7140.46	2.79	16.66	11.08	37.47	0.74
SDII 34	0.04	154.13	5.25	4.61	197.12	5130.29	3.06	13.84	5.57	13.85	0.53
SDII 36	0.00	154.85	4.46	2.30	209.58	5493.56	2.60	13.70	5.38	27.48	0.26
SDII 40	0.73	191.12	6.17	5.37	219.80	4823.81	1.47	10.30	6.60	22.08	0.45
VCDII 51A	0.77	191.34	4.33	4.39	222.66	4493.56	2.40	10.58	6.76	22.40	0.37
SDII 42	0.23	179.35	5.82	4.11	218.64	4472.39	1.69	10.90	5.42	16.23	0.25
VCDII 50A	0.24	174.55	4.96	3.57	189.72	3326.88	1.35	9.02	6.25	13.85	0.33
SDII 43	0.00	146.16	7.88	6.28	176.50	5164.49	1.26	11.26	9.11	22.73	0.80
VCDII 49A	0.53	195.09	6.28	4.93	236.85	6764.77	3.11	13.49	7.24	38.48	0.70
VCDII 48A	0.50	164.16	8.57	6.31	218.75	8512.77	2.66	12.39	7.31	47.85	1.06
VCDII 46A	0.02	154.98	5.33	3.61	171.82	5112.72	1.71	10.43	7.64	24.44	0.46
VCDII 44A	0.25	175.02	5.88	3.79	197.00	5815.60	1.00	8.48	4.70	12.86	0.53
VCDII 42A	0.00	158.94	5.15	4.19	172.85	6068.35	1.86	8.57	5.89	13.90	0.59
VCDII 40A	0.00	140.92	8.04	6.77	144.40	6640.61	2.32	11.50	7.46	16.68	0.95
SDII 51	0.49	174.83	6.52	5.11	172.14	5854.44	0.99	10.36	7.19	19.08	0.73
VCDII 37A	0.00	144.64	5.06	3.95	163.46	4537.04	1.39	8.45	3.93	13.15	0.49
VCDII 35A	0.00	167.24	4.82	3.06	150.04	4160.06	1.32	7.57	4.59	13.49	0.42
VCDII 33A	0.00	163.47	4.83	3.25	162.39	4565.79	1.77	8.82	5.47	14.92	0.46
VCDII 30A	0.03	149.62	4.39	3.33	138.78	3476.23	1.11	13.62	4.59	10.09	0.36
VCDII 27A	0.00	166.09	5.02	2.66	179.43	4483.10	1.85	9.85	3.90	22.87	0.45
VCDII 25A	1.20	170.94	8.50	8.37	186.10	8205.36	3.63	16.85	10.99	36.43	0.85
VCDII 22A	0.36	132.97	6.95	4.65	129.48	7041.65	2.84	14.57	9.23	47.93	0.48
VCDII 19A	0.37	148.23	7.16	5.43	169.48	7398.00	2.34	14.25	7.02	21.65	0.79
VCDII 16A	0.00	138.09	11.69	3.60	117.23	3736.70	1.51	11.39	5.44	13.43	0.65
VCDII 12A	0.00	149.75	6.79	3.28	144.84	4793.36	1.66	6.94	5.27	13.92	0.43
VCDII 10A	0.00	152.87	3.96	2.40	138.73	3849.05	1.45	7.66	5.45	14.87	0.36
VCDII 8A	0.27	168.80	4.48	3.81	145.16	4584.38	1.57	7.54	6.46	17.02	0.41
SD 42	0.16	126.21	6.50	5.72	177.16	5293.37	1.88	12.37	5.53	20.46	0.78
VCDII 6A	0.00	151.66	4.14	2.15	144.01	3711.27	1.63	8.05	4.41	15.89	0.27
SD 38	0.13	130.26	6.45	3.83	209.07	5433.19	1.62	11.00	5.81	17.32	0.54
SD 36	0.21	140.04	5.24	2.94	193.76	4845.21	1.22	11.61	6.02	20.50	0.53
SD 32	0.23	153.87	5.88	4.07	219.50	5665.44	1.12	12.01	4.66	16.93	0.48
SD 29	0.61	164.93	5.39	4.09	211.72	5264.20	1.91	10.62	5.25	17.39	0.48
SD 27	0.00	119.12	1.88	0.00	199.33	5161.48	1.24	12.01	5.65	15.35	0.59
SD 24	0.00	154.82	1.79	0.00	221.10	4818.50	2.02	11.17	5.72	18.61	0.49
SD 21	0.00	143.59	2.17	0.00	226.70	4925.86	0.97	11.63	5.69	7.73	0.65
SD 19	0.00	140.68	2.69	0.00	248.25	6540.24	1.25	11.74	5.97	11.26	0.67
SD 16	0.00	151.31	2.54	0.00	256.35	5632.83	1.42	18.00	5.60	16.38	0.60
SD 12	0.00	122.79	2.67	0.00	233.90	5659.86	1.22	11.73	7.72	12.33	0.56
SD 8	0.00	141.61	1.96	0.00	247.97	4650.27	1.99	10.74	6.60	18.12	0.63
SD 5	0.00	120.74	4.14	0.00	259.46	5605.30	2.36	12.02	5.82	14.32	0.64
SD 1	0.00	141.51	5.18	0.00	293.09	6323.71	2.61	14.83	6.08	25.27	0.88

Veveyse de Châtel - St. Denis section

Sample n°	Ge	As	Rb	Sr	Y	Zr	Nb	Mo	Ru	Pd	Ag
VCD 1A	0.05	1.38	7.13	945.77	6.09	1.87	0.01	0.27	0.00	0.05	0.10
VCD 3A	0.01	0.45	6.95	680.99	3.67	0.58	0.00	0.02	0.00	0.00	0.11
VCD 4A	0.00	0.56	4.39	705.00	3.16	0.78	0.00	0.25	0.01	0.01	0.06
VCD 6A	0.01	0.25	3.93	814.02	3.14	0.72	0.00	0.00	0.00	0.01	0.08
VCD 9A	0.01	0.13	3.61	723.05	2.56	0.68	0.00	0.10	0.00	0.00	0.07
VCD 13A	0.01	0.46	5.44	717.22	3.39	0.67	0.00	0.33	0.00	0.02	1.85
VCD 15A	0.01	0.64	4.10	665.64	4.32	0.52	0.00	0.08	0.00	0.01	0.09
VCD 18A	0.01	0.46	3.92	675.62	3.74	0.47	0.00	0.19	0.00	0.01	0.37
VCD 21A	0.01	0.66	4.56	690.19	3.72	0.62	0.00	0.34	0.00	0.01	0.08
VCD 24A	0.01	0.70	4.81	734.14	3.16	0.52	0.00	0.41	0.00	0.01	0.10
VCD 27A	0.01	1.24	6.38	757.45	4.33	0.71	0.00	0.21	0.01	0.04	0.02
VCD 29A	0.00	0.91	5.39	784.31	4.80	0.75	0.00	0.15	0.00	0.02	0.09
SDII 1	0.00	1.21	5.58	839.65	3.62	0.73	0.00	0.29	0.00	0.03	0.20
SDII 3	0.01	0.88	2.86	820.29	2.62	0.47	0.00	0.24	0.00	0.01	0.05
SDII 5	0.00	0.82	4.53	809.56	2.76	0.59	0.01	0.07	0.00	0.01	0.04
SDII 6	0.00	0.37	3.55	835.11	3.20	0.88	0.00	0.15	0.00	0.02	0.12
SDII 7c	0.01	0.36	4.29	776.18	3.75	0.70	0.00	0.18	0.00	0.01	0.05
SDII 10	0.01	0.85	5.88	831.73	3.81	0.69	0.00	0.19	0.00	0.02	0.09
SDII 11	0.03	0.66	6.13	829.47	4.34	0.50	0.00	0.47	0.00	0.02	0.12
SDII 13a	0.00	0.67	5.47	803.43	3.43	0.50	0.00	0.31	0.02	0.03	0.10
SDII 14	0.00	0.55	3.38	746.25	2.74	0.34	0.00	0.15	0.00	0.01	0.03
SDII 15	0.00	0.79	5.22	781.11	3.77	0.49	0.00	0.00	0.00	0.03	0.06
SDII 16b	0.02	0.56	4.72	756.99	4.80	0.37	0.00	0.00	0.01	0.02	0.06
SDII 18	0.01	0.67	4.14	814.03	3.29	0.37	0.00	0.26	0.01	0.03	0.03
SDII 19	0.01	0.76	5.42	743.20	3.97	0.67	0.00	0.04	0.00	0.02	0.06
SDII 21	0.00	0.47	3.53	933.39	3.73	0.45	0.00	0.14	0.03	0.02	0.05
SDII 23	0.01	0.47	4.65	810.30	3.34	0.32	0.00	0.00	0.02	0.02	0.07
SDII 25	0.01	0.62	4.95	859.09	3.43	0.43	0.01	0.02	0.01	0.02	0.06
SDII 27	0.02	0.51	4.53	872.59	6.46	0.83	0.00	0.00	0.00	0.00	0.06
SDII 28	0.04	1.53	5.70	889.17	7.55	0.86	0.00	0.06	0.00	0.00	0.26
SDII 30	0.04	0.32	4.20	802.87	6.94	2.00	0.00	0.00	0.00	0.00	0.02
SDII 33	0.06	0.95	6.08	893.37	11.12	0.96	0.00	0.12	0.00	0.01	0.18
SDII 34	0.00	0.88	4.84	829.75	6.99	0.58	0.00	0.00	0.00	0.00	0.07
SDII 36	0.00	1.28	2.60	777.77	7.44	0.75	0.00	0.01	0.00	0.00	0.21
SDII 40	0.03	0.70	3.76	930.05	9.52	0.83	0.00	0.00	0.00	0.04	0.09
VCDII 51A	0.00	0.61	3.03	1021.33	6.12	1.27	0.01	0.10	0.00	0.01	0.11
SDII 42	0.00	0.60	2.94	892.76	9.67	1.45	0.00	0.00	0.00	0.00	0.12
VCDII 50A	0.00	0.47	3.26	831.25	8.65	0.87	0.00	0.00	0.00	0.00	0.04
SDII 43	0.03	0.53	6.05	760.12	9.48	1.41	0.00	0.21	0.00	0.00	0.15
VCDII 49A	0.04	1.01	4.47	1076.51	7.82	1.10	0.01	0.00	0.00	0.00	0.20
VCDII 48A	0.00	1.00	6.37	981.60	10.08	1.60	0.00	0.00	0.00	0.00	0.48
VCDII 46A	0.00	0.45	4.58	777.32	8.49	0.99	0.00	0.00	0.00	0.00	0.00
VCDII 44A	0.00	0.58	2.80	1082.03	7.24	1.43	0.00	0.00	0.00	0.00	0.05
VCDII 42A	0.00	0.54	4.52	915.03	7.64	0.92	0.01	0.00	0.00	0.00	0.05
VCDII 40A	0.04	1.14	6.00	819.05	7.56	1.63	0.01	0.26	0.00	0.03	0.10
SDII 51	0.03	0.44	5.22	971.57	7.93	1.26	0.01	0.00	0.00	0.00	0.05
VCDII 37A	0.01	0.48	3.29	1011.60	6.84	1.02	0.00	0.00	0.00	0.00	0.03
VCDII 35A	0.00	0.44	2.18	952.53	5.87	1.56	0.01	0.01	0.00	0.00	0.07
VCDII 33A	0.00	0.57	2.48	1010.79	6.39	1.07	0.00	0.00	0.00	0.00	0.02
VCDII 30A	0.00	0.48	2.22	971.67	4.00	1.49	0.00	0.00	0.00	0.04	0.07
VCDII 27A	0.00	0.68	2.88	963.20	5.98	0.96	0.00	0.00	0.00	0.01	0.02
VCDII 25A	0.01	1.03	6.89	921.92	10.12	1.14	0.00	0.04	0.00	0.02	0.11
VCDII 22A	0.00	1.20	5.34	799.29	7.01	0.98	0.00	0.01	0.00	0.02	0.13
VCDII 19A	0.00	1.15	5.77	998.97	6.36	1.44	0.00	0.00	0.00	0.00	0.11
VCDII 16A	0.00	2.54	4.99	1028.28	5.64	1.17	0.00	1.22	0.00	0.00	0.04
VCDII 12A	0.01	1.13	3.58	1029.77	5.98	1.51	0.01	0.07	0.00	0.00	0.02
VCDII 10A	0.00	0.73	3.20	970.28	5.73	1.12	0.00	0.00	0.00	0.01	0.04
VCDII 8A	0.03	0.51	3.70	1009.81	5.22	1.15	0.00	0.00	0.00	0.01	0.05
SD 42	0.01	0.75	5.74	992.43	5.36	1.68	0.00	0.00	0.00	0.03	0.02
VCDII 6A	0.08	0.74	2.41	1035.02	4.27	1.27	0.00	0.00	0.00	0.05	0.02
SD 38	0.01	0.89	3.55	953.83	6.18	1.49	0.00	0.31	0.00	0.00	0.00
SD 36	0.02	0.38	3.46	990.37	4.44	1.53	0.00	0.00	0.00	0.02	0.00
SD 32	0.00	0.51	3.10	1010.83	6.10	1.59	0.00	0.00	0.00	0.00	0.00
SD 29	0.02	0.88	4.39	1007.31	5.63	1.47	0.00	0.07	0.00	0.06	0.02
SD 27	0.00	0.00	5.78	806.94	7.53	0.00	0.00	0.00	0.00	0.03	0.00
SD 24	0.01	0.00	5.23	826.45	7.56	0.00	0.00	0.00	0.00	0.04	0.00
SD 21	0.00	0.00	5.38	957.45	5.43	0.00	0.00	0.00	0.00	0.03	0.00
SD 19	0.01	0.00	4.78	963.45	6.09	0.00	0.00	0.00	0.00	0.02	0.00
SD 16	0.00	0.00	6.37	871.53	5.66	0.00	0.00	0.00	0.00	0.01	0.00
SD 12	0.03	0.00	5.47	908.80	7.11	0.00	0.01	0.00	0.00	0.03	0.00
SD 8	0.00	0.00	5.41	959.75	4.60	0.00	0.00	0.00	0.00	0.02	0.00
SD 5	0.01	0.05	7.22	968.84	6.55	0.00	0.01	0.00	0.00	0.04	0.00
SD 1	0.00	0.30	6.82	1056.67	6.19	0.00	0.00	0.00	0.00	0.03	0.00

Veveyse de Châtel - St. Denis section

Sample n°	Cd	Ba	Pb	Bi	Th	U
VCD 1A	0.00	17.21	2.22	0.07	0.83	0.64
VCD 3A	0.02	25.93	0.00	0.03	0.92	0.52
VCD 4A	0.03	20.22	0.00	0.02	0.66	0.59
VCD 6A	0.00	18.24	0.00	0.02	0.62	0.43
VCD 9A	0.00	14.82	0.00	0.02	0.50	0.42
VCD 13A	0.01	16.58	0.00	0.03	0.61	0.72
VCD 15A	0.00	15.15	0.00	0.04	0.91	0.54
VCD 18A	0.00	28.13	0.00	0.04	0.66	0.77
VCD 21A	0.03	19.95	0.00	0.05	0.64	0.76
VCD 24A	0.00	16.19	0.00	0.10	0.59	0.48
VCD 27A	0.04	18.71	4.67	0.04	0.94	0.65
VCD 29A	0.08	19.20	2.84	0.05	0.96	0.43
SDII 1	0.07	30.86	3.49	0.04	0.84	0.48
SDII 3	0.03	13.88	2.53	0.01	0.41	0.59
SDII 5	0.05	13.68	4.22	0.02	0.49	0.52
SDII 6	0.04	41.60	2.34	0.04	0.62	0.52
SDII 7c	0.08	86.76	2.27	0.05	0.53	0.45
SDII 10	0.03	14.84	5.20	0.10	0.80	0.53
SDII 11	0.02	15.84	0.00	0.29	0.68	0.48
SDII 13a	0.04	14.84	5.22	0.24	0.59	0.40
SDII 14	0.00	13.07	0.00	0.15	0.46	0.51
SDII 15	0.00	14.69	0.00	0.05	0.82	0.53
SDII 16b	0.00	14.24	0.00	0.05	0.60	0.59
SDII 18	0.00	14.29	0.00	0.05	0.53	0.54
SDII 19	0.28	13.62	6.48	0.03	0.85	0.38
SDII 21	0.00	28.26	0.00	0.04	0.69	0.68
SDII 23	0.00	25.49	0.00	0.03	0.73	0.71
SDII 25	0.00	22.05	1.87	0.05	0.75	0.57
SDII 27	0.00	15.57	1.96	0.01	0.93	0.40
SDII 28	0.00	17.89	4.59	0.05	1.15	0.53
SDII 30	0.00	47.36	1.81	0.01	1.13	0.48
SDII 33	0.07	22.17	3.37	0.07	1.39	0.74
SDII 34	0.00	23.59	2.69	0.04	0.96	0.53
SDII 36	0.00	19.10	3.48	0.00	0.53	0.53
SDII 40	0.00	30.40	1.49	0.07	0.60	0.61
VCDII 51A	0.09	19.51	2.24	0.04	0.54	0.42
SDII 42	0.00	16.10	2.10	0.09	0.60	0.47
VCDII 50A	0.03	18.50	1.34	0.04	0.88	0.64
SDII 43	0.11	23.05	2.24	0.45	0.78	0.64
VCDII 49A	0.14	49.20	1.64	0.05	1.01	0.60
VCDII 48A	0.17	64.60	2.68	0.04	1.29	0.60
VCDII 46A	0.03	32.28	1.25	0.06	1.11	0.75
VCDII 44A	0.00	16.67	0.78	0.06	0.56	0.56
VCDII 42A	0.05	17.77	0.89	0.15	0.75	0.53
VCDII 40A	0.07	17.09	1.47	0.44	0.80	0.73
SDII 51	0.00	47.59	1.47	0.04	0.94	0.49
VCDII 37A	0.00	14.85	0.86	0.02	0.63	0.60
VCDII 35A	0.02	12.96	1.16	0.04	0.51	0.39
VCDII 33A	0.00	14.52	1.51	0.05	0.82	0.40
VCDII 30A	0.00	11.65	0.96	0.02	0.51	0.39
VCDII 27A	0.00	14.85	0.89	0.05	0.70	0.37
VCDII 25A	0.00	23.57	2.43	0.08	2.15	0.70
VCDII 22A	0.12	16.22	3.26	0.10	1.46	0.88
VCDII 19A	0.00	14.76	2.73	0.12	1.37	0.59
VCDII 16A	0.00	12.87	1.13	0.47	0.67	0.94
VCDII 12A	0.05	14.03	1.19	0.03	0.75	0.68
VCDII 10A	0.02	12.62	1.59	0.02	0.90	0.53
VCDII 8A	0.03	12.20	1.28	0.04	0.90	0.46
SD 42	0.05	14.08	4.58	0.03	0.96	0.44
VCDII 6A	0.00	14.10	1.44	0.04	0.71	0.41
SD 38	0.04	12.36	1.47	0.03	0.75	0.48
SD 36	0.03	16.14	0.75	0.02	0.74	0.43
SD 32	0.05	13.27	1.30	0.01	0.91	0.41
SD 29	0.00	12.37	2.20	0.04	1.12	0.37
SD 27	0.01	34.71	2.43	0.00	1.28	0.49
SD 24	0.00	20.53	1.30	0.00	1.14	0.50
SD 21	0.00	43.57	1.61	0.00	1.00	0.36
SD 19	0.00	44.85	1.92	0.00	1.03	0.44
SD 16	0.00	53.02	2.43	0.00	1.66	0.37
SD 12	0.00	14.42	1.44	0.00	1.18	0.49
SD 8	0.00	14.99	1.56	0.00	0.90	0.37
SD 5	0.00	15.43	1.84	0.00	1.16	0.42
SD 1	0.00	26.08	3.05	0.00	1.07	0.46

Angles section

Stage	Ammonite zone	Sample n°	Li	Be	B	Na	Mg	Al	K	Ca
Late Hauterivian	*B. balearis*	AN 2	8.45	0.18	4.75	0.00	3287.44	3916.31	1136.70	323367.17
		AN 4	5.16	0.09	0.00	0.00	3227.88	2417.23	457.37	341985.39
		AN 6	5.74	0.09	0.00	0.00	3178.20	2538.43	507.22	313660.76
		AN 8	5.53	0.30	0.00	0.00	2963.97	2516.97	545.27	300111.66
		AN 10	5.13	0.38	0.00	0.00	3163.64	2133.77	574.96	294787.66
		AN 13	3.89	0.00	0.00	0.00	2805.37	1406.86	250.38	310244.85
		AN 15.1	1.74	0.12	0.00	0.00	2316.16	826.02	379.92	314738.03
		AN 16	2.22	0.00	0.00	0.00	2600.79	882.53	174.95	324834.25
		AN 18	4.55	0.13	0.00	0.00	2803.78	1812.45	453.81	304482.28
		AN 20	2.56	0.00	1.97	70.39	2454.92	1236.38	253.65	335994.98
		AN 23	3.17	0.06	0.00	61.94	2704.39	1640.56	268.48	311829.54
		AN 26	1.64	0.00	0.00	58.25	2274.58	932.56	231.03	315266.59
		AN 27.2	5.18	0.09	0.00	51.58	2874.22	2297.35	289.05	304613.01
		AN 29	2.04	0.16	0.00	44.52	2353.67	940.59	156.01	319387.57
		AN 31	2.03	0.16	0.00	50.50	2337.37	1058.54	189.77	312229.78
		AN 33	2.06	0.06	0.00	45.70	2450.01	826.04	136.07	312132.26
		AN 35	3.00	0.15	0.00	59.46	2544.41	1472.03	224.63	308406.57
	S. angulicostatum	AN 38	1.90	0.07	0.00	47.17	2343.64	816.32	141.93	311255.68
		AN 40	2.58	0.83	12.17	47.93	2408.90	1290.82	343.08	315058.40
		AN 43	3.30	0.28	0.00	53.19	2648.07	1358.53	268.36	322415.94
		AN 46	2.46	0.10	0.00	39.23	2272.56	995.98	180.83	317810.71
		AN 49.1	3.68	0.25	0.00	51.65	2504.79	1424.67	221.99	322821.68
		AN 50	2.89	0.22	0.00	42.73	2493.81	1261.20	169.84	321860.60
		AN 51	3.31	0.41	0.00	50.81	2502.49	1363.40	225.58	316779.16
		AN 52	3.41	0.10	0.00	51.46	2747.44	1334.60	202.48	321223.04
		AN 53.2	2.48	0.25	0.00	54.62	2810.44	1045.55	157.91	328330.15
	P. mortilleti	AN 55	2.21	0.29	0.00	41.41	2516.24	997.80	159.37	326593.51
		AN 62.1	3.49	0.42	13.79	54.58	2640.83	1567.33	261.99	343832.67
		AN 65.1	2.64	0.16	0.00	61.57	2780.41	1195.01	166.31	352172.22
		AN 68	3.96	0.29	0.00	67.56	2744.95	1523.86	267.21	328559.24
		AN 71	3.78	0.32	0.00	51.08	2719.47	1419.84	160.06	326548.78
Early Barremian	*A. kiliani*	AN 72	2.85	0.24	0.00	49.94	2514.08	1430.34	178.59	304389.55
		AN 75	3.16	0.22	0.00	76.06	2724.07	1372.37	165.86	330995.12
		AN 78	5.17	0.30	0.00	58.50	2982.13	1912.40	313.41	313443.09
		AN 81	4.63	0.19	0.00	82.30	2897.35	2003.95	236.00	317661.03
		AN 84	4.64	0.23	0.00	54.92	2973.93	1951.41	248.75	312377.94
		AN 87	9.68	0.38	16.59	60.66	3511.56	3549.52	514.11	321810.16
		AN 89	5.92	0.16	0.00	58.11	3247.40	2146.16	327.82	327771.29
		AN 90 haut	4.97	0.04	0.00	63.28	2893.81	1836.43	323.20	320463.38
		AN 92	4.47	0.10	0.00	49.20	2974.81	1776.00	231.15	324039.39
		AN 93 haut	3.29	0.00	0.00	58.17	3031.77	1515.50	229.07	328675.96
		AN 95 bas	4.12	0.10	0.00	61.54	3030.37	1610.47	306.34	307741.10
		AN 97	2.58	0.00	0.00	56.44	2816.42	1024.66	171.19	330125.06
		AN 98 haut	2.92	0.20	0.00	50.08	2564.18	1171.30	174.96	318471.49
	K. nicklesi	AN 101	5.50	0.18	0.00	57.65	3034.79	2222.73	419.16	302469.51
		AN 103	7.36	0.41	10.46	73.73	3782.29	2961.64	691.44	334742.80
		AN 104	4.60	0.11	0.65	74.51	3544.17	2020.31	396.58	359361.19
		AN 105	4.42	0.27	0.00	79.78	3301.83	1990.27	413.92	311657.89
		AN 108	4.12	0.14	0.00	68.40	2780.24	1729.31	291.10	321310.65
	N. pulchella	AN 109.4	4.55	0.34	0.00	65.90	3138.52	1815.18	384.43	307408.36
		AN 110.1b	3.68	0.51	0.00	73.61	2869.42	1518.54	307.65	299431.84
		AN 110.3c	2.29	0.23	0.00	55.08	2495.21	782.24	157.44	322476.14
		AN 110.4	2.88	0.10	0.00	56.99	2596.81	1043.38	241.33	314774.38
		AN 111.2	3.57	0.07	0.00	57.21	2739.29	1371.52	237.45	312900.74
		AN 111.5	5.89	0.37	13.52	71.38	2920.99	2319.23	472.68	334250.68
		AN 112.2	5.40	0.13	0.00	75.42	3025.49	2212.47	273.14	321171.77
	K. compressissima	AN 112.7	4.57	0.23	0.00	55.76	2965.40	2183.70	455.70	307412.02
		AN 114.2	2.54	0.07	0.00	52.45	2496.52	1336.50	240.45	312938.13
		AN 115	4.70	0.07	0.00	62.63	2983.30	2062.15	316.58	306409.35
		AN 117	2.62	0.13	0.00	47.65	2669.69	1221.77	212.71	315017.15
		AN 119	1.66	0.13	0.00	51.53	2450.38	632.71	130.08	326860.76
		AN 121	2.53	0.03	0.00	51.99	2683.17	1024.02	186.80	311033.22
		AN 123	3.26	0.03	0.00	50.03	2627.21	1377.40	294.44	310674.07

Angles section

Sample n°	Sc	Ti	V	Cr	Mn	Fe	Co	Ni	Cu	Zn	Ga
AN 2	0.35	135.31	7.78	6.69	113.27	4887.34	1.04	13.14	5.54	16.12	1.02
AN 4	0.28	159.81	4.88	3.87	126.05	5078.53	1.36	12.63	4.47	17.42	0.47
AN 6	0.23	138.43	5.04	3.68	125.52	5100.22	1.49	13.41	4.68	21.93	0.56
AN 8	0.33	151.94	5.03	4.79	111.07	4396.90	1.01	12.25	5.91	35.59	0.49
AN 10	0.34	149.05	4.87	4.44	98.42	3826.35	1.79	13.57	5.79	15.46	0.45
AN 13	0.22	147.36	3.64	3.29	102.95	3502.92	0.97	11.18	3.72	13.18	0.29
AN 15.1	0.12	150.25	2.62	2.75	110.05	2584.03	1.23	11.29	3.58	11.36	0.26
AN 16	0.08	140.07	2.75	2.33	98.35	2736.92	1.28	11.24	3.64	7.65	0.22
AN 18	0.17	150.92	3.89	3.70	95.35	4025.26	1.32	11.16	4.88	30.37	0.47
AN 20	0.00	166.12	3.43	3.41	103.02	2975.18	0.80	8.95	3.11	17.93	0.39
AN 23	0.00	154.17	4.13	3.61	104.56	3516.86	1.36	12.45	6.66	17.79	0.41
AN 26	0.00	158.73	2.92	3.79	98.86	3169.89	0.83	9.81	4.32	14.90	0.31
AN 27.2	0.00	137.07	4.64	4.43	105.31	4670.47	1.15	11.30	6.85	26.72	0.56
AN 29	0.00	136.69	2.70	2.63	97.02	3856.14	1.11	10.79	3.35	13.45	0.28
AN 31	0.00	142.49	3.04	3.18	98.53	3114.49	1.17	11.28	4.61	20.26	0.31
AN 33	0.00	160.39	2.71	3.11	78.40	2325.13	1.06	10.55	3.42	6.85	0.27
AN 35	0.00	147.21	4.02	2.99	87.11	3305.78	1.05	11.66	5.49	16.32	0.41
AN 38	0.00	161.75	2.45	2.39	87.22	5346.64	5.15	24.32	5.92	75.44	0.28
AN 40	1.80	164.86	4.15	3.30	93.55	4664.38	0.98	10.43	4.40	23.53	0.48
AN 43	0.15	164.95	3.97	3.81	92.36	3377.86	1.25	11.65	5.67	18.99	0.42
AN 46	0.00	161.38	2.85	2.90	94.18	2904.85	1.08	11.06	3.60	15.65	0.30
AN 49.1	0.00	147.27	4.18	3.00	87.84	3068.11	1.13	10.54	3.93	48.61	0.38
AN 50	0.00	149.26	3.45	2.65	104.03	3011.44	0.77	9.72	3.22	14.54	0.33
AN 51	0.00	159.10	4.62	3.48	99.00	3018.16	1.16	12.53	5.34	26.19	0.36
AN 52	0.00	161.89	8.93	2.14	92.79	6303.36	2.36	26.63	6.41	420.80	0.44
AN 53.2	0.00	153.45	7.43	1.99	91.02	4355.78	1.42	23.69	3.83	13.13	0.31
AN 55	0.00	158.97	4.75	2.35	98.84	2455.41	0.71	8.58	3.16	25.79	0.31
AN 62.1	0.13	153.12	4.79	2.45	124.79	3142.77	1.03	10.21	3.52	17.13	0.51
AN 65.1	0.13	142.51	4.38	1.87	133.63	2933.72	1.56	11.89	3.93	12.59	0.28
AN 68	0.20	148.04	4.61	3.13	124.29	3555.60	0.98	10.37	4.69	24.61	0.43
AN 71	0.04	138.53	4.22	2.40	115.98	3686.75	0.99	10.74	3.70	15.91	0.31
AN 72	0.11	148.08	4.61	2.22	114.61	3660.94	1.05	11.19	4.14	23.89	0.37
AN 75	0.04	154.88	3.57	2.76	116.82	3496.32	1.03	10.10	3.44	16.25	0.32
AN 78	0.04	141.09	5.00	3.40	118.02	4472.06	2.17	11.93	4.18	29.54	0.45
AN 81	0.08	132.04	5.30	2.83	126.13	4821.42	1.30	10.64	4.84	33.86	0.49
AN 84	0.00	145.95	4.88	2.44	124.77	4816.87	1.28	11.05	3.50	26.82	0.44
AN 87	0.41	157.95	7.34	5.31	138.73	5547.98	1.57	12.42	5.15	17.40	0.92
AN 89	0.36	133.21	5.17	3.48	141.27	4216.26	1.25	9.25	3.89	14.02	0.48
AN 90 haut	0.30	160.55	4.98	3.59	141.23	4775.30	1.79	13.17	4.52	18.55	0.44
AN 92	0.37	130.86	4.08	3.18	144.81	4468.41	1.34	11.60	4.55	12.24	0.45
AN 93 haut	0.25	145.34	3.59	3.52	145.98	3596.65	1.25	11.02	3.62	16.10	0.40
AN 95 bas	0.33	149.85	3.95	3.31	152.67	4886.94	1.47	10.65	5.80	17.18	0.38
AN 97	0.21	140.52	3.13	2.64	142.21	2738.02	1.11	11.56	3.85	15.57	0.26
AN 98 haut	0.27	152.28	3.49	2.71	149.96	3989.89	1.50	10.91	11.51	29.09	0.34
AN 101	0.38	143.89	4.92	3.65	147.00	4833.90	1.33	12.82	6.11	23.13	0.59
AN 103	0.20	162.67	6.88	4.53	173.01	5334.03	2.01	12.74	6.03	30.35	0.81
AN 104	0.16	172.96	5.15	4.06	168.05	4806.90	1.30	11.33	6.05	24.55	0.54
AN 105	0.27	149.01	4.47	3.79	151.32	5361.52	1.49	11.80	6.94	33.44	0.48
AN 108	0.30	137.19	5.81	3.37	151.40	5455.51	1.49	11.22	6.21	37.61	0.47
AN 109.4	0.29	163.05	4.14	3.04	129.95	3958.18	1.72	11.49	5.75	29.79	0.54
AN 110.1b	0.24	161.44	5.48	3.08	135.48	4272.76	1.73	13.14	5.34	52.45	0.40
AN 110.3c	0.13	148.50	3.99	2.64	143.05	2810.33	1.38	10.42	4.04	47.02	0.25
AN 110.4	0.10	153.02	5.03	2.88	136.19	3153.37	1.09	11.21	5.29	21.30	0.33
AN 111.2	0.16	155.74	5.36	2.58	142.83	3445.86	0.88	8.83	4.58	20.12	0.34
AN 111.5	0.24	0.00	7.64	3.26	158.55	4590.06	1.20	10.84	5.10	65.66	0.71
AN 112.2	0.25	0.00	6.66	2.52	148.20	4313.24	1.33	10.43	4.41	23.15	0.57
AN 112.7	0.26	0.00	5.55	2.41	158.58	4166.80	1.04	10.55	4.12	150.20	0.61
AN 114.2	0.29	0.00	4.61	1.80	143.79	5099.73	0.93	10.13	4.68	24.82	0.33
AN 115	0.32	0.00	6.43	2.57	145.08	4492.24	1.05	13.81	5.45	24.46	0.37
AN 117	0.26	0.00	4.16	1.87	138.69	3941.66	1.27	10.40	5.44	24.94	0.35
AN 119	0.18	0.00	3.10	1.55	127.46	2690.54	1.00	10.27	4.83	80.29	0.22
AN 121	0.16	0.00	3.38	1.86	142.71	2884.19	1.34	10.94	3.29	18.69	0.28
AN 123	0.24	0.00	4.26	2.53	141.11	3533.06	1.38	11.74	4.57	30.62	0.46

Angles section

Sample n°	Ge	As	Se	Rb	Sr	Y	Zr	Nb	Mo	Ru	Pd
AN 2	0.03	0.82	0.00	7.51	843.42	6.79	0.81	0.01	0.60	0.00	0.00
AN 4	0.04	0.65	0.00	3.47	870.39	6.21	0.51	0.00	0.26	0.00	0.00
AN 6	0.02	0.77	0.00	3.56	761.22	6.66	1.28	0.01	0.20	0.00	0.03
AN 8	0.02	0.44	0.00	4.53	697.20	6.90	0.62	0.00	0.33	0.00	0.00
AN 10	0.04	0.77	0.00	4.42	688.22	6.56	0.53	0.00	0.14	0.00	0.01
AN 13	0.00	0.29	0.00	2.05	701.89	5.31	0.47	0.00	0.11	0.00	0.00
AN 15.1	0.02	0.39	0.00	2.75	762.21	7.05	0.58	0.00	0.19	0.00	0.00
AN 16	0.02	0.36	0.00	1.61	747.35	5.00	0.79	0.00	0.14	0.00	0.02
AN 18	0.03	0.45	0.00	3.37	726.91	6.73	0.39	0.01	0.40	0.00	0.02
AN 20	0.00	0.25	8.25	2.81	778.56	6.33	0.48	0.00	0.45	0.00	0.01
AN 23	0.02	0.41	0.54	3.47	684.55	7.87	0.46	0.00	0.16	0.00	0.00
AN 26	0.00	0.30	4.62	2.66	775.63	7.30	0.58	0.00	0.18	0.00	0.01
AN 27.2	0.01	0.66	0.00	3.52	609.86	8.69	0.72	0.01	0.25	0.00	0.00
AN 29	0.00	0.73	1.51	2.02	734.37	6.88	0.44	0.00	0.44	0.00	0.00
AN 31	0.01	0.61	0.00	2.47	689.98	8.61	0.50	0.00	0.17	0.01	0.01
AN 33	0.00	0.40	0.00	1.67	675.91	5.45	0.54	0.00	0.11	0.01	0.01
AN 35	0.00	0.50	0.00	2.61	673.28	8.97	0.57	0.00	0.13	0.00	0.00
AN 38	0.01	1.49	0.00	1.67	741.69	6.99	0.46	0.00	1.02	0.00	0.00
AN 40	0.00	0.61	0.00	3.00	729.66	7.36	0.85	0.00	0.57	0.00	0.03
AN 43	0.03	0.57	0.00	3.11	630.61	7.58	0.49	0.01	0.24	0.00	0.00
AN 46	0.03	0.35	0.00	1.95	635.04	6.39	0.66	0.00	0.06	0.02	0.00
AN 49.1	0.02	0.43	0.00	2.81	585.25	7.06	0.43	0.00	0.10	0.03	0.01
AN 50	0.03	0.35	2.67	2.12	598.51	7.11	0.39	0.00	0.36	0.00	0.00
AN 51	0.03	0.86	4.79	2.67	597.89	6.18	0.90	0.00	0.59	0.01	0.01
AN 52	0.02	6.34	0.08	2.88	510.78	5.81	0.58	0.00	4.87	0.00	0.00
AN 53.2	0.05	3.84	0.00	2.39	520.89	5.78	0.54	0.00	4.61	0.01	0.02
AN 55	0.03	0.20	0.00	2.07	658.81	7.33	0.43	0.00	0.14	0.00	0.03
AN 62.1	0.03	0.64	0.00	2.79	724.49	6.33	0.59	0.00	0.44	0.00	0.00
AN 65.1	0.01	0.54	0.00	2.32	715.73	7.38	0.79	0.00	0.16	0.01	0.02
AN 68	0.00	0.46	0.00	2.74	663.96	7.46	1.23	0.00	0.20	0.00	0.01
AN 71	0.00	0.47	0.00	2.05	691.43	6.85	0.56	0.00	0.06	0.06	0.00
AN 72	0.02	0.31	0.00	2.23	651.78	6.87	0.67	0.00	0.00	0.00	0.02
AN 75	0.00	0.38	0.00	1.98	708.81	5.15	0.56	0.00	0.05	0.00	0.01
AN 78	0.00	0.62	0.00	4.39	728.97	6.13	0.67	0.00	0.17	0.00	0.01
AN 81	0.01	0.50	0.00	3.25	639.66	8.13	0.70	0.00	0.04	0.01	0.01
AN 84	0.00	0.42	0.00	3.24	738.54	5.69	0.68	0.00	0.18	0.00	0.01
AN 87	0.00	0.88	0.00	5.67	790.19	7.28	0.83	0.00	0.61	0.01	0.00
AN 89	0.03	0.61	0.00	3.75	845.66	6.71	0.88	0.00	0.21	0.00	0.01
AN 90 haut	0.00	0.86	0.00	4.23	827.72	6.46	0.60	0.00	0.29	0.12	0.00
AN 92	0.01	0.58	0.00	2.99	831.14	5.56	0.54	0.00	0.20	0.00	0.01
AN 93 haut	0.00	0.46	0.00	2.99	829.02	5.31	0.49	0.00	0.03	0.00	0.00
AN 95 bas	0.00	0.87	0.00	3.93	794.49	6.52	0.67	0.00	0.21	0.01	0.01
AN 97	0.00	0.42	0.00	2.04	973.11	7.02	0.46	0.01	0.07	0.05	0.01
AN 98 haut	0.01	0.75	0.00	2.28	904.69	8.10	0.56	0.00	0.21	0.00	0.00
AN 101	0.04	0.92	0.00	4.76	923.97	8.20	0.91	0.00	0.23	0.00	0.00
AN 103	0.01	1.02	1.05	6.92	1026.37	6.51	1.42	0.01	0.65	0.00	0.03
AN 104	0.02	1.10	0.00	4.72	1020.72	6.02	0.83	0.01	0.37	0.00	0.02
AN 105	0.01	1.22	0.00	4.68	959.18	6.56	0.61	0.00	0.63	0.00	0.02
AN 108	0.01	1.08	0.00	3.71	794.29	9.14	0.68	0.00	0.71	0.00	0.02
AN 109.4	0.00	1.14	0.00	4.09	837.51	7.10	0.85	0.00	0.69	0.00	0.04
AN 110.1b	0.04	1.36	0.00	3.19	763.01	8.38	1.11	0.00	1.11	0.00	0.03
AN 110.3c	0.03	0.67	0.00	1.67	758.64	5.43	0.41	0.00	0.33	0.00	0.03
AN 110.4	0.01	1.07	0.00	2.35	749.86	7.41	0.83	0.01	0.47	0.00	0.03
AN 111.2	0.03	0.87	0.00	2.49	659.47	6.89	0.63	0.00	0.12	0.00	0.00
AN 111.5	0.00	1.12	0.00	4.09	678.57	8.23	1.26	0.00	0.72	0.00	0.02
AN 112.2	0.04	0.55	0.00	2.86	709.91	8.07	1.03	0.00	0.17	0.01	0.02
AN 112.7	0.00	0.63	0.00	4.26	676.77	7.14	0.99	0.00	0.42	0.00	0.00
AN 114.2	0.03	0.88	0.00	2.68	667.09	5.71	0.62	0.00	0.41	0.01	0.01
AN 115	0.02	1.21	0.00	3.44	674.59	8.57	0.48	0.00	0.62	0.00	0.02
AN 117	0.00	0.74	0.00	2.60	713.90	6.88	0.49	0.00	0.30	0.01	0.02
AN 119	0.04	0.34	0.00	1.20	709.39	5.12	0.82	0.00	0.23	0.01	0.03
AN 121	0.04	0.32	0.00	2.12	692.85	5.66	0.34	0.00	0.12	0.00	0.00
AN 123	0.03	0.53	0.00	3.15	715.42	6.12	0.35	0.00	0.27	0.00	0.02

Angles section

Sample n°	Ag	Cd	Ba	Pb	Bi	Th	U
AN 2	0.03	0.02	22.44	1.52	0.38	0.94	0.57
AN 4	0.03	0.02	14.53	2.00	0.08	0.68	0.50
AN 6	0.10	0.03	65.98	2.35	0.05	0.68	0.60
AN 8	0.00	0.06	280.75	1.25	0.03	0.89	0.71
AN 10	0.08	0.02	10.98	1.54	0.03	0.79	0.88
AN 13	0.00	0.01	20.77	0.78	0.01	0.46	0.64
AN 15.1	0.03	0.03	12.44	1.05	0.01	0.43	0.57
AN 16	0.05	0.00	12.36	1.28	0.01	0.34	0.52
AN 18	0.00	0.05	182.27	0.63	0.00	0.49	0.55
AN 20	0.04	0.04	92.46	0.91	0.11	0.34	0.49
AN 23	0.08	0.07	89.85	1.48	0.07	0.61	0.91
AN 26	0.01	0.00	67.30	0.98	0.05	0.63	0.76
AN 27.2	0.03	0.11	51.67	1.91	0.05	0.89	0.62
AN 29	0.11	0.03	40.87	1.55	0.03	0.42	0.55
AN 31	0.06	0.02	10.78	1.24	0.03	0.50	0.67
AN 33	0.02	0.00	30.55	1.16	0.01	0.38	0.47
AN 35	0.01	0.09	16.88	1.62	0.02	0.55	1.02
AN 38	0.12	0.39	23.78	6.24	0.01	0.37	0.48
AN 40	0.98	0.20	111.45	1.99	0.43	0.37	0.63
AN 43	0.07	0.09	7.99	1.93	0.10	0.52	0.73
AN 46	0.02	0.04	19.60	0.96	0.03	0.39	0.49
AN 49.1	0.04	0.11	434.49	1.13	0.04	0.47	0.73
AN 50	0.01	0.06	18.35	1.21	0.03	0.35	0.49
AN 51	0.04	0.08	162.94	1.58	0.04	0.53	1.05
AN 52	0.08	2.12	28.61	5.73	0.02	0.44	1.43
AN 53.2	0.03	0.05	33.26	4.81	0.02	0.41	1.28
AN 55	0.01	0.03	145.25	1.02	0.01	0.37	2.07
AN 62.1	0.18	0.00	67.07	1.08	0.46	0.32	0.78
AN 65.1	0.03	0.00	16.17	2.06	0.10	0.34	0.98
AN 68	0.02	0.06	234.96	1.03	0.05	0.52	0.79
AN 71	0.00	0.00	28.19	1.22	0.04	0.49	0.89
AN 72	0.02	0.12	60.15	1.91	0.03	0.41	1.17
AN 75	0.00	0.02	42.23	1.15	0.03	0.47	0.53
AN 78	0.06	0.04	133.59	1.57	0.04	0.63	0.54
AN 81	0.00	0.08	18.14	1.51	0.03	0.59	0.73
AN 84	0.02	0.04	70.24	1.35	0.02	0.55	0.52
AN 87	0.02	0.04	45.60	2.05	0.40	0.90	0.59
AN 89	0.02	0.03	9.56	1.26	0.10	0.61	0.56
AN 90 haut	0.13	0.00	70.27	2.06	0.09	0.68	0.56
AN 92	0.02	0.04	9.58	2.37	0.05	0.64	0.40
AN 93 haut	0.04	0.02	71.79	1.36	0.05	0.62	0.37
AN 95 bas	0.07	0.06	10.86	1.74	0.03	0.67	0.51
AN 97	0.00	0.06	31.50	1.26	0.02	0.40	0.49
AN 98 haut	0.04	0.11	69.08	1.40	0.03	0.50	0.53
AN 101	0.03	0.04	16.78	2.21	0.05	0.72	0.71
AN 103	0.06	0.06	188.31	2.42	0.41	0.67	0.57
AN 104	0.05	0.06	89.63	2.22	0.11	0.60	0.52
AN 105	0.05	0.05	154.66	2.28	0.08	0.89	0.52
AN 108	0.08	0.08	243.36	2.20	0.06	0.76	0.89
AN 109.4	0.04	0.02	221.75	2.08	0.04	0.80	0.49
AN 110.1b	0.04	0.04	504.13	2.66	0.04	0.61	0.68
AN 110.3c	0.04	0.08	495.05	0.91	0.02	0.37	0.62
AN 110.4	0.05	0.07	82.91	1.77	0.02	0.49	1.04
AN 111.2	0.04	0.05	26.19	1.50	0.02	0.38	0.80
AN 111.5	0.14	0.09	658.66	1.86	0.39	0.51	1.22
AN 112.2	0.02	0.07	38.49	1.24	0.10	0.42	0.74
AN 112.7	0.06	0.08	1735.00	1.83	0.06	0.77	0.59
AN 114.2	0.08	0.04	106.07	1.43	0.04	0.50	0.68
AN 115	0.06	0.03	65.93	9.36	0.04	0.57	0.77
AN 117	0.07	0.05	70.71	1.36	0.03	0.44	0.60
AN 119	0.03	1.25	90.98	0.81	0.02	0.24	0.57
AN 121	0.02	0.06	95.90	0.99	0.02	0.33	0.54
AN 123	0.06	0.08	69.74	1.10	0.02	0.39	0.57

Angles section (continued)

Stage	Ammonite zone	Sample n°	Li	Be	B	Na	Mg	Al	K	Ca
Early Barremian	*C. darsi*	AN 125	7.79	0.38	15.49	61.26	3509.93	3542.98	471.02	319991.99
		AN 127	2.09	0.25	1.10	51.34	2599.86	922.12	124.77	344449.34
		AN 128	1.31	0.11	0.00	49.71	2513.30	569.70	103.27	340240.96
		AN 129	3.22	0.22	0.00	61.61	2664.20	1544.29	287.05	322019.75
		AN 131	2.56	0.31	0.00	59.10	2647.31	1103.69	179.05	323837.81
		AN 133	1.48	0.26	0.00	58.08	2586.04	601.54	102.50	331854.82
		AN 136.2	4.96	0.25	0.00	68.57	3206.77	2292.92	343.92	305011.27
		AN 138	2.22	0.22	0.00	49.90	2809.51	1018.22	172.16	316972.78
		AN 139d	1.07	0.14	0.00	105.99	3211.68	696.22	0.00	443280.19
Late Barremian	*H. uhligi*	AN 141.1	2.17	0.24	10.83	54.42	2259.32	913.11	288.66	347139.48
		AN 143.1a	1.87	0.15	1.15	47.58	2310.28	998.16	246.86	328958.52
		AN 144	3.01	0.27	0.00	50.73	2577.35	1318.56	257.05	316288.33
		AN 147.1	1.57	0.07	0.00	57.88	2371.55	831.67	176.97	325583.15
	H. sayni	AN 148	1.37	0.48	0.00	42.53	2065.31	550.86	181.55	323959.00
		AN 149.3	1.86	0.29	0.00	47.73	2174.77	954.07	232.40	320283.60
		AN 151.1	1.23	0.26	0.00	33.76	2053.74	614.02	185.50	339841.74
		AN 151.3	1.22	0.21	0.00	42.69	2211.88	477.21	84.20	330540.41
		AN 153.2	1.54	0.00	0.00	49.32	2164.70	760.66	214.88	328907.41
		AN 155.1a	2.14	0.11	0.00	69.77	2723.71	1920.68	0.00	346418.73
		AN 156.1	1.77	0.00	0.00	62.15	2710.80	1327.97	0.00	355728.53
		AN 156.4	1.01	0.00	0.00	63.09	2384.25	1231.49	0.00	337670.57
		AN 156.6	0.64	0.26	0.00	66.62	2389.40	748.28	0.00	341164.60
		AN 158	0.96	0.27	0.00	59.33	2535.78	1276.13	0.00	351732.97
	G. sartousiana	AN 160.3	1.33	0.50	0.00	70.48	2525.58	1183.97	0.00	339801.22
		AN 161.1	1.86	0.00	0.00	46.94	2688.91	1858.90	0.00	329273.33
		AN 161.2	0.29	0.00	0.00	79.78	2705.64	298.76	0.00	376884.65
		AN 163.1b	0.58	0.00	0.00	64.13	2192.80	606.88	0.00	343130.08
	H. feraudianus	AN 164.2	1.45	0.89	4.23	81.80	2587.99	946.42	0.00	361086.71
		AN 166 b	3.91	0.00	0.00	97.56	3000.64	1878.41	0.00	369043.37
	I. giraudi	AN 168.1	4.63	0.15	0.00	125.98	3226.22	2557.02	0.00	352054.48
		AN 170c	6.32	0.49	0.00	119.15	3795.68	3327.35	0.00	347546.27
		AN 172.1	5.66	0.47	0.00	120.86	3696.78	2289.66	0.00	379490.54
		AN 173	7.24	1.17	0.00	87.66	3586.55	3337.05	0.00	358768.92
		AN 176.1	5.85	0.00	0.00	105.91	3421.07	3261.41	0.00	352936.21
	M. sarasini	AN 177	4.72	0.00	0.00	85.11	3076.22	2215.84	0.00	367527.51
		AN 179.1	4.93	0.45	0.00	80.53	2935.26	3170.51	0.00	348272.78
		AN 181	4.54	1.07	10.81	118.22	3058.03	2458.60	0.00	404144.35
		AN 183	3.23	1.11	0.00	117.41	2779.91	1799.70	0.00	417171.86
		AN 185	2.68	1.19	0.00	154.19	2438.14	1174.28	0.00	386844.79
		AN 188	1.03	1.05	0.00	81.71	2564.56	821.77	0.00	392280.83
		AN 190	3.31	0.31	0.00	110.64	2766.49	2146.25	0.00	378373.99
		AN 192	3.41	1.00	2.22	94.99	2453.71	2196.56	0.00	378695.38
		AN 195	4.81	1.42	0.00	112.77	2506.81	2731.81	0.00	316916.35
		AN 196.2	6.46	0.12	0.00	107.21	2784.58	3320.45	0.00	314711.66
Early Aptian	*D. oglanlensis*	AN 197	1.80	0.11	0.00	89.53	2034.66	1420.99	0.00	316474.27
		AN 198	2.44	0.50	0.00	104.67	2370.24	1467.57	0.00	363152.93
		AN 200	2.82	0.00	0.00	79.72	2403.46	1551.79	0.00	349673.91
		AN 202 c	1.26	0.14	0.00	80.56	2121.32	748.56	0.00	355822.29
		AN 204	2.05	0.00	0.00	115.78	2323.26	1192.18	0.00	364100.51
		AN 206	2.66	0.97	0.00	117.76	2284.53	1974.63	0.00	348146.31
		AN 211	3.34	0.00	5.58	123.84	2250.43	1942.99	0.00	325138.16
		AN 214	0.95	0.55	0.00	106.63	2337.94	948.95	0.00	355086.85
		AN 216	1.24	0.00	0.00	93.35	2269.81	1024.72	0.00	335157.61

Angles section (continued)

Sample n°	Sc	Ti	V	Cr	Mn	Fe	Co	Ni	Cu	Zn	Ga
AN 125	0.27	146.65	6.99	3.81	135.55	5267.09	1.95	14.53	7.09	41.84	0.88
AN 127	0.01	156.92	4.27	1.98	123.27	3068.60	0.76	8.52	5.15	18.56	0.29
AN 128	0.00	147.06	3.24	1.69	131.92	2696.00	0.84	9.74	4.39	14.86	0.18
AN 129	0.13	141.68	4.25	2.28	151.36	4648.42	1.76	12.89	6.48	23.92	0.45
AN 131	0.01	155.46	8.34	1.90	120.47	3505.37	1.25	13.50	7.52	21.95	0.32
AN 133	0.00	162.11	3.10	2.01	118.83	3033.82	1.00	12.97	6.30	21.42	0.22
AN 136.2	0.19	140.99	4.88	2.89	137.90	5583.43	2.27	14.45	8.46	29.82	0.53
AN 138	0.12	153.18	3.41	1.17	125.96	3902.70	0.97	11.66	6.72	44.43	0.32
AN 139d	1.20	237.31	3.54	3.74	138.25	2954.51	0.94	11.87	4.86	26.74	0.19
AN 141.1	0.25	0.00	4.69	2.15	106.73	2469.15	1.22	11.99	5.09	32.21	0.37
AN 143.1a	0.54	0.00	3.79	1.90	100.11	2593.67	1.23	12.28	4.87	21.33	0.27
AN 144	0.28	0.00	3.38	2.04	102.41	3171.49	2.00	16.31	4.79	24.18	0.33
AN 147.1	0.34	0.00	3.57	1.99	90.68	2609.61	1.45	13.50	5.14	39.23	0.26
AN 148	0.41	0.00	3.56	2.06	87.63	1991.46	1.01	10.93	5.75	10.90	0.24
AN 149.3	0.66	0.00	4.20	2.12	82.28	2131.21	1.12	13.35	5.13	14.68	0.26
AN 151.1	0.23	0.00	2.72	1.87	85.02	1991.83	1.04	13.04	4.47	24.29	0.21
AN 151.3	0.19	0.00	2.50	1.82	96.35	2038.20	0.97	11.69	3.63	10.29	0.17
AN 153.2	0.18	0.00	3.28	2.35	81.47	2207.80	0.85	11.24	5.51	14.50	0.29
AN 155.1a	0.32	176.91	5.28	0.10	91.60	2674.92	1.46	21.16	5.34	45.06	0.38
AN 156.1	0.50	176.92	3.41	0.64	97.27	2342.03	1.06	6.44	4.02	9.05	0.24
AN 156.4	0.21	150.53	4.01	0.42	87.74	2416.94	1.16	8.09	5.73	24.14	0.19
AN 156.6	0.22	175.06	3.21	1.61	90.41	2267.52	0.86	7.23	6.53	21.88	0.16
AN 158	0.30	181.01	3.99	1.00	103.48	2948.36	1.54	10.41	5.21	16.34	0.19
AN 160.3	0.00	175.17	4.47	0.76	120.81	2578.50	1.37	9.07	5.80	15.64	0.30
AN 161.1	0.00	172.94	4.94	0.90	131.47	3263.63	1.67	10.22	4.22	46.58	0.31
AN 161.2	0.00	196.55	4.82	1.41	198.64	1978.30	1.28	6.20	2.81	25.81	0.05
AN 163.1b	0.00	177.49	5.73	1.03	130.91	2282.58	1.03	6.53	3.14	8.76	0.13
AN 164.2	0.00	183.53	6.73	2.07	130.65	1916.09	1.05	6.33	2.25	36.31	0.29
AN 166 b	0.41	181.10	7.48	2.07	144.21	5911.40	2.48	13.25	6.55	177.50	0.52
AN 168.1	0.49	189.65	7.12	2.32	139.74	3970.77	1.96	9.76	6.45	38.73	0.58
AN 170c	0.00	178.15	5.38	2.94	175.96	5445.23	1.43	6.73	7.77	47.58	0.58
AN 172.1	0.00	191.93	5.15	2.19	180.85	4593.45	1.86	6.32	6.83	25.39	0.62
AN 173	0.00	178.86	6.97	1.92	196.88	6732.48	1.69	8.85	6.27	21.27	0.63
AN 176.1	0.00	167.73	6.43	2.99	156.06	5725.45	2.58	10.25	10.50	25.73	0.77
AN 177	0.00	176.43	4.72	2.02	164.36	4973.01	1.42	8.85	7.34	26.92	0.46
AN 179.1	0.00	169.13	5.95	1.79	142.22	5019.51	0.86	11.55	5.05	21.62	0.52
AN 181	0.77	205.78	5.65	4.58	138.70	6878.14	2.28	10.90	10.18	67.08	0.52
AN 183	0.60	197.96	4.57	3.78	126.05	4147.11	1.65	8.25	7.85	29.59	0.43
AN 185	0.51	196.31	3.68	2.75	111.12	3282.55	1.25	8.78	4.38	15.70	0.28
AN 188	0.31	176.01	2.88	2.91	101.00	2901.40	1.90	8.15	4.76	20.01	0.20
AN 190	0.53	175.31	6.53	4.34	103.51	4784.98	1.68	12.26	8.92	24.29	0.57
AN 192	0.00	182.10	6.59	4.23	102.52	4323.00	1.45	7.52	7.11	16.27	0.57
AN 195	0.00	142.96	6.38	4.38	78.96	4009.98	1.37	6.95	9.39	37.73	0.64
AN 196.2	0.00	149.10	5.85	3.25	78.37	4532.15	1.71	9.48	9.14	16.54	0.64
AN 197	0.00	157.29	3.11	2.61	71.95	2671.78	0.99	6.85	6.64	78.38	0.28
AN 198	0.00	175.71	4.10	3.61	82.36	2838.46	1.10	8.13	6.50	18.73	0.28
AN 200	0.00	175.20	3.83	3.07	77.89	2808.44	1.05	6.98	6.13	14.53	0.42
AN 202 c	0.00	155.16	2.81	2.84	83.90	2286.21	1.02	8.76	9.43	18.84	0.27
AN 204	0.00	178.25	4.93	4.46	90.88	2945.70	1.91	8.73	6.57	23.40	0.31
AN 206	0.00	166.49	6.19	4.73	89.91	2975.89	1.56	9.38	6.92	20.27	0.61
AN 211	0.19	151.56	5.14	2.92	85.67	2576.83	1.03	7.51	7.37	21.32	0.61
AN 214	0.25	181.82	3.55	3.55	97.20	2612.55	0.85	6.31	7.27	22.85	0.31
AN 216	0.22	162.60	3.57	1.73	92.61	2419.91	0.97	6.64	4.42	17.26	0.30

Angles section (continued)

Sample n°	Ge	As	Se	Rb	Sr	Y	Zr	Nb	Mo	Ru	Pd
AN 125	0.04	1.06	0.74	4.87	702.25	9.93	1.12	0.00	0.73	0.00	0.01
AN 127	0.00	0.36	0.91	1.13	780.81	7.95	0.79	0.00	0.32	0.00	0.00
AN 128	0.02	0.42	0.00	1.07	708.06	5.74	1.00	0.00	0.34	0.01	0.00
AN 129	0.03	2.58	1.31	3.76	639.90	10.20	0.62	0.00	1.70	0.07	0.00
AN 131	0.01	0.95	4.29	2.05	706.61	8.77	0.96	0.00	0.73	0.00	0.00
AN 133	0.01	1.08	0.00	1.32	684.56	6.26	0.46	0.00	0.39	0.00	0.00
AN 136.2	0.00	1.94	0.00	4.20	548.71	9.51	0.71	0.01	0.47	0.00	0.00
AN 138	0.04	1.10	0.00	2.21	655.96	7.24	0.33	0.00	0.57	0.00	0.02
AN 139d	0.09	0.63	0.00	1.27	900.55	9.39	0.54	0.00	0.16	0.00	0.01
AN 141.1	0.03	0.50	0.00	2.39	696.98	7.11	0.84	0.00	0.69	0.00	0.03
AN 143.1a	0.01	0.46	0.00	1.86	662.22	9.76	0.56	0.00	0.36	0.00	0.01
AN 144	0.02	0.88	0.00	2.59	612.68	10.33	0.80	0.00	0.52	0.00	0.03
AN 147.1	0.01	0.83	0.00	1.86	639.40	9.02	0.48	0.00	0.27	0.00	0.02
AN 148	0.04	0.30	0.00	1.61	697.67	7.16	0.46	0.00	0.10	0.00	0.02
AN 149.3	0.03	0.46	0.00	2.11	647.89	7.86	1.07	0.00	0.12	0.00	0.02
AN 151.1	0.00	0.37	0.00	1.72	660.86	6.45	0.87	0.00	0.25	0.00	0.02
AN 151.3	0.02	0.48	0.00	1.07	695.46	10.70	0.33	0.00	0.20	0.00	0.02
AN 153.2	0.03	0.42	0.00	1.91	685.13	7.34	0.58	0.00	0.10	0.00	0.02
AN 155.1a	0.00	0.33	0.00	2.94	680.27	8.60	0.25	0.00	0.48	0.00	0.04
AN 156.1	0.00	0.13	0.00	2.22	702.15	10.71	0.20	0.00	0.41	0.00	0.00
AN 156.4	0.00	0.50	0.00	2.48	630.24	7.76	0.16	0.00	0.24	0.00	0.01
AN 156.6	0.00	0.36	0.00	2.19	682.41	7.92	0.25	0.00	0.45	0.00	0.01
AN 158	0.00	0.56	0.00	2.73	691.86	9.01	0.26	0.00	0.41	0.00	0.00
AN 160.3	0.02	0.84	0.00	2.66	677.75	8.52	0.07	0.00	0.18	0.00	0.02
AN 161.1	0.00	0.78	0.00	1.71	645.41	9.82	0.08	0.00	0.17	0.00	0.00
AN 161.2	0.00	0.19	0.00	0.69	762.74	6.87	0.10	0.00	0.00	0.00	0.00
AN 163.1b	0.00	0.27	0.00	1.48	763.13	6.98	0.14	0.00	0.19	0.00	0.00
AN 164.2	0.07	0.14	0.00	1.61	768.30	8.27	0.45	0.01	0.12	0.00	0.00
AN 166 b	0.00	2.00	0.00	3.01	851.25	11.75	0.43	0.00	0.54	0.00	0.06
AN 168.1	0.04	0.39	0.00	3.67	802.20	13.18	0.24	0.00	0.00	0.00	0.01
AN 170c	0.02	0.60	0.00	6.18	709.72	9.22	0.26	0.00	0.00	0.00	0.00
AN 172.1	0.05	0.39	0.00	3.35	786.02	7.15	0.25	0.00	0.06	0.00	0.00
AN 173	0.04	0.68	0.00	3.87	756.25	10.06	0.25	0.01	0.00	0.00	0.00
AN 176.1	0.10	0.96	0.00	5.48	766.57	12.79	0.44	0.00	0.00	0.00	0.01
AN 177	0.07	0.43	0.00	3.95	796.16	9.37	0.32	0.00	0.07	0.00	0.00
AN 179.1	0.06	0.30	0.00	3.79	778.68	17.67	0.21	0.00	0.00	0.00	0.03
AN 181	0.01	2.16	0.00	4.03	898.43	17.34	0.48	0.00	0.86	0.00	0.04
AN 183	0.03	0.84	0.00	3.25	834.10	14.34	0.41	0.00	0.00	0.00	0.00
AN 185	0.00	0.51	0.00	1.73	862.05	13.50	0.27	0.00	0.00	0.00	0.00
AN 188	0.09	1.23	0.00	1.72	847.35	5.87	0.29	0.00	0.34	0.00	0.03
AN 190	0.00	1.90	0.00	3.97	874.70	11.93	0.40	0.00	0.33	0.00	0.00
AN 192	0.03	1.13	0.00	3.80	845.72	12.11	0.28	0.00	1.06	0.00	0.00
AN 195	0.07	1.43	0.00	4.37	687.84	12.99	0.59	0.00	0.28	0.00	0.00
AN 196.2	0.07	0.70	0.00	5.09	702.61	18.34	0.37	0.00	0.32	0.00	0.02
AN 197	0.00	0.68	0.00	2.97	712.04	12.41	0.16	0.00	0.00	0.00	0.03
AN 198	0.05	0.52	0.00	3.21	827.31	10.45	0.30	0.01	0.00	0.00	0.00
AN 200	0.08	0.84	0.00	2.06	758.90	7.90	0.31	0.00	0.29	0.00	0.01
AN 202 c	0.04	0.32	0.00	2.46	781.99	8.25	0.16	0.00	0.58	0.00	0.00
AN 204	0.09	0.56	0.00	2.67	837.70	11.84	0.47	0.00	0.39	0.00	0.03
AN 206	0.07	1.31	0.00	4.65	771.84	9.30	0.65	0.00	0.33	0.00	0.01
AN 211	0.08	1.01	0.00	4.44	768.86	13.41	0.02	0.00	0.44	0.00	0.03
AN 214	0.04	0.91	0.00	2.53	815.93	8.32	0.19	0.00	0.20	0.00	0.04
AN 216	0.03	0.49	0.00	1.88	758.20	10.09	0.71	0.00	0.09	0.00	0.02

Angles section (continued)

Sample n°	Ag	Cd	Ba	Pb	Bi	Th	U
AN 125	0.07	0.05	397.96	1.94	0.38	0.80	0.96
AN 127	0.05	0.03	101.13	0.42	0.07	0.29	1.02
AN 128	0.04	0.07	44.62	0.69	0.04	0.25	0.76
AN 129	0.11	0.09	49.24	1.88	0.04	0.55	0.75
AN 131	0.03	0.03	124.55	1.47	0.03	0.49	0.84
AN 133	0.12	0.10	14.19	1.45	0.02	0.26	0.84
AN 136.2	0.12	0.07	100.58	3.71	0.05	0.84	0.61
AN 138	0.20	0.21	22.70	1.36	0.02	0.33	0.70
AN 139d	0.08	0.17	77.84	1.95	0.07	0.28	1.08
AN 141.1	0.04	0.22	20.38	1.17	0.37	0.26	0.66
AN 143.1a	0.04	0.10	92.68	0.70	0.08	0.31	0.69
AN 144	0.09	0.07	10.73	2.16	0.05	0.41	0.75
AN 147.1	0.07	0.26	69.96	1.37	0.09	0.29	1.26
AN 148	0.02	0.04	22.89	0.98	0.02	0.23	1.03
AN 149.3	0.04	0.06	25.00	1.07	0.02	0.29	0.83
AN 151.1	0.04	0.10	32.74	2.42	0.01	0.24	0.67
AN 151.3	0.02	0.02	10.12	0.79	0.00	0.17	0.70
AN 153.2	0.13	0.04	32.28	0.85	0.01	0.26	0.74
AN 155.1a	0.09	0.00	537.87	1.35	0.17	0.28	0.77
AN 156.1	0.06	0.00	12.63	1.04	0.08	0.28	0.69
AN 156.4	0.12	0.06	12.82	1.06	0.04	0.46	0.79
AN 156.6	0.06	0.02	19.60	1.41	0.06	0.45	1.09
AN 158	0.10	0.00	19.10	1.31	0.03	0.30	0.97
AN 160.3	0.02	0.05	15.13	1.41	0.00	0.45	1.08
AN 161.1	0.01	0.00	540.92	0.82	0.00	0.39	0.81
AN 161.2	0.03	0.00	174.61	0.77	0.00	0.22	1.88
AN 163.1b	0.00	0.00	52.68	1.10	0.00	0.23	1.19
AN 164.2	0.05	0.00	528.88	0.72	0.40	0.20	1.27
AN 166 b	0.98	1.70	64.69	5.47	0.17	0.38	2.70
AN 168.1	0.13	0.00	301.94	1.77	0.11	0.65	1.67
AN 170c	0.09	0.00	415.52	2.19	0.09	0.91	0.38
AN 172.1	0.06	0.00	188.78	1.57	0.05	0.50	0.41
AN 173	0.11	0.00	38.85	2.14	0.03	0.50	0.72
AN 176.1	0.08	0.00	58.20	2.27	0.06	0.91	0.59
AN 177	0.10	0.00	28.80	1.74	0.04	0.60	0.41
AN 179.1	0.01	0.00	55.12	1.74	0.03	0.59	0.73
AN 181	0.11	0.22	440.48	3.92	0.55	0.69	0.91
AN 183	0.06	0.00	35.11	2.11	0.28	0.34	0.99
AN 185	0.00	0.00	27.20	1.92	0.08	0.34	0.77
AN 188	0.01	0.12	77.01	0.98	0.07	0.24	0.69
AN 190	0.06	0.21	26.20	2.29	0.09	0.65	1.47
AN 192	0.21	0.02	14.26	1.92	0.59	0.50	1.20
AN 195	0.07	0.08	292.87	2.52	0.16	0.76	1.17
AN 196.2	0.04	0.00	16.45	2.26	0.10	0.81	1.42
AN 197	0.00	0.12	1092.72	1.15	0.04	0.72	0.65
AN 198	0.02	0.12	20.79	1.65	0.06	0.42	1.13
AN 200	0.01	0.00	21.74	1.38	0.06	0.36	0.70
AN 202 c	0.03	0.00	135.97	0.80	0.02	0.34	0.63
AN 204	0.00	0.16	46.72	1.69	0.02	0.43	1.75
AN 206	0.09	0.07	25.54	1.57	0.03	0.61	1.38
AN 211	0.05	0.09	120.36	0.86	0.49	0.44	0.97
AN 214	0.07	0.22	45.43	1.17	0.12	0.41	0.80
AN 216	0.02	0.20	25.95	1.22	0.06	0.34	0.95

Phosphorus data

Fiume-Bosso section

Stage	Ammonite zone	Sample n°	Depth (m)	Sed. Rate	P (ppm)	P (MAR)
Late Hauterivian	*B. balearis - P. ligatus*	FB 2	0.24		90.73	
		FB 5	1.71		96.43	
		FB 8	3.29		74.79	
		FB 12	4.61	1.10	118.73	0.33
		FB 15	5.98	1.55	113.32	0.44
		FB 21	8.37	1.65	85.34	0.35
		FB 28	9.41	0.75	90.37	0.17
		FB 33	10.37	0.90	91.96	0.21
		FB 41	11.48	1.00	106.79	0.27
		FB 45	12.66	0.85	77.60	0.16
		FB 50	13.72	1.00	82.07	0.21
		FB 55	14.64	1.35	92.50	0.31
		FB 59	15.31	0.95	88.27	0.21
		FB 65	16.38	0.80	69.59	0.14
		FB 71	17.75	1.25	107.01	0.33
		FB 79	18.82	1.20	76.30	0.23
		FB 89	19.92	1.45	105.89	0.38
		FB 94	20.84	0.65	81.59	0.13
		FB 99	21.77	1.05	98.47	0.26
		FB 104	22.73	0.85	95.05	0.20
		FB 109	23.78	0.80	82.86	0.17
		FB 123*	25.81	0.75	96.55	0.18
	P. Angulicostata	FB 128a	26.71	1.20	80.12	0.24
		FB 134a	27.81	1.15	75.09	0.22
		FB 136	28.36	1.15	86.84	0.25
		FB 139	28.93	0.63	95.75	0.15
		FB 371	29.07	0.63	90.53	0.14
	P. catulloi (subzone)	FB 373a	29.17	0.63	95.40	0.15
		FB 373 d	29.47	0.63	107.10	0.17
		FB 375	29.53	0.82	104.16	0.21
		FB 378	29.64	0.82	63.63	0.13
		FB 380 b	29.80	0.82	66.48	0.14
		FB 382 a	30.00	0.82	68.37	0.14
		FB 382 c	30.12	0.82	61.83	0.13
		FB 385	30.39	1.17	83.52	0.24
		FB 387 b	30.79	1.17	80.70	0.24
		FB 391	31.14	1.17	105.01	0.31
		FB 396 b	32.60	1.13	79.15	0.22
		FB 402 b	33.56	1.35	76.05	0.26
		FB 410	34.64	1.50	85.84	0.32
Early Barremian	*S. hugii*	FB 417	35.80	1.85	76.23	0.35
		FB 424	37.20	1.85	71.44	0.33
		FB 430a	38.27	1.65	62.54	0.26
		FB 433	39.43	1.45	70.21	0.25
		FB 440 a	40.43	1.60	91.27	0.37
		FB 448 b	41.71	1.60	83.17	0.33
		FB 451 a	42.73	1.10	77.04	0.21
		FB 454 b	43.91	0.85	72.72	0.15
		FB 459b	44.68	1.30	86.95	0.28
		FB 464 a	45.73	1.50	58.46	0.22
		FB 469	46.75	1.50	76.00	0.29
		FB 473b	47.69	1.25	71.21	0.22
		FB 480a	48.62	0.80	71.30	0.14
		FB 487	49.54	1.30	74.09	0.24
		FB 494b	50.59	0.45	79.63	0.09
		FB 499a	51.35		68.84	

Sed. Rate = Sedimentation rate, expressed in cm/kyr

Veveyse de Châtel - St. Denis section

Stage	Ammonite zone	Sample n°	Depth (m)	Sed. Rate	P (ppm)	P (MAR)
Late Hauterivian	*sayni*	VCD 1A	1.50	2.80	206.44	1.45
		VCD 3A	3.40	2.80	324.97	2.27
		VCD 4A	4.50	2.80	180.95	1.27
		VCD 6A	5.75	2.80	237.49	1.66
		VCD 9A	7.90	2.80	238.83	1.67
		VCD 13A	9.70	2.80	243.60	1.71
		VCD 15A	11.30	2.80	236.16	1.65
		VCD 18A	12.50	2.80	194.99	1.36
		VCD 21A	13.50	2.80	225.74	1.58
		VCD 24A	15.00	2.80	189.80	1.33
		VCD 27A	16.20	2.80	198.90	1.39
		VCD 29A	16.90	2.80	196.77	1.38
	ligatus	SDII 1	18.80	2.50	156.16	0.98
		SDII 3	20.10	2.50	178.51	1.12
		SDII 5	22.00	2.50	189.92	1.19
		SDII 6	23.00	2.50	187.89	1.17
		SDII 7c	24.50	2.50	222.05	1.39
		SDII 10	26.90	2.50	311.12	1.94
		SDII 11	28.00	2.50	253.43	1.58
		SDII 13a	28.80	2.50	216.95	1.36
		SDII 14	29.80	2.50	220.03	1.38
		SDII 15	31.50	2.50	246.17	1.54
	balearis	SDII 16b	32.60	3.19	238.14	1.90
		SDII 18	33.80	3.19	260.74	2.08
		SDII 19	35.10	3.19	383.05	3.05
		SDII 21	36.70	3.19	205.98	1.64
		SDII 23	38.20	3.19	219.00	1.75
		SDII 25	40.30	3.19	266.80	2.13
		SDII 27	42.20	3.19	263.31	2.10
		SDII 28	43.50	3.19	305.60	2.44
		SDII 30	44.30	3.19	243.68	1.94
		SDII 33	47.30	3.19	435.67	3.47
		SDII 34	49.30	3.19	230.95	1.84
		SDII 36	50.90	3.19	186.30	1.49
		SDII 40	52.90	3.19	169.55	1.35
		VCDII 51A	54.20	3.19	160.25	1.28
	angulicostata auct.	SDII 42	54.50	3.75	154.74	1.45
		VCDII 50A	54.80	3.75	187.46	1.76
		SDII 43	55.20	3.75	191.89	1.80
		VCDII 49A	55.50	3.75	162.68	1.53
		VCDII 48A	56.10	3.75	210.10	1.97
		VCDII 46A	57.75	3.75	240.04	2.25
		VCDII 44A	59.10	3.75	152.03	1.43
		VCDII 42A	60.40	3.75	180.82	1.70
		VCDII 40A	62.10	3.75	204.70	1.92
		SDII 51	62.80	3.75	192.51	1.80
		VCDII 37A	63.40	3.75	197.24	1.85
		VCDII 35A	64.50	3.75	143.61	1.35
		VCDII 33A	65.60	3.75	176.41	1.65
		VCDII 30A	67.50	3.75	156.89	1.47
		VCDII 27A	68.70	3.75	288.18	2.70
		VCDII 25A	70.20	3.75	293.30	2.75
		VCDII 22A	71.60	3.75	199.29	1.87
		VCDII 19A	73.30	3.75	180.91	1.70
		VCDII 16A	75.50	3.75	135.34	1.27
		VCDII 12A	76.90	3.75	133.23	1.25
		VCDII 10A	78.40	3.75	123.73	1.16
		VCDII 8A	80.00	3.75	186.95	1.75
		SD 42	81.60	3.75	293.27	2.75
		VCDII 6A	82.50	3.75	191.44	1.79
		SD 38	85.00	3.75	235.32	2.21
		SD 36	86.00	3.75	187.55	1.76
		SD 32	88.30	3.75	200.54	1.88
		SD 29	90.30	3.75	200.11	1.88
		SD 27	91.20	3.75	190.06	1.78
		SD 24	92.90	3.75	233.00	2.18
Early Barremian	*hugii*	SD 21	94.20	5.00	203.23	2.54
		SD 19	97.20	5.00	189.75	2.37
		SD 16	98.80	5.00	212.21	2.65
		SD 12	99.70	5.00	199.23	2.49
		SD 8	102.60	5.00	191.79	2.40
		SD 5	103.80	5.00	199.57	2.49
		SD 1	105.40	5.00	185.84	2.32

Sed. Rate = Sedimentation rate, expressed in cm/kyr

Angles section

Stage	Ammonite zone	Sample n°	Depth (m)	Sed. Rate	P (ppm)	P (MAR)
Late Hauterivian	*B. balearis*	AN 2	0.57	2.54	208.85	1.32
		AN 4	2.54	2.54	179.05	1.14
		AN 6	4.55	2.54	211.17	1.34
		AN 8	6.12	2.54	251.97	1.60
		AN 10	7.83	2.54	218.98	1.39
		AN 13	9.95	2.54	176.94	1.12
		AN 15.1	11.75	2.54	190.90	1.21
		AN 16	13.23	2.54	143.52	0.91
		AN 18	14.89	2.54	222.00	1.41
		AN 20	16.26	2.54	179.45	1.14
		AN 23	17.52	2.54	254.98	1.62
		AN 26	19.37	2.54	200.15	1.27
		AN 27.2	20.60	2.54	196.39	1.24
		AN 29	22.61	2.54	173.82	1.10
		AN 31	23.99	2.54	209.96	1.33
		AN 33	25.43	2.54	175.41	1.11
		AN 35	27.27	2.54	237.92	1.51
	S. angulicostatum	AN 38	28.86	1.73	190.07	0.82
		AN 40	30.16	1.73	242.83	1.05
		AN 43	31.68	1.73	197.78	0.85
		AN 46	33.09	1.73	186.50	0.80
		AN 49.1	35.14	1.73	209.54	0.90
		AN 50	35.95	1.73	194.22	0.84
		AN 51	36.54	1.73	236.38	1.02
		AN 52	37.25	1.73	163.43	0.71
		AN 53.2	38.45	1.73	150.00	0.65
	P. mortilleti	AN 55	39.09	1.35	169.54	0.57
		AN 62.1	42.75	1.35	177.47	0.60
		AN 65.1	44.41	1.82	165.04	0.75
		AN 68	46.95	1.82	185.90	0.85
		AN 71	48.89	1.82	166.21	0.76
Early Barremian	*A. kiliani*	AN 72	49.67	2.65	169.61	1.12
		AN 75	52.03	2.65	138.67	0.92
		AN 78	54.96	2.65	174.95	1.16
		AN 81	56.97	2.65	186.02	1.23
		AN 84	59.37	2.65	146.56	0.97
		AN 87	62.09	2.65	163.05	1.08
		AN 89	64.13	2.65	141.42	0.94
		AN 90 haut	65.93	2.65	165.05	1.09
		AN 92	68.72	2.65	152.23	1.01
		AN 93 haut	70.61	2.65	147.80	0.98
		AN 95 bas	73.06	2.65	179.29	1.51
		AN 97	75.63	2.65	170.44	1.44
		AN 98 haut	77.22	2.65	161.56	1.36
	K. nicklesi	AN 101	79.74	3.38	185.00	1.56
		AN 103	82.76	3.38	178.06	1.50
		AN 104	84.77	3.38	168.31	1.42
		AN 105	86.36	3.38	228.08	1.92
		AN 108	91.16	3.38	232.93	1.97
	N. pulchella	AN 109.4	93.52	2.44	174.87	1.07
		AN 110.1b	95.07	2.44	186.10	1.13
		AN 110.3c	98.00	2.44	151.72	0.92
		AN 110.4	99.66	2.44	165.62	1.01
		AN 111.2	101.21	2.44	185.08	1.13
		AN 111.5	102.87	2.44	185.73	1.13
		AN 112.2	105.06	2.44	168.16	1.02
	K. compressissima	AN 112.7	108.51	2.56	203.94	1.31
		AN 114.2	111.70	2.56	179.98	1.15
		AN 115	113.42	2.56	158.08	1.01
		AN 117	114.97	2.56	158.29	1.01
		AN 119	116.66	2.56	147.01	0.94
		AN 121	118.53	2.56	160.58	1.03
		AN 123	119.84	2.56	181.41	1.16

Sed. Rate = Sedimentation rate, expressed in cm/kyr

Angles section (continued)

Stage	Ammonite zone	Sample n°	Depth (m)	Sed. Rate	P (ppm)	P (MAR)
Early Barremian	*C. darsi*	AN 125	121.89	2.87	147.42	1.06
		AN 127	123.65	2.87	177.38	1.27
		AN 128	124.85	2.87	159.07	1.14
		AN 129	125.62	2.87	199.79	1.43
		AN 131	127.70	2.87	167.50	1.20
		AN 133	130.00	2.87	196.05	1.41
		AN 136.2	131.97	2.87	203.44	1.46
		AN 138	133.17	2.87	241.61	1.73
		AN 139d	134.69	2.87	175.89	1.26
Late Barremian	*H. uhligi*	AN 141.1	136.21	2.08	205.95	1.07
		AN 143.1a	138.22	2.08	237.81	1.24
		AN 144	140.65	2.08	158.64	0.83
		AN 147.1	142.66	2.08	237.07	1.23
	H. sayni	AN 148	144.04	1.96	181.33	0.89
		AN 149.3	145.42	1.96	236.06	1.16
		AN 151.1	146.93	1.96	174.95	0.86
		AN 151.3	148.23	1.96	181.08	0.89
		AN 153.2	149.93	1.96	168.14	0.83
		AN 155.1a	151.41	1.96	180.51	0.89
		AN 156.1	152.82	1.96	188.56	0.93
		AN 156.4	155.01	1.96	178.12	0.87
		AN 156.6	156.63	1.96	171.98	0.84
		AN 158	158.75	1.96	184.79	0.91
	G. sartousiana	AN 160.3	160.44	2.31	247.55	1.43
		AN 161.1	160.84	2.31	165.73	0.96
		AN 161.2	161.54	2.31	199.27	1.15
		AN 163.1b	163.30	2.31	165.81	0.96
	H. feraudianus	AN 164.2	164.92	1.56	154.25	0.60
		AN 166 b	166.27	1.56	234.10	0.91
	I. giraudi	AN 168.1	167.92	1.80	296.19	1.33
		AN 170c	169.30	1.80	231.74	1.04
		AN 172.1	170.64	1.80	139.33	0.63
		AN 173	172.19	1.80	183.44	0.82
		AN 176.1	175.26	1.80	199.83	0.90
	M. sarasini	AN 177	176.74	2.30	191.42	1.10
		AN 179.1	178.30	2.30	185.86	1.07
		AN 181	180.34	2.30	161.24	0.93
		AN 183	181.75	2.30	195.08	1.12
		AN 185	183.66	2.30	150.66	0.87
		AN 188	186.34	2.30	132.17	0.76
		AN 190	187.96	2.30	174.63	1.00
		AN 192	189.62	2.30	214.21	1.23
		AN 195	192.48	2.30	216.05	1.24
		AN 196.2	193.79	2.30	181.75	1.05
Early Aptian	*D. oglanlensis*	AN 197	195.16	2.25	160.45	0.90
		AN 198	196.15	2.25	170.70	0.96
		AN 200	197.77	2.25	123.32	0.69
		AN 202 c	199.43	2.25	147.11	0.83
		AN 204	200.76	2.25	157.82	0.89
		AN 206	202.04	2.25	180.39	1.01
		AN 211	204.67	2.25	150.16	0.84
		AN 214	206.39	2.25	131.31	0.74
		AN 216	207.70	2.25	119.06	0.67

Sed. Rate = Sedimentation rate, expressed in cm/kyr

Gorgo a Cerbara section

Stage	Magnetochron	Sample n°	Depth (m)	Sed. Rate	P (ppm)	P (MAR)
Early Aptian	*M-0*	GC 50	69.80	0.12	264.14	0.08
Late Barremian	*M-1n*	GC 51	68.90	0.21	245.72	0.13
		GC 52	68.40	0.15	265.57	0.10
		BA 01	67.80	0.07	610.01	0.10
		BA 02	67.20	0.42	289.50	0.30
		BA 03	66.50	0.62	293.73	0.45
		BA 04	66.00	0.62	259.31	0.40
		BA 05	65.00	0.22	369.06	0.20
		BA 06	64.00	0.33	273.86	0.23
		BA 07	63.10	0.35	360.28	0.32
		BA 08	62.50	0.52	350.21	0.46
		BA 09	61.80	0.58	381.18	0.55
		BA 10	61.00	0.30	298.96	0.23
		BA 11	60.00	0.82	259.30	0.53
		BA 12	58.80	0.66	275.04	0.45
		BA 13	58.00	0.66	283.90	0.47
		BA 14	57.00	0.48	250.09	0.30
		BA 15	55.90	0.48	212.65	0.26
		BA 16	54.70	0.58	284.31	0.41
		BA 50	50.80	0.38	257.54	0.25
		BA 49	49.90	0.69	225.52	0.39
	M-1	BA 48	48.00	0.65	197.57	0.32
		BA 47	46.70	0.66	272.86	0.45
		BA 46	45.00	0.76	313.65	0.59
	M-2	BA 45	43.50	0.82	209.07	0.43
		BA 44	42.00	0.75	238.56	0.45
		BA 43	40.10	0.89	242.34	0.54
		BA 42	37.90	0.62	247.73	0.38
		BA 41	35.90	0.55	244.72	0.34
		BA 40	34.60	0.49	267.85	0.33
Early Barremian	*M-3*	BA 39	33.50	0.89	303.70	0.68
		BA 38	32.20	0.82	375.61	0.77
		BA 37	30.50	1.07	279.34	0.75
		BA 36	28.90	0.89	282.08	0.63
		BA 35	27.10	0.33	232.15	0.19
		BA 34	25.70	0.33	248.95	0.21
		BA 33	24.00	0.41	264.11	0.27
		BA 32	23.20	0.34	295.46	0.25
		BA 31	22.30	0.69	307.29	0.53
		BA 30	20.50	0.62	348.40	0.54
		BA 29	19.50	0.34	259.38	0.22
		BA 28	18.20	0.62	198.51	0.31
		BA 27	17.10	1.07	257.69	0.69
		BA 26	15.70	0.46	220.91	0.25
		BA 25	13.20	0.76	263.31	0.50
		BA 24	11.10	0.76	327.00	0.62
		BA 23	9.60	0.34	214.72	0.18
Late Hauterivian	*M-4*	BA 22	8.10	0.82	271.90	0.56
		BA 21	6.70	0.41	328.12	0.34
		BA 20	5.70	0.34	385.88	0.33
		BA 19	4.50	0.55	259.88	0.36
		BA 18	2.50	0.55	276.37	0.38
		BA 17	0.90	0.41	247.77	0.26

Sed. Rate = Sedimentation rate, expressed in cm/kyr

Curriculum Vitae

Stéphane Bodin

Sedimentologist and geochemist

Institute of Geology and Hydrogeology
University of Neuchâtel
Rue Emile-Argand 11, CP 158
2009 Neuchâtel
Switzerland

stephane.bodin@unine.ch

RESEARCH FOCUS

- Rapid and long-term global changes
- Oceanic anoxic events
- Interaction between carbonate platform factory and palaeoceanographic conditions
- Palaeoproductivity and palaeoredox proxies
- Palaeoenvironmental reconstructions

EDUCATION

Pending **PhD in Geology.** Laboratory of Geochemical and Environmental Analyses, University of Neuchâtel, Institute of Geology, Switzerland.

2002 **"DEA" (Master equivalent),** major in Geochemistry. University Louis Pasteur, Strasbourg I, Centre de Géochimie de la Surface, France. Graduated with distinction.

2001 **"Maîtrise" of Science in Geology,** major in Geochemistry. University Louis Pasteur, Strasbourg I, Centre de Géochimie de la Surface, France. Graduated with distinction.

2000 **"Licence" (Bachelor equivalent) of Science in Geology.** University Louis Pasteur, Strasbourg I, Centre de Géochimie de la Surface, France. Graduated with distinction.

1999 **"DEUG", major in Life and Earth Sciences.** University Louis Pasteur, Strasbourg I, Centre de Géochimie de la Surface, France.

1995 **Scientific "Baccalauréat"**, major in Life and Earth Sciences, Lycée Kléber, Strasbourg, France. Graduated with distinction.

RESEARCH EXPERIENCE

October 2002 – present

Laboratory of Geochemical and Environmental Analyses, University of Neuchâtel, Institute of Geology, Switzerland.
PhD under the supervision of Prof. Karl B. Föllmi.

"Palaeoceanographic and palaeoclimatic changes during the late Hauterivian – Barremian and their impact on the Northern Tethyan margin: a combined sedimentological and geochemical approach."

August – September 2002

TotalFinaElf company, La Défense, Paris, France.
Internship under the supervision of Dr. Christian Blanpied.

Bibliography research, seismic profiles and well-log interpretations, and report on the "Snowball Earth" theory and its link to petroleum resources.

January – June 2002

Laboratory of Paleoenvironment and Sedimentary Basin Tectonic, Centre de Géochimie de la surface, University Louis Pasteur, Strasbourg I, France.
Master's under the supervision of Dr. Philippe Duringer.

Translated title "Are the Permian rhyolitic flows from the Nideck (Vosges, France) tephras? Volcano-sedimentary study of one of the principal volcanoes of Alsace."

April – June 2001

Laboratory of Paleoenvironment and Sedimentary Basin Tectonic, Centre de Géochimie de la surface, University Louis Pasteur, Strasbourg I, France.
Supervisors: Dr. Jean-François Ghienne & Dr. Philippe Duringer.

Translated title "Syn-sedimentary deformations associated to the Limberg volcanic activity (Kaiserstuhl massif, Germany)."

SKILLS

Geology

Basin and platform carbonate sedimentology
Sequence stratigraphy
Palaeoceanography
Palaeoproductivity and palaeredox proxies
Volcano-sedimentology

Laboratory

ICP-MS analyses
Phosphorus analyses with the SEDEX method
Rock-Eval 6 organic carbon analyses

TEACHING EXPERIENCE

October 2002 – present

General Geology practical classes (1st year students), University of Neuchâtel.
Sedimentology practical classes (2nd year students), University of Neuchâtel.
Geological Cartography and Field Sedimentology excursions guide (1st, 2nd and 3rd year students), University of Neuchâtel.
Geochemistry practical classes (3rd year students), University of Neuchâtel.

June 2002

Geological Cartography and Field Sedimentology excursions co-leader (3rd year students), University Louis Pasteur, Strasbourg I.

ORGANISATION OF CONFERENCE

September 2005

Member of the organization committee for the **"7th International Symposium on the Cretaceous"** held in Neuchâtel (Switzerland).
Co-editor of the Abstract volume and field trip co-leader.

AWARD

April 2006

IAS Young Scientists' Outstanding Paper Award (Best student oral presentation at the EGU Vienna April 2006).

REFEREED PAPERS

Bodin S., Godet A., Föllmi K.B., Vermeulen J., Arnaud H., Strasser A., Fiet N. & Adatte, T. (2006) The Late Hauterivian Faraoni oceanic anoxic event in the western Tethys: Evidence from phosphorus burial rates. *Palaeogeography, Palaeoclimatology, Palaeoecology 235, 245-264*.

Godet A., **Bodin S.**, Föllmi K.B., Vermeulen J., Gardin S., Fiet N., Adatte T., Berner Z., Stüben D. & Van de Schootbrugge B. (2006) Evolution of the marine stable carbon-isotope record during the early Cretaceous: A focus on the late Hauterivian and Barremian in the Tethyan realm. *Earth and Planetary Science Letters 242, 254-271*.

Bodin S., Godet A., Vermeulen J., Linder P. & Föllmi K.B. (2006) Biostratigraphy, sedimentology and sequence stratigraphy of the latest Hauterivian – Early Barremian drowning episode of the Northern Tethyan margin (Altmann Member, Helvetic nappes, Switzerland). *Eclogae Geologicae Helvetiae 99, 157-174*.

Bodin S., Vermeulen J., Godet A. & Föllmi K.B. (2006) New data on the age of the installation of the Urgonian-type carbonates along the northern Tethyan margin: Biostratigraphy of the Chopf Member (Helvetic Alps, eastern Switzerland). *Comptes rendus de Géosciences 338, 727-733*.

Bodin S., Godet A., Matera V., Steinmann P., Vermeulen J., Gardin S., Adatte T., Coccioni R. & Föllmi K.B. (in press) Enrichment of redox-sensitive trace metals (U, V, Mo, As) associated with the late Hauterivian Faraoni oceanic anoxic event. *International Journal of Earth Sciences. DOI: 10.1007/s00531-006-0091-9*

Föllmi K.B., Godet A., **Bodin S.** & Linder P. (2006) Interactions between environmental change and shallow-water carbonate build-up along the northern Tethyan margin and their impact on the early Cretaceous carbon-isotope record. *Paleoceanography 21, PA4211*.

NON PEER-REVIEWED PAPERS

Godet A., Blanc-Aletru M.C., **Bodin S.**, Adatte T. & Föllmi, K.B. (2005) The Hauterivian - Barremian of the Western Swiss Jura around Neuchâtel. In: The Hauterivian - Lower Aptian sequence stratigraphy from Jura platform to Vocontian basin: a multidisciplinary approach (Eds. Adatte T. *et al.*), *Géologie Alpine, Série Spéciale "Colloques et Excursions" n°7, pp. 79-96*.

Bodin S., Godet A., Adatte T. & Föllmi K.B. (2005) Palaeoceanographic and palaeoclimatic changes of the northern tethyan realm during the Hauterivian - Barremian: New insight from the Angles section (SE France). In: The Hauterivian - Lower Aptian sequence stratigraphy from Jura

platform to Vocontian basin: a multidisciplinary approach (Eds. Adatte T. *et al.*), *Géologie Alpine, Série Spéciale "Colloques et Excursions" n°7, pp. 138-146.*

SUBMITTED PAPERS

Godet A., **Bodin S.**, Adatte T. & Föllmi K.B. (submitted) Platform-induced clay-mineral fractionation along a northern Tethyan basin-platform transect: implication for the interpretation of Early Cretaceous climate change. *Cretaceous Research.*

PAPERS IN PREPARATION

Bodin S., Fiet N., Matera V., Godet A., Clément A., Jansen N.M.M. & Föllmi K.B. An integrated approach to palaeoceanographic changes during the Early Cretaceous in the western Tethyan realm and their link to carbonate-platform factory changes and drowning.

Bodin S., Pittet B., Godet A., Matera V. & Föllmi K.B. Milankovitch-type cyclicity of Rare Earth Elements concentration in the carbonate of the Angles section (Late Hauterivian – Early Barremian, SE France).

Godet A., **Bodin S.**, Stille P., Adatte T., Van de Schootbrugge B., Matera V. & Föllmi K.B. Strontium-isotopes stratigraphy of the Urgonian Formation from the Western Swiss Jura: implication for the evolution of the Early Cretaceous northern Tethyan carbonate platforms.

PRESENTATIONS AT CONFERENCES (as first author)

Bodin S., Godet A., Adatte T., Matera V., Vermeulen J., Steinmann P. & Föllmi K.B. (2004) A record of the Late Hauterivian – Barremian palaeoenvironmental crisis (Faraoni and Mid-Barremian Event levels) in the Helvetic Alps. 32nd International Geological Congress, Florence, Italy, August 20-28, 2004. *Oral presentation.*

Bodin S., Godet A., Föllmi K.B., Adatte T., Matera V., Vermeulen J., Steinmann P. & Gardin S. (2004) Understanding the carbonate platform drowning event D3 of the Helvetics Alps: New insight from pelagic sections. Reunion des Sciences de la Terre, Strasbourg, France, 20-25 Septembre 2004. *Oral presentation.*

Bodin S., Godet A., Vermeulen J., Adatte T., Matera V., Steinmann P., Gardin S. & Föllmi K.B. (2005) The Altmann Beds (Late Hauterivian – Early Barremian, Helvetic realm): new perspectives and paleoceanographic interpretations. Thirteenth SwissSed, Fribourg, Switzerland, 29 January 2005. *Oral presentation.*

Bodin S., Godet A., Vermeulen J. & Föllmi K.B. (2005) The drowning of the Helvetic platform during the Hauterivian – Barremian transition (Altmann Beds, Switzerland). Sediment 05, Gwatt, Switzerland, 18-20 July 2005. *Oral presentation.*

Bodin S., Godet A., Vermeulen J., Adatte T., Matera V., Steinmann P., Gardin S., Fiet N. & Föllmi K.B. (2005) Palaeoceanographic changes in the western Tethys during the Late Hauterivian – Barremian : Evidences from geochemical tools. 7th International Symposium on the Cretaceous, Neuchâtel, Switzerland, 5-9 September 2005. *Oral presentation.*

Bodin S., Godet A., Vermeulen J. & Föllmi K.B. (2005) The drowning of the Helvetic platform during the Hauterivian – Barremian transition (Altmann Beds, Switzerland): A reevaluation. 7th International Symposium on the Cretaceous, Neuchâtel, Switzerland, 5-9 September 2005. *Poster presentation.*

Bodin S., Godet A. & Föllmi K.B. (2005) An integrated approach to carbonate platform factory changes and drowning: Example from the Hauterivian – Barremian transition in the western Tethyan realm. Réunion thématique du Groupe Français du Crétacé, Paris, France, 5-6 Décembre 2005. *Oral presentation*.

Bodin S., Godet A. & Föllmi K.B. (2006) Phosphogenesis and silicification associated to condensation events: an example from the Hauterivian – Barremian transition along the northern Tethyan margin (Helvetic realm, Switzerland). EGU General Assembly, Geophysical Research Abstracts, Volume 8, Vienna, Austria, 2-7 April 2006. *Oral presentation*.

LANGUAGES

French	Mother tongue
English	Good command
German	Basic knowledge

HOBBIES

Cultural	Theater (acted for 5 years)
Sports	Soccer, volleyball, tennis, table tennis, squash

REFERENCES

Prof. Karl B. Föllmi karl.foellmi@unine.ch
University of Neuchâtel +41 32 718 2655
Institute of Geology
Emile-Argand, 11
CP 158
CH-2009 Neuchâtel
Switzerland

Dr. Christian Blanpied christian.blanpied@total.com
Total, Exploration & Production +33 1 47 44 47 56
2 place de la Coupole
La Défense 6, Cedex 45
F-92078 Paris La Défense
France

Dr. Philippe Duringer duringer@illite.u-strasbg.fr
Université Louis Pasteur +33 3 90 24 04 28
Centre de Géochimie de la Surface
CNRS UMR 7517
Institut de Géologie
1 rue Blessig
F-67084 Strasbourg Cedex
France

Abstract

The goal of this PhD study was to decipher the mechanisms responsible for changes in the carbonate platform factory accompanied by incipient drowning. For this purpose, a peculiar condensed level called the Altmann Member, which recorded the northern Tethyan margin drowning during the latest Hauterivian – Early Barremian, and which is now locked up in the Helvetic realm, was studied. Indeed, this horizon is situated at the verge of a major change in the carbonate platform production mode. On one hand, during the Hauterivian, heterotrophic organisms such as crinoids and bryozoans dominated the northern Tethyan carbonate platforms. On the other hand, phototrophic organisms such as corals, green algae and rudists dominated during the Late Barremian. This important transition and its documentation in the shelf and basinal realms of the Tethys offered the framework of this study.

Helvetic realm: A first step was to establish as precisely as possible the time range of the Late Hauterivian – Barremian sediments in the Helvetic realm. Thanks to numerous ammonite findings, it was possible to determine that the Altmann Member spans from the *Pseudothurmannia seitzi* (latest Hauterivian) to the *Coronites darsi* (latest Early Barremian) ammonite zones. The onset of the Schrattenkalk Formation is dated by sequence stratigraphy correlation and by ammonite findings in the Chopf Member. This event is dated as belonging to the *Gerhardtia sartousiana* zone.

Sedimentology and sequence stratigraphy studies helped to determine the unfolding of the Altmann Member drowning episode, which has proceeded in two steps. The first one is coeval with the Faraoni event, which was thus far only reported from basinal settings. The second step is coeval with the Barremian second-order sea-level rise occurring at the Early – Late Barremian transition. During the Early Barremian second-order sea-level lowstand, the Helvetic platform was submitted to winnowing currents leading to the formation of phosphatized crusts.

Basin sections: In order to understand the link between carbonate platform factory changes and drowning events, geochemical studies were done on bulk-rock and belemnite samples from (hemi-) pelagic sections. These include redox-sensitive trace metals, phosphorus, carbon and oxygen isotopes. Four sections were chosen: the Angles section, SE France, which is the Barremian stratotype section; the Veveyse de Châtel – St. Denis section, Ultrahelvetic realm, Switzerland: the Fiume-Bosso and Gorgo a Cerbara sections, Umbria-Marche basin, Italy. These four sections offer a good coverage of the western Tethys and allow thus to establish general trends in the paleoceanographic conditions of the western Tethys at that time.

Enrichments of redox-sensitive trace metals were used to trace oceanic anoxic events during the Late Hauterivian – Early Barremian, because numerous black-shale horizons are recognized in the corresponding rocks. Only one level, corresponding to the Faraoni Level, was identified as the result of an oceanic anoxic event. This result is confirmed by the C/P ratio that shows a positive shift associated to the Faraoni Level.

Phosphorus burial rates were used to trace nutrient contents in the ocean during the Late Hauterivian – Barremian. They have resulted in a tripartite division of trophic conditions during the studied time interval. Thus, the middle Late Hauterivian is associated to mesotrophic conditions, the latest Hauterivian – Early Barremian to eutrophic conditions and the Late Barremian to oligotrophic conditions.

Bulk rock carbon isotopes were investigated in order to obtain information about the carbon cycle and its link to the carbonate platform. It appears that the bulk-rock carbon isotope signal in basinal sections situated close to the northern Tethyan margin is strongly influenced by carbonate factory changes due to carbonate platform shedding into the basin. During the time of heterozoan-dominated platform growth, the pelagic carbon isotope signal is buffered by the shedding of calcite-dominated fragments and dissolved inorganic carbon. During the time of photozoan-dominated platform growth, the pelagic carbon isotope signal is pushed to heavier values due to the export of aragonite.

Finally, in order to better understand the interactions between palaeoenvironmental changes and carbonate platform, an integrated approach, coupling numerous geochemical data as well as clay minerals, sea-level changes and others information, was done. This approach allows to conclude that changes in the northern Tethyan carbonate platform factory were driven by the overall nutrient content in seawater. During times of oligotrophic conditions, photozoan carbonate systems dominated the neritic realm whereas during times of meso-eutrophic conditions, heterozoan carbonate systems developed. Moreover, carbonate platform drowning events were linked to changes in ocean current pattern during time of sea-level highstand, together with high seawater nutrient levels. These changes have favored winnowing of platform-surface sediments and the deposition of phosphate-rich layers, and precluded carbonate platform growth along the northern Tethyan margin.